ENGINEERING ADULT NEUROGENESIS AND GLIOGENESIS

EDITED BY: Fraser James Sim, Annalisa Buffo, Daniel A. Peterson and Christophe Heinrich

PUBLISHED IN: Frontiers in Neuroscience, Frontiers in Cellular Neuroscience, Frontiers in Molecular Neuroscience and Frontiers in Neuroanatomy

frontiers Research Topics

frontiers

ISSN 1664-8714
ISBN 978-2-88966-510-5
DOI 10.3389/978-2-88966-510-5

About Frontiers

Frontiers is more than just an open-access publisher of scholarly articles: it is a pioneering approach to the world of academia, radically improving the way scholarly research is managed. The grand vision of Frontiers is a world where all people have an equal opportunity to seek, share and generate knowledge. Frontiers provides immediate and permanent online open access to all its publications, but this alone is not enough to realize our grand goals.

Frontiers Journal Series

The Frontiers Journal Series is a multi-tier and interdisciplinary set of open-access, online journals, promising a paradigm shift from the current review, selection and dissemination processes in academic publishing. All Frontiers journals are driven by researchers for researchers; therefore, they constitute a service to the scholarly community. At the same time, the Frontiers Journal Series operates on a revolutionary invention, the tiered publishing system, initially addressing specific communities of scholars, and gradually climbing up to broader public understanding, thus serving the interests of the lay society, too.

Dedication to Quality

Each Frontiers article is a landmark of the highest quality, thanks to genuinely collaborative interactions between authors and review editors, who include some of the world's best academicians. Research must be certified by peers before entering a stream of knowledge that may eventually reach the public - and shape society; therefore, Frontiers only applies the most rigorous and unbiased reviews.
Frontiers revolutionizes research publishing by freely delivering the most outstanding research, evaluated with no bias from both the academic and social point of view. By applying the most advanced information technologies, Frontiers is catapulting scholarly publishing into a new generation.

What are Frontiers Research Topics?

Frontiers Research Topics are very popular trademarks of the Frontiers Journals Series: they are collections of at least ten articles, all centered on a particular subject. With their unique mix of varied contributions from Original Research to Review Articles, Frontiers Research Topics unify the most influential researchers, the latest key findings and historical advances in a hot research area! Find out more on how to host your own Frontiers Research Topic or contribute to one as an author by contacting the Frontiers Editorial Office: frontiersin.org/about/contact

ENGINEERING ADULT NEUROGENESIS AND GLIOGENESIS

Topic Editors:
Fraser James Sim, University at Buffalo, United States
Annalisa Buffo, University of Turin, Italy
Daniel A. Peterson, Rosalind Franklin University of Medicine and Science, United States
Christophe Heinrich, INSERM U1208 Institut Cellule Souche et Cerveau, France

Citation: Sim, F. J., Buffo, A., Peterson, D. A., Heinrich, C., eds. (2021). Engineering Adult Neurogenesis and Gliogenesis. Lausanne: Frontiers Media SA.
doi: 10.3389/978-2-88966-510-5

Table of Contents

frontiers in Neuroanatomy

ORIGINAL RESEARCH
published: 06 November 2017
doi: 10.3389/fnana.2017.00094

The BAF45D Protein Is Preferentially Expressed in Adult Neurogenic Zones and in Neurons and May Be Required for Retinoid Acid Induced PAX6 Expression

Chao Liu[1,2,3*†], *Ruyu Sun*[1,2,3†], *Jian Huang*[4†], *Dijuan Zhang*[1,2,3], *Dake Huang*[1], *Weiqin Qi*[1], *Shenghua Wang*[1,2,3], *Fenfen Xie*[1,2,3], *Yuxian Shen*[1] and *Cailiang Shen*[4*]

[1] School of Basic Medical Sciences, Anhui Medical University, Hefei, China, [2] Department of Histology and Embryology, Anhui Medical University, Hefei, China, [3] Institute of Stem Cell and Tissue Engineering, Anhui Medical University, Hefei, China, [4] Department of Spine Surgery, The First Affiliated Hospital of Anhui Medical University, Hefei, China

OPEN ACCESS

Edited by:
Daniel A. Peterson, Rosalind Franklin University of Medicine and Science, United States

Reviewed by:
Richard S. Nowakowski, Florida State University College of Medicine, United States
Tobias David Merson, Australian Regenerative Medicine Institute (ARMI), Australia

***Correspondence:**
Chao Liu
chaol1974@ahmu.edu.cn
Cailiang Shen
shencailiang1616@163.com

[†] These authors have contributed equally to this work.

Received: 06 July 2017
Accepted: 13 October 2017
Published: 06 November 2017

Citation:
Liu C, Sun R, Huang J, Zhang D, Huang D, Qi W, Wang S, Xie F, Shen Y and Shen C (2017) The BAF45D Protein Is Preferentially Expressed in Adult Neurogenic Zones and in Neurons and May Be Required for Retinoid Acid Induced PAX6 Expression. Front. Neuroanat. 11:94. doi: 10.3389/fnana.2017.00094

Adult neurogenesis is important for the development of regenerative therapies for human diseases of the central nervous system (CNS) through the recruitment of adult neural stem cells (NSCs). NSCs are characterized by the capacity to generate neurons, astrocytes, and oligodendrocytes. To identify key factors involved in manipulating the adult NSC neurogenic fate thus has crucial implications for the clinical application. Here, we report that BAF45D is expressed in the subgranular zone (SGZ) of the dentate gyrus, the subventricular zone (SVZ) of the lateral ventricle, and the central canal (CC) of the adult spinal cord. Coexpression of BAF45D with glial fibrillary acidic protein (GFAP), a radial glial like cell marker protein, was identified in the SGZ, the SVZ and the adult spinal cord CC. Quantitative analysis data indicate that BAF45D is preferentially expressed in the neurogenic zone of the LV and the neurons of the adult CNS. Furthermore, during the neuroectoderm differentiation of H9 cells, BAF45D is required for the expression of PAX6, a neuroectoderm determinant that is also known to regulate the self-renewal and neuronal fate specification of adult neural stem/progenitor cells. Together, our results may shed new light on the expression of BAF45D in the adult neurogenic zones and the contribution of BAF45D to early neural development.

Keywords: BAF45D, adult neural stem cell, subgranular zone, subventricular zone, ependymal cells, PAX6

INTRODUCTION

Adult neurogenesis is important for driving structural plasticity of the brain through addition and integration of new neurons from adult neural stem cells (NSCs; Sailor et al., 2017), which can selfrenew and generate neurons, astrocytes, and oligodendrocytes (Gage, 2000; Ma et al., 2009). Aberrant modulation of the differentiation potential of NSCs residing in the central canal of the spinal cord contributes to cell loss and neural circuitry dysfunction following spinal cord injury (Sabelstrom et al., 2014). Disruption of the adult neurogenesis contributes to neurodegenerative, psychiatric, and cognitive diseases of central nervous system (CNS; Apple et al., 2017; Horgusluoglu et al., 2017). Therefore, it is crucial to develop regenerative therapies through employing the adult

NSCs. Classically, adult NSCs can be identified in two discrete brain regions: the subgranular zone (SGZ) of hippocampal dentate gyrus (DG) and the subventricular zone (SVZ), which lines the lateral wall of the lateral ventricle (LV; Fuentealba et al., 2012; Apple et al., 2017; Horgusluoglu et al., 2017). In the hippocampal DG, the SGZ is located at the interface of the granule cell layer (GCL) and the hilus (Hil) and contains NSCs, which reside in a layer about three nuclei wide, including the basal cell band of GCL and two nuclei wide zone into the Hil (Balu and Lucki, 2009). Actually, there are different types of cells in the SGZ and the SVZ (Varela-Nallar and Inestrosa, 2013; Bonaguidi et al., 2016). Among the cells, the GFAP-expressing cells are believed to function as NSCs and are vital for the adult neurogenesis (Doetsch et al., 1999; Chojnacki et al., 2009; Mandyam, 2013; Varela-Nallar and Inestrosa, 2013; Bonaguidi et al., 2016). To identify key factors involved in manipulating the NSCs in the adult brain has important implications for the therapy of CNS diseases (Liu and Song, 2016; Ren et al., 2017). However, uncertainty about the identity of the adult NSCs remains.

Brg1/Brm-associated factor (BAF) chromatin remodeling complex arranges a switch in subunit composition between the neural subtype-specific BAF complexes to determine neural development and neural differentiation (Ronan et al., 2013; Narayanan and Tuoc, 2014). BAF45D, also known as DPF2, belongs to BAF45 family proteins, subunits of the BAF complexes, which include BAF45A, BAF45B, BAF45C, and BAF45D (Lessard et al., 2007). It is known that BAF45D mRNA is present in the developing cerebral cortex of mouse embryos at embryonic day 14 (E14; Gabig et al., 1998). In adult mouse brain, the presence of BAF45D in the hippocampus has also been addressed (Gabig et al., 1998). It is already known that BAF complex interacts with PAX6, a neurogenic fate determinant, and determines neurogenesis of adult NSCs (Ninkovic et al., 2013; Gotz et al., 2016). PAX6 is also a human neuroectoderm determinant (Zhang et al., 2010). Neuroectoderm is the primordium of human nervous system (Gammill and Bronner-Fraser, 2003).Moreover, PAX6 also contributes to brain structure and function in human adults (Yogarajah et al., 2016). Thus, in current study, we want to explore if BAF45D is expressed in adult nervous system and plays a role in PAX6 expression.

Here our data suggest that BAF45D is expressed in the SGZ of the adult DG, the SVZ of the adult LV and the spinal cord central canal. Coexpression of BAF45D and GFAP was identified in some of the cells in the SGZ, the ependymal cells of the SVZ, dorsal third ventricle (D3V) and the spinal cord central canal. Moreover, BAF45D is preferentially expressed in the neurons of the adult CNS. Further analysis revealed that retinoid acid (RA) downregulates OCT4 and upregulates PAX6, a neurogenic fate determinant, together with an upregulation of BAF45D during the neuroectoderm differentiation of H9 cells but fails to downregulate OCT4 and upregulates PAX6 upon knockdown of BAF45D. Besides, BAF45D siRNA does not affect significantly the expression of GATA6, an endoderm marker protein. These data may shed new light on the expression of BAF45D in adult neurogenic zones and function of BAF45D in early neural development.

Abbreviations: CNS, central nervous system; NSC, neural stem cell; SGZ, subgranular zone; DG, dentate gyrus; SVZ, sub ventricular zone; LV, lateral ventricle; GFAP, glial fibrillary acidic protein; OPC, oligodendrocyte precursor; BAF, Brg1/Brm-associated factor; ESC, embryonic stem cell; IH, immunohistochemistry; IF, immunofluorescence; IB, immunoblotting; RA, retinoid acid; D3V, dorsal third ventricle; RGL, Radial glial-like cell; SN, substantia nigra; PD, Parkinson's disease. EP, ependymal cells; NEP, non-ependymal cells. LP: lateral posterior thalamic nucleus; ZI: zona incerta; DLG: dorsal lateral geniculate nucleus.

EXPERIMENTAL PROCEDURES

Animals

Animals were acquired according to previously described (Duan et al., 2013). The adult mice (10–12 weeks old, weight 25–30 g) of C57/BL6 were obtained from the Experimental Animal Centre of Anhui Province.

Tissue Preparation

The preparation of adult animal tissues was performed as previously described (Duan et al., 2013; Lacroix et al., 2014). Briefly, the adult mice were anesthetized and sacrificed. Then the tissues of the brains and the spinal cords were dissected and post-fixed overnight in 4% paraformaldehyde at 4°C. Serial sections of 5 μm thickness were cut using a Leica microtome and mounted on CITOGLAS adhesion microscope slides.

Cell Cultures

A human embryonic stem cell line, H9 cells, was cultured as previously described (Liu et al., 2015). Briefly, H9 cells were maintained on Matrigel (BD Bioscience, Bedford, MA) in mTeSR medium (Stem Cell Technologies, Vancouver, BC, Canada) supplemented with 50 units per milliliter penicillin and 50 μg per milliliter streptomycin under 5% CO2 in a humidified incubator. The medium was changed daily and the cells were passaged at a ratio of 1:4.

H9 Cell Neuroectoderm Differentiation

H9 cells were infected transiently by lentiviruses containing negative control (NC) siRNA and BAF45D siRNA #25540, and were subjected to all-trans retinoic acid (RA, Sigma) induced neuroectoderm differentiation according to our previous protocol (Liu et al., 2015). Briefly, undifferentiated H9 cells were cultured in mTeSR supplemented with 10 mM Y-27632 at 37°C for 1 h. Then the cells were digested using accutase (Millipore) and washed with mTeSR. The cells were then centrifugated at 500 rpm/min and resuspended in 1 mL mTeSR. Then the cell suspension was incubated with 10 μL of concentrated GFP-expressing lentivirus containing DPF2 siRNAs (LV-DPF2 siRNA #25,540; Genechem, Shanghai, China) at 37°C for 1 h. Finally, the infected cells were supplemented with 10 mM Y-27,632 and replated on Matrigel-coated 6-well plates. The medium were change with mTeSR daily. When the lentivirus-infected H9 cells grew to 60–70% confluence, the cells were seeded in 6-well plates pre-coated with Matrigel at a ratio of 1:2 and maintained in mTeSR medium. The next day (d1), cells were exposure by all-trans retinoic acid at 10 μM in mTeSR medium. For a

3-day induction, the culture medium was refreshed with mTeSR medium containing 10 μM every day. At d4, the H9 cells were lysed and the lysates were subjected to IB.

Immunohistochemistry (IH) Assay

IH assay was performed as previously described (Duan et al., 2013; Lacroix et al., 2014). The sections were blocked with 3% goat serum and then incubated with mouse anti-PAX6 antibody (1:200, Millipore, Temecula, CA, USA) and rabbit anti-BAF45D (1:100, Proteintech, Chicago, IL, USA) antibodies overnight at 4°C. A NIKON Eclipse 80i fluorescent microscope and a NIKON Eclipse Ti-S inverted fluorescence microscope were used for visualization.

Immunofluorescence (IF) Assay

IF assay for tissue samples was performed according to a previous protocol (Gao and Chen, 2013). The samples were incubated with rabbit anti-BAF45D (1:100, Proteintech, Chicago, IL, USA), mouse anti-GFAP (1:100, Proteintech, Chicago, IL, USA), mouse anti-NEUN (1:100, Millipore, Belecula, CA, USA) and mouse anti-beta-III-tubulin (1:200, Millipore, Belecula, CA, USA) overnight at 4°C. After washed with PBS, the samples were incubated with Alexa Flour-488 anti-mouse (1:500) and Alexa Fluor-594 anti-rabbit (1:500) antibodies. The nuclei were counterstained with 4, 6-diamidino-2-phenylindole (DAPI). A NIKON Eclipse 80i fluorescence microscope and a NIKON Eclipse Ti-S inverted fluorescence microscope were used for visualization. In some cases, a Leica DMI6000CS confocal microscope was used for the visualization. More descriptions of the antibodies used for IF were shown in Table S1.

Immunoblotting (IB) Assay

The lysates of fresh tissues and the H9-derived cells were subjected to IB assay according to the previous protocol (Liu et al., 2012; Tripathi and Mishra, 2012). Then the proteins were detected using indicated antibodies. Antibodies used for IB are as follows: mouse anti-GFAP (1:500, Proteintech, Chicago, IL, USA), mouse anti-NEUN (1:500, Millipore, Belecula, CA, USA), rabbit anti-BAF45D (1:500, Proteintech, Chicago, IL, USA), rabbit anti-GATA6 (1:100, Abcam, New Territories, HK), mouse anti-OCT4 (1:1000, Santa Cruz Biotechnology, Santa Cruz, CA, USA), rabbit anti-PAX6 (1:500, Millipore, Belecula, CA, USA) and rabbit anti-GAPDH (1:2000, Proteintech, Chicago, IL, USA) antibodies. More descriptions of the antibodies used for IB were shown in Table S1.

Ethics Approval

All animal experiments were approved by the Anhui Medical University Experimental Animal Ethics Committee. The NIH Guide for the care and use of laboratory animals (National Institutes of Health Publications, No. 80-23, revised 1978) was followed for the acquisition and care of animals.

Statistics

The statistical analysis was performed using SPSS17.0 software. Data for comparison of two groups were implemented by independent sample *T*-test and/or one-way ANOVA. For the proportion data belong to two groups of independent samples, we performed non-parametric statistics using Mann–Whitney *U*-test. The data are presented as the mean ± standard deviation. Statistical significance was accepted at $p < 0.05$.

RESULTS

BAF45D Is Expressed in the SGZ of Adult Mouse Hippocampal DG

The SGZ of the hippocampal DG is a classical adult NSC niche. We performed HE staining and IH assay using the sections of the adult mouse brain cut in a sagittal plane, in which the CA1, CA2, CA3, and DG regions are shown (Figures S1A–C). Within the DG, both the SGZ and the GCL are also shown (Figure S1B). According to the IH assay data, as compared to the PBS control (Figures S1D–F), PAX6-immunopositive signals, although weak, were detected in the SGZ (Figures S1G–I). BAF45D-immunopositive signals were detected in the cells of the CA1, CA2, CA3, and the DG regions (**Figure 1A**). BAF45D is expressed mainly in the nuclei of the SGZ and GCL cells of the DG (**Figure 1B**). The 2–3 layers of the nuclei next to the hilus are shown (**Figure 1C**, dashed circles). We next performed IF assay using anti-NEUN and anti-BAF45D antibodies. The data indicates that BAF45D and NEUN, a mature neuron marker, are coexpressed in most of the DG cells (**Figures 1D–H**, arrows).

These results suggest that BAF45D is a nuclear protein that is expressed in the SGZ of the adult mouse hippocampus.

BAF45D and GFAP Are Coexpressed in the Adult DG

The adult NSCs in the SGZ, like radial glial cells, are characterized by the expression of GFAP (Fuentealba et al., 2012; Horgusluoglu et al., 2017). To further examine if the BAF45D-positvie cells are potential NSCs, we performed IF assay for BAF45D and GFAP using the sections of the DG and non-DG regions. The non-DG regions include lateral posterior thalamic nucleus (LP), zona incerta (ZI), and dorsal lateral geniculate nucleus (DLG). Consistent with our IH assay results, the expression of BAF45D was detected in the nuclei of most of the DG cells, while a lot of GFAP-positive cells in the Hil regions express few or no BAF45D (**Figure 2A**). As we expected, although most of the BAF45D-positive cells in the DG are GFAP-negative (**Figure 2B**, arrows), coexpression of both BAF45D (**Figure 2B**, arrows) and GFAP (**Figure 2B**, triangles) were detected in some of the SGZ cells that are next to the hilus. However, in the non-DG region (**Figures 2D–F**), BAF45D was found in the nuclei of some of the neural cells, which display clear nucleoli and are also devoid of GFAP expression (**Figure 2E**, arrows). Moreover, few or no BAF45D-positive signals were detected in the nuclei (**Figures 2E,F**, arrowheads) of the GFAP-positive cells (**Figures 2E,F**, triangles). Through the quantitative assay, while BAF45D is expressed in almost 80% of the DG cells, it is expressed only in no more than 40% of the non-DG cells (**Figure 2G**). On the

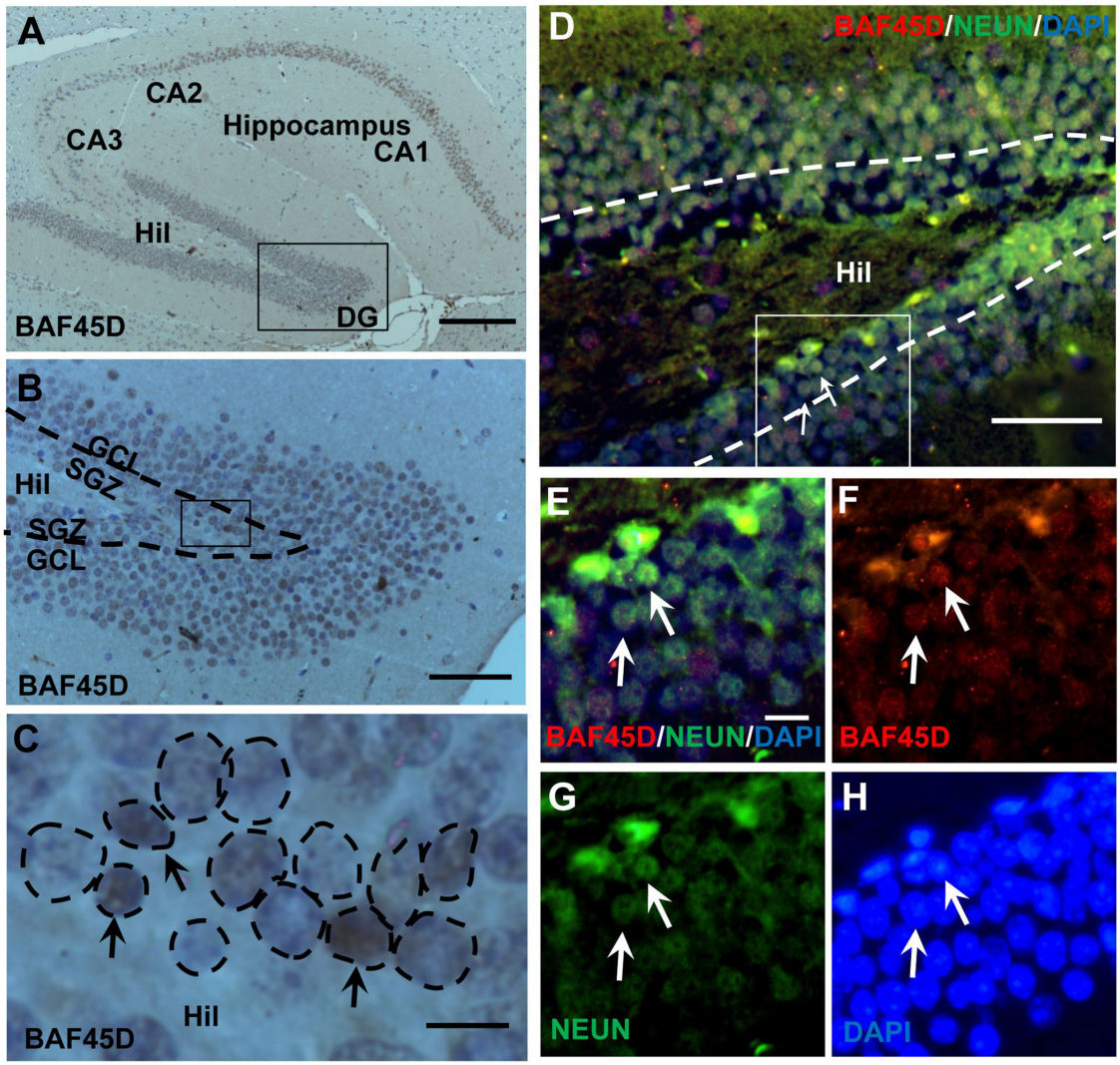

FIGURE 1 | Expression of BAF45D in the adult hippocampal DG. **(A–C)** The sagittal sections (lateral 1.08 mm according to Paxinos and Franklin, 2001.) of the adult mouse brain were subjected to IH assay using anti-BAF45D antibodies. The BAF45D-immunopositive signals in the CA1, CA2, CA3, and DG regions of the hippocampus were shown **(A)**. Hil, hilus of the DG. Panel **(B)** is a higher magnification of the inlet in **(A)**. Panel **(C)** is a higher magnification of the inlet in **(B)**. The DG is characterized by the SGZ and the granule cell layer (GCL) **(B)**. The nuclear architecture of the SGZ is shown. The arrows indicate the BAF45D-immunopositive cells and the dashed circles indicate the various types of the nuclei **(C)**. **(D–G)** The DG section was subjected to IF assay using the indicated antibodies. Panel **(E)** is a higher magnification of the inlet in **(D)**. **(F–H)** are the indicated different signal channels that merged in **(E)**, respectively. Bar = 200 μm **(A)**, 50 μm **(B,D)**, and 10 μm **(C,E)**, respectively. The nuclei (blue) were counterstained by DAPI.

contrary, the number of the GFAP-positive cells in the non-DG regions is much more than that in the DG region (**Figure 2G**).

These results suggest that BAF45D may be expressed as a nuclear protein of the GFAP-expressing NSCs in the SGZ of the adult mouse hippocampal DG.

BAF45D Is Expressed in the Ependymal Cells of the Adult Brain LV

The SVZ zone along the LV is another classical adult NSC niche (Bonaguidi et al., 2016), in which the ependymal cells are essential niche components for neurogenesis under injury conditions (Carlen et al., 2009; Paez-Gonzalez et al., 2011). To examine the expression of BAF45D in the LV ependymal cells, the sagittal sections of adult mouse brain were subjected to IH assay with anti-BAF45D antibodies (**Figure 3A**). The results indicate that the BAF45D-immunopositive signals were detected in the ependymal cells that line both the dorsal wall and SVZ region (**Figures 3B,B1,B2**) of the LV, including the subependymal cells. Notably, the ependymal cells and the subependymal cells of the SVZ region form a specific nuclear architecture (**Figures 3E,F,G**, dashed circles), which is different from that of the dorsal wall (**Figures 3C,D**). At higher magnification, the BAF45D-immunopositive signals were identified mainly in the nuclei

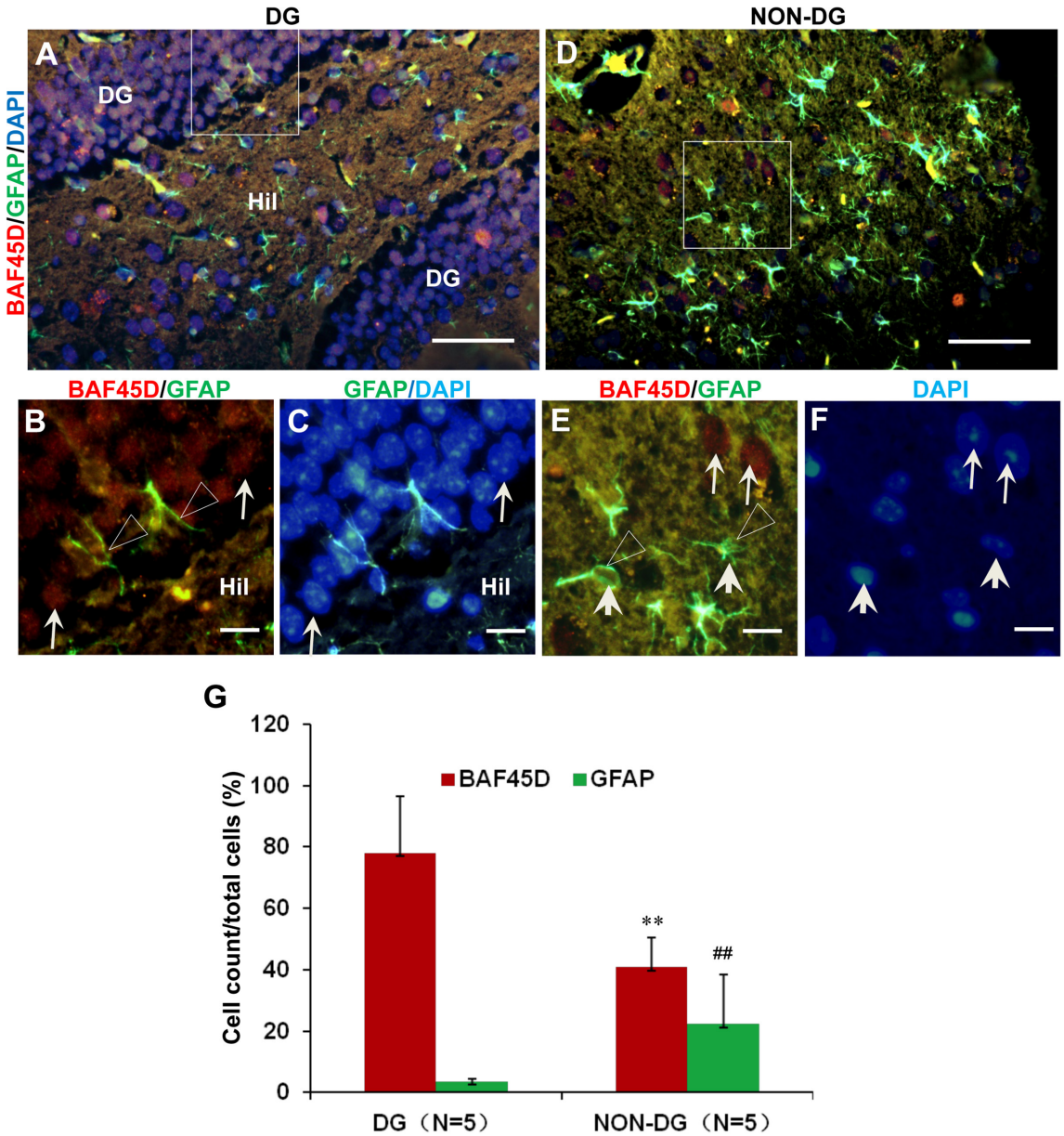

FIGURE 2 | Coexpression of BAF45D and GFAP in the adult DG. **(A–C)** IF assay for the expression of BAF45D and GFAP in the DG. Panel **(B)** is a higher magnification of the merged red and green channels in the inlet in **(A)**. Panel **(C)** is a higher magnification of the merged green and blue channels in the inlet in **(A)**. The BAF45D-immunopositive signals (red) (**B**, arrows) and the GFAP-immunopositive signals (green) (**B**, triangles) were shown. **(D–F)** IF assay for the expression of BAF45D and GFAP in the non-DG regions. Panel **(E)** is a higher magnification of the merged red and green channels of the inlet in **(D)**. Panel **(F)** is a higher magnification of the blue channel of the inlet in **(D)**. The BAF45D-immunopositive signals (red) (**E**, arrows) and the GFAP-immunopositive signals (green) (**E**, triangles) were also shown. The nuclei (blue) were counterstained by DAPI **(A,C,D,F)**. Bar = 50 μm **(A,D)** and 10 μm **(B,C,E,F)**, respectively. **(G)** Quantitative assay of the ratio of the BAF45D-positive and the GFAP-positive cells in the indicated regions. Five to six mices per group were analyzed. The non-parametric statistics using Mann–Whitney *U*-test was performed using SPSS software. $^{**}P < 0.01$, $^{\#\#}P < 0.01$, as compared to the DG region.

(**Figures 3D,F,G**, arrows). Moreover, the cilia-like structures on the apical surface of some of the ependymal cells were identified at higher magnification (**Figure 3D**, arrowheads).

These results suggest that BAF45D is expressed as a nuclear protein in both the ependymal cells and subependymal cells of the adult mouse LV.

BAF45D and GFAP Are Coexpressed in the Ependymal Cells of the Adult Brain LV

Because accumulating experimental evidences suggest that GFAP-expressing SVZ astrocytes may behave as NSCs (Bonaguidi et al., 2016), we therefore investigated the expression of both BAF45D and GFAP in the SVZ ependymal

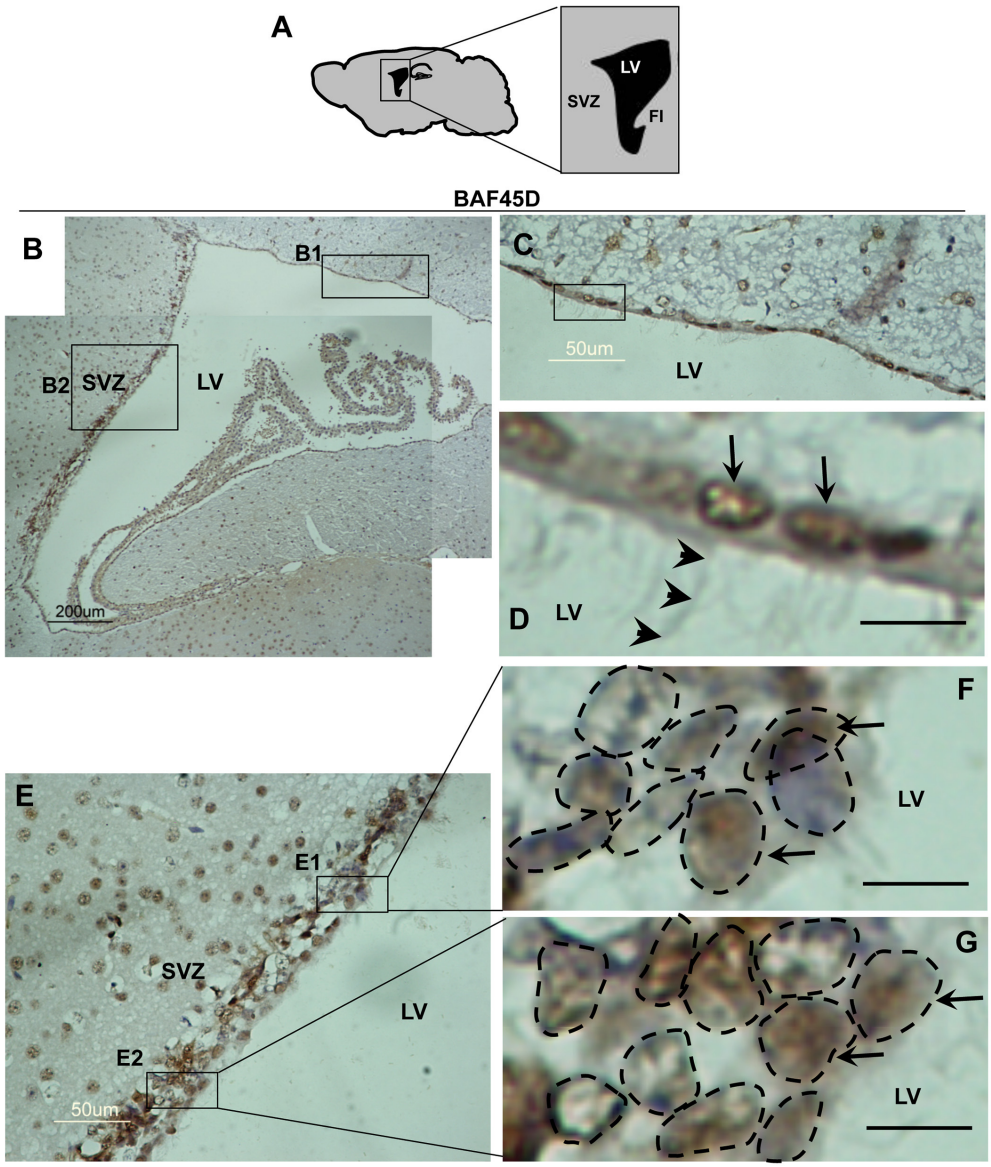

FIGURE 3 | Expression of BAF45D in the ependymal cells of the adult LV. **(A)** Schematic representation of the sagittal plane (lateral 1.08 mm) of the adult mouse brain, highlighting the SVZ and LV. FI, fimbria of the hippocampus. **(B)** IH assay for examining the expression of BAF45D in the ependymal cells of the adult mouse LV. The SVZ and the LV are shown. Panel **(C)** is a higher magnification of the inlet **(B1)**. Panel **(D)** is a higher magnification of the inlet in **(C)**. The BAF45D-immunopositive signals in the nuclei of the dorsal wall ependymal cells are shown (**D**, arrows). The arrowheads indicate the cilia-like structures on the apical surface of the cells **(D)**. Panel **(E)** is a higher magnification of the inlet **(B2)**. Panel **(F)** is a higher magnification of the inlet **(E1)**. Panel **(G)** is a higher magnification of the inlet **(E2)**. The arrows indicate the BAF45D-immunopositive nuclei of the SVZ ependymal cells. The different types of the nuclei in the SVZ are shown (**F,G**, dashed circles). Bar= 10 μm **(D–G)**.

cells using the sections of the adult mouse brain cut in a coronal plane(**Figure 4A**). The expression of GFAP in the LV region was shown (**Figure 4B**). As expected, coexpression of BAF45D and GFAP in the ependymal cells was identified (**Figures 4C–G**). Localization of BAF45D is mainly in the nuclei (**Figures 4D,E,G**, arrows), while the GFAP expression is mainly in the cytoplasm and the cell processes (**Figures 4D,F**, triangles). This finding is similar with that of the D3V ependymal cells, which express both BAF45D and GFAP, with the BAF45D-immunopositive signals mainly found in the nuclei (Figures S2B–D, arrows) and the coexpressed GFAP-immunopositive signals found in the cytoplasm and cell processes (Figures S2C,E, triangles).The nucleus architecture of the LV is also shown (**Figure 4G**, dashed circles). Moreover, the nucleus architecture of the D3V, which is composed of one layer cells that are positive for both BAF45D and GFAP, seems different from that of the LV (Figure S2). Besides, there are some of the BAF45D-positive cells express

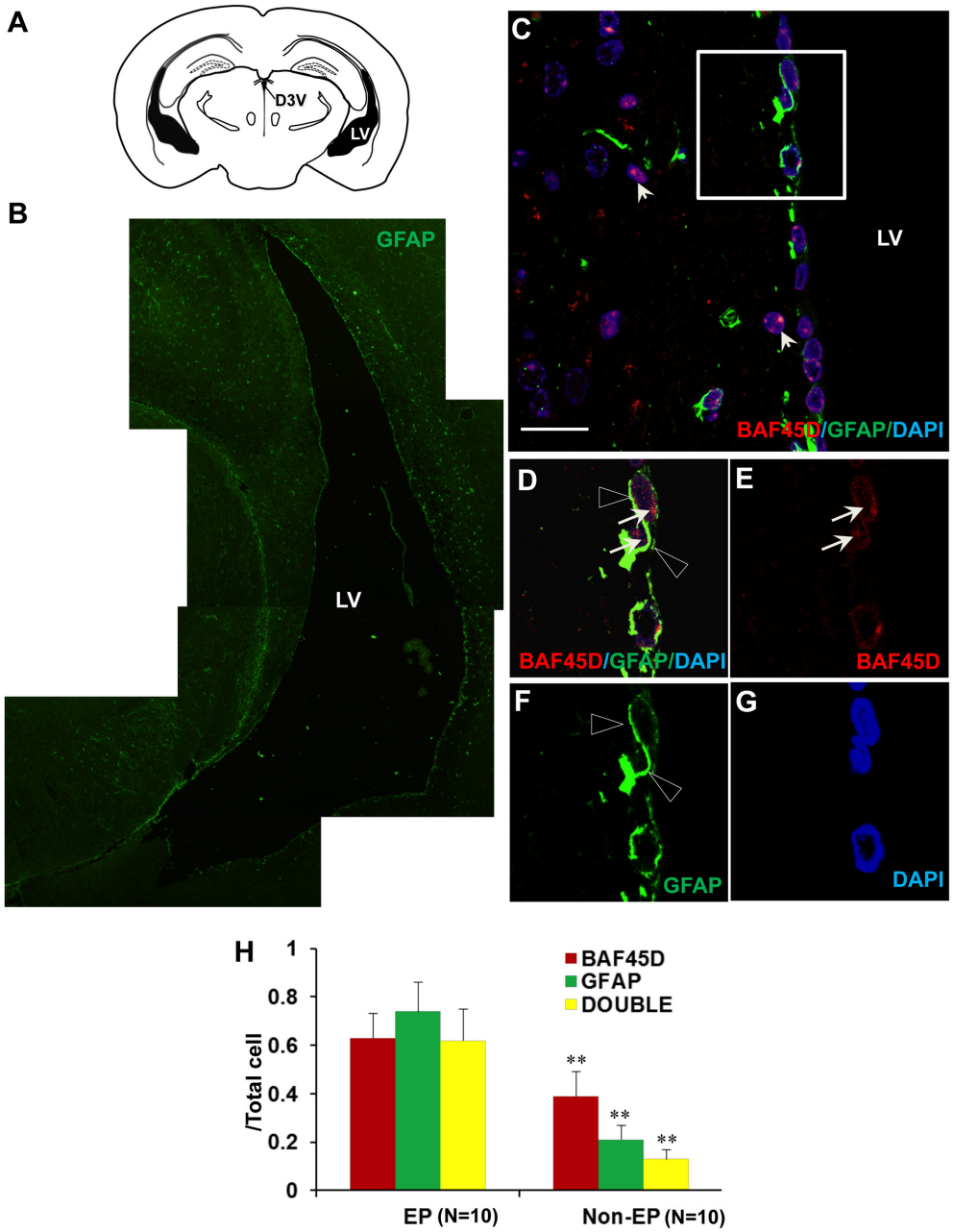

FIGURE 4 | Coexpression of BAF45D and GFAP in the ependymal cells of the adult brain LV. **(A)** The schematic representation of the coronal plane (interaural 1.34 mm and bregma −2.46 mm) of the adult mouse brain, highlighting the LV and the dorsal third ventricle (D3V). **(B)** IF assay using anti-GFAP antibody for the LV. **(C–G)** The coexpression of BAF45D and GFAP in the ependymal cells of the LV. C is a subregion of the lateral wall of the LV taken by the confocal microscope. Panel **(D)** is a higher magnification of the inlet in **(C)**. **(E–G)** are the indicated different signal channels that merged in **(D)**, respectively. The BAF45D-immunopositive signals (**D,E**, arrows) and the GFAP-immunopositive signals (**D,F**, triangles) are shown. The arrowheads indicate the cells that are positive for BAF45D but negative for GFAP **(C)**. The nuclei are counterstained by DAPI. Bar = 20 μm **(C)**. **(H)** The quantitative analysis of the ratio of the BAF45D-positvie cells, the GFAP-positive cells and the double-positive cells to the total cells in the ependymal cells and the non-ependymal cells. Five to six mices per group were analyzed. Ten different areas of the lateral wall of the LVs were selected randomly for visualization. Data for comparison were implemented by independent sample *T*-test. EP, ependymal cells; NEP, non-ependymal cells. $^{**}P < 0.01$ as compared to the EP.

no GFAP in the non-ependymal region (**Figures 4D–F**, arrowheads). At last, the results of the quantitative analysis indicate that among the total cells, the BAF45D-positvie cells, the GFAP-positive cells and the double-positive cells in the ependymal region are more than those in the non-ependymal region (**Figure 4H**).

These results suggest that BAF45D is expressed as a nuclear protein in GFAP-expressing NSCs lining the ventricular walls of the adult mouse brain.

BAF45D Is Expressed in the Ependymal Cells of the Adult Spinal Cord CC

The central canal (CC) ependymal cells may also behave like NSCs (Fu et al., 2003; Panayiotou and Malas, 2013). To determine if BAF45D is also expressed in the CC ependymal cells, the cross sections of the adult mouse spinal cord were subjected to IH assay using anti-BAF45D antibodies (**Figures 5A–D**). The results proved the expression of BAF45D in the nuclei of some of the neural cells (**Figure 5C**, arrows) and the CC ependymal cells (**Figure 5D**, arrows), while there are still some of the neural cells seem BAF45D-negative (**Figures 5C,D**, arrowheads). Next we performed IF assay to check if the CC ependymal cells express both BAF45D and GFAP. As the data revealed, coexpression of BAF45D and GFAP was found in some of the CC ependymal cells (**Figures 5E,F,H**, arrowheads and triangles). While some of the GFAP-positive neural cells have few or no expression of BAF45D (**Figures 5E,F,H**, triangles), there are also some BAF45D-positive neural cells express no GFAP (**Figures 5E–H**, arrows).

These results suggest that BAF45D is expressed as a nuclear protein in putative GFAP-expressing NSCs lining the CC of the adult mouse spinal cord.

BAF45D Is Preferentially Expressed in the Mature Neurons of the Adult Mouse Brain

We next want to know if BAF45D is differentially expressed between mature neurons and astrocytes. We thus performed IF assay using anti-NEUN and anti-GFAP antibodies together with anti-BAF45D antibodies. The brain sections are similar with the coronal section used in **Figure 4**. The examined brain parts include the LP (laterorostral, mediocaudal, and mediorostral parts), the ZI (dorsal and ventral parts) and the DLG. The data indicate that the colocalization of BAF45D and NEUN was identified in the nuclei (**Figures 6A,B,D**, arrows). The colocalization of cytoplasmic BAF45D and NEUN was also shown (**Figures 6A,B,D**, arrowheads). However, BAF45D-positive cells express few or no GFAP (**Figures 6E–H**, arrows), while few or no expression of BAF45D was detected in the nuclei of the GFAP-expressing astrocytes (**Figures 6E,F,H**, triangles). By the quantitative assay among the total cells, the ratio of the BAF45D-expressing neurons is higher than that of the BAF45D-expressing astrocytes, and the ratio of the neurons that are positive for both BAF45D and NEUN is much more than that of the astrocytes that are positive for both BAF45D and GFAP, although the ratio of the neurons has no significant differences from that of the astrocytes (**Figure 6I**).

These results suggest that BAF45D is preferentially expressed in the mature neurons of the adult mouse brain.

BAF45D Is Preferentially Expressed in the Mature Neurons of the Adult Spinal Cord

To prove the different BAF45D expression between neurons and astrocytes, we performed IF assay using the transverse sections of the adult mouse spinal cord. The expression of BAF45D, together with GFAP, NEUN and BETA-III-tubulin was examined. The results showed that while GFAP is expressed in both the gray matter and the white matter (Figures S3A–D), BAF45D together with beta-III-tubulin are mainly expressed in the gray matter (Figures S3E–H). Consistent with the findings in the adult brain, the BAF45D is expressed in both the nuclei and the cytoplasm of some of the cells (**Figures 7A,C,D**, arrows and arrowheads), while the GFAP-expressing astrocytes have few or no BAF45D expression (**Figures 7B,D**, triangles). Among the neurons, colocalization of BAF45D and NEUN was identified in the nuclei (**Figures 7E,H**, arrows), and coexpression of BAF45D and beta-III-tubulin in the neurons was also detected (**Figures 7I–L**, arrows and triangles). Moreover, colocalization of beta-III-tubulin with BAF45D in the cytoplasm was also shown (**Figures 7I–L**, arrowheads). The expression of BAF45D, GFAP and NEUN in the adult hippocampus and spinal cord has been confirmed by IB assay (Figure S4).

These results suggest that BAF45D is preferentially expressed in the neurons of the adult mouse spinal cord.

BAF45D Is Required for PAX6 Expression during the Differentiation of H9 Cells Induced by RA

We had reported that BAF45D is involved in RA-induced H9 cell general differentiation (Liu et al., 2015). Here, the expression of BAF45D in the NSC niches may imply that BAF45D can determine NSC commitment. PAX6 contributes to both embryonic and adult neurogenesis (Osumi et al., 2008). Therefore, we next performed a RA-induced differentiation of human embryonic stem cell line, H9 cells. The expression of PAX6 and BAF45D was examined along with the induction. To address if BAF45D is required for the expression of PAX6, the H9 cells were first infected by lentiviruses containing NC siRNA and BAF45D #25540 siRNA, respectively, followed by the RA-induced differentiation. Because the data of the differentiation of H9 cells have 3 time points, we thus speculated that it may be more reliable to evaluate the overall expression of the indicated proteins at 3 time points but not at a single time point. Therefore, we analyzed the average relative expression of the indicated proteins at d0, d1, and d3. As expected, RA induced upregulation of PAX6 (**Figure 8A**, top panel, lane 1-lane 3) and BAF45D (**Figure 8A**, third panel, lane 1-lane 3) together with a downregulation of OCT4 (**Figure 8A**, fourth panel, lane 1-lane 3) from day 1 to day 3 in the NC siRNA group. Interestingly, RA failed to upregulate PAX6 expression (**Figure 8A**, top panel, lane 4-lane 6) and downregulate OCT4 expression (**Figure 8A**, fourth panel, lane 4-lane 6) in the BAF45D siRNA group (**Figure 8A**, third panel, lane 4-lane 6). Quantitative analysis of the expression of the indicated proteins at the different time points relative to that of day 0 further supports the requirement of BAF45D for the PAX6 induction (**Figure 8B**). Upon the BAF45D knockdown, PAX6 was significantly downregulated and OCT4 was upregulated significantly at the same time. However, expression of GATA 6, an endoderm marker protein (Tiyaboonchai et al., 2017),

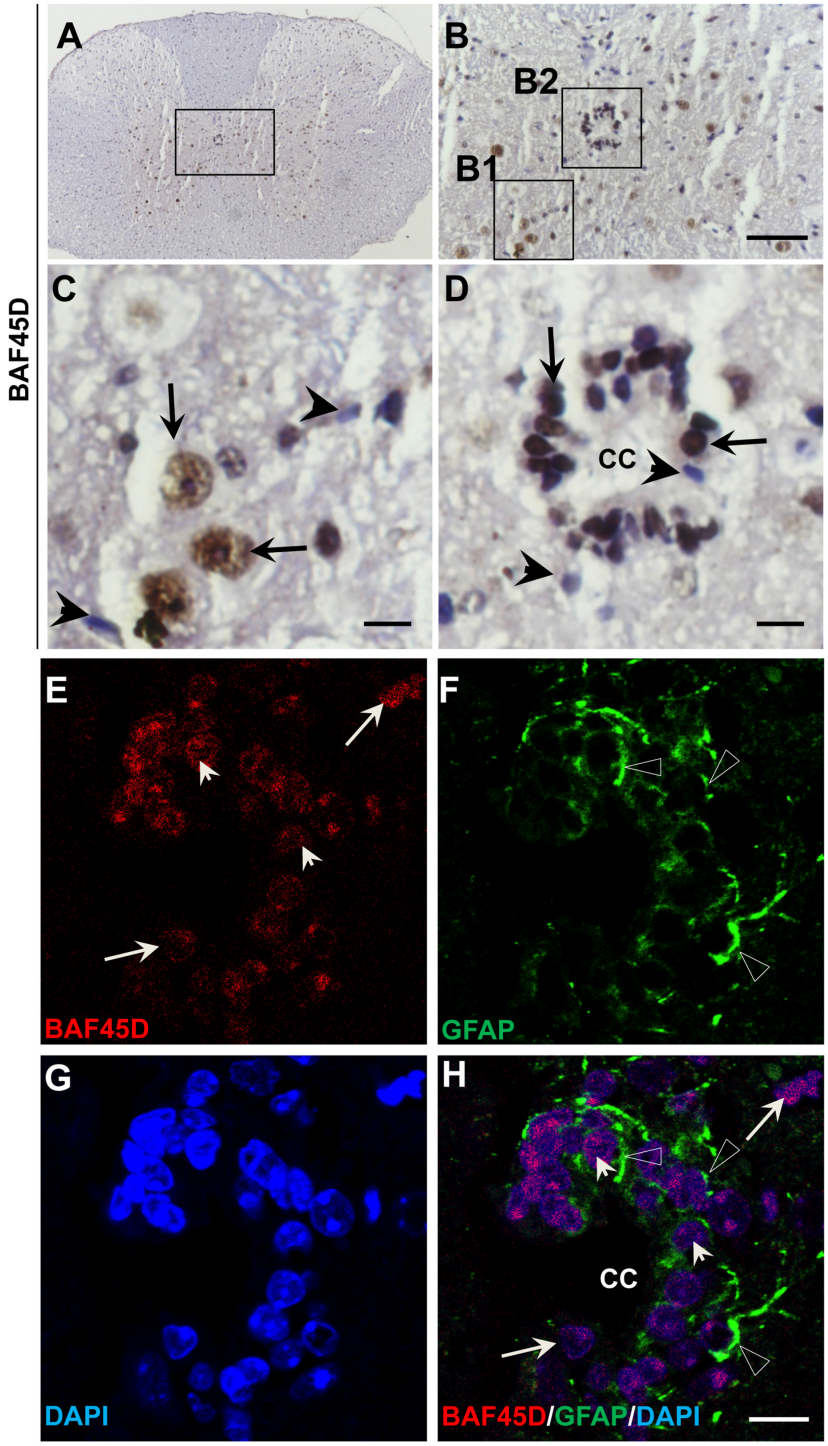

FIGURE 5 | BAF45D is expressed in the ependymal cells of the adult spinal cord CC. **(A–D)** The cross sections of the adult mouse spinal cord were subjected to IH assay using anti-BAF45D antibodies. Panel **(B)** is the higher magnification of the inlet in **(A)**. **(C,D)** are higher magnifications of the inlets **(B1,B2)**, respectively. The arrows indicate the BAF45D-immunopositive nuclei of the non-ependymal cells **(C)** and the ependymal cells of the CC **(D)**. The arrowheads indicate the BAF45D-immunonegative nuclei **(C,D)**. Bar = 50 μm **(B)** and 10 μm **(C,D)**. **(E–H)**, A confocal visualization of the expression of BAF45D in the GFAP-positive cells. The triangles indicate the robust expression of GFAP in the cell processes **(F,H)**.The arrowheads indicate the BAF45D-positive cell nuclei that have the coexpressed GFAP-positive cell processes **(E,H)**. While the arrows indicate the BAF45D-positive nuclei that have few or no expression of GFAP **(E,H)**.

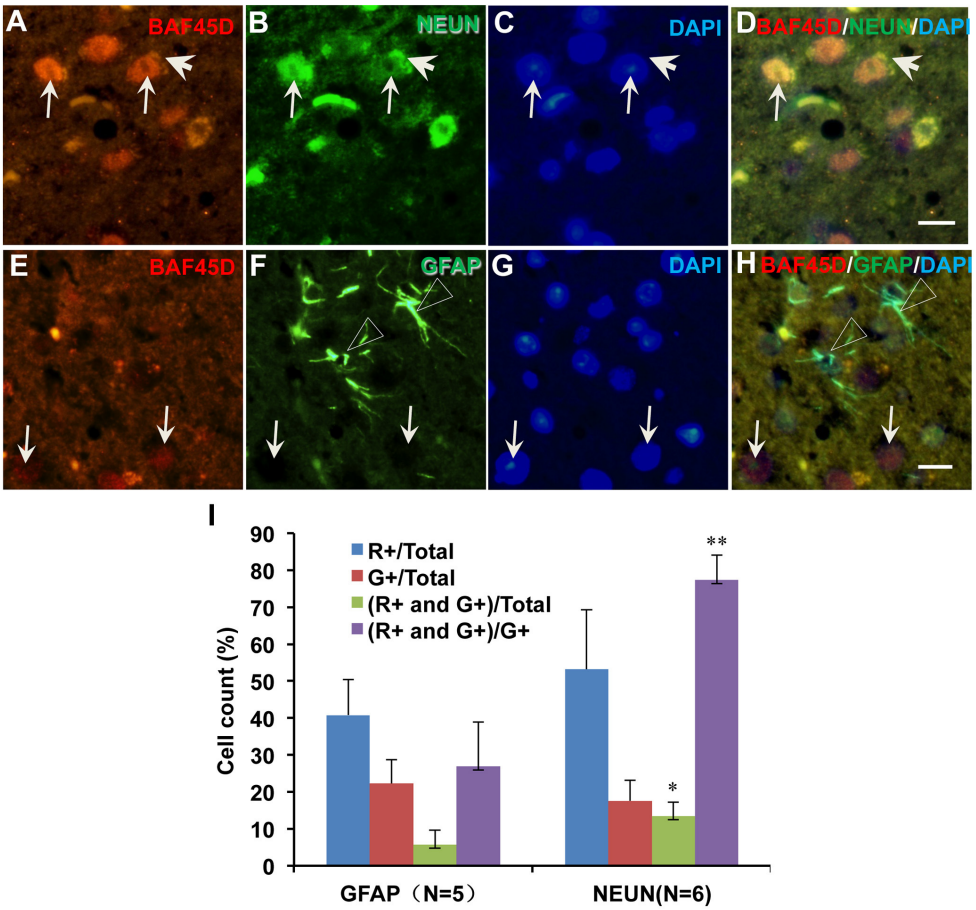

FIGURE 6 | Expression of BAF45D in the neurons and astrocytes in the adult mouse brain. The brain sections are similar with the coronal section used in **Figure 4**. The examined brain parts include the LP (lateroorostral, mediocaudal, and mediorostral parts), the ZI (dorsal and ventral parts) and the DLG. **(A–D)** Expression of BAF45D and NEUN in the neurons of the adult mouse brain. The arrows indicate the coexpression of the BAF45D and NEUN (**A,B,D**, arrows) in the nuclei which have clear nucleoli (**C**, arrows). **(E–H)** Expression of BAF45D and GFAP in the astrocytes of the adult mouse brain. The BAF45D-immunopositive nuclei show few or no GFAP-immunopositive signals (**E,G,H**, arrows). The GFAP-immunopositive cells were shown (**F,H**, triangles), which have few or no expression of BAF45D **(E,G,H)**. Bar = 10 μm. **(I)** Quantitative assay of the ratio of the cells that are positive for red channel (R+), green channel (G+), red and green channel (R+ and G+) among the total cells and the cells positive only for green channel (G+), respectively. Five to six mices per group were analyzed. The non-parametric statistics using Mann–Whitney *U*-test was performed using SPSS software. $^{*}P < 0.05$, $^{**}P < 0.01$, as compared to the GFAP.

seems not affected significantly by the BAF45D knockdown (**Figure 8B**).

These results suggest that RA-induced PAX6 expression in the H9 cells depends on BAF45D.

DISCUSSION

Here, we have characterized a new BAF45 family member, BAF45D, which is expressed in adult mouse brain NSC niches. We identified the first time the expression of BAF45D in the SGZ of the DG through both IH and IF assays (**Figure 1**). Moreover, coexpression of GFAP and BAF45D was also detected in the SGZ (**Figure 2**). Thus, we speculate that the cells that are double positive for both BAF45D and GFAP in the SGZ may be potential NSCs. It was reported that the ependymal cells forms a simple ciliated epithelium that lines the ventricular surface of the CNS, extending from the lateral ventricles to the filum terminale (Del Bigio, 2010), and also functioned as NSCs (Johansson et al., 1999). Recent progresses suggest that the ependymal cells in the SVZ may be a cell type showing NSC characterizations (Bonaguidi et al., 2016).

Next, we found that coexpression of BAF45D and GFAP in the ependymal cells of the LV and the D3V (**Figure 4**, Figure S2), also in the ependymal cells of the adult spinal cord CC (**Figure 5**). Allen Brain Atlas had been reported to be used for gene expression analysis in the adult mouse brain (Lein et al., 2007). We thus explored the online database of the Allen Brain Atlas (http://www.brain-map.org). The in situ hybridization (ISH) data of *BAF45D* gene expression in C57BL/6J adult mouse brain (http://mouse.brain-map.org/experiment/show/68301353, sagittal section) imply that *BAF45D* is preferentially expressed in the hippocampal DG. The *BAF45D*-positive cell nuclei can

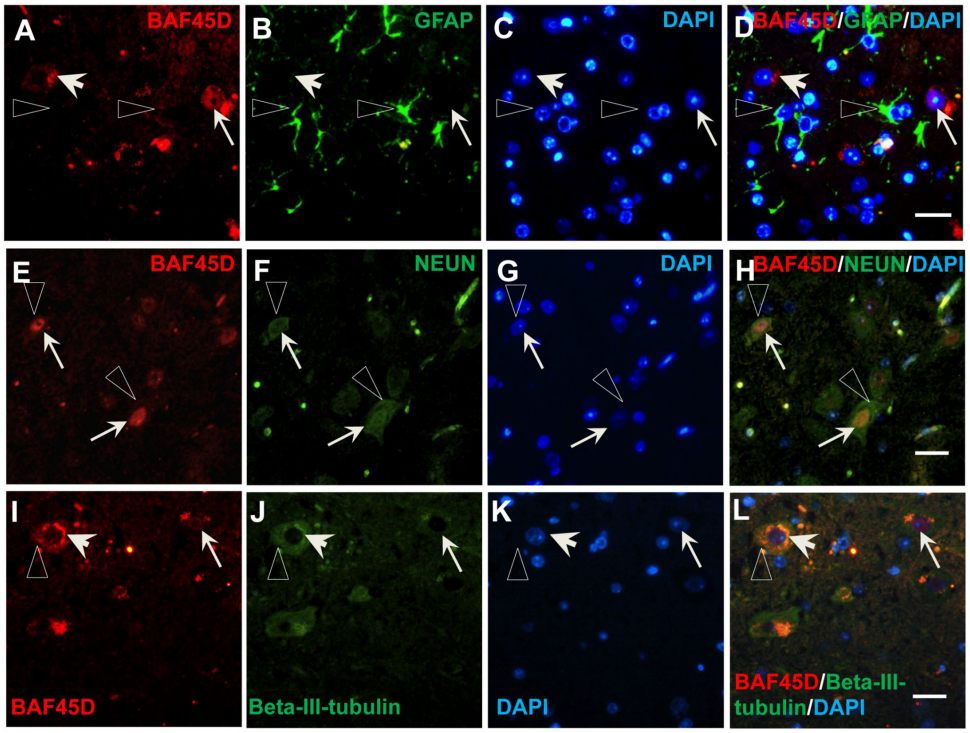

FIGURE 7 | Expression of BAF45D in the neurons and astrocytes of the adult spinal cord. **(A–D)** The expression of BAF45D in the GFAP-positive astrocytes. The arrows indicate the BAF45D-positive cells **(A,C,D)**. While the arrowheads indicate the cell nuclei have few or no expression of BAF45D **(A,C,D)**, the triangles indicate the robust expression of GFAP in the cell processes **(B,D)**. **(E–H)** The expression of BAF45D in the NEUN-positive neurons. The arrows indicate the BAF45D-positive cell nuclei **(E,H)**, which are also positive for NEUN **(F,H)**. The triangles indicate the expression of NEUN in the cell cytoplasm **(B,D)**. **(I–L)** The expression of BAF45D in the beta-III-tubulin-positive neurons. The arrows indicate the BAF45D-positive cell nuclei **(I,L)**. Colocalization of beta-III-tubulin, which is expressed in the cytoplasm (triangles, **J,L**), with the cytoplasmic BAF45D was shown (**I–L**, arrowheads). Bar = 10 μm.

be identified in the SGZ region, which corroborates our data that BAF45D protein is expressed in the SGZ of the DG in the C57BL/6 adult mouse brain. Next, we also explored the ISH data of *GFAP* gene expression in the adult mouse brain (http://mouse.brain-map.org/experiment/show/79913385, sagittal section). Although, the expression pattern of *GFAP* is largely different from that of *BAF45D*, *GFAP* is also expressed in a few cells in the SGZ of the DG and the ependymal cells lining the LV, which is confirmed by another ISH data of *GFAP* expression (http://mouse.brain-map.org/experiment/show/79591671, coronal section). These findings are consistent with our data of the GFAP expression pattern and may also support the possibility of the coexpression of BAF45D and GFAP in the ependymal cells of the LV. Because ablation of GFAP-positive cells results in loss of NSCs in adult brain (Morshead et al., 2003) and GFAP-expressing cells can behave as NSC niche cells (Jiao and Chen, 2008). Our data here may suggest that the ependymal cells express both BAF45D and GFAP are more likely adult NSCs (Johansson et al., 1999). Adult NSCs can generate neurons, astrocytes and oligodendrocytes. Interestingly, among the GFAP-expressing cells other than the NSC-like cells, the expression of BAF45D is weak or even undetectable. On the contrary, among the neurons, BAF45D colocalizes or coexpresses with NEUN and beta-III-tubulin, two neuron marker proteins. The quantitative analysis data further indicate BAF45D is preferentially expressed in neurons in the adult mouse CNS (**Figures 6**, **7**). Our finding that BAF45D is more highly expressed in neurons than astrocytes in non-neurogenic regions raises the possibility that the expression of BAF45D in putative adult NSCs could play a role in neuronal fate determination during adult neurogenesis, which is to be explored in our future study.

PAX6 is also a neuroectoderm marker protein (Bhinge et al., 2014; Liu et al., 2014). We therefore investigated BAF45D expression during the H9 cell neuroectoderm differentiation induced by RA. According to our data, RA induces the significant upregulation of PAX6 in the H9-derived cells (**Figure 8**). This is in line with previous report that RA is sufficient to induce neuroectoderm (Parsons et al., 2012). It is known that the balance between neurogenesis and NSC self-renewal depends on the PAX6 levels (Pourabdolhossein et al., 2017). According to our data, the upregulation of PAX6 levels induced by RA is dependent on BAF45D, suggesting the first time that BAF45D, as a subunit of BAF complex, is involved in RA-PAX6 signaling pathway regulating neuroectoderm development. Although some of the PAX6-positive cells can be detected until adult life, the intensity of PAX6 expression decreases with the development of the

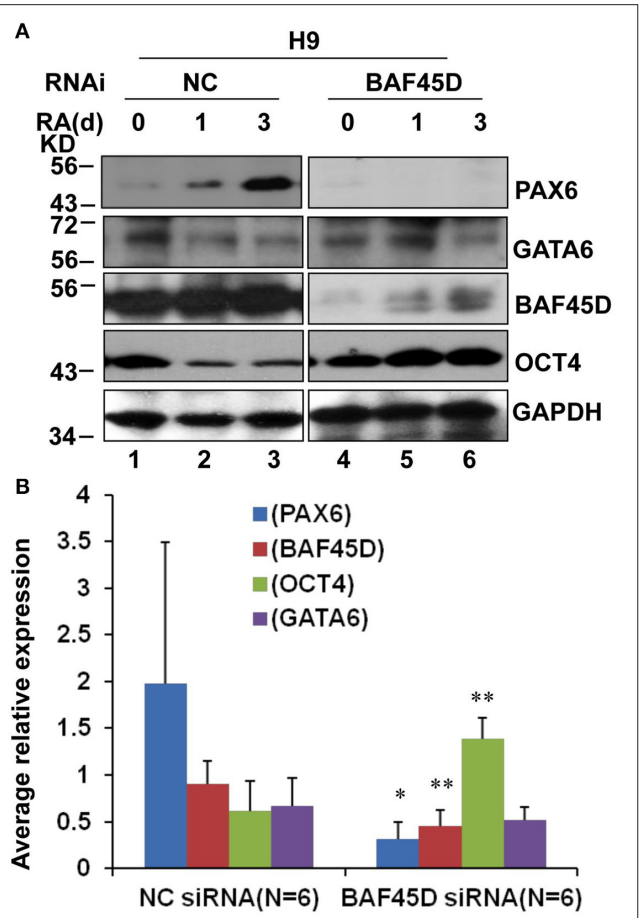

FIGURE 8 | BAF45D is required for the expression of PAX6 during the RA-induced H9 cell neuroectoderm differentiation. **(A)** H9 cells infected by lentiviruses containing negative control (NC) siRNA and BAF45D #25540 siRNA were subjected to a 3-day differentiation induced by RA (1 μM). The H9-derived cells were harvested at the different time points and subjected to IB assay for the indicated proteins. **(B)** Quantitative analysis of the average expression of the indicated proteins at the different time points (d0, d1, and d3) relative to the expression at the beginning (d0) ($n = 6$). Data for comparison were implemented by one-way ANOVA. $^{*}P < 0.05$, $^{**}P < 0.01$, compared to the NC siRNA group.

brain (Duan et al., 2013). This is consistent with our result that although weak, PAX6-positive signals are expressed in the adult hippocampal DG. PAX6 contributes to both embryonic and adult neurogenesis (Osumi et al., 2008), possibly rely on the regulation of transcription factors that required for neurogenic fate specification (Ninkovic et al., 2013; Agoston et al., 2014). In our previous study, nuclear distribution of BAF45D has been addressed in H9 cells *in vitro* (Liu et al., 2015). Here our data confirmed the nuclear distribution of BAF45D in the SGZ and SVZ cells of the adult brain and the ependymal cells of the adult spinal cord *in vivo,* which may be crucial for its transcription regulation. Besides, as a subunit of the chromatin remodeling complex, nuclear localization is also of importance for its epigenetic regulation in neurogenesis (Narayanan and Tuoc, 2014; Yao et al., 2016).

Recent report showed that the PAX6-expressing cells increased significantly as a result of acute injury in the adult human brain. Moreover, PAX6 mutations are correlated with memory dysfunction, with the most severe genotypes have the most widespread differences in a greater age-related decrease in frontoparietal cortex thickness (Yogarajah et al., 2016). In the substantia nigra (SN) from patients with Parkinson's disease (PD), the number of PAX6-positive cells was reduced compared to age and sex matched control. Furthermore, PAX6 protects SH-SY5Y cells from PD relevant neurotoxins through inhibiting apoptosis and oxidative stress (Thomas et al., 2016). Thus, our data here may imply that the BAF45D may have significant implications for contribute to PAX6 expression, which may have significant implications for treatment of neurodegenerative diseases.

Taken together, our results here may be a step forward to understand the expression of BAF45D in the adult neurogenic zones and the contribution of BAF45D to early neural development.

AUTHOR CONTRIBUTIONS

CL: Conceived the study; CL, YS, and CS: Supervised the study; CL: Designed experiments; CL, RS, JH, DZ: Performed experiments; CL, RS, JH, DZ: Analyzed data; DH, WQ, SW, FX: Provided materials; CL: Wrote the manuscript.

ACKNOWLEDGMENTS

This project was sponsored by a grant from the National Natural Science Foundation of the People's Republic of China (31271159), a Key Program of Academic Funding for Outstanding Talents in Colleges and Universities of Anhui Province (gxbjZD2016030). It was also supported by a Provincial /Ministerial Key Laboratory Cultivation Project of Anhui Medical University (SBSYS-1404).

SUPPLEMENTARY MATERIAL

The Supplementary Material for this article can be found online at: https://www.frontiersin.org/articles/10.3389/fnana.2017.00094/full#supplementary-material

REFERENCES

Agoston, Z., Heine, P., Brill, M. S., Grebbin, B. M., Hau, A. C., Kallenborn-Gerhardt, W., et al. (2014). Meis2 is a Pax6 co-factor in neurogenesis and dopaminergic periglomerular fate specification in the adult olfactory bulb. *Development* 141, 28–38. doi: 10.1242/dev.097295

Apple, D. M., Fonseca, R. S., and Kokovay, E. (2017). The role of adult neurogenesis in psychiatric and cognitive disorders. *Brain Res.* 1655, 270–276. doi: 10.1016/j.brainres.2016.01.023

Balu, D. T., and Lucki, I. (2009). Adult hippocampal neurogenesis: regulation, functional implications, and contribution to disease pathology. *Neurosci. Biobehav. Rev.* 33, 232–252. doi: 10.1016/j.neubiorev.2008.08.007

Bhinge, A., Poschmann, J., Namboori, S. C., Tian, X., Jia Hui Loh, S., Traczyk, A., et al. (2014). MiR-135b is a direct PAX6 target and specifies human neuroectoderm by inhibiting TGF-beta/BMP signaling. *EMBO J.* 33, 1271–1283. doi: 10.1002/embj.201387215

Bonaguidi, M. A., Stadel, R. P., Berg, D. A., Sun, J., Ming, G. L., and Song, H. (2016). Diversity of Neural Precursors in the Adult Mammalian Brain. *Cold Spring Harb. Perspect. Biol.* 8:a018838. doi: 10.1101/cshperspect.a018838

Carlen, M., Meletis, K., Goritz, C., Darsalia, V., Evergren, E., Tanigaki, K., et al. (2009). Forebrain ependymal cells are Notch-dependent and generate neuroblasts and astrocytes after stroke. *Nat. Neurosci.* 12, 259–267. doi: 10.1038/nn.2268

Chojnacki, A. K., Mak, G. K., and Weiss, S. (2009). Identity crisis for adult periventricular neural stem cells: subventricular zone astrocytes, ependymal cells or both? *Nat. Rev. Neurosci.* 10, 153–163. doi: 10.1038/nrn2571

Del Bigio, M. R. (2010). Ependymal cells: biology and pathology. *Acta Neuropathol.* 119, 55–73 doi: 10.1007/s00401-009-0624-y

Doetsch, F., Caille, I., Lim, D. A., Garcia-Verdugo, J. M., and Alvarez-Buylla, A. (1999). Subventricular zone astrocytes are neural stem cells in the adult mammalian brain. *Cell* 97, 703–716. doi: 10.1016/S0092-8674(00)80783-7

Duan, D., Fu, Y., Paxinos, G., and Watson, C. (2013). Spatiotemporal expression patterns of Pax6 in the brain of embryonic, newborn, and adult mice. *Brain Struct. Funct.* 218, 353–372. doi: 10.1007/s00429-012-0397-2

Fu, H., Qi, Y., Tan, M., Cai, J., Hu, X., Liu, Z., et al. (2003). Molecular mapping of the origin of postnatal spinal cord ependymal cells: evidence that adult ependymal cells are derived from Nkx6.1+ ventral neural progenitor cells. *J. Comp. Neurol.* 456, 237–244. doi: 10.1002/cne.10481

Fuentealba, L. C., Obernier, K., and Alvarez-Buylla, A. (2012). Adult neural stem cells bridge their niche. *Cell Stem. Cell.* 10, 698–708. doi: 10.1016/j.stem.2012.05.012

Gabig, T. G., Crean, C. D., Klenk, A., Long, H., Copeland, N. G., Gilbert, D. J., et al. (1998). Expression and chromosomal localization of the requiem gene. *Mamm. Genome* 9, 660–665. doi: 10.1007/s003359900840

Gage, F. H. (2000). Mammalian neural stem cells. *Science* 287, 1433–1438. doi: 10.1126/science.287.5457.1433

Gammill, L. S., and Bronner-Fraser, M. (2003). Neural crest specification: migrating into genomics. *Nat. Rev. Neurosci.* 4, 795–805. doi: 10.1038/nrn1219

Gao, X., and Chen, J. (2013). Moderate traumatic brain injury promotes neural precursor proliferation without increasing neurogenesis in the adult hippocampus. *Exp. Neurol.* 239, 38–48. doi: 10.1016/j.expneurol.2012.09.012

Gotz, M., Nakafuku, M., and Petrik, D. (2016). Neurogenesis in the developing and adult brain-similarities and key differences. *Cold Spring Harb. Perspect. Biol.* 8:a018853. doi: 10.1101/cshperspect.a018853

Horgusluoglu, E., Nudelman, K., Nho, K., and Saykin, A. J. (2017). Adult neurogenesis and neurodegenerative diseases: a systems biology perspective. *Am. J. Med. Genet. B Neuropsychiatr. Genet.* 174, 93–112. doi: 10.1002/ajmg.b.32429

Jiao, J., and Chen, D. F. (2008). Induction of neurogenesis in nonconventional neurogenic regions of the adult central nervous system by niche astrocyte-produced signals. *Stem Cells* 26, 1221–1230. doi: 10.1634/stemcells.2007-0513

Johansson, C. B., Momma, S., Clarke, D. L., Risling, M., Lendahl, U., and Frisen, J. (1999). Identification of a neural stem cell in the adult mammalian central nervous system. *Cell* 96, 25–34. doi: 10.1016/S0092-8674(00)80956-3

Lacroix, S., Hamilton, L. K., Vaugeois, A., Beaudoin, S., Breault-Dugas, C., Pineau, I., et al. (2014). Central canal ependymal cells proliferate extensively in response to traumatic spinal cord injury but not demyelinating lesions. *PLoS ONE* 9:e85916. doi: 10.1371/journal.pone.0085916

Lein, E. S., Hawrylycz, M. J., Ao, N., Ayres, M., Bensinger, A., Bernard, A., et al. (2007). Genome-wide atlas of gene expression in the adult mouse brain. *Nature* 445, 168–176. doi: 10.1038/nature05453

Lessard, J., Wu, J. I., Ranish, J. A., Wan, M., Winslow, M. M., Staahl, B. T., et al. (2007). An essential switch in subunit composition of a chromatin remodeling complex during neural development. *Neuron* 55, 201–215. doi: 10.1016/j.neuron.2007.06.019

Liu, C., Sun, Y., Arnold, J., Lu, B., and Guo, S. (2014). Synergistic contribution of SMAD signaling blockade and high localized cell density in the differentiation of neuroectoderm from H9 cells. *Biochem. Biophys. Res. Commun.* 452, 895–900. doi: 10.1016/j.bbrc.2014.08.137

Liu, C., Zhang, D., Shen, Y., Tao, X., Liu, L., Zhong, Y., et al. (2015). DPF2 regulates OCT4 protein level and nuclear distribution. *Biochim. Biophys. Acta* 1853, 3279–3293. doi: 10.1016/j.bbamcr.2015.09.029

Liu, H., and Song, N. (2016). Molecular mechanism of adult neurogenesis and its association with human brain diseases. *J. Cent. Nerv. Syst. Dis.* 8, 5–11. doi: 10.4137/JCNSD.S32204

Liu, L., Liu, C., Zhong, Y., Apostolou, A., and Fang, S. (2012). ER stress response during the differentiation of H9 cells induced by retinoic acid. *Biochem. Biophys. Res. Commun.* 417, 738–743. doi: 10.1016/j.bbrc.2011.12.026

Ma, D. K., Bonaguidi, M. A., Ming, G. L., and Song, H. (2009). Adult neural stem cells in the mammalian central nervous system. *Cell Res.* 19, 672–682. doi: 10.1038/cr.2009.56

Mandyam, C. D. (2013). The interplay between the hippocampus and amygdala in regulating aberrant hippocampal neurogenesis during protracted abstinence from alcohol dependence. *Front. Psychiatry* 4:61. doi: 10.3389/fpsyt.2013.00061

Morshead, C. M., Garcia, A. D., Sofroniew, M. V., and van Der Kooy, D. (2003). The ablation of glial fibrillary acidic protein-positive cells from the adult central nervous system results in the loss of forebrain neural stem cells but not retinal stem cells. *Eur. J. Neurosci.* 18, 76–84 doi: 10.1046/j.1460-9568.2003.02727.x

Narayanan, R., and Tuoc, T. C. (2014). Roles of chromatin remodeling BAF complex in neural differentiation and reprogramming. *Cell Tissue Res.* 356, 575–584. doi: 10.1007/s00441-013-1791-7

Ninkovic, J., Steiner-Mezzadri, A., Jawerka, M., Akinci, U., Masserdotti, G., Petricca, S., et al. (2013). The BAF complex interacts with Pax6 in adult neural progenitors to establish a neurogenic cross-regulatory transcriptional network. *Cell. Stem Cell* 13, 403–418. doi: 10.1016/j.stem.2013.07.002

Osumi, N., Shinohara, H., Numayama-Tsuruta, K., and Maekawa, M. (2008). Concise review: Pax6 transcription factor contributes to both embryonic and adult neurogenesis as a multifunctional regulator. *Stem Cells* 26, 1663–1672. doi: 10.1634/stemcells.2007-0884

Paez-Gonzalez, P., Abdi, K., Luciano, D., Liu, Y., Soriano-Navarro, M., Rawlins, E., et al. (2011). Ank3-dependent SVZ niche assembly is required for the continued production of new neurons. *Neuron* 71, 61–75. doi: 10.1016/j.neuron.2011.05.029

Panayiotou, E., and Malas, S. (2013). Adult spinal cord ependymal layer: a promising pool of quiescent stem cells to treat spinal cord injury. *Front. Physiol.* 4:340. doi: 10.3389/fphys.2013.00340

Parsons, X. H., Parsons, J. F., and Moore, D. A. (2012). Genome-scale mapping of MicroRNA signatures in human embryonic stem cell neurogenesis. *Mol. Med. Ther.* 1:105. doi: 10.4172/2324-8769.1000105

Pourabdolhossein, F., Gil-Perotin, S., Garcia-Belda, P., Dauphin, A., Mozafari, S., Tepavcevic, V., et al. (2017). Inflammatory demyelination induces ependymal modifications concomitant to activation of adult (SVZ) stem cell proliferation. *Glia* 65, 756–772. doi: 10.1002/glia.23124

Ren, Y., Ao, Y., O'Shea, T. M., Burda, J. E., Bernstein, A. M., Brumm, A. J., et al. (2017). Ependymal cell contribution to scar formation after spinal cord injury is minimal, local and dependent on direct ependymal injury. *Sci. Rep.* 7:41122. doi: 10.1038/srep41122

Ronan, J. L., Wu, W., and Crabtree, G. R. (2013). From neural development to cognition: unexpected roles for chromatin. *Nat. Rev. Genet.* 14, 347–359. doi: 10.1038/nrg3413

Sabelstrom, H., Stenudd, M., and Frisen, J. (2014). Neural stem cells in the adult spinal cord. *Exp. Neurol.* 260, 44–49. doi: 10.1016/j.expneurol.2013.01.026

Sailor, K. A., Schinder, A. F., and Lledo, P. M. (2017). Adult neurogenesis beyond the niche: its potential for driving brain plasticity. *Curr. Opin. Neurobiol.* 42, 111–117. doi: 10.1016/j.conb.2016.12.001

Thomas, M. G., Welch, C., Stone, L., Allan, P., Barker, R. A., and White, R. B. (2016). PAX6 expression may be protective against dopaminergic cell loss in Parkinson's disease. *CNS Neurol. Disord. Drug Targets* 15, 73–79. doi: 10.2174/1871527314666150821101757

Tiyaboonchai, A., Cardenas-Diaz, F. L., Ying, L., Maguire, J. A., Sim, X., Jobaliya, C., et al. (2017). GATA6 plays an important role in the induction of human definitive endoderm, development of the pancreas, and functionality of pancreatic beta cells. *Stem Cell Rep.* 8, 589–604. doi: 10.1016/j.stemcr.2016.12.026

Tripathi, R., and Mishra, R. (2012). Aging-associated modulation in the expression of Pax6 in mouse brain. *Cell Mol. Neurobiol.* 32, 209–218. doi: 10.1007/s10571-011-9749-3

Varela-Nallar, L., and Inestrosa, N. C. (2013). Wnt signaling in the regulation of adult hippocampal neurogenesis. *Front. Cell Neurosci.* 7:100. doi: 10.3389/fncel.2013.00100

Yao, B., Christian, K. M., He, C., Jin, P., Ming, G. L., and Song, H. (2016). Epigenetic mechanisms in neurogenesis. *Nat. Rev. Neurosci.* 17, 537–549. doi: 10.1038/nrn.2016.70

Yogarajah, M., Matarin, M., Vollmar, C., Thompson, P. J., Duncan, J. S., Symms, M., et al. (2016). PAX6, brain structure and function in human adults: advanced MRI in aniridia. *Ann. Clin. Transl. Neur.* 3, 314–330. doi: 10.1002/acn3.297

Zhang, X., Huang, C. T., Chen, J., Pankratz, M. T., Xi, J., Li, J., et al. (2010). Pax6 is a human neuroectoderm cell fate determinant. *Cell Stem Cell* 7, 90–100. doi: 10.1016/j.stem.2010.04.017

Conflict of Interest Statement: The authors declare that the research was conducted in the absence of any commercial or financial relationships that could be construed as a potential conflict of interest.

frontiers in Cellular Neuroscience

ORIGINAL RESEARCH
published: 12 March 2018
doi: 10.3389/fncel.2018.00057

Mob2 Insufficiency Disrupts Neuronal Migration in the Developing Cortex

Adam C. O'Neill[1,2], Christina Kyrousi[3], Melanie Einsiedler[2], Ingo Burtscher[2,4], Micha Drukker[2,5], David M. Markie[6], Edwin P. Kirk[7], Magdalena Götz[2,8,9], Stephen P. Robertson[1] and Silvia Cappello[3]**

[1]Department of Women's and Children's Health, University of Otago, Dunedin, New Zealand, [2]Helmholtz Center, Institute of Stem Cell Research, Munich, Germany, [3]Max Planck Institute of Psychiatry, Munich, Germany, [4]Helmholtz Center Munich, Institute of Diabetes and Regeneration Research, Garching, Germany, [5]Helmholtz Center, iPSC Core Facility, Munich, Germany, [6]Department of Pathology, University of Otago, Dunedin, New Zealand, [7]Sydney Children's Hospital, University of New South Wales and New South Wales Health Pathology, Randwick, NSW, Australia, [8]Physiological Genomics, Biomedical Center, Ludwig-Maximilians-University, Munich, Germany, [9]Excellence Cluster of Systems Neurology (SYNERGY), Munich, Germany

Disorders of neuronal mispositioning during brain development are phenotypically heterogeneous and their genetic causes remain largely unknown. Here, we report biallelic variants in a Hippo signaling factor—*MOB2*—in a patient with one such disorder, periventricular nodular heterotopia (PH). Genetic and cellular analysis of both variants confirmed them to be loss-of-function with enhanced sensitivity to transcript degradation via nonsense mediated decay (NMD) or increased protein turnover via the proteasome. Knockdown of *Mob2* within the developing mouse cortex demonstrated its role in neuronal positioning. Cilia positioning and number within migrating neurons was also impaired with comparable defects detected following a reduction in levels of an upstream modulator of Mob2 function, Dchs1, a previously identified locus associated with PH. Moreover, reduced Mob2 expression increased phosphorylation of Filamin A, an actin cross-linking protein frequently mutated in cases of this disorder. These results reveal a key role for Mob2 in correct neuronal positioning within the developing cortex and outline a new candidate locus for PH development.

Keywords: Mob2, Hippo pathway, periventricular heterotopia, cortical development, exome sequencing

OPEN ACCESS

Edited by:
Christophe Heinrich, INSERM U1208 Institut Cellule Souche et Cerveau, France

Reviewed by:
Alfonso Represa, INSERM UMR1249 Institut de Neurobiologie de la Méditerranée, France
Fiona Francis, INSERM UMRS839 Institut du Fer à Moulin, France

****Correspondence:***
Stephen P. Robertson
stephen.robertson@otago.ac.nz
Silvia Cappello
silvia_cappello@psych.mpg.de

Received: *02 December 2017*
Accepted: *19 February 2018*
Published: *12 March 2018*

Citation:
O'Neill AC, Kyrousi C, Einsiedler M, Burtscher I, Drukker M, Markie DM, Kirk EP, Götz M, Robertson SP and Cappello S (2018) Mob2 Insufficiency Disrupts Neuronal Migration in the Developing Cortex. Front. Cell. Neurosci. 12:57. doi: 10.3389/fncel.2018.00057

INTRODUCTION

During mammalian brain development, new neurons are produced from germinal niches lining the lateral ventricles of the cerebral cortex. From here, neurons must migrate to the outer cortical plate (CP), where they establish connections, contributing to normal brain function (Götz and Huttner, 2005). Broadly grouped, these crucial processes begin with neurogenesis, followed by neuronal migration, differentiation and spatial organization to establish connectivity (Komuro and Rakic, 1998; Kriegstein and Noctor, 2004). Disruption of these developmental processes can lead to a range of neurodevelopment conditions, the understanding of which can inform on the mechanisms governing normal brain development.

Periventricular nodular heterotopia (PH) is a phenotypically heterogeneous condition of cortical development characterized by a failure of neurons to populate the outer cortex of the brain, resulting in heterotopic positioning along their sites of origin—the margins of the lateral ventricles (Guerrini and Dobyns, 2014). Although variants in eight genes have been

shown to cause PH, these only account for ∼26% of sporadic cases (Fox et al., 1998; Sheen et al., 2004; Parrini et al., 2006; Cappello et al., 2013; Conti et al., 2013; Broix et al., 2016; Alcantara et al., 2017; Oegema et al., 2017). An important etiological role for genetics is, however, hypothesized in many of the remaining individuals with PH (Mandelstam et al., 2013). Mutations in the gene *FLNA*, encoding the F-actin binding protein FilaminA, represent the main cause for established monogenic forms of PH accounting for almost all familial X-linked presentations (Fox et al., 1998). A rare autosomal recessive form of PH with associated microcephaly has also been described in six individuals (Sheen et al., 2004; Bardón-Cancho et al., 2014). The causative gene associated with this phenotype is *ARFGEF2*, with all mutations to date being loss-of-function. *In vitro* studies have shown that *ARFGEF2*, encoding ADP-ribosylation factor guanine nucleotide exchange factor 2 (or BIG2), regulates vesicle formation from the Golgi and trafficking to the cellular surface. BIG2 is also reported to regulate the transport of FLNA to its appropriate cellular compartment (Shin et al., 2005).

Mutations in the atypical cadherin receptor ligands *FAT4* and *DCHS1* have also been shown to cause PH (Cappello et al., 2013). FAT4 and DCHS1 function upstream of the MST kinase (aka Hippo) of the Hippo signaling pathway to control two main functions—cellular polarity and proliferation; with nuclear YAP promoting cell proliferation. Although much interest in recent years has focused on the function of the MST kinases and their downstream effectors—NDR1/2 and Yap (Hergovich, 2012), the heterotopic neurons produced upon FAT4 and DCHS1 knockdown could be mitigated by the simultaneous knockdown of Yap (Cappello et al., 2013). These results suggested that disrupted proliferation was the dominant mechanism for the altered neuronal distribution. However, a role for NDR1/2, a separate branch of the Hippo signaling pathway, could also be involved, but as yet, this possibility remains unexplored. Most recently, missense mutations leading to substitutions in the HECT domain of the E3 ubiquitin ligase, NEDD4L, were also implicated in the cause of PH with *in vivo* mouse studies highlighting dysregulation of mTOR and AKT signaling pathways (Broix et al., 2016).

In this study, we hypothesized that existing knowledge of the genetic pathways underpinning PH could be exploited to prioritize variants found in the genes of patients with PH by exome sequencing. Although such genes fall short of proof-of-pathogenicity on genetic grounds, the aim of this strategy is to identify candidate genes with experimentally validated deleterious biallelic variants for more in-depth targeted re-sequencing analyses that further test their causative potential of PH.

MATERIALS AND METHODS

Subject Ascertainment and Ethical Approval

All study participants were ascertained by physician-initiated referral and consented to participate under a University of Otago consent protocol. Ethical approval was obtained from the Southern Regional Ethics Committee O03/016 and the New Zealand Multicenter Ethics Committee MEC08/08/094.

Whole-Exome Sequencing

Whole-exome sequencing was carried out by Otogenetics Corporation (Norcross, GA, USA). Sequencing libraries were prepared from genomic DNA extracted from leukocytes of parents and patients using Wizard® Genomic DNA Purification Kit (Promega, Cat. A1620) following the manufacturer's instructions. Library DNA was exome enriched using the Agilent SureSelect Human All Exon V4+UTRs capture kit, and sequenced on an Illumina Hiseq2000, Illumina, San Diego, CA, USA using 100 bp paired-end reads. Alignment of the sequenced DNA fragments to the Ensembl Genome Browser human genome assembly (GRCh37) was carried out using the Burrows-Wheeler Aligner (MEM algorithm) v.0.7.12. After alignments were produced for each individual separately, the data was locally realigned around indels followed by base quality score recalibration consistent with Genome Analysis Tool Kit (GATK) Best Practices (version 3.4–46; Broad Institute). Duplicate reads were removed using PICARD (version 1.140; Broad Institute). Individual variant calling was undertaken using the GATK HaplotypeCaller, followed by joint genotyping and variant quality score recalibration to produce a multisample variant call format file (vcf).

VCF gene context annotation was added using SnpEff v.4.1L. Allele frequencies were obtained from 1000 Genomes Project phase 1, NHLBI GO Exome Sequencing Project (ESP) ESP6500 and the Exome Aggregation Consortium (ExAC) via the GATK VariantAnnotator. All alignments with loci bearing putative *de novo* variants were extracted from the multisample VCF using GATK SelectVariants and SnpSift v.4.1L (SnpEff) that met the following criteria: (1) the read depth should be $\geq$8 within the patient; (2) at least 20% of the reads should carry the alternate allele; (3) <5% of the reads in either parent should carry the alternative allele; (4) at least two alleles must be observed in the proband; (5) the genotype quality (GQ) score for the offspring should be 99; and (6) the normalized, phred-scaled genotype likelihood (PL) scores in both parents for the three possible genotypes 0/0, 0/1 and 1/1, where 0 is the reference allele and 1 is the alternative allele, should be >0, >20 and >20, respectively. Candidate *de novo* variants were also absent from population controls, including a set of 107 internally sequenced controls and the individuals whose single nucleotide variant data are reported in the Genome Aggregation Database (gnomAD; Lek et al., 2016). All candidate *de novo* variants were Sanger sequenced using the relevant proband and parents for confirmation.

Putative recessive variants were extracted from the VCF that met the following criteria: (1) the read depth should be $\geq$8 or 20 for compound heterozygous or homozygous alternate genotype calls in the patient, respectively; (2) at least 20% and 90% of the reads in the patient should carry the alternate allele for candidate compound heterozygous and homozygous genotypes, respectively; (3) in the parents, at least one individual requires a read depth $\geq$30; and (4) candidate recessive variants should not be present in population controls, including a set of 107 internally

sequenced controls and the individuals whose single nucleotide variant data are reported in the Genome Aggregation Database (gnomAD; Lek et al., 2016). All candidate recessive variants were Sanger sequenced using the relevant proband and parents for confirmation.

Framework for Identifying a Recessive Candidate for Functional Follow Up Studies

To prioritize validated recessive variants for functional investigations that assess the effect of the various changes we used the following criteria: (1) remove any candidate in an individual already reported to have a *de novo* event; (2) at least one of the recessive variants is required to be a stop gain/loss, canonical splice site, or a small out of frame insertion/deletion; and (3) using each of the remaining candidate gene names as key word, functional studies were mined from the literature described in Pubmed to determine if interactions with pre-established PH loci and their cognate proteins was described. Although not suggesting any given candidate satisfying this criterion will be confirmed as a contributor to PH etiology, in this study one gene—*MOB2*—was identified as having properties warranting further analysis. Once identified, the minor allele frequency cut off was relaxed to 2% in the 65 large cohort to survey for additional variants within this gene. This, however, did not identify any further variants of significant excess to that expected from control estimates within the ExAC and gnomAD datasets (Lek et al., 2016).

Cell Culture

C2C12, HEK293, patient and control fibroblasts were cultured in DMEM Dulbecco's Modified Eagles Medium (DMEM; Gibco®) supplemented with 10% fetal bovine serum (FBS) and 1% L-glutamine at 37°C in humidified 5% CO_2.

Reprogramming of Human Fibroblasts to Induced Pluripotent Stem Cells (iPSCs HMGU1)

Induced pluripotent stem cells (iPSCs) were reprogrammed from human newborn foreskin fibroblasts (CRL-2522, ATCC). 2.5×10^5 NuFF3-RQ IRR human newborn foreskin feeder fibroblasts (GSC-3404, GlobalStem) were seeded per well of a 6-well tissue culture dish with advanced MEM (12491015, Thermo Fisher Scientific) supplemented with 5% HyClone FBS (SV30160.03HI, GE Healthcare), 1% MEM NEAA and GlutaMAX (11140050; 35050061 Thermo Fisher Scientific). On day 1, 70%–80% confluent CRL-2522 fibroblasts were dissociated using 0.25% Trypsin-EDTA (25200056, Life Technologies), counted and seeded on the NuFF3-RQ cells at two different densities: 2×10^4 cells/well and 4×10^4 cells/well. On day 2, the medium was changed to Pluriton Reprogramming Medium (00–0070, Stemgent) supplemented with 500 ng/mL carrier-free B18R Recombinant Protein (03–0017, Stemgent). On days 3–18, a cocktail of modified mRNAs (mmRNAs) containing *OCT4, SOX2, LIN28, C-MYC*, and *KLF* mmRNAs at a 3:1:1:1:1 stoichiometric ratio was transfected daily. For that purpose, the mmRNAs were mixed in a total volume of 105 μL and were combined with a mix of 92 μL Opti-MEM I Reduced Serum Medium and 13 μL Lipofectamine RNAiMAX Transfection Reagent (31985062, Thermo Fisher Scientific) after separate incubation at RT for 15 min. Cells were transfected for 4 h, washed and fresh reprogramming medium supplemented with B18R was added to the cultures. The mmRNAs with the following modifications: 5-Methyl CTP, a 150 nt poly-A tail, ARCA cap and Pseudo-UTP were obtained from the RNA CORE unit of the Houston Methodist Hospital. Five days after the first transfection, the first morphological changes were noticed, while the first iPSC colonies appeared by day 12–15. On day 16, the medium was changed to STEMPRO hESC SFM (A1000701, Thermo Fisher Scientific) for 5 days. Harvesting of the iPSC colonies was performed after 40 min incubation at 37°C with 2 mg/ml Collagenase Type IV (17104019, Thermo Fisher Scientific) solution in DMEM/F12 (31331093, Thermo Fisher Scientific). The iPSCs were plated on γ-irradiated mouse embryonic fibroblasts (MEFs) and grown in STEMPRO hESC SFM for 10 additional passages. After that the iPSCs were further cultured in a feeder-free culture system, using mTeSR1 (05850, StemCell Technologies) on plates coated with LDEV-Free Geltrex (A1413302, Thermo Fisher Scientific). The control iPSC line HMGU1 was generated in the iPSC Core Facility, Helmholtz Center Munich.

iPSC Culture

iPSCs were cultured at 37°C, 5% CO_2 and ambient oxygen level on Geltrex coated plates in mTeSR1 medium with daily medium change. For passaging, iPSC colonies were incubated with StemPro Accutase Cell Dissociation Reagent (A1110501, Life Technologies) diluted 1:4 in PBS for 4 min. Pieces of colonies were washed off with DMEM/F12, centrifuged for 5 min at 300× *g* and resuspended in mTeSR1 supplemented with 10 μM Rock inhibitor Y-27632 (2HCl; 72304, StemCell Technologies) for the first day.

Cerebral Organoid Generation

Cerebral organoids were generated starting from 9000 single iPSCs/well in 96 well tissue culture plates as previously described (Lancaster et al., 2013). Upon their formation, organoids were cultured in 10 cm dishes on an orbital shaker at 37°C, 5% CO_2 and ambient oxygen level with medium changes twice a week.

Transfection of Human Cells

Expression constructs were transiently transfected into C2C12, HEK293 and fibroblast cells with Lipofectamine™ 2000 (Invirogen, Cat. # 11668-019) according to the manufacturer's instructions. siRNA constructs were transiently transfected into human fibroblasts with Lipofectamine RNAiMAX (Invitrogen, Cat. # 13778-075) according to the manufacturer's instructions.

Protein Extraction

Cells were lysed after 20 h post transfection in 1× phosphate buffered saline (PBS), 1% (v/v) Triton-X100 and Complete Protease Inhibitor (Roche) on ice for 20 min. Cell debris was then pelleted through centrifugation at 13,000 rpm 4°C for

10 min. Twenty microliter of protein lysate was combined with protein loading dye (final concentration: 50 mM Tris pH 6.8, 10% glycerol, 2% SDS, 6% 2-mercaptoethanol and 1% w/v Bromo blue) and denatured at 95°C for 5 min.

SDS-Page and Western Blot

Protein lysate was separated by polyacrylamide gel electrophoresis using a mini-PROTEAN Tetra Cell system (BioRad Laboratories, Hercules, CA, USA). The samples were run through on a 7%–10% running gel, depending on the size of the proteins being separated, and a 5% stacking gel. Gel electrophoresis was performed for 1–2 h at 200 V in running buffer (25 mM Tris base, 192 mM Glycine, 0.1% (v/v) SDS), with 4 μL Precision Plus Protein Dual Colour Standard (BioRad, Cat. # 161-0734) loaded to determine protein size and monitor electrophoresis speed. Proteins were transferred to a nitrocellulose membrane (0.25 or 0.45 micron, depending on protein size, Pierce) using the Min Trans-Blot Electrophoretic Transfer Cell (BioRad Laboratories, Hercules, CA, USA) at 25 V and 50 V for 1.5 h each in transfer buffer (25 mM Tris, 0.19 M Glycine, 10% (v/v) isopropanol). The membrane was then blocked in 5% non-fat milk powder in PBS-T (PBS, 0.05% (v/v) Tween20) for 30 min with shaking at 30 rpm (Ratek platform shaker). The appropriate primary antibody was then diluted into fresh 5% (w/v) non-fat milk powder in PBS-T and incubated with the membrane overnight at 4°C and 30 rpm. The following day the membrane was washed once in PBS-T before incubation with secondary antibody to horseradish peroxidase diluted into fresh 5% non-fat milk powder in PBS-T for 1 h at 30 rpm. The membrane was then washed five times for 5 min in PBS-T before detecting bands with SuperSignal West Pico Chemiluminscent Substrate (Pierce, Cat. # 34080) on Kodak BioMax XAR Film size 8 (Kodak, Cat. # 165-1454). Total FLNA (mouse, Abcam, Cat. #ab188350, 1:3000) and phospho-Filamin A (Ser2152; rabbit, Cell Signalling Technology, Cat. #4761S, 1:1000) were used to assess phosphorylated levels of FLNA at site serine 2152.

Nonsense Mediated RNA Decay

Age-matched control and patient fibroblasts were cultured in T-25 flask (Falcon, Cat. # 353108). Once at 80% confluency, minimal growth media was substituted (DMEM, 1% FCS, 1% L-glutamine) and cells were cultured for a further 12 h. After 12 h incubation media was substituted for DMEM, 10% FCS, 1% L-glutamine and either solvent alone (DMSO) or 150 μg/mL cycloheximide (CHX) in DMSO. Cells were then incubated for a further 4 h after which time media was removed and cells washed with PBS, before RNA isolation. *MOB2* expression was then assayed by RT-qPCR using gene specific primers. House-keeping normalized *MOB2* expression in patient fibroblasts was compared to control DMSO treatment using the delta-delta Ct method.

Proteasome Inhibition

HEK293 cells plated at 80% confluency in 24-well plates (Falcon, Cat. # 353047) were transiently transfected with a bicistronic vector expressing both the green fluorescent protein (GFP) and wild-type (WT) or mutant (Glu227Lys) *MOB2*. Twenty-four hours after transfection media was removed and cells gently washed with PBS. Media containing DMEM, 10% FCS, 1% L-glutamine and either solvent alone (0.01% DMSO) or the proteasome inhibitor, 1 μM MG132 (Sigma-Aldrich, Cat. # C2211), in DMSO for 24 h. After which point total cell lysates were prepared and subjected to Western blot analysis using MOB2 (mouse, LSBio, Cat. #LS-C184588, 1:5000), GFP (mouse, OriGene, Cat. # TZ150041, 1:5000) and GAPDH (rabbit, Sigma-Aldrich, Cat. # G9545, 1:3000).

Apoptosis Assay

Age-matched control and patient fibroblasts were cultured in T-25 flask (Falcon, Cat. # 353108). Once at 80% confluency, cells were treated with 0.5% trypsin (Sigma-Aldrich, Cat. # 59418C) and reverse transfection protocol was carried out in a 24-well plate with cells re-plated at the appropriate densities. Media contained DMEM, 10% FCS and 1% L-glutamine and 30 nM siRNA scrambled or against *MOB2* (Sigma-Aldrich, Cat. # SIC001-10NMOL and SASI_Hs01_00177399) pre-mixed in Lipofectamine RNAiMAX (Invitrogen, Cat. # 13778-075) according to the manufacturer's instructions. Samples not treated with siRNA were only provided the Lipofectamine RNAiMAX mixture. Twenty-four hours after transfection media was removed, cells gently washed with PBS and then placed in DMEM, 10% FCS, 1% L-glutamine and 200 μM camptothecin (Merck-Millipore, Cat. # 208925). Total cell lysates were prepared 0, 8, 15 and 24 h post camptothecin treatment (200 μM) and processed for immunoblotting using cleaved-PARP (mouse, BD-Pharmigen, Cat. # 552596, 1:1000) and GAPDH (rabbit, Sigma-Aldrich, Cat. # G9545, 1:3000).

Mouse Lines

All the animals used in this work were kept in the animal facility of the Helmholtz Center Munich and Max Planck Institute of Psychiatry. All the experimental procedures were performed in accordance with German and European Union guidelines. Animals were maintained on a 12 h light-dark cycle. The day of vaginal plug was considered as embryonic day 0 (E0). In this study the C57Bl/6J mouse line was used.

Anesthesia

To perform *in utero* operations, mice were anesthetized by subcutaneous injection of a solution containing: Fentanyl (0.05 mg/kg), Midazolam (5 mg/kg) and Medetomidine (0.5 mg/kg). The anesthesia was terminated with a subcutaneous injection of a solution composed of Buprenorphine (0.1 mg/kg), Atipamezol (1.5 mg/kg) and Flumazenil (0.5 mg/kg).

In Utero Electroporation

Surgery was performed on animals in accordance with the guidelines of Government of Upper Bavaria under licence numbers 55.2-1-54-2532-79-11 and 55.2-1-54-2532-79-2016. E13 pregnant dams were anesthetized and operated on as previously described (Saito, 2006). In brief, the shaved abdomen was opened by caesarean section in order to expose the uterine horns. These were kept wet and warm by continuous application of pre-warmed saline. Endotoxin free vectors—diluted to

1.5 μg/μL—were mixed in Fast green (2.5 mg/μL, Sigma). One microliter of mix was injected into the ventricle with the aid of glass capillaries (self-made with a micropipette puller). DNA was electroporated into the lateral ventricle of the telencephalon with four pulses of 38 mV for 100 ms each. At the end of the entire electroporation procedure, the uterine horns were repositioned into the abdominal cavity, which was then filled with pre-warmed saline. The abdominal wall was closed by surgical sutures (Ethicon, Cat. # K832H). Anesthesia is reversed as described above and animals were monitored appropriately. At E16 (3 days post electroporation (3 dpe)) operated animals were sacrificed by cervical dislocation. Embryos were placed in HBSS (Hank's Balanced Salt Solution—Gibco, Life Technologies) supplemented with 10 mM Hepes (Gibco, Life Technologies). Embryos were dissected and brains fixed. pSuper-GFP (Oligoengine) were used as the control plasmid. *Mob2* targeting miRNA-expressing constructs (miRNA1 (5′-ctatactgcaggttgatgtgg-3′) and miRNA2 (5′-aataggagcaagcagcaggtg-3′)) were cloned into the pSuper-GFP vector (Blockit, Invitrogen) according to the manufacturer's instructions. Plasmids were subsequently recombined into PCAGGS destination vector (Invitrogen Gateway®-adapted expression vector, Cat. # K493600). shRNAs against *Dchs1* and *Yap* have been described previously (Cappello et al., 2013). To visualize the cilia, we electroporated a plasmid encoding *Arl13b* fused with tagRFP (*Arl13b*-tagRFP). Nucleus-cilia coupling was assessed in migrating neurons in the upper bin (CP2).

Electroporation of Cerebral Organoids

Cerebral organoids were kept in antibiotic-free conditions prior to electroporation. Electroporations were performed in cerebral organoids at the 44 days stage after the initial plating of the cells and fixed 7 dpe. During the electroporation cerebral organoids were placed in an electroporation chamber (Harvard Apparatus, Holliston, MA, USA) under a stereoscope and using a glass microcapillary 1–2 μL of plasmid DNAs at final concentration of 1 μg/μL was injected together with Fast Green (0.1%, Sigma) into different ventricles of the organoids. Cerebral organoids were subsequently electroporated with five pulses applied at 80 V for 50 ms each at intervals of 500 ms using the Electroportator ECM830 (Harvard Apparatus). Following electroporation cerebral organoids were kept for additional 24 h in antibiotic-free media, and then changed into the normal media until fixation. Cerebral organoids were fixed using 4% PFA for 1 h at 4°C, cryopreserved with 30% sucrose and then stored in −20°C. For immunofluorescence, 16 μm cryosections were prepared.

Immunofluorescence of Mouse Cortical Tissue

Mouse cortical tissues were fixed in 4% paraformaldehyde for 20 min at 4°C followed by washing in PBS three times 10 min. Tissues were allowed to sink in 30% sucrose overnight and then embedded into molds (Polysciences, Cat. # 18646A-1) using Tissue-Tek (Hartenstein, Cat. # TTEK) and frozen on dry ice. Tissue was then stored at −20°C until it was cryosectioned in 20 μm sections with a Cryostat (Leica). Sections were blocked and permeabilized in 0.25% Triton-X100, 4% normal donkey serum in PBS. Sections were then incubated with primary antibodies in 0.1% Triton-X100, 4% normal donkey serum at the following dilutions: GFP (chick, Aves Lab, Cat. # GFP-1020, 1:500). Sections were incubated overnight at 4°C. The next day slides were washed three times in PBS and then treated as per the manufacturer's instructions with the appropriate secondary fluorophore antibodies.

Immunofluorescence of Human Cerebral Organoids

Tissues were processed as per mouse cortical tissue. Before sections were blocked they were post-fixed with 4% PFA for 10 mins, permeabilized in 0.3% Triton-X100 and then blocked with 0.1% Tween, 3% BSA and 10% normal goat serum. Sections then incubated with primary antibodies diluted in blocking solution. GFP (chick, Aves Lab, Cat. # GFP-1020, 1:1000) and RFP (rbb, Rockland 1:1000, Cat. # 600-401-379).

Quantification and Statistical Analysis

All analyses were performed using at least three different animals of each genotype and the total number of cells counted is shown below each treatment bar in each graph of the figure. Data are represented as mean ± SEM. Statistical significance was assessed using Mann-Whitney U test, exact binomial test or one-way ANOVA with Tukey HSD correction as indicated.

RESULTS

Identifying Candidate Loci With Biallelic Variants in Patients With PH for Functional Tests

To begin identifying candidate variants in PH, we analyzed the coding region of the genome (the exome) in 65 patients with the condition and their unaffected parents. Although *de novo* variants have a strong association in neurodevelopmental conditions, to simplify interpretation in this study we restricted our analysis to rare biallelic variants whereby at least one of the altered alleles was required to be a stop gain/loss or a small out of frame insertion/deletion predictive of loss-of-function (materials and methods). Of the 17 rare biallelic genotypes identified in the 65 patients, only five satisfied these criteria (Supplementary Table S1). Functional studies mined from the literature database Pubmed, with each of the five candidate gene names as key word, identified no evidence for any locus that indicated a described functional interaction with pre-established PH loci and their cognate proteins. There was, however, functional evidence for one locus modulating immediate components of the Hippo signaling pathway, through which the protein products of the known PH genes *FAT4* and *DCHS1* signals (Cappello et al., 2013)—*MOB2*.

The MOB family of proteins are both evolutionary conserved and well-defined regulators of the Hippo signaling pathway (Hergovich, 2012). Specifically, the sole identified interacting partners of MOB2 are the kinases NDR1/2 of the Hippo signaling pathway (Hergovich et al., 2005; Kohler et al., 2010;

Hergovich, 2012). As per the Online Mendelian Inheritance in Man database (OMIM), variants in the *MOB* family of genes have not been associated with any disease to date.

Biallelic Variants Reduce *MOB2* Transcript and Protein Levels *in Vitro*

Patient 1203, a female, identified here with biallelic variants in *MOB2* was born to healthy non-consanguineous parents. She first presented with epilepsy and learning difficulties. A brain MRI scan revealed bilateral nodular PH of the lateral ventricles (**Figure 1A**). Specifically, patient 1203 has two variants in *MOB2*, a frameshift variant leading to the introduction of a stop codon and a missense variant (c.207delC, p.Phe69Phefs*127; and c.679G > A, p.Glu227Lys; RefSeq NM_001172223 (GRCh37)), respectively (**Figure 1B**). Neither variant is present within the Genome Aggregation Database (gnomAD; Lek et al., 2016). Sanger validations of the parental genotypes identified they were in *trans* in the proband with each parent being heterozygous for only one of the two variants (**Figure 1B**). Both variants show patterns of strong evolutionary conservation (**Figure 1C**).

Analysis of gene constraint using information from the ExAC database (Lek et al., 2016) showed evidence of intolerance against LoF variants in *MOB2*. The constraint metric pLI for this gene in ExAC is 0.64. While scores greater than 0.9 are regarded as indicating extreme intolerance to LoF, the number of predicted LoF variants in ExAC is quite small (7.3, with a single variant actually observed). It is noteworthy that in the much larger gnomAD database, there are only six LoF alleles in total, two of which are located in the final exon, indicating that the resulting transcripts are unlikely to be targeted for nonsense-mediated decay. Taken together, this information indicates that LoF variants in *MOB2* are likely to have a deleterious effect.

The nonsense variant identified in individual 1203, c.207delC, predicts a premature termination codon within exon two and degradation via post-transcriptional mechanisms involving nonsense mediated decay (NMD; Nagy and Maquat, 1998). To formally determine if NMD is activated in response to the c.207delC allele, quantitative RT-PCR of *MOB2* transcripts was carried out on mRNA extracted from patient 1203 fibroblasts. Compared to *MOB2* expression in two age-matched control fibroblast lines, we identified a significant ($P < 0.001$) four-fold reduction in gene expression (**Figure 1D**). Treating fibroblasts with CHX, a known NMD suppressor (Carter et al., 1995), induced a significant 2.6-fold increase ($P < 0.001$) in *MOB2* transcript relative to vehicle-treated patient cells (**Figure 1D**).

To investigate any potential detrimental effects conferred by the missense variant (c.679G > A) identified in patient 1203, total protein lysate of HEK293 cells overexpressing the MOB2 constructs (WT or p.Glu227Lys) linked bicistronically to GFP were analyzed by Western blot (**Figure 1E**). Analysis of total protein lysate 24-h post transfection identified a significant ($P < 0.001$) 10-fold reduction in mutant MOB2 protein harboring the p.Glu227Lys change, relative to WT control (**Figure 1F**).

In light of these results, we hypothesized that the missense variant, p.Glu227Lys, destabilizes MOB2 resulting in its degradation. In eukaryotic cells, the ubiquitin-dependent proteasome system is the main pathway responsible for selective intracellular protein degradation in response to mis-folding (Nandi et al., 2006). To determine whether this pathway was activated here, HEK293 cells expressing human *MOB2* variants (WT or p.Glu227Lys) were treated with the proteasome inhibitor MG132. Quantitative analysis 24-h post MG132 treatment identified a significant ($P < 0.01$) increase in mutant MOB2 protein harboring the p.Glu227Lys change, relative to vehicle-only treated cells also overexpressing this form of protein (**Figures 1E,F**). No significant change in total MOB2 abundance was detected between MG132 and vehicle treated HEK293 cells overexpressing the WT protein (**Figures 1E,F**). No change in transfection efficiency (reported by untagged-GFP encoded on the same bicistronic vector) was identified between any of the treatment groups (**Figure 1E**).

Direct assessment of the detrimental effect conferred by the missense variant (p.Glu227Lys) in patient 1203 fibroblasts was precluded given the undetectable levels of endogenous MOB2 in control cells. However, reduced MOB2 levels enhance the susceptibility of cells to apoptosis *in vitro* (Kohler et al., 2010). Camptothecin is a potent inducer of apoptosis operating through the inhibition of DNA topoisomerase (Tazi et al., 1997). Thus, to assess altered levels of susceptibility to apoptosis in patient 1203 fibroblasts, cells were treated for 8, 15 and 24 h with camptothecin, after which total protein lysate was isolated and probed with an antibody against cleaved poly ADP-ribose polymerase (PARP)—a protein cleaved directly by caspase-3 upon apoptosis induction (Supplementary Figure S1). Cleaved-PARP was detected 24 h post camptothecin treatment in age-matched control fibroblasts. In contrast, cleaved-PARP was detected 7 h earlier, at 8 h post camptothecin treatment, in patient 1203 fibroblasts (Supplementary Figure S1). This enhanced susceptibility to apoptosis observed in patient 1203 fibroblasts, relative to controls, was comparable to that seen in age-matched control fibroblasts transfected with siRNA targeting *MOB2* (Supplementary Figure S1).

Taken together, these data suggest that both variants identified in *MOB2* of patient 1203 are LoF with NMD and proteasome-dependent protein degradation acting to reduce MOB2 levels.

Mob2 Knockdown *in Vivo* Alters Neuronal Distribution Within the Developing Mouse Cortex and Induces Nucleus-Cilia Uncoupling

Data defining brain structures that express *Mob2* suggest a potential role of this gene in cortical development (Lein et al., 2007; Miller et al., 2014). To test this directly we assessed the effects of knocking *Mob2* down during mouse cortical development. Specifically, we injected a bi-cistronic vector expressing EGFP and validated miRNAs directed against *Mob2* (Supplementary Figure S2) into the ventricular neuroepithelium of embryonic day 13 embryos (E13) using *in utero* electroporation. Three days post electroporation (3 dpe; E16) the electroporated cortices were cross-sectioned into five

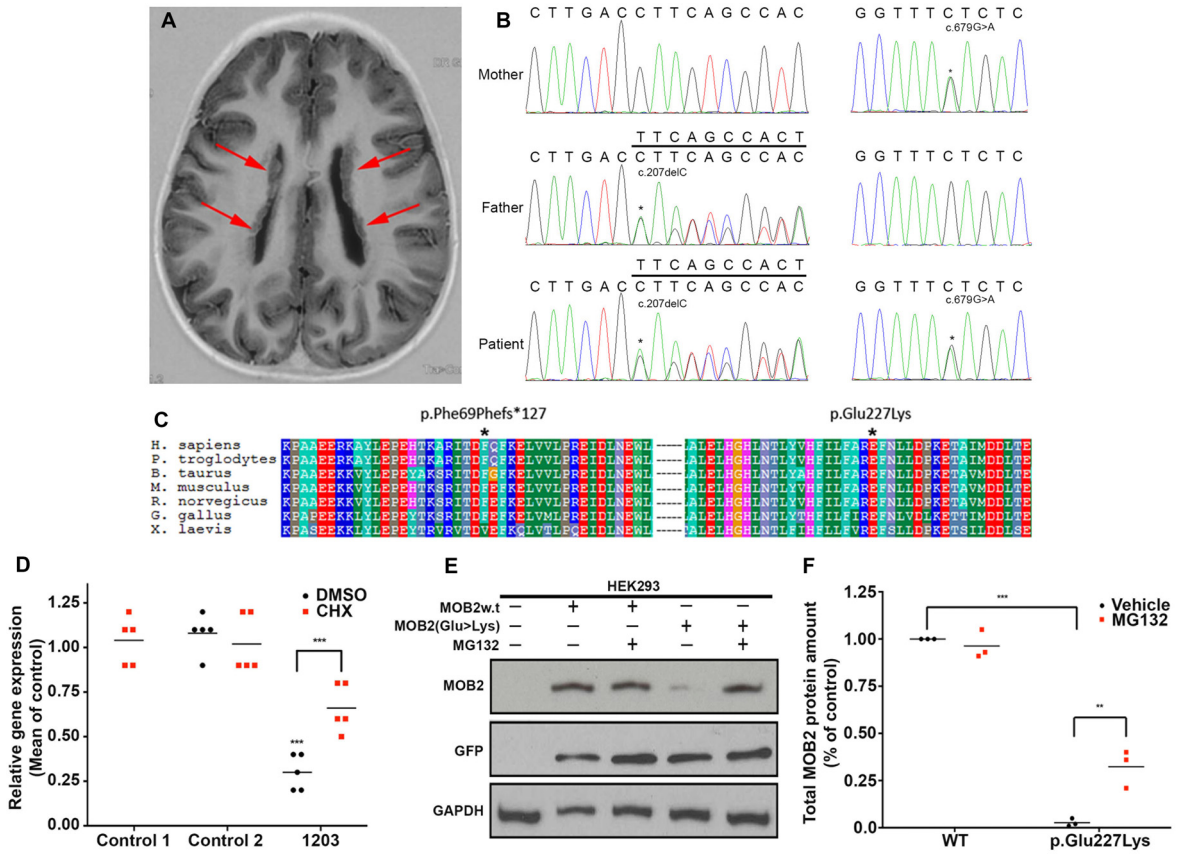

FIGURE 1 | Biallelic variants in *MOB2* affect mRNA and protein stability *in vitro*. **(A)** Brain MRI scan of patient 1203, showing the presence of bilateral periventricular nodular heterotopia (PH; red arrows). **(B)** Sequence traces illustrating the *MOB2* sequence variants c.679G > A, present in mother and patient, and c.207delC, present in father and patient. **(C)** Multiple sequence alignment (ClustalX) of the human MOB2 protein against various species. Columns are colored by conservation and property. *Denotes the positions of the mutated residues—Phe69 and Glu227—substituted by each of the alleles discovered in individual 1203. **(D)** Mean expression of *MOB2* in age-matched controls and individual 1203 (n = 5) fibroblasts when treated with vehicle/DMSO (black circles) and cycloheximide (CHX; red squares), as determined by real-time PCR. Expression was normalized against *GAPDH* and *DIMT1* housekeeping genes in the same sample using the relative standard curve method. Values were then subsequently normalized to control 1 DMSO treatment using the delta-delta Ct method. **(E)** HEK293 cells were transiently transfected with a bi-cistronic vector expressing both the green fluorescent protein (GFP) and wild-type (w.t) or mutant (Glu227Lys) *MOB2*. At 24 h after transfection, cells were treated with DMSO, or the proteasome inhibitor, MG132, for 24 h, after which total cell lysates were prepared and subjected to western blot analysis using anti-MOB2, anti-GFP and anti-GAPDH as a loading control. **(F)** Quantifications representing three biological replicates of **(E)** summarizing total MOB2 protein amount with or without MG132 treatment. Lysosomal degradation pathways may account for the remaining degraded MOB2. $^{**}P < 0.01$; $^{***}P < 0.001$, Mann-Whitney U test.

equally sized bins (approximately corresponding to the different two proliferative zones, intermediate zone (IZ) and upper and lower CP) for analysis. Here, we identified an increased fraction of EGFP-expressing cells in bin 1, corresponding to the ventricular surface (VZ) relative to the vector-only control cortices, with a correspondingly decrease in EGFP-expressing cells in bin 5, corresponding to the outer CP (CP2; **Figures 2A–C**; $P < 0.05$). No change to the total number of GFP+ cells in either condition was observed. These patterns suggest that reduced *Mob2* levels alter the distribution of neuronal cells within the developing cortex.

The predominant mode of radial neuronal migration within the developing cortex is glial-guided locomotion, regulated by coupled/coordinated movement of the cilia/centrosome and nucleus within the neuron (Marin and Rubenstein, 2003). The kinases NDR1/2 are known modulators of cilia/centrosome dynamics, induced by changes in MOB2 activity *in vitro* (Hergovich et al., 2009). Given this insight and the redistribution patterns observed in cells upon decreased *Mob2* levels *in utero*, we hypothesized that knockdown of *Mob2* could alter cilia/centrosome dynamics. To test this, developing mouse cortices were electroporated with a plasmid encoding the cilia specific protein—Arl13b (Higginbotham et al., 2012)—fused to tagRFP (Arl13b-tagRFP), together with either the plasmid expressing EGFP/control or miRNA targeting *Mob2* bi-cistronically linked to EGFP (**Figures 2D–G**). In migrating neurons expressing the control vector, the mean distance between the nucleus and cilia (defined by Arl13b-tagRFP) was 3.5 μm, consistent with distances reported in previous studies (Insolera et al., 2014). In migrating neurons expressing hair-pins

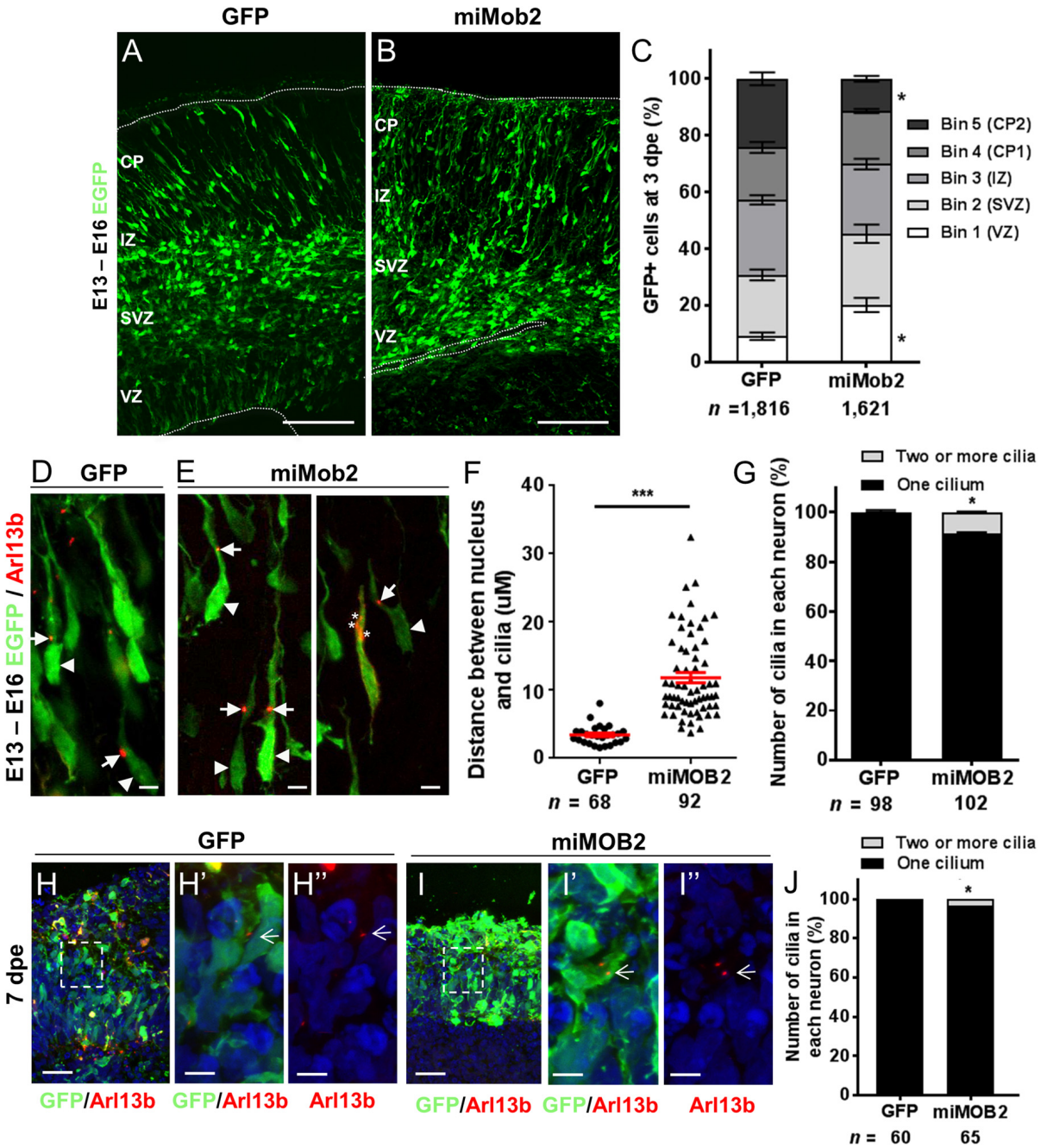

FIGURE 2 | *Mob2* knockdown alters neuronal cell distribution and nucleus-cilia coupling. Coronal micrograph sections of E16 mouse cerebral cortices electroporated at E13 with EGFP/empty vector control **(A)** or miRNAs targeting *Mob2* **(B)**. **(C)** Quantification of the distribution of EGFP-expressing (EGFP+) cells transfected with EGFP/empty vector alone or miRNAs targeting *Mob2* 3 days after electroporation (mean ± SEM). The cortex was subdivided into five equal width bins approximately corresponding to VZ (bin 1), SVZ (bin 2), IZ (bin 3) and CP (bins 4 and 5). CP, cortical plate; IZ, intermediate zone; SVZ, subventricular zone; VZ, ventricular zone; dpe, days post electroporation. At least three embryos were analyzed for each condition. n, total number of GFP+ cells counted per condition. **(D,E)** Representative images of migrating neurons in E16 cortices (3 dpe) electroporated with EGFP/control or miRNA targeting *Mob2* (green) and Arl13b-tagRFP (red) located within bin 5 (CP2). Arrow heads indicate the cell bodies and arrows indicate the cilia labeled by Arl13b-tagRFP. Asterisks show the position of three cilia within a neuron. **(F)** Quantification of the distance between the cilia and nucleus (micrometers) in neurons. Each dot represents a neuron and red lines indicate mean ± SEM. **(G)** Quantification of the number of cilia in each neuron. **(H,I)** Micrographs sections of day 51 human cerebral organoids electroporated at day 44 with EGFP/empty vector control or miRNA targeting *MOB2* (green) and Arl13b-tagRFP (red). White arrows indicate the cilia labeled by Arl13b-tagRFP. **(J)** Quantification of the percentage of cells with more than one cilium of organoids transfected with EGFP/empty vector control (GFP) or miRNAs targeting *Mob2*. Data taken from at least three ventricular structures. **(C,F,G)** Mann-Whitney U test, **(J)** Exact binomial test; $^{*}p < 0.05$, $^{***}p < 0.001$. Scale bar represents **(A,B)** 100 μm, **(D,E)** 10 μm, **(H,I)** 25 μm and **(H′,H″,I′,I″)** 5 μm.

targeting *Mob2* and co-electroporated with a construct encoding *Arl13b-tagRFP*, however, a significant 3-fold increase in distance between the nucleus and cilia was observed (mean distant 11.84 μm; $P < 0.001$) relative to the control (**Figure 2F**).

Every migrating neuron contains a primary cilium attached to the centrosome (basal body; Louvi and Grove, 2011). Of the 102 migrating neurons analyzed that express both miRNAs directed against *Mob2* and Arl13b-tagRFP, eight had evidence for the presence of two or more cilia, a significant increase compared to the 98 neurons expressing both the control vector and Arl13b-tagRFP of which two had more than one cilium (**Figure 2G**; $P < 0.05$). Defects in cilia number were also observed in human cerebral organoid cultures upon *MOB2* knockdown, further suggesting that correct levels of this protein are essential for maintenance of this organelle in human neurons (**Figures 2H,H′,H″,I,I′,I″,J**). Taken together, these results suggest that knockdown of *Mob2* during E13–E16 of murine brain development, *in utero*, uncouples coordinated movement between the cilium and nucleus and may interfere with the regulation of cilia/centrosome duplication; changes that could ultimately impair effective neuronal migration in a subpopulation of neurons, similarly to what occurs in PH.

Dchs1 Knockdown Induces Nucleus-Cilia Uncoupling Within the Developing Mouse Cortex *in Vivo*

FAT4 and DCHS1 are directly implicated in the cause of Van Maldergem syndrome, a developmental disorder characterized by PH (Cappello et al., 2013) and function upstream of MOB2 in the Hippo signaling pathway (Hergovich, 2012). Given this, and the altered cellular distribution and nucleus-cilia uncoupling observed upon *Mob2* knockdown in mouse embryonic cortices, we investigated if dysregulation of other genes involved in the regulation of the Hippo pathway and in which mutations were associated with PH also altered these uncoupling events. Indeed, knockdown of *Dchs1* by *in utero* electroporation induced cilia defects in the developing mouse cortex (**Figures 3A,A′,B,B′,C**). In particular, the position and/or number of cilia in migrating neurons was aberrant upon *Dchs1* downregulation. Strikingly, unlike the altered proliferation phenotype induced by knockdown of this factor (Cappello et al., 2013), this effect could not be remedied by simultaneous reduction of *Yap* expression (**Figures 3C,D,D′,D″,D‴**). As the Hippo signaling pathway is composed of two arms, the Yap arm and Mob2 arm (**Figure 5**; Hergovich, 2012), these results suggest that the changes previously observed upon *Dchs1* knockdown *in utero* with respect to proliferation related directly to the regulation of Yap (Cappello et al., 2013). In contrast, defects in nucleus-cilia coupling could be independently determined by interference with Mob2 function in migrating neurons.

Enhanced FLNA Phosphorylation at Serine2152 After *Mob2* Knockdown *in Vitro*

In addition to regulating cilia/centrosome dynamics, Ndr1/2 kinases control actin-cytoskeletal arrangements and inhibit murine mitogen-activated protein kinases 1 and 2 (MEKK1 and MEKK2) by binding directly to residues 1169–1488 and 342–619 at their respective carboxy-termini (Enomoto et al., 2008). Interestingly, conditional depletion of *Mekk4* in the developing mouse forebrain impairs neuroependymal integrity and induces PH (Sarkisian et al., 2006). The same study also detected enhanced FlnA phosphorylation at Ser^{2152} in cells conditionally depleted of *Mekk4* (Sarkisian et al., 2006). Phosphorylation at Ser^{2152} is an important regulator of FLNA function (Loy et al., 2003). Given this insight we hypothesized a link between MOB2, NDR1/2, MEKK4 and FLNA.

Although Ndr1/2 directly binds to the carboxyl-terminus of MEKK1 and MEKK2, the study by Enomoto et al. did not investigate the binding potential of this kinase to the additional MEKK family proteins—i.e., MEKK3 and MEKK4 (Enomoto et al., 2008). Human peptide sequence alignments for this family of proteins show that the carboxyl-terminal region has the most conserved portion, with MEKK2, MEKK3 and MEKK4 having 42%, 44% and 33% sequence identity relative to MEKK1, respectively (Supplementary Figure S3). Notably, sites of highest conservation co-locate with the binding domain of NDR1/2 (Supplementary Figure S3, yellow highlight).

In light of the carboxyl-terminus conservation within the MEKK family of proteins and the reported role for Mekk4 in regulating FlnA phosphorylation at Ser^{2152} (Sarkisian et al., 2006), we next hypothesized that changes in Mob2 would alter FlnA phosphorylation at Ser^{2152}. Although total FlnA protein levels were unchanged after *Mob2* knockdown in C2C12 cells *in vitro*, a significant 1.6-fold increase in FlnA phosphorylated at Ser^{2152} was observed ($P = 0.028$; **Figures 4A,B**). In addition, protein lysate isolated from fibroblasts of patient 1203 had a 2-fold increase in FlnA phosphorylated at Ser^{2152} relative to an age-matched control ($P = 0.014$; **Figures 4A,B**). *Mob2* also regulates *FlnA* mRNA expression, with a significant 2.0-fold decrease ($P < 0.001$) detected by qRT-PCR upon transfection of miRNA targeted against *Mob2* in C2C12 cells *in vitro* (**Figure 4C**). Together, these results suggest that altered *Mob2* expression can modulate FlnA phosphorylation and are similar to those observed upon *Mekk4* knockdown reported elsewhere (Sarkisian et al., 2006).

DISCUSSION

Next-generation sequencing approaches in families with two or more affected individuals have proven to be extraordinarily effective for identifying novel recessive causes of developmental conditions, including those of neurodevelopment (Yu et al., 2013; Karaca et al., 2015). In non-consanguineous families with a single affected individual (as true for the majority of patients with PH), however, this approach is difficult, and requires innovative strategies to investigate the relative contribution of candidate variants. Here, we have employed a framework that exploits reported functional interactions with loci already implicated in PH causation as a further filter through which to stratify putative biallelic candidates. Although not suggesting any given candidate satisfying this criterion will be confirmed as a contributor to PH etiology, in this study one

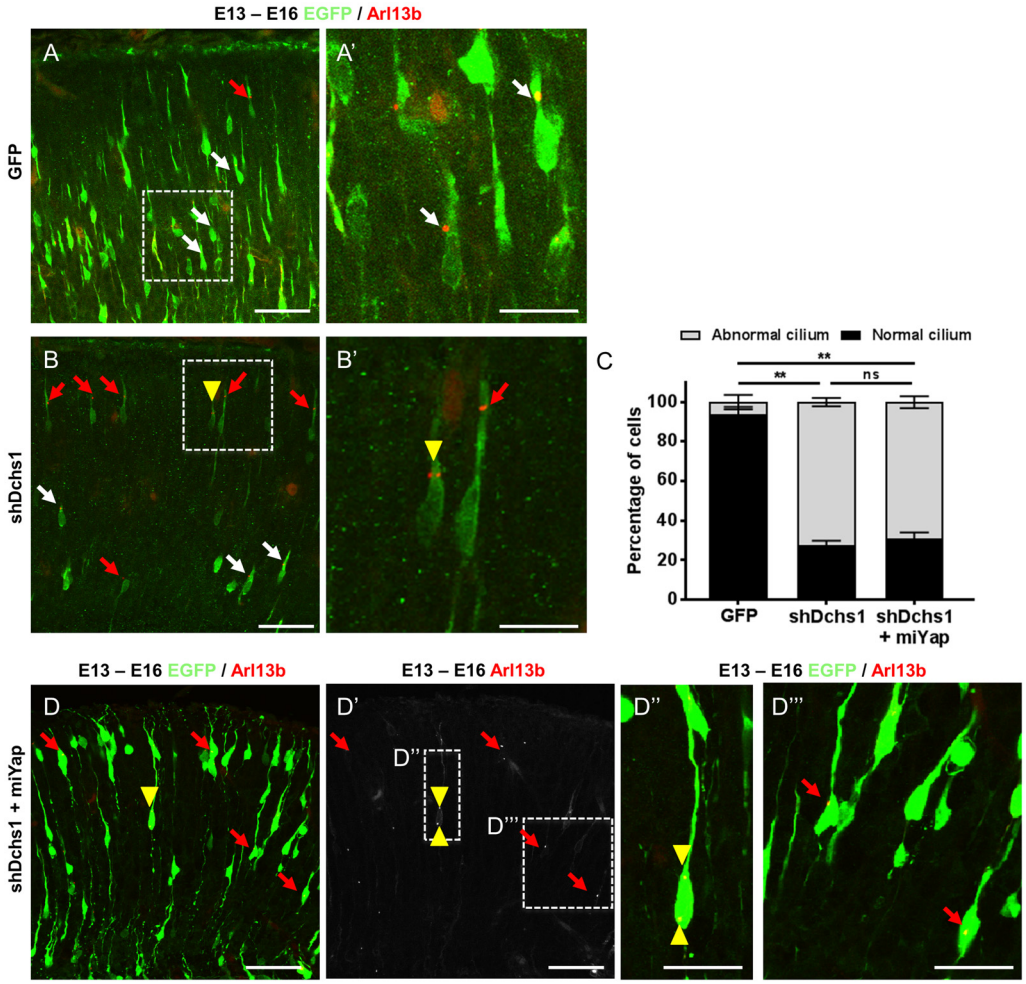

FIGURE 3 | *Dchs1* knockdown in the developing mouse cortex alters nucleus-cilia coupling that cannot be rescued by *Yap* knockdown. **(A,B,D)** Representative images of migrating neurons located within bin 5 (CP2) in E16 cortices (3 dpe) electroporated with EGFP/control, miRNA targeting *Yap* and/or shRNA targeting *Dchs1* (green) and Arl13b-tagRFP (red). White and red arrows indicate migrating neurons with correct or abnormal nucleus-cilia coupling as defined by position, respectively. Yellow arrow head shows migrating neurons with multiple cilia. **(C)** Quantification of the percentage of cells with abnormal nucleus-cilia coupling. Results represented as mean (± SEM). One-way ANOVA with Tukey HSD correction; $^{**}p < 0.001$; ns, not significant. Scale bar represents **(A,B,D,D′)** 50 μm and **(A′,B′,D″,D‴)** 20 μm.

gene—*MOB2*—was identified as having properties warranting further analysis. Functional assessment of the *MOB2* variants identified in this individual showed both to be LoF alleles. There is evidence for constraint against LoF variants in *MOB2*, as indicated by the probability of being loss-of-function intolerant (pLI) metric in the ExAC dataset being greater than 0.1 (pLI score = 0.64), as well as the very small number of LoF alleles in the gnomAD database (Lek et al., 2016). This, together with the altered cellular distribution observed after knockdown of *Mob2* within the developing mouse cortex, suggests this gene is a potential biallelic risk-conferring candidate in PH etiology with further functional and genetic analyses being warranted. However, only through the identification of more patients with *MOB2* insufficiency and PH can a direct causal association be determined.

In addition to the altered cellular distribution induced by *Mob2* knockdown, impairments in nucleus-cilia coupling were also observed. Interestingly, this phenotype was observed not only in the developing mouse cortex *in vivo*, but also in a human specific cortical development model—cerebral organoids (Lancaster et al., 2013)—suggesting that the role of Mob2 in determining cilia number and position is conserved in mammals. Given the similarities of this phenotype to that observed after *Dchs1* knockdown, a known factor of the Hippo signaling pathway and PH etiology, we hypothesize a role for cilia and MOB2 in cortical development, a prediction that is strengthened by the inability to remedy the effects of this alteration through simultaneous knockdown of Yap. While disruption of actin dynamics and cell adhesion has been a dominant theme in mechanistic studies on the pathogenesis of PH to date, the link to cilia described here could represent an unappreciated role for this organelle in the development of some forms of this particular cortical malformation.

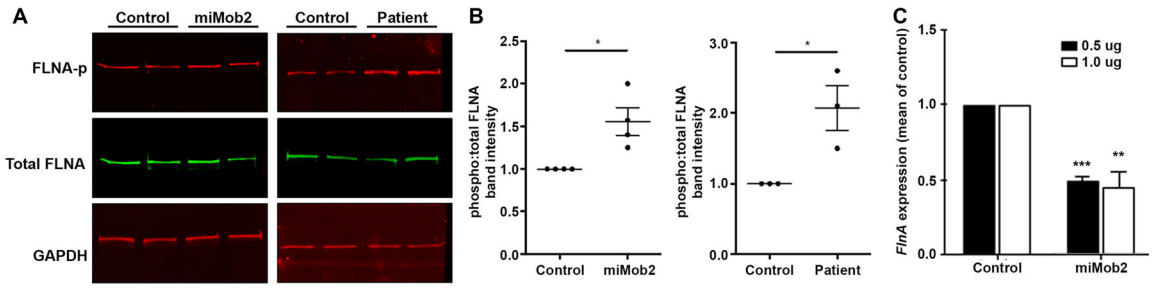

FIGURE 4 | *Mob2* knockdown increases FlnA phosphorylation at Ser^{2152} *in vitro*. **(A)** C2C12 cells were transiently transfected with EGFP/empty vector control or miRNAs targeting *Mob2* (left panel). At 24 h after transfection, cell lysates were prepared and subjected to Western blot analysis using the indicated antibodies. Right panel shows results for the same experiment but performed on age-matched control or patient 1203 fibroblasts. **(B)** Quantifications representing three biological replicates of **(A)** summarizing the proportion of phosphorylated Flna at residue 2152 relative to total FLNA and normalized against the loading control Gapdh in C2C12 or age-matched fibroblast controls. Results represented as mean (± SEM). **(C)** Mean (± SEM) *FlnA* expression in C2C12 cells expressing control or *Mob2* targeting hairpins at the indicated amounts. Expression was normalized against the control using the delta-delta Ct method, as determined by real-time PCR. Expression was normalized against *Gapdh* and *Dimt1* housekeeping genes in the same sample using the relative standard curve method. Mann-Whitney U test; $^{*}P < 0.05$, $^{**}P < 0.005$, $^{***}P < 0.001$.

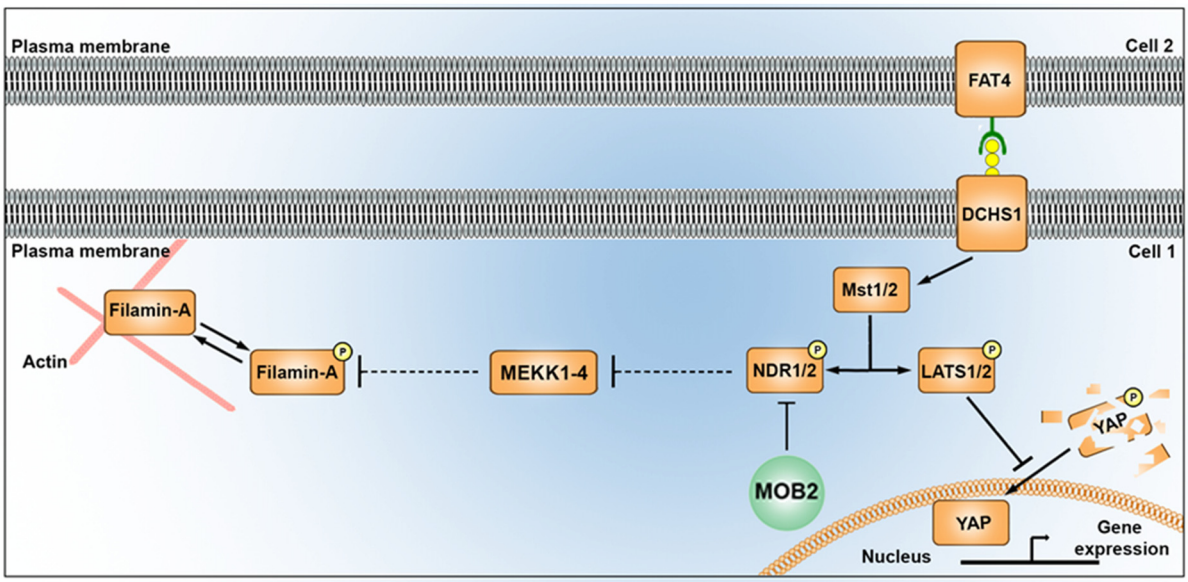

FIGURE 5 | Alterations in the mammalian Hippo signaling pathway alter FLNA phosphorylation. A schematic depicting the potential link between the Hippo signaling pathway and FLNA phosphorylation as outlined in this study. MST1/2 kinases (also known as "Hippo"), activated by FAT4/DCHS1, induces phosphorylation of YAP and NDR kinases. Phosphorylation of YAP leads to its degradation in the cytoplasm, while reduced activity of MST (e.g., via loss of DCHS1 activity) attenuates YAP phosphorylation and results in its translocation in the nucleus where it promotes changes to transcription. Phosphorylation of NDR1/2 facilitates its kinase activity. NDR1/2 kinases are further modulated by MOB1 (not shown) and MOB2 either positively or negatively, respectively. NDR1/2 kinases regulate the phosphorylation of the MEKK family of proteins, known modulators of FLNA phosphorylation (at site Ser^{2152}) and activity. In addition to disrupting nucleus-cilia coupling, reduced levels of MOB2 where seen in this study to induce changes in FLNA phosphorylation. A feature which could be mediated by the MEKK kinases given the associated supporting information.

LATS and NDR kinases are central parts of the Hippo signaling pathway in multicellular eukaryotes (Hergovich and Hemmings, 2009; Pan, 2010; Sudol and Harvey, 2010; Badouel and McNeill, 2011). Despite the importance of the NDR arm of the Hippo pathway in regulating cellular morphogenesis in eukaryotes (Kohler et al., 2010; Lin et al., 2011), the downstream targets of this kinase remain largely unknown (Ultanir et al., 2012). NDR1/2 has been experimentally identified to regulate MEKK1/2 kinase activity (**Figure 5**) and MEKK4 is a known regulator of FLNA phosphorylation (specifically at site Ser^{2152}), a deficiency of which has been implicated in the formation of PH in the mouse cortex (Sarkisian et al., 2006; Enomoto et al., 2008). To our knowledge, a link between FLNA activity and the Hippo tumur suppressor pathway has not been described previously. Thus in this study, the association of: (1) NDR1/2 with MEKK1/2 carboxyl-terminal binding (Enomoto et al., 2008);

(2) the *Mekk4*$^{-/-}$ conditional mouse knockout inducing a PH phenotype (Sarkisian et al., 2006); and (3) the carboxyl-terminal conserved sequence between MEKK1, 2, 3 and 4 (suggesting NDR1/2 can bind and regulate all four MEKK kinases), prompted investigations into the potential link between MOB2, NDR1/2, MEKK4 and FLNA. Functional studies described here identified a contribution from MOB2 in modulating FLNA activity, suggesting a potential link between these two prominent pathways implicated in PH etiology (**Figure 5**). Future experiments will be required to mechanistically explore this link and indeed determine if MEKK4, or another kinase in this family, is involved. Nonetheless, FLNA phosphorylation at site Ser^{2152} has been documented to impair FLNA turnover and impairing actin cytoskeletal remodeling; features that ultimately affect neuronal migration (Sarkisian et al., 2006).

Through a framework exploiting information from known loci involved in PH, we have identified a novel candidate locus—*MOB2*—conferring potential inherited risk to PH. While functional studies and screens within larger cohorts are needed to explore this link further, we also describe a role for Mob2 in directing cortical development and present evidence that suggests that these two pathways implicated in PH etiology (i.e., FLNA and Hippo signaling) are linked.

AUTHOR CONTRIBUTIONS

ACO, SPR and SC conceived and designed the experiments. ACO, CK, SC and ME performed the experiments. ACO and DMM analyzed the whole-exome sequencing data. IB provided the Arl13b-tagRFP vector. MD supplied the control iPSC line HMGU1. EPK clinically evaluated the patient and provided clinical samples. MG and SPR provided funding. All authors edited and approved the manuscript.

ACKNOWLEDGMENTS

SPR is supported by funding from Health Research Council of NZ and Curekids NZ. ACO was supported by a grant from the DAAD foundation of the German Research Council and by a University of Otago Postgraduate Scholarship Award. SC is supported by funding from the German Research Foundation (DFG CA 1205/2-1). We thank the family for their participation in this study. The Exome Aggregation Consortium are acknowledged for access to data.

SUPPLEMENTARY MATERIAL

The Supplementary Material for this article can be found online at: https://www.frontiersin.org/articles/10.3389/fncel.2018.00057/full#supplementary-material

Online Resources

Allen Mouse Brain Atlas database: http://mouse.brain-map.org/
Allen Human Brain Science Atlas: http://www.brainspan.org/
Exome Aggregation Consortium (ExAC), Cambridge, MA, USA http://exac.broadinstitute.org
PubMed, https://www.ncbi.nlm.nih.gov/pubmed/
Online Mendelian Inheritance in Man (OMIM), http://www.omim.org/
1000 Genomes, http://www.1000genomes.org
Burrows-Wheeler Aligner, http://bio-bwa.sourceforge.net/
Ensembl Genome Browser, http://www.ensembl.org/index.html
GATK, http://www.broadinstitute.org/gatk/
GenBank, http://www.ncbi.nlm.nih.gov/genbank/
NHLBI Exome Sequencing Project (ESP) Exome Variant Server, ESP6500, http://evs.gs.washington.edu/EVS/
Picard, http://broadinstitute.github.io/picard/

REFERENCES

Alcantara, D., Timms, A. E., Gripp, K., Baker, L., Park, K., Collins, S., et al. (2017). Mutations of AKT3 are associated with a wide spectrum of developmental disorders including extreme megalencephaly. *Brain* 140, 2610–2622. doi: 10.1093/brain/awx203

Badouel, C., and McNeill, H. (2011). SnapShot: the hippo signaling pathway. *Cell* 145, 484.e1–484.e1. doi: 10.1016/j.cell.2011.04.009

Bardón-Cancho, E. J., Muñoz-Jiménez, L., Vázquez-López, M., Ruíz-Martín, Y., García-Morín, M., and Barredo-Valderrama, E. (2014). Periventricular nodular heterotopia and dystonia due to an ARFGEF2 mutation. *Pediatr. Neurol.* 51, 461–464. doi: 10.1016/j.pediatrneurol.2014.05.008

Broix, L., Jagline, H., Ivanova, E., Schmucker, S., Drouot, N., Clayton-Smith, J., et al. (2016). Mutations in the HECT domain of NEDD4L lead to AKT-mTOR pathway deregulation and cause periventricular nodular heterotopia. *Nat. Genet.* 48, 1349–1358. doi: 10.1038/ng.3676

Cappello, S., Gray, M. J., Badouel, C., Lange, S., Einsiedler, M., Srour, M., et al. (2013). Mutations in genes encoding the cadherin receptor-ligand pair DCHS1 and FAT4 disrupt cerebral cortical development. *Nat. Genet.* 45, 1300–1308. doi: 10.1038/ng.2765

Carter, M. S., Doskow, J., Morris, P., Li, S., Nhim, R. P., Sandstedt, S., et al. (1995). A regulatory mechanism that detects premature nonsense codons in T-cell receptor transcripts *in vivo* is reversed by protein synthesis inhibitors *in vitro*. *J. Biol. Chem.* 270, 28995–29003. doi: 10.1074/jbc.270.48.28995

Conti, V., Carabalona, A., Pallesi-Pocachard, E., Parrini, E., Leventer, R. J., Buhler, E., et al. (2013). Periventricular heterotopia in 6q terminal deletion syndrome: role of the *C6orf70* gene. *Brain* 136, 3378–3394. doi: 10.1093/brain/awt249

Enomoto, A., Kido, N., Ito, M., Morita, A., Matsumoto, Y., Takamatsu, N., et al. (2008). Negative regulation of MEKK1/2 signaling by serine-threonine kinase 38 (STK38). *Oncogene* 27, 1930–1938. doi: 10.1038/sj.onc.1210828

Fox, J. W., Lamperti, E. D., Eksioglu, Y. Z., Hong, S. E., Feng, Y., Graham, D. A., et al. (1998). Mutations in filamin 1 prevent migration of cerebral cortical neurons in human periventricular heterotopia. *Neuron* 21, 1315–1325. doi: 10.1016/s0896-6273(00)80651-0

Götz, M., and Huttner, W. B. (2005). The cell biology of neurogenesis. *Nat. Rev. Mol. Cell Biol.* 6, 777–788. doi: 10.1038/nrm1739

Guerrini, R., and Dobyns, W. B. (2014). Malformations of cortical development: clinical features and genetic causes. *Lancet Neurol.* 13, 710–726. doi: 10.1016/s1474-4422(14)70040-7

Hergovich, A. (2012). Mammalian Hippo signalling: a kinase network regulated by protein-protein interactions. *Biochem. Soc. Trans.* 40, 124–128. doi: 10.1042/BST20110619

Hergovich, A., Bichsel, S. J., and Hemmings, B. A. (2005). Human NDR kinases are rapidly activated by MOB proteins through recruitment to the plasma membrane and phosphorylation. *Mol. Cell. Biol.* 25, 8259–8272. doi: 10.1128/mcb.25.18.8259-8272.2005

Hergovich, A., and Hemmings, B. A. (2009). Mammalian NDR/LATS protein kinases in hippo tumor suppressor signaling. *Biofactors* 35, 338–345. doi: 10.1002/biof.47

Hergovich, A., Kohler, R. S., Schmitz, D., Vichalkovski, A., Cornils, H., and Hemmings, B. A. (2009). The MST1 and hMOB1 tumor suppressors control

human centrosome duplication by regulating NDR kinase phosphorylation. *Curr. Biol.* 19, 1692–1702. doi: 10.1016/j.cub.2009.09.020

Higginbotham, H., Eom, T. Y., Mariani, L. E., Bachleda, A., Hirt, J., Gukassyan, V., et al. (2012). Arl13b in primary cilia regulates the migration and placement of interneurons in the developing cerebral cortex. *Dev. Cell* 23, 925–938. doi: 10.1016/j.devcel.2012.09.019

Insolera, R., Shao, W., Airik, R., Hildebrandt, F., and Shi, S. H. (2014). SDCCAG8 regulates pericentriolar material recruitment and neuronal migration in the developing cortex. *Neuron* 83, 805–822. doi: 10.1016/j.neuron.2014.06.029

Karaca, E., Harel, T., Pehlivan, D., Jhangiani, S. N., Gambin, T., Coban Akdemir, Z., et al. (2015). Genes that affect brain structure and function identified by rare variant analyses of mendelian neurologic disease. *Neuron* 88, 499–513. doi: 10.1016/j.neuron.2015.09.048

Kohler, R. S., Schmitz, D., Cornils, H., Hemmings, B. A., and Hergovich, A. (2010). Differential NDR/LATS interactions with the human MOB family reveal a negative role for human MOB2 in the regulation of human NDR kinases. *Mol. Cell. Biol.* 30, 4507–4520. doi: 10.1128/MCB.00150-10

Komuro, H., and Rakic, P. (1998). Distinct modes of neuronal migration in different domains of developing cerebellar cortex. *J. Neurosci.* 18, 1478–1490.

Kriegstein, A. R., and Noctor, S. C. (2004). Patterns of neuronal migration in the embryonic cortex. *Trends Neurosci.* 27, 392–399. doi: 10.1016/j.tins.2004.05.001

Lancaster, M. A., Renner, M., Martin, C. A., Wenzel, D., Bicknell, L. S., Hurles, M. E., et al. (2013). Cerebral organoids model human brain development and microcephaly. *Nature* 501, 373–379. doi: 10.1038/nature12517

Lein, E. S., Hawrylycz, M. J., Ao, N., Ayres, M., Bensinger, A., Bernard, A., et al. (2007). Genome-wide atlas of gene expression in the adult mouse brain. *Nature* 445, 168–176. doi: 10.1038/nature05453

Lek, M., Karczewski, K. J., Minikel, E. V., Samocha, K. E., Banks, E., Fennell, T., et al. (2016). Analysis of protein-coding genetic variation in 60,706 humans. *Nature* 536, 285–291. doi: 10.1038/nature19057

Lin, C. H., Hsieh, M., and Fan, S. S. (2011). The promotion of neurite formation in Neuro2A cells by mouse Mob2 protein. *FEBS Lett.* 585, 523–530. doi: 10.1016/j.febslet.2011.01.003

Louvi, A., and Grove, E. A. (2011). Cilia in the CNS: the quiet organelle claims center stage. *Neuron* 69, 1046–1060. doi: 10.1016/j.neuron.2011.03.002

Loy, C. J., Sim, K. S., and Yong, E. L. (2003). Filamin-A fragment localizes to the nucleus to regulate androgen receptor and coactivator functions. *Proc. Natl. Acad. Sci. U S A* 100, 4562–4567. doi: 10.1073/pnas.0736237100

Mandelstam, S. A., Leventer, R. J., Sandow, A., McGillivray, G., van Kogelenberg, M., Guerrini, R., et al. (2013). Bilateral posterior periventricular nodular heterotopia: a recognizable cortical malformation with a spectrum of associated brain abnormalities. *Am. J. Neuroradiol.* 34, 432–438. doi: 10.3174/ajnr.a3427

Marin, O., and Rubenstein, J. L. (2003). Cell migration in the forebrain. *Annu. Rev. Neurosci.* 26, 441–483. doi: 10.1146/annurev.neuro.26.041002.131058

Miller, J. A., Ding, S. L., Sunkin, S. M., Smith, K. A., Ng, L., Szafer, A., et al. (2014). Transcriptional landscape of the prenatal human brain. *Nature* 508, 199–206. doi: 10.1038/nature13185

Nagy, E., and Maquat, L. E. (1998). A rule for termination-codon position within intron-containing genes: when nonsense affects RNA abundance. *Trends Biochem. Sci.* 23, 198–199. doi: 10.1016/s0968-0004(98)01208-0

Nandi, D., Tahiliani, P., Kumar, A., and Chandu, D. (2006). The ubiquitin-proteasome system. *J. Biosci.* 31, 137–155. doi: 10.1007/BF02705243

Oegema, R., Baillat, D., Schot, R., van Unen, L. M., Brooks, A., Kia, S. K., et al. (2017). Human mutations in integrator complex subunits link transcriptome integrity to brain development. *PLoS Genet.* 13:e1006809. doi: 10.1371/journal.pgen.1006809

Pan, D. (2010). The hippo signaling pathway in development and cancer. *Dev. Cell* 19, 491–505. doi: 10.1016/j.devcel.2010.09.011

Parrini, E., Ramazzotti, A., Dobyns, W. B., Mei, D., Moro, F., Veggiotti, P., et al. (2006). Periventricular heterotopia: phenotypic heterogeneity and correlation with Filamin A mutations. *Brain* 129, 1892–1906. doi: 10.1093/brain/awl125

Saito, T. (2006). *In vivo* electroporation in the embryonic mouse central nervous system. *Nat. Protoc.* 1, 1552–1558. doi: 10.1038/nprot.2006.276

Sarkisian, M. R., Bartley, C. M., Chi, H., Nakamura, F., Hashimoto-Torii, K., Torii, M., et al. (2006). MEKK4 signaling regulates filamin expression and neuronal migration. *Neuron* 52, 789–801. doi: 10.1016/j.neuron.2006.10.024

Sheen, V. L., Ganesh, V. S., Topcu, M., Sebire, G., Bodell, A., Hill, R. S., et al. (2004). Mutations in ARFGEF2 implicate vesicle trafficking in neural progenitor proliferation and migration in the human cerebral cortex. *Nat. Genet.* 36, 69–76. doi: 10.1038/ng1276

Shin, H. W., Shinotsuka, C., and Nakayama, K. (2005). Expression of BIG2 and analysis of its function in mammalian cells. *Meth. Enzymol.* 404, 206–215. doi: 10.1016/s0076-6879(05)04020-6

Sudol, M., and Harvey, K. F. (2010). Modularity in the Hippo signaling pathway. *Trends Biochem. Sci.* 35, 627–633. doi: 10.1016/j.tibs.2010.05.010

Tazi, J., Rossi, F., Labourier, E., Gallouzi, I., Brunel, C., and Antoine, E. (1997). DNA topoisomerase I: customs officer at the border between DNA and RNA worlds? *J. Mol. Med.* 75, 786–800. doi: 10.1007/s001090050168

Ultanir, S. K., Hertz, N. T., Li, G., Ge, W. P., Burlingame, A. L., Pleasure, S. J., et al. (2012). Chemical genetic identification of NDR1/2 kinase substrates AAK1 and Rabin8 Uncovers their roles in dendrite arborization and spine development. *Neuron* 73, 1127–1142. doi: 10.1016/j.neuron.2012.01.019

Yu, T. W., Chahrour, M. H., Coulter, M. E., Jiralerspong, S., Okamura-Ikeda, K., Ataman, B., et al. (2013). Using whole-exome sequencing to identify inherited causes of autism. *Neuron* 77, 259–273. doi: 10.1016/j.neuron.2012.11.002

Conflict of Interest Statement: The authors declare that the research was conducted in the absence of any commercial or financial relationships that could be construed as a potential conflict of interest.

frontiers in Neuroscience

ORIGINAL RESEARCH
published: 20 April 2018
doi: 10.3389/fnins.2018.00220

Transcriptional Profiling of Ligand Expression in Cell Specific Populations of the Adult Mouse Forebrain That Regulates Neurogenesis

Kasum Azim[1], Rainer Akkermann[1], Martina Cantone[2], Julio Vera[2], Janusz J. Jadasz[1] and Patrick Küry[1]*

[1] *Department of Neurology, Neuroregeneration, Medical Faculty, Heinrich-Heine-University, Düsseldorf, Germany,*
[2] *Laboratory of Systems Tumor Immunology, Department of Dermatology, Friedrich-Alexander-Universität Erlangen-Nürnberg, Erlangen, Germany*

In the adult central nervous system (CNS), the subventricular zone (SVZ) of the forebrain is the largest and most active source of neural stem cells (NSCs) that generates mainly neurons and few glial cells lifelong. A large body of evidence has shed light on the distinct families of signaling ligands (i.e., morphogens, growth factors, secreted molecules that alter signaling pathways) in regulating NSC biology. However, most of the research has focused on the mRNA expression of individual or few signaling ligands and their pathway components in specific cell types of the CNS in the context of neurogenesis. A single unifying study that underlines the expression of such molecules comprehensively in different cell types in spatial contexts has not yet been reported. By using whole genome transcriptome datasets of individual purified cell specific populations of the adult CNS, the SVZ niche, NSCs, glial cells, choroid plexus, and performing a bioinformatic meta-analysis of signaling ligands, their expression in the forebrain was uncovered. Therein, we report that a large plethora of ligands are abundantly expressed in the SVZ niche, largely from the vasculature than from other sources that may regulate neurogenesis. Intriguingly, this sort of analysis revealed a number of ligands with unknown functions in neurogenesis contexts that warrants further investigations. This study therefore serves as a framework for investigators in the field for understanding the expression patterns of signaling ligands and pathways regulating neurogenesis.

Keywords: neural stem cells, subventricular zone, neurogenesis, gliogenesis, growth/trophic factors, ligands, morphogens

OPEN ACCESS

Edited by:
Daniel A. Peterson,
Rosalind Franklin University of Medicine and Science, United States

Reviewed by:
Annalisa Buffo,
Università degli Studi di Torino, Italy
Mariagrazia Grilli,
Università degli Studi del Piemonte Orientale, Italy

****Correspondence:***
Kasum Azim
kasumazim@gmail.com

Specialty section:
This article was submitted to Neurogenesis, a section of the journal Frontiers in Neuroscience

Received: *15 December 2017*
Accepted: *20 March 2018*
Published: *20 April 2018*

Citation:
Azim K, Akkermann R, Cantone M, Vera J, Jadasz JJ and Küry P (2018) Transcriptional Profiling of Ligand Expression in Cell Specific Populations of the Adult Mouse Forebrain That Regulates Neurogenesis. Front. Neurosci. 12:220. doi: 10.3389/fnins.2018.00220

INTRODUCTION

In the adult brain, the subventricular zone (SVZ) of the lateral ventricles is one of the main reservoirs of adult neural stem cells (NSCs) that generate new neurons and glial cells throughout life. SVZ-NSCs are present in quiescent phenotypes (qNSCs) and upon activation form activated NSCs (aNSCs) that give rise to transiently amplifying progenitors (TAPs) that will generate neurons via a highly migratory neuroblast stage. Newly generated neuroblasts migrate away from the SVZ along the rostral migratory stream and differentiate into interneurons mainly, and also a

few glutamatergic neurons (Doetsch et al., 1999; Quiñones-Hinojosa et al., 2006; Brill et al., 2009). Depending on the transcriptional and signaling cues, SVZ-NSCs will additionally generate oligodendrocytes and astrocytes that invade the surrounding parenchyma (Menn et al., 2006; Benner et al., 2013), suggesting that there may be specialized subtypes of lineage restricted NSCs.

The SVZ is located around a spatially complex ventricular system and consists of a heterogeneous cell population, as a number of studies have identified that specific neuronal and glial subtypes are generated from discrete domains of the SVZ throughout life (reviewed in Fiorelli et al., 2015; Azim et al., 2016). This implies that regionally segregated NSCs are primed in a time-controlled manner for the generation of glial and neuronal subtypes, proposing that transcriptional mechanisms are additionally modulated by external stimuli that guide NSC fate. Such add-on regulators include microRNAs, exosomes containing proteins or RNAs, extracellular matrix constituents, additional and soluble secreted factors reviewed in Wakabayashi et al. (2014), Batiz et al. (2015), and Faissner and Reinhard (2015), the latter being one of the most studied in the field.

Identifying the source and expression patterns of signaling ligands with their role in NSC biology represents an important step in developing innovative strategies for manipulating germinal regions in health and disease. A number of earlier studies have described the expression patterns of signaling ligands by classical *in situ* experiments. For example in studies of young adult rodents, bone morphogenetic proteins (BMP4/7) were detected in glial-like cells in the vicinity of the SVZ (Peretto et al., 2004). Another classical ligand, epidermal growth factor (EGF) is expressed and secreted at somewhat distant sources from the SVZ, i.e., the striatum (Lazar and Blum, 1992). Other key ligands such as FGF2 have been shown to be expressed in the SVZ (Frinchi et al., 2008; Azim et al., 2012), whereas Shh is uniquely transported to ventral regions of the SVZ by axons projected from the ventral forebrain (Ihrie et al., 2011). The vasculature has been considered as a trophic source for maintaining or expanding NSC phenotypes (Thored et al., 2007; Tavazoie et al., 2008; Ottone et al., 2014; Crouch et al., 2015), but the expression levels of vascular-derived ligands in respect to other cell types are not fully understood. Moreover, additional secreted ligands are dispersed by the cerebral spinal fluid (CSF) (Thouvenot et al., 2006; Marques et al., 2011) and its flow is a major determinant of neurogenesis/gliogenesis (Silva-Vargas et al., 2016). Although these studies have given vital insights into some ligand expression, a thorough and systematic investigation of ligands across a variety of cell types has not yet been reported.

The increasing availability of whole genome transcriptome (WGT) datasets consisting of purified cell types of the young adult forebrain and of cells that constitute the SVZ niche, facilitates meta-analyses for the description of large scale expression patterns of signaling ligands involved in neurogenic processes. To this end, we present data analyses performed by focusing exclusively on ligands across multiple datasets that include adjacent glial cells, choroid plexus, NSCs and cells that comprise the SVZ niche (i.e., vasculature cells, ependymal cells, TAPs and neuroblasts). A number of region specific hallmarks in ligand expression were found and its transcriptome landscape could be mapped with enriched ligands presented for further future analysis. Most notably, a novel finding was that endothelia expressed a large number of transcripts, including key ligands the expression of which was apparently more abundant than previously thought. Intriguingly, data generated revealed a number of ligands that have not yet been studied in the context of adult neurogenesis/gliogenesis and warrants further studies. Altogether, these findings will aid investigators in the field by providing expression levels of key genes and families across a variety of cell types and may promote future functional insights.

Abbreviations: SVZ, subventricular zone; NSCs, neural stem cells; TAPs, transiently amplifying progenitors; TFs, transcription factors; WGT, whole genome transcriptome; NPs, neural precursors; FDR, false discovery rate; PCA, principle components plots; qNSCs, quiescent NSCs; aNSCs, activated NSCs; CSF, cerebral spinal fluid; CP, choroid plexus; MGs, microglia; aNSCs, active neural stem cells; qNSCs, quiescent neural stem cells; Astros, astrocytes; OLs, oligodendrocytes (mature); PCs, pericytes; END, endothelia.

METHODS

Datasets Incorporated Into the Study

Mouse Affymetrix datasets that have been reposited in GEO Pubmed (GSE numbers), representing NSCs of different subtypes (GSE54653) [postnatal day (P) ∼70] (Codega et al., 2014); neural precursors (NPs)\TAPs, neuroblasts and ependymal cells (GSE18765) (P60) (Beckervordersandforth et al., 2010); oligodendroglia at different stages of development (GSE9566) (P16) (Cahoy et al., 2008); endothelial pericytes from the cerebral cortex (GSE47067; GSE48209) (∼P70) (Nolan et al., 2013; Coppiello et al., 2015); (GSE29284) (Olson and Soriano, 2011); choroid plexus (GSE82308) (P60) (Silva-Vargas et al., 2016); astrocytes (GSE35338) (P30-35) (Zamanian et al., 2012); microglia (GSE58483) (∼P60) (Israelsson et al., 2014) have been used. Of note, datasets of subtypes of neurons from different mouse forebrain regions that project axons and innervate the SVZ, have been generated using different platforms and were therefore excluded in this analysis in order to minimize any false positives. Datasets were processed for Robust Multi-array Average (RMA) normalization on CARMA software suite (https://carmaweb.genome.tugraz.at/carma/) comprehensive R- and bioconductor-based web service for microarray data analysis (Rainer et al., 2006), and additionally via R/Bioconductor using standard procedures. The Benjamini and Hochberg false discovery rate (FDR) was used to calculate *p*-values. The final gene lists contain all genes with FDR of 5% and >1.8 fold changes. Genefilter, heatmap.2 method implemented in the gplots, and pcamethods package was used for generating gene lists, and principle components analysis (PCA) using the statistics software R (R Development Core Team, 2008). The Venn diagram was made using http://www.interactivenn.net. Previous gene lists representing essential signaling ligands were used for further filtering parameters (Azim et al., 2017). All imported datasets were quality checked on a PCA plot for control- and housekeeping genes in discriminating overlapping properties and discarding datasets that were distant in the plot. The function

of individual genes was classified using the resource http://www.genecards.org.

An analysis was performed for over-enrichment within these categories: (1) autocrine/paracrine signaling of NSCs (qNSCs; aNSCs); (2) adjacent glial ligand expression [microglia, astrocytes, mature oligodendrocytes (mOLs) and oligodendrocyte progenitor cells (OPCs)]; (3) secretion from the choroid plexus and (4) secretion from the niche, i.e., pericytes, endothelia, ependymal cells, neuroblasts and TAPs. Between these four groups, an enrichment analysis was performed. For example, for comparing expression profiles enriched in autocrine/paracrine NSC signaling, these datasets were compared with the remaining three categories. Similarly, this was then also done for enrichment for the remaining three groups. In this analysis, the four resulting gene lists were processed for further analysis and heatmaps were assembled applying default criteria. The cells that form the niche, i.e., endothelia, pericytes, neuroblasts and TAPs were grouped together as reported by other studies (Kokovay et al., 2010; Ottone et al., 2014; Crouch et al., 2015; Fiorelli et al., 2015). Ligand mRNA from endothelia and pericytes overlapped considerably, and the same was evident for neuroblasts and TAPs that otherwise expressed fewer ligand transcripts.

Secretome Pathways

The four different categories of ligands were further studied for functional analysis enrichment using the freely available Reactome (defined here as secretome) database using the latest version of the mouse-annotated database (Pathan et al., 2015). Using default settings, data was exported for each group and sorted by their *p*-values. Pathways with overlapping sets of genes were processed by taking the most significant in the list. In general, the minimal numbers of genes studied per pathway was "2," except for those of the NSC category which a few obtained were only "1" and are stated with double asterisks in graphs. The top 10 are presented in order (clock-wise) of their significance and pathway terms shortened to fit in pie charts constructed using the genes associated with pathway terms in the data. Any obtained pathways with *p*-values (Hypergeometric test) >0.01 were discarded. For evaluating the pathways more enriched according to the genes populating the four groups we used ClueGO, a plugin of the freely available software Cytoscape (http://www.cytoscape.org). Each group of genes was represented as a separate cluster, and we performed an analysis by setting the same set of parameters and ran a pathway enrichment analysis of all genes' groups together. For graphical representation purposes, differences among the enrichment analysis of the single cluster were selected.

RESULTS

A Road Map of Signaling Ligand Expression in the Mouse Forebrain

We incorporated and cross normalized a number of whole genome transcriptome datasets that have been generated from earlier studies using the same Affymetrix platform and at comparable ages. Using these datasets we performed an analysis to examine transcripts that are significantly altered across these groups taking into account recent gene lists of exclusively secreted signaling ligands, inhibitory signaling molecules, morphogens and trophic factors (Azim et al., 2017), resulting in 310 probes in total that were $\leq$5% FDR. Four groups for comparison were generated consisting of (1) qNSCs and aNSCs, termed as "NSCs," (2) microglia, astrocytes and oligodendroglia termed as "adjacent," (3) choroid plexus (CP), (4) endothelia, pericytes, TAPs, neuroblasts and ependymal cells, termed as "niche" (Mirzadeh et al., 2008). In cases where transcripts were represented by more than one probe, only the probe with the highest FDR value was analyzed further. Firstly, PCA was done against significant probes (**Figure 1A**), which designated all glial cells, pericytes, TAPs and neuroblasts exhibiting similar hallmarks, whereas qNSCs and aNSCs as well as the CP were unrelated. Surprisingly, endothelial cells showed dramatically distinct and distant covariance in their expression signatures. The four groups were compared with each other and plotted as Venn diagram (**Figure 1B**) revealing various degrees of overlaps. Intriguingly, ∼60% of all ligand transcripts were derived from the niche, followed by adjacent (18%), CP (∼12.5%), and NSCs (∼9.5%), revealing that the niche itself is likely the most important signaling determinant in regulating neurogenesis/gliogenesis. All transcripts significantly different in this analysis were plotted on a HC heatmap which illustrates that the largest and overwhelming source of ligands are endothelial cells in the forebrain (**Figure 1C**). A gene ontology "secretome" (Reactome pathway) analysis was performed subsequently on these four groupings (niche, adjacent, CP, and NSCs) to examine gross differences amongst the genes related as % of the total genes expressed by different regions. In this analysis, potential sharing in regulated pathways amongst the four groupings were analyzed. Indeed, many of the ligands overlapped with ligands that target class A/1 (G protein coupled receptors) GPCRs, hemostasis (i.e., vascular-like and anti-inflammatory) and ligands that target Erbb4 receptors being common to all with the exception of the CP. But then some ligand expression patterns were rather unique. For example, ligands associated with ISG15 mechanisms (antiviral and immune-like pathways) were enriched in both the niche and CP (**Figure 1D**). Others, such as ligands targeting BMP and Notch2 signaling were upregulated in the niche and NSCs, respectively (**Figure 1D**). Altogether this implies that certain ligands detected in the four different groups exhibit a degree of redundancy whereas some ligand signatures show an extent of exclusiveness to a particular region or cell type, i.e., NSCs vs. the niche.

Signaling Ligand Enrichment in NSCs

Compared with all other groups, NSCs expressed relatively few ligands. Such ligands are shared in expression between other cell types analyzed including their downstream progenitors, TAPs and NBs, which is unlike the expression patterns of transcription factors that are shared between progenitors and NSCs (Azim et al., 2015). The small proportion of ligands enriched in NSCs implies that in the context of normal adult differentiation and maturation, NSCs appear to be mainly supported by external cues rather than providing direct stimuli to their environment in an auto- or paracrine manner. This is due to NSCs expressing relatively fewer transcripts compared to other sources or regions.

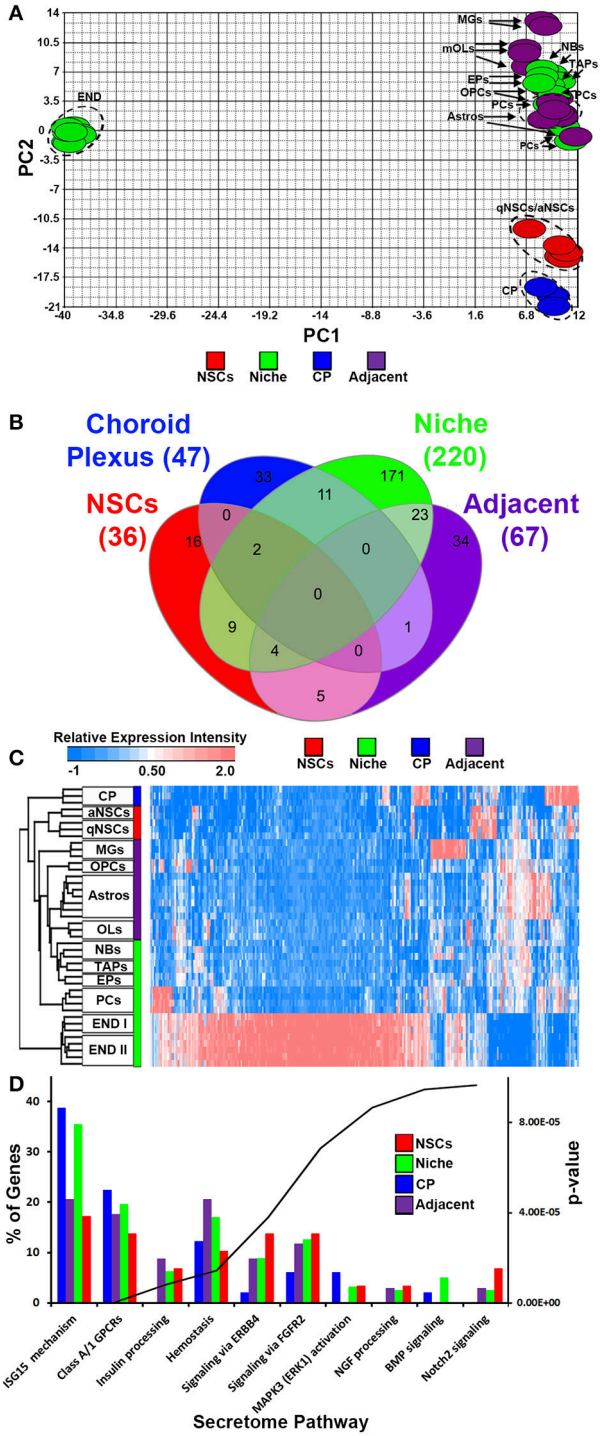

FIGURE 1 | Ligand mRNA heterogeneity in purified cell populations of the adult mouse forebrain. **(A)** PCA ordering of ligands exclusively and significantly ($p < 5\%$ FDR) enriched throughout the different cell populations. Colors show the groupings of different cell populations. **(B)** Venn diagram of the 4 different groups displaying overlaps and specificity of significantly enriched genes (1.8 fold change; $p < 5\%$ FDR). **(C)** HC heatmap of all significantly enriched ligands in the analysis. **(D)** The ligand genes of the 4 different groups were classified using Reactome Pathway Analysis in ClueGO. The top 10 pathways (out of 17 obtained) were plotted and ranked according to their *p*-values. Data are shown as a percentage of ligands per pathway term. Red, green, blue and purple colors used are for groups containing NSCs, niche, choroid plexus and adjacent glial cells respectively. CP, choroid plexus; aNSCs, activated neural stem cells; qNSCs, quiescent neural stem cells; MGs, microglia; OPCs, oligodendrocytes precursor cells; Astros, astrocytes; OLs, oligodendrocytes (mature); NBs, neuroblasts; TAPs, transiently amplifying progenitors; EPs, ependymal; PCs, pericytes; END I, Endothelia 1; END II, Endothelia 2.

Some transcripts were found to be highly abundant in NSCs compared to other cell types, with few transcripts shared between endothelia and astrocytes (**Figure 2A**). The secretome analysis was used to identify which signaling pathways are associated with the ligand transcripts detected in NSCs and arranged by their significance. This revealed pathways associated with Notch2 signaling, rapid depolarization (i.e., *Fgfs*), chemokines and ligands that stimulate Akt signaling via PIP3 (*Hgf, Nrg2*). The remaining pathways were narrowly significant due to the lower number of ligand genes expressed in NSCs (**Figure 2B**). The top five most highly enriched transcripts in NSCs in this analysis were *Dkk3, Efnb2, Igfbp5 Ptn*, and *Mdk* with most of them being uniquely expressed in NSCs compared to other cell types sampled (**Figure 2C**). *Dkk3* and *Efnb2* have been described previously as being enriched in the walls of the SVZ (Diep et al., 2004) as well as in a high-to-low expression gradient from the wall to the striatum (Ottone et al., 2014), respectively, thus confirming our findings. Most ligands were homogeneous to NSCs, whereas some were enriched in either qNSCs or aNSCs (highlighted in **Supplementary Figure 1**). Additional ligands which were not pursued further included *Hgf, Fgf13, Jag1, Fgf11, Vegfa, Bmp1, Inhbb*, that are likely to control neurogenesis/gliogenesis in an autocrine/paracrine manner (**Supplementary Figure 1**).

Signaling Ligand Enrichment in Glial Cells of Adjacent Tissues

Glial cells in the vicinity of the SVZ lateral and dorsal walls will contribute to neurogenesis/gliogenesis as previously demonstrated for astrocytes, oligodendrocytes and microglia (reviewed in Morrens et al., 2012; Su et al., 2014). Probes significantly enriched in glial cells were plotted on a heatmap revealing overlaps between OLs, OPCs, and astrocytes with cells in the niche. Of note, microglia expressed a number of unique ligands and clustered at a distance compared to other glial cells that were similar in their proximities (**Figure 3A**). According to the secretome analysis, at least half of the major pathways associated with glial ligands resembled immune-like signaling events via the detected chemokine and interleukin transcripts whereas some ligands point to common proliferative and survival functions via pathways involving Akt, RAF/MAP kinases. For example, *Angpt1, Fgf1, Hbegf*, and *Hgf* genes were upregulated in these cells, suggesting that some promote EGF-like functions (**Figure 3B**, **Supplementary Figure 2**). Within the pathway "ligand-receptor interactions," *Hhip* and *Shh* that are enriched in oligodendroglia appeared highly significant. Ligands (*C4b, Chrdl1, Csf1, Il6*) which contribute to IGF regulation,

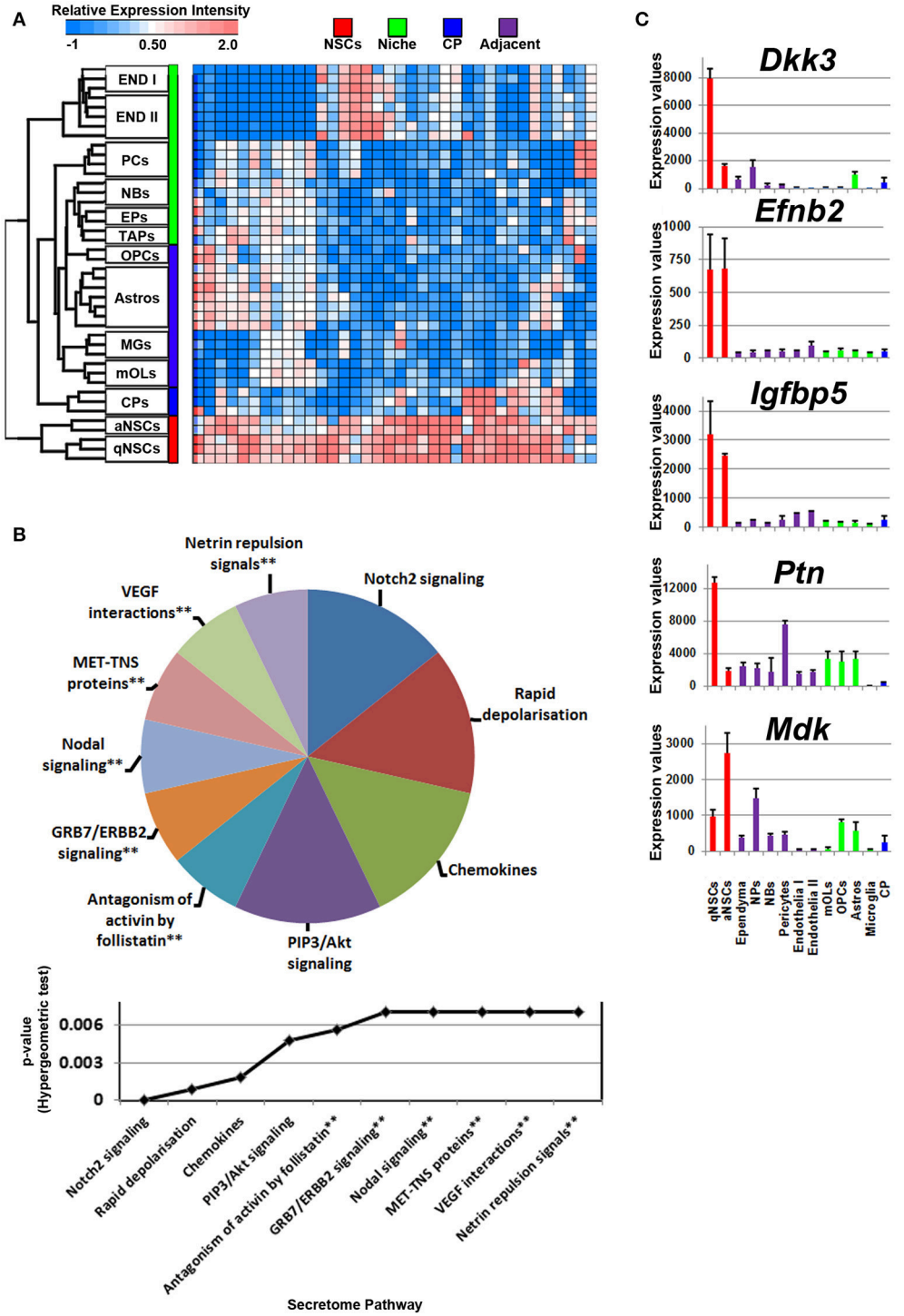

FIGURE 2 | Autocrine/paracrine ligand mRNA enrichment in NSCs. **(A)** The transcriptome of significantly enriched (1.8 fold change; $p < 5\%$ FDR) ligands in both qNSCs and aNSCs are displayed as a heatmap and plotted with the remaining datasets. Some ligand genes show similar or lower mRNA enrichment with other cell types. **(B)** These were further characterized using Reactome Pathway for classifying broadly the functions and signaling networks of ligand mRNA detected in the analysis. The top 10 pathways were selected and ranked clockwise by their *p*-values and plotted below as a histogram. Note: double asterisks signify only 1 ligand mRNA associated within the pathway. **(C)** The top most enriched genes are shown in histograms with in their antilog expression values across multiple cell types showing overall elevated expression in NSCs. Red, green, blue and purple colors used are for groups containing NSCs, niche, choroid plexus and adjacent glial cells respectively. CP, choroid plexus; aNSCs, active neural stem cells; qNSCs, quiescent neural stem cells; MGs, microglia; OPCs, oligodendrocytes precursor cells; Astros, astrocytes; OLs, oligodendrocytes (mature); NBs, neuroblasts; TAPs, transiently amplifying progenitors; EPs, ependymal; PCs, pericytes; END I, Endothelia 1; END II, Endothelia 2.

transport, uptake by Igfbps, i.e., sequestering *Igfs* by *Igfbps*, imply some mode of trophic factor modulation. Overall, *Wnt7b, Hbegf, IL18, Ccl3*, and *Shh* are the top five major ligands enriched in adjacent glial cells (**Figure 3C**), deciphering novel highly enriched transcripts involved in glial to niche/NSC signaling.

Signaling Ligand Enrichment in the Choroid Plexus

The cerebral spinal fluid (CSF) is formed mainly by the choroid plexus (CP), an epithelial-like structure present internally around the brain ventricles that expresses and secretes a number of signaling ligands throughout life which is why this structure is considered an important regulator of development, differentiation and maturation (Silva-Vargas et al., 2016). Ligands enriched in the CP were plotted on a heatmap (**Figure 4A**). Consistent with their morphology and classification as mural cells, a subset of signaling ligands were found to overlap in expression with those deriving from the vasculature (**Figure 4A**), therefore suggesting that many ligands enriched in expression in the CP are also synthesized by endothelia and pericytes. The secretome pathway analysis revealed some "pro-neurogenic" terms as being upregulated and specific to CP such as signaling via IGFRs, non-integrin membrane-ECM interactions and PI5P/PP2A/IER3-PI3K/Akt. A number of terms which emerged as being significant in the analysis were due to the expression of *Igfs* and *Igfbps* that were vastly abundant in the CP (**Figure 4B**). Of note, the top five CP enriched ligands are *Igf2, Tgfb2, Twsg1, Bmp6*, and *Angptl2* (**Figure 4C**) and were almost exclusively expressed in the CP. Other ligands with relative abundant expression in the CP include *Fgf2, Gas6, Pdgfa, Pdgfd, Tgfb2, Bmp7*, all of which have previously been confirmed elsewhere as major neurogenic determinants (Marques et al., 2011; **Supplementary Figure 3**).

Signaling Ligand Enrichment in the Niche

The PCA described earlier showed that endothelia are distinct from any other cell type included in the analysis whereas the others showed some degree of relatedness (**Figure 1A**). Accordingly, the niche that consists of progenitors, neuroblasts, ependymal- and cells of the vasculature should contain the largest cohort of signaling ligand transcripts. The analysis was done by incorporating datasets of endothelial cells derived from two different studies as a control and as a consequence essentially the same expression patterns were observed (see Materials and Methods). Of note, datasets of niche-specific astrocytes (also termed as B2 astrocytes), a smaller proportion of cells in the niche that may also contribute to neurogenesis/gliogenesis (Platel and Bordey, 2016), are not yet available in any platform.

Indeed, most of the ligands detected were expressed in the niche (**Figure 1B**) and moreover, as anticipated, the vast majority of ligands were abundantly expressed in endothelia (**Figure 5A**). Furthermore, some ligands were partly shared with other cell types (white or red hot spots of **Figure 5A**) but the overall majority of ligands were unique in expression to endothelia, slightly overlapping with pericytes. Altogether, the niche itself and particularly endothelia display the most abundant expression of signaling ligands, although the extent of their functionality in neurogenesis is not understood.

The secretome pathway analysis revealed only a few overlapping pathways as seen for NSCs, glial cells and the CP. Aside from *Fgf2* which was highly abundant in the CP, the 10 other members of the FGF-family of proteins were enriched in the niche, which resulted in several different pathways associated with Fgf-signaling (**Figure 5B**). For the first time, a pathway enrichment for "Wnt signaling" was also evident since several Wnt mRNAs are expressed in endothelia. This enrichment analysis also revealed a variety of other pro-neurogenic pathways that were lowly ranked but still emerged as significant such as signaling by BMP, ERBB2, glycoprotein hormones, or via Eph-Ephrin interactions. Very few inhibitory pathways were observed from endothelia, with the notable exception of "negative regulation of TCF-dependent signaling by WNT ligand antagonists," suggesting an overall trophic nature of niche derived signals (**Figure 5B**). The top five ligands detected in the niche were almost exclusively derived from the vasculature (**Figure 5C**) and corresponded to *Vegfc, Ccl7, Igfbp1, Egfl7,* and *Tnfsf4*. The top 5 most enriched ligands were ranked into their respective known ligand families and the top 10 most abundant family members are presented in **Table 1** for their first glance preview. Here, a number of ligands from the same families have overlapping functions for example, *Wnt7a* and *Wnt8b* (Choe et al., 2015), and multiple members of the Fgf-family of ligands (Ornitz and Itoh, 2015).

Ligands enriched in ependymal or NPs were overall very few, implying that these cells expressed fewer ligands. Another important neurogenic ligand, *Egf,* of which the expression was higher in TAPs and neuroblasts, although likely resulting from the large variability within these datasets, was not significantly changed. Similarly, the expression of *Cntf* was high in TAPs, neuroblasts and astrocytes, but only in astrocytes the expression was stable among the replicates. Generally, with the inclusion of endothelia and pericytes in the analysis, very few ligands show any enrichment in neuroblasts or TAPs or the entire niche vs. the other region/cell types demonstrating that the vasculature contains abundant sources of ligand mRNA (see also **Supplementary Figure 4**).

DISCUSSION

Much of the information regarding ligand expression in adult neurogenic niches has been yielded from classical *in situ* experiments which provided a gross overview on their expression at the anatomical level. The ever increasing availability of cell purified WGT datasets in GEO enables thorough meta-analyses to be performed for identifying gene expression patterns of interest. Such an approach is relevant for understanding the basic biology behind upstream developmental/neural turnover purposes and could therefore facilitate target identification for therapeutic intervention.

Here, we present a thorough signaling ligand expression analysis across a variety of cell types present in neurogenic niches, glial cells and choroid plexus. Identified ligand patterns were then

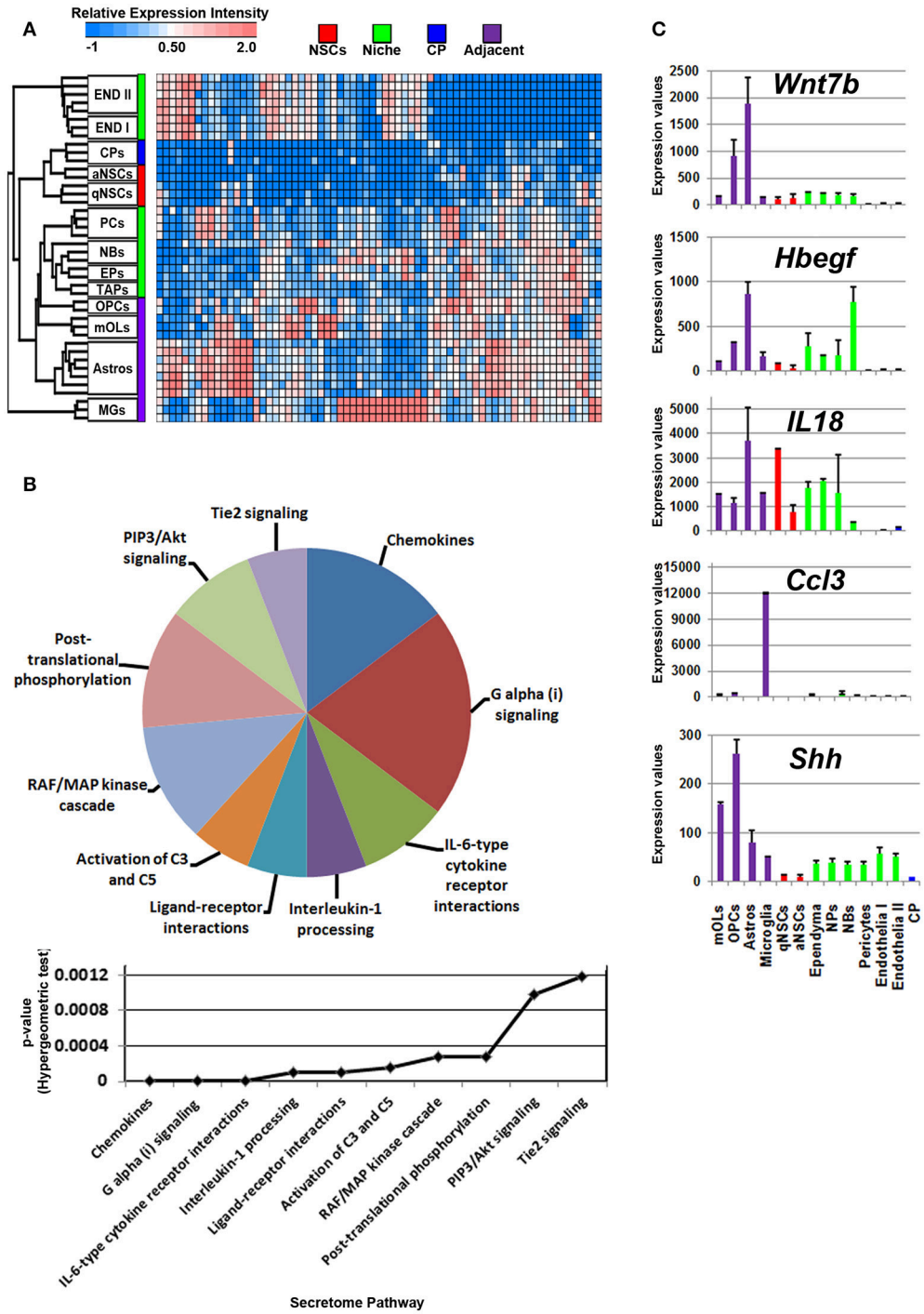

FIGURE 3 | Enrichment of ligand mRNA derived from adjacent glial cells. **(A)** The transcriptome of ligands significantly (1.8 fold change; $p < 5\%$ FDR) enriched in subpopulations of glial cells are displayed as a heatmap and plotted with the remaining datasets. Ligands enriched in MGs are highly expressed in these cells compared to other cells types whereas those in astrocyte and oligodendroglia show some exclusiveness in their expression and some shared expression with other cells. **(B)** These were further characterized using Reactome Pathway for classifying broadly the functions and signaling networks of ligand mRNA detected in the analysis and their *p*-values plotted below as a histogram. **(C)** The top most enriched genes are shown in histograms with in their antilog expression values across multiple cell types showing overall elevated expression in different glial cells. Red, green, blue and purple colors used are for groups containing NSCs, niche, choroid plexus and adjacent glial cells, respectively. CP, choroid plexus; aNSCs, active neural stem cells; qNSCs, quiescent neural stem cells; MGs, microglia; OPCs, oligodendrocytes precursor cells; Astros, astrocytes; OLs, oligodendrocytes (mature); NBs, neuroblasts; TAPs, transiently amplifying progenitors; EPs, ependymal; PCs, pericytes; END I, Endothelia 1; END II, Endothelia 2.

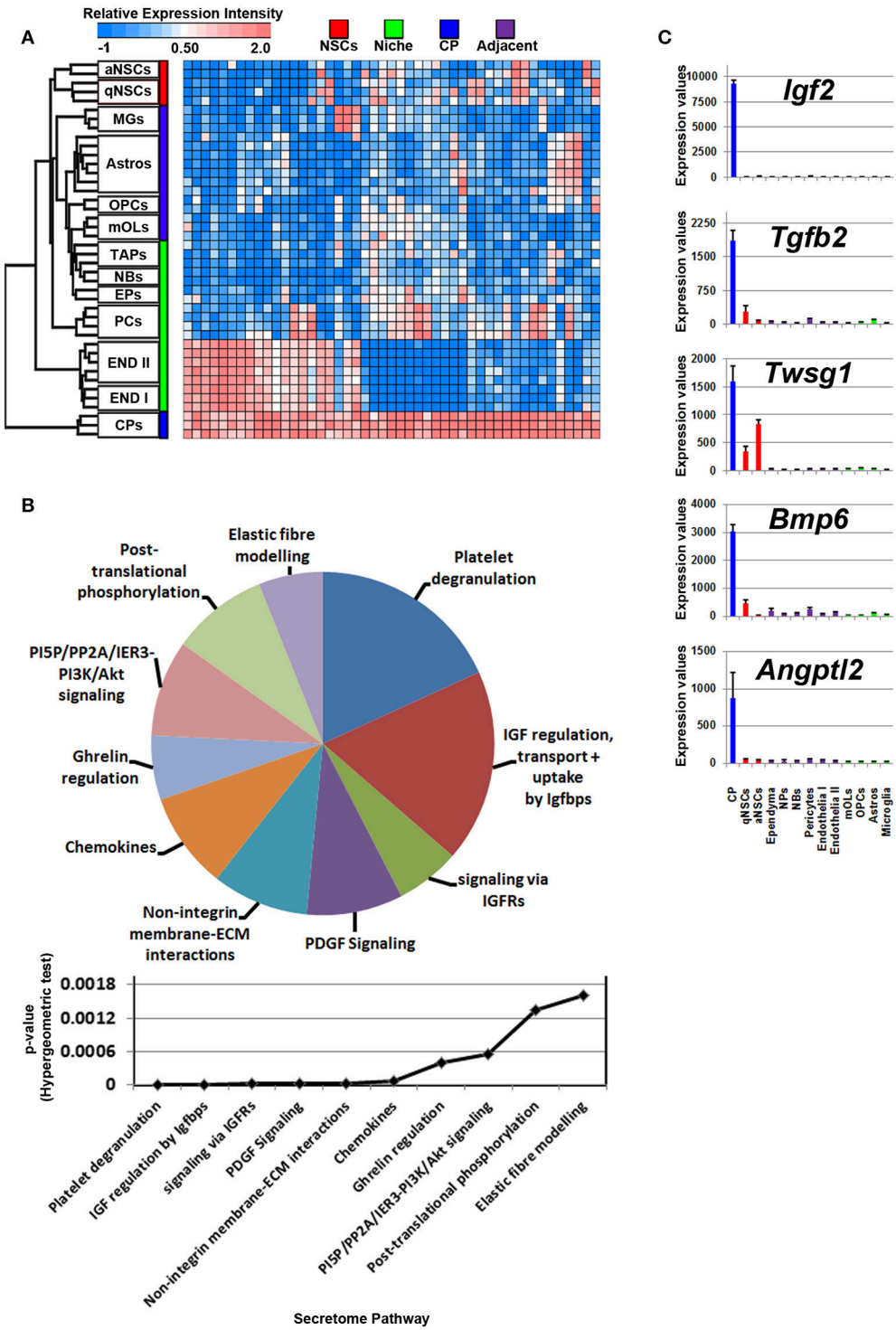

FIGURE 4 | Ligand mRNA enrichment in the CP. **(A)** The transcriptome of ligand mRNA significantly enriched (1.8 fold change; $p < 5\%$ FDR) in the CP are displayed as a heatmap and plotted with the remaining datasets. Some ligand genes are abundant in the CP with some shared expression in vasculature. **(B)** These were further characterized using Reactome Pathway for classifying broadly the functions and signaling networks of ligand mRNA detected in the analysis and their *p*-values plotted below as a histogram. **(C)** The top most enriched genes are shown in histograms with in their antilog expression values across multiple cell types showing overall elevated expression in the CP. Red, green, blue and purple colors used are for groups containing NSCs, niche, choroid plexus and adjacent glial cells, respectively. CP, choroid plexus; aNSCs, active neural stem cells; qNSCs, quiescent neural stem cells; MGs, microglia; OPCs, oligodendrocytes precursor cells; Astros, astrocytes; OLs, oligodendrocytes (mature); NBs, neuroblasts; TAPs, transiently amplifying progenitors; EPs, ependymal; PCs, pericytes; END I, Endothelia 1; END II, Endothelia 2.

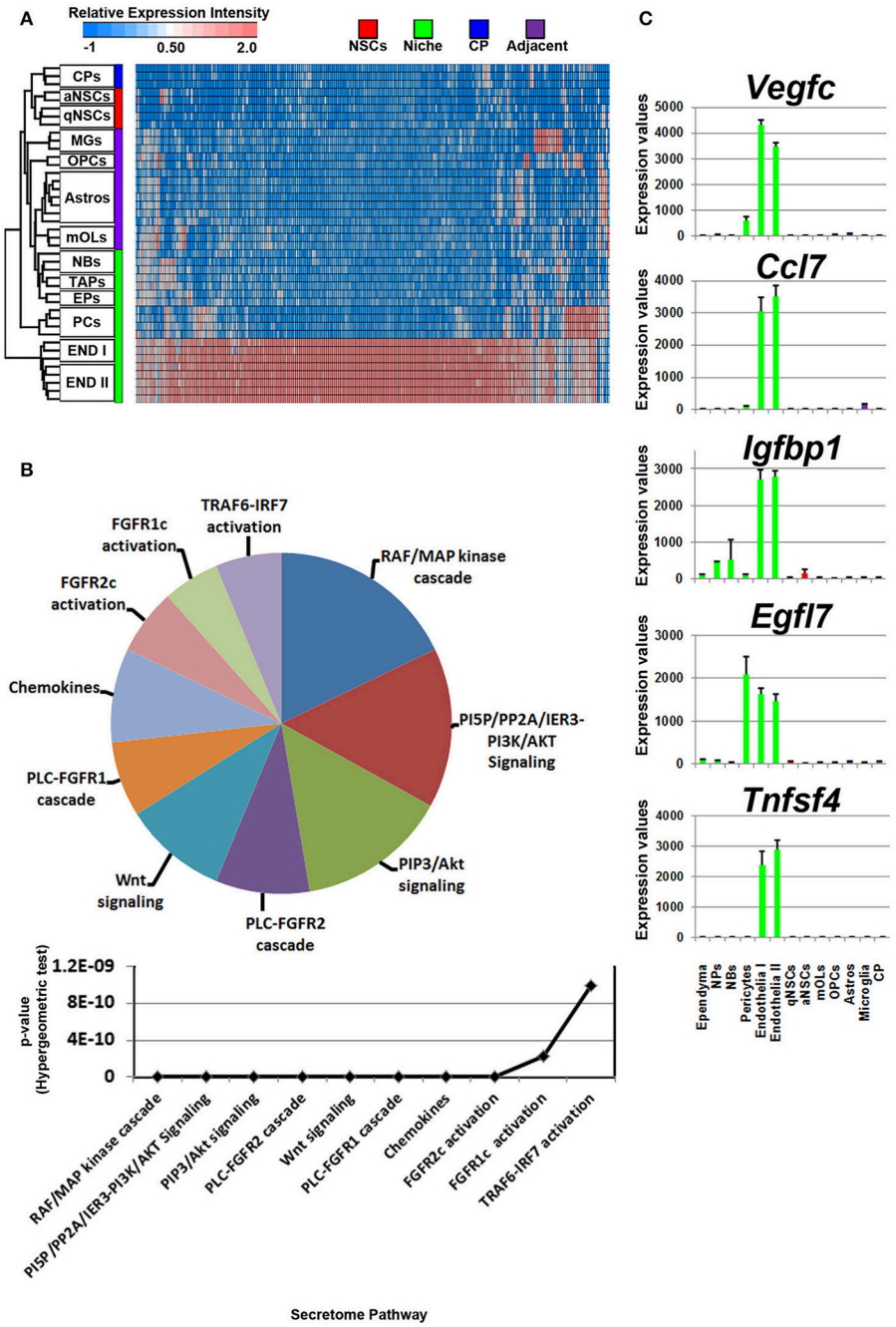

FIGURE 5 | Ligand mRNA enrichment in cells that constitute the niche**. (A)** The transcriptome of ligand mRNA significantly enriched (1.8 fold change; $p < 5\%$ FDR) in the cells derived from the niche are displayed as a heatmap and plotted with the remaining datasets. The majority of ligand mRNA detected in this analysis is derived from endothelia. **(B)** These were further characterized using Reactome Pathway for classifying broadly the functions and signaling networks of ligand mRNA detected in the analysis and their *p*-values plotted below as a histogram. **(C)** The top most enriched genes are shown in histograms with in their antilog expression values across multiple cell types showing overall elevated expression in different glial cells. Red, green, blue and purple colors used are for groups containing NSCs, niche, choroid plexus and adjacent glial cells, respectively. CP, choroid plexus; aNSCs, active neural stem cells; qNSCs, quiescent neural stem cells; MGs, microglia; OPCs, oligodendrocytes precursor cells; Astros, astrocytes; OLs, oligodendrocytes (mature); NBs, neuroblasts; TAPs, transiently amplifying progenitors; EPs, ependymal; PCs, pericytes; END I, Endothelia 1; END II, Endothelia 2.

TABLE 1 | Ligands enriched in the niche were classified by the signaling families they are grouped in.

Immune Related			Wnts		
Gene symbol	**Fold change**	***p*-value**	**Gene symbol**	**Fold change**	***p*-value**
Tnfsf4	10.8	3.1E−08	*Wnt5a*	8.0	8.2E−13
C1qtnf4	7.7	2.6E−06	*Wnt7a*	5.8	1.3E−18
Ifna11	4.9	2.2E−07	*Frzb*	4.8	7.9E−07
C1ra	4.7	3.4E−05	*Wnt8b*	4.7	2.4E−06
Ifng	4.5	3.5E−07	*Rspo2*	2.9	4.0E−07
BMP/TGFβ			**Interleukins**		
Gene symbol	**Fold change**	***p*-value**	**Gene symbol**	**Fold change**	***p*-value**
Grem2	8.6	2.7E−07	*Il7*	5.4	3.7E−06
Tgfb3	6.3	1.4E−09	*Il34*	4.2	3.9E−13
Gdf11	4.8	4.1E−08	*Il1a*	3.7	5.2E−04
Nog	4.3	2.1E−05	*Il23a*	3.4	3.7E−03
Bmp5	4.2	4.3E−07	*Il1f5*	3.3	9.4E−09
Chemokines			**FGFs**		
Gene symbol	**Fold change**	***p*-value**	**Gene symbol**	**Fold change**	***p*-value**
Ccl7	17.1	4.1E−10	*Fgf6*	5.7	1.4E−07
Cxcl5	3.8	1.4E−06	*Fgf3*	5.6	8.4E−07
Ccl11	3.6	4.5E−07	*Fgf18*	5.3	6.4E−05
Cxcl3	3.5	2.7E−06	*Fgfl*	4.6	3.4E−03
Ccl5	3.1	2.3E−06	*Fgf4*	4.4	9.2E−09
Prolactins			**EGF-like**		
Gene symbol	**Fold change**	***p*-value**	**Gene symbol**	**Fold change**	***p*-value**
Prl2c2	8.5	1.4E−07	*Edil3*	5.1	8.7E−08
Pr l2a1	5.5	3.1E−08	*Epgn*	4.4	3.3E−08
Pr l2b1	5.2	4.3E−08	*Vwce*	3.3	2.4E−07
Pr l3d1	4.8	1.8E−09	*Btc*	3.0	1.3E−04
Prl7a2	4.6	5.1E−08	*Nrg2*	2.3	2.2E−12
Hormone-like			**IGF family and regulation**		
Gene symbol	**Fold change**	***p*-value**	**Gene symbol**	**Fold change**	***p*-value**
Grp	5.4	4.5E−06	*Igfbpl1*	15.3	5.0E−08
Adm	4.4	2.2E−06	*Insl*	9.8	8.8E−16
Gcg	4.2	9.1E−07	*Igfbp4*	6.1	1.2E−04
Gast	3.9	7.8E−06	*Igfl*	5.4	1.0E−05
Tshb	3.8	7.4E−10	*Igfbpl*	4.1	1.1E−07

The top 10 most abundant ligand families are summarized and each ligand per family is ranked in order from high-to-low. The top 5 ligands per group are presented.

correlated with information on matching receptor expression taking into account that multiple receptors for each family of ligands can exist (for example the >25 known receptors for Wnt ligands that are spatiotemporally expressed in the SVZ; Harrison-Uy and Pleasure, 2012). Nevertheless, exposed ligand/receptor couples may reveal important, currently unrecognized signaling events contributing to adult neuro- and gliogenic activities. The nature of the analysis performed, i.e., examining region-specific hallmarks within multiple datasets, allowed the detection of transcripts with a degree of specificity rather than transcripts that are shared in expression broadly across a variety of cell types.

The goal of this study was to describe enrichment of ligands in defined regions or subpopulations of cells in close proximity to the walls of the SVZ that regulate aspects of neurogenesis/gliogenesis. Datasets used in the study were derived from acutely isolated cells, using as similar procedures as possible, thereby eliminating any potential false-positives. Future studies involving single cell sequencing of all known cell types that are present close to neurogenic regions will address any potential caveats. To date, such a resource is available but lacks datasets of cells constituting the niche, i.e., NSCs, progenitors (Zeisel et al., 2015). However, the results also indicate that cocktails of ligands triggering multiple intracellular signaling networks might be operating during the distinctive steps of NSC differentiation– a notion that should be considered for future functional studies. Our key findings of the most abundant ligands identified in CNS regions or cell types are summarized in **Figure 6**.

The Vasculature Constitutes an Important Determinant of Neurogenic Processes

A novel finding in this study was the identification of over 200 ligand mRNAs enriched in cells that form the niche, whilst the bulk of these transcripts are attributed to endothelia in contrast to ependymal cells, TAPs and neuroblasts. This might partially result from the little information available regarding ligand expression in ependymal cells, TAPs or neuroblasts in the adult SVZ which is currently limited to a combined number of 10 transcripts. In this regard it is of interest to note that for example *Nog*, a Bmp inhibitor previously reported to be expressed in mainly ependymal cells (Lim et al., 2000), has in the present study been found to be abundant in endothelia with low expression in any other cell type. *Efnb3* encoding the Ephrin-B3 ligand binding to Eph tyrosine kinase receptors revealed to be expressed in both neuroblasts and ependymal cells, a finding confirming the patterns of expression at the protein level (Theus et al., 2010). In another study sampling postnatal neuroblasts close to the walls of the SVZ and those migrating to the olfactory bulb, also only few ligands have been identified (Khodosevich et al., 2009), similar to the adult SVZ-neuroblasts examined here.

Endothelia expressed virtually all known major pathway ligands and several members of any given family. This included at least 18 members of prolactins, 18 chemokines, 12 Fgfs, at least 11 Wnt ligands (canonical and non-canonical), and 24 Bmp/TGFβ-related transcripts. On the other hand, many of the ligands enriched in pericytes overlap with those of endothelia or correspond to related family members, suggesting a certain degree of redundancy among endothelia and pericytes. Inhibitory-like ligands were broadly classified as "ligands" in both endothelia and pericytes, and only appeared at relatively

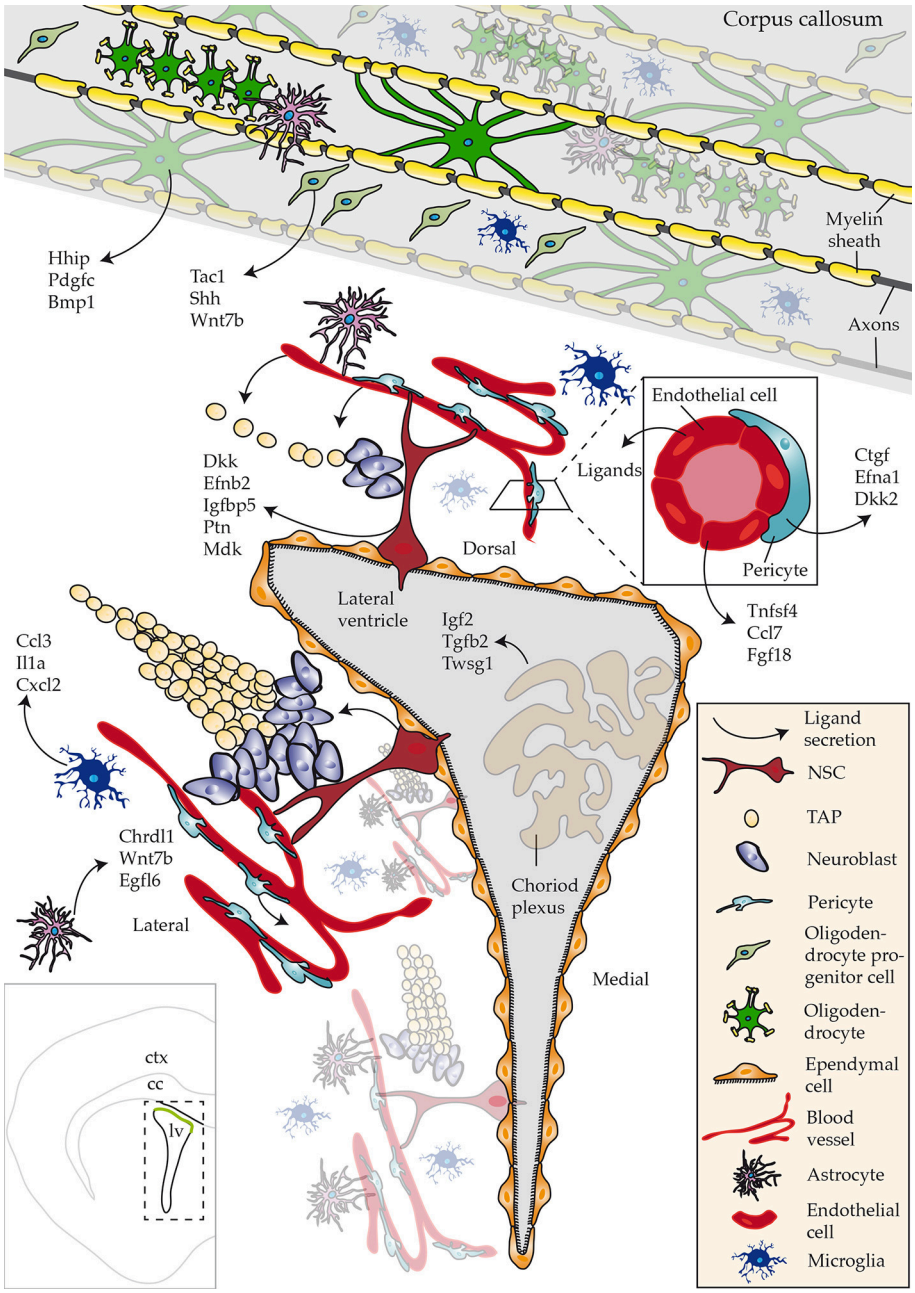

FIGURE 6 | Schematic overview of ligands identified that regulate adult neurogenesis**.** An overview of ligands detected with a focus on novel ligand expression in studied regions and cell types. Bottom left hand corner inset shows an overview of a coronal section of the brain highlighting the lateral ventricle (lv), corpus callosum (cc) and cortex (ctx).

low percentages, thus, demonstrating the large extent of trophic support from the vasculature.

Of note, the used WGT datasets of endothelia or pericytes were suboptimal as SVZ specific expression profiles are currently not available, so that the datasets analyzed in this study were derived from the adult cortex (Nolan et al., 2013; Coppiello et al., 2015). It is anticipated that some degree of heterogeneity of the vasculature in different CNS compartments exists. However, analysis of endothelia purified from the cortex, heart and liver have not reported any marked differences in ligand expression, in contrast to transcriptional regulators that are differentially expressed in endothelia of different origins (Coppiello et al., 2015). Information regarding endothelial heterogeneity in the CNS is restricted to a few studies that show *Vegfa, Vegfb,* and *App* appearing to be expressed at similar levels among endothelia from SVZ and cortex (Crouch et al., 2015; Sato et al., 2017).

The absence of SVZ specific datasets is even further deplorable, as it has been suggested that the cortical vasculature is non-neurogenic, assumingly due to astrocytic end-feet interactions with blood vessels (Ninkovic and Götz, 2013).

Still, the finding that over 200 ligands enriched exclusively in endothelia and pericytes, is intriguing and supports earlier observations on endothelia of non-neurogenic as well as neurogenic origins shown to enhance aNSC proliferation compared to qNSCs and TAPs *in vitro* (Crouch et al., 2015). At the same time, specific ligands such as Jagged1- and EphrinB2-signaling derived from the vasculature were shown to maintain NSC quiescence (Ottone et al., 2014). Multiple regulatory modes on neurogenesis/gliogenesis are likely to occur and await further functional description. In this regard spatio-temporal combinations and synergistic effects will have to be taken into account.

Cell Intrinsic Environmental Cues That Maintain NSCs

Neural stem cells (NSCs) during postnatal or embryonic development express fewer transcripts for ligands compared to adult NSCs, (Azim et al., 2015). It has to be mentioned that the NSC datasets analyzed here are mainly derived from the lateral wall whereas those originating from the dorsal wall are likely to show additional heterogeneity in ligand expression as described for region specific postnatal NSCs (Azim et al., 2015). Despite these limitations, the profiles of a few key candidates were obtained. For example, the abundant expression of the Wnt pathway antagonist, *Dkk3* in qNSCs implies a broad autocrine or paracrine mode of negative regulation in neurogenesis/gliogenesis (Zhu et al., 2014), and, presumably with other Wnt antagonists such as *Srfp1* that is also highly expressed in qNSCs, represses dorsal SVZ identities. Similarly, the chemoattractant *Ptn* has recently been described in drawing glioma cells toward the SVZ prior to further invasion (Qin et al., 2017). Although poorly studied in terms of neurogenic/gliogenic functionality, its elevated expression in qNSCs signifies that it may guide other cells in the vicinity of qNSCs for further trophic support.

Cues Deriving From Adjacent Glial Cells That May Regulate NSC Behavior

Subpopulations of glial cells close to SVZ walls contribute to NSC behavior (reviewed in Morrens et al., 2012; Su et al., 2014). The secretome pathway analysis showed that many of the glial-derived ligands resemble "inflammatory," "chemokine," or "immune-like" pathways consistent with known micro- and astroglial expression signatures (Ribeiro Xavier et al., 2015). It is anticipated that some of these ligands will have pro-neurogenic functions, whereas others such as for example *IL18* may impair neurogenesis/gliogenesis (Crampton et al., 2012). Overall, the immune-related nature of the bulk of these ligands as we are used to know them may have to be reconsidered as they appear to exert non-immune related functions in the physiologically normal brain. Other detected ligands such as TNFα and IFNβ have been shown to promote oligodendrogenesis at the expense of neurogenesis (Tepavcevic et al., 2011; reviewed in Covacu and Brundin, 2015).

Long Distance-Regulation of Neurogenic Processes by the CP

The CP has long been regarded as an important source of ligand secretion into the CSF amongst its well-known functions in maintaining CSF constituents. It is noteworthy that the protruding cilia of NSCs directly contact the CSF in regulating NSC behavior (reviewed in Lun et al., 2015) and that ligands derived from the CP guide neuroblast migration by widespread dispersion into the SVZ tissue via the CSF flow (Sawamoto et al., 2006). Therefore, ligands secreted from the CP will not only affect NSCs, but also cells close to the lateral ventricle walls. One aim of the present study was to determine the expression profiles of ligand mRNA in the CP compared to other cell types sampled. This would define which expressed ligands are relatively unique to the CP and which are only additionally expressed by the CP as a supplementary source confirming their known expression patterns elsewhere (Marques et al., 2011). Furthermore, by sampling a number of other WGT datasets, at least these analyzed ligand mRNA expression profiles are uniquely confined to the CP. A large number of CP ligands are also shared in expression with their mural counterparts, endothelia and pericytes such as for example *Bmp5, Bmp7* and *Fgf,* implying a "surplus" mode of ligand generation.

CONCLUSION

In the present study, we could address the unsolved issue of ligand expression in the major neurogenic niche of the forebrain, the SVZ. Our results have unraveled an unexpected level of diversity and complexity in ligand expression that is likely to orchestrate the distinct neurogenic processes such as survival, proliferation, maintenance, and fate acquisition. The key findings based on the datasets used in this study imply that the niche is an important source of signaling regulation. Some other ligands could additionally be engaged in long-range communication, particularly those emanating from the CP to cells that reside in the niche acting as a means for further regulating aspects of NSCs. As many of the here described novel ligands have not yet been tested for functionality on NSCs, future studies are warranted not only in regard of matching receptor profiles but also in terms of neurogenic and/or gliogenic functions. In the case of neurogenesis in the human SVZ, it will be interesting to compare human-derived datasets of NSCs and niche components. This would enable focusing on novel ligands common to both species for functional studies in mouse in order to eventually be used for therapeutical interventions in humans. Moreover, the data presented here will serve as a guidepost for future studies on related cell populations following disease or in ageing.

AUTHOR CONTRIBUTIONS

KA: conceptualization, data curation, formal analysis, funding acquisition, investigation, methodology, project administration, supervision; RA: writing, data curation, formal analysis, investigation, methodology; MC: data curation, formal analysis, funding acquisition, investigation, methodology;

JJ: writing, visualization, investigation, methodology; JV: funding acquisition, project administration, supervision; PK: funding acquisition, investigation, methodology, project administration, supervision, validation, writing.

FUNDING

This work was supported by the German Research Council (DFG; SPP1757/KU1934/2_1, KU1934/5-1; AZ/115/1-1/Ve642/1-1), the Christiane and Claudia Hempel Foundation for clinical stem cell research, the German Academic Exchange Service (DAAD), the Swiss National Funds (P300PA_171224). The MS Center at the Department of Neurology is supported in part by the Walter and Ilse Rose Foundation and the James and Elisabeth Cloppenburg, Peek & Cloppenburg Düsseldorf Foundation.

ACKNOWLEDGMENTS

We wish to thank Dr. Gareth Williams at the Wolfson Centre of Age Related Diseases, KCL London, UK for proof checking the Secreteome analysis and Prof. Benedikt Berninger at the Institute of Physiological Chemistry, JV University of Mainz for critical evaluation of the manuscript.

SUPPLEMENTARY MATERIAL

The Supplementary Material for this article can be found online at: https://www.frontiersin.org/articles/10.3389/fnins.2018.00220/full#supplementary-material

Supplementary Figure 1 | A transcriptomic map of ligand expression in NSCs. All transcripts enriched in NSCs across multiple cell types presented as a heatmap. Red, white and blue are relative intensity expression of 2, 0.5, and −1 respectively. Gene symbols in red, light red and black show enrichment (≥1.8 fold change; ≤5% FDR) in qNSCs, aNSCs or homogenous expression to both subpopulations. CP, choroid plexus; aNSCs, active neural stem cells; qNSCs, quiescent neural stem cells; MGs, microglia; OPCs, oligodendrocytes precursor cells; Astros, astrocytes; OLs, oligodendrocytes (mature); NBs, neuroblasts; TAPs, transiently amplifying progenitors; EPs, ependymal; PCs, pericytes; END I, Endothelia 1; END II, Endothelia 2.

Supplementary Figure 2 | A transcriptomic map of ligand expression in adjacent glial cell**s**. All transcripts enriched in glial cells across multiple cell types presented as a heatmap. Red, white and blue are relative intensity expression of 2, 0.5, and −1 respectively. CP, choroid plexus; aNSCs, active neural stem cells; qNSCs, quiescent neural stem cells; MGs, microglia; OPCs, oligodendrocytes precursor cells; Astros, astrocytes; OLs, oligodendrocytes (mature); NBs, neuroblasts; TAPs, transiently amplifying progenitors; EPs, ependymal; PCs, pericytes; END I, Endothelia 1; END II, Endothelia 2.

Supplementary Figure 3 | A transcriptomic map of ligand expression in the choroid plexus. All transcripts enriched in the CP across multiple cell types presented as a heatmap. Red white and blue are relative intensity expression of 2, 0.5 and −1 respectively. CP, choroid plexus; aNSCs, active neural stem cells; qNSCs, quiescent neural stem cells; MGs, microglia; OPCs, oligodendrocytes precursor cells; Astros, astrocytes; OLs, oligodendrocytes (mature); NBs, neuroblasts; TAPs, transiently amplifying progenitors; EPs, ependymal; PCs, pericytes; END I, Endothelia 1; END II, Endothelia 2.

Supplementary Figure 4 | A transcriptomic map of ligand expression in the niche. The top 100 transcripts enriched in cells that constitute the niche across multiple cell types presented as a heatmap. Red, white and blue are relative intensity expression of 2, 0.5, and −1 respectively. CP, choroid plexus; aNSCs, active neural stem cells; qNSCs, quiescent neural stem cells; MGs, microglia; OPCs, oligodendrocytes precursor cells; Astros, astrocytes; OLs, oligodendrocytes (mature); NBs, neuroblasts; TAPs, transiently amplifying progenitors; EPs, ependymal; PCs, pericytes; END I, Endothelia 1; END II, Endothelia 2.

REFERENCES

Azim, K., Angonin, D., Marcy, G., Pieropan, F., Rivera, A., Donega, V., et al. (2017). Pharmacogenomic identification of small molecules for lineage specific manipulation of subventricular zone germinal activity. *PLoS Biol.* 15:e2000698. doi: 10.1371/journal.pbio.2000698

Azim, K., Berninger, B., and Raineteau, O. (2016). Mosaic subventricular origins of forebrain oligodendrogenesis. *Front. Neurosci.* 10:107. doi: 10.3389/fnins.2016.00107

Azim, K., Hurtado-Chong, A., Fischer, B., Kumar, N., Zweifel, S., Taylor, V., et al. (2015). Transcriptional hallmarks of heterogeneous neural stem cell niches of the subventricular zone. *Stem Cells* 33, 2232–2242. doi: 10.1002/stem.2017

Azim, K., Raineteau, O., and Butt, A. M. (2012). Intraventricular injection of FGF-2 promotes generation of oligodendrocyte-lineage cells in the postnatal and adult forebrain. *Glia* 60, 1977–1990. doi: 10.1002/glia.22413

Bátiz, L. F., Castro, M. A., Burgos, P. V., Velásquez, Z. D., Muñoz, R. I., Lafourcade, C. A., et al. (2015). Exosomes as novel regulators of adult neurogenic niches. *Front. Cell. Neurosci.* 9:501. doi: 10.3389/fncel.2015.00501

Beckervordersandforth, R., Tripathi, P., Ninkovic, J., Bayam, E., Lepier, A., Stempfhuber, B., et al. (2010). *In vivo* fate mapping and expression analysis reveals molecular hallmarks of prospectively isolated adult neural stem cells. *Cell Stem Cell* 7, 744–758. doi: 10.1016/j.stem.2010.11.017

Benner, E. J., Luciano, D., Jo, R., Abdi, K., Paez-Gonzalez, P., Sheng, H., et al. (2013). Protective astrogenesis from the SVZ niche after injury is controlled by Notch modulator Thbs4. *Nature* 497, 369–373. doi: 10.1038/nature12069

Brill, M. S., Ninkovic, J., Winpenny, E., Hodge, R. D., Ozen, I., Yang, R., et al. (2009). Adult generation of glutamatergic olfactory bulb interneurons. *Nat. Neurosci.* 12, 1524–1533. doi: 10.1038/nn.2416

Cahoy, J. D., Emery, B., Kaushal, A., Foo, L. C., Zamanian, J. L., Christopherson, K. S., et al. (2008). A transcriptome database for astrocytes, neurons, and oligodendrocytes: a new resource for understanding brain development and function. *J. Neurosci.* 28, 264–278. doi: 10.1523/JNEUROSCI.4178-07.2008

Choe, Y., Pleasure, S. J., and Mira, H. (2015). Control of Adult Neurogenesis by Short-Range Morphogenic-Signaling Molecules. *Cold Spring Harb. Perspect. Biol.* 8:a018887. doi: 10.1101/cshperspect.a018887

Codega, P., Silva-Vargas, V., Paul, A., Maldonado-Soto, A. R., Deleo, A. M., Pastrana, E., et al. (2014). Prospective identification and purification of quiescent adult neural stem cells from their *in vivo* niche. *Neuron* 82, 545–559. doi: 10.1016/j.neuron.2014.02.039

Coppiello, G., Collantes, M., Sirerol-Piquer, M. S., Vandenwijngaert, S., Schoors, S., Swinnen, M., et al. (2015). Meox2/Tcf15 heterodimers program the heart capillary endothelium for cardiac fatty acid uptake. *Circulation* 131, 815–826. doi: 10.1161/CIRCULATIONAHA.114.013721

Covacu, R., and Brundin, L. (2015). Effects of neuroinflammation on neural stem cells. *Neuroscientist.* 23, 27–39 doi: 10.1177/1073858415616559

Crampton, S. J., Collins, L. M., Toulouse, A., Nolan, Y. M., and O'Keeffe, G. W. (2012). Exposure of foetal neural progenitor cells to IL-1beta impairs their proliferation and alters their differentiation-a role for maternal inflammation? *J. Neurochem.* 120, 964–973. doi: 10.1111/j.1471-4159.2011.07634.x

Crouch, E. E., Liu, C., Silva-Vargas, V., and Doetsch, F. (2015). Regional and stage-specific effects of prospectively purified vascular cells on the adult V-SVZ neural stem cell lineage. *J. Neurosci.* 35, 4528–4539. doi: 10.1523/JNEUROSCI.1188-14.2015

Diep, D. B., Hoen, N., Backman, M., Machon, O., and Krauss, S. (2004). Characterisation of the Wnt antagonists and their response to conditionally

activated Wnt signalling in the developing mouse forebrain. *Brain Res. Dev. Brain Res.* 153, 261–270. doi: 10.1016/j.devbrainres.2004.09.008

Doetsch, F., Caillé, I., Lim, D. A., García-Verdugo, J. M., and Alvarez-Buylla, A. (1999). Subventricular zone astrocytes are neural stem cells in the adult mammalian brain. *Cell* 97, 703–716. doi: 10.1016/S0092-8674(00)80783-7

Faissner, A., and Reinhard, J. (2015). The extracellular matrix compartment of neural stem and glial progenitor cells. *Glia* 63, 1330–1349. doi: 10.1002/glia.22839

Fiorelli, R., Azim, K., Fischer, B., and Raineteau, O. (2015). Adding a spatial dimension to postnatal ventricular-subventricular zone neurogenesis. *Development* 142, 2109–2120. doi: 10.1242/dev.119966

Frinchi, M., Bonomo, A., Trovato-Salinaro, A., Condorelli, D. F., Fuxe, K., Spampinato, M. G., et al. (2008). Fibroblast growth factor-2 and its receptor expression in proliferating precursor cells of the subventricular zone in the adult rat brain. *Neurosci. Lett.* 447, 20–25. doi: 10.1016/j.neulet.2008.09.059

Harrison-Uy, S. J., and Pleasure, S. J. (2012). Wnt signaling and forebrain development. *Cold Spring Harb. Perspect. Biol.* 4:a008094. doi: 10.1101/cshperspect.a008094

Ihrie, R. A., Shah, J. K., Harwell, C. C., Levine, J. H., Guinto, C. D., Lezameta, M., et al. (2011). Persistent sonic hedgehog signaling in adult brain determines neural stem cell positional identity. *Neuron* 71, 250–262. doi: 10.1016/j.neuron.2011.05.018

Israelsson, C., Kylberg, A., Bengtsson, H., Hillered, L., and Ebendal, T. (2014). Interacting chemokine signals regulate dendritic cells in acute brain injury. *PLoS ONE* 9:e104754. doi: 10.1371/journal.pone.0104754

Khodosevich, K., Seeburg, P. H., and Monyer, H. (2009). Major signaling pathways in migrating neuroblasts. *Front. Mol. Neurosci.* 2:7. doi: 10.3389/neuro.02.007.2009

Kokovay, E., Goderie, S., Wang, Y., Lotz, S., Lin, G., Sun, Y., et al. (2010). Adult SVZ lineage cells home to and leave the vascular niche via differential responses to SDF1/CXCR4 signaling. *Cell Stem Cell* 7, 163–173. doi: 10.1016/j.stem.2010.05.019

Lazar, L. M., and Blum, M. (1992). Regional distribution and developmental expression of epidermal growth factor and transforming growth factor-alpha mRNA in mouse brain by a quantitative nuclease protection assay. *J. Neurosci.* 12, 1688–1697.

Lim, D. A., Tramontin, A. D., Trevejo, J. M., Herrera, D. G., García-Verdugo, J. M., and Alvarez-Buylla, A. (2000). Noggin antagonizes BMP signaling to create a niche for adult neurogenesis. *Neuron* 28, 713–726. doi: 10.1016/S0896-6273(00)00148-3

Lun, M. P., Monuki, E. S., and Lehtinen, M. K. (2015). Development and functions of the choroid plexus-cerebrospinal fluid system. *Nat. Rev. Neurosci.* 16, 445–457. doi: 10.1038/nrn3921

Marques, F., Sousa, J. C., Coppola, G., Gao, F., Puga, R., Brentani, H., et al. (2011). Transcriptome signature of the adult mouse choroid plexus. *Fluids Barriers CNS* 8:10. doi: 10.1186/2045-8118-8-10

Menn, B., Garcia-Verdugo, J. M., Yaschine, C., Gonzalez-Perez, O., Rowitch, D., and Alvarez-Buylla, A. (2006). Origin of oligodendrocytes in the subventricular zone of the adult brain. *J. Neurosci.* 26, 7907–7918. doi: 10.1523/JNEUROSCI.1299-06.2006

Mirzadeh, Z., Merkle, F. T., Soriano-Navarro, M., Garcia-Verdugo, J. M., and Alvarez-Buylla, A. (2008). Neural stem cells confer unique pinwheel architecture to the ventricular surface in neurogenic regions of the adult brain. *Cell Stem Cell* 3, 265–278. doi: 10.1016/j.stem.2008.07.004

Morrens, J., W., Van Den Broeck, and Kempermann, G. (2012). Glial cells in adult neurogenesis. *Glia* 60, 159–174. doi: 10.1002/glia.21247

Ninkovic, J., and Götz, M. (2013). Fate specification in the adult brain–lessons for eliciting neurogenesis from glial cells. *BioEssays* 35, 242–252. doi: 10.1002/bies.201200108

Nolan, D. J., Ginsberg, M., Israely, E., Palikuqi, B., Poulos, M. G., James, D., et al. (2013). Molecular signatures of tissue-specific microvascular endothelial cell heterogeneity in organ maintenance and regeneration. *Dev. Cell* 26, 204–219. doi: 10.1016/j.devcel.2013.06.017

Olson, L. E., and Soriano, P. (2011). PDGFRbeta signaling regulates mural cell plasticity and inhibits fat development. *Dev. Cell* 20, 815–826. doi: 10.1016/j.devcel.2011.04.019

Ornitz, D. M., and Itoh, N. (2015). The Fibroblast Growth Factor signaling pathway. *Wiley Interdiscip. Rev. Dev. Biol.* 4, 215–266. doi: 10.1002/wdev.176

Ottone, C., Krusche, B., Whitby, A., Clements, M., Quadrato, G., Pitulescu, M. E., et al. (2014). Direct cell-cell contact with the vascular niche maintains quiescent neural stem cells. *Nat. Cell Biol.* 16, 1045–1056. doi: 10.1038/ncb3045

Pathan, M., Keerthikumar, S., Ang, C. S., Gangoda, L., Quek, C. Y., Williamson, N. A., et al. (2015). FunRich: an open access standalone functional enrichment and interaction network analysis tool. *Proteomics* 15, 2597–2601. doi: 10.1002/pmic.201400515

Peretto, P., Dati, C., De Marchis, S., Kim, H. H., Ukhanova, M., Fasolo, A., et al. (2004). Expression of the secreted factors noggin and bone morphogenetic proteins in the subependymal layer and olfactory bulb of the adult mouse brain. *Neuroscience* 128, 685–696. doi: 10.1016/j.neuroscience.2004.06.053

Platel, J. C., and Bordey, A. (2016). The multifaceted subventricular zone astrocyte: from a metabolic and pro-neurogenic role to acting as a neural stem cell. *Neuroscience* 323, 20–28. doi: 10.1016/j.neuroscience.2015.10.053

Qin, E. Y., Cooper, D. D., Abbott, K. L., Lennon, J., Nagaraja, S., Mackay, A., et al. (2017). Neural precursor-derived pleiotrophin mediates subventricular zone invasion by Glioma. *Cell* 170, 845 e19–859 e19. doi: 10.1016/j.cell.2017.07.016

Quiñones-Hinojosa, A., Sanai, N., Soriano-Navarro, M., Gonzalez-Perez, O., Mirzadeh, Z., Gil-Perotin, S., et al. (2006). Cellular composition and cytoarchitecture of the adult human subventricular zone: a niche of neural stem cells. *J. Comp. Neurol.* 494, 415–434. doi: 10.1002/cne.20798

Rainer, J., Sanchez-Cabo, F., Stocker, G., Sturn, A., and Trajanoski, Z. (2006). CARMAweb: comprehensive R- and bioconductor-based web service for microarray data analysis. *Nucleic Acids Res.* 34, W498–W503. doi: 10.1093/nar/gkl038

Ribeiro Xavier, A. L., Kress, B. T., Goldman, S. A., Lacerda de Menezes, J. R., and Nedergaard, M. (2015). A distinct population of microglia supports adult neurogenesis in the subventricular zone. *J. Neurosci.* 35, 11848–11861. doi: 10.1523/JNEUROSCI.1217-15.2015

Sato, Y., Uchida, Y., Hu, J., Young-Pearse, T. L., Niikura, T., and Mukouyama, Y. S. (2017). Soluble APP functions as a vascular niche signal that controls adult neural stem cell number. *Development* 144, 2730–2736. doi: 10.1242/dev.143370

Sawamoto, K., Wichterle, H., Gonzalez-Perez, O., Cholfin, J. A., Yamada, M., Spassky, N., et al. (2006). New neurons follow the flow of cerebrospinal fluid in the adult brain. *Science* 311, 629–632. doi: 10.1126/science.1119133

Silva-Vargas, V., Maldonado-Soto, A. R., Mizrak, D., Codega, P., and Doetsch, F. (2016). Age-dependent niche signals from the choroid plexus regulate adult neural stem cells. *Cell Stem Cell* 19, 643–652. doi: 10.1016/j.stem.2016.06.013

Su, P., Zhang, J., Zhao, F., Aschner, M., Chen, J., and Luo, W. (2014). The interaction between microglia and neural stem/precursor cells. *Brain Res. Bull.* 109, 32–38. doi: 10.1016/j.brainresbull.2014.09.005

Tavazoie, M., Van der Veken, L., Silva-Vargas, V., Louissaint, M., Colonna, L., Zaidi, B., et al. (2008). A specialized vascular niche for adult neural stem cells. *Cell Stem Cell* 3, 279–288. doi: 10.1016/j.stem.2008.07.025

Tepavcević, V., Lazarini, F., Alfaro-Cervello, C., Kerninon, C., Yoshikawa, K., Garcia-Verdugo, J. M., et al. (2011). Inflammation-induced subventricular zone dysfunction leads to olfactory deficits in a targeted mouse model of multiple sclerosis. *J. Clin. Invest.* 121, 4722–4734. doi: 10.1172/JCI59145

Theus, M. H., Ricard, J., Bethea, J. R., and Liebl, D. J. (2010). EphB3 limits the expansion of neural progenitor cells in the subventricular zone by regulating p53 during homeostasis and following traumatic brain injury. *Stem Cells* 28, 1231–1242. doi: 10.1002/stem.449

Thored, P., Wood, J., Arvidsson, A., Cammenga, J., Kokaia, Z., and Lindvall, O. (2007). Long-term neuroblast migration along blood vessels in an area with transient angiogenesis and increased vascularization after stroke. *Stroke* 38, 3032–3039. doi: 10.1161/STROKEAHA.107.488445

Thouvenot, E., Lafon-Cazal, M., Demettre, E., Jouin, P., Bockaert, J., and Marin, P. (2006). The proteomic analysis of mouse choroid plexus secretome reveals a high protein secretion capacity of choroidal epithelial cells. *Proteomics* 6, 5941–5952. doi: 10.1002/pmic.200600096

Wakabayashi, T., Hidaka, R., Fujimaki, S., Asashima, M., and Kuwabara, T. (2014). MicroRNAs and epigenetics in adult neurogenesis. *Adv. Genet.* 86, 27–44. doi: 10.1016/B978-0-12-800222-3.00002-4

Zamanian, J. L., Xu, L., Foo, L. C., Nouri, N., Zhou, L., Giffard, R. G., et al. (2012). Genomic analysis of reactive astrogliosis. *J. Neurosci.* 32, 6391–6410. doi: 10.1523/JNEUROSCI.6221-11.2012

Zeisel, A., Muñoz-Manchado, A. B., Codeluppi, S., Lonnerberg, P., La Manno, G., Jureus, A., et al. (2015). Brain structure. Cell types in the mouse cortex and hippocampus revealed by single-cell RNA-seq. *Science* 347, 1138–1142. doi: 10.1126/science.aaa1934

Zhu, Y., Demidov, O. N., Goh, A. M., Virshup, D. M., Lane, D. P., and Bulavin, D. V. (2014). Phosphatase WIP1 regulates adult neurogenesis and WNT signaling during aging. *J. Clin. Invest.* 124, 3263–3273. doi: 10.1172/JCI73015

Conflict of Interest Statement: The authors declare that the analysis performed in the absence of any commercial or financial relationships that could be construed as a potential conflict of interest.

The handling Editor and reviewer AB declared their involvement as co-editors in the Research Topic, and confirm the absence of any other collaboration

frontiers in Cellular Neuroscience

ORIGINAL RESEARCH
published: 08 June 2018
doi: 10.3389/fncel.2018.00155

Direct Reprogramming of Adult Human Somatic Stem Cells Into Functional Neurons Using *Sox2*, *Ascl1*, and *Neurog2*

Jessica Alves de Medeiros Araújo[1], *Markus M. Hilscher*[1†], *Diego Marques-Coelho*[1,2], *Daiane C. F. Golbert*[1], *Deborah A. Cornelio*[3], *Silvia R. Batistuzzo de Medeiros*[3], *Richardson N. Leão*[1] *and Marcos R. Costa*[1*]

[1] *Brain Institute, Federal University of Rio Grande do Norte, Natal, Brazil,* [2] *Bioinformatics Multidisciplinary Environment, IMD, Federal University of Rio Grande do Norte, Natal, Brazil,* [3] *Laboratório de Biologia Molecular e Genômica, Centro de Biociências, Federal University of Rio Grande do Norte, Natal, Brazil*

OPEN ACCESS

Edited by:
Christophe Heinrich, INSERM U1208 Institut Cellule Souche et Cerveau, France

Reviewed by:
Zhiping P. Pang, Rutgers University, The State University of New Jersey, United States
Carol Schuurmans, Sunnybrook Health Science Centre, Canada

***Correspondence:**
Marcos R. Costa
mrcosta@neuro.ufrn.br

†Present Address:
Markus M. Hilscher, Institute for Analysis and Scientific Computing, Vienna University of Technology, Vienna, Austria

Received: *23 April 2018*
Accepted: *17 May 2018*
Published: *08 June 2018*

Citation:
Araújo JAM, Hilscher MM, Marques-Coelho D, Golbert DCF, Cornelio DA, Batistuzzo de Medeiros SR, Leão RN and Costa MR (2018) Direct Reprogramming of Adult Human Somatic Stem Cells Into Functional Neurons Using Sox2, Ascl1, and Neurog2. Front. Cell. Neurosci. 12:155. doi: 10.3389/fncel.2018.00155

Reprogramming of somatic cells into induced pluripotent stem cells (iPS) or directly into cells from a different lineage, including neurons, has revolutionized research in regenerative medicine in recent years. Mesenchymal stem cells are good candidates for lineage reprogramming and autologous transplantation, since they can be easily isolated from accessible sources in adult humans, such as bone marrow and dental tissues. Here, we demonstrate that expression of the transcription factors (TFs) SRY (sex determining region Y)-box 2 (*Sox2*), Mammalian achaete-scute homolog 1 (*Ascl1*), or Neurogenin 2 (*Neurog2*) is sufficient for reprogramming human umbilical cord mesenchymal stem cells (hUCMSC) into induced neurons (iNs). Furthermore, the combination of *Sox2/Ascl1* or *Sox2/Neurog2* is sufficient to reprogram up to 50% of transfected hUCMSCs into iNs showing electrical properties of mature neurons and establishing synaptic contacts with co-culture primary neurons. Finally, we show evidence supporting the notion that different combinations of TFs (*Sox2/Ascl1* and *Sox2/Neurog2*) may induce multiple and overlapping neuronal phenotypes in lineage-reprogrammed iNs, suggesting that neuronal fate is determined by a combination of signals involving the TFs used for reprogramming but also the internal state of the converted cell. Altogether, the data presented here contribute to the advancement of techniques aiming at obtaining specific neuronal phenotypes from lineage-converted human somatic cells to treat neurological disorders.

Keywords: induced neurons, lineage reprogramming, human mesenchymal stem cells, umbilical cord, proneural genes

INTRODUCTION

Reprogramming of somatic cells into induced pluripotent stem cells (iPS) that can generate all three major embryonic lineages, stem cells and even a new animal has revolutionized research in regenerative medicine in recent years (Takahashi and Yamanaka, 2006; Okita et al., 2007). Somatic cells isolated from different sources can be converted into iPS (Meissner et al., 2007; Aoi et al., 2008; Hanna et al., 2008; Espejel et al., 2010; Imamura et al., 2010), which in turn can be converted into specific cell types including neurons (Wernig et al., 2008; Kuzmenkin et al., 2009; Mizuno et al., 2010; Zhang et al., 2013).

However, generation of iPS and further differentiation into neuronal cells is time consuming and the cells retain tumorigenic potential (Takahashi and Yamanaka, 2006; Okita et al., 2007).

In contrast, direct lineage reprogramming of somatic cells is a fast process and bypasses the pluripotent stage associated with tumor transformation. Astrocytes isolated from the postnatal cerebral cortex of mice were the first cells to be directly reprogrammed into induced neurons (iNs) following expression of the transcription factor (TF) Neurogenin 2 (*Neurog2*) or Mammalian achaete-scute homolog 1 (*Mash1/Ascl1*) (Berninger et al., 2007; Heinrich et al., 2011). Subsequently, the list of murine cell types liable to lineage reprogramming into iNs grew substantially, including non-neural cells, such as mouse fibroblasts and hepatocytes (Vierbuchen et al., 2010; Marro et al., 2011). However, non-neural cells typically require more than one TF to achieve a full neuronal conversion.

Direct reprogramming of human somatic cells into neurons can also be achieved through expression of *Ascl1* in combination with other TFs (Ambasudhan et al., 2011; Son et al., 2011; Karow et al., 2012). It has also been reported that expression of *Ascl1* or *Neurog2* alone is sufficient to induce conversion of human fibroblasts into induced neurons (Chanda et al., 2014; Gascón et al., 2016), but the efficiency of this process is low (<10%). Moreover, the phenotypes of iNs obtained through direct cell lineage reprogramming using human cells remains largely elusive. Pinpointing strategies capable of producing iNs exhibiting defined neurochemical phenotypes is a critical step towards translation of the lineage reprogramming techniques into clinics.

Here, we show that the expression of the transcription factor SRY (sex determining region Y)-box 2 (*Sox2*), *Ascl1* or *Neurog2* is sufficient to lineage-convert a small fraction of human umbilical cord mesenchymal stem cells (hUCMSCs) into iNs. In contrast, the co-expression of either *Sox2/Ascl1* or *Sox2/Neurog2* is sufficient to convert a large fraction of hUCMSCs (up to 50%) into iNs displaying electrophysiological hallmarks of mature neurons and establishing synaptic contacts with other cells. Furthermore, we show that iNs may express transcripts associated with the acquisition of different neurochemical phenotypes, independently of the combination of transcription factors used. Also, *Sox2/Ascl1* and *Sox2/Neurog2* may induce the expression of genes involved in the acquisition of the same neurochemical phenotypes, suggesting that iNs fate during lineage-conversion is influenced by other aspects than the transcription factors used. Collectively, our data indicate that hUCMSCs are good candidates for lineage reprogramming into iNs, but more studies are required to further advance protocols capable of producing iNs with a particular phenotype.

MATERIALS AND METHODS

Cell Culture

Human multipotent mesenchymal stem cells (hMSC) were isolated from umbilical cords donated with informed consent of the pregnant mothers at maternity Januário Cicco, Federal University of Rio Grande do Norte, Natal, Brazil. The study was approved by the Research Ethics Committee of the Federal University of Rio Grande do Norte (Project Number 508.459), and in strict agreement with Brazilian law (Resolution 196/96). All subjects gave written informed consent in accordance with the Declaration of Helsinki.

In this study, Wharton's jelly mesenchymal stem cells were isolated from umbilical cord. Following isolation from the subendothelium vein, according to the method previously published (Duarte et al., 2012), the remaining umbilical cord tissue was cut in small pieces and washed with phosphate-buffered saline (PBS; 137 mM NaCl, 2.7 mM KCl, 4.3 mM Na_2HPO_4, and 1.47 mM KH_2PO_4; Merck), supplemented with 3% antibiotic–antimycotic solution (prepared with 10,000 units/ml penicillin G sodium, 10,000 μg/ml streptomycin sulfate and 25 μg/ml amphotericin B; HyClone). Then, the tissue was centrifuged at 200 g for 10 min, and the pellet resuspended in 10 mL of 0.1% collagenase type IV (Worthington) diluted in PBS. After that, the explants were incubated for 16 h at 37°C in a water bath. The tissue was centrifuged again at 200 g for 10 min, the pellet washed twice with PBS and then gently dissociated in a digestion solution containing 0.25% trypsin and 0.02% EDTA (Invitrogen) for 15 min at room temperature. To interrupt trypsin activity, we added fetal bovine serum (FBS; HyClone). Once again, the cell suspension was centrifuged, and the cell pellet resuspended in minimum essential medium a (α MEM; Gibco Invitrogen) supplemented with 10% FBS and 1% antibiotic solution. Cells were plated onto T25 tissue culture flasks (TPP) and these cultures maintained at 37°C in a humidified atmosphere containing 5% CO_2. After 2 or 4 days, the medium was changed and non-adherent cells were removed. Cultures consisting of small, adherent and spindle shaped fibroblastoid cells reaching 60–70% of confluence were detached and subcultured at 4,000 cells/cm^2.

Characterization of hMSCs

The cells isolated from Wharton's jelly human umbilical cord were characterized as MSCs, according to the criteria proposed by the International Society for Cellular Therapy (Horwitz et al., 2005; Dominici et al., 2006). The hMSCs were labeled with a panel of monoclonal antibodies against several cell markers, including CD105-FITC, CD90PE-Cy5 (Bioscience), CD73PE, CD34PE, HLA-DR-FITC, CD45-FITC, and CD14PE (Becton Dickinson's). Briefly, the cells were detached of the tissue culture plates using 0.25% trypsin/EDTA, washed, and homogenized with PBS. They were then incubated with monoclonal antibody for 30 min in darkness at room temperature. At the end of this period, the cell suspension was centrifuged, washed in PBS, and re-suspended in cold fixing solution, 0.5% formaldehyde in PBS. For each test, isotype-matched monoclonal antibodies were used as negative controls (IgG1-FITC, PE, and PE-Cy5; Becton Dickinson's). The fluorescence intensity of labeled cells was determined with a fluorescence-activated cell analyzer (FACScan) using cell quest software (Cell Quest™ Software, Becton Dickinson Immunocytometry Systems), a total of 20,000 events for each sample were recorded. The following parameters were considered: forward scatter in linear scale (which evaluates cell size), side scatter in linear scale (assessing

cell complexity), and cell marker expression in fluorescence analysis by FL1, FL2, and FL3 in logarithmical scale, representing the antigen–antibody reaction conjugated to FITC, PE, and PE-Cy5, respectively. Results were expressed as a percentage of cells labeled with monoclonal antibodies. Osteogenic, adipogenic, and chondrogenic differentiation assays were carried out according to methodology previously published (Duarte et al., 2012).

Plasmids

The pro-neural genes *Ascl1*, *Neurog2,* or *Sox2* were expressed under control of an internal chicken β-actin promoter with cytomegalovirus enhancer (pCAG) together with DsRed or GFP behind an internal ribosomal entry site (pCAG-Ascl1-IRES-DsRed, pCAG-Neurog2-IRES-DsRed, and pCAG-Sox2-IRES-GFP). For control experiments, cultures were transfected with plasmids encoding only DsRed or GFP (pCAG-IRES-DsRed or pCAG-IRES-GFP) (Heinrich et al., 2010; Karow et al., 2012). Plasmid stocks were prepared in *Escherichia coli* and purified using the endotoxin-free Maxiprep plasmid kit (Invitrogen). DNA concentration was adjusted to 1 μg/μL in TE buffer endotoxin free, and plasmids were stored at −20°C.

Transfection

For transfections, hMSC were seeded in 24-well plates onto poly-D-lysine (Sigma-Aldrich) and laminin (L-2020; Sigma Aldrich) coated glass coverslips at a density of 3×10^4 cells per well in 0.5 mL α MEM (Gibco) supplemented with 10% fetal bovine serum (FBS) and 1% antibiotic solution (penicillin/streptomycin). The cells were grown in these conditions for 1–3 days until 70–80% confluent.

Both DNA plasmids (1 μg/μL) and a lipophilic cationic reagent (Lipofectamine 2000, Invitrogen) were diluted in 50 μL Opti-MEM (Reduced Serum Medium, Invitrogen). Mixtures were incubated for 5 min and then combined for a further 20 min according to the manufacturer's instructions. Complexes were added to the cells in a total volume of 0.5 mL Opti-MEM (Gibco) and incubated at 37°C in a humidified atmosphere containing 5% CO_2 for 10–12 h. Antibiotics and serum were not used during transfection procedures.

Co-culture With Hippocampal Neurons

For co-culture experiments, mouse hippocampus at postnatal day 0 to 4 (P0-4) were dissected in ice-cold PBS and dissociated in a the digestion solution for 10 min at 37°C. Trypsin action was interrupted with fetal bovine serum and the tissue dissociated mechanically with a fire-polished glass Pasteur pipette. The suspension was then centrifuged at 200 g for 5 min and washed twice in DMEM/F12 10% FBS in DMEM/F12 medium (Gibco). Mouse hippocampal cells were added to the human cultures 1–2 days after transfection at a density of 50,000 cells per well. The local University Animal Care and Use Committee (CEUA/UFRN) approved experiments involving mice. All experiments were carried out in accordance with international guidelines and regulations for animal use.

Immunocytochemistry

Cell cultures were fixed in 4% paraformaldehyde (PFA) in PBS for 15 min at room temperature. Primary antibodies were diluted in PBS, 0.5% Triton X-100 and 5% normal goat serum. Specimens were incubated overnight at 4°C. After three washes with PBS, cells were incubated with species-specific secondary antibodies conjugated to fluorophores for 2 h at room temperature. Once again, samples were washed with PBS three times. For nuclei staining, cells were incubated for 5 min with 0.1 μg/mL DAPI (4′6′-diamino-2-phenylindone) in PBS 0.1 M. Coverslips were finally mounted onto a glass slide with a mounting medium (Aqua Poly/Mount; Polysciences). The following primary antibodies and dilutions were used: chicken anti-Green Fluorescent Protein (GFP, Aves Labs, 1:1,000), rabbit anti-Red Fluorescent Protein (RFP, Rockland, 1:1,000), mouse anti-major microtubule associated protein (MAP2; Sigma, 1:500), guinea pig polyclonal anti-vesicular GABA transporter (vGAT, Synaptic Systems, 1:200), and polyclonal anti-vesicular glutamate transporter 1 (vGLUT11, Synaptic Systems, 1:1,000).

Electrophysiology

Cell cultures with induced neurons were transferred to a recording chamber mounted on the stage of a microscope equipped with a water immersion 40X objective (Zeiss Examiner. A1, 1 NA) and perfused with oxygenated external solution (1–1.25 ml/min) at 37°C. Data were acquired using a patch-clamp amplifier Axopatch 200B (Molecular Devices) in current or voltage clamp mode, a 16-bit data acquisition card (National Instruments), and WinWCP or WinEDR software implemented by Dr. John Dempster (University of Strathclyde). Patch-pipettes of borosilicate glass capillaries (GC150F-10 Harvard Apparatus) were pulled on a vertical puller (Narishige) with resistances from 5–7 MΩ. Pipettes were filled with internal solution (∼290 Osm) containing (in mM) 130 K^+-gluconate, 7 NaCl, 0.1 EGTA, 0.3 $MgCl_2$, 0.8 $CaCl_2$, 2 Mg-ATP, 0.5 NaGTP, 10 HEPES, and 2 EGTA (pH 7.2 adjusted with KOH 1M). The external solution (∼300 Osm) contained (in mM) 120 NaCl, 3 KCl, 1.2 $MgCl_2$, 2.5 $CaCl_2$, 23 $NaHCO_3$, 5 HEPES, and 11 Glucose (pH 7.4 adjusted with NaOH 1M).

Patch-clamped cells were measured for input resistance, resting membrane potential, and capacitance. Recordings were analyzed with custom routines in MATLAB. Action potentials were triggered by 400-ms depolarizing current injections from 100 pA, 400 ms, with 10 pA increments. The first fired action potential in response to minimal current injection was analyzed for amplitude (peak to afterhyperpolarization voltage), half-width (halfway between threshold voltage and peak), and afterhyperpolarization amplitude (threshold to minimum of voltage trough between the first and the second action potential in a spike train). Instantaneous and steady-state voltage were analyzed in response to hyperpolarizing current injections (−100 pA, 400 ms). Excitatory postsynaptic currents were analyzed for amplitude and rise time in free-run traces of 150 s. Active and passive electrophysiological membrane properties, including action potential parameters were analyzed using a Student's unpaired, two-tailed *t*-test.

Calcium Imaging

Calcium imaging was performed on human MSC 3 weeks post-transfection using Oregon green 488 BAPTA-1 (Invitrogen, 10 μM). Imaging was performed in physiological saline solution containing (in mM) 140 NaCl, 5 KCl, 2 $MgCl_2$, 2 $CaCl_2$, 10 HEPES, 10 glucose, and 6 sucrose (pH 7.35). Images were acquired approximately every 10 ms using a scientific CMOS camera (Andor). The microscope was controlled by Micro-Manager software together with the image processor ImageJ. Changes in fluorescence were measured for individual cells and average of the first 10 time-lapse images for each region of interest (ROI) was defined as initial fluorescence (F0).

Single Cell RT-qPCR

After electrophysiological recordings, the cell was sucked into the recording pipette. Pipettes were quickly removed and broken into 1.5 mL tubes containing 20 U of RNase inhibitor and 8.3 mM DTT. Samples were frozen immediately on dry ice and stored at −80°C. Immediately after thaw, the samples were treated to eliminate contaminating DNA molecules. Complementary DNA (cDNA) synthesis and pre-amplified reactions were performed with the RT^2 PreAMP cDNA Synthesis Kit following the manufacturer's procedure (QIAGEN). Amplification was performed on the Applied Biosystems ViiA 7 Real-Time PCR (Applied Biosystems). RT^2 Profiler PCR Array were customized in 96-well plates, designed for analyzing the expression of the following genes: Choline O-acetyltransferase (*CHAT*), Tyrosine hydroxylase (*TH*), Tryptophan hydroxylase 2 (*TPH2*), Vesicular glutamate transporter 1 (*VGLUT1* or *SLC17A7*), GABA Vesicular transporter (*VGAT* or *SLC32A1*), FEZ family zinc finger 2 (*FEZF2*), T-box brain 1 (*TBR1*), SATB homeobox 2 (*SATB2*), COUP-TF-interacting protein 2 (*CTIP2* or *BCL11B*), Platelet-derived growth factor receptor, beta polypeptide (*PDGFRB*), Thy-1 cell surface antigen (*THY-1*), Atonal homolog 8 (*ATOH8*), Neurogenic differentiation 1 (*NEUROD1*), Glyceraldehyde-3-phosphate dehydrogenase (*GAPDH*), and Hypoxanthine phosphoribosyltransferase 1 (*HPRT1*). The RT-qPCR was performed using the RT^2 profiler PCR customized array (QIAGEN). Each array included genomic DNA control primer set, reverse transcription control, positive PCR control to report the efficiency of the polymerase chain reaction itself, and the endogenous reference genes *GAPDH* and *HPRT1*.

Analysis of Single-Cell RT-qPCR

A single-cell RT-qPCR pre-processing was performed based on method described by Ståhlberg et al. (2013). Melting curve analysis performed elimination of false positives. Next, relative quantities were calculated using a cycle of quantification cutoff (Cq-cutoff) and relative-quantities of cDNA molecule equation. Missing data were imputed with absolute value 0.5, followed by conversion to log_2-scale. Mean center and auto scale, for each gene mean center and auto scale were calculated separately using log_2-values. Heat map and Principal Component Analysis (PCA) were used to visualize expression differences between groups. Statistical analysis and plotting were performed using the software R version 3.3.3.

Statistical Analysis

All statistical data are presented as the mean ± standard error of the mean (SEM) of at least three independent experiments. Statistically significant differences were assessed by Student's unpaired *t*-test or one-way Analysis of variance (ANOVA), comparing two or more groups, respectively. $P < 0.05$ was considered a significant difference (*).

RESULTS

Direct Lineage Reprogramming of Human Umbilical Cord MSCs

Mesenchymal stem cells (MSCs) can be isolated from different sources in adult humans, including the bone marrow and umbilical cord (Ding et al., 2011). These cells are highly plastic, retaining the potential to generate chondroblasts, adipocytes, and osteoblasts (Caplan, 1991; Dominici et al., 2006; Afanasyev et al., 2010; Keating, 2012). In order to characterize the cells isolated from Wharton's jelly umbilical cord, we first evaluated the expression of MSC-specific antigens using flow cytometry. Virtually all cells exhibited expression of CD105, CD73, and CD90 markers, and lacked the expression of hematopoietic lineage markers, such as CD14, CD34, and CD45 (Supplementary Figures 1A–I). The MSCs also demonstrated capacity for osteogenic, adipogenic, and chondrogenic differentiation (Supplementary Figures 1J–L). Given this versatility, we hypothesized that expression of neurogenic transcription factors in MSCs could directly reprogram these cells into neurons. To test this possibility, we transfected plasmids carrying the genes encoding for *Sox2*, *Neurog2,* or *Ascl1* into human umbilical cord mesenchymal stem cells (hUCMSCs) using lipophilic cationic reagent. To monitor transduced cells, all vectors carried a fluorescent protein (GFP or DsRed) under control of an internal chicken β-actin promoter with cytomegalovirus enhancer (pCAG). Vectors expressing GFP or DsRed alone were used as control (**Figures 1A,B**). One day after transfection, cultured medium of hUCMSCs was replaced with neuronal differentiation medium containing B27. In this medium, most transfected hUCMSCs underwent cell death precluding analysis of lineage reprogramming (Supplementary Figure 2). To overcome this limitation, we co-cultured neonatal mouse hippocampal cells with hUCMSCs. We found an average of about 50% GFP+/DsRed+ hUCMSC per field 15 days after transfection and in the presence of co-cultured neonatal mouse hippocampal cells. In contrast, the average number of GFP+/DsRed+ hUCMSCs in the absence of co-cultured cells was <4% (Supplementary Figure 2). Low number of cells was also observed in Hucmsc cultures transfected with control plasmids, indicating that the cell death under these culture conditions was independent of lineage-reprogramming. It is likely that the withdrawal of serum performed after transfection (aiming at the differentiation of induced neurons) affects the survival of hUCMSCs, whereas addition of co-cultured cells, somehow, counteracts this cell-death effect. We, therefore, concluded that co-cultures are necessary to support hUCMSC in the culture conditions used.

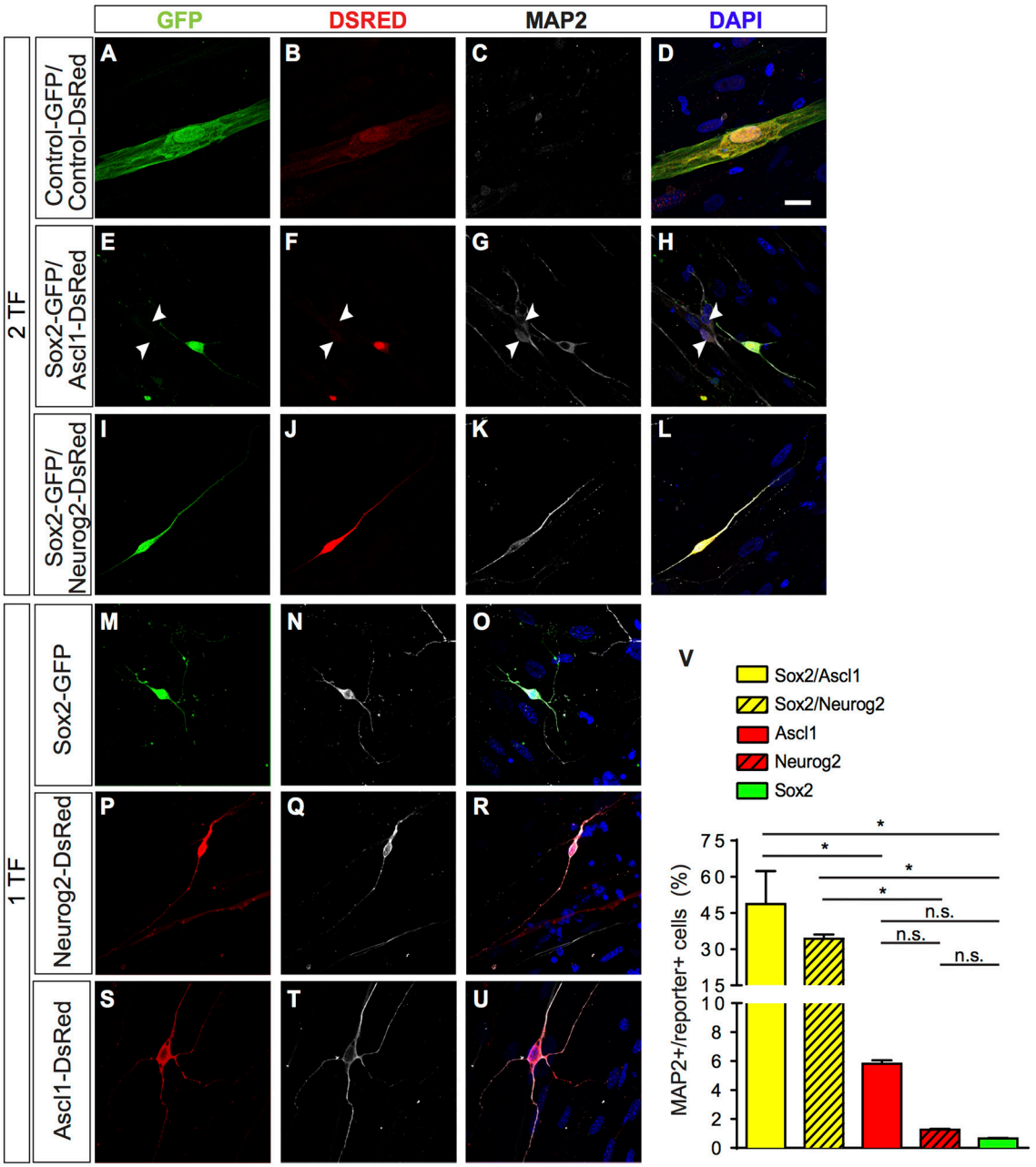

FIGURE 1 | Direct lineage reprogramming of hUCMSC into iN by forced expression of *Sox2, Ascl1*, or *Neurog2* alone, *Sox2/Ascl1* or *Sox2/Neurog2*. **(A–U)** Immunostaining for DSRED (red), GFP (green), MAP2 (white), and DAPI (blue), 15 days post transfection (dpt). Scale bar represents 20μm. **(A–D)** Example of hUCMSC transfected with control plasmids encoding only reporter proteins GFP and DSRED. Note that cell displayed classical mesenchymal cell morphologies and did not express MAP2. **(E–H)** Example of hUCMSC transfected with *Sox2* and *Ascl1* (white arrows indicate hippocampal neurons expressing MAP2). **(I–L)** hUCMSC transfected with *Sox2* and *Neurog2*. **(M–O)** hUCMSC transfected with only *Sox2*. **(P–R)** hMSC transfected with only *Neurog2*. **(S–U)** hUCMSC transfected with only *Ascl1*. **(V)** Histograms show the percentage of induced neurons, measured by the number of expressing MAP2 cells over the total number of reporter positive cells. Data are presented as mean ± s.e.m. from three independent experiments. ANOVA followed by Dunn's post-hoc test, $^*p < 0.05$; no statistically significant difference (n.s.). hUCMSC transfected with control plasmids did not express MAP2, thereby the bar is not being shown.

A few days after transfection, we observed that some hUCMSCs transfected with proneural genes acquired neuronal-like morphology. To confirm this possible lineage conversion of hUCMSCs into iNs, we further analyzed the expression of the neuronal-specific microtubule-associate protein 2 (MAP2) 15 days after transfection with proneural genes (**Figure 1**). A fraction of cells transfected with proneural genes expressed MAP2 and acquired small-round cell bodies and thin and

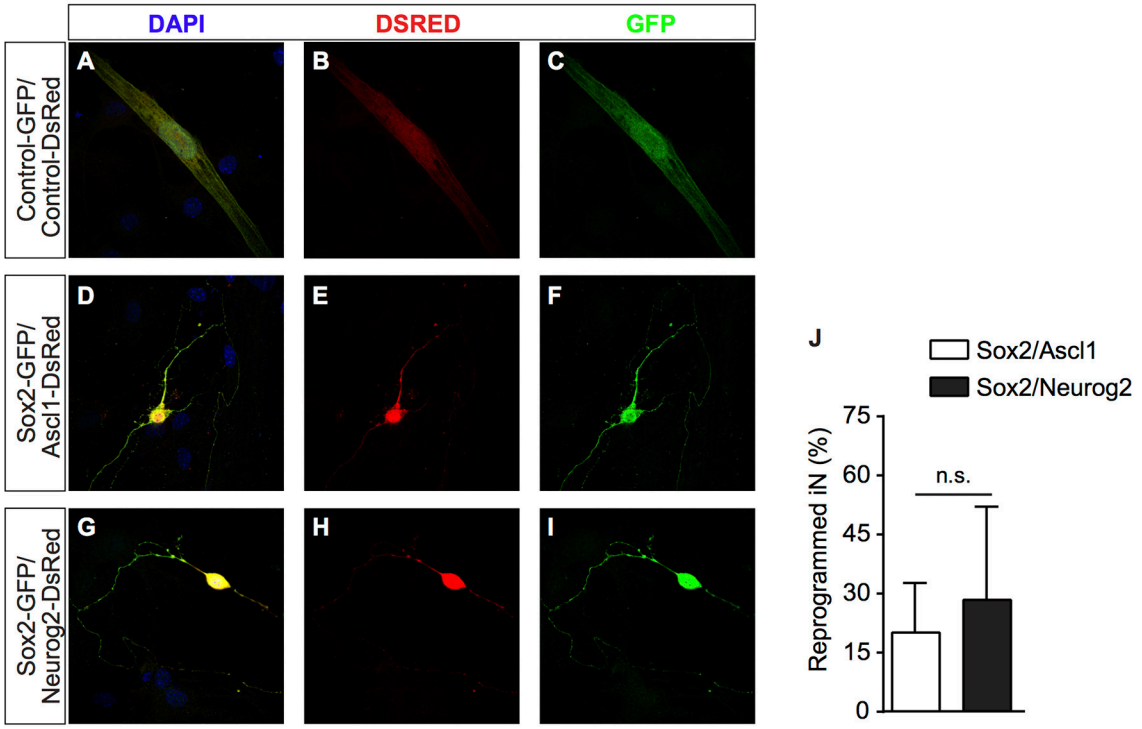

FIGURE 2 | After transfection, cells were grown on astrocyte monolayers which provide support to hUCMSCs-derived iNs. **(A–C)** hUCMSCs transfected with control, **(D–F)** *Sox2/Ascl1*, or **(G–I)** *Sox2/Neurog2*. **(J)** Histogram shows the percentage of hUCMSCs-derived iNs. Data are presented as mean ± s.e.m. from three independent experiments, Student's unpaired *t*-test, no statistically significant difference (n.s.). hUCMSC transfected with control plasmids were not reprogramed into induced neurons, therefore the bar is not being shown.

long processes, resembling immature neurons. Whereas, hUCMSCs transfected with control plasmids displayed classical mesenchymal cell morphologies and did not express MAP2 (**Figures 1A–U**). Expression of *Sox2*, *Ascl1*, or *Neurog2* alone was sufficient to reprogram hUCMSCs into iNs, albeit at low rates (**Figure 1V**). However, the combination of *Sox2* and *Ascl1* increased the efficiency of reprogramming up to 49%, whereas the combination of *Sox2* and *Neurog2* increased the efficiency up to 35% (**Figure 1V**). We obtained these results using Wharton's jelly mesenchymal stem cells isolated from tree different donors and did not observed any heterogeneity in the potential of reprogramming (data not shown). These data indicate that single proneural TFs have potential to elicit lineage reprogramming of hUCMSCs into iNs, but that the synergistic action of the TFs *Sox2/Ascl1* or *Sox2/Neurog2* is sufficient to induce neuronal phenotype in a high number of hUCMSCs.

It has been shown that cells from the mesenchymal lineage can fuse with other cell types in culture (Terada et al., 2002; Alvarez-Dolado et al., 2003). To rule out the possibility that hUCMSCs could be fusing with mouse hippocampal neurons present in our co-cultures, we performed similar experiments co-culturing reprogrammed hUCMSCs with purified postnatal mouse cortical astrocytes (Heinrich et al., 2011). Similar to cultures containing neonatal hippocampal cells, we observed that hUCMSCs transfected with *Sox2/Ascl1* or *Sox2/Neurog2* survived in astrocyte monolayers and acquired neuronal-like morphologies (**Figures 2A–I**). Thus, lineage reprogramming of hUCMSCs into iN after *Sox2/Ascl1* or *Sox2/Neurog2* expression is unlikely to be attributed to cell fusion with primary co-cultured neurons. However, we observed a lower lineage conversion efficiency when plating hUCMSCs on astrocytes (**Figure 2J**) compared to hippocampal cells suggesting that additional factors released by co-cultured neurons may affect either the reprogramming efficiency or survival of iNs.

Functional Properties of Induced Neurons

To investigate if iNs could establish synaptic connections with neighboring neurons, we studied the dynamics of calcium transients using calcium sensitive dye imaging (Rosenberg and Spitzer, 2011). We measured the spontaneous changes in fluorescence intensity ($\Delta F/F0$) during the total period of imaging (17 s) and compared their responses with primary murine hippocampal neurons. We found that both human iNs and mouse hippocampal neurons present in the co-culture displayed fast calcium-transients as indicated by rapid variations in the fluorescence (**Figures 3A–I**, Supplementary Movies 1, 2). The iNs reprogrammed with *Sox2/Ascl1*, *Sox2/Neurog2*, and the mouse hippocampal neurons showed a mean variation in fluorescence intensity of 39.66% (**Figure 3J**, gray bar), 33.05% (**Figure 3J**, blue bar), of 60.83% (**Figure 3J**, white bar), respectively. In contrast, the change in fluorescence intensity observed in hUCMSCs transfected with control plasmids presented a mean value of

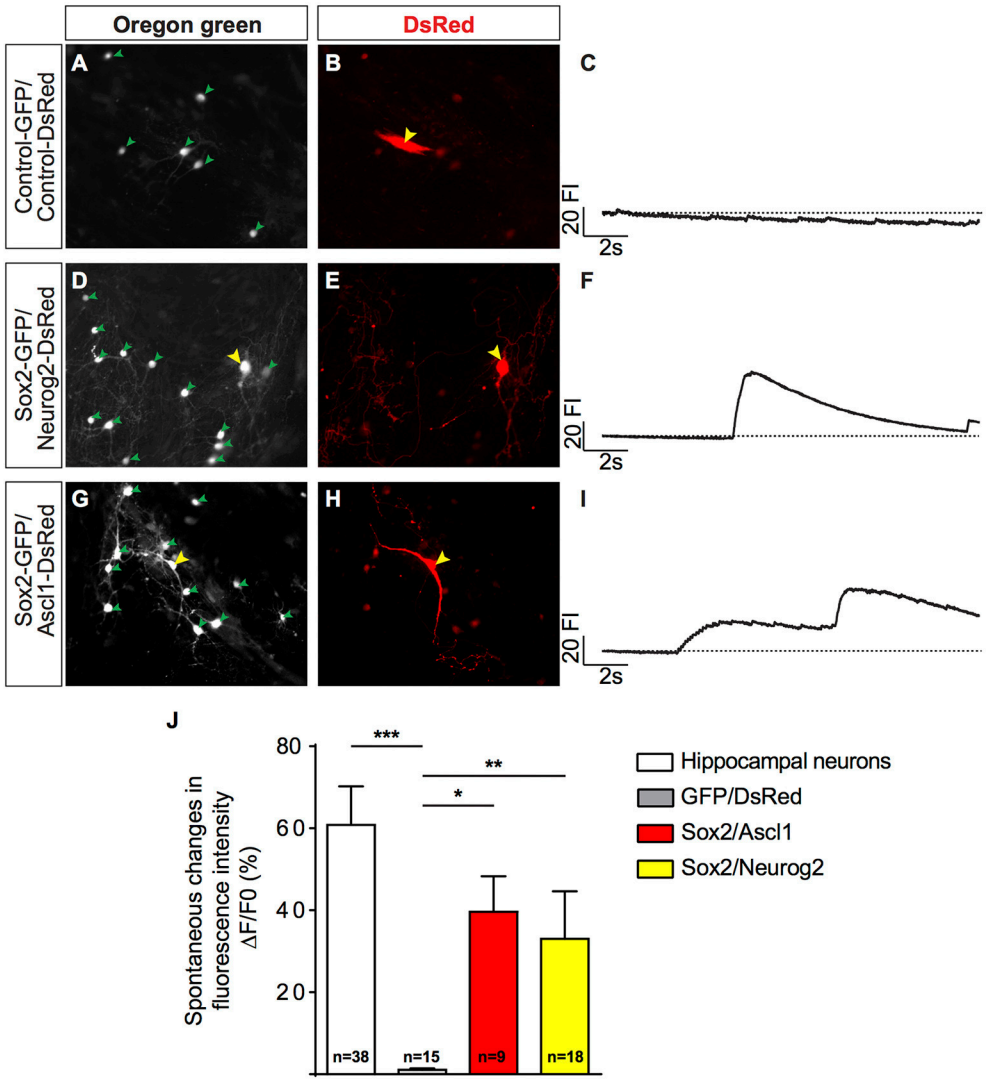

FIGURE 3 | Human MSC lineage-converted iNs show fast calcium transients. **(A,B)** hUCMSCs transfected with control plasmids encoding only reporter proteins GFP and DSRED 23 dpt (yellow arrow). **(D,E)** hUCMSCs transfected with *Sox2* and *Neurog2* with neuronal morphology 23 dpt (yellow arrow). **(G,H)** Example of hUCMSCs transfected with *Sox2* and *Ascl1* with neuronal morphology 23 dpt (yellow arrow). Note the presence of mouse hippocampal neurons (green arrowheads) in the same fields. **(C,F,I)** Representative traces of time course calcium-transients of transfected hUCMSCs are shown by spontaneous variations in the fluorescence intensity (FI). **(J)** Histograms show the mean change in fluorescence of mouse hippocampal neurons and iNs. Responses were calculated as the change in fluorescence (1F) over the initial fluorescence (F0). Number of cells analyzed is indicated in the bars for each group. (ANOVA followed by Tukey's *post-hoc* test, $^{*}p < 0.05$; $^{**}p < 0.01$; $^{***}p < 0.001$).

1.1% (**Figure 3J**, black bar), significantly lower than the responses observed in iNs and hippocampal neurons (ANOVA followed by Tukey's post-test, $p < 0.0001$). These observations indicate that hUCMSCs-derived iNs present fast calcium transients qualitatively similar of those observed in primary neurons.

Notably, this sudden increase in fluorescence intensity in hUCMSC-derived iNs was temporally synchronized mouse hippocampal neurons in the same field of observation (**Figures 4A–I**). To quantify this phenomenon, we measured the percentage of hippocampal neurons showing elevation in the fluorescence intensity within a time-range (ms) of the fluorescence fluctuation observed in a single iN within the same field of observation. The time of the iN calcium transient was considered as $t = 0$. We found that the majority of mouse hippocampal neurons showed changes in fluorescence intensity within 15 ms of fluctuations observed in iNs (**Figure 4J**), indicating a strong synchronization of calcium transients among primary neurons and iNs. Such a strong synchronization within the frame of milliseconds may suggest that cells are synaptically connected (Dawitz et al., 2011). To further confirm that hUCMSCs-derived iNs could receive synaptic inputs, we performed patch clamp recordings on these cells.

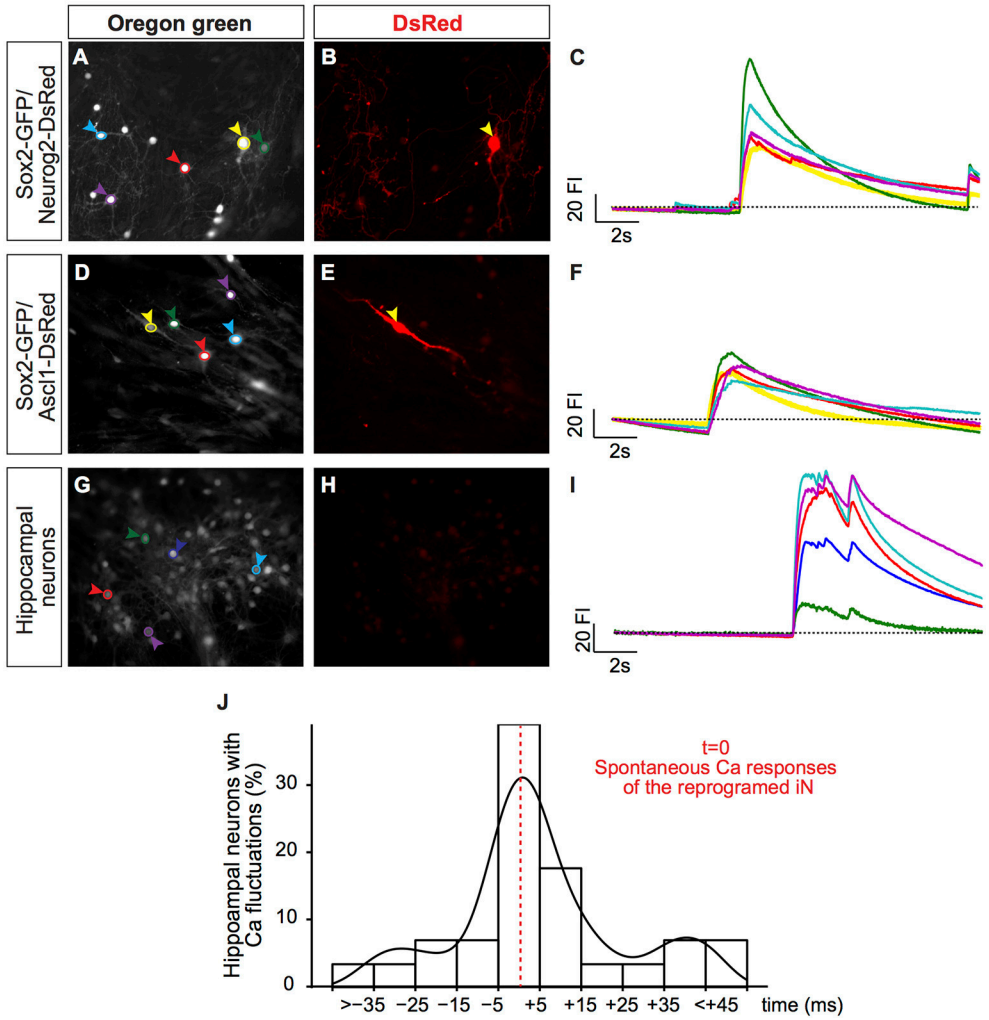

FIGURE 4 | Synchronization of calcium transients between iNs and primary neurons. **(A,D,G)** Photomicrographs show hUCMSC cultures 23 dpt and labeled with BAPTA Oregon Green. Colored circles delimit the regions of interest (ROI) where fluorescence intensity (FI) was measured (colored arrowheads). **(B,E,H)** Photomicrographs of the same fields show DsRed expression. Yellow arrowheads **(A,B, D,E)** point to hUCMSC-derived iNs. Blue, red, green and purple arrowheads point to primary hippocampal neurons. **(C,F,I)** Graphics show spontaneous calcium transients. The color of ROIs in the left panel **(A,D,G)** corresponds to the color of each trace in the right panel **(C,F,I)**. The traces show spontaneous variations in the FI during 17s of recording. **(J)** Histogram shows percentage of hippocampal neurons that respond within a range time difference (ms) in the same area, $t = 0$ was considered the time of spontaneous calcium responses of the reprogrammed iN present in the same field of imaging. Density curve is represented in black.

We performed patch-clamp recordings on iNs reprogrammed with one transcription factor (1 TF; $n = 5$) and compared their active and passive properties to cells reprogrammed with two transcription factors (2 TF; $n = 10$). Cells with 1 TF had a mean input resistance of 726 ± 119 MΩ, resting membrane potential of −61 ± 2 mV and capacitance of 22 ± 2 pF. Out of the 5 cells, 2 responded with regular spiking pattern (**Figure 5A**, top left), 1 responded with startle onset (**Figure 5A**, top right), and 2 with a spikelet in response to depolarizing current injections (0–100 pA, 400 ms, with 10 pA increments). Spikes were analyzed for action potential amplitude, action potential half-width and afterhyperpolarization amplitude. Spikes of cells with 1 TF had a mean action potential amplitude of 44 ± 8 mV, action potential half-width of 13 ± 0.5 ms and afterhyperpolarization amplitude of −6 ± 2 mV (**Figure 5C**). In comparison, cells reprogrammed with 2 TF had a mean input resistance of 605 ± 110 MΩ ($p = 0.51$), resting membrane potential of −59 ± 2 mV ($p = 0.54$) and capacitance of 26 ± 1 pF ($p = 0.13$). Of the 10 cells with 2 TF, 6 responded with regular spiking pattern and 4 responded with startle onset (0–100 pA, 400 ms, with 10 pA increments). Spikes of cells with 2 TF had a mean action potential amplitude of 76 ± 3 mV ($p = 0.0004$), action potential half-width of 4 ± 1 ms ($p = 0.0006$) and afterhyperpolarization amplitude of −11 ± 2 mV ($p = 0.22$; **Figure 5B**). While hyperpolarizing current injections (0 to −100 pA, 400 ms, with 10 pA decrements) caused some cells to rebound ($n = 3$), prominent membrane sags could only be detected in cells transfected with *Sox2/Neurog2* ($n = 7$; **Figure 5B**, right) suggesting that these cells have a sizeable

hyperpolarization-activated current. Comparing instantaneous and steady state voltage in response to negative current injections (−100 pA, 400 ms) showed a significant difference between instantaneous (−71 ± 2 mV) and steady state (−66 ± 1 mV) values ($p = 0.0427$).

We also observed spontaneous excitatory postsynaptic currents (EPSCs) in iN during voltage clamp (**Figure 5D**), suggesting that lineage-reprogrammed iNs could receive synaptic contacts from other neurons. We compared the first 100 events of 1 TF cells and 2 TF cells against each other. Postsynaptic currents of cells with 1 TF had an amplitude of 82 ± 9.7 pA and rise time of 11 ± 0.4 ms. The postsynaptic currents of cells with 2 TF had an amplitude of 86 ± 15.1 pA ($p = 0.8312$) and a mean rise time of 9 ± 0.3 ms ($p = 0.0211$).

Sox2/Neurog2 and *Sox2/Ascl1* Induce Different Neuronal Phenotypes in hUCMSCs

Next, we set out to evaluate the expression of messenger RNAs (mRNA) of genes commonly expressed in either hMSCs or neurons. To that, we collected single cells using a glass-micropipette, isolated the total mRNA, reverse transcribed, and pre-amplified cDNAs that were used in RT-qPCR reactions. We observed that the average expression level of common MSCs genes *THY1* and *PDGFB* was decreased in the iNs (Supplementary Figure 3A), whereas the expression of the neuronal genes *ATHO8* or *NEUROD1* increased after expression of *Sox2/Ascl1* or *Sox2/Neurog2* in hMSCs, respectively (Supplementary Figure 3B). Combined with our previous observations, these data indicate that hMSCs were effectively converted into iNs by forced expression of proneural TFs.

To evaluate the possible phenotypes adopted by hMSC-derived iNs, we analysed the expression of known genes expressed by cholinergic (*CHAT*), dopaminergic (*TH*), serotoninergic (*TPH2*), glutamatergic (*SLC17A7*), and GABAergic (*SLC32A1*) neurons, as well as genes encoding for transcription factors associated with specific classes of glutamatergic neurons within the cerebral cortex (*FEZF2* and *BCL11B*—corticofugal neurons; *TBR1*—cortico-thalamic neurons; *SATB2*—callosal neurons). Relative expression of these transcripts was calculated using a cycle of quantification cutoff (Cq-cutoff) and relative-quantities of cDNA molecule equation (Ståhlberg et al., 2013). Next, we used unsupervised PCA analysis to classify iNs obtained from hUCMSCs expressing either *Sox2/Neurog2* or *Sox2/Ascl1*. We observed that the expression levels of the transcripts for *CHAT, TH, TPH2, SLC17A7*, *SLC32A1, FEZF2*, *BCL11B, TBR1,* and *SATB2* could not clearly distinguish the two populations of cells (**Figure 6A**), indicating that similar genes were regulated by both combinations of TFs in hUCMSCs-derived iNs. Indeed, we observed that both *Sox2/Ascl1* and *Sox2/Neurog2* could induce the expression of genes associated with distinct neurochemical phenotypes in hUCMSCs-derived iNs, although some phenotypes were more commonly observed for a given TF combination. For instance, *Sox2/Ascl1* generated more iNs expressing high levels of *TPH2*, whereas *Sox2/Neurog2* generated more *CHAT* expressing iNs. Nevertheless, the expression of all transcripts analyzed was regulated by both combinations of TFs, suggesting that *Ascl1* and *Neurog2* do not have a unique role in the phenotypic specification of lineage reprogrammed hUCMSC-derived iNs (**Figure 6B**). These data suggest that the expression of *Sox2/Ascl1* or *Sox2/Neurog2* in hUCMSC activates a transcriptional program associated with loss of mesenchymal phenotype and acquisition of multiple neuronal phenotypes.

To further evaluate the neurochemical phenotypes of hUCMSC-derived iNs, we investigated the expression of SLC17A7 (Vesicular Glutamate Transporter 1 or VGLUT1) and SLC32A1 (GABA Vesicular Transporter or VGAT) using immunocytochemistry (**Figure 7**). We observed that only a few *Sox2/Ascl1*-derived iNs showed expression of VGAT fifteen days after reprogramming (**Figures 7I–L**), whereas most of the hUCMSC-derived iNs did not express any of these markers days after (**Figures 7M–Y**). Although iNs expressed MAP2 15 days after transfection with proneural genes (**Figure 1**), expression of vesicular neurotransmitter transporters is likely to occur at later stages of neuronal differentiation. Further analyses and immunostaining for other vesicular transporters isoforms are necessary to confirm the phenotypes of hUCMSCs-derived iNs.

DISCUSSION

Direct lineage reprogramming of human somatic cells into neurons is a promising strategy to advance cell-based therapies to treat neurological disorders, as well as to study the basic mechanisms of neuronal differentiation. In this work, we further expand the list of cells suitable for direct lineage reprogramming using transcription factors. More importantly, we show that combined expression of either *Neurog2*/*Sox2* or *Ascl1*/*Sox2* is sufficient to convert human MSCs into iNs displaying electrophysiological properties typical of neuronal cells. Finally, we show that these two combinations of transcription factors may elicit diverse and non-exclusive neuronal phenotypes in reprogrammed cells.

Human MSCs are versatile cells, capable of differentiation into adipocytes, chondrocytes, and osteoblasts (Horwitz et al., 2005; Dominici et al., 2006). This potential, combined with the fact that hMSC can be easily isolated from adult donors, has encouraged researchers to further exploit the versatility of reprogramming MSCs to other lineages, such as muscle and neural cells for therapeutic purposes (Fan et al., 2011; Kwon et al., 2016). However, the capacity to convert MSCs into fully functional neurons using extrinsic signals remains a matter of intense debate.

Here, we show that forced expression of *Ascl1*, *Neurog2,* or *Sox2* alone is sufficient to convert hUCMSCs into iNs expressing key neuronal proteins and exhibiting electrophysiological properties of mature neurons. Importantly, combination of *Neurog2* or *Ascl1* with *Sox2* significantly increases the rate of hUCMSC conversion into iNs (up to 35% with *Sox2/Neurog2* and 49% with *Sox2/Ascl1*). This efficiency is similar to the conversion

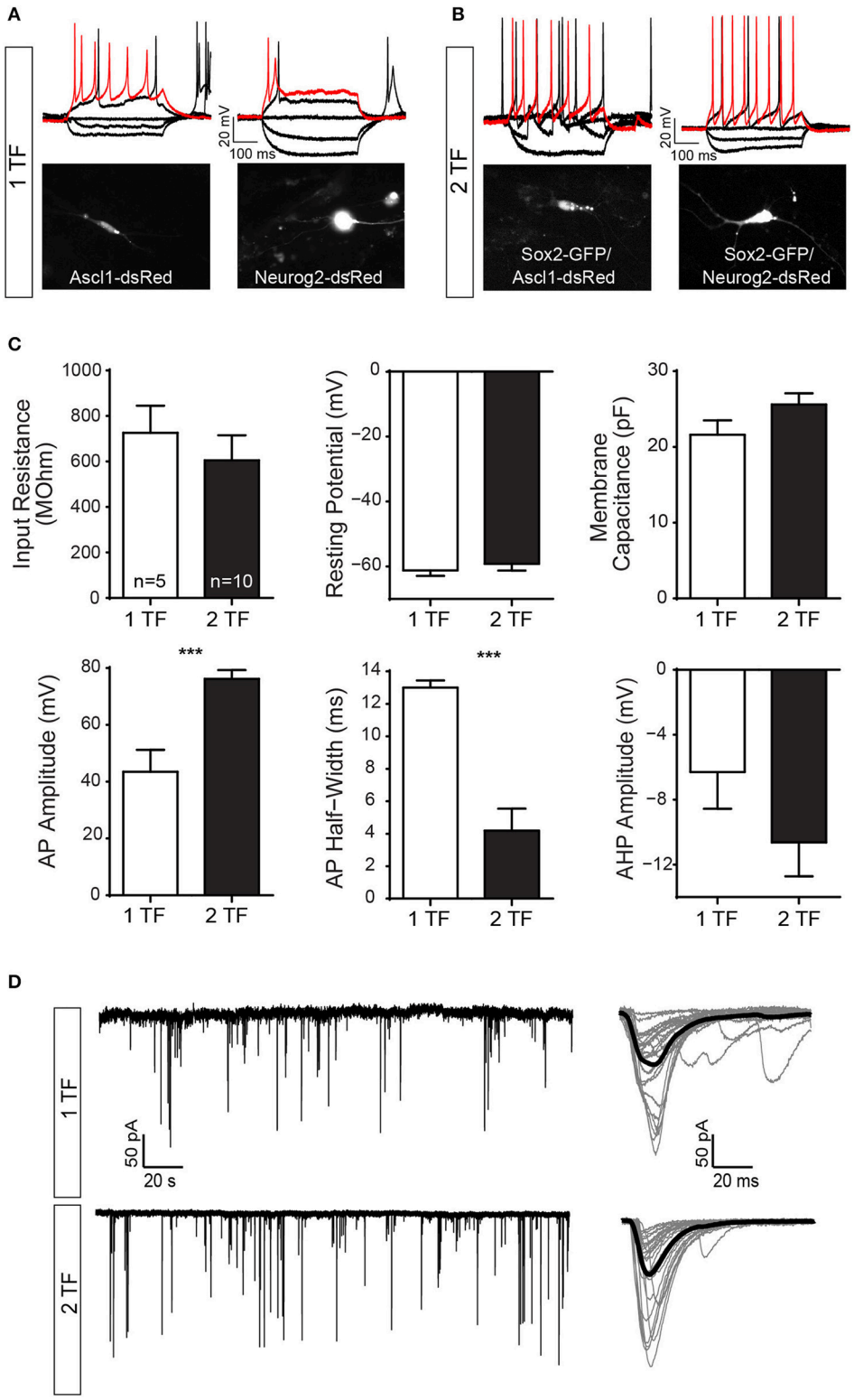

FIGURE 5 | hUCMSCs-derived iNs show electrical properties of mature neurons and establish synaptic contacts with co-culture mouse primary neurons. Electrophysiological properties of cells reprogrammed with one transcription factor (1 TF) compared to cells reprogrammed with two transcription factors (2 TF). **(A)** Current clamp traces from cells with 1 TF (left: *Ascl11*; right: *Neurog2*) showing regular spiking pattern (left), and startle onset (right) in response to depolarizing

(Continued)

FIGURE 5 | current injections [50 pA (black), 100 pA (red), 400 ms]. **(B)** Example of current clamp traces from cells with 2 TF (left: *Sox2/Ascl1*; right: *Sox2/Neurog2*) responding with a regular spiking pattern (black: 50 pA; red: 100pA; 400 ms). Note that hyperpolarizing current injections caused some cells to rebound (−50 and −100 pA, 400 ms). Fluorescence images of the recorded cells are displayed below. **(C)** Bar graphs showing mean and SEM input resistance, resting membrane potential and capacitance (top) as well as mean action potential (AP) amplitude, AP half-width and afterhyperpolarization (AHP) amplitude (bottom) for cells with 1 TF (white bars) and 2 TF (black bars) respectively (Student's unpaired *t*-test, $^{***}p < 0.001$). **(D)** Example of voltage clamp trace (free run) showing spontaneous EPSCs of a reprogramed 1TF iN (top, left) and a 2TF iN (bottom, left). Single postsynaptic currents are plot in gray (right) and the corresponding mean trace is shown in black ($n = 25$).

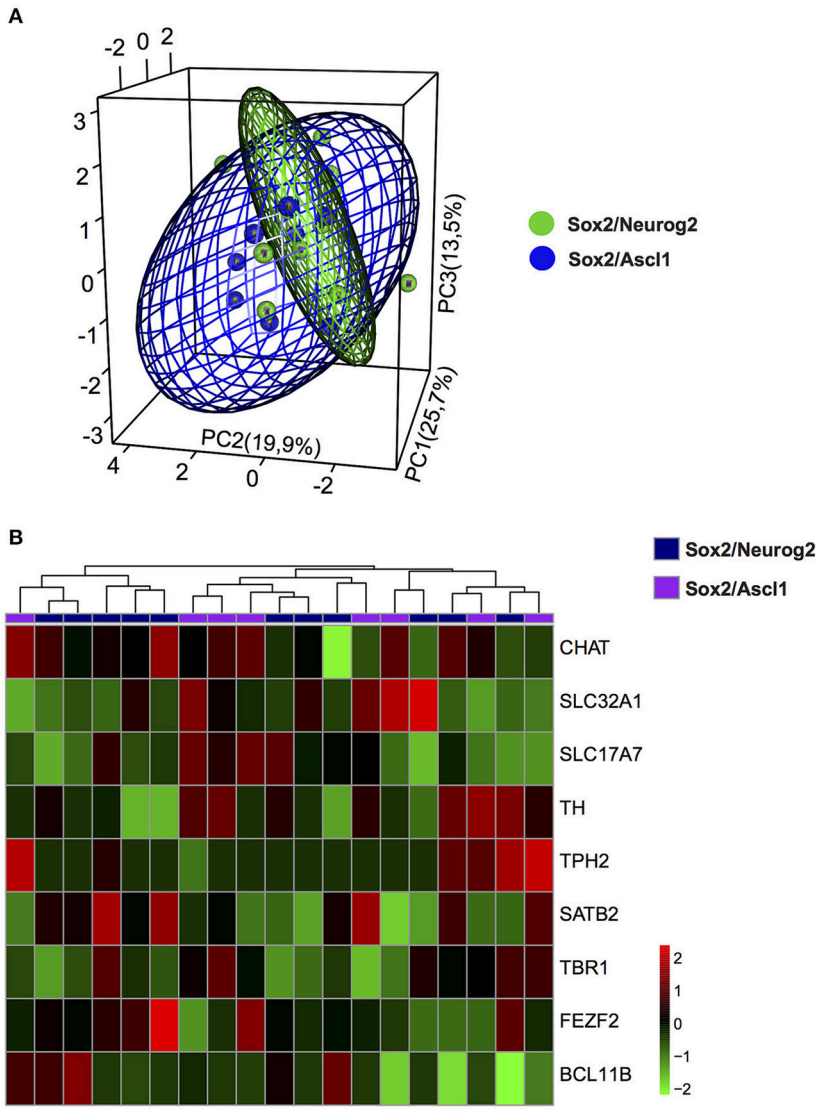

FIGURE 6 | Phenotypic specification of lineage reprogrammed hUCMSC-derived iNs. **(A)** Principal component analysis (PCA) of gene expression among cells reprogrammed with *Sox2/Neurog2* or *Sox2/Ascl1*. Genes used in the PCA are involved in neurotransmitter identity. Note the significant overlap between the two cell populations, suggesting that expression of either *Sox2/Neurog2* or *Sox2/Ascl1*/ may elicit similar neuronal phenotypes. **(B)** Heat map showing the relative expression of 9 genes involved in the specification of different neuronal phenotypes. Observe the variable expression of genes essential for the specification of distinct neurotransmitter identities in iNs derived from hUCMSCs lineage-converted through the expression of either *Sox2/Neurog2* or *Sox2/Ascl1*. Choline O-acetyltransferase (CHAT), Tyrosine hydroxylase (TH), Tryptophan hydroxylase 2 (TPH2), Vesicular Glutamate Transporter 1 (VGLUT1 or SLC17A7), GABA Vesicular Transporter (VGAT or SLC32A1), FEZ family zinc finger 2 (FEZF2), T-box brain 1 (TBR1), SATB homeobox 2 (SATB2), COUP-TF-Interacting Protein 2 (CTIP2 or BCL11B).

of human pericytes into iNs using *Sox2/Ascl1* (Karow et al., 2012) and significantly higher than the conversion rate of human fibroblasts into iNs using *Ascl1* or *Neurog2* alone (Chanda et al., 2014; Gascón et al., 2016) or the combination *Ascl1/Brn2/Myt1* (Caiazzo et al., 2011; Pang et al., 2011; Wapinski et al., 2013). However, the latter can be increased by using micro-RNAs, co-expression of *Bcl-2* and small molecule treatment (Yoo et al., 2011; Ladewig et al., 2012; Gascón et al., 2016).

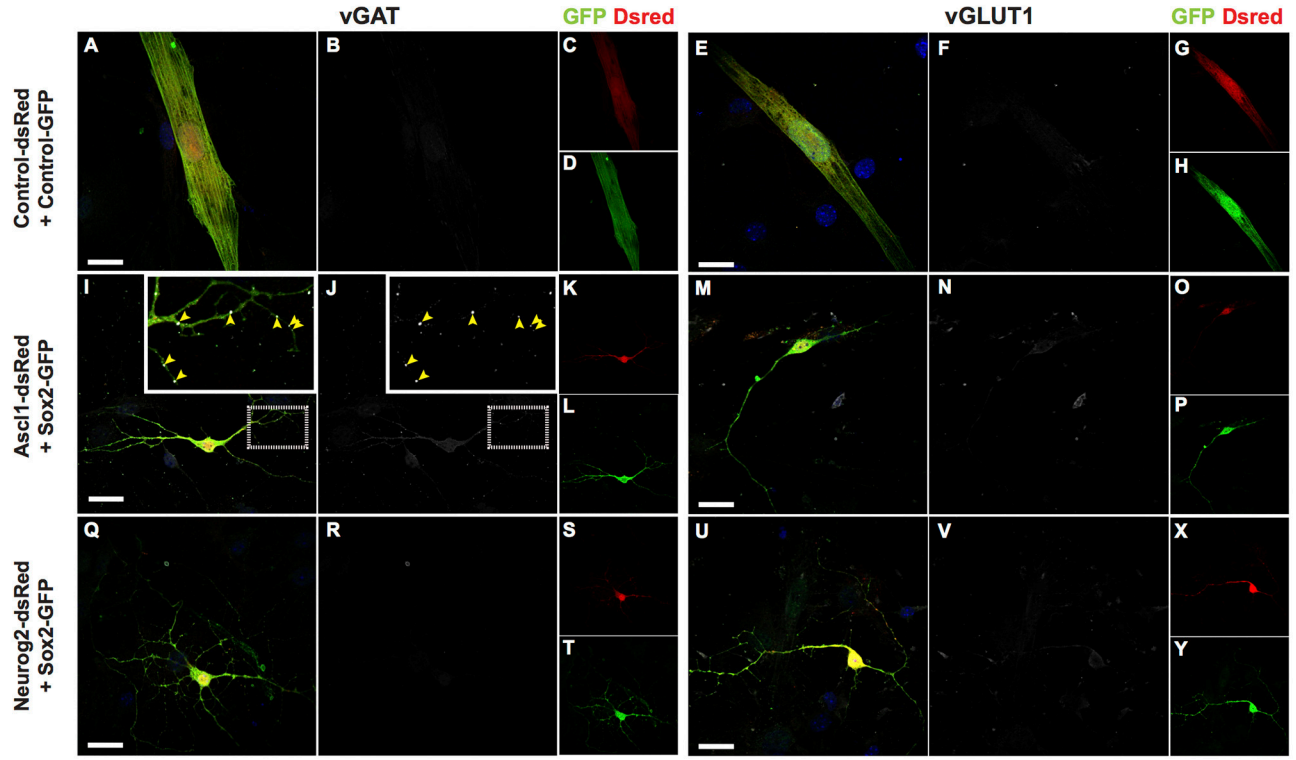

FIGURE 7 | Protein expression of vesicular transporters of lineage reprogrammed hUCMSC-derived iNs. Immunostaining for DSRED (red), GFP (green), vGAT (white; left panel) or vGLUT1 (white; right panel) and DAPI (blue), 15 days post transfection (dpt). Scale bar represents 20μm. **(A–H)** hUCMSC transfected with control plasmids encoding only reporter proteins GFP and DSRED. Note that cells displayed classical mesenchymal cell morphologies and did not express neither vGAT or vGLUT1. **(I–P)** hUCMSC transfected with *Sox2* and *Ascl1*. **(Q–Y)** hUCMSC transfected with *Sox2* and *Neurog2*. **(I,J)** Observe the expression of the vesicular GABA transporter (VGAT) in *Sox2/Ascl1*-derived iN (yellow arrows). The inset shows a high magnification view of the boxed area.

Single expression of *Ascl1* is sufficient to convert other human somatic cells into iNs (Chanda et al., 2014). This potential of *Ascl1* is attributed to its ability to recognize and bind to the regulatory elements of its target genes even when they are nucleosome-bound (Wapinski et al., 2017). In contrast, the same pioneering activity has not been shown to *Neurog2*, which is believed to bind exclusively to accessible regulatory elements within the genome. This could help to explain the prominent potential of *Neurog2* to lineage-reprogram astrocytes (Berninger et al., 2007; Heinrich et al., 2010; Chouchane et al., 2017) and pluripotent stem cells (Zhang et al., 2013) in comparison to mouse embryonic fibroblasts into iNs (Gascón et al., 2016).

Our results indicate that a fraction of hUCMSCs (1–2%) has an epigenetic state compatible with the binding of NEUROG2 to regulatory elements of neuronal genes, allowing for the conversion into iNs. However, combination with *Sox2*, which has a well-known role in chromatin modification of Neurog2-target genes (Amador-Arjona et al., 2015), largely increases the efficiency of neuronal conversion mediated by *Neurog2* (∼35%). Similarly, combination with *Sox2* increases the percentage of hUCMSCs converted by *Ascl1* into iNs by an order of magnitude. These observations suggest that key regulatory elements of neuronal genes identified by ASCL1 and NEUROG2 are not accessible in the vast majority of hUCMSCs cultured under the conditions described in this study.

In addition to the low frequency of neuronal conversion elicited in hUCMSC by forced expression of *Ascl1* or *Neurog2* alone, iNs also display electrophysiological properties less robust compared to iNs generated using *Sox2/Ascl1* or *Sox2/Neurog2*. In fact, the action potential of iNs reprogrammed with a single TF has a smaller amplitude and a shorter half-width as compared to iNs reprogrammed with 2 TFs (*Sox2/Ascl1* or *Sox2/Neurog2*), indicating that the latter express a more complete set of ion channels. It is possible that these differences represent a delay in the maturation of single-TF iNs. Alternatively, the combination of *Sox2/Ascl1* or *Sox2/Neurog2* may be necessary to induce the complete transcriptional cascade required for thorough neuronal maturation. Calcium transients are implicated in distinct aspects of neuronal differentiation by regulating neurotransmitter phenotype, dendritic morphology, and axonal growth and guidance (Rosenberg and Spitzer, 2011). While control-transfected hUCMSCs never displayed fast calcium transients, both *Sox2/Ascl1*- and *Sox2/Neurog2*-iNs showed spontaneous fast calcium transients, indicative of synaptic activity (Bonifazi et al., 2009). Likewise, the calcium transients of primary neurons and iNs are synchronized, suggesting that these cells are synaptically connected. Together, these findings suggest that hUCMSCs are lineage-converted into iNs capable of firing action potentials and establishing pre- and post-synaptic compartments.

The cellular and molecular mechanisms of direct lineage reprogramming remain largely unknown. It has been reported that the metabolic state is particularly important in direct neuronal reprogramming of somatic cells into iNs. Accordingly, co-expression of *Bcl2/Neurog2* or *Bcl2/Ascl1* greatly enhances the conversion efficiency of astrocytes into iNs by inhibiting lipid peroxidation, consistent with a caspase-independent role. Similarly, co-expression of *Bcl-2* alongside *Ascl1* improves the rates of lineage conversion of mouse embryonic fibroblast into iNs, demonstrating that the metabolic shift is necessary to support survival of lineage-converted iNs (Gascón et al., 2016). Our data suggest that mouse astrocytes and hippocampal neurons may contribute to enhance hUCMSCs survival during lineage conversion. Future experiments should elucidate whether Bcl2 co-expression or small molecules treatment would allow for the conversion of *Sox2/Neurog2*- or *Sox2/Ascl1*-iNs from hUCMSCs even in the absence of co-cultured cells.

Despite the large number of studies showing the conversion of human somatic cells into iNs, it remains largely unknown what is the phenotype of reprogrammed neurons (Ambasudhan et al., 2011; Pang et al., 2011; Son et al., 2011; Karow et al., 2012; Chanda et al., 2014; Hu et al., 2015). Moreover, it is still unclear whether different TFs could induce particular neuronal fates in lineage-converted cells. Here, we show that lineage-reprogrammed hUCMSCs generate iNs expressing genes associated with the acquisition of diverse neurotransmitter identities, regardless of the use of *Sox2/Ascl1* or *Sox2/Neurog2*. These different combinations of TFs can regulate similar sets of genes, suggesting that *Sox2/Ascl1* and *Sox2/Neurog2* are not sufficient to drive unambiguous neurotransmitter identities in hUCMSCs-derived iNs. However, the expression of genes associated with a specific neuronal phenotype is only an indication of the possible phenotype of the iNs. Future experiments using electrophysiological and pharmacological techniques are necessary to confirm the phenotypes of hUCMSCs-derived iNs.

According to the notion that *Neurog2* and *Ascl1* may be sufficient to induce a pro-neuronal program during somatic cell lineage reprogramming but not be sufficient to determine a specific phenotype of the iN, studies of the developing central nervous system reveal that those TFs may be associated with diverse neuronal phenotypes. For instance, while in the telencephalon, *Neurog2* plays important roles for the specification of glutamatergic neurons (Schuurmans and Guillemot, 2002). Progenitors in the cerebellum and spinal cord express *Neurog2* generate GABAergic and cholinergic neurons, respectively (Bertrand et al., 2002). Similarly, progenitors expressing *Ascl1* contribute to different neuronal lineages in the cerebral cortex, cerebellum, and retina (Chouchane and Costa, 2018). Most protocols aiming at obtaining fibroblast-derived iNs with a particular phenotype through direct lineage reprogramming require the use of several TFs (Victor et al., 2014; Blanchard et al., 2015).

Expression of either Ascl1 and Neurog2 in cortical astrocytes leads to the activation of transcriptional networks with only a small subset of shared target genes (Masserdotti et al., 2015), which could partly explain the role of those TFs in instructing different iNs phenotypes (Berninger et al., 2007; Heinrich et al., 2010). However, co-expression of Ascl1, Myt1L, and Brn2 induces a glutamatergic neuronal fate in fibroblast-derived iNs (Vierbuchen et al., 2010), whereas Neurog2 drives motor neuron differentiation associated with forskolin and dorsomorphin treatments in the same cells (Liu et al., 2013), suggesting that the fate-specification of iNs is not only dependent on the TF used. Recent work in our laboratory using direct lineage reprogramming of mouse astrocytes isolated from different brain regions further supports the versatile roles of *Neurog2* and *Ascl1* to affect the phenotypes of iNs (Chouchane et al., 2017). While cerebral cortex astrocytes reprogrammed into iNs with *Neurog2* adopt mostly a glutamatergic fate, cerebellum astrocyte-derived iNs show GABAergic phenotypes. Taken together, these data indicate that the cell of origin with its specific epigenetic landscape can influence the final fate of iNs.

A comprehensive understanding of the molecular mechanisms involved in the acquisition of particular neurochemical phenotypes will greatly improve the protocols for lineage reprogramming of human somatic cells into iNs, allowing for the generation of homogeneous neuronal populations that could be later used in cell-based therapies.

AUTHOR CONTRIBUTIONS

All authors reviewed the manuscript. JAMA contributed to design, performed most of the experiments, analyzed the data, discussed the results, and wrote the manuscript. DAC performed isolation and characterization of hUCMSC. SRBM assisted and provided financial support with isolation and characterization of hUCMSC. RNL performed electrophysiology experiments. MMH analyzed electrophysiology experiments data, discussed the results, and helped writing the manuscript. DCFG performed qPCR experiments. DM-C analyzed the single cell qPCR data. MRC provided financial support, directed the project, conceived the experiment, analyzed data, discussed the results, and wrote the manuscript.

FUNDING

This work was supported by Conselho Nacional de Desenvolvimento Científico e Tecnológico (CNPq) and Coordenação de Aperfeiçoamento de Pessoal de Nível Superior (CAPES).

ACKNOWLEDGMENTS

We thank Ana Raquel for her excellent technical help. The umbilical cord cells were obtained through the Laboratório de Biologia Molecular e Genômica (Natal, Brazil), we thank Susana Moreira and Tatiana Bressel for their assistance providing the cells.

SUPPLEMENTARY MATERIAL

The Supplementary Material for this article can be found online at: https://www.frontiersin.org/articles/10.3389/fncel.2018.00155/full#supplementary-material

REFERENCES

Afanasyev, B. V., Elstner, E. E., and Zander, A. R. (2010). A. J. Friedenstein, founder of the mesenchymal stem cell concept. *Cell. Ther. Transpl.* 1, 35–38. doi: 10.3205/ctt-2009-en-000029.01

Alvarez-Dolado, M., Pardal, R., Garcia-Verdugo, J. M., Fike, J. R., Lee, H. O., Pfeffer, K., et al. (2003). Fusion of bone-marrow-derived cells with Purkinje neurons, cardiomyocytes and hepatocytes. *Nature* 425, 968–973. doi: 10.1038/nature02069

Amador-Arjona, A., Cimadamore, F., Huang, C. T., Wright, R., Lewis, S., Gage, F. H., et al. (2015). SOX2 primes the epigenetic landscape in neural precursors enabling proper gene activation during hippocampal neurogenesis. *Proc. Natl. Acad. Sci. U.S.A.* 112, E1936–E1945. doi: 10.1073/pnas.1421480112

Ambasudhan, R., Talantova, M., Coleman, R., Yuan, X., Zhu, S., Lipton, S. A., et al. (2011). Direct reprogramming of adult human fibroblasts to functional neurons under defined conditions. *Cell Stem Cell* 9, 113–118. doi: 10.1016/j.stem.2011.07.002

Aoi, T., Yae, K., Nakagawa, M., Ichisaka, T., Okita, K., Takahashi, K., et al. (2008). Generation of pluripotent stem cells from adult mouse liver and stomach cells. *Science* 321, 699–702. doi: 10.1126/science.1154884

Berninger, B., Costa, M. R., Koch, U., Schroeder, T., Sutor, B., Grothe, B., et al. (2007). Functional properties of neurons derived from *in vitro* reprogrammed postnatal astroglia. *J. Neurosci.* 27, 8654–8664. doi: 10.1523/JNEUROSCI.1615-07.2007

Bertrand, N., Castro, D. S., and Guillemot, F. (2002). Proneural genes and the specification of neural cell types. *Nat. Rev. Neurosci.* 3, 517–530. doi: 10.1038/nrn874

Blanchard, J. W., Eade, K. T., Szucs, A., Lo Sardo, V., Tsunemoto, R. K., Williams, D., et al. (2015). Selective conversion of fibroblasts into peripheral sensory neurons. *Nat. Neurosci.* 18, 25–35. doi: 10.1038/nn.3887

Bonifazi, P., Goldin, M., Picardo, M. A., Jorquera, I., Cattani, A., Bianconi, G., et al. (2009). GABAergic hub neurons orchestrate synchrony in developing hippocampal networks. *Science* 326, 1419–1424. doi: 10.1126/science.1175509

Caiazzo, M., Dell'Anno, M. T., Dvoretskova, E., Lazarevic, D., Taverna, S., Leo, D., et al. (2011). Direct generation of functional dopaminergic neurons from mouse and human fibroblasts. *Nature* 476, 224–227. doi: 10.1038/nature10284

Caplan, A. (1991). Mesenchymal stem cells. *J. Orthop. Res.* 9, 641–650. doi: 10.1002/jor.1100090504

Chanda, S., Ang, C. E., Davila, J., Pak, C., Mall, M., Lee, Q. Y., et al. (2014). Generation of induced neuronal cells by the single reprogramming factor ASCL1. *Stem Cell Rep.* 3, 282–296. doi: 10.1016/j.stemcr.2014.05.020

Chouchane, M., and Costa, M. R. (2018). Instructing neuronal identity during CNS development and astroglial-lineage reprogramming: roles of NEUROG2 and ASCL1. *Brain Res.* doi: 10.1016/j.brainres.2018.02.045. [Epub ahead of print].

Chouchane, M., Melo de Farias, A. R., Moura, D. M. S., Hilscher, M. M., Schroeder, T., Leão, R. N., et al. (2017). Lineage reprogramming of astroglial cells from different origins into distinct neuronal subtypes. *Stem Cell Rep.* 9, 162–176. doi: 10.1016/j.stemcr.2017.05.009

Dawitz, J., Kroon, T., Hjorth, J. J., and Meredith, R. M. (2011). Functional calcium imaging in developing cortical networks. *J. Vis. Exp.* 56, 1–8. doi: 10.3791/3550

Ding, D.-C., Shyu, W.-C., and Lin, S.-Z. (2011). Mesenchymal stem cells. *Cell Transplant.* 20, 5–14. doi: 10.3727/096368910X

Dominici, M., Le Blanc, K., Mueller, I., Slaper-Cortenbach, I., Marini, F., Krause, D., et al. (2006). Minimal criteria for defining multipotent mesenchymal stromal cells. *Int. Soc. Cell. Ther. Posit. Stat. Cytother.* 8, 315–317. doi: 10.1080/14653240600855905

Duarte, D. M., Cornélio, D. A., Corado, C., Medeiros, V. K., de Araújo L. A., Cavalvanti, G. B. Jr. et al., (2012). Chromosomal characterization of cryopreserved mesenchymal stem cells from the human subendothelium umbilical cord vein. *Regen. Med.* 7, 147–157. doi: 10.2217/rme.11.113

Espejel, S., Roll, G. R., McLaughlin, K. J., Lee, A. Y., Zhang, J. Y., Laird, D. J., et al. (2010). Induced pluripotent stem cell-derived hepatocytes have the functional and proliferative capabilities needed for liver regeneration in mice. *J. Clin. Invest.* 120, 3120–3126. doi: 10.1172/JCI43267

Fan, C. G., Zhang, Q. J., and Zhou, J. R. (2011). Therapeutic potentials of mesenchymal stem cells derived from human umbilical cord. *Stem Cell Rev.* 7, 195–207. doi: 10.1007/s12015-010-9168-8

Gascón, S., Murenu, E., Masserdotti, G., Ortega, F., Russo, G. L., Petrik, D., et al. (2016). Identification and successful negotiation of a metabolic checkpoint in direct neuronal reprogramming. *Cell Stem Cell* 18, 396–409. doi: 10.1016/j.stem.2015.12.003

Hanna, J., Markoulaki, S., Schorderet, P., Carey, B. W., Beard, C., Wernig, M., et al. (2008). Direct reprogramming of terminally differentiated mature B lymphocytes to pluripotency. *Cell* 133, 250–264. doi: 10.1016/j.cell.2008.03.028

Heinrich, C., Blum, R., Gascón, S., Masserdotti, G., Tripathi, P., Sánchez, R., et al. (2010). Directing astroglia from the cerebral cortex into subtype specific functional neurons. *PLoS Biol.* 8:e373. doi: 10.1371/journal.pbio.1000373

Heinrich, C., Gascón, S., Masserdotti, G., Lepier, A., Sanchez, R., Simon-Ebert, T., et al. (2011). Generation of subtype-specific neurons from postnatal astroglia of the mouse cerebral cortex. *Nat. Protoc.* 6, 214–228. doi: 10.1038/nprot.2010.188

Horwitz, E. M., Le Blanc, K., Dominici, M., Mueller, I., Slaper-Cortenbach, I., Marini, F. C., et al. (2005). Clarification of the nomenclature for MSC: the International Society for Cellular Therapy position statement. *Cytotherapy* 7, 393–395. doi: 10.1080/14653240500319234

Hu, W., Qiu, B., Guan, W., Wang, Q., Wang, M., Li, W., et al. (2015). Direct conversion of normal and Alzheimer's disease human fibroblasts into neuronal cells by small molecules. *Cell Stem Cell* 17, 204–212. doi: 10.1016/j.stem.2015.07.006

Imamura, M., Aoi, T., Tokumasu, A., Mise, N., Abe, K., Yamanaka, S., et al. (2010). Induction of primordial germ cells from mouse induced pluripotent stem cells derived from adult hepatocytes. *Mol. Reprod. Dev.* 77, 802–811. doi: 10.1002/mrd.21223

Karow, M., Sánchez, R., Schichor, C., Masserdotti, G., Ortega, F., Heinrich, C., et al. (2012). Reprogramming of pericyte-derived cells of the adult human brain into induced neuronal cells. *Cell Stem Cell* 11, 471–476. doi: 10.1016/j.stem.2012.07.007

Keating, A. (2012). Mesenchymal stromal cells: new directions. *Cell Stem Cell* 10, 709–716. doi: 10.1016/j.stem.2012.05.015

Kuzmenkin, A., Liang, H., Xu, G., Pfannkuche, K., Eichhorn, H., Fatima, A., et al. (2009). Functional characterization of cardiomyocytes derived from murine induced pluripotent stem cells *in vitro*. *FASEB J.* 23, 4168–4180. doi: 10.1096/fj.08-128546

Kwon, A., Kim, Y., Kim, M., Kim, J., Choi, H., Jekarl, D. W., et al. (2016). Tissue-specific differentiation potency of mesenchymal stromal cells from perinatal tissues. *Sci. Rep.* 6, 1–11. doi: 10.1038/srep23544

Ladewig, J., Mertens, J., Kesavan, J., Doerr, J., Poppe, D., Glaue, F., et al. (2012). Small molecules enable highly efficient neuronal conversion of human fibroblasts. *Nat. Methods* 9, 575–578. doi: 10.1038/nmeth.1972

Liu, M. L., Zang, T., Zou, Y., Chang, J. C., Gibson, J. R., Huber, K. M., et al. (2013). Small molecules enable neurogenin 2 to efficiently convert human fibroblasts into cholinergic neurons. *Nat Commun* 4:2183. doi: 10.1038/ncomms3183

Marro, S., Pang, Z. P., Yang, N., Tsai, M. C., Qu, K., Chang, H. Y., et al. (2011). Direct lineage conversion of terminally differentiated hepatocytes to functional neurons. *Cell Stem Cell* 9, 374–382. doi: 10.1016/j.stem.2011.09.002

Masserdotti, G., Gillotin, S., Sutor, B., Drechsel, D., Irmler, M., Jørgensen, H. F., et al. (2015). Transcriptional mechanisms of proneural factors and REST in regulating neuronal reprogramming of astrocytes. *Cell Stem Cell* 17, 74–88. doi: 10.1016/j.stem.2015.05.014

Meissner, A., Wernig, M., and Jaenisch, R. (2007). Direct reprogramming of genetically unmodified fibroblasts into pluripotent stem cells. *Nat. Biotechnol.* 25, 1177–1181. doi: 10.1038/nbt1335

Mizuno, Y., Chang, H., Umeda, K., Niwa, A., Iwasa, T., Awaya, T., et al. (2010). Generation of skeletal muscle stem/progenitor cells from murine induced pluripotent stem cells. *FASEB J.* 24, 2245–2253. doi: 10.1096/fj.09-137174

Okita, K., Ichisaka, T., and Yamanaka, S. (2007). Generation of germline-competent induced pluripotent stem cells. *Nature* 448, 313–317. doi: 10.1038/nature05934

Pang, Z. P., Yang, N., Vierbuchen, T., Ostermeier, A., Fuentes, D. R., Yang, T. Q., et al. (2011). Induction of human neuronal cells by defined transcription factors. *Nature* 476, 220–223. doi: 10.1038/nature10202

Rosenberg, S. S., and Spitzer, N. C. (2011). Calcium signaling in neuronal development. *Cold Spring Harb. Perspect. Biol.* 3, 1–13. doi: 10.1101/cshperspect.a004259

Schuurmans, C., and Guillemot, F. (2002). Molecular mechanisms underlying cell fate specification in the developing telencephalon. *Curr. Opin. Neurobiol.* 12, 26–34. doi: 10.1016/S0959-4388(02)00286-6

Son, E. Y., Ichida, J. K., Wainger, B. J., Toma, J. S., Rafuse, V. F., Woolf, C. J., et al. (2011). Conversion of mouse and human fibroblasts into functional spinal motor neurons. *Cell Stem Cell* 9, 205–218. doi: 10.1016/j.stem.2011.07.014

Ståhlberg, A., Rusnakova, V., Forootan, A., Anderova, M., and Kubista, M. (2013). RT-qPCR work-flow for single-cell data analysis. *Methods* 59, 80–88. doi: 10.1016/j.ymeth.2012.09.007

Takahashi, K., and Yamanaka, S. (2006). Induction of pluripotent stem cells from mouse embryonic and adult fibroblast cultures by defined factors. *Cell* 126, 663–676. doi: 10.1016/j.cell.2006.07.024

Terada, N., Hamazaki, T., Oka, M., Hoki, M., Mastalerz, D. M., Nakano, Y., et al. (2002). Bone marrow cells adopt the phenotype of other cells by spontaneous cell fusion. *Nature* 416, 542–545. doi: 10.1038/nature730

Victor, M. B., Richner, M., Hermanstyne, T. O., Ransdell, J. L., Sobieski, C., Deng, P., et al. (2014). Generation of human striatal neurons by MicroRNA-dependent direct conversion of fibroblasts. *Neuroresource* 84, 311–323. doi: 10.1016/j.neuron.2014.10.016

Vierbuchen, T., Ostermeier, A., Pang, Z. P., Kokubu, Y., Südhof, T. C., and Wernig, M. (2010). Direct conversion of fibroblasts to functional neurons by defined factors. *Nature* 463, 1035–1041. doi: 10.1038/nature08797

Wapinski, O. L., Lee, Q. Y., Chen, A. C., Li, R., Corces, M. R., Ang, C. E., et al. (2017). Rapid chromatin switch in the direct reprogramming of fibroblasts to neurons. *Cell Rep.* 20, 3236–3247. doi: 10.1016/j.celrep.2017.09.011

Wapinski, O. L., Vierbuchen, T., Qu, K., Lee, Q. Y., Chanda, S., Fuentes, D. R., et al. (2013). Hierarchical mechanisms for direct reprogramming of fibroblasts to neurons. *Cell* 155, 621–635. doi: 10.1016/j.cell.2013.09.028

Wernig, M., Zhao, J. P., Pruszak, J., Hedlund, E., Fu, D., Soldner, F., et al. (2008). Neurons derived from reprogrammed fibroblasts functionally integrate into the fetal brain and improve symptoms of rats with Parkinson's disease. *Proc. Natl. Acad. Sci. U.S.A.* 105, 5856–5861. doi: 10.1073/pnas.0801677105

Yoo, A. S., Sun, A. X., Li, L., Shcheglovitov, A., Portmann, T., Li, Y., et al. (2011). MicroRNA-mediated conversion of human fibroblasts to neurons. *Nature* 476, 228–231. doi: 10.1038/nature10323

Zhang, Y., Pak, C., Han, Y., Ahlenius, H., Zhang, Z., Chanda, S., et al. (2013). Rapid single-step induction of functional neurons from human pluripotent stem cells. *Neuron* 78, 785–798. doi: 10.1016/j.neuron.2013.05.029

Conflict of Interest Statement: The authors declare that the research was conducted in the absence of any commercial or financial relationships that could be construed as a potential conflict of interest.

frontiers in Neuroscience

MINI REVIEW
published: 02 August 2018
doi: 10.3389/fnins.2018.00522

Mechanistic Insights Into MicroRNA-Induced Neuronal Reprogramming of Human Adult Fibroblasts

Ya-Lin Lu[1,2] *and Andrew S. Yoo*[1]*

[1] Department of Developmental Biology, School of Medicine, Washington University in St. Louis, St. Louis, MO, United States, [2] Program in Developmental, Regenerative and Stem Cell Biology, School of Medicine, Washington University in St. Louis, St. Louis, MO, United States

The use of transcriptional factors as cell fate regulators are often the primary focus in the direct reprogramming of somatic cells into neurons. However, in human adult fibroblasts, deriving functionally mature neurons with high efficiency requires additional neurogenic factors such as microRNAs (miRNAs) to evoke a neuronal state permissive to transcription factors to exert their reprogramming activities. As such, increasing evidence suggests brain-enriched miRNAs, miR-9/9* and miR-124, as potent neurogenic molecules through simultaneously targeting of anti-neurogenic effectors while allowing additional transcription factors to generate specific subtypes of human neurons. In this review, we will focus on methods that utilize neuronal miRNAs and provide mechanistic insights by which neuronal miRNAs, in synergism with brain-region specific transcription factors, drive the conversion of human fibroblasts into clinically relevant subtypes of neurons. Furthermore, we will provide insights into the age signature of directly converted neurons and how the converted human neurons can be utilized to model late-onset neurodegenerative disorders.

Keywords: microRNA, chromatin, neuronal conversion, reprogramming, neurogenesis, disease modeling, human neurons

OPEN ACCESS

Edited by:
Annalisa Buffo,
Università degli Studi di Torino, Italy

Reviewed by:
Dimitra Thomaidou,
Pasteur Hellenic Institute, Greece
Massimiliano Caiazzo,
Utrecht University, Netherlands

***Correspondence:**
Andrew S. Yoo
yooa@wustl.edu

Specialty section:
This article was submitted to Neurogenesis, a section of the journal Frontiers in Neuroscience

Received: *28 May 2018*
Accepted: *12 July 2018*
Published: *02 August 2018*

Citation:
Lu Y-L and Yoo AS (2018) Mechanistic Insights Into MicroRNA-Induced Neuronal Reprogramming of Human Adult Fibroblasts. Front. Neurosci. 12:522. doi: 10.3389/fnins.2018.00522

INTRODUCTION

Overcoming epigenetic barriers through direct cellular reprogramming has allowed scientists to rapidly acquire cell types of interest for regenerative therapies and disease modeling. Direct conversion of mouse fibroblasts into functional neurons have been demonstrated through the use of transcription factors (Vierbuchen et al., 2010; Son et al., 2011; Chanda et al., 2014; Blanchard et al., 2015). Empirically, however, obtaining mature human neurons from adult human fibroblasts with transcription factors have been challenging (Caiazzo et al., 2011). To enhance reprogramming efficiency and to promote neuronal maturation, small chemical molecules (Ladewig et al., 2012; Liu et al., 2013; Pfisterer et al., 2016; Smith et al., 2016) and RNA molecules, miRNAs (Ambasudhan et al., 2011; Yoo et al., 2011; Victor et al., 2014; Abernathy et al., 2017), have been used in conjunction with transcription factors to robustly generate functional neurons from human fibroblasts. The mechanism(s) by which miR-9/9* and miR-124 collectively drive robust neuronal fate conversion remains an ongoing investigation, but through examining transcriptome and

epigenetic changes at the genome-wide level, we attempt to elucidate how miRNAs promote the neuronal identity during direct conversion of human fibroblasts to neurons.

miRNAs AS POTENT CELL FATE REGULATORS

Traditionally, transcription factors, in particular, pioneer transcription factors, have been viewed as regulators and determinants of cell fate. With domains that can interact directly with chromatin and/or other modifier proteins, transcription factors have been widely used for cellular reprogramming (Iwafuchi-Doi and Zaret, 2014, 2016), including the generation of induced pluripotent stem cells (iPSC) from somatic cells (Takahashi and Yamanaka, 2006). Increasing studies across different cellular contexts have revealed that miRNAs are also potent cell fate regulators as miRNAs not only target large repertoire of genes in genetic networks but also epigenetic regulators necessary for the remodeling of the chromatin (Yoo et al., 2009; Ivey and Srivastava, 2010; Gruber and Zavolan, 2013; Rajman and Schratt, 2017). Subsequently, miRNAs have been used to generate iPSCs (Anokye-Danso et al., 2011), cardiomyocytes (Jayawardena et al., 2012), and neurons (Yoo et al., 2011) from fibroblasts.

miR-9/9* AND miR-124 ARE NEUROGENIC MOLECULES

The acquisition of neuronal fate requires the downregulation of the neuron-restrictive silencer factor (NRSF) or repressor element-1 silencing transcription factor (REST) that represses neuronal genes in non-neuronal cells, including the neuron-specific miRNAs, miR-9/9*, and miR-124 (miR-9/9*-124) (Lagos-Quintana et al., 2002; Lim et al., 2005; Conaco et al., 2006; Deo et al., 2006). Both miR-9/9* and miR-124 are highly abundant in neuronal tissues (Lagos-Quintana et al., 2002; Lim et al., 2005; He et al., 2012), and are essential for neuronal differentiation (Cheng et al., 2009; Dajas-Bailador et al., 2012; Xue Q. et al., 2016) and the maintenance of neuronal identity through the repression of anti-neural genes including cofactors of the REST complex, RCOR1 and SCP1 (Visvanathan et al., 2007; Packer et al., 2008). As overexpression of miR-9/9* (Leucht et al., 2008; Zhao et al., 2009) and/or miR-124 (Krichevsky et al., 2006; Cheng et al., 2009; Akerblom et al., 2012) in stem cells or neural progenitors resulted in the precocious acquisition of neuronal fate, demonstrating the function of miRNAs in the activation of neuronal program (Lim et al., 2005). Ectopic expression of miR-9/9*-124 was also shown to drive the direct conversion of primary human dermal fibroblasts into functional neurons (Yoo et al., 2011). Therefore, knockdown of REST is sufficient to promote neuronal identity in part due to miR-9/9*-124-dependent mechanisms (Drouin-Ouellet et al., 2017). Furthermore, miR-9/9*-124 orchestrates the reduction of REST protein stability during neuronal reprogramming to promote chromatin accessibility of neuronal loci (Lee et al., 2018) and induction of neuronal genes (Abernathy et al., 2017; Drouin-Ouellet et al., 2017; Lee et al., 2018). Interestingly, miR-124 alone has also been used in neuronal conversion with the help of transcription factors (Ambasudhan et al., 2011; Jiang et al., 2015). Here, we review current understanding of the properties of miR-9/9* and miR-124 in both developmental and cellular reprogramming contexts highlighting their synergistic roles in coordinating the molecular switching of several critical non-neuronal to neuronal components during mammalian neurogenesis. We will mainly focus on the molecular switches critical in epigenetic regulation such as chromatin remodeling and DNA methylation, and transcriptome dynamics such as alternative splicing underlying the adoption of the neuronal identity. Our discussion will also include molecular pathways that occur during *in vivo* neurogenesis and are also recapitulated in the miRNA-directed reprogramming of human fibroblasts into neurons for the successful overcoming of cell fate barriers.

miRNAs ORCHESTRATE THE COMPOSITION OF BAF CHROMATIN REMODELING COMPLEXES

Spatial and temporal reciprocity of homologous gene or isoform expression during neurogenesis is a recurring theme. Previous studies have indicated that the neurogenic and reprogramming activity of miR-9/9* and miR-124 may be in part through the direct targeting of subunits of the ATP-dependent BRG/BRM associated factor (BAF) chromatin remodeling complexes (Yoo et al., 2009; Staahl and Crabtree, 2013; Staahl et al., 2013). Mammalian BAF complexes are large multi-subunit complexes combinatorically assembled in a cell type-dependent manner. The combinatorial assembly of different homologs and splice variants of BAF subunit families confers functional specificity as each subunit contains functional domains that recognized DNA and/or modified histones (Wu et al., 2009; Zheng et al., 2012). For example, embryonic stem cell (ESC) BAF (esBAF) is characterized by BAF53a and a homodimer of BAF155, as opposed to a heterodimer of BAF155 and BAF170 in differentiated cells (Wang et al., 1996a,b; Ho et al., 2009b). The esBAF complex is involved in maintaining pluripotency by establishing an ESC-specific chromatin state permissive for transcription factors and signaling molecules to access ESC-associated genes (Ho et al., 2009a; Kidder et al., 2009). Although BAF complexes are traditionally known to antagonize the function of polycomb repressive complexes (PRC) to promote chromatin accessibility for gene activation (Kennison, 1995; Ho et al., 2011), studies have also suggested that BAF complexes can synergize with PRC for gene regulation (Ho et al., 2011).

The BAF complex is crucial for mammalian nervous system as mutations in BAF subunits have been implicated in neurological disorders such as Coffin-Siris syndrome due to mutations in BRG1 and BRM (Tsurusaki et al., 2012; Ronan et al., 2013), and SS18L1/CREST in amyotrophic lateral sclerosis (ALS) (Chesi et al., 2013). During neural development, several BAF complex subunit switches to form the neuron-specific BAF (nBAF) complex (Staahl and Crabtree, 2013). The assembly

of the nBAF complex requires the switching of progenitor subunits (BAF53a, BAF45a, and SS18) to neuronal subunits (BAF53b, BAF45b or BAF45c, and SS18L1/CREST) between the proliferating ventricular zone and the post-mitotic zone (Olave, 2002; Lessard et al., 2007; Wu et al., 2007; Yoo et al., 2009; Staahl et al., 2013). These molecular switches also occur during miRNA-mediated direct conversion of human fibroblasts into neurons (Staahl et al., 2013), in which the reciprocal switching of BAF53a to BAF53b is directly orchestrated by miR-9/9* and miR-124 (Yoo et al., 2009; Staahl et al., 2013; **Figure 1**). The assembly of the nBAF complex is essential for proper neuronal function in learning and memory as loss of function of either BAF53b or SS18L1/CREST dramatically reduced dendritic outgrowth and morphology (Aizawa et al., 2004; Wu et al., 2007; Staahl et al., 2013; Vogel-Ciernia et al., 2013). The function of chromatin remodeling by BAF complex was also found to be critical for neuronal reprogramming as loss of BRG1 during miRNA-mediated

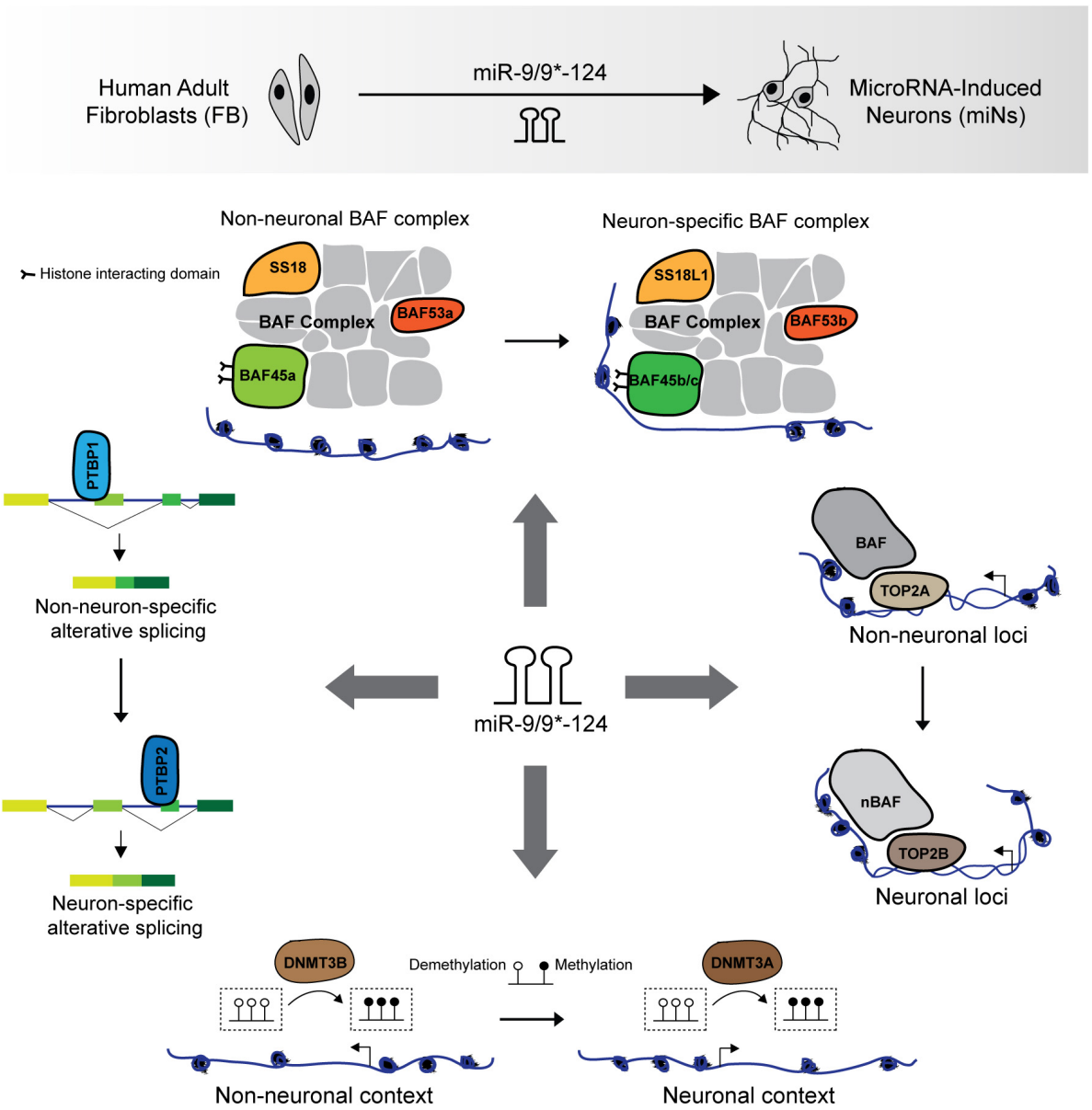

FIGURE 1 | MiR-9/9*-124-mediated neuronal reprogramming of human adult fibroblasts. Ectopic expression of miR-9/9*-124 in human adult fibroblasts leads to the switching of several non-neuronal to neuronal components for neural fate acquisition. MiRNAs orchestrate the genetic switching of epigenetic regulators including the BAF complex subunits (BAF53a, BAF45a, and SS18 to BAF53b, BAF45b/c, and SS18L1/CREST), TOP2A to TOP2B, and DNMT3B to DNMT3A. These coordinated molecular switches underlie the establishment of a neuronal epigenetic landscape during neuronal reprogramming. Additionally, the switching of PTB proteins, from PTBP1 to PTBP2, mediated by miR-124 activates neuron-specific alternative splicing program.

reprogramming abolished the chromatin landscape permissive to the activation of the neuronal program (Abernathy et al., 2017).

SWITCHING OF CHROMATIN MODIFIERS ARE CRUCIAL FOR CELL FATE CONVERSION

The switching of other homologous epigenetic regulators also occur during neurogenesis and neuronal reprogramming, though may not be direct targets of miR-9/9*-124. These include the switching of DNA topoisomerase II (TOP2) that functions to decatenate and catenate chromatin, from non-neuronal TOP2A to neuronal TOP2B (Watanabe et al., 1994; Tsutsui et al., 2001a; Tiwari et al., 2012; Thakurela et al., 2013). TOP2A is expressed in mitotic cells and interacts with BAF complexes to modulate chromatin accessibility (Tsutsui et al., 2001b; Dykhuizen et al., 2013; Wijdeven et al., 2015; Miller et al., 2017). On the other hand, TOP2B is required for neuronal differentiation *in vitro* and *in vivo* (Yang, 2000; Tsutsui et al., 2001b; Tiwari et al., 2012). Consistent with neuronal differentiation, miR-9/9*-124 instruct the similar switch of TOP2 homologs during neuronal reprogramming of human adult fibroblasts by inducing a rapid reduction of TOP2A in fibroblasts for the selective expression TOP2B in converted neurons (Abernathy et al., 2017; **Figure 1**).

Similarly, the reconfiguration of the epigenetic landscape during neuronal reprogramming also involves changes in DNA methylation patterns (Abernathy et al., 2017). Regarding the reprogramming activities of the miRNAs, it has been shown that ectopic expression of miR-9/9*-124 in fibroblasts recapitulated the molecular switching of *de novo* methyltransferases, DNMT3B to DNMT3A, similarly, to neural differentiation *in vivo* (Feng et al., 2005; Watanabe et al., 2006; Abernathy et al., 2017; **Figure 1**). DNMT3A has been implicated in various aspects of neuronal development, including synaptic plasticity (Feng et al., 2010; Colquitt et al., 2014), but it remains unclear how DNMT3A modulates gene expression in the nervous system. Although DNA methylation is viewed as a repressive mark, methylation marks deposited by DNMT3A have also been associated with enhanced gene expression through antagonizing PRC2 activity (Wu et al., 2010). The dramatic change in DNA methylation profile in miRNA-induced neurons also involves the induction of a family of demethylase, ten–eleven translocation (TET) family proteins (TET1/2/3) (Abernathy et al., 2017), implicated in neuronal development (Hahn et al., 2013; Zhang et al., 2013). It should be noted, however, what additional molecules interact with DNMT3A and TET proteins during neuronal reprogramming to influence DNA methylation at specific loci remains largely unknown.

Although the mechanisms underlying the switching of epigenetic effectors remain to be precisely defined, it is clear that miR-9/9*-124 promote neuronal identity during the direct reprogramming of human fibroblasts through establishing an epigenetic state permissive for the downstream acquisition of neuronal fate. The reciprocal temporal and spatial switching of chromatin modifiers observed both during neurogenesis and neuronal reprogramming highlight the complex and dynamic epigenetic regulations required to overcome cell fate barriers.

miR-124-MEDIATED PTB SWITCHING REGULATES NEURONAL SPLICING PROFILE

In addition to epigenetic regulators, post-transcriptional regulation of gene expression appears to be integral for neuronal reprogramming. The expression of PTB (polypyrimidine tract-binding) proteins, PTBP1 and PTBP2, are mutually exclusive and exhibit reciprocal switching during neural fate acquisition (Boutz et al., 2007). PTB proteins are RNA-binding proteins that bind to U-rich tracts primarily in introns for the post-transcriptional regulation of mRNAs, including alternative splicing (Wagner and Garcia-Blanco, 2001; Keppetipola et al., 2012). PTBP1 is expressed in non-neuronal cells and neural progenitors whereas the expression of its neuronal homolog, PTBP2 (nPTB), a splicing target of PTBP1, is primarily restricted to post-mitotic neurons in the nervous system (Boutz et al., 2007; Makeyev et al., 2007). PTBP1 represses PTBP2 expression by introducing a premature stop through the skipping of PTBP2 exon (Boutz et al., 2007). During development, the expression of miR-124 at the onset of neurogenesis mediates the switching of PTB proteins by targeting the 3′UTR of PTBP1, thereby alleviating PTBP1-mediated repression of PTBP2 in neurons (Makeyev et al., 2007). Although PTB proteins exhibit functional redundancy (Spellman et al., 2007), PTBP2 in neurons are essential for the proper splicing of various transcripts involved in neuronal function (Boutz et al., 2007; Licatalosi et al., 2012; Zheng et al., 2012; Li et al., 2014). Interestingly, ablating PTBP1 function in several cell types, including mouse embryonic fibroblasts, though insufficient in human fibroblasts, led to the direct conversion into neurons (Xue et al., 2013; Xue Y. et al., 2016), suggesting the significance of PTBP2 for the induction of neuronal fate. In addition to the activation of PTBP2 upon neural fate acquisition, PTBP2 level attenuates later in development for neuronal maturation (Li et al., 2014; Xue Y. et al., 2016). The attenuation of PTBP2 can be recapitulated with sequential knockdown of both PTB proteins resulting in the reprogramming of human fibroblasts into neurons (Xue Y. et al., 2016). The proposed mechanism is that PTBP2 reduction initiates a regulatory loop that activates downstream BRN2 for miR-9 expression, which dampens PTBP2 activity through 3′UTR targeting (Xue Y. et al., 2016). Altogether, PTBP2 level is dynamically regulated throughout neuronal differentiation and is essential as PTBP2 knockout results in neuronal death (Li et al., 2014).

THE USE OF miRNA-INDUCED NEURONAL GROUND STATE FOR SUBTYPE-SPECIFIC NEURONAL REPROGRAMMING

As neurological disorders affect distinct neuronal subtypes, the generation of neuronal subtypes has been of interest not

only for dissecting the underlying mechanisms behind subtype-specific neuronal conversion, but also for the implication of the reprogrammed neurons in disease modeling. MiR-9/9*-124 have been shown to induce a "default" neuronal state characterized by enhanced accessibility of chromatin regions encompassing neuronal genes (**Figure 2**). These regions include genes specifically expressed in distinct neuronal subtypes, yet remain inactivated, thereby providing the chromatin environment that is open and permissive for subtype-defining inputs of transcription factors (Abernathy et al., 2017). Furthermore, unlike iPSC-based reprogramming methods, direct neuronal conversion bypasses an embryonic intermediate (Lapasset et al., 2011; Miller et al., 2013), thereby retaining the age signatures of starting fibroblasts including the epigenetic clock (Horvath, 2013), age-associated changes in transcriptome and microRNAs, reactive oxygen species (ROS) levels, DNA damage and telomere lengths (Mertens et al., 2015; Huh et al., 2016; Tang et al., 2017). As direct neuronal conversion can faithfully recapitulate age-associated phenotypes, directly reprogrammed neurons hold promise in the modeling of adult-onset neurodegenerative diseases and necessitates the control of subtype-specificity during neuronal reprogramming.

The use of synergism between miRNAs and subtype-defining transcription factors to obtain subtype-specific neurons has been successful in generating cortical neurons (Yoo et al., 2011), striatal medium spiny neurons (MSN) (Victor et al., 2014), and spinal cord motor neurons (Abernathy et al., 2017; **Figure 2**). For instance, heterogeneous population of excitatory and inhibitory neurons belonging to the cortex can be obtained with the use of miR-9/9*-124 in combination with NEUROD2, ASCL1, and MYT1L (DAM) cocktail from adult fibroblasts (Yoo et al., 2011). However, it remains to be tested whether layer-enriched transcription factors would be able to further guide the cortical lineage to neurons with layer-specific identities. Since previous studies demonstrated the plasticity of cortical neurons being able to transition between cortical layer fates (Rouaux and Arlotta, 2010, 2013; De la Rossa et al., 2013), it raises the potential that a similar approach may be taken in a cellular reprogramming context.

An enriched population of striatal MSN, the neuronal subtype primarily degenerated in Huntington's disease (HD), can be derived using miR-9/9*-124 in conjunction with CTIP2, DLX1/2, and MYT1L (CDM) factors (Victor et al., 2014). More than

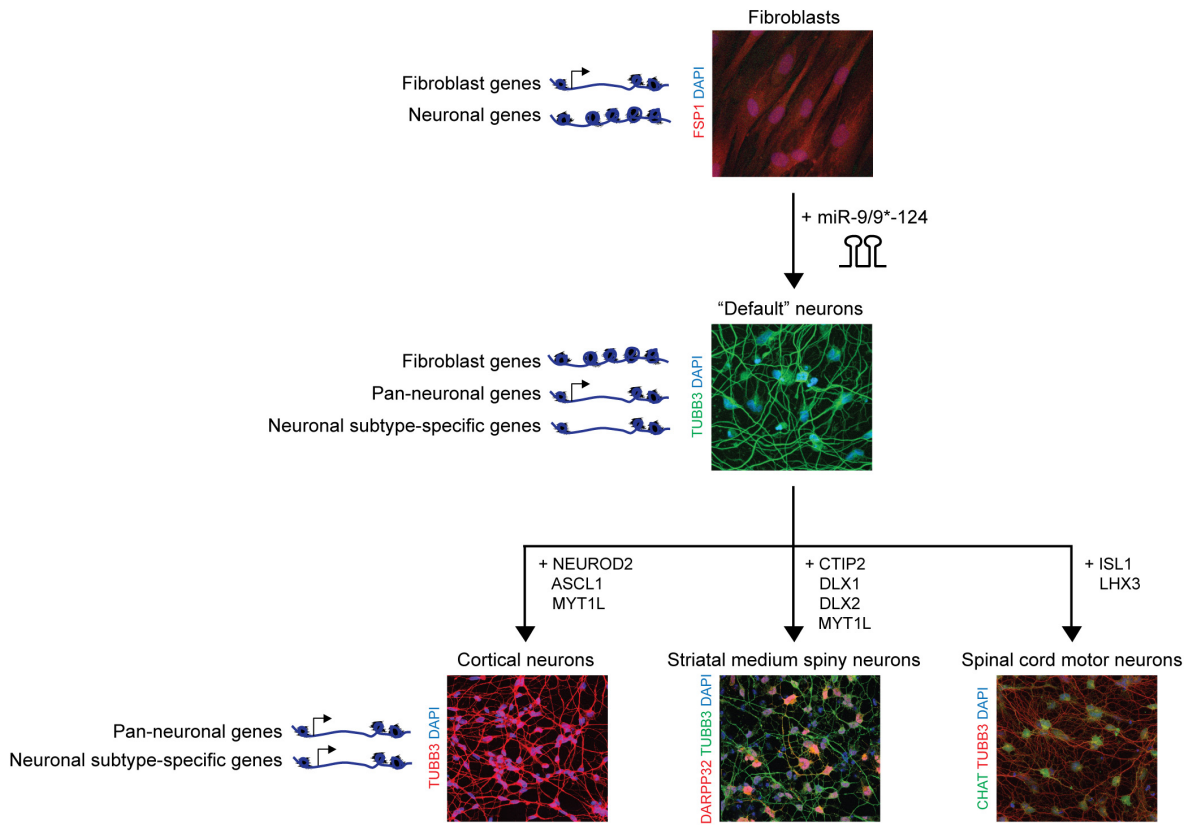

FIGURE 2 | Synergism between microRNAs and transcription factors for subtype-specific neuronal reprogramming of human adult fibroblasts. MiR-9/9*-124 mediate the erasure of fibroblast fate through remodeling of a fibroblast-specific chromatin landscape and transcriptome profile and promote a neuronal chromatin landscape and transcriptome. MiRNA alone generates a default neuronal state characterized by the reconfiguration of the chromatin state permissive to the subtype-defining inputs of transcription factors. With distinct combinations of transcription factors, the miRNA-based conversion have been successfully employed to generate cortical neurons (Yoo et al., 2011), striatal medium spiny neurons (Victor et al., 2014), and spinal cord motor neurons (Abernathy et al., 2017).

70% of cells express DARPP32, a marker of MSNs, and when injected into the stratum of mouse pups, the converted MSNs incorporate and project to the substantia nigra and globus pallidus *in vivo* with electrophysiological properties similar to neighboring endogenous mouse MSNs (Victor et al., 2014). Interestingly, applying the MSN-specific neuronal conversion approach in fibroblast samples from symptomatic patients has proven to be successful in generating patient-specific MSNs manifesting hallmark HD pathology, including HTT aggregation, spontaneous neuronal death, and increased DNA damage (Victor et al., 2018). Importantly, the manifestation of HD-associated phenotypes was dependent on the specificity of the type of neurons generated and the age status in converted neurons, further highlighting the importance of age and subtype-specificity in modeling adult-onset diseases (Victor et al., 2018).

Spinal cord motor neurons are most susceptible to degeneration in amyotrophic lateral sclerosis (ALS) and spinal muscular atrophy (SMA) diseases, and devising a conversion protocol could be instrumental to the study and modeling of motor neuron (MN) diseases. Using a combination of NEUROG1, SOX11, ISL1, and LHX3 (NSIL), MNs can be generated from fibroblasts of ALS patients in which the patient-derived MNs manifest various ALS pathologies, including FUS protein mislocalization and neuronal degeneration (Liu et al., 2016). Alternatively, miRNAs in conjunction with two transcription factors, ISL1 and LHX3, have been shown to generate functional mature MNs that display transcriptional signatures similar to *in vivo* mouse spinal MNs (Abernathy et al., 2017). Despite the robustness in generating a highly enriched population of spinal cord MNs, it remains to be demonstrated whether the MNs derived through the miRNA-induced neuronal state can be used to model ALS or SMA.

The use of transcription factors only, ASCL1, NURR1, and LMX1A, to directly convert fibroblasts of healthy and Parkinson's disease (PD) patients into dopaminergic cells is possible but with limited efficiency in human cells (Caiazzo et al., 2011). Interestingly, reprogramming efficiency improved with the addition of neuronal miRNA, miR-124, and shRNA against p53, to the transcription factor cocktail using adult fibroblasts (Jiang et al., 2015). One of the proposed mechanisms behind this enhancement is due to the activation of TET proteins, in particular TET1, during reprogramming, as knockdown of TET1 results in increased cell death while overexpression enhances the overall number of TUBB3 and TH positive cells (Jiang et al., 2015). The induction of TET family members has also been observed in miR-9/9*-124-mediated reprogramming (Abernathy et al., 2017).

The generation of additional neuronal subtypes, including serotonergic neurons for the study of neuropsychiatric disorders such as schizophrenia (Vadodaria et al., 2016; Xu et al., 2016) and sensory neurons for the study of pain sensation (Blanchard et al., 2015; Wainger et al., 2015) have been demonstrated using the transcription factor approach. It remains to be tested whether miR-9/9*-124 could be combined with similar transcription factors to enhance overall conversion efficiency in human cells.

SUMMARY

MiR-9/9*-124-mediated direct conversion of human adult fibroblasts into functional neurons reconfigures and establishes a pan-neuronal epigenetic landscape permissive on which brain region-enriched transcription factors can act and generate specific neuronal subtype. MiR-9/9*-124 are potent neurogenic molecules as they mediate numerous genetic switches that occur during neurogenesis, in which many include epigenetic players and pro-neurogenic effectors that are important to overcome cell fate barriers and activate neuronal fate programs. As miRNAs regulate expression of multiple genes, the pro-neural environment established by the miRNAs allow for the use of this paradigm for the study of neural fate acquisition. To better understand and address the role of brain-enriched miRNAs, examining miRNA-mRNA network would provide invaluable insights to the acquisition of neuronal fate. Though much remains to be uncovered, with the maintenance of age of starting fibroblasts preserved after cellular conversion, modeling age-dependent neurodegenerative diseases through direct reprogramming allows for the faithful recapitulation of age-associated pathogenesis for mechanistic studies of the disease.

AUTHOR CONTRIBUTIONS

Y-LL planned, researched, and wrote the manuscript. AY planned and edited the manuscript.

FUNDING

AY is supported by the Andrew B and Virginia C. Craig Faculty Fellowship Endowment, NIH Director's Innovator Award (DP2NS083372-01), Missouri Spinal Cord Injury/Disease Research Program (SCIDRP), Cure Alzheimer's Fund (CAF), Presidential Early Career Award for Scientists and Engineers (PECASE), and NIA (RF1AG056296).

ACKNOWLEDGMENTS

We thank Matheus B. Victor for providing images of reprogrammed cortical and medium spiny neurons, and Daniel G. Abernathy for providing the image of reprogrammed motor neurons.

REFERENCES

Abernathy, D. G., Kim, W. K., McCoy, M. J., Lake, A. M., Ouwenga, R., Lee, S. W., et al. (2017). MicroRNAs induce a permissive chromatin environment that enables neuronal subtype-specific reprogramming of adult human fibroblasts. *Cell Stem Cell* 21, 332.e9–348.e9. doi: 10.1016/j.stem.2017.08.002

Aizawa, H., Hu, S.-C., Bobb, K., Balakrishnan, K., Ince, G., Gurevich, I., et al. (2004). Dendrite development regulated by CREST, a calcium-regulated transcriptional activator. *Science* 303, 197–202. doi: 10.1126/science.1089845

Akerblom, M., Sachdeva, R., Barde, I., Verp, S., Gentner, B., Trono, D., et al. (2012). MicroRNA-124 is a subventricular zone neuronal fate determinant. *J. Neurosci.* 32, 8879–8889. doi: 10.1523/JNEUROSCI.0558-12.2012

Ambasudhan, R., Talantova, M., Coleman, R., Yuan, X., Zhu, S., Lipton, S. A., et al. (2011). Direct reprogramming of adult human fibroblasts to functional neurons under defined conditions. *Cell Stem Cell* 9, 113–118. doi: 10.1016/j.stem.2011.07.002

Anokye-Danso, F., Trivedi, C. M., Juhr, D., Gupta, M., Cui, Z., Tian, Y., et al. (2011). Highly efficient miRNA-mediated reprogramming of mouse and human somatic cells to pluripotency. *Cell Stem Cell* 8, 376–388. doi: 10.1016/j.stem.2011.03.001

Blanchard, J. W., Eade, K. T., Szűcs, A., Lo Sardo, V., Tsunemoto, R. K., Williams, D., et al. (2015). Selective conversion of fibroblasts into peripheral sensory neurons. *Nat. Neurosci.* 18, 25–35. doi: 10.1038/nn.3887

Boutz, P. L., Stoilov, P., Li, Q., Lin, C.-H., Chawla, G., Ostrow, K., et al. (2007). A post-transcriptional regulatory switch in polypyrimidine tract-binding proteins reprograms alternative splicing in developing neurons. *Genes Dev.* 21, 1636–1652. doi: 10.1101/gad.1558107

Caiazzo, M., Dell'Anno, M. T., Dvoretskova, E., Lazarevic, D., Taverna, S., Leo, D., et al. (2011). Direct generation of functional dopaminergic neurons from mouse and human fibroblasts. *Nature* 476, 224–227. doi: 10.1038/nature10284

Chanda, S., Ang, C. E., Davila, J., Pak, C., Mall, M., Lee, Q. Y., et al. (2014). Generation of induced neuronal cells by the single reprogramming factor ASCL1. *Stem Cell Rep.* 3, 282–296. doi: 10.1016/j.stemcr.2014.05.020

Cheng, L.-C., Pastrana, E., Tavazoie, M., and Doetsch, F. (2009). miR-124 regulates adult neurogenesis in the subventricular zone stem cell niche. *Nat. Neurosci.* 12, 399–408. doi: 10.1038/nn.2294

Chesi, A., Staahl, B. T., Jovičić, A., Couthouis, J., Fasolino, M., Raphael, A. R., et al. (2013). Exome sequencing to identify de novo mutations in sporadic ALS trios. *Nat. Neurosci.* 16, 851–855. doi: 10.1038/nn.3412

Colquitt, B. M., Markenscoff-Papadimitriou, E., Duffié, R., and Lomvardas, S. (2014). Dnmt3a regulates global gene expression in olfactory sensory neurons and enables odorant-induced transcription. *Neuron* 83, 823–838. doi: 10.1016/j.neuron.2014.07.013

Conaco, C., Otto, S., Han, J.-J., and Mandel, G. (2006). Reciprocal actions of REST and a microRNA promote neuronal identity. *Proc. Natl. Acad. Sci. U.S.A.* 103, 2422–2427. doi: 10.1073/pnas.0511041103

Dajas-Bailador, F., Bonev, B., Garcez, P., Stanley, P., Guillemot, F., and Papalopulu, N. (2012). microRNA-9 regulates axon extension and branching by targeting Map1b in mouse cortical neurons. *Nat. Neurosci.* 15, 697–699. doi: 10.1038/nn.3082

De la Rossa, A., Bellone, C., Golding, B., Vitali, I., Moss, J., Toni, N., et al. (2013). In vivo reprogramming of circuit connectivity in postmitotic neocortical neurons. *Nat. Neurosci.* 16, 193–200. doi: 10.1038/nn.3299

Deo, M., Yu, J.-Y., Chung, K.-H., Tippens, M., and Turner, D. L. (2006). Detection of mammalian microRNA expression by in situ hybridization with RNA oligonucleotides. *Dev. Dyn.* 235, 2538–2548. doi: 10.1002/dvdy.20847

Drouin-Ouellet, J., Lau, S., Brattås, P. L., Rylander Ottosson, D., Pircs, K., Grassi, D. A., et al. (2017). REST suppression mediates neural conversion of adult human fibroblasts via microRNA-dependent and -independent pathways. *EMBO Mol. Med.* 9, 1117–1131. doi: 10.15252/emmm.201607471

Dykhuizen, E. C., Hargreaves, D. C., Miller, E. L., Cui, K., Korshunov, A., Kool, M., et al. (2013). BAF complexes facilitate decatenation of DNA by topoisomerase IIα. *Nature* 497, 624–627. doi: 10.1038/nature12146

Feng, J., Chang, H., Li, E., and Fan, G. (2005). Dynamic expression of de novo DNA methyltransferases Dnmt3a and Dnmt3b in the central nervous system. *J. Neurosci. Res.* 79, 734–746. doi: 10.1002/jnr.20404

Feng, J., Zhou, Y., Campbell, S. L., Le, T., Li, E., Sweatt, J. D., et al. (2010). Dnmt1 and Dnmt3a maintain DNA methylation and regulate synaptic function in adult forebrain neurons. *Nat. Neurosci.* 13, 423–430. doi: 10.1038/nn.2514

Gruber, A. J., and Zavolan, M. (2013). Modulation of epigenetic regulators and cell fate decisions by miRNAs. *Epigenomics* 5, 671–683. doi: 10.2217/epi.13.65

Hahn, M. A., Qiu, R., Wu, X., Li, A. X., Zhang, H., Wang, J., et al. (2013). Dynamics of 5-hydroxymethylcytosine and chromatin marks in mammalian neurogenesis. *Cell Rep.* 3, 291–300. doi: 10.1016/j.celrep.2013.01.011

He, M., Liu, Y., Wang, X., Zhang, M. Q., Hannon, G. J., and Huang, Z. J. (2012). Cell-type-based analysis of microRNA profiles in the mouse brain. *Neuron* 73, 35–48. doi: 10.1016/j.neuron.2011.11.010

Ho, L., Jothi, R., Ronan, J. L., Cui, K., Zhao, K., and Crabtree, G. R. (2009a). An embryonic stem cell chromatin remodeling complex, esBAF, is an essential component of the core pluripotency transcriptional network. *Proc. Natl. Acad. Sci. U.S.A.* 106, 5187–5191. doi: 10.1073/pnas.0812888106

Ho, L., Miller, E. L., Ronan, J. L., Ho, W. Q., Jothi, R., and Crabtree, G. R. (2011). esBAF facilitates pluripotency by conditioning the genome for LIF/STAT3 signalling and by regulating polycomb function. *Nat. Cell Biol.* 13, 903–913. doi: 10.1038/ncb2285

Ho, L., Ronan, J. L., Wu, J., Staahl, B. T., Chen, L., Kuo, A., et al. (2009b). An embryonic stem cell chromatin remodeling complex, esBAF, is essential for embryonic stem cell self-renewal and pluripotency. *Proc. Natl. Acad. Sci. U.S.A.* 106, 5181–5186. doi: 10.1073/pnas.0812889106

Horvath, S. (2013). DNA methylation age of human tissues and cell types. *Genome Biol.* 14:R115. doi: 10.1186/gb-2013-14-10-r115

Huh, C. J., Zhang, B., Victor, M. B., Dahiya, S., Batista, L. F., Horvath, S., et al. (2016). Maintenance of age in human neurons generated by microRNA-based neuronal conversion of fibroblasts. *eLife* 5:e18648. doi: 10.7554/eLife.18648

Ivey, K. N., and Srivastava, D. (2010). MicroRNAs as regulators of differentiation and cell fate decisions. *Cell Stem Cell* 7, 36–41. doi: 10.1016/j.stem.2010.06.012

Iwafuchi-Doi, M., and Zaret, K. S. (2014). Pioneer transcription factors in cell reprogramming. *Genes Dev.* 28, 2679–2692. doi: 10.1101/gad.253443.114

Iwafuchi-Doi, M., and Zaret, K. S. (2016). Cell fate control by pioneer transcription factors. *Development* 143, 1833–1837. doi: 10.1242/dev.133900

Jayawardena, T. M., Egemnazarov, B., Finch, E. A., Zhang, L., Payne, J. A., Pandya, K., et al. (2012). MicroRNA-mediated in vitro and in vivo direct reprogramming of cardiac fibroblasts to cardiomyocytes. *Circ. Res.* 110, 1465–1473. doi: 10.1161/CIRCRESAHA.112.269035

Jiang, H., Xu, Z., Zhong, P., Ren, Y., Liang, G., Schilling, H. A., et al. (2015). Cell cycle and p53 gate the direct conversion of human fibroblasts to dopaminergic neurons. *Nat. Commun.* 6:10100. doi: 10.1038/ncomms10100

Kennison, J. A. (1995). The polycomb and trithorax group proteins of drosophila: trans-regulators of homeotic gene function. *Annu. Rev. Genet.* 29, 289–303. doi: 10.1146/annurev.ge.29.120195.001445

Keppetipola, N., Sharma, S., Li, Q., and Black, D. L. (2012). Neuronal regulation of pre-mRNA splicing by polypyrimidine tract binding proteins, PTBP1 and PTBP2. *Crit. Rev. Biochem. Mol. Biol.* 47, 360–378. doi: 10.3109/10409238.2012.691456

Kidder, B. L., Palmer, S., and Knott, J. G. (2009). SWI/SNF-Brg1 regulates self-renewal and occupies core pluripotency-related genes in embryonic stem cells. *Stem Cells* 27, 317–328. doi: 10.1634/stemcells.2008-0710

Krichevsky, A. M., Sonntag, K.-C., Isacson, O., and Kosik, K. S. (2006). Specific microRNAs modulate embryonic stem cell-derived neurogenesis. *Stem Cells* 24, 857–864. doi: 10.1634/stemcells.2005-0441

Ladewig, J., Mertens, J., Kesavan, J., Doerr, J., Poppe, D., Glaue, F., et al. (2012). Small molecules enable highly efficient neuronal conversion of human fibroblasts. *Nat. Methods* 9, 575–578. doi: 10.1038/nmeth.1972

Lagos-Quintana, M., Rauhut, R., Yalcin, A., Meyer, J., Lendeckel, W., and Tuschl, T. (2002). Identification of tissue-specific microRNAs from mouse. *Curr. Biol.* 12, 735–739. doi: 10.1016/S0960-9822(02)00809-6

Lapasset, L., Milhavet, O., Prieur, A., Besnard, E., Babled, A., Ait-Hamou, N., et al. (2011). Rejuvenating senescent and centenarian human cells by reprogramming through the pluripotent state. *Genes Dev.* 25, 2248–2253. doi: 10.1101/gad.173922.111

Lee, S. W., Oh, Y. M., Lu, Y.-L., Kim, W. K., and Yoo, A. S. (2018). MicroRNAs overcome cell fate barrier by reducing EZH2-controlled rest stability during

neuronal conversion of human adult fibroblasts. *Dev. Cell* 46, 73.e7–84.e7. doi: 10.1016/j.devcel.2018.06.007

Lessard, J., Wu, J. I., Ranish, J. A., Wan, M., Winslow, M. M., Staahl, B. T., et al. (2007). An essential switch in subunit composition of a chromatin remodeling complex during neural development. *Neuron* 55, 201–215. doi: 10.1016/j.neuron.2007.06.019

Leucht, C., Stigloher, C., Wizenmann, A., Klafke, R., Folchert, A., and Bally-Cuif, L. (2008). MicroRNA-9 directs late organizer activity of the midbrain-hindbrain boundary. *Nat. Neurosci.* 11, 641–648. doi: 10.1038/nn.2115

Li, Q., Zheng, S., Han, A., Lin, C.-H., Stoilov, P., Fu, X.-D., et al. (2014). The splicing regulator PTBP2 controls a program of embryonic splicing required for neuronal maturation. *eLife* 3:e01201. doi: 10.7554/eLife.01201

Licatalosi, D. D., Yano, M., Fak, J. J., Mele, A., Grabinski, S. E., Zhang, C., et al. (2012). Ptbp2 represses adult-specific splicing to regulate the generation of neuronal precursors in the embryonic brain. *Genes Dev.* 26, 1626–1642. doi: 10.1101/gad.191338.112

Lim, L. P., Lau, N. C., Garrett-Engele, P., Grimson, A., Schelter, J. M., Castle, J., et al. (2005). Microarray analysis shows that some microRNAs downregulate large numbers of target mRNAs. *Nature* 433, 769–773. doi: 10.1038/nature03315

Liu, M.-L., Zang, T., and Zhang, C.-L. (2016). Direct lineage reprogramming reveals disease-specific phenotypes of motor neurons from human ALS patients. *Cell Rep.* 14, 115–128. doi: 10.1016/j.celrep.2015.12.018

Liu, M.-L., Zang, T., Zou, Y., Chang, J. C., Gibson, J. R., Huber, K. M., et al. (2013). Small molecules enable neurogenin 2 to efficiently convert human fibroblasts into cholinergic neurons. *Nat. Commun.* 4:2183. doi: 10.1038/ncomms3183

Makeyev, E. V., Zhang, J., Carrasco, M. A., and Maniatis, T. (2007). The MicroRNA miR-124 promotes neuronal differentiation by triggering brain-specific alternative pre-mRNA splicing. *Mol. Cell* 27, 435–448. doi: 10.1016/j.molcel.2007.07.015

Mertens, J., Paquola, A. C. M., Ku, M., Hatch, E., Böhnke, L., Ladjevardi, S., et al. (2015). Directly reprogrammed human neurons retain aging-associated transcriptomic signatures and reveal age-related nucleocytoplasmic defects. *Cell Stem Cell* 17, 705–718. doi: 10.1016/j.stem.2015.09.001

Miller, E. L., Hargreaves, D. C., Kadoch, C., Chang, C.-Y., Calarco, J. P., Hodges, C., et al. (2017). TOP2 synergizes with BAF chromatin remodeling for both resolution and formation of facultative heterochromatin. *Nat. Struct. Mol. Biol.* 24, 344–352. doi: 10.1038/nsmb.3384

Miller, J. D., Ganat, Y. M., Kishinevsky, S., Bowman, R. L., Liu, B., Tu, E. Y., et al. (2013). Human iPSC-based modeling of late-onset disease via progerin-induced aging. *Cell Stem Cell* 13, 691–705. doi: 10.1016/j.stem.2013.11.006

Olave, I. (2002). Identification of a polymorphic, neuron-specific chromatin remodeling complex. *Genes Dev.* 16, 2509–2517. doi: 10.1101/gad.992102

Packer, A. N., Xing, Y., Harper, S. Q., Jones, L., and Davidson, B. L. (2008). The bifunctional microRNA miR-9/miR-9* regulates rest and CoREST and is downregulated in Huntington's disease. *J. Neurosci.* 28, 14341–14346. doi: 10.1523/JNEUROSCI.2390-08.2008

Pfisterer, U., Ek, F., Lang, S., Soneji, S., Olsson, R., and Parmar, M. (2016). Small molecules increase direct neural conversion of human fibroblasts. *Sci. Rep.* 6:38290. doi: 10.1038/srep38290

Rajman, M., and Schratt, G. (2017). MicroRNAs in neural development: from master regulators to fine-tuners. *Development* 144, 2310–2322. doi: 10.1242/dev.144337

Ronan, J. L., Wu, W., and Crabtree, G. R. (2013). From neural development to cognition: unexpected roles for chromatin. *Nat. Rev. Genet.* 14, 347–359. doi: 10.1038/nrg3413

Rouaux, C., and Arlotta, P. (2010). Fezf2 directs the differentiation of corticofugal neurons from striatal progenitors in vivo. *Nat. Neurosci.* 13, 1345–1347. doi: 10.1038/nn.2658

Rouaux, C., and Arlotta, P. (2013). Direct lineage reprogramming of post-mitotic callosal neurons into corticofugal neurons in vivo. *Nat. Cell Biol.* 15, 214–221. doi: 10.1038/ncb2660

Smith, D. K., Yang, J., Liu, M.-L., and Zhang, C.-L. (2016). Small molecules modulate chromatin accessibility to promote NEUROG2-mediated fibroblast-to-neuron reprogramming. *Stem Cell Rep.* 7, 955–969. doi: 10.1016/j.stemcr.2016.09.013

Son, E. Y., Ichida, J. K., Wainger, B. J., Toma, J. S., Rafuse, V. F., Woolf, C. J., et al. (2011). Conversion of mouse and human fibroblasts into functional spinal motor neurons. *Cell Stem Cell* 9, 205–218. doi: 10.1016/j.stem.2011.07.014

Spellman, R., Llorian, M., and Smith, C. W. J. (2007). Crossregulation and functional redundancy between the splicing regulator PTB and its paralogs nPTB and ROD1. *Mol. Cell* 27, 420–434. doi: 10.1016/j.molcel.2007.06.016

Staahl, B. T., and Crabtree, G. R. (2013). Creating a neural specific chromatin landscape by npBAF and nBAF complexes. *Curr. Opin. Neurobiol.* 23, 903–913. doi: 10.1016/j.conb.2013.09.003

Staahl, B. T., Tang, J., Wu, W., Sun, A., Gitler, A. D., Yoo, A. S., et al. (2013). Kinetic analysis of npBAF to nBAF switching reveals exchange of SS18 with CREST and integration with neural developmental pathways. *J. Neurosci.* 33, 10348–10361. doi: 10.1523/JNEUROSCI.1258-13.2013

Takahashi, K., and Yamanaka, S. (2006). Induction of pluripotent stem cells from mouse embryonic and adult fibroblast cultures by defined factors. *Cell* 126, 663–676. doi: 10.1016/j.cell.2006.07.024

Tang, Y., Liu, M.-L., Zang, T., and Zhang, C.-L. (2017). Direct reprogramming rather than iPSC-based reprogramming maintains aging hallmarks in human motor neurons. *Front. Mol. Neurosci.* 10:359. doi: 10.3389/fnmol.2017.00359

Thakurela, S., Garding, A., Jung, J., Schübeler, D., Burger, L., and Tiwari, V. K. (2013). Gene regulation and priming by topoisomerase IIα in embryonic stem cells. *Nat. Commun.* 4:2478. doi: 10.1038/ncomms3478

Tiwari, V. K., Burger, L., Nikoletopoulou, V., Deogracias, R., Thakurela, S., Wirbelauer, C., et al. (2012). Target genes of topoisomerase II regulate neuronal survival and are defined by their chromatin state. *Proc. Natl. Acad. Sci. U.S.A.* 109, E934–E943. doi: 10.1073/pnas.1119798109

Tsurusaki, Y., Okamoto, N., Ohashi, H., Kosho, T., Imai, Y., Hibi-Ko, Y., et al. (2012). Mutations affecting components of the SWI/SNF complex cause Coffin-Siris syndrome. *Nat. Genet.* 44, 376–378. doi: 10.1038/ng.2219

Tsutsui, K., Tsutsui, K., Hosoya, O., Sano, K., and Tokunaga, A. (2001a). Immunohistochemical analyses of DNA topoisomerase II isoforms in developing rat cerebellum. *J. Comp. Neurol.* 431, 228–239.

Tsutsui, K., Tsutsui, K., Sano, K., Kikuchi, A., and Tokunaga, A. (2001b). Involvement of DNA topoisomerase IIβ in neuronal differentiation. *J. Biol. Chem.* 276, 5769–5778. doi: 10.1074/jbc.M008517200

Vadodaria, K. C., Mertens, J., Paquola, A., Bardy, C., Li, X., Jappelli, R., et al. (2016). Generation of functional human serotonergic neurons from fibroblasts. *Mol. Psychiatry* 21, 49–61. doi: 10.1038/mp.2015.161

Victor, M. B., Richner, M., Hermanstyne, T. O., Ransdell, J. L., Sobieski, C., Deng, P.-Y., et al. (2014). Generation of human striatal neurons by microRNA-dependent direct conversion of fibroblasts. *Neuron* 84, 311–323. doi: 10.1016/j.neuron.2014.10.016

Victor, M. B., Richner, M., Olsen, H. E., Lee, S. W., Monteys, A. M., Ma, C., et al. (2018). Striatal neurons directly converted from Huntington's disease patient fibroblasts recapitulate age-associated disease phenotypes. *Nat. Neurosci.* 21, 341–352. doi: 10.1038/s41593-018-0075-7

Vierbuchen, T., Ostermeier, A., Pang, Z. P., Kokubu, Y., Südhof, T. C., and Wernig, M. (2010). Direct conversion of fibroblasts to functional neurons by defined factors. *Nature* 463, 1035–1041. doi: 10.1038/nature08797

Visvanathan, J., Lee, S., Lee, B., Lee, J. W., and Lee, S.-K. (2007). The microRNA miR-124 antagonizes the anti-neural REST/SCP1 pathway during embryonic CNS development. *Genes Dev.* 21, 744–749. doi: 10.1101/gad.1519107

Vogel-Ciernia, A., Matheos, D. P., Barrett, R. M., Kramár, E. A., Azzawi, S., Chen, Y., et al. (2013). The neuron-specific chromatin regulatory subunit BAF53b is necessary for synaptic plasticity and memory. *Nat. Neurosci.* 16, 552–561. doi: 10.1038/nn.3359

Wagner, E. J., and Garcia-Blanco, M. A. (2001). Polypyrimidine tract binding protein antagonizes exon definition. *Mol. Cell. Biol.* 21, 3281–3288. doi: 10.1128/MCB.21.10.3281-3288.2001

Wainger, B. J., Buttermore, E. D., Oliveira, J. T., Mellin, C., Lee, S., Saber, W. A., et al. (2015). Modeling pain in vitro using nociceptor neurons reprogrammed from fibroblasts. *Nat. Neurosci.* 18, 17–24. doi: 10.1038/nn.3886

Wang, W., Cote, J., Xue, Y., Zhou, S., Khavari, P. A., Biggar, S. R., et al. (1996a). Purification and biochemical heterogeneity of the mammalian SWI-SNF complex. *EMBO J.* 15, 5370–5382.

Wang, W., Xue, Y., Zhou, S., Kuo, A., Cairns, B. R., and Crabtree, G. R. (1996b). Diversity and specialization of mammalian SWI/SNF complexes. *Genes Dev.* 10, 2117–2130. doi: 10.1101/gad.10.17.2117

Watanabe, D., Uchiyama, K., and Hanaoka, K. (2006). Transition of mouse de novo methyltransferases expression from Dnmt3b to Dnmt3a during neural progenitor cell development. *Neuroscience* 142, 727–737. doi: 10.1016/j.neuroscience.2006.07.053

Watanabe, M., Tsutsui, K., Tsutsui, K., and Inoue, Y. (1994). Differential expressions of the topoisomerase IIa and IIb mRNAs in developing rat brain. *Neurosci. Res.* 19, 51–57. doi: 10.1016/0168-0102(94)90007-8

Wijdeven, R. H., Pang, B., van der Zanden, S. Y., Qiao, X., Blomen, V., Hoogstraat, M., et al. (2015). Genome-wide identification and characterization of novel factors conferring resistance to topoisomerase II poisons in cancer. *Cancer Res.* 75, 4176–4187. doi: 10.1158/0008-5472.CAN-15-0380

Wu, H., Coskun, V., Tao, J., Xie, W., Ge, W., Yoshikawa, K., et al. (2010). Dnmt3a-dependent nonpromoter DNA methylation facilitates transcription of neurogenic genes. *Science* 329, 444–448. doi: 10.1126/science.1190485

Wu, J. I., Lessard, J., and Crabtree, G. R. (2009). Understanding the words of chromatin regulation. *Cell* 136, 200–206. doi: 10.1016/j.cell.2009.01.009

Wu, J. I., Lessard, J., Olave, I. A., Qiu, Z., Ghosh, A., Graef, I. A., et al. (2007). Regulation of dendritic development by neuron-specific chromatin remodeling complexes. *Neuron* 56, 94–108. doi: 10.1016/j.neuron.2007.08.021

Xu, Z., Jiang, H., Zhong, P., Yan, Z., Chen, S., and Feng, J. (2016). Direct conversion of human fibroblasts to induced serotonergic neurons. *Mol. Psychiatry* 21, 62–70. doi: 10.1038/mp.2015.101

Xue, Q., Yu, C., Wang, Y., Liu, L., Zhang, K., Fang, C., et al. (2016). miR-9 and miR-124 synergistically affect regulation of dendritic branching via the AKT/GSK3β pathway by targeting Rap2a. *Sci. Rep.* 6:26781. doi: 10.1038/srep26781

Xue, Y., Ouyang, K., Huang, J., Zhou, Y., Ouyang, H., Li, H., et al. (2013). Direct conversion of fibroblasts to neurons by reprogramming PTB-regulated microRNA circuits. *Cell* 152, 82–96. doi: 10.1016/j.cell.2012.11.045

Xue, Y., Qian, H., Hu, J., Zhou, B., Zhou, Y., Hu, X., et al. (2016). Sequential regulatory loops as key gatekeepers for neuronal reprogramming in human cells. *Nat. Neurosci.* 19, 807–815. doi: 10.1038/nn.4297

Yang, X. (2000). DNA topoisomerase II and neural development. *Science* 287, 131–134. doi: 10.1126/science.287.5450.131

Yoo, A. S., Staahl, B. T., Chen, L., and Crabtree, G. R. (2009). MicroRNA-mediated switching of chromatin-remodelling complexes in neural development. *Nature* 460, 642–646. doi: 10.1038/nature08139

Yoo, A. S., Sun, A. X., Li, L., Shcheglovitov, A., Portmann, T., Li, Y., et al. (2011). MicroRNA-mediated conversion of human fibroblasts to neurons. *Nature* 476, 228–231. doi: 10.1038/nature10323

Zhang, R.-R., Cui, Q.-Y., Murai, K., Lim, Y. C., Smith, Z. D., Jin, S., et al. (2013). Tet1 regulates adult hippocampal neurogenesis and cognition. *Cell Stem Cell* 13, 237–245. doi: 10.1016/j.stem.2013.05.006

Zhao, C., Sun, G., Li, S., and Shi, Y. (2009). A feedback regulatory loop involving microRNA-9 and nuclear receptor TLX in neural stem cell fate determination. *Nat. Struct. Mol. Biol.* 16, 365–371. doi: 10.1038/nsmb.1576

Zheng, S., Gray, E. E., Chawla, G., Porse, B. T., O'Dell, T. J., and Black, D. L. (2012). PSD-95 is post-transcriptionally repressed during early neural development by PTBP1 and PTBP2. *Nat. Neurosci.* 15, 381–388. doi: 10.1038/nn.3026

Conflict of Interest Statement: The authors declare that the research was conducted in the absence of any commercial or financial relationships that could be construed as a potential conflict of interest.

frontiers in Neuroscience

PERSPECTIVE
published: 26 September 2018
doi: 10.3389/fnins.2018.00646

The Use of Stem Cell-Derived Neurons for Understanding Development and Disease of the Cerebellum

*Samuel P. Nayler and Esther B. E. Becker**

Department of Physiology, Anatomy and Genetics, University of Oxford, Oxford, United Kingdom

The cerebellum is a fascinating brain structure, containing more neurons than the rest of the brain combined. The cerebellum develops according to a highly orchestrated program into a well-organized laminar structure. Much has been learned about the underlying genetic networks controlling cerebellar development through the study of various animal models. Cerebellar development in humans however, is significantly protracted and more complex. Given that the cerebellum regulates a number of motor and non-motor functions and is affected in a wide variety of neurodevelopmental and neurodegenerative disorders, a better understanding of human cerebellar development is highly desirable. Pluripotent stem cells offer an exciting new tool to unravel human cerebellar development and disease by providing a dynamic and malleable platform, which is amenable to genetic manipulation and temporally unrestricted sampling. It remains to be seen, however, whether *in vitro* neuronal cultures derived from pluripotent stem cells fully recapitulate the formation and organization of the developing nervous system, with many reports detailing the functionally immature nature of these cultures. Nevertheless, recent advances in differentiation protocols, cell-sampling methodologies, and access to informatics resources mean that the field is poised for remarkable discoveries. In this review, we provide a general overview of the field of neuronal differentiation, focusing on the cerebellum and highlighting conceptual advances in understanding neuronal maturity, including a discussion of both current and emerging methods to classify, and influence neuroanatomical identity and maturation status.

Keywords: cerebellum, stem cell, organoid, differentiation, ataxia, neuronal, Purkinje cell, granule cell

OPEN ACCESS

Edited by:
Annalisa Buffo,
Università degli Studi di Torino, Italy

Reviewed by:
Mikio Hoshino,
National Center of Neurology and Psychiatry, Japan
Jan Cendelin,
Charles University, Czechia

***Correspondence:**
Esther B. E. Becker
esther.becker@dpag.ox.ac.uk

Specialty section:
This article was submitted to Neurogenesis, a section of the journal Frontiers in Neuroscience

Received: *13 July 2018*
Accepted: *29 August 2018*
Published: *26 September 2018*

Citation:
Nayler SP and Becker EBE (2018) The Use of Stem Cell-Derived Neurons for Understanding Development and Disease of the Cerebellum. Front. Neurosci. 12:646. doi: 10.3389/fnins.2018.00646

INTRODUCTION

The development of the nervous system is guided by temporally programmed, spatially distinct morphogen gradients. *In vitro* reproduction of these cues can be achieved in pluripotent stem cells (PSCs), facilitating cellular differentiation into distinct neuronal and glial subtypes (Zhang et al., 2001; Wichterle et al., 2002). The advent of induced PSC (iPSC) technology has greatly advanced the field by enabling the *in vitro* derivation of PSCs from almost any somatic cell type. This has allowed for the generation of iPSCs from patients and thus linkage of *in vitro* cellular phenotypes to distinct clinical presentations. Over recent years, enormous progress has been made

in differentiating patient and control PSCs into cortical (Brennand et al., 2015), motor (Dimos et al., 2008; Sances et al., 2016), and dopaminergic (Woodard et al., 2014; Sandor et al., 2017) neurons. Moreover, three-dimensional (3D) PSC-derived organoid cultures offer exciting possibilities to study brain development, evolution, and abnormalities that underlie developmental disorders (Kelava and Lancaster, 2016; Camp and Treutlein, 2017).

Despite these technological breakthroughs, the potential of PSC-derived neuronal models remains far from fully realized. Current challenges include the development of standardized, robust protocols for differentiation, as well as classification strategies that can effectively relate *in vitro*-derived cell types to their *in vivo* counterparts, including assessing their state of maturity. Thus far, PSC-derived models have mainly been utilized to explore very early stages of brain development associated with disorders, including correct neural tube polarization and apico-basal polarity establishment (Yoon et al., 2014), microcephaly (Lancaster et al., 2013), and Zika-related viral infection (Dang et al., 2016; Garcez et al., 2016; Qian et al., 2016). PSC-derived neuronal cells are usually not exposed to the same range of environmental stimuli, which aid in the development of neurons within the correct physiological context of the developing brain *in vivo*. It therefore remains to be established whether PSC-derived neuronal models are able to recapitulate late developmental events including the formation of complex cellular interactions and neuronal networks. Finally, the degree to which a given disease can be recreated in synthetic *in vitro* environments remains an important consideration.

Methodologies to generate cerebellar neurons from human PSCs and to model cerebellar disorders are beginning to emerge (Muguruma et al., 2015; Ishida et al., 2016; Sundberg et al., 2018; Watson et al., 2018). Here, we review the current state of the field and highlight conceptual advances that will help to establish relevant model systems for the study of cerebellar development and disease using PSCs.

RECAPITULATION OF CEREBELLAR ONTOGENESIS *IN VITRO*

The cerebellum is one of the first brain structures to emerge and develops over a long period of time until the first postnatal years (Wang and Zoghbi, 2001). Following generation of the neural plate and tube, the developing embryonic brain begins to organize into three distinct compartments, the prosencephalon, mesencephalon, and rhombencephalon (Hatten and Heintz, 1995; Wassef, 2013). Development of the cerebellar anlage is dependent on fibroblast growth factor (FGF) signaling from the isthmic organizer, which is located at the mid-hindbrain boundary (MHB) and demarcated by the expression of distinct transcription factors including OTX2, GBX2, EN1/2, and PAX2 (Wang and Zoghbi, 2001; Butts et al., 2014; Leto et al., 2016). Unique to cerebellar development, progenitors are generated in two distinct germinal zones in rhombomere 1; the ventricular zone (VZ) gives rise to GABAergic neurons [Purkinje cells (PCs), interneurons, GABA-ergic cerebellar nuclei neurons], whereas all glutamatergic neurons [granule cells (GCs), unipolar brush cells, glutamatergic cerebellar nuclei neurons] are generated from the rhombic lip (RL) (Hoshino et al., 2013; Butts et al., 2014; Leto et al., 2016). Embryonic and postnatal cerebellar development are driven by both symmetric and asymmetric division and migration of progenitors and subsequent neuronal differentiation, ultimately giving rise to a highly organized structure containing more neurons than the rest of the brain combined. In the human brain, 80% of the total number of neurons in the brain, i.e., approximately 69 billion neurons, are found in the cerebellum (Herculano-Houzel, 2009). By week 15 of development, the human cerebellum already shows remarkable complexity (**Figure 1**).

Early studies using mouse embryonic stem cells (ESCs) aimed to recapitulate the signals that occur during *in vivo* cerebellar development for the *in vitro* differentiation of cerebellar neurons. Initial studies focussed on the stepwise addition of growth factors and mitogens including FGF8 and retinoic acid (RA) to initiate cerebellar patterning and differentiation (Salero and Hatten, 2007). Notably, medium conditioned by primary cultured cerebellar cells improved survival and induced the expression of mature markers in differentiated ESC-derived cerebellar cultures.

Su et al. (2006) pioneered an approach utilizing serum-free culture of embryoid body-like aggregates (SFEB) in combination with dorsalizing activity of bone morphogenetic protein (BMP) signaling. This approach gave rise to progenitors of both germinal zones (RL and VZ), including ATOH1/MATH1-positive GC precursors and cerebellar neurons expressing the PC markers L7/PCP2 and Calbindin.

The SFEB methodology was subsequently refined, yielding a 30-fold improvement in PC production, ostensibly due to the more precise way in which the conditions resembled the local self-inductive signaling events operational during development of the cerebellum *in vivo* (Muguruma et al., 2010). Additionally, this study advanced understanding of both FGF2 and Insulin as caudalizing factors assisting in MHB pre-patterning. 75% of neural rosettes expressed the cell-surface marker Kirrel2/NEPH3, a downstream target of PTF1α, which is expressed in all VZ progenitors (Leto et al., 2016). This allowed isolation by flow cytometry and expansion of a purified population of PC progenitors. Importantly, this study also showed orthotopic integration of ESC-derived PCs into the mouse cerebellum following *in utero* electroporation into the sub-ventricular space at E15.5 (Muguruma et al., 2010). Remarkably, these PCs exhibited engraftment, proper cell polarity, and projections as well as expression of synaptic markers. Whilst surviving transplantation, purified Kirrel2-positive cells could not be maintained alone *in vitro*, but required co-culture with RL-derived GCs for their further differentiation, and maturation. This is consistent with other studies reporting a drastic improvement in ESC-derived PC generation through co-culture with dissociated cerebellar cultures or organotypic slice cultures of whole mouse cerebellum (Tao et al., 2010), and highlights the need for an appropriate trophic environment for the *in vitro* culture of neuronal subpopulations.

More recent studies have further developed these protocols for the differentiation of cerebellar neurons derived from human

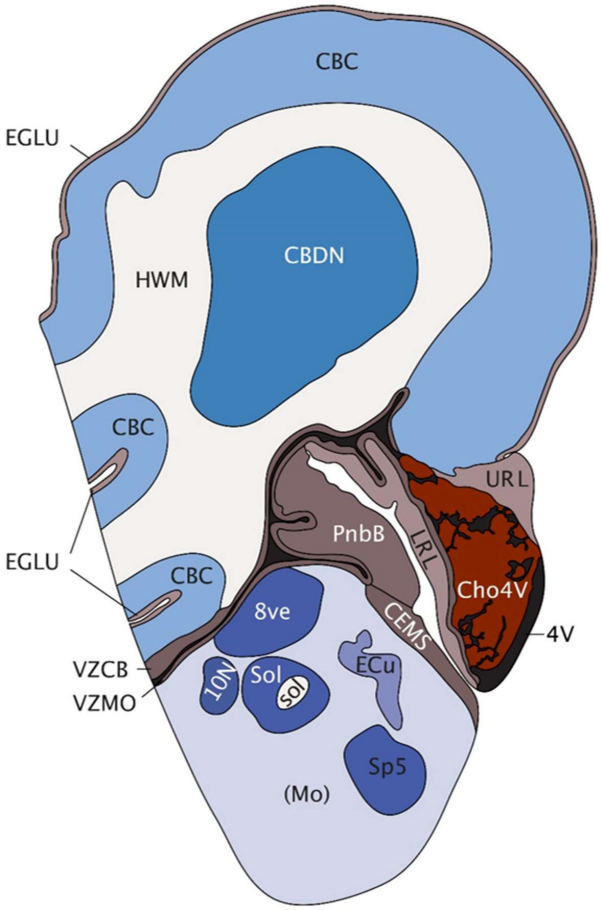

FIGURE 1 | Saggital depiction of human hindbrain at post-conception week 15. EGLU, external granule layer; CBC, cerebellar cortex; HWM, white matter of hindbrain; CBDN, cerebellar deep nuclei; 4V, fourth ventricle; VZCB, ventricular matrix zone of cerebellum; VZMO, ventricular matrix zone of medulla; URL, upper rhombic lip; LRL, lower rhombic lip; Cho4V, choroid plexus of the fourth ventricle; PnbB, pontobulbar body; CEMS, caudal (posterior) extramural migratory stream; Mo, medulla oblongata; 8ve, vestibular nuclei in medulla; 10N [(dorsal motor nucleus of the vagus, vagal nucleus)], Sol, solitary nucleus; sol, solitary tract; Ecu, external cuneate nucleus; Sp5, spinal trigeminal matrix. Image taken with permission from the Allen Brain Atlas (http://atlas.brain-map.org) [Accessed 2018].

PSCs. Based on the method by Salero and Hatten (Salero and Hatten, 2007), Erceg et al. (2010) treated embryoid bodies (EBs) aggregated from hESCs with FGF8b and RA, followed by a multi-stage-specific application of growth factors and mitogens. This protocol utilized a manual selection process to isolate polarized neuroepithelium and extended a number of the stages, yielding cerebellar cells expressing markers of GCs, PCs, and glial cells. A subsequent transcriptomic analysis on iPSCs differentiated according to this protocol showed that their transcriptomic signature most closely resembled the human fetal cerebellum at 22 weeks of development, when compared to temporally and spatially discrete regions of the human brain (Nayler et al., 2017).

Ishida et al. (2016) applied their earlier-developed mouse ESC protocol for the generation of cerebellar neurons from human ESCs and subsequently human iPSCs. By day 35 approximately 28% of cells expressed Kirrel2, forming rosettes that resembled polarized neuroepithelial tissue. Unlike the murine protocol, exogenous inhibition of ventralizing Hedgehog signals with cyclopamine was not required for the specification of human Kirrel2-positive cells. However, similar to the murine protocol, Kirrel2-positive cells required co-culture with murine RL-derived cerebellar cultures to promote survival and further differentiation. This suggests that there are factors necessary for long-term growth and maturation of human PCs that are still unknown. Nevertheless, this protocol marks a major conceptual leap and offers a more economically feasible protocol for the differentiation of human cerebellar cells than previously available, with fewer sources of experimental variability. Recently, an adaptation of the protocol was reported that eliminates sorting of Kirrel2-positive cells and employs co-culture of E18.5 mouse cerebellar progenitors rather than RL-derived cultures (Watson et al., 2018). As early as day 35 of differentiation, subpopulations of iPSC-derived cells expressed markers of the two cerebellar germinal zones. Calbindin-positive PC progenitors were detected from day 50 onward with 10% of human cells staining positive by day 70 of differentiation.

Another approach made use of human iPSC-EBs that were treated early with FGF2, Insulin, and cyclopamine, resulting in 10% of cells expressing Kirrel2 after 20 days (Wang et al., 2015). Further maturation of isolated Kirrel2-positive cells was achieved through co-culture with rat organotypic slices (P9–10). However, significant electrophysiological activity of the iPSC-derived neurons was observed only following co-culture with human fetal cerebellar slices (16–23 post-conception weeks).

More recently, an alternative protocol was published using both FGF8b and FGF2 to instigate cerebellar patterning (Sundberg et al., 2018). Greater yields (61–91%) of maturing PCs, positive for L7/PCP2, were obtained using immunopanning for the specific cell surface antigen Thy-1 instead of cell sorting for Kirrel2. Cultures were maintained for up to 140 days in the presence of postnatal mouse GCs and displayed expression of mature synaptic markers and electrical activity.

Most of the published protocols to date focus on the generation of PCs from human PSCs, while the differentiation into other cerebellar cell types remains relatively unexplored. The addition of FGF19 and SDF1 to SFEB cultures has been reported to promote the spontaneous generation of polarized neural tube-like structures with a three-layer cytoarchitecture reminiscent of the embryonic cerebellum (Muguruma et al., 2015). This suggests that human ESC-derived cerebellar progenitors show significant potential for self-organization. However, the potential of organoid cultures to recapitulate the full cerebellar ontogenesis remains to be further explored.

Another challenge remains the long-term culture and maturation of human PSC-derived cerebellar neurons without the presence of mouse co-cultures. Mature phenotypes of PSC-derived PCs have so far only been demonstrated in co-culture or, more convincingly, by transplantation of differentiated cells into mouse cerebellum, where signaling factors, and the local micro-environment coax them toward terminal differentiation and/or integration with the host cerebellar

circuitry (See **Supplementary Table 1** for summary). While this demonstrates the potential of the PSC-derived neurons to mature into functioning cerebellar neurons, it also highlights the need to better understand the factors that promote the maturation of PSC-derived cerebellar neurons. A growing number of methods exist for reverse-engineering specific cellular micro-environments and the cells and molecules which constitute these (Murrow et al., 2017). It is likely that the combination of these technologies will be instrumental in elucidating key conditions that promote long-term survival and maturation of PSC-derived cerebellar neurons. These methodologies might also be exploited to identify factors that could increase the neurogenic potential of the mature cerebellum, which is believed to be one of the most static structures in the brain (Ponti et al., 2008).

EMERGING TECHNOLOGIES FOR ENGINEERING NEURAL STEM CELL MICRO-ENVIRONMENTS

When modeling brain development *in vitro*, one should be cognizant of the trade-off between purity and complexity of neuronal cultures (Kelava and Lancaster, 2016), with 'pure' cultures representing a facile state that does not exist in nature. For example, a pure population of PCs, while facilitating stringent biochemical analyses, would not be informative in terms of modeling developmental and physiological processes that are dependent on the interaction with other neurons, or glial cells. Physiologically relevant insight will therefore likely require recapitulation of local niches, including the presence and interactions of astrocytes, neurons, microglia, and potentially vasculature. Such an approach has been pioneered by combining neural precursors, endothelial cells, mesenchymal stem cells and microglia/macrophage progenitors in chemically defined polyethylene-glycol hydrogels (Schwartz et al., 2015). This exemplified a model system comprising a milieu of independently engineered cell types, striving to recapitulate the complex interplay of these cells and their collective response to a range of compounds as a method for drug screening and discovery. Moreover, 3D printing of cells will be helpful to reconstruct the spatial relationship of different cell populations (Graham et al., 2017; Gu et al., 2017; Yanagi et al., 2017). The potential for isolation by bead-sorting or flow cytometry and recombination in a controlled deposition by 3D printing makes it technically feasible to generate cellular constructs in which the organization of cells is specified by the user. In addition, the use of bioengineering approaches to recreate physiologically relevant chemical signaling gradients or varied physical parameters such as surface tension may be advantageous. Prime examples would be the recapitulation of concentration gradients of Sonic Hedgehog or Reelin, known to direct cerebellar migration, and patterning. Such an approach would be aided by the use of devices, such as bioreactors featuring cells in serial array, to allow the study of paracrine/autocrine signaling (Titmarsh et al., 2016). Combined with genetic-reporters this allows combinatorial factor screening in order to monitor cell-fate commitment to systematically optimize culture conditions (Titmarsh et al., 2013).

Organoids show extraordinary promise in recapitulating the complex architecture of the developing brain. An interesting recent example of this is the addition of Matrigel to the organoid culture environment, which appears to mimic the basement membrane (Lancaster et al., 2017). It will be intriguing to apply this to cerebellar organoids, where Laminin, β1-integrins and dystroglycans of the basement membrane have a distinct role in astroglial specialization (Nguyen et al., 2013; Leto et al., 2016). However, organoid technology faces several limitations surrounding the maturity reached following differentiation, intrinsic heterogeneity, and size constraints with oxygen and nutrient diffusion (Okkelman et al., 2017; Quadrato et al., 2017). The latter might be overcome using vascularized organoids (Mansour et al., 2018; Pham et al., 2018). The cerebellum is a prime candidate for this technology, given that it is one of the most highly vascularized sites in the brain. A recent development involved *in vitro* patterning and fusion of adjacent brain areas to mimic migration and long-range developmental interactions (Bagley et al., 2017). Approaches such as this may shed light on developmental disorders of the cerebellum involving abnormal migration and positioning of cerebellar precursor cells. A summary of key approaches that could be utilized synergistically with organoid technology is shown in **Figure 2**.

NEURONAL CLASSIFICATION STRATEGIES USING TRANSCRIPTOMIC DATA

Major efforts to identify molecular markers for discrete sub-populations of cerebellar cells at distinct points in time have come from studies of the mouse (Sato et al., 2008; Ha et al., 2012). An early example of this, GENSAT, made use of eGFP-BAC transgenic mice to isolate and identify patterns of epoch/cell-type specific gene expression (Heintz, 2004). While a number of genetic-reporters have been utilized to study differentiation and facilitate experimental handling, their widespread adoption in human systems has been slow. This may be explained by the notion that cell-type specific markers are often facile in the context of PSC differentiation, owing to non-equivalent time scales, species-specific ontological differences, and the lack of spatial congruence as a means for anatomical orientation. The rapid development of increasingly affordable expression-profiling strategies combined with powerful cell-sampling methodologies, including laser-capture-microdissection, cell-surface marker isolation by FACS, barcoding, and microfluidic capture of single cells have dramatically changed what is now experimentally possible.

Large data repositories are driving approaches to isolate spatio-temporal signatures that can be used to move to a fuller understanding of the neuroanatomical identity and maturity of human neurons following differentiation (Kang et al., 2011; Miller et al., 2014). Data repositories [e.g., Allen Brain Atlas

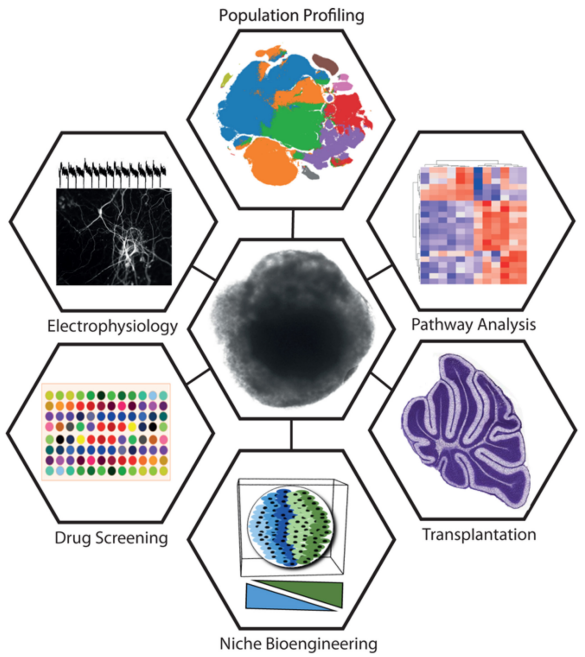

FIGURE 2 | Summary of key approaches being utilized synergistically with organoid technology. A cerebellar organoid is shown in the center. Approaches clockwise from top: Rapid developments in single-cell sequencing technologies drive new methods of population profiling. Shown is a tSNE plot constructed from the 10X Million Cell Dataset (data accessible at NCBI GEO database, accession GSM2453144). Pathway analysis is a broad set of approaches commonly utilizing differential expression and gene-set enrichment analysis methods to identify coordinately dysregulated genes as representative of specific pathway perturbations. Transplantation offers a means to test cellular plasticity, lineage commitment, and factors required for terminal differentiation (figure depicting P14 mouse cerebellum has been adapted from the Allen Brain Atlas). Niche bioengineering allows the *in vitro* reconstruction of elements of the *in vivo* niche, using approaches such as 3D printing, hydrogels, microfabricated devices, and co-culture. Drug screening stands to benefit from organoids by providing physiologically relevant surrogate model systems for the organ of interest for high-throughput testing. Electrophysiology is a widely adopted tool for establishing neuronal maturity and connectivity (trace adapted from Nayler et al., 2017).

(ABA), Stemformatics, Zenbu, CbGRITS, CDT-DB], and analysis tools offer means to inform unbiased classification strategies (Sato et al., 2008; Chen et al., 2013; Sunkin et al., 2013; Wells et al., 2013; Severin et al., 2014; Stein et al., 2014; van de Leemput et al., 2014; Ha et al., 2015). For example, statistical comparisons to ABA datasets from discrete brain regions have provided an important framework to evaluate the temporal and spatial identity of differentiated PSCs (Brennand et al., 2015; Pasca et al., 2015; Nayler et al., 2017). These tools and resources will be instrumental in elucidating factors that could be targeted to promote the maturation of cerebellar neurons beyond an embryonic stage.

While many of these datasets utilize whole population-based sampling, recent advances in microfluidic technologies and sequencing chemistry have led to robust methodologies for the sampling of single cells, which might reconcile a number of the current limitations (Jaitin et al., 2014; Habib et al., 2016). Fine-scale sampling of individual cells will allow population profiling and delineation of cell-type-specific markers and thus the identification and isolation of cells characteristic of their *in vivo* counterparts at specific developmental windows.

CONCLUSION

In this article, we describe the major methods related to PSC-derived models of the cerebellum, including their provenance from early developmental biology studies. While the majority of differentiation protocols share some methodological overlap (primary neurulation, MHB specification, cerebellar patterning, and terminal differentiation/maturation), it appears that there are a number of distinct ways to achieve these goals. Waddington's 'Epigenetic Landscape' theory (Waddington, 1939) has often been used to illustratively map the concept of lineage specification. This remains highly relevant in the context of cerebellar differentiation, given the varying protocols used to derive cerebellar neurons with seemingly different input requirements. Further understanding of the pathways and processes that govern cerebellar self-organization will be critical to producing the next generation of PSC-derived models of the developing cerebellum. Challenges will include the recapitulation of the laminar structure of the cerebellar cortex, with its distinct configuration of neuronal and non-neuronal cells, and highly stereotyped circuits. Moreover it will be interesting to demonstrate whether formation of cerebellar organoids into lobules, including the organization of cerebellar circuits in parasagittal compartments is possible. Another highly desirable goal, particularly in light of eventual potential therapeutic use of PSC-derived neuronal cells, is the elimination of xenogeneic culture methodologies. In the absence of current protocols this advanced for cerebellar differentiation, we have discussed several methodologies that are poised to advance the field, including the next generation of classification strategies.

One of the major motivations driving cerebellar PSC research forward is the potential for creating patient-specific models and better understanding cerebellar disorders (Watson et al., 2015). Recent examples highlight the exciting future direction of the field, with advances in creating iPSC models for spinocerebellar ataxia type 6 (SCA6) and Tuberous sclerosis complex (TSC), an autism spectrum disorder (Ishida et al., 2016; Sundberg et al., 2018). SCA6 patient-derived PCs showed vulnerability to triiodothyronine depletion, which could be suppressed with thyrotropin-releasing hormone and riluzole (Ishida et al., 2016), underscoring that patient-derived cells can be used to identify unknown early disease phenotypes, and as potential drug screening tools. Similarly, the disease phenotypes in TSC patient-derived PCs including abnormal differentiation, synaptic dysfunction and hypoexcitability, could be rescued by treatment with the mTOR inhibitor rapamycin (Sundberg et al., 2018).

Together, despite the remaining challenges in the field, and given the recent history of success in the field, we are

extremely optimistic about the future of PSC-derived models in advancing our knowledge about cerebellar development and providing invaluable model systems to better understand and treat cerebellar disorders.

AUTHOR CONTRIBUTIONS

SN and EB wrote the manuscript. SN made and adapted figures with guidance from EB.

FUNDING

SN is the recipient of a fellowship from the Oxford Nuffield Medical Trust. Research in the Becker laboratory is supported by the Royal Society, the Wellcome Trust, the Rosetrees Trust, the John Fell OUP Research Fund and BrAshAT.

ACKNOWLEDGMENTS

We would like to thank members of the lab for their comments on the manuscript.

SUPPLEMENTARY MATERIAL

The Supplementary Material for this article can be found online at: https://www.frontiersin.org/articles/10.3389/fnins.2018.00646/full#supplementary-material

REFERENCES

Bagley, J. A., Reumann, D., Bian, S., Levi-Strauss, J., and Knoblich, J. A. (2017). Fused cerebral organoids model interactions between brain regions. *Nat. Methods* 14, 743–751. doi: 10.1038/nmeth.4304

Brennand, K., Savas, J. N., Kim, Y., Tran, N., Simone, A., Hashimoto-Torii, K., et al. (2015). Phenotypic differences in hiPSC NPCs derived from patients with schizophrenia. *Mol. Psychiatry* 20, 361–368. doi: 10.1038/mp.2014.22

Butts, T., Green, M. J., and Wingate, R. J. (2014). Development of the cerebellum: simple steps to make a 'little brain'. *Development* 141, 4031–4041. doi: 10.1242/dev.106559

Camp, J. G., and Treutlein, B. (2017). Human development: advances in mini-brain technology. *Nature* 545, 39–40. doi: 10.1038/545039a

Chen, E. Y., Tan, C. M., Kou, Y., Duan, Q., Wang, Z., Meirelles, G. V., et al. (2013). Enrichr: interactive and collaborative HTML5 gene list enrichment analysis tool. *BMC Bioinformatics* 14:128. doi: 10.1186/1471-2105-14-128

Dang, J., Tiwari, S. K., Lichinchi, G., Qin, Y., Patil, V. S., Eroshkin, A. M., et al. (2016). Zika virus depletes neural progenitors in human cerebral organoids through activation of the innate immune receptor TLR3. *Cell Stem Cell* 19, 258–265. doi: 10.1016/j.stem.2016.04.014

Dimos, J. T., Rodolfa, K. T., Niakan, K. K., Weisenthal, L. M., Mitsumoto, H., Chung, W., et al. (2008). Induced pluripotent stem cells generated from patients with ALS can be differentiated into motor neurons. *Science* 321, 1218–1221. doi: 10.1126/science.1158799

Erceg, S., Ronaghi, M., Zipancic, I., Lainez, S., Rosello, M. G., Xiong, C., et al. (2010). Efficient differentiation of human embryonic stem cells into functional cerebellar-like cells. *Stem Cells Dev.* 19, 1745–1756. doi: 10.1089/scd.2009.0498

Garcez, P. P., Loiola, E. C., Madeiro da Costa, R., Higa, L. M., Trindade, P., Delvecchio, R., et al. (2016). Zika virus impairs growth in human neurospheres and brain organoids. *Science* 352, 816–818. doi: 10.1126/science.aaf6116

Graham, A. D., Olof, S. N., Burke, M. J., Armstrong, J. P. K., Mikhailova, E. A., Nicholson, J. G., et al. (2017). High-resolution patterned cellular constructs by droplet-based 3D printing. *Sci. Rep.* 7:7004. doi: 10.1038/s41598-017-06358-x

Gu, Q., Tomaskovic-Crook, E., Wallace, G. G., and Crook, J. M. (2017). 3D bioprinting human induced pluripotent stem cell constructs for in situ cell proliferation and successive multilineage differentiation. *Adv. Healthc. Mater.* 6, doi: 10.1002/adhm.201700175

Ha, T., Swanson, D., Larouche, M., Glenn, R., Weeden, D., Zhang, P., et al. (2015). CbGRiTS: cerebellar gene regulation in time and space. *Dev. Biol.* 397, 18–30. doi: 10.1016/j.ydbio.2014.09.032

Ha, T. J., Swanson, D. J., Kirova, R., Yeung, J., Choi, K., Tong, Y., et al. (2012). Genome-wide microarray comparison reveals downstream genes of Pax6 in the developing mouse cerebellum. *Eur. J. Neurosci.* 36, 2888–2898. doi: 10.1111/j.1460-9568.2012.08221.x

Habib, N., Li, Y., Heidenreich, M., Swiech, L., Avraham-Davidi, I., Trombetta, J. J., et al. (2016). Div-seq: single-nucleus RNA-seq reveals dynamics of rare adult newborn neurons. *Science* 353, 925–928. doi: 10.1126/science.aad7038

Hatten, M. E., and Heintz, N. (1995). Mechanisms of neural patterning and specification in the developing cerebellum. *Annu. Rev. Neurosci.* 18, 385–408. doi: 10.1146/annurev.ne.18.030195.002125

Heintz, N. (2004). Gene expression nervous system atlas (GENSAT). *Nat. Neurosci.* 7:483. doi: 10.1038/nn0504-483

Herculano-Houzel, S. (2009). The human brain in numbers: a linearly scaled-up primate brain. *Front. Hum. Neurosci.* 3:31. doi: 10.3389/neuro.09.031.2009

Hoshino, M., Seto, Y., and Yamada, M. (2013). "Specification of cerebellar and precerebellar neurons," in *Handbook of the Cerebellum and Cerebellar Disorders*, eds M. Manto, D. L. Gruol, J. D. Schmahmann, N. Koibuchi, and F. Rossi (Berlin: Springer), 75–87. doi: 10.1007/978-94-007-1333-8_5

Ishida, Y., Kawakami, H., Kitajima, H., Nishiyama, A., Sasai, Y., Inoue, H., et al. (2016). Vulnerability of purkinje cells generated from spinocerebellar ataxia type 6 patient-derived iPSCs. *Cell Rep.* 17, 1482–1490. doi: 10.1016/j.celrep.2016.10.026

Jaitin, D. A., Kenigsberg, E., Keren-Shaul, H., Elefant, N., Paul, F., Zaretsky, I., et al. (2014). Massively parallel single-cell RNA-seq for marker-free decomposition of tissues into cell types. *Science* 343, 776–779. doi: 10.1126/science.1247651

Kang, H. J., Kawasawa, Y. I., Cheng, F., Zhu, Y., Xu, X., Li, M., et al. (2011). Spatio-temporal transcriptome of the human brain. *Nature* 478, 483–489. doi: 10.1038/nature10523

Kelava, I., and Lancaster, M. A. (2016). Stem cell models of human brain development. *Cell Stem Cell* 18, 736–748. doi: 10.1016/j.stem.2016.05.022

Lancaster, M. A., Corsini, N. S., Wolfinger, S., Gustafson, E. H., Phillips, A. W., Burkard, T. R., et al. (2017). Guided self-organization and cortical plate formation in human brain organoids. *Nat. Biotechnol.* 35, 659–666. doi: 10.1038/nbt.3906

Lancaster, M. A., Renner, M., Martin, C. A., Wenzel, D., Bicknell, L. S., Hurles, M. E., et al. (2013). Cerebral organoids model human brain development and microcephaly. *Nature* 501, 373–379. doi: 10.1038/nature12517

Leto, K., Arancillo, M., Becker, E. B., Buffo, A., Chiang, C., Ding, B., et al. (2016). Consensus paper: cerebellar development. *Cerebellum* 15, 789–828. doi: 10.1007/s12311-015-0724-2

Mansour, A. A., Goncalves, J. T., Bloyd, C. W., Li, H., Fernandes, S., Quang, D., et al. (2018). An in vivo model of functional and vascularized human brain organoids. *Nat. Biotechnol.* 36, 432–441. doi: 10.1038/nbt.4127

Miller, J. A., Ding, S. L., Sunkin, S. M., Smith, K. A., Ng, L., Szafer, A., et al. (2014). Transcriptional landscape of the prenatal human brain. *Nature* 508, 199–206. doi: 10.1038/nature13185

Muguruma, K., Nishiyama, A., Kawakami, H., Hashimoto, K., and Sasai, Y. (2015). Self-organization of polarized cerebellar tissue in 3D culture of human pluripotent stem cells. *Cell Rep.* 10, 537–550. doi: 10.1016/j.celrep.2014.12.051

Muguruma, K., Nishiyama, A., Ono, Y., Miyawaki, H., Mizuhara, E., Hori, S., et al. (2010). Ontogeny-recapitulating generation and tissue integration of ES cell-derived Purkinje cells. *Nat. Neurosci.* 13, 1171–1180. doi: 10.1038/nn.2638

Murrow, L. M., Weber, R. J., and Gartner, Z. J. (2017). Dissecting the stem cell niche with organoid models: an engineering-based approach. *Development* 144, 998–1007. doi: 10.1242/dev.140905

Nayler, S. P., Powell, J. E., Vanichkina, D. P., Korn, O., Wells, C. A., Kanjhan, R., et al. (2017). Human iPSC-derived cerebellar neurons from a patient with ataxia-telangiectasia reveal disrupted gene regulatory networks. *Front. Cell. Neurosci.* 11:321. doi: 10.3389/fncel.2017.00321

Nguyen, H., Ostendorf, A. P., Satz, J. S., Westra, S., Ross-Barta, S. E., Campbell, K. P., et al. (2013). Glial scaffold required for cerebellar granule cell migration is dependent on dystroglycan function as a receptor for basement membrane proteins. *Acta Neuropathol. Commun.* 1:58. doi: 10.1186/2051-5960-1-58

Okkelman, I. A., Foley, T., Papkovsky, D. B., and Dmitriev, R. I. (2017). Live cell imaging of mouse intestinal organoids reveals heterogeneity in their oxygenation. *Biomaterials* 146, 86–96. doi: 10.1016/j.biomaterials.2017.08.043

Pasca, A. M., Sloan, S. A., Clarke, L. E., Tian, Y., Makinson, C. D., Huber, N., et al. (2015). Functional cortical neurons and astrocytes from human pluripotent stem cells in 3D culture. *Nat. Methods* 12, 671–678. doi: 10.1038/nmeth.3415

Pham, M. T., Pollock, K. M., Rose, M. D., Cary, W. A., Stewart, H. R., Zhou, P., et al. (2018). Generation of human vascularized brain organoids. *Neuroreport* 29, 588–593. doi: 10.1097/WNR.0000000000001014

Ponti, G., Peretto, P., and Bonfanti, L. (2008). Genesis of neuronal and glial progenitors in the cerebellar cortex of peripuberal and adult rabbits. *PLoS One* 3:e2366. doi: 10.1371/journal.pone.0002366

Qian, X., Nguyen, H. N., Song, M. M., Hadiono, C., Ogden, S. C., Hammack, C., et al. (2016). Brain-region-specific organoids using mini-bioreactors for modeling ZIKV exposure. *Cell* 165, 1238–1254. doi: 10.1016/j.cell.2016.04.032

Quadrato, G., Nguyen, T., Macosko, E. Z., Sherwood, J. L., Min Yang, S., Berger, D. R., et al. (2017). Cell diversity and network dynamics in photosensitive human brain organoids. *Nature* 545, 48–53. doi: 10.1038/nature22047

Salero, E., and Hatten, M. E. (2007). Differentiation of ES cells into cerebellar neurons. *Proc. Natl. Acad. Sci. U.S.A.* 104, 2997–3002. doi: 10.1073/pnas.0610879104

Sances, S., Bruijn, L. I., Chandran, S., Eggan, K., Ho, R., Klim, J. R., et al. (2016). Modeling ALS with motor neurons derived from human induced pluripotent stem cells. *Nat. Neurosci.* 19, 542–553. doi: 10.1038/nn.4273

Sandor, C., Robertson, P., Lang, C., Heger, A., Booth, H., Vowles, J., et al. (2017). Transcriptomic profiling of purified patient-derived dopamine neurons identifies convergent perturbations and therapeutics for Parkinson's disease. *Hum. Mol. Genet.* 26, 552–566. doi: 10.1093/hmg/ddw412

Sato, A., Sekine, Y., Saruta, C., Nishibe, H., Morita, N., Sato, Y., et al. (2008). Cerebellar development transcriptome database (CDT-DB): profiling of spatio-temporal gene expression during the postnatal development of mouse cerebellum. *Neural Netw.* 21, 1056–1069. doi: 10.1016/j.neunet.2008.05.004

Schwartz, M. P., Hou, Z., Propson, N. E., Zhang, J., Engstrom, C. J., Santos Costa, V., et al. (2015). Human pluripotent stem cell-derived neural constructs for predicting neural toxicity. *Proc. Natl. Acad. Sci. U.S.A.* 112, 12516–12521. doi: 10.1073/pnas.1516645112

Severin, J., Lizio, M., Harshbarger, J., Kawaji, H., Daub, C. O., Hayashizaki, Y., et al. (2014). Interactive visualization and analysis of large-scale sequencing datasets using ZENBU. *Nat. Biotechnol.* 32, 217–219. doi: 10.1038/nbt.2840

Stein, J. L., de la Torre-Ubieta, L., Tian, Y., Parikshak, N. N., Hernandez, I. A., Marchetto, M. C., et al. (2014). A quantitative framework to evaluate modeling of cortical development by neural stem cells. *Neuron* 83, 69–86. doi: 10.1016/j.neuron.2014.05.035

Su, H. L., Muguruma, K., Matsuo-Takasaki, M., Kengaku, M., Watanabe, K., and Sasai, Y. (2006). Generation of cerebellar neuron precursors from embryonic stem cells. *Dev. Biol.* 290, 287–296. doi: 10.1016/j.ydbio.2005.11.010

Sundberg, M., Tochitsky, I., Buchholz, D. E., Winden, K., Kujala, V., Kapur, K., et al. (2018). Purkinje cells derived from TSC patients display hypoexcitability and synaptic deficits associated with reduced FMRP levels and reversed by rapamycin. *Mol. Psychiatry* doi: 10.1038/s41380-018-0018-4 [Epub ahead of print].

Sunkin, S. M., Ng, L., Lau, C., Dolbeare, T., Gilbert, T. L., Thompson, C. L., et al. (2013). Allen brain atlas: an integrated spatio-temporal portal for exploring the central nervous system. *Nucleic Acids Res.* 41, D996–D1008. doi: 10.1093/nar/gks1042

Tao, O., Shimazaki, T., Okada, Y., Naka, H., Kohda, K., Yuzaki, M., et al. (2010). Efficient generation of mature cerebellar Purkinje cells from mouse embryonic stem cells. *J. Neurosci. Res.* 88, 234–247. doi: 10.1002/jnr.22208

Titmarsh, D. M., Glass, N. R., Mills, R. J., Hidalgo, A., Wolvetang, E. J., Porrello, E. R., et al. (2016). Induction of human iPSC-derived cardiomyocyte proliferation revealed by combinatorial screening in high density microbioreactor arrays. *Sci. Rep.* 6:24637. doi: 10.1038/srep24637

Titmarsh, D. M., Ovchinnikov, D. A., Wolvetang, E. J., and Cooper-White, J. J. (2013). Full factorial screening of human embryonic stem cell maintenance with multiplexed microbioreactor arrays. *Biotechnol. J.* 8, 822–834. doi: 10.1002/biot.201200375

van de Leemput, J., Boles, N. C., Kiehl, T. R., Corneo, B., Lederman, P., Menon, V., et al. (2014). CORTECON: a temporal transcriptome analysis of in vitro human cerebral cortex development from human embryonic stem cells. *Neuron* 83, 51–68. doi: 10.1016/j.neuron.2014.05.013

Waddington, C. H. (1939). *An Introduction to Modern Genetics*. London: George Allen & Unwin.

Wang, S., Wang, B., Pan, N., Fu, L., Wang, C., Song, G., et al. (2015). Differentiation of human induced pluripotent stem cells to mature functional Purkinje neurons. *Sci. Rep.* 5:9232. doi: 10.1038/srep09232

Wang, V. Y., and Zoghbi, H. Y. (2001). Genetic regulation of cerebellar development. *Nat. Rev. Neurosci.* 2, 484–491. doi: 10.1038/35081558

Wassef, M. (2013). "Specification of the cerebellar territory," in *Handbook of the Cerebellum and Cerebellar Disorders*, eds M. Manto, D. L. Gruol, J. D. Schmahmann, N. Koibuchi, and F. Rossi (Berlin: Springer), 3–21. doi: 10.1007/978-94-007-1333-8_1

Watson, L. M., Wong, M. M., and Becker, E. B. (2015). Induced pluripotent stem cell technology for modelling and therapy of cerebellar ataxia. *Open Biol.* 5:150056. doi: 10.1098/rsob.150056

Watson, L. M., Wong, M. M. K., Vowles, J., Cowley, S. A., and Becker, E. B. E. (2018). A simplified method for generating purkinje cells from human-induced pluripotent stem cells. *Cerebellum* 17, 419–427. doi: 10.1007/s12311-017-0913-2

Wells, C. A., Mosbergen, R., Korn, O., Choi, J., Seidenman, N., Matigian, N. A., et al. (2013). Stemformatics: visualisation and sharing of stem cell gene expression. *Stem Cell Res.* 10, 387–395. doi: 10.1016/j.scr.2012.12.003

Wichterle, H., Lieberam, I., Porter, J. A., and Jessell, T. M. (2002). Directed differentiation of embryonic stem cells into motor neurons. *Cell* 110, 385–397. doi: 10.1016/S0092-8674(02)00835-8

Woodard, C. M., Campos, B. A., Kuo, S. H., Nirenberg, M. J., Nestor, M. W., Zimmer, M., et al. (2014). iPSC-derived dopamine neurons reveal differences between monozygotic twins discordant for Parkinson's disease. *Cell Rep.* 9, 1173–1182. doi: 10.1016/j.celrep.2014.10.023

Yanagi, Y., Nakayama, K., Taguchi, T., Enosawa, S., Tamura, T., Yoshimaru, K., et al. (2017). In vivo and ex vivo methods of growing a liver bud through tissue connection. *Sci. Rep.* 7:14085. doi: 10.1038/s41598-017-14542-2

Yoon, K. J., Nguyen, H. N., Ursini, G., Zhang, F., Kim, N. S., Wen, Z., et al. (2014). Modeling a genetic risk for schizophrenia in iPSCs and mice reveals neural stem cell deficits associated with adherens junctions and polarity. *Cell Stem Cell* 15, 79–91. doi: 10.1016/j.stem.2014.05.003

Zhang, S. C., Wernig, M., Duncan, I. D., Brustle, O., and Thomson, J. A. (2001). In vitro differentiation of transplantable neural precursors from human embryonic stem cells. *Nat. Biotechnol.* 19, 1129–1133. doi: 10.1038/nbt1201-1129

Conflict of Interest Statement: The authors declare that the research was conducted in the absence of any commercial or financial relationships that could be construed as a potential conflict of interest.

frontiers in Neuroscience

MINI REVIEW
published: 02 November 2018
doi: 10.3389/fnins.2018.00800

Regenerative Approaches in Huntington's Disease: From Mechanistic Insights to Therapeutic Protocols

Jenny Sassone[1], Elsa Papadimitriou[2] and Dimitra Thomaidou[2]**

[1] *Vita-Salute University and San Raffaele Scientific Institute, Milan, Italy,* [2] *Department of Neurobiology, Hellenic Pasteur Institute, Athens, Greece*

Huntington's Disease (HD) is a neurodegenerative disorder caused by a CAG expansion in the exon-1 of the IT15 gene encoding the protein Huntingtin. Expression of mutated Huntingtin in humans leads to dysfunction and ultimately degeneration of selected neuronal populations of the striatum and cerebral cortex. Current available HD therapy relies on drugs to treat chorea and control psychiatric symptoms, however, no therapy has been proven to slow down disease progression or prevent disease onset. Thus, although 24 years have passed since HD gene identification, HD remains a relentless progressive disease characterized by cognitive dysfunction and motor disability that leads to death of the majority of patients, on average 10–20 years after its onset. Up to now several molecular pathways have been implicated in the process of neurodegeneration involved in HD and have provided potential therapeutic targets. Based on these data, approaches currently under investigation for HD therapy aim on the one hand at getting insight into the mechanisms of disease progression in a human-based context and on the other hand at silencing mHTT expression by using antisense oligonucleotides. An innovative and still poorly investigated approach is to identify new factors that increase neurogenesis and/or induce reprogramming of endogenous neuroblasts and parenchymal astrocytes to generate new healthy neurons to replace lost ones and/or enforce neuroprotection of pre-existent striatal and cortical neurons. Here, we review studies that use human disease-in-a-dish models to recapitulate HD pathogenesis or are focused on promoting *in vivo* neurogenesis of endogenous striatal neuroblasts and direct neuronal reprogramming of parenchymal astrocytes, which combined with neuroprotective protocols bear the potential to re-establish brain homeostasis lost in HD.

Keywords: Huntington's disease, iPCs, direct reprogramming, neuroprotection, *in vivo* reprogramming, miRNAs

OPEN ACCESS

Edited by:
Annalisa Buffo,
Università degli Studi di Torino, Italy

Reviewed by:
Karine Merienne,
Centre National de la Recherche Scientifique (CNRS), France
Dario Besusso,
Institute of Neuroscience (CAS), China

****Correspondence:***
Dimitra Thomaidou
thomaidou@pasteur.gr
Jenny Sassone
sassone.jenny@hsr.it

Specialty section:
This article was submitted to Neurogenesis, a section of the journal Frontiers in Neuroscience

Received: *29 June 2018*
Accepted: *15 October 2018*
Published: *02 November 2018*

Citation:
Sassone J, Papadimitriou E and Thomaidou D (2018) Regenerative Approaches in Huntington's Disease: From Mechanistic Insights to Therapeutic Protocols. Front. Neurosci. 12:800. doi: 10.3389/fnins.2018.00800

INTRODUCTION

Huntington's Disease (HD) is an autosomal-dominant neurodegenerative disorder with prevalence of ∼7–11 per 100,000 in the caucasian population (Spinney, 2010). It is caused by abnormal expansion of a trinucleotide CAG repeat in exon 1 of the HTT gene (MacDonald et al., 1993) and is characterized by severe motor, cognitive and psychiatric symptoms. HD neuropathology

is characterized by preferential degeneration of GABAergic medium spiny neurons (MSNs) of the striatum and, in a lesser extent, of pyramidal projection neurons in cortical layers V, VI, and III, innervating the striatum (Cudkowicz and Kowall, 1990). Neurodegeneration in HD is preceded by a long period of neuronal dysfunction, associated with transcriptional and epigenetic changes resulting in progressive loss of striatal identity (Seredenina and Luthi-Carter, 2012; Langfelder et al., 2016). Neurodegeneration in HD may also be accompanied by decreased striatal neurogenesis, a fact that may also account for part of HD symptomatology (Ernst et al., 2014). As of now, molecular mechanisms underlying HD pathogenesis remain elusive, and no therapeutic treatments are currently available beyond clinical symptomatic management.

An effective therapy in HD may use a combined approach of cell *trans*-differentiation and neuroprotection. The following chapters review the main identified molecular pathways and potential therapeutic targets which can lead to the development of cell reprogramming and neuroprotective protocols (**Figure 1**).

CELL REPLACEMENT APPROACHES IN ANIMAL MODELS OF HD

A variety of rodent models have been created to recapitulate neuropathological features and symptoms of either juvenile, early adult, or adult human HD (Mangiarini et al., 1996; Slow et al., 2003) and to develop cell therapy protocols using renewable cell sources, including fetal neural stem cells (NSCs), embryonic stem cells (ESCs), induced pluripotent stem cells (iPSCs) and induced neural stem cells (iNSCs) for brain repair in HD (for review see (Tartaglione et al., 2017). The majority of recent transplantation studies were performed using the Quinolinic Acid (QA) excitotoxic lesion model, as it induces a selective loss of striatal MSNs with a relative preservation of interneurons, largely resembling the neuropathological features of human HD (Beal et al., 1991). In these studies human progenitor cells, either hESCs or hiPSCs were, prior to their transplantation, *in vitro* differentiated to striatal progenitors or immature MSNs, either through directed differentiation protocols modulating the levels of extrinsic developmental signals, such as BMP/TGFβ (Carri et al., 2013), Sonic Hedgehog (SHH) and Activin A (Arber et al., 2015) or by forced expression of transcription factors (TFs) involved in MSNs differentiation, such as GSX2 and EBF1 (Faedo et al., 2017). In these studies, transplantation of the enriched populations of striatal progenitors resulted in their functional integration into the lesioned striatum, a subpopulation of which differentiated to DARPP-32^{+} MSNs (Arber et al., 2015), extended fibers over a long distance (Faedo et al., 2017), projected to the substantia nigra and received GABAergic and glutamatergic inputs, leading to restoration of apomorphine-induced rotational behavior (Ma et al., 2012). In a very recent study, a hydrogel scaffold has been used for the more effective, rapid and scalable directed differentiation of human iPSCs to striatal progenitors in three-dimensional (3D) organoid-like structures (Adil et al., 2018). 3D-derived striatal progenitors grafted into R6/2 HD mice (Mangiarini et al., 1996), developed an MSN-like phenotype and formed synaptic connections with host cells, resulting in improvement of mice motor coordination (Adil et al., 2018). Although the use of human cells – in particular healthy hESCs that partially overcomes the problem of dealing with a diseased system – bears potential for cell replacement, studies are still in a preliminary stage and more rigorous testing of human cell directed differentiation on 2D and 3D culture systems and transplantation in various HD animal models is needed to assess both circuit reconstruction and behavioral recovery in HD.

IN VITRO DIFFERENTIATION FOR HD MODELING

Whilst HD rodent models have undoubtedly yielded much useful data, the nature of these systems makes insights gained from such a stand-alone model limited when it comes to translation in human patients. On the other hand, cell transplantation has only partially restored lost function in pre-clinical models and clinical trials. To this end the discovery and advancement of iPSCs technology has allowed for a more thorough study of human HD on a cellular and developmental level. The first iPSC lines were generated from HD patients (Park et al., 2008) and since then, many iPSC-based human HD cell models with different CAG repeat lengths have been generated, among which, the ones generated by the HD iPSC Consortium are the best characterized (Jeon et al., 2012; The HD iPSC Consortium, 2012). HD iPSCs and the neural cell types derived from them recapitulate some disease phenotypes found in both human patients and animal models, such as altered cell growth (Jeon et al., 2012), cell adhesion, survival, electrophysiological properties, metabolism (The HD iPSC Consortium, 2012), protein clearance (proteasomal, autophagic), oxidative stress/antioxidant response (Szlachcic et al., 2015) and mitochondrial fragmentation (Guo et al., 2013). Interestingly, gene expression studies have revealed that neurons derived from HD iPSCs exhibit deregulated signaling pathways directly related to development and neurogenesis. Conforti et al., 2018 showed that early telencephalic induction and late neural identity are affected in cortical and striatal populations obtained from HD iPSC lines. It was also reported for the first time using cortical organoids that large CAG expansion causes complete failure of the neuro-ectodermal acquisition, while cells carrying shorter CAG repeats show gross abnormalities in neural rosette formation as well as disrupted cytoarchitecture (Conforti et al., 2018). Interestingly, gene-expression analysis revealed that control organoids overlapped with differentiated human fetal cortical areas, while HD organoids correlated with the immature ventricular / subventricular zone (Conforti et al., 2018). Along the same lines, recent data using isogenic human embryonic stem cell (hESC) lines, suggest that HD is caused by chromosomal instability and begins far earlier than expected as a dominant-negative loss-of function, rather than through the broadly accepted gain-of toxic function mechanism (Ruzo et al., 2018). This evidence supports the hypothesis that an early neurodevelopmental

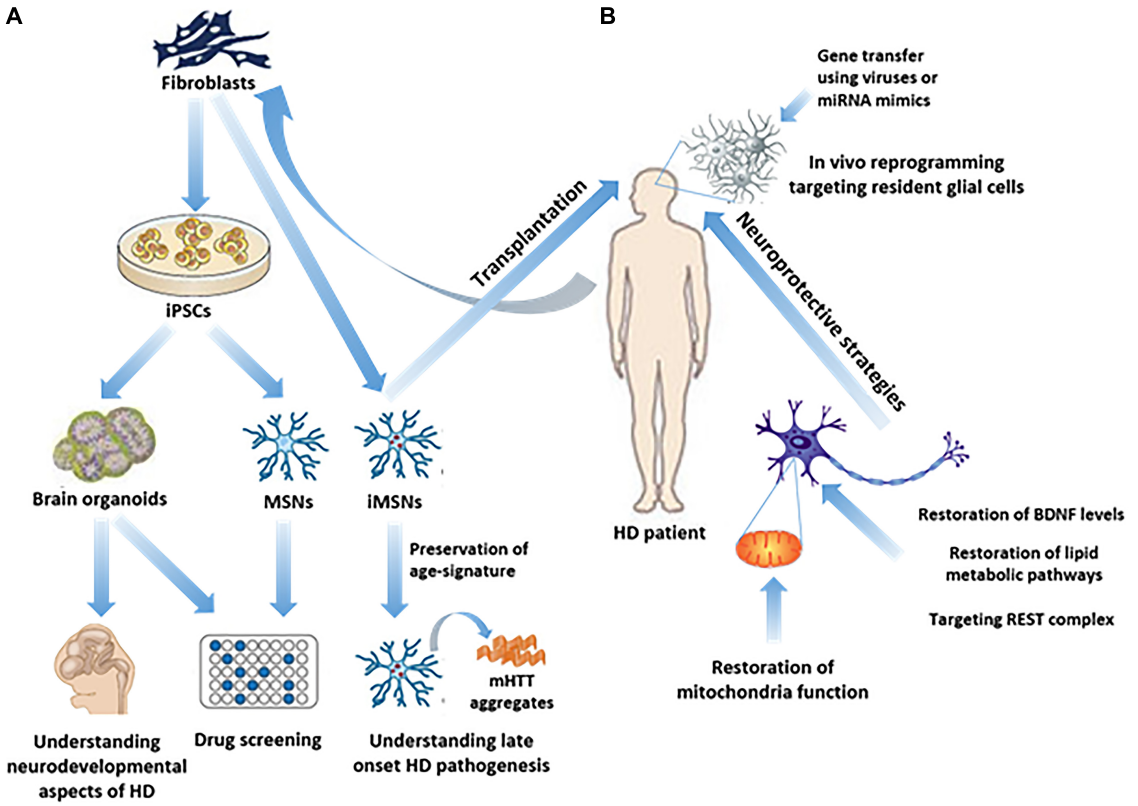

FIGURE 1 | Study of HD pathogenesis and possible therapeutic approaches in humans. **(A)** iPSC technology has made it possible to generate *in vitro* brain organoids or subtype specific neuronal populations related to HD, such as MSNs, from HD patients' fibroblasts, thus enabling the study of the neurodevelopmental aspects of HD, as well as drug screening. Direct reprogramming of patients' fibroblasts to induced-MSNs (iMSNs) facilitated the study of late onset HD pathogenesis, since iMSNs retain age-related signatures. **(B)** *In vivo* regenerative approaches as possible therapeutic strategies, including transplantation of iMSNs or direct reprogramming of resident glial cells into induced neurons in the striatum, remain to be further explored. On the other hand, neuroprotective approaches have been more extensively explored aiming either at targeting REST complex activity, or at the restoration of BDNF levels, lipid metabolic pathways or mitochondrial function.

defect exists in HD and could contribute to the later adult neurodegenerative phenotype (Lim et al., 2017; Wiatr et al., 2018).

Considering this pathological phenotype, PSCs, including iPSCs and ESCs, have been used to screen for HD therapies. A screen in wild type human ESCs-derived neural stem cells (NSCs) for chemical inhibitors of the transcriptional repressor REST resulted in the identification of one potent compound, named X5050, able to increase the expression of neuronal genes targeted by REST in wild type neural cells (Charbord et al., 2013). Acute intraventricular delivery of this small molecule increased the expression of the key neurotrophic factor BDNF, being depleted during disease progression (Zuccato et al., 2001), as well as, several other REST-regulated genes in the prefrontal cortex of mice with QA-induced striatal lesions (Charbord et al., 2013), highlighting its potential therapeutic value in HD. In another study led by the HD iPSC Consortium, RNA-seq analysis in iPSC-derived neural cultures revealed consistent deficits related to neurodevelopmental gene networks and led to the identification of a small molecule, isoxazole-9 (Isx-9), that targeted several of these dysregulated networks and successfully normalized CAG repeat-associated phenotypes in both juvenile- and adult-onset HD iPSC-derived neural cultures, as well as cognition and synaptic pathology in R6/2 HD mice (Lim et al., 2017).

Hence, these results highlight that ESC/iPSC are promising cellular models for the investigation of the molecular defects underlying HD pathogenesis and the screening of compounds for HD therapies. Important caveat remains the need for optimization of human iPSC models, including reprogramming and differentiation protocols, for the purposes of consistent observation. Importantly, given the fact that human iPSCs become rejuvenated by erasing epigenetic aging signatures (Mertens et al., 2015), they seem more appropriate for studying early onset diseases and this is probably the reason that the majority of results obtained from studies using iPSCs is derived from individuals with juvenile onset HD (>60 CAGs) rather than with adult onset HD (39–60 CAGs) (Park et al., 2008; Guo et al., 2013; Szlachcic et al., 2015). The contribution of epigenetic aging signature in the appearance of HD pathology is also supported by the finding that human iPSC-derived lines with expansion lower than 60 CAG repeats, corresponding to late onset HD pathology, don't exhibit major observable pathological phenotypes (Mattis and Svendsen, 2018).

Direct Reprogramming in HD: Preservation of Age-Related Signatures

Accordingly it has been recently established that modeling an adult-onset disorder might require the maintenance of aging signatures. Along this line, direct reprogramming approaches that result in the production of neuronal types that retain donor age-dependent aging signatures, such as age-specific transcriptional profiles, nucleo-cytoplasmic compartmentalization and an aged DNA methylation epigenetic clock (Mertens et al., 2015), seem to be appropriate human models for the study of HD, which is primarily an adult-onset disease. Victor et al., 2014 reported for the first time the direct reprogramming of human fibroblasts into induced-MSNs (i-MSNS), by force-expressing neurogenic miRNAs miR-9/9*−miR-124 together with the TFs CTIP2, DLX1/2, and MYT1L. Interestingly, when the i-MSNs were transplanted into the mouse striatum they survived for more than 6 months and projected to their correct targets (Victor et al., 2014). Recently the same group expanded this protocol for the *in vitro* generation of i-MSNs from healthy and HD-patients' fibroblasts (Victor et al., 2018). Remarkably, HD neurons generated in this manner displayed inclusion-body formation, mitochondrial and metabolic dysfunction and cell death, mirroring the defects occurring in the striatum of HD patients. By contrast, heMSNs derived by direct conversion of human HD embryonic fibroblasts (HEFs), produced by differentiation of HD-iPSCs, exerted a milder HD phenotype with lower mHTT aggregation, supporting the notion that the age-related decline in protein homeostasis could contribute to HD pathology. Taken together the findings of this study presented for the first time a patient-based platform of MSNs for the study of the age-related mechanisms of late onset HD pathogenesis and proved that in a human context cellular age is an essential component underlying the manifestation of HD phenotypes and that age-associated reduction in protein homeostasis levels is primarily responsible for mHTT aggregation in HD i-MSNs.

IN VIVO REPROGRAMMING FOR HD THERAPY

A novel strategy for cell replacement therapy for HD is the concept of *in vivo* cell reprogramming in the striatum, which is the area mostly affected. Increasing evidence indicates that astrocytes within the striatal parenchyma can undergo endogenous *trans*-differentiation into neuroblasts after stroke or QA-mediated excitotoxic lesion that induces selective loss of striatal MSNs (Magnusson et al., 2014; Nato et al., 2015), revealing the intrinsic existence of a latent neurogenic capacity in the adult striatum. These cells were found to express markers of immature newborn neurons like ASCL1 or DCX, while some of them developed into mature $NeuN^+$ neurons, several of which expressed MSN TFs (Luzzati et al., 2011) and the MSN marker neuronal nitric oxide synthase (nNOS), while they formed synaptic connections (Magnusson et al., 2014). However, most newborn neurons generated in both studies have a short life-span and fail to express markers of fully differentiated striatal neurons, either due to their precocious death or lack of proper commitment, but attain complex and specific morphologies (Magnusson et al., 2014; Nato et al., 2015). Additionally, studies in early and late onset HD genetic models have revealed the presence of newborn neurons in the striatal area, that have either ectopically migrated from the SVZ (Kohl et al., 2010) or have originated from selective proliferation in the striatal area, respectively (Kandasamy et al., 2015). Importantly, intraventricular administration of BDNF/Noggin in R6/2 mice enhanced striatal neurogenesis and delayed motor impairment, implicating induced neurogenesis as an important contributor to functional recovery (Cho et al., 2007). Along the same lines, continuous administration of FGF2 in R6/2 mice not only stimulated SVZ neurogenesis and newborn neurons' recruitment to the striatum, but also provided neuroprotection and prolonged survival of striatal neurons (Jin et al., 2005). In parallel, *in vivo* reprogramming has been a promising approach for the conversion of glial cells (astrocytes, NG2 glia and pericytes) into more mature, subtype-specific neurons under defined conditions using specific TFs both in the injured cortex (Heinrich et al., 2010, 2014; Guo et al., 2014) and normal striatum (Niu et al., 2013; Torper et al., 2013, 2015). In some of those studies the induced neurons were electrophysiologically functional and could integrate into the endogenous circuitry (Guo et al., 2014; Torper et al., 2015), highlighting the potential of this approach in producing functionally mature neurons *in vivo*. Recently the *in vivo* direct reprogramming approach has been successfully employed in a mouse model of Parkinson's disease (Rivetti Di Val Cervo et al., 2017). In this study a combination of the TFs NEUROD1, ASCL1, and LMX1A with the microRNA miR-218 was used in order to reprogram adult striatal astrocytes into induced dopaminergic neurons that were shown to be excitable and managed to correct some aspects of motor behavior *in vivo*. However, it must be kept in mind that enhancement of endogenous neurogenesis, or *in vivo* reprogramming do not address the fact that mHTT is not targeted and is widely expressed throughout the brain, so a primary neurodegenerative process can occur in newly generated cells. However, as HD is an age related disease, a high rate of new neurogenesis may lead to tissue rejuvenation providing substantial benefit. Thus, *in vivo* direct reprogramming remains a promising approach for the production of healthy MSNs in the striatum with interesting and still largely unexplored potential, especially if the reprogramming process is combined with gene therapy strategies aiming at the down-regulation of mHTT in the reprogrammed newborn neurons. To this end, approaches to reduce mHTT levels *in vivo* in animal HD models are being tested over the last decade using either intrastriatal rAAV-mediated delivery of anti-mHTT shRNAs (Rodriguez-Lebron et al., 2005), antisense oligonucleotides (ASO) that catalyze RNase H-mediated degradation of mHTT mRNA (Kordasiewicz et al., 2012), or more recently miRNA-based mHTT mRNA-lowering using AAV viral vectors (Miniarikova et al., 2017). All these approaches so far (recently reviewed in Miniarikova et al., 2018) show promising results in alleviating HD symptomatology in animal models and could potentially

be combined with regenerative therapeutic strategies and/or neuroprotective molecules in order to further enhance their therapeutic effect on HD progression. To this end, a recently released drug trial using the antisense oligonucleotide, IONIS-HTT_R that targets Huntingtin mRNA and suppresses mutant HTT production, has shown promise as a potential disease-modifying HD therapy (Tabrizi et al., 2018).

THE ROLE OF miRNAs IN HD THERAPEUTIC APPROACHES

As already mentioned, miRNAs (miR-9/9*, miR-124, miR-218) have been already used in direct reprogramming protocols in combination with TFs to produce induced-striatal, cortical or motor neurons. Interestingly, besides their promising use in direct reprogramming protocols to slow down HD progression, miRNAs are also implicated in HD pathology and it has been very recently reported that disease-specific miRNAs have been detected in the cerebrospinal fluid (CSF) of HD patients (Reed et al., 2017) and could be potentially used as early HD prognostic markers. The perturbation of the neural miRNA system observed in HD, in many cases occurs through a mechanism involving the REST complex. REST complex targets include the neuronal specific microRNAs miR-9/9*, miR-29a, miR-29b, miR-124 and miR-132 (Johnson and Buckley, 2009), all being dysregulated in human HD samples, or mouse models of HD. Conversely, components of the REST complex are targets for down-regulation by certain neurogenic miRNAs, such as miR-9/9* and miR-124, suggesting that their neurogenic potential is at least in part due to challenging REST complex levels and/or activity (Visvanathan et al., 2007; Packer et al., 2008), a concept that may have far reaching implications regarding experimental therapeutic strategies for HD. miR-124 is the most abundant miRNA in both the embryonic and adult CNS, acting globally to increase the expression levels of neuronal genes through several different pathways, including repression of anti-neural transcriptional repressor REST complex (Visvanathan et al., 2007). Dysregulation of miR-124 has been shown in many CNS disorders and conditions, including CNS tumors, inflammation and stroke (Sun et al., 2015). During HD progression in particular, the levels of miR-124, as well as other neurogenic miRNAs, are significantly reduced (Johnson and Buckley, 2009), resulting in disorganization of the neurogenic program. On the other hand miR-124 enhances striatal neurogenesis in HD, as striatal stereotaxic injection of miR-124 mimics increased striatal cells' proliferation and improved motor function of R6/2 mice (Liu et al., 2015), while exosomal delivery of miR-124 in a mouse model of ischemia led to an increase in cortical neurogenesis and ameliorated the injury (Yang et al., 2017). However, the neurogenic/ neuroprotective potential of miR-124 in HD remains to be further studied, as in a recent study exosome-based delivery of miR-124 in the striatum of R6/2 mice did not lead to a behavioral improvement (Lee et al., 2017). In light of the evidence provided that the neural miRNA system is affected during HD progression, the mechanism of action of specific brain-enriched miRNAs in instructing or reinforcing neurogenesis or *in vivo* neuronal reprogramming would lead to the identification of new therapeutic strategies to combat HD.

NEUROPROTECTION AS A MEANS TO REDUCE OR PREVENT NEURONAL DEGENERATION IN HD

It is obvious from recent studies that although significant advances have been made in the identification of molecular pathways and screening of potential drug targets using stem cells and reprogramming technologies (for review see (Connor, 2018), a stand-alone therapeutic strategy cannot reverse HD progression. Promoting neuronal replacement from endogenous sources and fostering neuroprotection of existing neurons are distinct but complementary strategies in view of devising an effective therapy in HD. Coupling these two approaches, ideally along with – as already mentioned – a strategy for the downregulation of mHTT, could have profound clinical impact. On the one hand induced-newborn neurons will rejuvenate the injured striatum, but require substantial support for their long-time survival and incorporation into the existing neural networks, while on the other hand the existing mature neurons need also support in order to alleviate their degeneration due to the wide presence of mHTT in the diseased brain. Thus, molecular mechanisms enhancing neurogenesis and neuroprotection represent valuable candidates in the field.

Neuroprotective Protocols Aimed at Restoring BDNF Levels

Countless evidence shows that BDNF or BDNF/TRKB signaling is reduced in HD due to a mHTT-mediated mechanism. Produced by cortical neurons, BDNF promotes neuronal growth, survival of striatal neurons and plasticity. mHTT causes changes in vesicular transport of BDNF and transcriptional down-regulation of the BDNF gene. Indeed, BDNF levels are decreased in HD mouse models and in the brains of HD patients (Zuccato and Cattaneo, 2014). Restoration of BDNF levels is of interest in HD and delivery of BDNF through viral or stem-cell vehicles has shown some potential in inducing striatal neuronal regeneration, delaying motor impairment and extending survival in HD mouse models (Cho et al., 2007), but delivering a protein-based therapeutic to the CNS remains an important challenge. Because BDNF acts principally through binding to TRKB receptors, one approach is the developing of TRKB agonists and TRKB monoclonal antibodies. Several experimental compounds have been tested in HD mouse models and provided promising neuroprotective effects (Wild and Tabrizi, 2014). In particular small molecule modulation of p75NTR TRKB receptor has been shown to effectively reduce HD phenotype in mouse models providing evidence that targeting p75NTR may be an effective strategy for HD treatment (Simmons et al., 2013, 2016). Another innovative approach to restore BDNF levels is by inhibiting the formation of the REST-mSIN3 complex that is required for BDNF transcriptional repression. One compound has been identified, and encouraging results obtained in mHTT knock-in NSC lines

(Conforti et al., 2013). Alternatively, as already discussed, neurogenic miRNAs and in particular miR-9/9* and miR-124 could serve as therapeutic agents to target the REST complex, as they have been both shown to down-regulate either REST itself (Packer et al., 2008) or other REST cofactors (Visvanathan et al., 2007). Thus, a combination of chemical compounds and miRNAs reducing REST complex formation may prove effective for HD treatment.

Neuroprotective Approaches Acting on Metabolic Pathways

A big number of studies has highlighted mitochondrial defects leading to impaired energy metabolism and cellular oxidative stress in HD models and tissues of HD patients (Guedes-Dias et al., 2016; Liot et al., 2017). In this context, a potential target is the peroxisome proliferator-activated receptor (PPAR) gamma coactivator 1 alpha (PGC-1α), a transcriptional co-regulator of many nuclear-encoded mitochondrial genes. Expression of PGC-1α and its target genes get reduced in HD tissues and drugs able to activate PPAR nuclear receptors exert neuroprotective effects in both cellular and mouse HD models (Chiang et al., 2012). The ATPase valosin-containing protein (VCP), is another molecular target for HD as treatment with the HV-3 VCP deriving peptide that abolishes mHTT/VCP interaction corrects excessive mitophagy and reduces cell death in *in vitro* and *in vivo* HD models (Guo et al., 2016). Finally, a mitochondrial pathway which when targeted may provide neuroprotection in HD and other polyglutamine diseases is the activation of anti-apoptotic proteins belonging to B-cell lymphoma 2 (BCL2) family. As *in vitro* and *in vivo* models of HD and HD patients' tissues show alterations in BCL2 family protein expression and localization (Sassone et al., 2013), it was suggested that inhibition of selected BCL2 family proteins may provide neuroprotection. Interestingly, BCL2 has been shown to act as a key factor for the improvement of glial-to-neuron direct reprogramming *in vitro* and *in vivo* by reducing cell death occurring due to the metabolic state transition of reprogrammed cells (Gascón et al., 2016).

Evidence also shows abnormal lipid metabolic pathways in HD and suggests that the development of new targets to restore their balance may act to ameliorate some HD symptoms (Desplats et al., 2007). A lipid pathway that dysfunctions in HD is the cholesterol metabolic pathway, as the expression of genes involved in the cholesterol biosynthetic pathway and the levels of cholesterol, lanosterol, lathosterol and 24S-hydroxycholesterol were found to be reduced in the brain of HD mouse models (Arenas et al., 2017). A recent study revealed a new cholesterol-targeting therapeutic strategy for HD through identifying abnormally low levels of the enzyme cholesterol 24-hydroxylase (CYP46A1) in HD models and in post-mortem brain tissues of HD patients. Delivery of CYP46A1 into the striatum of HD models decreased neuronal atrophy and improved motor deficits, implying that restoring CYP46A1 activity promises a new therapeutic approach in HD (Boussicault et al., 2016). Interestingly a nanoparticle-based cholesterol delivering strategy was able to restore synaptic and cognitive impairment in R6/2 HD mice, supporting the idea that therapies aimed to restore brain cholesterol level may have a significant impact in HD treatment (Valenza et al., 2015).

CONCLUSION

Recent achievements in iPSC technology have contributed substantially to the understanding of the HD pathology and the screening for potential therapeutic molecules for HD. Furthermore, the advancements in *in vivo* neuronal reprogramming in different regions of the CNS, such as the cortex, the striatum, the spinal cord and the midbrain have opened new possibilities for the treatment of neurodegenerative diseases. Benefiting from those advances, a possible new approach for the treatment of HD could be a combination of promoting neuronal replacement from endogenous sources by direct reprogramming along with fostering neuroprotection by restoring BDNF levels or metabolic dysfunction of existing neurons, ideally in conjunction with the promising strategy of the down-regulation of mHTT levels.

AUTHOR CONTRIBUTIONS

JS and EP planned and wrote the manuscript. DT planned, wrote, and edited the manuscript.

FUNDING

This study was supported by Fondation Santé 2017–2018 Grant, Stavros Niarhos Foundation 2017–2019 Grant and Greek Ministry of Education KRIPIS-II Grant to DT.

REFERENCES

Adil, M. M., Gaj, T., Rao, A. T., Kulkarni, R. U., Fuentes, C. M., Ramadoss, G. N., et al. (2018). hPSC-Derived Striatal Cells Generated Using a Scalable 3D Hydrogel Promote Recovery in a Huntington Disease Mouse Model. *Stem Cell Reports* 10, 1481–1491. doi: 10.1016/j.stemcr.2018.03.007

Arber, C., Precious, S. V., Cambray, S., Risner-Janiczek, J. R., Kelly, C., Noakes, Z., et al. (2015). Activin A directs striatal projection neuron differentiation of human pluripotent stem cells. *Development* 142, 1375–1386. doi: 10.1242/dev.117093

Arenas, F., Garcia-Ruiz, C., and Fernandez-Checa, J. C. (2017). Intracellular cholesterol trafficking and impact in neurodegeneration. *Front. Mol. Neurosci.* 10:382. doi: 10.3389/fnmol.2017.00382

Beal, M. F., Ferrante, R. J., Swartz, K. J., and Kowall, N. W. (1991). Chronic quinolinic acid lesions in rats closely resemble Huntington's disease. *J. Neurosci.* 11, 1649–1659. doi: 10.1523/JNEUROSCI.11-06-01649.1991

Boussicault, L., Alves, S., Lamazière, A., Planques, A., Heck, N., Moumné, L., et al. (2016). CYP46A1, the rate-limiting enzyme for cholesterol degradation, is neuroprotective in Huntington's disease. *Brain* 139(Pt 3), 953–970. doi: 10.1093/brain/awv384

Carri, A. D., Onorati, M., Lelos, M. J., Castiglioni, V., Faedo, A., Menon, R., et al. (2013). Developmentally coordinated extrinsic signals drive human pluripotent stem cell differentiation toward authentic DARPP-32+ medium-sized spiny neurons. *Development* 140, 301–312. doi: 10.1242/dev.084608

Charbord, J., Poydenot, P., Bonnefond, C., Feyeux, M., Casagrande, F., Brinon, B., et al. (2013). High throughput screening for inhibitors of REST in neural derivatives of human embryonic stem cells reveals a chemical compound that promotes expression of neuronal genes. *Stem Cells* 31, 1816–1828. doi: 10.1002/stem.1430

Chiang, M. C., Chern, Y., and Huang, R. N. (2012). PPARgamma rescue of the mitochondrial dysfunction in Huntington's disease. *Neurobiol. Dis*. 45, 322–328. doi: 10.1016/j.nbd.2011.08.016

Cho, S. R., Benraiss, A., Chmielnicki, E., Samdani, A., Economides, A., and Goldman, S. A. (2007). Induction of neostriatal neurogenesis slows disease progression in a transgenic murine model of Huntington disease. *J. Clin. Invest*. 117, 2889–2902. doi: 10.1172/JCI31778

Conforti, P., Besusso, D., Bocchi, V. D., Faedo, A., Cesana, E., Rossetti, G., et al. (2018). Faulty neuronal determination and cell polarization are reverted by modulating HD early phenotypes. *Proc. Natl. Acad. Sci. U.S.A*. 115, E762–E771. doi: 10.1073/pnas.1715865115

Conforti, P., Zuccato, C., Gaudenzi, G., Ieraci, A., Camnasio, S., Buckley, N. J., et al. (2013). Binding of the repressor complex REST-mSIN3b by small molecules restores neuronal gene transcription in Huntington's disease models. *J. Neurochem*. 127, 22–35. doi: 10.1111/jnc.12348

Connor, B. (2018). Concise review: the use of stem cells for understanding and treating Huntington's Disease. *Stem Cells* 36, 146–160. doi: 10.1002/stem.2747

Cudkowicz, M., and Kowall, N. W. (1990). Degeneration of pyramidal projection neurons in Huntington's disease cortex. *Ann. Neurol.* 27, 200–204. doi: 10.1002/ana.410270217

Desplats, P. A., Denny, C. A., Kass, K. E., Gilmartin, T., Head, S. R., Sutcliffe, J. G., et al. (2007). Glycolipid and ganglioside metabolism imbalances in Huntington's disease. *Neurobiol. Dis*. 27, 265–277. doi: 10.1016/j.nbd.2007.05.003

Ernst, A., Alkass, K., Bernard, S., Salehpour, M., Perl, S., Tisdale, J., et al. (2014). Neurogenesis in the striatum of the adult human brain. *Cell* 156, 1072–1083. doi: 10.1016/j.cell.2014.01.044

Faedo, A., Laporta, A., Segnali, A., Galimberti, M., Besusso, D., Cesana, E., et al. (2017). Differentiation of human telencephalic progenitor cells into MSNs by inducible expression of Gsx2 and Ebf1. *Proc. Natl. Acad. Sci. U.S.A*. 114, E1234–E1242. doi: 10.1073/pnas.1611473114

Gascón, S., Murenu, E., Masserdotti, G., Ortega, F., Russo, G. L., Petrik, D., et al. (2016). Identification and successful negotiation of a metabolic checkpoint in direct neuronal reprogramming. *Cell Stem Cell* 18, 396–409. doi: 10.1016/j.stem.2015.12.003

Guedes-Dias, P., Pinho, B. R., Soares, T. R., de Proença, J., Duchen, M. R., and Oliveira, J. M. A. (2016). Mitochondrial dynamics and quality control in Huntington's disease. *Neurobiol. Dis.* 90, 51–57. doi: 10.1016/j.nbd.2015.09.008

Guo, X., Disatnik, M., Monbureau, M., Shamloo, M., Mochly-rosen, D., and Qi, X. (2013). Inhibition of mitochondrial fragmentation diminishes Huntington' s disease – associated neurodegeneration. *J. Clin. Invest.* 123, 5371–5388. doi: 10.1172/JCI70911DS1

Guo, X., Sun, X., Hu, D., Wang, Y. J., Fujioka, H., Vyas, R., et al. (2016). VCP recruitment to mitochondria causes mitophagy impairment and neurodegeneration in models of Huntington's disease. *Nat. Commun.* 7:12646. doi: 10.1038/ncomms12646

Guo, Z., Zhang, L., Wu, Z., Chen, Y., Wang, F., and Chen, G. (2014). In vivo direct reprogramming of reactive glial cells into functional neurons after brain injury and in an Alzheimer's disease model. *Cell Stem Cell* 14, 188–202. doi: 10.1016/j.stem.2013.12.001

Heinrich, C., Bergami, M., Gascón, S., Lepier, A., Viganò, F., Dimou, L., et al. (2014). Sox2-mediated conversion of NG2 glia into induced neurons in the injured adult cerebral cortex. *Stem Cell Reports* 3, 1000–1014. doi: 10.1016/j.stemcr.2014.10.007

Heinrich, C., Blum, R., Gascón, S., Masserdotti, G., Tripathi, P., Sánchez, R., et al. (2010). Directing astroglia from the cerebral cortex into subtype specific functional neurons. *PLoS Biol.* 8:e1000373. doi: 10.1371/journal.pbio.1000373

Jeon, I., Lee, N., Li, J. Y., Park, I. H., Park, K. S., Moon, J., et al. (2012). Neuronal properties, in vivo effects, and pathology of a Huntington's disease patient-derived induced pluripotent stem cells. *Stem Cells* 30, 2054–2062. doi: 10.1002/stem.1135

Jin, K., LaFevre-Bernt, M., Sun, Y., Chen, S., Gafni, J., Crippen, D., et al. (2005). FGF-2 promotes neurogenesis and neuroprotection and prolongs survival in a transgenic mouse model of Huntington's disease. *Proc. Natl. Acad. Sci. U.S.A*. 102, 18189–18194. doi: 10.1073/pnas.0506375102

Johnson, R., and Buckley, N. J. (2009). Gene dysregulation in Huntington's disease: REST, microRNAs and beyond. *Neuromolecular Med.* 11, 183–199. doi: 10.1007/s12017-009-8063-4

Kandasamy, M., Rosskopf, M., Wagner, K., Klein, B., Couillard-Despres, S., Reitsamer, H. A., et al. (2015). Reduction in subventricular zone-derived olfactory bulb neurogenesis in a rat model of huntington's disease is accompanied by striatal invasion of neuroblasts. *PLoS One* 10:e0116069. doi: 10.1371/journal.pone.0116069

Kohl, Z., Regensburger, M., Aigner, R., Kandasamy, M., Winner, B., Aigner, L., et al. (2010). Impaired adult olfactory bulb neurogenesis in the R6/2 mouse model of Huntington's disease. *BMC Neurosci.* 11:114. doi: 10.1186/1471-2202-11-114

Kordasiewicz, H. B., Stanek, L. M., Wancewicz, E. V., Mazur, C., McAlonis, M. M., Pytel, K. A., et al. (2012). Sustained therapeutic reversal of huntington's disease by transient repression of huntingtin synthesis. *Neuron* 1031–1044. doi: 10.1016/j.neuron.2012.05.009

Langfelder, P., Cantle, J. P., Chatzopoulou, D., Wang, N., Gao, F., Al-Ramahi, I., et al. (2016). Integrated genomics and proteomics define huntingtin CAG length-dependent networks in mice. *Nat. Neurosci.* 19, 623–633. doi: 10.1038/nn.4256

Lee, S.-T., Im, W., Ban, J.-J., Lee, M., Jung, K.-H., Lee, S. K., et al. (2017). Exosome-based delivery of miR-124 in a Huntington's Disease model. *J. Mov. Disord.* 10, 45–52. doi: 10.14802/jmd.16054

Lim, R. G., Salazar, L. L., Wilton, D. K., King, A. R., Stocksdale, J. T., Sharifabad, D., et al. (2017). Developmental alterations in Huntington's disease neural cells and pharmacological rescue in cells and mice. *Nat. Neurosci.* 20, 648–660. doi: 10.1038/nn.4532

Liot, G., Valette, J., Pépin, J., Flament, J., and Brouillet, E. (2017). Energy defects in Huntington's disease: Why "in vivo" evidence matters. *Biochem. Biophys. Res. Commun*. 483, 1084–1095. doi: 10.1016/j.bbrc.2016.09.065

Liu, T., Im, W., Mook-Jung, I., and Kim, M. (2015). MicroRNA-124 slows down the progression of huntington's disease by promoting neurogenesis in the striatum. *Neural Regen. Res.* 786–791. doi: 10.4103/1673-5374.156978

Luzzati, F., de Marchis, S., Parlato, R., Gribaudo, S., Schütz, G., Fasolo, A., et al. (2011). New striatal neurons in a mouse model of progressive striatal degeneration are generated in both the subventricular zone and the striatal parenchyma. *PLoS One* 6:e25088. doi: 10.1371/journal.pone.0025088

Ma, L., Hu, B., Liu, Y., Vermilyea, S. C., Liu, H., Gao, L., et al. (2012). Human embryonic stem cell-derived GABA neurons correct locomotion deficits in quinolinic acid-lesioned mice. *Cell Stem Cell* 10, 455–464. doi: 10.1016/j.stem.2012.01.021

MacDonald, M. E., Ambrose, C. M., Duyao, M. P., Myers, R. H., Lin, C., Srinidhi, L., et al. (1993). A novel gene containing a trinucleotide repeat that is expanded and unstable on Huntington's disease chromosomes. *Cell* 72, 971–983. doi: 10.1016/0092-8674(93)90585-E

Magnusson, J. P., Göritz, C., Tatarishvili, J., Dias, D. O., Smith, E. M. K., Lindvall, O., et al. (2014). A latent neurogenic program in astrocytes regulated by Notch signaling in the mouse. *Science* 346, 237–241. doi: 10.1126/science.346.6206.237

Mangiarini, L., Sathasivam, K., Seller, M., Cozens, B., Harper, A., Hetherington, C., et al. (1996). Exon I of the HD gene with an expanded CAG repeat is sufficient to cause a progressive neurological phenotype in transgenic mice. *Cell* 87, 493–506. doi: 10.1016/S0092-8674(00)81369-0

Mattis, V. B., and Svendsen, C. N. (2018). Huntington modeling improves with age. *Nat. Neurosci.* 21, 301–303. doi: 10.1038/s41593-018-0086-4

Mertens, J., Paquola, A. C. M., Ku, M., Hatch, E., Böhnke, L., Ladjevardi, S., et al. (2015). Directly reprogrammed human neurons retain aging-associated transcriptomic signatures and reveal age-related nucleocytoplasmic defects. *Cell Stem Cell* 17, 705–718. doi: 10.1016/j.stem.2015.09.001

Miniarikova, J., Evers, M. M., and Konstantinova, P. (2018). Translation of MicroRNA-based huntingtin-lowering therapies from preclinical studies to the clinic. *Mol. Ther*. 26, 947–962. doi: 10.1016/j.ymthe.2018.02.002

Miniarikova, J., Zimmer, V., Martier, R., Brouwers, C. C., Pythoud, C., Richetin, K., et al. (2017). AAV5-miHTT gene therapy demonstrates suppression of mutant huntingtin aggregation and neuronal dysfunction in a rat model of Huntington's disease. *Gene Ther.* 24, 630–639. doi: 10.1038/gt.2017.71

Nato, G., Caramello, A., Trova, S., Avataneo, V., Rolando, C., Taylor, V., et al. (2015). Striatal astrocytes produce neuroblasts in an excitotoxic model of Huntington's disease. *Development* 142, 840–845. doi: 10.1242/dev.116657

Niu, W., Zang, T., Zou, Y., Fang, S., Smith, D. K., Bachoo, R., et al. (2013). *In vivo* reprogramming of astrocytes to neuroblasts in the adult brain. *Nat. Cell Biol.* 15, 1164–1175. doi: 10.1038/ncb2843

Packer, A. N., Xing, Y., Harper, S. Q., Jones, L., and Davidson, B. L. (2008). The bifunctional microRNA miR-9/miR-9* regulates REST and CoREST and is downregulated in Huntington's disease. *J. Neurosci.* 28, 14341–14346. doi: 10.1523/JNEUROSCI.2390-08.2008

Park, I.-H., Arora, N., Huo, H., Maherali, N., Ahfeldt, T., Shimamura, A., et al. (2008). Disease-specific induced pluripotent stem cells. *Cell* 134, 877–886. doi: 10.1016/j.cell.2008.07.041

Reed, E. R., Latourelle, J. C., Bockholt, J. H., Bregu, J., Smock, J., Paulsen, J. S., et al. (2017). MicroRNAs in CSF as prodromal biomarkers for Huntington disease in the PREDICT-HD study. *Neurology* 90, e264–e272. doi: 10.1212/WNL.0000000000004844

Rivetti Di Val Cervo, P., Romanov, R. A., Spigolon, G., Masini, D., Martín-Montañez, E., Toledo, E. M., et al. (2017). Induction of functional dopamine neurons from human astrocytes *in vitro* and mouse astrocytes in a Parkinson's disease model. *Nat. Biotechnol.* 35, 444–452. doi: 10.1038/nbt.3835

Rodriguez-Lebron, E., Denovan-Wright, E. M., Nash, K., Lewin, A. S., and Mandel, R. J. (2005). Intrastriatal rAAV-mediated delivery of anti-huntingtin shRNAs induces partial reversal of disease progression in R6/1 Huntington's disease transgenic mice. *Mol. Ther.* 12, 618–633. doi: 10.1016/j.ymthe.2005.05.006

Ruzo, A., Croft, G. F., Metzger, J. J., Galgoczi, S., Gerber, L. J., Pellegrini, C., et al. (2018). Chromosomal instability during neurogenesis in Huntington's disease. *Development* 142:dev156844. doi: 10.1242/dev.156844

Sassone, J., Maraschi, A., Sassone, F., Silani, V., and Ciammola, A. (2013). Defining the role of the Bcl-2 family proteins in Huntington's disease. *Cell Death Dis.* 4:e772. doi: 10.1038/cddis.2013.300

Seredenina, T., and Luthi-Carter, R. (2012). What have we learned from gene expression profiles in Huntington's disease? *Neurobiol. Dis.* 45, 83–98. doi: 10.1016/j.nbd.2011.07.001

Simmons, D. A., Belichenko, N. P., Ford, E. C., Semaan, S., Monbureau, M., Aiyaswamy, S., et al. (2016). A small molecule p75NTRligand normalizes signalling and reduces Huntington's disease phenotypes in R6/2 and BACHD mice. *Hum. Mol. Genet.* 25, 4920–4938. doi: 10.1093/hmg/ddw316

Simmons, D. A., Belichenko, N. P., Yang, T., Condon, C., Monbureau, M., Shamloo, M., et al. (2013). A Small Molecule TrkB Ligand Reduces Motor Impairment and Neuropathology in R6/2 and BACHD Mouse Models of Huntington's Disease. *J. Neurosci.* 33, 18712–18727. doi: 10.1523/JNEUROSCI.1310-13.2013

Slow, E. J., van Raamsdonk, J., Rogers, D., Coleman, S. H., Graham, R. K., Deng, Y., et al. (2003). Selective striatal neuronal loss in a YAC128 mouse model of Huntington disease. *Hum. Mol. Genet.* 12, 1555–1567. doi: 10.1093/hmg/ddg169

Spinney, L. (2010). Uncovering the true prevalence of Huntington's disease. *Lancet Neurol.* 9, 760–761. doi: 10.1016/S1474-4422(10)70160-5

Sun, Y., Luo, Z.-M., Guo, X.-M., Su, D.-F., and Liu, X. (2015). An updated role of microRNA-124 in central nervous system disorders: a review. *Front. Cell. Neurosci.* 9:193. doi: 10.3389/fncel.2015.00193

Szlachcic, W. J., Switonski, P. M., Krzyzosiak, W. J., Figlerowicz, M., and Figiel, M. (2015). Huntington disease iPSCs show early molecular changes in intracellular signaling, the expression of oxidative stress proteins and the p53 pathway. *Dis. Model. Mech.* 8, 1047–1057. doi: 10.1242/dmm.019406

Tabrizi, S., Leavitt, B., Kordasiewicz, H., Czech, C., Swayze, E., Norris, D. A., et al. (2018). Effects of IONIS-HTTRx in patients with early Huntington's disease, results of the first HTT-lowering drug trial (CT.002). *Paper presented at the 2018 American Academy of Neurology Annual Meeting*, Los Angeles, CA.

Tartaglione, A. M., Popoli, P., and Calamandrei, G. (2017). Regenerative medicine in Huntington's disease: Strengths and weaknesses of preclinical studies. *Neurosci. Biobehav. Rev.* 77, 32–47. doi: 10.1016/j.neubiorev.2017.02.017

The HD iPSC Consortium (2012). Induced pluripotent stem cells from patients with huntington's disease show CAG-repeat-expansion-associated phenotypes. *Cell Stem Cell* 11, 264–278. doi: 10.1016/j.stem.2012.04.027

Torper, O., Ottosson, D. R., Pereira, M., Lau, S., Cardoso, T., Grealish, S., et al. (2015). Invivo reprogramming of striatal NG2 glia into functional neurons that integrate into local host circuitry. *Cell Rep.* 12, 474–481. doi: 10.1016/j.celrep.2015.06.040

Torper, O., Pfisterer, U., Wolf, D. A., Pereira, M., Lau, S., Jakobsson, J., et al. (2013). Generation of induced neurons via direct conversion in vivo. *Proc. Natl. Acad. Sci. U.S.A.* 10, 7038–7043. doi: 10.1073/pnas.1303829110

Valenza, M., Chen, J. Y., Di Paolo, E., Ruozi, B., Belletti, D., Ferrari Bardile, C., et al. (2015). Cholesterol-loaded nanoparticles ameliorate synaptic and cognitive function in Huntington's disease mice. *EMBO Mol. Med.* 7, 1547–1564. doi: 10.15252/emmm.201505413

Victor, M. B., Richner, M., Hermanstyne, T. O., Ransdell, J. L., Sobieski, C., Deng, P. Y., et al. (2014). Generation of human striatal neurons by microrna-dependent direct conversion of fibroblasts. *Neuron* 84, 311–323. doi: 10.1016/j.neuron.2014.10.016

Victor, M. B., Richner, M., Olsen, H. E., Lee, S. W., Monteys, A. M., Ma, C., et al. (2018). Striatal neurons directly converted from Huntington's disease patient fibroblasts recapitulate age-associated disease phenotypes. *Nat. Neurosci.* 21, 341–352. doi: 10.1038/s41593-018-0075-7

Visvanathan, J., Lee, S., Lee, B., Lee, J. W., and Lee, S. K. (2007). The microRNA miR-124 antagonizes the anti-neural REST/SCP1 pathway during embryonic CNS development. *Genes Dev.* 21, 744–749. doi: 10.1101/gad.1519107

Wiatr, K., Szlachcic, W. J., Trzeciak, M., Figlerowicz, M., and Figiel, M. (2018). Huntington disease as a neurodevelopmental disorder and early signs of the disease in stem cells. *Mol. Neurobiol.* 55, 3351–3371. doi: 10.1007/s12035-017-0477-7

Wild, E. J., and Tabrizi, S. J. (2014). Targets for future clinical trials in Huntington's disease: What's in the pipeline? *Mov. Disord.* 29, 1434–1445. doi: 10.1002/mds.26007

Yang, J., Zhang, X., Chen, X., Wang, L., and Yang, G. (2017). Exosome mediated delivery of miR-124 promotes neurogenesis after Ischemia. *Mol. Ther. Nucleic Acids* 7, 278–287. doi: 10.1016/j.omtn.2017.04.010

Zuccato, C., and Cattaneo, E. (2014). Huntington's Disease. *Handb. Exp. Pharmacol.* 220, 357–409. doi: 10.1007/978-3-642-45106-5_14

Zuccato, C., Ciammola, A., Rigamonti, D., Leavitt, B. R., Goffredo, D., Conti, L., et al. (2001). Loss of huntingtin-mediated BDNF gene transcription in Huntington's disease. *Science* 293, 493–498. doi: 10.1126/science.1059581

Conflict of Interest Statement: The authors declare that the research was conducted in the absence of any commercial or financial relationships that could be construed as a potential conflict of interest.

frontiers in Neuroscience

REVIEW
published: 05 November 2018
doi: 10.3389/fnins.2018.00707

MicroRNAs Engage in Complex Circuits Regulating Adult Neurogenesis

*Laura Stappert, Frederike Klaus and Oliver Brüstle**

Institute of Reconstructive Neurobiology, Life & Brain Center, University of Bonn Medical Center, Bonn, Germany

The finding that the adult mammalian brain is still capable of producing neurons has ignited a new field of research aiming to identify the molecular mechanisms regulating adult neurogenesis. An improved understanding of these mechanisms could lead to the development of novel approaches to delay cognitive decline and facilitate neuroregeneration in the adult human brain. Accumulating evidence suggest microRNAs (miRNAs), which represent a class of post-transcriptional gene expression regulators, as crucial part of the gene regulatory networks governing adult neurogenesis. This review attempts to illustrate how miRNAs modulate key processes in the adult neurogenic niche by interacting with each other and with transcriptional regulators. We discuss the function of miRNAs in adult neurogenesis following the life-journey of an adult-born neuron from the adult neural stem cell (NSCs) compartment to its final target site. We first survey how miRNAs control the initial step of adult neurogenesis, that is the transition of quiescent to activated proliferative adult NSCs, and then go on to discuss the role of miRNAs to regulate neuronal differentiation, survival, and functional integration of the newborn neurons. In this context, we highlight miRNAs that converge on functionally related targets or act within cross talking gene regulatory networks. The cooperative manner of miRNA action and the broad target repertoire of each individual miRNA could make the miRNA system a promising tool to gain control on adult NSCs in the context of therapeutic approaches.

Keywords: microRNAs, adult neurogenesis, hippocampus, neural stem cells, neurons, feedback loops, miRNA convergence

OPEN ACCESS

Edited by:
Christophe Heinrich, INSERM U1208 Institut Cellule Souche et Cerveau, France

Reviewed by:
Dieter Chichung Lie, Friedrich Alexander Universität Erlangen Nürnberg, Germany
Krishna Vadodaria, Salk Institute for Biological Studies, United States

***Correspondence:**
Oliver Brüstle
r.neuro@uni-bonn.de

Specialty section:
This article was submitted to Neurogenesis, a section of the journal Frontiers in Neuroscience

Received: *03 July 2018*
Accepted: *18 September 2018*
Published: *05 November 2018*

Citation:
Stappert L, Klaus F and Brüstle O (2018) MicroRNAs Engage in Complex Circuits Regulating Adult Neurogenesis. Front. Neurosci. 12:707. doi: 10.3389/fnins.2018.00707

INTRODUCTION

Neural stem cells (NSCs) are self-renewing, multipotent progenitors that generate all neurons and glial cells of the mammalian central nervous system (CNS). In the adult mammalian brain, a limited number of adult neural stem cells (aNSCs) persists in the subventricular zone (SVZ) of the lateral ventricles and the subgranular zone (SGZ) in the hippocampal dentate gyrus as the two main neurogenic niches (**Figures 1A–C**). The composition and functionality of these germinal zones has been most extensively studied in rodents (reviewed by Kempermann et al., 2015; Pino et al., 2017). Similar regions containing neurogenic progenitor cells have been described in the SVZ and dentate gyrus of the adult human brain (Eriksson et al., 1998; Roy et al., 2000; Nunes et al., 2003). Neurogenesis within the human SVZ declines during infancy (Sanai et al., 2011), whereas several studies have pointed to a quite substantial generation of dentate granule neurons in humans

throughout life (Spalding et al., 2013; Boldrini et al., 2018). This view has been challenged by a recent report suggesting that hippocampal neurogenesis decreases dramatically after the first years of life in both humans and macaques [Sorrells et al. (2018); see also Kempermann et al. (2018) for a statement regarding the recent discussion on the relevance of adult hippocampal neurogenesis in humans]. Nevertheless, there is a strong interest in understanding the mechanisms regulating adult neurogenesis (reviewed by Kempermann et al., 2015; Peng and Bonaguidi, 2018). Research in this regard is motivated by the fact that the hippocampus is involved in memory and learning, which led to the hypothesis that adult neurogenesis could play an important role in cognition (reviewed by Gonçalves et al., 2016). Furthermore, a series of studies revealed that adult hippocampal neurogenesis in rodents can be modulated by experiential and environmental conditions as well as by aging (reviewed by Toda and Gage, 2018). Altered hippocampal neurogenesis has been linked to a number of pathological conditions, such as ischemia- or epilepsy-induced insults, mood disorders, and neurodegenerative diseases (reviewed by Pino et al., 2017).

Adult neurogenesis involves multiple steps that have to be tightly regulated, i.e., aNSC activation, proliferation, differentiation into neural progeny as well as survival, migration, and functional maturation of the adult-born neurons (**Figure 1D**). Recent evidence indicate that microRNAs (miRNAs) can be placed in midst of the regulatory mechanisms operating in adult neurogenesis (reviewed by Lopez-Ramirez and Nicoli, 2014; Murao et al., 2016; Encinas and Fitzsimons, 2017). miRNAs are short (22 nucleotide long) single-stranded RNA molecules that post-transcriptionally repress gene expression by complementary binding to mRNA targets (reviewed by Bartel, 2009). miRNA genes are transcribed as hairpin-shaped transcripts, called pri-miRNAs, which are sequentially processed to liberate the mature miRNAs (**Figure 2**). Some pri-miRNAs are polycistronic and encode for several mature miRNAs (reviewed by Olive et al., 2015). The final and essential cleavage step of miRNA biogenesis is carried out by the ribonuclease Dicer, and genetic ablation studies for Dicer have been used to assess the overall importance of the miRNA system. Mature miRNAs are then loaded onto Argonaut (Ago) proteins to form the RNA-induced silencing complex (RISC) through which they target mRNAs for translational inhibition or mRNA degradation. miRNAs often come as families whose members share a common seed sequence and are thought to have similar functions (**Figure 2**) (reviewed by Ha and Kim, 2014). During brain development, miRNAs regulate neural progenitor proliferation, neurogenic and gliogenic differentiation as well as maturation and functional integration of neurons (reviewed by Bian et al., 2013; Barca-Mayo and De Pietri Tonelli, 2014; Stappert et al., 2014). Likewise, miRNAs play important roles in regulating cell fate decisions in the adult SVZ and SGZ (reviewed by Lopez-Ramirez and Nicoli, 2014; Murao et al., 2016) and have been linked to diseases associated with these compartments, e.g., epilepsy (Bielefeld et al., 2017), stroke (Khoshnam et al., 2017), and neurodegenerative disorders (Qiu et al., 2014).

In many cases, miRNAs act in concert with transcription factors and chromatin modifiers to control gene expression in NSCs (of embryonic or adult origin), thereby affecting NSC number and their ability to generate differentiated progeny.

In this review, we discuss the physiological role of miRNAs during adult neurogenesis following the route from aNSC maintenance to neuronal differentiation and maturation of newborn neurons. Given its discussed relevance for human neurogenesis and cognition, we will mainly focus on hippocampal neurogenesis. However, in some cases we will also refer to data generated in other compartments, e.g., the adult SVZ or the developing brain, to highlight important principles of miRNA function during neurogenesis (see **Figure 1D** and **Tables 1**, **2** for an overview of the functions of the miRNAs presented here). In the first part, we depict how miRNAs control the balance between quiescent and activated aNSCs contributing to homeostasis and plasticity in response to neurogenic stimuli. In the second part, we describe how miRNAs influence the neurogenic output of the aNSC niche by modulating neuronal differentiation, survival, and functional integration. In this context, we delineate the interactions of miRNAs with gene regulatory networks controlling adult neurogenesis and focus on miRNAs that converge by targeting functionally associated genes. We end by summarizing the diverse roles of miRNAs during adult neurogenesis and discuss the importance of target multiplicity and miRNA cooperativity as key features of the miRNA system. Finally, we speculate how miRNAs may contribute to aNSC heterogeneity and give an outlook on how knowledge on miRNA-based regulation could be further increased and eventually exploited to facilitate neuroregeneration in the adult human brain.

MicroRNAs Regulating Activation and Proliferation of Adult Neural Stem Cells

Adult NSCs reside in a specialized microenvironment, the stem cell niche, which is composed of different cell types and extracellular matrix molecules and provides extracellular signals to regulate NSC homeostasis and differentiation (reviewed by Llorens-Bobadilla and Martin-Villalba, 2017). In the currently prevalent view, aNSCs are slowly dividing radial glia-like precursor cells that express *Nestin*, *Gfap*, as well as *Sox2* and are in close contact with the vasculature. The radial glia-like precursor cells of the dentate gyrus SGZ are further characterized by basal processes that span the granule cell layer. The radial glia-like NSCs (SVZ: type B cells, SGZ: type 1 cells) generate fast-dividing committed intermediate progenitors (IPCs, SVZ: type C cells, SGZ: type 2 cells), which then give rise to neuroblasts (SVZ: type A cells, SGZ: type 3 cells) (Doetsch et al., 1997; Seri et al., 2004; and reviewed by Pino et al., 2017) (see **Figures 1B,C** for an overview of the lineage relationships and nomenclature in the SVZ and SGZ). The SVZ neuroblasts migrate along the rostral migratory stream to the olfactory bulb where they differentiate into olfactory interneurons. The dentate gyrus neuroblasts generated from the SGZ move up into the granule cell layer before they differentiate into mature granule neurons (**Figures 1A–C**) (reviewed by Pino et al., 2017).

The majority of aNSCs is quiescent, which seems to be important to ensure long-term homeostasis of the niche

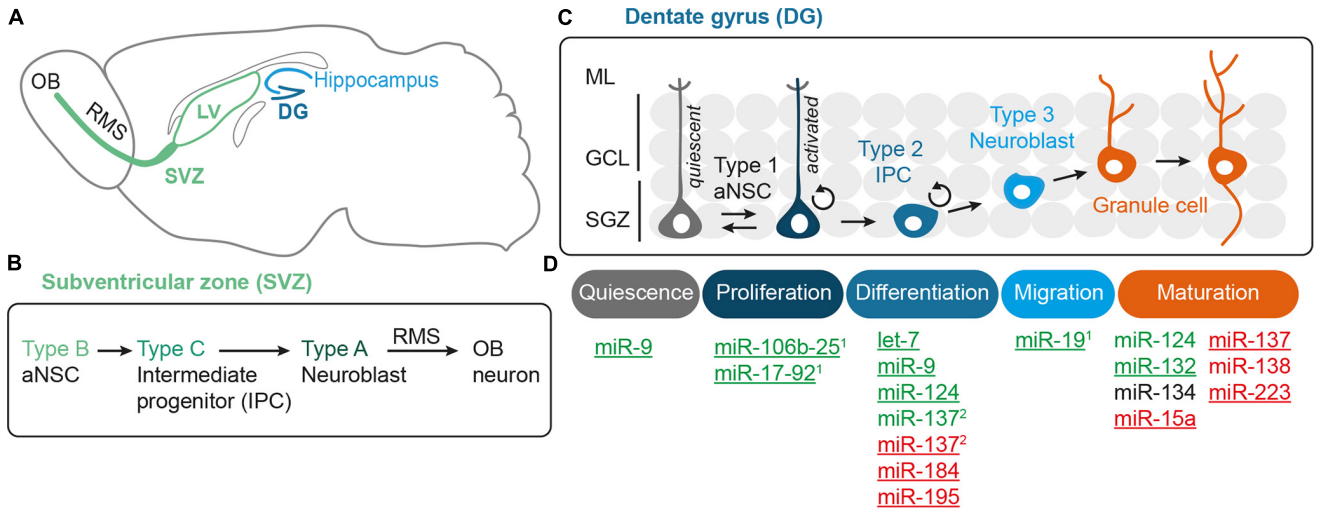

FIGURE 1 | MicroRNAs as key regulators of the multistep process of adult neurogenesis. **(A)** The adult mouse brain contains two main neurogenic niches, i.e., the subventricular zone (SVZ) of the lateral ventricle (LV), which produces neurons for the olfactory bulb (OB), and the subgranular zone (SGZ) of the hippocampal dentate gyrus (DG). **(B)** The adult neural stem cells (aNSCs) of the subventricular zone are called type B cells. They give rise to intermediate progenitors (IPCs, type C cells), which after a few cell cycles develop into type A neuroblasts that migrate along the rostral migratory stream (RMS) to the OB before terminal differentiation (Doetsch et al., 1997). **(C)** The aNSCs of the SGZ of the dentate gyrus are called type 1 cells and the IPCs to which they develop are designated as type 2, the neuroblasts as type 3 cells (Seri et al., 2004). The neuroblasts generated from the SGZ migrate up into the granule cell layer (GCL), where they maturate into granule cells, extend dendrites into the molecular layer (ML), and grow axons. **(D)** Adult neurogenesis is a multistep process that begins with activation of quiescent aNSCs to re-enter cell cycling, followed by a proliferation phase of aNSCs, which eventually develop into IPCs and further differentiate into neuroblasts. The last steps of adult neurogenesis involve neuroblast migration and functional maturation into terminally differentiated neurons. For all these steps, regulatory miRNAs have been identified that either have a positive (green), negative (red), or modulatory (black) effect. Underlined miRNAs have been studied in the context of adult neurogenesis, whereas the function of the other miRNAs has been inferred from studies addressing developmental neurogenesis. The miRNAs miR-106b-25$^{(1)}$, miR-17-92$^{(1)}$ and miR-19$^{(1)}$ belong to the family of polycistronic miR-17 clusters. There are divergent results for miRNA-137$^{(2)}$, which was found to have a pro-differentiation effect in embryonic NSCs (Sun et al., 2011), but an anti-differentiation effect in adult NSCs (Szulwach et al., 2010).

throughout the life span of the organism. However, a small fraction of aNSCs has been shown to proliferate quite rapidly, and it has been suggested that aNSCs transition between activated proliferative and quiescent states (**Figure 1C**; Lugert et al., 2010). The number of aNSCs shuttling between these two states is modulated by neurogenic stimuli and during aging (van Praag et al., 1999; Lugert et al., 2010; Encinas et al., 2011). In fact, neurogenic activity seems to decline with age, whereby it is still unresolved whether this is due to an exhaustion of aNSCs, which once activated eventually lose their self-renewal capacity and terminally differentiate (Encinas et al., 2011; Ziebell et al., 2018), or an increased quiescence of the aNSCs pool (Lugert et al., 2010; and reviewed by Giachino and Taylor, 2015).

MicroRNAs Controlling the Balance Between Quiescent and Activated Proliferative aNSCs

There are many factors known to control the proliferative capacity of aNSCs (reviewed by Beckervordersandforth et al., 2015) including transcription factors and signaling pathways, such as Notch, BMP, Wnt, and insulin/IGF signaling. While for many of the players involved regulatory miRNAs have been identified, we will focus on such miRNA–target interactions that have been explicitly studied in the context of adult neurogenesis.

One pathway that is regulated by many miRNAs and plays a key role in controlling aNSCs proliferation is Notch signaling (reviewed by Giachino and Taylor, 2015). High Notch levels protect aNSC from activation as shown by studies in mouse SVZ (Kawaguchi et al., 2013) and SGZ (Semerci et al., 2017) as well as in zebrafish aNSCs (Chapouton et al., 2010). While studying adult neurogenesis in the zebrafish brain, which exhibits a widespread neurogenic capacity and contains regions similar to the rodent SVZ and SGZ, Katz et al. (2016) found that miR-9 potentiates Notch signaling to maintain aNSC quiescence. This function of miR-9 stands in apparent contrast to its previously described pro-differentiation effect in embryonic (reviewed by Roese-Koerner et al., 2017) and adult NSCs (Zhao et al., 2009; Kim et al., 2015) (see also **Table 1**). The proposed role of miR-9 during aNSC quiescence in zebrafish may, however, reflect a non-canonical function of miR-9 since Katz et al. (2016) found that miR-9 is actively transported to the nucleus by binding of miR-9-Ago complexes to the shuttle protein TNRC6 and that this nuclear concentration is critical for aNSC quiescence. Interestingly, nuclear localization of miR-9 was also detected in a subset of cells in the SVZ and SGZ neurogenic niche in the mouse brain, suggesting that the role of miR-9 in regulating aNSC quiescence might be conserved (Katz et al., 2016). Furthermore, nuclear concentration of miR-9 was also found to be increased in older versus younger mice, pointing to an age-dependent shift of the subcellular localization of miR-9 (Katz et al., 2016).

Another example of a miRNA-target pair implicated in aNSC maintenance is let-7 and *Hmga2*. miRNA let-7 and its target gene *Hmga2* show an inverse expression pattern in the murine

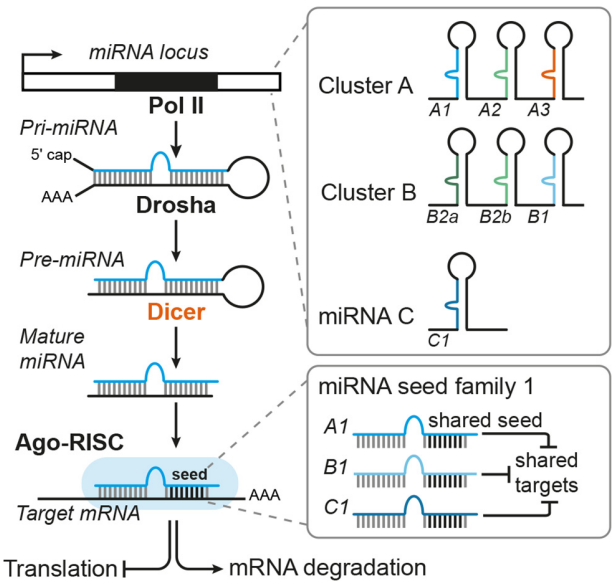

FIGURE 2 | Canonical miRNA biogenesis and function. miRNA genes are transcribed by RNA Polymerase II (Pol II) and then processed by the sequential action of Drosha and Dicer to liberate the mature miRNA duplex, which is then loaded onto Argonaut proteins (Ago) to form the RNA-induced silencing complex (RISC). As part of the RISC, miRNAs can bind to target mRNAs whereby binding of the miRNA seed sequence is the key requirement for mRNA target recognition. Thus, miRNAs with the same seed sequence are thought to target overlapping sets of mRNAs and are assigned to the same miRNA seed family. miRNA genes can be either monocistronic (miRNA C) or polycistronic (clusters A and B) containing several miRNAs that are usually expressed as one pri-miRNA transcript. Some polycistronic clusters comprise miRNA homologs that have emerged via duplication events (cluster B with miR-B2a, B2b as homologous miRNAs) whereas other clusters consist of miRNAs belonging to different seed families (here exemplarily designated as seed family 1 (in blue) with miRNAs A1, B1, C1, and seed family 2 (in green) with miRNAs A2, B2a, and B2b). For more details on miRNA biogenesis and polycistronic miRNA clusters, see the reviews from Ha and Kim (2014) and Olive et al. (2015), respectively.

SVZ during aging (Nishino et al., 2008). HMGA2 is a member of the high mobility group protein family that modulates gene expression as part of the enhanceosome (reviewed by Pfannkuche et al., 2009). Nishino et al. (2008) showed that HMGA2 promotes the proliferative capacity of fetal and adult NSCs by repressing expression of *Ink4a/Arf* locus, which encodes for the cell cycle inhibitors p16 (*Cdkn2a*) and p19 (*Cdkn2d*). However, HMGA2 seems not to bind to the *Ink4a/Arf* locus and it is not yet clear how HMGA2 represses expression of *Ink4/Arf*. Expression of *Hmga2* declines during aging, and premature loss of *Hmga2* impairs self-renewal in *in vitro* cultured forebrain aNSCs, which may contain both SVZ and SGZ aNSCs. Nishino et al. (2008) further found that *Hmga2* expression is regulated by let-7, whose expression increases with age. Furthermore, overexpression of let-7 decreases the proliferative capacity of *in vitro* cultured forebrain aNSCs mimicking the effect of *Hmga2* loss. Thus, the interaction of HMGA2 and let-7 may couple aNSC self-renewal and aging.

Quiescence of aNSCs is also regulated by FOXO3, which was initially identified as an age- and longevity-associated factor downstream of insulin/IGF signaling (reviewed by Martins et al., 2015). FOXO3 is necessary to maintain quiescent aNSCs in both the SVZ and SGZ (Paik et al., 2009; Renault et al., 2009) and was suggested to interact with the polycistronic miR-106b-25 cluster. This cluster is encoded in an intronic region of the protein-coding *Mcm7* gene, which is one of the FOXO3 target genes (Brett et al., 2011). In turn, miR-25, generated by the miR-106b-25 cluster, is critical for the proliferative capacity of *in vitro* cultured forebrain aNSC and is predicted to target *Foxo3* mRNA. Thus, miR-25 and FOXO3 might form a feedback loop regulating the self-renewal capacity of aNSCs (Brett et al., 2011). Unfortunately, the impact of miR-25 on *Foxo3* has not yet been experimentally validated. Nevertheless, an interaction between IGF signaling, FOXO3, and miR-25 to regulate NSC proliferation seems an attractive scenario, which might even be evolutionary conserved as the *C. elegans* ortholog of miR-25, cel-miR-253, has been shown to couple proliferation of blast cells to the nutritional state downstream of IGF signaling (Kasuga et al., 2013). Interestingly, ectopic expression of miR-25 can even re-instate cell cycling of post-mitotic zebrafish neurons (Rodriguez-Aznar et al., 2013). The relevant target gene in this context is p57 (*Cdkn1c*), which has been shown to pace adult hippocampal neurogenesis in mice by controlling aNSCs quiescence (Furutachi et al., 2013).

Taken together, these findings indicate the importance of miRNAs in regulating activation and proliferation of aNSCs, which is key for long-term homeostasis of the adult neurogenic niche.

MicroRNAs Regulating aNSC Activation Downstream of Neurogenic Modulators

Hippocampal neurogenesis is modulated by several physiological stimuli, such as physical exercise, environmental conditions, learning, and aging. Physical activation, for instance, has been shown to promote neurogenesis by inducing cell cycle entry of quiescent aNSCs (Lugert et al., 2010), while exposing mice to enriched environment enhances the survival of new neurons (van Praag et al., 1999). Interestingly, it has been demonstrated that exposure of mice to an enriched environment also leads to altered miRNA expression profiles in the hippocampus (Barak et al., 2013). In total, 29% of the miRNAs, including miR-124, were found to be down-regulated in response to enriched environment, while 8% (including miR-132 as the most increased miRNA) were up-regulated (Barak et al., 2013). Many of the differentially expressed miRNAs also showed an inverse differential expression in a mouse model for Alzheimer's disease, which has been associated with impaired adult hippocampal neurogenesis. These data point to an important role of miRNAs in conferring plasticity of hippocampal neurogenesis in response to modulatory signals.

In further support of this, the polycistronic miR-17-92 cluster, which shares miRNA seed family members with the miR-106b-25 cluster, was recently shown to regulate hippocampal neurogenesis in a mouse model of chronic stress (Jin et al., 2016). Stress and mood-related disorders have adverse effects on the neurogenic activity of the hippocampus, while antidepressant

TABLE 1 | MicroRNAs modulating proliferation and differentiation during adult neurogenesis.

MicroRNA	Main model system	Observed main effect	miRNA regulator	Target mRNA	Reference
let-7b	Mouse primary neonatal forebrain NSCs	let-7 decreases NSC proliferation		*Hmga2*	Nishino et al., 2008
	Mouse embryonic VZ, **primary adult forebrain NSCs**	**let-7 promotes neuronal differentiation**		***Tlx, CyclinD1 (Ccnd1)***	Zhao et al., 2010
miR-17-92 cluster	**Nestin-CreER miR-17-92 KO/OE mice, adult hippocampus**	**miR-17-92 promotes aNSC proliferation and rescues stress-induced impairment of neurogenesis**		***Sgk1***	Jin et al., 2016
miR-25 (miR-106b-25) cluster	**Mouse primary adult forebrain NSCs**	**miR-25 promotes aNSC proliferation**	**FOXO3**	***Foxo3* (predicted)**	Brett et al., 2011
miR-9	Mouse embryonic VZ, **primary adult forebrain NSCs**	**miR-9 promotes neuronal differentiation**	**TLX**	***Tlx***	Zhao et al., 2009
	Human embryonal carcinoma cell line	miR-9/9* and the REST silencing complex form a double negative feedback loop	REST	*Rest, CoRest (Rcor2)*	Packer et al., 2008
	Human neuroblastoma cell line	miR-9 expression is inhibited by Rest in undifferentiated cells and promoted by CREB in differentiated cells, miR-9 targets *Rest* forming a feedback loop	REST, CREB	*Rest*	Laneve et al., 2010
	Mouse primary neonatal NSCs, adult SVZ	**miR-9 OE promotes neuronal differentiation; miR-9 decreases Notch signaling dependent on FOXO1**	**FOXO1 (predicted)**	***Foxo1***	Kim et al., 2015
	Adult zebrafish brain	**Nuclear localized non-canonical miR-9 maintains aNSC quiescence**	**TNRC6 (for nuclear shuttling)**	**Notch signaling (indirect positive effect)**	Katz et al., 2016
miR-124	Mouse embryonal carcinoma cell line	REST prevents miR-124 expression in neural progenitors	REST		Conaco et al., 2006
	Chick neural tube, mouse embryonal carcinoma cell line	miR-124 promotes neuronal differentiation	REST	*Scp1*	Visvanathan et al., 2007
	Mouse adult SVZ: injection of miR-124 OE retrovirus, infusion of miR-124 inhibitor	**miR-124 promotes neuronal differentiation and is necessary for SVZ regeneration**		***Sox9***	Cheng et al., 2009
	Mouse adult SVZ: injection of miR-124 OE/sponge lentivirus	**miR-124 OE leads to precocious neuronal differentiation and aNSC exhaustion; miR-124 inhibition represses neuronal differentiation and promotes glial differentiation**			Akerblom et al., 2012
miR-137	**Mouse primary adult forebrain NSCs, DG retroviral injection**	**miR-137 OE promotes aNSC proliferation and represses neuronal differentiation**	**MECP2**	***Ezh2***	Szulwach et al., 2010
	Mouse embryonic NSCs, *in utero* electroporation into the lateral ventricle	miR-137 OE inhibits NSC proliferation and accelerates neuronal differentiation	TLX (via LSD1)	*Lsd1*	Sun et al., 2011
miR-184	**Mouse primary adult DG NSCs, DG retroviral injection**	**miR-184 promotes aNSC proliferation**	**MBD1**	***Numbl***	Liu et al., 2010
miR-195	**Mouse primary adult DG NSCs, DG retroviral injection**	**miR-195 promotes aNSC proliferation**	**MBD1**	***Mbd1***	Liu et al., 2013

Overview of miRNAs (in ascending numerical order) discussed in this review that modulate proliferation and differentiation of (adult) neural progenitor cells, their upstream regulators, target mRNAs, and the model systems they have been studied in. Findings relating to adult neurogenesis are highlighted in bold. (a) NSC, (adult) neural stem cells; DG, dentate gyrus; KO, knockout; OE, overexpression; SVZ, subventricular zone; VZ, ventricular zone.

TABLE 2 | Putative impact of miRNAs on neuronal migration and neuronal morphogenesis in the context of adult neurogenesis.

MicroRNA	Main model system	Observed main effect	miRNA regulator	Target mRNA	Reference
miR-15a	**Floxed *Mecp2* mice, DG retroviral grafting of Cre-GFP/miR-15a sponge,** primary neonatal cortical/hippocampal neurons	**miR-15a impairs dendrite maturation, miR-15a inhibition rescues *Mecp2*-deficiency-induced neuronal maturation deficits**	**MECP2**	***Bdnf***	Gao et al., 2015
miR-19	**Mouse primary adult DG NSCs, DG and SVZ retroviral injection**	**miR-19 promotes migration of neurons**		***Rapgef2***	Han et al., 2016
miR-124	Rat primary embryonic hippocampal neurons	miR-124 increases axonal and dendrite complexity		*Rhog*	Franke et al., 2012
miR-132	Rat primary neonatal cortical neurons	CREB induces miR-132 expression downstream of BDNF, miR-132 promotes neurite outgrowth	CREB	p250Gap (*Arhgap32)*	Vo et al., 2005
	Rat primary neonatal cortical neurons	miR-132 and MECP2 form a feedback mechanism via BDNF	BDNF via CREB	*Mecp2*	Klein et al., 2007
	Rat primary neonatal hippocampal neurons	miR-132 promotes dendrite growth and spine maturation		p250Gap (*Arhgap32)*	Wayman et al., 2008
	Floxed miR-213/132 mice and GFP-Cre DG retroviral injection	**Deletion of miR-132 decreases dendrite length and arborization**			Magill et al., 2010
miR-134	Rat primary embryonic cortical/hippocampal neurons	miR-134 decreases size of dendritic spines	BDNF (indirect effect)	*Limk1*	Schratt et al., 2006
	***Sirt1* KO/Nestin-Cre mice, adult hippocampal lentiviral injection**	**miR-134 knockdown rescues *Sirt1*-deficiency-induced LTP and memory defects**	**SIRT1**	***Creb***	Gao et al., 2010
	Mecp2 KO/OE mice, mouse primary embryonic cortical neurons	*Mecp2* OE inhibits dendrite growth and pri-miR-134 processing; miR-134 OE rescues dendrite growth defect	MECP2		Cheng T.-L. et al., 2014
miR-134 part of miR-379-410 cluster	Rat primary embryonic cortical/hippocampal neurons	miR-379-410 expression is regulated by neuronal activity via MEF2; miR-134 promotes dendrite outgrowth	MEF2	*Pum2*	Fiore et al., 2009
miR-137	**Mouse DG retroviral injection,** primary embryonic hippocampal neurons	**miR-137 OE inhibits dendrite morphogenesis**		***Mib1***	Smrt et al., 2010
miR-138	Rat primary embryonic cortical/hippocampal neurons	miR-138 decreases size of dendritic spines		*Apt1*	Siegel et al., 2009
miR-223	**Retroviral injection of miR-223 sponge into mouse DG,** miR-223 OE in human fetal NPCs	**miR-223 inhibits dendrite outgrowth**			Harraz et al., 2014

List of the miRNAs (in ascending numerical order) and their respective up-stream regulators and target mRNAs associated with regulating neuron migration and morphogenesis during neurogenesis. Findings directly related to adult neurogenesis are highlighted in bold. DG, dentate gyrus; KO, knockout; LTP, long-term potentiation; NSC, neural stem cells; OE, overexpression; SVZ, subventricular zone.

treatment may reverse this impairment. In fact, mood and psychiatric disorders have been associated with dysfunctional hippocampal neurogenesis (reviewed by Mahar et al., 2014). Mouse transgenic gain- and loss-of-function models revealed that miR-17-92 is required for aNSC proliferation in the dentate gyrus and that alterations of miR-17-92 expression have a strong impact on hippocampal neurogenesis and evoke changes in stress and anxiety-related behavioral tests. Mice depleted for miR-17-92 showed a reduced hippocampal neurogenic activity and exhibited anxiety-like behavior. It was further shown that miR-17-92 targets *Sgk1*, a downstream effector of glucocorticoid receptor signaling involved in cellular stress response, and that miR-17-92 can rescue the impairment of neural progenitor proliferation induced by corticosterone treatment (Jin et al., 2016). Expression of miR-17-92 itself is down-regulated upon chronic stress suggesting miR-17-92 as a physiological effector of stress-impaired hippocampal neurogenesis. Of note, miR-17-92 expression in aNSCs might change during aging as indicated by a recent study reporting a reduced miR-17-92 expression in neurogenic niches of old versus young *N. furzeri* fish (Terzibasi Tozzini et al., 2014).

MicroRNAs Modulate Adult Neuronal Differentiation by Acting in Concert With Gene Expression Regulators

Activated aNSCs give rise to IPCs, which then differentiate into neuroblasts that further mature into the respective neurons, i.e., olfactory bulb neurons (generated from the SVZ) and dentate granule cells (generated from the SGZ) (**Figure 1**). miRNAs have been shown to regulate the transition from proliferation to neuronal differentiation both during embryonic and adult neurogenesis. In this context, miRNAs are often found to interact with gene expression regulators forming feedback loops as we delineate in the following paragraphs. In fact, a recurrent feature of the miRNA's mode of action is that several miRNAs act on the same transcriptional regulator, which in turn modulates the expression of its regulatory miRNAs, thereby forming feedback loops to fine-tune gene expression (reviewed by Arora et al., 2013; Lopez-Ramirez and Nicoli, 2014; Osella et al., 2014; Murao et al., 2016).

MicroRNA-124 and miR-9 Are Part of a Gene Regulatory Network Controlling Developmental and Adult Neurogenesis

One of the most studied miRNAs expressed in the brain are miR-124 and miR-9, which are not only able to induce neuronal differentiation of embryonic NSCs (reviewed by, e.g., Akerblom and Jakobsson, 2014; Roese-Koerner et al., 2013) but can even instruct a neurogenic gene expression program in non-neuronal cells (Yoo et al., 2011). Both miR-124 and miR-9 are widely expressed in the mouse adult brain including the hippocampus (Bak et al., 2008) and play important roles during adult neurogenesis. miRNA-124 has been shown to promote neuronal differentiation in the mouse SVZ by targeting the transcription factor SOX9 (Cheng et al., 2009). Stable overexpression of miR-124 in the mouse SVZ initially boosts neuronal differentiation but ultimately leads to premature exhaustion of the aNSC pool and loss of neurogenic activity (Akerblom et al., 2012). miRNA-9 is also expressed in the adult mouse SVZ, where it promotes neuronal differentiation (Zhao et al., 2009; Kim et al., 2015). One of the *bona fide* miR-9 targets identified in this context is *Foxo1*, which is related to *Foxo3*, and was shown to maintain aNSC self-renewal by acting in concert with Notch signaling (Kim et al., 2015). These findings are in contrast to the suggested role of miR-9 in maintaining quiescence in the zebrafish neurogenic niche (Katz et al., 2016), and it is not clear whether miR-9 impacts on both aNSC quiescence and differentiation in the adult mouse brain.

miRNA-124 and miR-9 have been shown to interact with an overlapping set of gene expression regulators that play important roles during NSC differentiation (reviewed by Stappert et al., 2014). Several of the transcription factors interacting with miR-124 and miR-9, e.g., REST and TLX, are also relevant in the context of adult neurogenesis. We will center our discussion on the miRNA-based circuitry formed around REST and TLX (**Figures 3A,B**).

Both miR-124 and miR-9 are connected to the anti-neural transcription factor REST (Conaco et al., 2006; Visvanathan et al., 2007; Packer et al., 2008; Laneve et al., 2010). While in undifferentiated cells high levels of REST prevent the expression of miR-9 and miR-124, these miRNAs are up-regulated during differentiation and enforce their own expression by targeting *Rest* and its cofactors *CoRest* (*Rcor2*) and *Scp1* (**Figure 3A**; Conaco et al., 2006; Visvanathan et al., 2007; Packer et al., 2008; Laneve et al., 2010). In the murine dentate gyrus, *Rest* is down-regulated during the transition of aNSCs to neuroblasts before it is up-regulated again in mature hippocampal granule cells (Gao et al., 2011). Adult NSC-specific depletion of *Rest* in the dentate gyrus results in premature differentiation and exhaustion of the aNSC pool (Gao et al., 2011). Of note, *Rest*-depleted aNSCs also show tremendous differences in their miRNA expression profile suggesting that dysregulation of miRNAs may at least in part underlie the imbalance of aNSC maintenance and differentiation induced by *Rest*-deficiency (Gao et al., 2012).

Another important transcription factor interacting with miRNAs to control NSC proliferation and differentiation is the nuclear receptor TLX (*Nr2e1*). TLX is expressed in neurogenic regions during development and adulthood, and its presumed function is to prevent premature differentiation and maintain the undifferentiated self-renewing state of NSCs (reviewed by Islam and Zhang, 2015). Conditional ablation of *Tlx* in dentate gyrus aNSCs does not induce differentiation, but results in precocious cell cycle exit of aNSCs that enter a quiescent inactive state (Shi et al., 2004; Zhang et al., 2008; Niu et al., 2011). Studies performed in mouse primary forebrain aNSCs revealed that miR-9 and let-7 promote neuronal and glial differentiation by targeting *Tlx* (Zhao et al., 2009, 2010). *In utero* electroporation into the lateral ventricles to overexpress miR-9 or let-7 during embryonic development resulted in a similar effect with a decrease of proliferative cells and an increase of differentiating, migrating cells (Zhao et al., 2009, 2010), indicating that miR-9 and let-7 induce differentiation both during developmental and adult neurogenesis. Interestingly, TLX has a direct repressive effect on

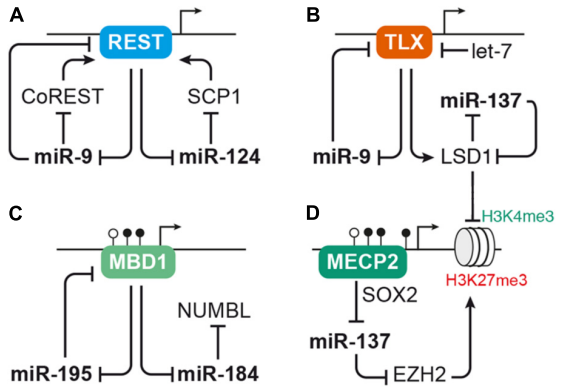

FIGURE 3 | MicroRNAs interact with transcription factors and epigenetic regulators to control aNSC proliferation and differentiation. **(A)** The transcriptional repressor REST serves as regulatory hub for several miRNAs, including pro-neural miR-9 and miR-124. REST represses expression of miR-9 and miR-124, which in turn interfere with the activity of the Rest complex by targeting *Rest* or its cofactors *CoRest* and *Scp1*. **(B)** Another transcription factor interacting with miRNAs in the context of NSC self-renewal and differentiation is TLX. TLX has a direct repressive effect on miR-9 expression and also inhibits expression of miR-137 via recruiting the histone demethylase LSD1. The activity of TLX itself is regulated by miR-9 as well as let-7, which both target *Tlx*, and miR-137, which targets *Lsd1*. **(C–D)** miRNAs often interact with epigenetic regulators, such as mediators of DNA methylation and histone modifiers. **(C)** Expression of miR-184 and miR-195 is suppressed by binding of the methyl-CpG-binding protein MBD1 to their genomic loci. miRNA-195, in turn, binds to *Mbd1* mRNA forming a negative feedback loop, while miR-184 targets *Numbl*. **(D)** MECP2 cooperates with the neural progenitor transcription factor SOX2 to repress miR-137 expression. miRNA-137 may regulate global gene transcription through repressing the expression of histone modifiers, i.e., EZH2, which induces repressive H3K27 trimethylation (me3) marks, and LSD1, which erases activating H3K4me3 marks. LSD1 and MECP2 are also recruited by the REST/CoREST complex, thus forming another node through which the miRNAs discussed here may cross talk with each other. For sake of simplicity, these interactions were not depicted here. For a detailed review on the cross talk between miRNAs and epigenetic regulators, see Jobe et al. (2012).

miR-9 expression forming a negative feedback loop (**Figure 3**; Zhao et al., 2009). Furthermore, TLX also represses miR-137 by recruiting the histone demethylase LSD1 (*Kdm1a*) to the miR-137 locus. *Lsd1* is highly expressed in mouse aNSCs and declines during neuronal differentiation. Inhibition of LSD1 results in a decrease of aNSC proliferation *in vitro* as well as in the adult dentate gyrus (Sun et al., 2010). Experiments in embryonic NSCs revealed that miR-137 promotes neuronal differentiation by targeting *Lsd1* (Sun et al., 2011), thus adding another loop to the feedback circuity formed around TLX (**Figure 3B**).

MicroRNAs Interacting With Epigenetic Regulators to Balance aNSC Proliferation and Differentiation

Another recurring theme in the context of miRNA-based regulation is the interplay of miRNAs and epigenetic regulators, such as chromatin modifiers (reviewed by Jobe et al., 2012; Lopez-Ramirez and Nicoli, 2014; Murao et al., 2016). miRNA-137, for instance, was reported to target the histone methyltransferase EZH2. EZH2 is part of the polycomb group protein complex involved in epigenetic remodeling by histone methylation. In line with that, overexpression of miR-137 in aNSCs resulted in an overall reduction of H3K27 tri-methylation (Szulwach et al., 2010). The same study also reported an increase of aNSC proliferation at the expense of neuronal differentiation upon miR-137 overexpression (Szulwach et al., 2010), which is opposed to the pro-differentiation function of miR-137 reported in embryonic NSCs (Sun et al., 2011). It was further shown that expression of miR-137 in aNSCs depends on the action of another epigenetic regulator, the DNA methyl-CpG-binding protein MECP2, which in cooperation with SOX2 retains miR-137 expression (Szulwach et al., 2010). Thus, miR-137 may act in concert with several epigenetic regulators (LSD1, MECP2, and EZH2) to control global gene expression (**Figures 3B,D**). The question is, though, which of these targets are responsible for the distinct effects of miR-137 during proliferation and differentiation of NSCs.

Another example for the interaction of miRNAs with epigenetic regulators is the interaction of the methyl-CpG-binding protein MBD1 with miR-184 and miR-195 in dentate gyrus aNSCs (**Figure 3C**; Liu et al., 2010, 2013). *Mbd1* is abundantly expressed in the adult brain with highest concentrations in the SGZ of the dentate gyrus. In line with that, *Mbd1*-deficient mice display reduced adult neurogenic activity and impaired hippocampal function (Zhao et al., 2003). Adult NSCs lacking *Mbd1* accumulate at the level of IPCs and fail to transition to the neuronal fate (Jobe et al., 2017). Besides regulating the expression of lineage differentiation-associated protein-coding genes (Jobe et al., 2017), MBD1 was also found to repress the expression of miR-184 and miR-195 by direct binding to their proximal genomic regions (Liu et al., 2010, 2013). Both miR-184 and miR-195 have been shown to promote aNSC proliferation at the expense of neuronal differentiation *in vitro* as well as *in vivo*. *Bona fide* targets identified in this context were *Numbl* for miR-184 (Liu et al., 2010) and *Mbd1* for miR-195, representing yet another example of a negative feedback loop to reinforce miRNA expression (Liu et al., 2013). Additionally, there seems to be some functional redundancy between the two MBD1-regulated miRNAs, miR-195 and miR-184, as the effect induced by miR-195 overexpression could be rescued by miR-184 inhibition (Liu et al., 2013).

MicroRNAs Regulating Survival in the Adult Neurogenic Niche

An important feature determining the neurogenic output of aNSC is the survival of their neuronal progeny. In fact, under normal conditions, the majority of newborn dentate gyrus neurons undergoes apoptosis within the first days of their life with apoptotic neurons being cleared out by microglia (Sierra et al., 2010; reviewed by Kim and Sun, 2011). Several miRNAs have been shown to regulate survival-associated genes, making them an interesting target for neuroprotective or cell replacement strategies in neurodegenerative diseases (Zhang et al., 2018), stroke (Sun et al., 2017), and epilepsy (Schouten et al., 2015; Yuan et al., 2016; Bielefeld et al., 2017).

A series of studies has been focusing on the impact of global miRNA loss using conditional knockout mouse (cKO) lines for

Dicer, the key enzyme of miRNA biogenesis (e.g., Davis et al., 2008; De Pietri Tonelli et al., 2008; Hébert et al., 2010; Konopka et al., 2010; Li et al., 2011; Cheng S. et al., 2014). While these studies came to sometimes contradictory results [see Barca-Mayo and De Pietri Tonelli (2014) for a detailed comparison], many of them report that *Dicer* depletion in the embryonic mouse forebrain reduces forebrain growth, increases apoptosis, and leads to premature death of the animals (Davis et al., 2008; De Pietri Tonelli et al., 2008; Hébert et al., 2010; Li et al., 2011). Likewise, specific deletion of *Dicer* in forebrain (cortical and hippocampal) neurons at postnatal stages also resulted in enhanced apoptosis and neuronal loss (Konopka et al., 2010; Cheng S. et al., 2014). Taken together, these findings indicate that a functional miRNA system is critical for neuron survival, but they do not provide direct information on the impact of the miRNA system on the generation and survival of adult-born neurons.

This question was recently assessed by two studies, in which *Dicer* was specifically deleted in aNSCs (Cernilogar et al., 2015; Pons-Espinal et al., 2017). In the first study, *Dicer* was inactivated by delivery of Cre recombinase into primary neural progenitors isolated from the adult SVZ or by retroviral injection into the adult hippocampus of $Dicer^{flox/flox}$ mice. Both *in vitro* as well as *in vivo* an increase in doublecortin *Dcx* expression was noted, hinting to an enhanced neuronal differentiation upon *Dicer* deletion (Cernilogar et al., 2015). However, the authors also observed a reduced viability of *Dicer*-depleted cells in their *in vivo* experiments. Pons-Espinal et al. (2017) used the Split-Cre approach developed by Beckervordersandforth et al. (2014) to selectively inactivate *Dicer* in aNSCs in the dentate gyrus and performed experiments on primary aNSCs isolated from $Dicer^{flox/flox}$ mice that were nucleofected with Cre recombinase. In contrast to the earlier study by Cernilogar et al. (2015), they observed an impaired neurogenic activity and a bias toward astrocytic differentiation. Furthermore, they noted a reduced survival of *Dicer*-depleted aNSCs both *in vivo* as well as *in vitro*, while the proliferative capacity of *in vitro* cultured aNSCs was not affected. This is in line with previous studies on embryonic NSCs reporting that the ability for NSC self-renewal in culture does not depend on Dicer activity (De Pietri Tonelli et al., 2008; Andersson et al., 2010). These *Dicer* cKO embryonic NSCs were, however, compromised with regard to their differentiation capacity (Andersson et al., 2010). Furthermore an increased cell loss was observed during differentiation of *Dicer*-depleted NSCs (embryonic or adult) indicating that differentiated cells are more sensitive toward global miRNA loss than undifferentiated cells (De Pietri Tonelli et al., 2008; Pons-Espinal et al., 2017).

These two findings prompted the hypothesis that a functional miRNA system is particularly important for cell fate transitions (De Pietri Tonelli et al., 2008; Andersson et al., 2010). Following this notion, Pons-Espinal et al. (2017) focused on a pool of 11 miRNAs (including miR-124 and miR-134) that was found to be highly up-regulated during early neuronal differentiation and asked whether these miRNAs could rescue the bias toward astrocytic differentiation and the impaired neuronal differentiation of *Dicer* cKO aNSCs (Pons-Espinal et al., 2017). Interestingly, they found that only combined delivery of all 11 miRNAs, but not subsets of them, was able to rescue the *Dicer* deletion phenotypes (Pons-Espinal et al., 2017). By combining proteomics and *in silico* miRNA target gene prediction they further found that quite a number of targets are shared by at least 2 of the 11 miRNAs, which led them to speculate that these 11 miRNAs may have a cooperative function targeting an overlapping set of genes to induce neuronal differentiation of aNSC. In fact, cooperative binding of several miRNAs to the same target mRNA is an important feature of the miRNAs' mode of action and may create functional redundancy (reviewed by Barca-Mayo and De Pietri Tonelli, 2014). However, the data generated by Pons-Espinal et al. (2017) suggest that the level of redundancy among the 11 miRNA is rather low since only the combination of all miRNAs was able to compensate for *Dicer* cKO and not the individual miRNAs.

MicroRNAs Regulating Migration and Neurite Morphogenesis of Adult-Born Neurons

MicroRNAs also influence functional integration of the neuronal progeny, i.e., migration to their final homing site, neuronal morphogenesis, and synaptogenesis. Immature neuroblasts that arise from the SGZ first have to migrate up into the granule cell layer before they start extending dendrites toward the molecular layer of the dentate gyrus and grow axons that target the CA3 region of the hippocampus, approximately 1 week after their birth (**Figure 1C**) (Zhao et al., 2006). The maturation process in adult neurogenesis differs from that of embryonic neurogenesis in that adult-born neurons have to integrate into already existing coordinated neuronal networks and that they receive synaptic inputs early on. As shown for mouse hippocampal neurogenesis, immature adult granule cells initially receive excitatory GABAergic inputs, which become inhibitory by 2 weeks after their birth (reviewed by Gonçalves et al., 2016). Around the same time, immature adult-born granule cells also receive glutamatergic input, start developing dendritic spines, and establish efferent and afferent synapses with the local neuron network (reviewed by Deng et al., 2010). Neurons that fail to develop strong synaptic connections will undergo selective apoptosis (Tashiro et al., 2006; and reviewed by Kim and Sun, 2011). Finally, by 8 weeks after their birth, adult-born granule neurons are considered to be fully mature and are indistinguishable from their earlier-born neighbors (Laplagne et al., 2006; and reviewed by Deng et al., 2010).

The molecular mechanisms guiding adult-generated granule cells to their final homing site in the granule cell layer and their mode of migration have not yet been completely resolved. Interestingly, it has been reported that adult-born dentate gyrus neuroblasts first undergo tangential migration along the blood vasculature in the SGZ followed by radial migration to reach the granule cell layer (Sun et al., 2015). While miRNAs have been shown to regulate various genes involved in neuron migration during development (reviewed by Rajman and Schratt, 2017), there is only one study that specifically assessed the impact of miRNAs in the context of adult-born neuron migration (Han et al., 2016). In this study, Han et al. (2016) discovered that

elevated levels of miR-19 increased cell migration of *in vitro* cultured hippocampal neural progenitors. They further showed that ectopic expression of miR-19 in the dentate gyrus triggered newborn granule cells to migrate deeper into the granule cell layer. Likewise, neuroblasts generated from the SVZ were found to cover longer distances within the RMS upon miR-19 overexpression. These data indicate that miR-19 promotes migration of adult-born neurons (Han et al., 2016). This function seems to be at least in part mediated by miR-19 targeting *Rapgef2*, which regulates cell migration by modulating the activity of RAP proteins (Han et al., 2016). Knock-down of *Rapgef2* in neural progenitors mimicked the effect of miR-19 overexpression as it promoted migration of *in vitro* cultured neural progenitors and newborn granule cells in the dentate gyrus granule cell layer. Since abnormal migration of adult-born hippocampal neurons was also described in schizophrenia (Duan et al., 2007; Kim et al., 2009), and rare inherited copy number variants of *RAPGEF2* have been associated with familiar schizophrenia (Xu et al., 2009), Han et al. (2016) went on to study the role of miR-19 and *RAPGEF2* in schizophrenia patient-derived hippocampal neural progenitor cells (SZ-NPCs). Indeed, they found that miR-19 is up-regulated in SZ-NPCs and that the regulation of *RAPGEF2* by miR-19 is conserved in humans (Han et al., 2016). miRNA-19 belongs to the family of polycistronic miR-17 clusters, including also miR-17-92 and miR-106b-25b, which have been shown to be important for aNSC proliferation (Brett et al., 2011; Jin et al., 2016). Hence, it would be interesting to assess whether the other members of the miR-17 clusters are also altered in schizophrenia and whether they contribute to the disease.

After the immature neuroblasts have reached the granule cell layer, they develop into mature neurons, extend dendrites and axons, and establish synaptic contacts. Numerous miRNA-target pairs have been identified to regulate neurite outgrowth and morphogenesis as well as synaptic plasticity (e.g., reviewed by Bicker et al., 2014; Hu and Li, 2017; Rajman and Schratt, 2017). Some miRNAs even show a specific synaptic localization, and several miRNAs are regulated in response to neuronal activity (reviewed by Hu and Li, 2017). Here, we focus on those miRNAs that have been shown to regulate neuronal morphogenesis of hippocampal neurons. Due to the limited number of studies addressing morphogenesis of adult-generated neurons, we also include studies on the role of miRNAs regulating neurite formation and maturation in the developing hippocampus (see **Table 2** for an overview of the miRNAs discussed). In the following paragraphs, we highlight examples of miRNAs that converge on functionally related targets or are regulated by the same set of transcription factors (**Figure 4**).

One common pathway through which miRNAs modulate neuronal morphogenesis is Rho GTPase signaling (**Figure 4A**). Rho GTPase-mediated remodeling of the actin cytoskeleton is important for regulating several aspects of neuronal morphogenesis (reviewed by Stankiewicz and Linseman, 2014) including dendritic spine maturation of hippocampal neurons (Vadodaria et al., 2013). miRNA-124 promotes axonal and dendrite complexity of rat embryonic hippocampal neurons by inhibiting expression of *Rhog* GTPase (Franke et al., 2012). miRNA-134 negatively affects the size of dendritic spines of *in vitro* cultured embryonic rat hippocampal neurons by targeting *Limk1*, which regulates actin filament dynamics via inhibition of ADF/cofilin (Schratt et al., 2006). In addition,

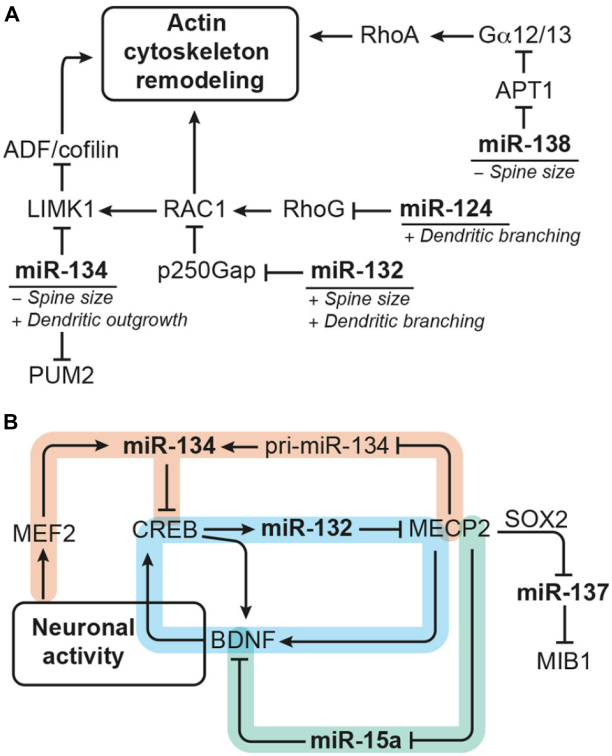

FIGURE 4 | miRNAs modulating dendrite morphogenesis converge by targeting components of the actin remodeling complex and cross talk with each other via neuronal activity-dependent gene regulatory networks. **(A)** miRNA-124, miR-132, miR-134, and miR-138 have divergent effects on dendrite morphogenesis by targeting different components of the actin remodeling pathway. miRNA-124 and miR-134 reduce the activity of RAC1/LIMK1 signaling, whereby miR-124 targets *RhoG* and miR-134 targets *Limk1*. miRNA-132, in contrast, increases RAC1/LIMK1 activity by inhibiting p250Gap-mediated repression of RAC1. miRNA-138 increases Gα12/13 palmitoylation and downstream RhoA signaling by targeting the mRNA coding for the depalmitoylation enzyme APT1. An additional target of miR-134 is the translational repressor PUM2 (Pumilio2) through which miR-134 promotes overall dendritogenesis. **(B)** Many of the miRNAs modulating dendrite morphogenesis engage in regulatory circuits with transcription regulators that respond to neuronal activity. One such regulatory circuit is formed around miR-132 (highlighted in blue), whose expression is induced by CREB downstream of neuronal activity. miRNA-132 itself may influence CREB activation via interfering with MECP2-induced expression of *Bdnf*, which forms a positive feedback loop with CREB. The regulation of miR-134 expression (in orange) seems to be more complex: miR-134 expression was found to be induced by MEF2 downstream of neuronal activity and inhibited by MECP2, which interferes with pri-miR-134 processing. miRNA-134, in turn, targets *Creb* and may thereby provide a negative feedback signal for activity-induced gene expression and also influence miR-132 transcription. Another regulatory hub involves miR-15a (in green), the expression of which is inhibited by MECP2. miRNA-15a targets *Bdnf* mRNA, thereby providing an alternative route through which MECP2 promotes *Bdnf* expression. MECP2 further represses expression of miR-137 by cooperating with SOX2. miRNA-137 inhibits neuronal maturation and dendrite morphogenesis by targeting the ubiquitin ligase MIB1.

miR-134 was shown to have a growth-promoting effect on dendrites, which is mediated by Pumilio2 (*Pum2*), a translational repressor involved in dendritogenesis (Fiore et al., 2009). miRNA-132 enhances dendrite growth and spine maturation of *in vitro* cultured neonatal rat hippocampal neurons by inhibiting expression of the Rho GTPase activating protein p250Gap (*Arhgap32*), which results in an increased RAC actin remodeling signal and LIMK1 activation (Wayman et al., 2008). Furthermore, miR-138 has been described to negatively regulate the size of dendritic spines by targeting the mRNA coding for the depalmitoylation enzyme APT1 (Siegel et al., 2009). Inhibition of *Apt1* expression by miR-138 leads to an increased palmitolyation and membrane-tethering of G protein Gα12/13, which activates RhoA signaling – another component of the actin remodeling pathway.

MicroRNA expression is modulated by transcriptional regulators, and many of the miRNAs involved in dendrite morphogenesis have been found to be targets of neuronal activity-associated gene regulatory networks. The transcription factors operating in those gene regulatory networks are by themselves often subject to miRNA regulation. Experiments in rat hippocampal neurons showed that expression of the polycistronic miR-379-410 cluster, which also contains miR-134, is induced by the transcription factor MEF2 in response to membrane depolarization or BDNF treatment (Fiore et al., 2009). However, BDNF treatment was also shown to relieve miR-134-mediated repression of *Limk1* in dendrites of embryonic rat hippocampal neurons via a yet unknown mechanism (Schratt et al., 2006). Another miRNA up-regulated in response to neuronal activity is miR-132, the expression of which is induced by the transcription factor CREB. CREB contributes to activity-induced refinement of dendrite morphology and is regulated by miR-134 (Gao et al., 2010). In addition, miR-132 fine-tunes BDNF-mediated CREB activation by targeting *Mecp2*, which induces *Bdnf* (Klein et al., 2007). Recently, it has also been shown that MECP2 can directly interact with the miRNA processing machinery to inhibit the expression of mature miR-134 (Cheng T.-L. et al., 2014). Thus, miR-132 and miR-134 may cross talk in the context of dendrite morphogenesis through CREB and MECP2 (**Figure 4B**). MECP2 also interacts with SOX2 to retain the expression of miR-137 (Szulwach et al., 2010), which negatively regulates neuronal maturation and dendrite morphogenesis by targeting the mRNA coding for ubiquitin ligase MIB1 (Smrt et al., 2010). MECP2 was further shown to act as a repressor of miR-15a expression, and miR-15a inhibits dendrite maturation of developmental- and adult-born hippocampal neurons by targeting *Bdnf* (Gao et al., 2015). Thus, MECP2-mediated repression of miR-15a represents an indirect route to promote *Bdnf* expression downstream of MECP2 (**Figure 4B**).

It is important to note that most of the experiments discussed above were performed in primary cultures of rodent embryonic or neonatal hippocampal neurons (**Table 2**), thus addressing the effect of miRNAs on neurons born in an early developmental phase. However, the same miRNA-target pairs might be also involved in regulating neurite morphogenesis during adult neurogenesis. Depletion of the miR-132 genomic loci in dentate gyrus aNSCs, for instance, was shown to reduce dendrite complexity of neuronal progenies demonstrating that miR-132 has a positive effect on dendrite maturation both during embryonic and adult hippocampal neurogenesis (Magill et al., 2010). In contrast, miR-137 and miR-15a were demonstrated to have a negative effect on dendrite maturation of adult-born dentate granule cells (Smrt et al., 2010; Gao et al., 2015). Another miRNA specifically studied in the context of adult neurogenesis and neuronal maturation is miR-223. Inhibition of miR-223 in dentate gyrus aNSCs by retroviral miRNA sponge injection resulted in an increased dendrite length, while overexpression of miR-223 in human embryonic stem cell-derived neurons had the opposite effect, suggesting that miR-223 also regulates neuronal morphogenesis both during developmental and adult neurogenesis (Harraz et al., 2014).

Taken together, these examples of miRNAs-target pairs that cross talk at different hierarchy levels illustrate once more the complexity and the importance of the miRNA system for adult neurogenesis. Furthermore, many of the miRNAs involved in neuronal morphogenesis discussed above have also been linked to neurological disorders, like Alzheimer's disease (miR-132, miR-138), Huntington's disease (miR-132, miR-137, miR-138), psychiatric disorders (miR-132, miR-134, miR-137, miR-138), and epilepsy (miR-134, miR-138) (reviewed by, e.g., Bicker et al., 2014). It is therefore tempting to speculate that dysregulation of miRNAs and altered neuronal morphogenesis may contribute to the disease pathology.

A Synopsis of the Diverse Roles of MicroRNAs in Adult Neurogenesis

Adult neurogenesis is a multistep process comprising activation of quiescent aNSCs, their differentiation into committed progenitor cells, neuronal survival, migration and functional integration of newborn neurons (**Figure 1D**). Transitions along these steps are accompanied by dynamic gene expression changes (Llorens-Bobadilla et al., 2015; Shin et al., 2015; Dulken et al., 2017; and reviewed by Beckervordersandforth et al., 2015). As discussed in this review and also in other reports (e.g., reviewed by Lopez-Ramirez and Nicoli, 2014; Murao et al., 2016), miRNAs are an integral part of the gene regulatory networks driving these changes. Although not all interactions discussed here have been experimentally validated in the context of adult neurogenesis, many of the individual factors involved, e.g., miR-124, miR-9, let-7, and miR-137 on the one side and REST, TLX, and LSD1 on the other side, have been shown to play important roles during adult neurogenesis (see **Figure 3** and **Table 1** for an overview). Thus, the emerging picture is that miRNAs are frequently engaged in feedback loops with transcription factors and epigenetic regulators importantly involved in regulating adult neurogenesis.

By doing so, miRNAs provide an additional layer to control gene expression programs and may help to ensure the robustness of such programs by dampening perturbations and reducing noise (reviewed by Arora et al., 2013; Lopez-Ramirez and Nicoli, 2014; Osella et al., 2014; Murao et al., 2016). However, miRNAs are also involved in remodeling gene expression programs during

neural lineage progression (reviewed by Herranz and Cohen, 2010; Peláez and Carthew, 2012). miRNAs may even exert an instructive effect on cell fate as impressively demonstrated by the finding that miR-9/9* and miR-124 can induce neuronal conversion of fibroblasts (Yoo et al., 2011). Furthermore, global miRNA loss by *Dicer* depletion seems to evoke stronger effects in differentiating cells than in self-renewing NSCs (derived from either embryonic and adult origin), suggesting that cell fate transitions show a particular dependency on miRNA-based regulation (De Pietri Tonelli et al., 2008; Andersson et al., 2010; Pons-Espinal et al., 2017).

However, some of the miRNA functions might be context-dependent. For instance, miR-9 was found to maintain quiescence of aNSCs in the zebrafish brain (Katz et al., 2016), while in mouse aNSCs it promotes neuronal differentiation of aNSCs (Zhao et al., 2009; Kim et al., 2015). These divergent observations might be due to the different experimental model systems employed but may also reflect two different modes of action of miR-9, i.e., cytoplasmic miR-9 promotes neuronal differentiation via canonical targeting of *Tlx* and *Foxo1* (Zhao et al., 2009; Kim et al., 2015), while nuclear miR-9 maintains aNSC quiescence (Katz et al., 2016). Another example of a miRNA eliciting context-dependent effects is miR-137, which was found to promote differentiation of embryonic NSCs (Sun et al., 2010) but inhibits differentiation of adult NSCs (Szulwach et al., 2010).

MicroRNAs Converge on Shared Targets to Control Adult Neurogenesis

Many miRNAs have been reported to have rather mild effects on their target genes (Baek et al., 2008; Selbach et al., 2008). Yet, each miRNA might target several hundreds of mRNAs (Lewis et al., 2005; Lim et al., 2005). This "multiplicity" of miRNA targets means that, although the effect of an individual miRNA on a given target might be rather weak, this miRNA might still exert a meaningful biological effect by acting on different genes with overlapping functions (Barca-Mayo and De Pietri Tonelli, 2014; Fischer et al., 2015). Another important feature of miRNA function is "cooperativity," which describes that most mRNAs possess binding sites for multiple miRNAs (Barca-Mayo and De Pietri Tonelli, 2014; Schmitz et al., 2014; Fischer et al., 2015). Cooperative binding of several miRNAs to the same target mRNA creates functional redundancy and might compensate for the rather mild repression mediated by individual miRNAs on that given target. It has been suggested that by the interplay of multiplicity and cooperativity, miRNAs may have "converging functions" defined as synergic action of a single miRNA or several miRNAs on multiple targets that belong to the same pathway or are exerting redundant functions (Barca-Mayo and De Pietri Tonelli, 2014). For instance, miR-9 and miR-124 have been shown to drive neuronal differentiation of NSCs by converging on *Rest*, *Baf53a*, and components of the Notch signaling cascade as common target genes (reviewed by Stappert et al., 2014). Other examples of miRNAs with convergent functions and mentioned in this review in the context of adult neurogenesis are let-7 and miR-9, which both target *Tlx* (**Figure 3B** and **Table 1**; Zhao et al., 2009, 2013), and miR-184 and miR-195, which are both regulated by MBD1 and promote aNSC proliferation (**Figure 3C** and **Table 1**; Liu et al., 2010, 2013). Furthermore, several miRNAs (i.e., miR-124, miR-132, miR-134, and miR-138) have been found to be involved in dendrite morphogenesis by targeting components of the actin remodeling pathway as common denominator (**Figure 4A** and **Table 2**; Schratt et al., 2006; Wayman et al., 2008; Siegel et al., 2009; Franke et al., 2012). Another mechanism to coordinate miRNA function is to couple the expression of several miRNAs to a common transcription regulator as shown for MECP2, which regulates the expression of various miRNAs involved in dendrite morphogenesis (**Figure 4B**; Szulwach et al., 2010; Cheng T.-L. et al., 2014; Gao et al., 2015). miRNA cooperativity may be also reflected by the genomic localization of miRNA genes (reviewed by Olive et al., 2015). Many miRNAs are located in polycistronic clusters that encode for members of different miRNA seed families (**Figure 2**), as is the case for the paralog clusters miR-17-92, miR-160b-25, and miR-106a-363. Interestingly, these clusters encode for miRNAs with distinct functions in adult neurogenesis. For example, miR-25 promotes aNSC proliferation (Brett et al., 2011), whereas miR-19 enhances neuroblast migration (Han et al., 2016; **Figure 1D**). It would be interesting to assess the extent of co-expression of these miRNAs and their seed family members in the aNSC compartments.

Taken together, these examples illustrate how miRNAs act in concert with gene regulatory networks and also cooperate with each other by targeting functionally related genes. However, most of the reports mentioned above have focused on the action of a single miRNA-target pair. Future studies should also investigate the cooperative function of miRNAs in the context of adult neurogenesis, as it was addressed by Pons-Espinal et al. (2017).

MicroRNAs May Contribute to Heterogeneity in the aNSC Niche

Neural progenitors within the adult neurogenic niche are a heterogeneous population that can be distinguished by their cell cycle status (quiescence versus activated cells), by their differentiation potential (neurogenic or gliogenic), and their differentiation stage (aNSCs, IPCs, and neuroblasts) (reviewed by Giachino and Taylor, 2015; Bonaguidi et al., 2016). miRNAs might be importantly involved in conferring aNSC heterogeneity. miRNA-9, for instance, is specifically found in the nucleus of a subset of quiescent aNSCs in the adult brain of zebrafish and mouse (Katz et al., 2016). Disruption of the nuclear localization of miR-9 leads to an increased activation of aNSCs suggesting that this particular expression pattern of miR-9 is crucial for aNSC quiescence (Katz et al., 2016). In addition, miRNAs are involved in biasing embryonic NSCs to either neurogenic or gliogenic differentiation (reviewed by Rajman and Schratt, 2017; Shimazaki and Okano, 2018). It is well perceivable that these miRNAs might have a similar role in aNSCs. In fact, it is not yet clear whether aNSCs are truly multipotent or whether several neural precursor populations with variable differentiation potencies (neurogenic or gliogenic) exist within the NSC niche (reviewed by Bonaguidi et al., 2016), and it might well be that miRNAs could contribute to this heterogenic differentiation potency. Indeed, in their aNSC-specific *Dicer*-knockout model,

Pons-Espinal et al. (2017) discovered a shift toward astrogial differentiation at the expense of neuronal differentiation, which could be rescued by combined delivery of 11 miRNAs.

Recent advances regarding single cell tracing and single cell transcriptomics have led to the assignment of specific gene expression profiles to different cell states and further demonstrated the presence of diverse cell states along the process of adult neurogenesis (Llorens-Bobadilla et al., 2015; Shin et al., 2015; Dulken et al., 2017). These analyses revealed that aNSCs do not exist in only two stages (quiescent and activated aNSCs) but instead move through a continuum of different stages during activation (Llorens-Bobadilla et al., 2015; Dulken et al., 2017). It was further shown that aNSC activation is associated with increased protein synthesis (Llorens-Bobadilla et al., 2015; Shin et al., 2015) as well as with vast expression changes in genes associated with energy metabolism, transcriptional regulation, and signaling pathway integration (Shin et al., 2015). Since miRNAs provide an important mechanism to control mRNA–protein output, and many signaling pathway components as well as transcription factors are regulated by miRNAs, it would be interesting to also analyze miRNA profiles at a single cell level and to assess to what extent miRNA expression in the adult neurogenic niche reflects aNSC heterogeneity.

MicroRNAs May Contribute to Homeostasis in the aNSC Niche in Healthy and Disease Conditions

Although there is currently a controversial discussion about the extent and role of adult neurogenesis in humans (Boldrini et al., 2018; Sorrells et al., 2018; and reviewed by Kempermann et al., 2018), there remains a strong interest to decipher the molecular mechanisms governing adult neurogenesis and to identify novel tools to gain control over this process. This direction of research is driven by the idea to recruit aNSCs as endogenous cell source replacing the cells lost due to aging, acute lesions, or neurodegenerative diseases (reviewed by Lindvall and Kokaia, 2010). Since miRNAs have been shown to regulate aNSC activation, proliferation, and differentiation and may thereby contribute to the homeostatic regulation in the adult neurogenic niche, they could be envisioned as targets to harness aNSCs for therapeutics approaches. Promising candidates might be miR-9, let-7, miR-106b-25, and miR-17-92, which regulate the balance between quiescence and activation of aNSCs (Nishino et al., 2008; Brett et al., 2011; Jin et al., 2016; Katz et al., 2016). miRNAs might be even involved in conferring plasticity of adult hippocampal neurogenesis in response to environmental signals as shown for miR-17-92 and stress (Jin et al., 2016). Furthermore, miRNAs might also impact on age-dependent decline of adult neurogenesis, and a number of miRNAs have been found to interact with important aNSC regulators that are also associated with aging, including HMGA2, FOXO1, FOXO3, and TLX (Nishino et al., 2008; Zhao et al., 2009, 2010; Brett et al., 2011; Kim et al., 2015). In addition, a functional miRNA system seems to be important to sustain adult neurogenesis and survival within the neurogenic niche (Cernilogar et al., 2015; Pons-Espinal et al., 2017). Finally, numerous miRNAs are dysregulated in pathophysiological conditions associated with dysfunctional hippocampal neurogenesis, such as epilepsy (reviewed by Bielefeld et al., 2017), stroke (reviewed by Khoshnam et al., 2017), and neurodegenerative diseases (reviewed by Qiu et al., 2014). These miRNAs might represent promising targets to not only tackle the primary cause of the disease but to also counteract the disease-induced impairment of adult neurogenesis.

From an evolutionary perspective, it is noteworthy that adult neurogenesis appears to be less pronounced in human compared to rodent brain (e.g., Sanai et al., 2011; Sorrells et al., 2018). The miRNA-target pairs discussed in this review were all identified in rodents, but considering their sequence similarity they should be largely conserved in humans. Nevertheless, there is quite some evolutionary pressure on the miRNA regulome as indicated by the presence of primate-specific miRNAs (Awan et al., 2017), the evolution of miRNA binding sites on mRNA targets (Gardner and Vinther, 2008), and the acquisition of novel factors regulating miRNA-associated processes across evolution (Pratt and Price, 2016). Thus, elucidating the differences in miRNA-based regulation of murine versus human adult neurogenesis might eventually enable the promotion of adult neurogenesis in humans and their exploitation for regenerative purposes.

AUTHOR CONTRIBUTIONS

LS, FK, and OB wrote the manuscript and designed the figures.

FUNDING

Work in the laboratory of OB was supported by the EU [Seventh Framework Program HEALTH-F4-2013-602278-NeuroStemCellRepair; Horizon2020 grant 667301-COSYN and European Cooperation in Science and Technology (COST) grant CA16210-MINDDS]; the German Federal Ministry of Education and Research (BMBF) within the framework of the e:Med research and funding concept (grant 01ZX1314A-IntegraMent); the German Federal Ministry of Education and Research (BMBF) grant 01EK1603A-Neuro2D3; the North Rhine Westphalian Program "LifeSciences.NRW"; European Regional Development Fund (EFRE) (grant EFRE-0800978-SCF III); the National Institutes of Health (award 1R01NS100514) and the Stem Cell Network North Rhine Westphalia (start-up financing for interdisciplinary and multi-site projects-323-40000513). LS was supported by the BONFOR program.

REFERENCES

Akerblom, M., and Jakobsson, J. (2014). MicroRNAs as neuronal fate determinants. *Neuroscientist* 20, 235–242. doi: 10.1177/1073858413497265

Akerblom, M., Sachdeva, R., Barde, I., Verp, S., Gentner, B., Trono, D., et al. (2012). MicroRNA-124 is a subventricular zone neuronal fate determinant. *J. Neurosci.* 32, 8879–8889. doi: 10.1523/JNEUROSCI.0558-12.2012

Andersson, T., Rahman, S., Sansom, S. N., Alsiö, J. M., Kaneda, M., Smith, J., et al. (2010). Reversible block of mouse neural stem cell differentiation in the absence of dicer and microRNAs. *PLoS One* 5:e13453. doi: 10.1371/journal.pone.0013453

Arora, S., Rana, R., Chhabra, A., Jaiswal, A., and Rani, V. (2013). miRNA-transcription factor interactions: a combinatorial regulation of gene expression. *Mol. Genet. Genomics* 288, 77–87. doi: 10.1007/s00438-013-0734-z

Awan, H. M., Shah, A., Rashid, F., and Shan, G. (2017). Primate-specific long non-coding RNAs and microRNAs. *Genom. Proteom. Bioinform.* 15, 187–195. doi: 10.1016/j.gpb.2017.04.002

Baek, D., Villén, J., Shin, C., Camargo, F. D., Gygi, S. P., and Bartel, D. P. (2008). The impact of microRNAs on protein output. *Nature* 455, 64–71. doi: 10.1038/nature07242

Bak, M., Silahtaroglu, A., Møller, M., Christensen, M., Rath, M. F., Skryabin, B., et al. (2008). MicroRNA expression in the adult mouse central nervous system. *RNA* 14, 432–444. doi: 10.1261/rna.783108

Barak, B., Shvarts-Serebro, I., Modai, S., Gilam, A., Okun, E., Michaelson, D. M., et al. (2013). Opposing actions of environmental enrichment and Alzheimer's disease on the expression of hippocampal microRNAs in mouse models. *Transl. Psychiatry* 3:e304. doi: 10.1038/tp.2013.77

Barca-Mayo, O., and De Pietri Tonelli, D. (2014). Convergent microRNA actions coordinate neocortical development. *Cell. Mol. Life Sci.* 71, 2975–2995. doi: 10.1007/s00018-014-1576-5

Bartel, D. P. (2009). MicroRNAs: target recognition and regulatory functions. *Cell* 136, 215–233. doi: 10.1016/j.cell.2009.01.002

Beckervordersandforth, R., Deshpande, A., Schäffner, I., Huttner, H. B., Lepier, A., Lie, D. C., et al. (2014). In vivo targeting of adult neural stem cells in the dentate gyrus by a split-cre approach. *Stem Cell Rep.* 2, 153–162. doi: 10.1016/j.stemcr.2014.01.004

Beckervordersandforth, R., Zhang, C.-L., and Lie, D. C. (2015). Transcription-factor-dependent control of adult hippocampal neurogenesis. *Cold Spring Harb. Perspect. Biol.* 7:a018879. doi: 10.1101/cshperspect.a018879

Bian, S., Xu, T.-L., and Sun, T. (2013). Tuning the cell fate of neurons and glia by microRNAs. *Curr. Opin. Neurobiol.* 23, 928–934. doi: 10.1016/j.conb.2013.08.002

Bicker, S., Lackinger, M., Weiß, K., and Schratt, G. (2014). MicroRNA-132, -134, and -138: a microRNA troika rules in neuronal dendrites. *Cell. Mol. Life Sci.* 71, 3987–4005. doi: 10.1007/s00018-014-1671-7

Bielefeld, P., Mooney, C., Henshall, D. C., and Fitzsimons, C. P. (2017). miRNA-mediated regulation of adult hippocampal neurogenesis; implications for epilepsy. *BPL* 3, 43–59. doi: 10.3233/BPL-160036

Boldrini, M., Fulmore, C. A., Tartt, A. N., Simeon, L. R., Pavlova, I., Poposka, V., et al. (2018). Human hippocampal neurogenesis persists throughout aging. *Stem Cell* 22, 589.e5–599.e5. doi: 10.1016/j.stem.2018.03.015

Bonaguidi, M. A., Stadel, R. P., Berg, D. A., Sun, J., Ming, G.-L., and Song, H. (2016). Diversity of neural precursors in the adult mammalian brain. *Cold Spring Harb. Perspect. Biol.* 8:a18838-20. doi: 10.1101/cshperspect.a018838

Brett, J. O., Renault, V. M., Rafalski, V. A., Webb, A. E., and Brunet, A. (2011). The microRNA cluster miR-106b∼25 regulates adult neural stem/progenitor cell proliferation and neuronal differentiation. *Aging* 3, 108–124. doi: 10.18632/aging.100285

Cernilogar, F. M., Di Giaimo, R., Rehfeld, F., Cappello, S., and Lie, D. C. (2015). RNA interference machinery-mediated gene regulation in mouse adult neural stem cells. *BMC Neurosci.* 16:60. doi: 10.1186/s12868-015-0198-7

Chapouton, P., Skupien, P., Hesl, B., Coolen, M., Moore, J. C., Madelaine, R., et al. (2010). Notch activity levels control the balance between quiescence and recruitment of adult neural stem cells. *J. Neurosci.* 30, 7961–7974. doi: 10.1523/JNEUROSCI.6170-09.2010

Cheng, L.-C., Pastrana, E., Tavazoie, M., and Doetsch, F. (2009). miR-124 regulates adult neurogenesis in the subventricular zone stem cell niche. *Nat. Neurosci.* 12, 399–408. doi: 10.1038/nn.2294

Cheng, S., Zhang, C., Xu, C., Wang, L., Zou, X., and Chen, G. (2014). Age-dependent neuron loss is associated with impaired adult neurogenesis in forebrain neuron-specific Dicer conditional knockout mice. *Int. J. Biochem. Cell Biol.* 57, 186–196. doi: 10.1016/j.biocel.2014.10.029

Cheng, T.-L., Wang, Z., Liao, Q., Zhu, Y., Zhou, W.-H., Xu, W., et al. (2014). MeCP2 suppresses nuclear microRNA processing and dendritic growth by regulating the DGCR8/Drosha complex. *Dev. Cell* 28, 547–560. doi: 10.1016/j.devcel.2014.01.032

Conaco, C., Otto, S., Han, J.-J., and Mandel, G. (2006). Reciprocal actions of REST and a microRNA promote neuronal identity. *Proc. Natl. Acad. Sci. U.S.A.* 103, 2422–2427. doi: 10.2307/30048143

Davis, T. H., Cuellar, T. L., Koch, S. M., Barker, A. J., Harfe, B. D., McManus, M. T., et al. (2008). Conditional loss of dicer disrupts cellular and tissue morphogenesis in the cortex and hippocampus. *J. Neurosci.* 28, 4322–4330. doi: 10.1523/JNEUROSCI.4815-07.2008

De Pietri Tonelli, D., Pulvers, J. N., Haffner, C., Murchison, E. P., Hannon, G. J., and Huttner, W. B. (2008). miRNAs are essential for survival and differentiation of newborn neurons but not for expansion of neural progenitors during early neurogenesis in the mouse embryonic neocortex. *Development* 135, 3911–3921. doi: 10.1242/dev.025080

Deng, W., Aimone, J. B., and Gage, F. H. (2010). New neurons and new memories: how does adult hippocampal neurogenesis affect learning and memory? *Nat. Rev. Neurosci.* 11, 339–350. doi: 10.1038/nrn2822

Doetsch, F., García-Verdugo, J. M., and Alvarez-Buylla, A. (1997). Cellular composition and three-dimensional organization of the subventricular germinal zone in the adult mammalian brain. *J. Neurosci.* 17, 5046–5061. doi: 10.1523/JNEUROSCI.17-13-05046.1997

Duan, X., Chang, J. H., Ge, S., Faulkner, R. L., Kim, J. Y., Kitabatake, Y., et al. (2007). Disrupted-in-schizophrenia 1 regulates integration of newly generated neurons in the adult brain. *Cell* 130, 1146–1158. doi: 10.1016/j.cell.2007.07.010

Dulken, B. W., Leeman, D. S., Boutet, S. C., Hebestreit, K., and Brunet, A. (2017). Single-cell transcriptomic analysis defines heterogeneity and transcriptional dynamics in the adult neural stem cell lineage. *Cell Rep.* 18, 777–790. doi: 10.1016/j.celrep.2016.12.060

Encinas, J. M., and Fitzsimons, C. P. (2017). Gene regulation in adult neural stem cells, current challenges and possible applications. *Adv. Drug Deliv. Rev.* 120, 118–132. doi: 10.1016/j.addr.2017.07.016

Encinas, J. M., Michurina, T. V., Peunova, N., Park, J.-H., Tordo, J., Peterson, D. A., et al. (2011). Division-coupled astrocytic differentiation and age-related depletion of neural stem cells in the adult hippocampus. *Cell Stem Cell* 8, 566–579. doi: 10.1016/j.stem.2011.03.010

Eriksson, P. S., Perfilieva, E., Björk-Eriksson, T., Alborn, A. M., Nordborg, C., Peterson, D. A., et al. (1998). Neurogenesis in the adult human hippocampus. *Nat. Med.* 4, 1313–1317. doi: 10.1038/3305

Fiore, R., Khudayberdiev, S., Christensen, M., Siegel, G., Flavell, S. W., Kim, T.-K., et al. (2009). Mef2-mediated transcription of the miR379–410 cluster regulates activity-dependent dendritogenesis by fine-tuning Pumilio2 protein levels. *EMBO J.* 28, 697–710. doi: 10.1038/emboj.2009.10

Fischer, S., Handrick, R., Aschrafi, A., and Otte, K. (2015). Unveiling the principle of microRNA-mediated redundancy in cellular pathway regulation. *RNA Biol.* 12, 238–247. doi: 10.1080/15476286.2015.1017238

Franke, K., Otto, W., Johannes, S., Baumgart, J., Nitsch, R., and Schumacher, S. (2012). miR-124-regulated RhoG reduces neuronal process complexity via ELMO/Dock180/Rac1 and Cdc42 signalling. *EMBO J.* 31, 2908–2921. doi: 10.1038/emboj.2012.130

Furutachi, S., Matsumoto, A., Nakayama, K. I., and Gotoh, Y. (2013). p57 controls adult neural stem cell quiescence and modulates the pace of lifelong neurogenesis. *EMBO J.* 32, 970–981. doi: 10.1038/emboj.2013.50

Gao, J., Wang, W.-Y., Mao, Y.-W., Gräff, J., Guan, J.-S., Pan, L., et al. (2010). A novel pathway regulates memory and plasticity via SIRT1 and miR-134. *Nature* 466, 1105–1109. doi: 10.1038/nature09271

Gao, Y., Su, J., Guo, W., Polich, E. D., Magyar, D. P., Xing, Y., et al. (2015). Inhibition of miR-15a promotes BDNF expression and rescues dendritic maturation deficits in MeCP2-deficient neurons. *Stem Cells* 33, 1618–1629. doi: 10.1002/stem.1950

Gao, Z., Ding, P., and Hsieh, J. (2012). Profiling of REST-dependent microRNAs reveals dynamic modes of expression. *Front. Neurosci.* 6:67. doi: 10.3389/fnins.2012.00067

Gao, Z., Ure, K., Ding, P., Nashaat, M., Yuan, L., Ma, J., et al. (2011). The master negative regulator REST/NRSF controls adult neurogenesis by restraining the neurogenic program in quiescent stem cells. *J. Neurosci.* 31, 9772–9786. doi: 10.1523/JNEUROSCI.1604-11.2011

Gardner, P. P., and Vinther, J. (2008). Mutation of miRNA target sequences during human evolution. *Trends Genet.* 24, 262–265. doi: 10.1016/j.tig.2008.03.009

Giachino, C., and Taylor, V. (2015). Notching up neural stem cell homogeneity in homeostasis and disease. *Front. Neurosci.* 8:32. doi: 10.3389/fnins.2014.00032

Gonçalves, J. T., Schafer, S. T., and Gage, F. H. (2016). Adult neurogenesis in the hippocampus: from stem cells to behavior. *Cell* 167, 897–914. doi: 10.1016/j.cell.2016.10.021

Ha, M., and Kim, V. N. (2014). Regulation of microRNA biogenesis. *Nat. Rev. Mol. Cell Biol.* 15, 509–524. doi: 10.1038/nrm3838

Han, J., Kim, H. J., Schafer, S. T., Paquola, A., Clemenson, G. D., Toda, T., et al. (2016). Functional implications of miR-19 in the migration of newborn neurons in the adult brain. *Neuron* 91, 79–89. doi: 10.1016/j.neuron.2016.05.034

Harraz, M. M., Xu, J.-C., Guiberson, N., Dawson, T. M., and Dawson, V. L. (2014). MiR-223 regulates the differentiation of immature neurons. *Mol. Cell Ther.* 2, 18–19. doi: 10.1186/2052-8426-2-18

Hébert, S. S., Papadopoulou, A. S., Smith, P., Galas, M.-C., Planel, E., Silahtaroglu, A. N., et al. (2010). Genetic ablation of Dicer in adult forebrain neurons results in abnormal tau hyperphosphorylation and neurodegeneration. *Hum. Mol. Genet.* 19, 3959–3969. doi: 10.1093/hmg/ddq311

Herranz, H., and Cohen, S. M. (2010). MicroRNAs and gene regulatory networks: managing the impact of noise in biological systems. *Genes Dev.* 24, 1339–1344. doi: 10.1101/gad.1937010

Hu, Z., and Li, Z. (2017). miRNAs in synapse development and synaptic plasticity. *Curr. Opin. Neurobiol.* 45, 24–31. doi: 10.1016/j.conb.2017.02.014

Islam, M. M., and Zhang, C.-L. (2015). TLX: a master regulator for neural stem cell maintenance and neurogenesis. *Biochim. Biophys. Acta* 1849, 210–216. doi: 10.1016/j.bbagrm.2014.06.001

Jin, J., Kim, S.-N., Liu, X., Zhang, H., Zhang, C., Seo, J.-S., et al. (2016). miR-17-92 cluster regulates adult hippocampal neurogenesis, anxiety, and depression. *Cell Rep.* 16, 1653–1663. doi: 10.1016/j.celrep.2016.06.101

Jobe, E. M., Gao, Y., Eisinger, B. E., Mladucky, J. K., Giuliani, C. C., Kelnhofer, L. E., et al. (2017). Methyl-CpG-binding protein MBD1 regulates neuronal lineage commitment through maintaining adult neural stem cell identity. *J. Neurosci.* 37, 523–536. doi: 10.1523/JNEUROSCI.1075-16.2016

Jobe, E. M., McQuate, A. L., and Zhao, X. (2012). Crosstalk among epigenetic pathways regulates neurogenesis. *Front. Neurosci.* 6:59. doi: 10.3389/fnins.2012.00059

Kasuga, H., Fukuyama, M., Kitazawa, A., Kontani, K., and Katada, T. (2013). The microRNA miR-235 couples blast-cell quiescence to the nutritional state. *Nature* 497, 503–506. doi: 10.1038/nature12117

Katz, S., Cussigh, D., Urbán, N., Blomfield, I., Guillemot, F., Bally-Cuif, L., et al. (2016). A nuclear role for miR-9 and argonaute proteins in balancing quiescent and activated neural stem cell states. *Cell Rep.* 17, 1383–1398. doi: 10.1016/j.celrep.2016.09.088

Kawaguchi, D., Furutachi, S., Kawai, H., Hozumi, K., and Gotoh, Y. (2013). Dll1 maintains quiescence of adult neural stem cells and segregates asymmetrically during mitosis. *Nat. Commun.* 4:1880. doi: 10.1038/ncomms2895

Kempermann, G., Gage, F. H., Aigner, L., Song, H., Curtis, M. A., Thuret, S., et al. (2018). Human adult neurogenesis: evidence and remaining questions. *Cell Stem Cell* 23, 25–30. doi: 10.1016/j.stem.2018.04.004

Kempermann, G., Song, H., and Gage, F. H. (2015). Neurogenesis in the adult hippocampus. *Cold Spring Harb. Perspect. Biol.* 7:a18812-14. doi: 10.1101/cshperspect.a018812

Khoshnam, S. E., Winlow, W., Farbood, Y., Moghaddam, H. F., and Farzaneh, M. (2017). Emerging roles of microRNAs in ischemic stroke: as possible therapeutic agents. *J. Stroke* 19, 166–187. doi: 10.5853/jos.2016.01368

Kim, D.-Y., Hwang, I., Muller, F. L., and Paik, J.-H. (2015). Functional regulation of FoxO1 in neural stem cell differentiation. *Cell Death. Differ.* 22, 2034–2045. doi: 10.1038/cdd.2015.123

Kim, J. Y., Duan, X., Liu, C. Y., Jang, M.-H., Guo, J. U., Pow-anpongkul, N., et al. (2009). DISC1 regulates new neuron development in the adult brain via modulation of AKT-mTOR signaling through KIAA1212. *Neuron* 63, 761–773. doi: 10.1016/j.neuron.2009.08.008

Kim, W. R., and Sun, W. (2011). Programmed cell death during postnatal development of the rodent nervous system. *Dev. Growth Differ.* 53, 225–235. doi: 10.1111/j.1440-169X.2010.01226.x

Klein, M. E., Lioy, D. T., Ma, L., Impey, S., Mandel, G., and Goodman, R. H. (2007). Homeostatic regulation of MeCP2 expression by a CREB-induced microRNA. *Nat. Neurosci.* 10, 1513–1514. doi: 10.1038/nn2010

Konopka, W., Kiryk, A., Novak, M., Herwerth, M., Parkitna, J. R., Wawrzyniak, M., et al. (2010). MicroRNA loss enhances learning and memory in mice. *J. Neurosci.* 30, 14835–14842. doi: 10.1523/JNEUROSCI.3030-10.2010

Laneve, P., Gioia, U., Andriotto, A., Moretti, F., Bozzoni, I., and Caffarelli, E. (2010). A minicircuitry involving REST and CREB controls miR-9-2 expression during human neuronal differentiation. *Nucleic Acids Res.* 38, 6895–6905. doi: 10.1093/nar/gkq604

Laplagne, D. A., Espósito, M. S., Piatti, V. C., Morgenstern, N. A., Zhao, C., van Praag, H., et al. (2006). Functional convergence of neurons generated in the developing and adult hippocampus. *PLoS Biol.* 4:e409. doi: 10.1371/journal.pbio.0040409

Lewis, B. P., Burge, C. B., and Bartel, D. P. (2005). Conserved seed pairing, often flanked by adenosines, indicates that thousands of human genes are microRNA targets. *Cell* 120, 15–20. doi: 10.1016/j.cell.2004.12.035

Li, Q., Bian, S., Hong, J., Kawase-Koga, Y., Zhu, E., Zheng, Y., et al. (2011). Timing specific requirement of microRNA function is essential for embryonic and postnatal hippocampal development. *PLoS One* 6:e26000. doi: 10.1371/journal.pone.0026000.g009

Lim, L. P., Lau, N. C., Garrett-Engele, P., Grimson, A., Schelter, J. M., Castle, J., et al. (2005). Microarray analysis shows that some microRNAs downregulate large numbers of target mRNAs. *Nature* 433, 769–773. doi: 10.1038/nature03315

Lindvall, O., and Kokaia, Z. (2010). Stem cells in human neurodegenerative disorders — Time for clinical translation? *J. Clin. Invest.* 120, 29–40. doi: 10.1172/JCI40543

Liu, C., Teng, Z.-Q., McQuate, A. L., Jobe, E. M., Christ, C. C., von Hoyningen-Huene, S. J., et al. (2013). An epigenetic feedback regulatory loop involving microRNA-195 and MBD1 governs neural stem cell differentiation. *PLoS One* 8:e51436. doi: 10.1371/journal.pone.0051436

Liu, C., Teng, Z.-Q., Santistevan, N. J., Szulwach, K. E., Guo, W., Jin, P., et al. (2010). Epigenetic regulation of miR-184 by MBD1 governs neural stem cell proliferation and differentiation. *Cell Stem Cell* 6, 433–444. doi: 10.1016/j.stem.2010.02.017

Llorens-Bobadilla, E., and Martin-Villalba, A. (2017). Adult NSC diversity and plasticity: the role of the niche. *Curr. Opin. Neurobiol.* 42, 68–74. doi: 10.1016/j.conb.2016.11.008

Llorens-Bobadilla, E., Zhao, S., Baser, A., Saiz-Castro, G., Zwadlo, K., and Martin-Villalba, A. (2015). Single-cell transcriptomics reveals a population of dormant neural stem cells that become activated upon brain injury. *Stem Cell* 17, 329–340. doi: 10.1016/j.stem.2015.07.002

Lopez-Ramirez, M. A., and Nicoli, S. (2014). Role of miRNAs and epigenetics in neural stem cell fate determination. *Epigenetics* 9, 90–100. doi: 10.4161/epi.27536

Lugert, S., Basak, O., Knuckles, P., Haussler, U., Fabel, K., Götz, M., et al. (2010). Quiescent and active hippocampal neural stem cells with distinct morphologies respond selectively to physiological and pathological stimuli and aging. *Cell Stem Cell* 6, 445–456. doi: 10.1016/j.stem.2010.03.017

Magill, S. T., Cambronne, X. A., Luikart, B. W., Lioy, D. T., Leighton, B. H., Westbrook, G. L., et al. (2010). microRNA-132 regulates dendritic growth and arborization of newborn neurons in the adult hippocampus. *Proc. Natl. Acad. Sci. U.S.A.* 107, 20382–20387. doi: 10.1073/pnas.1015691107

Mahar, I., Bambico, F. R., Mechawar, N., and Nobrega, J. N. (2014). Stress, serotonin, and hippocampal neurogenesis in relation to depression and antidepressant effects. *Neurosci. Biobehav. Rev.* 38, 173–192. doi: 10.1016/j.neubiorev.2013.11.009

Martins, R., Lithgow, G. J., and Link, W. (2015). Long live FOXO: unraveling the role of FOXO proteins in aging and longevity. *Aging Cell* 15, 196–207. doi: 10.1111/acel.12427

Murao, N., Noguchi, H., and Nakashima, K. (2016). Epigenetic regulation of neural stem cell property from embryo to adult. *NEPIG* 5, 1–10. doi: 10.1016/j.nepig.2016.01.001

Nishino, J., Kim, I., Chada, K., and Morrison, S. J. (2008). Hmga2 promotes neural stem cell self-renewal in young but not old mice by reducing p16Ink4a and p19Arf expression. *Cell* 135, 227–239. doi: 10.1016/j.cell.2008.09.017

Niu, W., Zou, Y., Shen, C., and Zhang, C. L. (2011). Activation of postnatal neural stem cells requires nuclear receptor TLX. *J. Neurosci.* 31, 13816–13828. doi: 10.1523/JNEUROSCI.1038-11.2011

Nunes, M. C., Roy, N. S., Keyoung, H. M., Goodman, R. R., McKhann, G., Jiang, L., et al. (2003). Identification and isolation of multipotential neural progenitor cells from the subcortical white matter of the adult human brain. *Nat. Med.* 9, 439–447. doi: 10.1038/nm837

Olive, V., Minella, A. C., and He, L. (2015). Outside the coding genome, mammalian microRNAs confer structural and functional complexity. *Sci. Signal.* 8:re2. doi: 10.1126/scisignal.2005813

Osella, M., Riba, A., Testori, A., Corà, D., and Caselle, M. (2014). Interplay of microRNA and epigenetic regulation in the human regulatory network. *Front. Genet.* 5:345. doi: 10.3389/fgene.2014.00345

Packer, A. N., Xing, Y., Harper, S. Q., Jones, L., and Davidson, B. L. (2008). The bifunctional microRNA miR-9/miR-9* regulates REST and CoREST and is downregulated in Huntington's disease. *J. Neurosci.* 28, 14341–14346. doi: 10.1523/JNEUROSCI.2390-08.2008

Paik, J.-H., Ding, Z., Narurkar, R., Ramkissoon, S., Muller, F., Kamoun, W. S., et al. (2009). FoxOs cooperatively regulate diverse pathways governing neural stem cell homeostasis. *Cell Stem Cell* 5, 540–553. doi: 10.1016/j.stem.2009.09.013

Peláez, N., and Carthew, R. W. (2012). Biological robustness and the role of microRNAs: a network perspective. *Curr. Top. Dev. Biol.* 99, 237–255. doi: 10.1016/B978-0-12-387038-4.00009-4

Peng, L., and Bonaguidi, M. A. (2018). Function and dysfunction of adult hippocampal neurogenesis in regeneration and disease. *Am. J. Pathol.* 188, 23–28. doi: 10.1016/j.ajpath.2017.09.004

Pfannkuche, K., Summer, H., Li, O., Hescheler, J., and Dröge, P. (2009). The high mobility group protein HMGA2: a co-regulator of chromatin structure and pluripotency in stem cells? *Stem Cell Rev. Rep.* 5, 224–230. doi: 10.1007/s12015-009-9078-9

Pino, A., Fumagalli, G., Bifari, F., and Decimo, I. (2017). New neurons in adult brain: distribution, molecular mechanisms and therapies. *Biochem. Pharmacol.* 141, 4–22. doi: 10.1016/j.bcp.2017.07.003

Pons-Espinal, M., de Luca, E., Marzi, M. J., Beckervordersandforth, R., Armirotti, A., Nicassio, F., et al. (2017). Synergic functions of miRNAs determine neuronal fate of adult neural stem cells. *Stem Cell Rep.* 8, 1046–1061. doi: 10.1016/j.stemcr.2017.02.012

Pratt, T., and Price, D. J. (2016). Junk DNA used in cerebral cortical evolution. *Neuron* 90, 1141–1143. doi: 10.1016/j.neuron.2016.06.007

Qiu, L., Zhang, W., Tan, E.-K., and Zeng, L. (2014). Deciphering the function and regulation of microRNAs in Alzheimer's disease and Parkinson's disease. *ACS Chem. Neurosci.* 5, 884–894. doi: 10.1021/cn500149w

Rajman, M., and Schratt, G. (2017). MicroRNAs in neural development: from master regulators to fine-tuners. *Development* 144, 2310–2322. doi: 10.1242/dev.144337

Renault, V. M., Rafalski, V. A., Morgan, A. A., Salih, D. A. M., Brett, J. O., Webb, A. E., et al. (2009). FoxO3 regulates neural stem cell homeostasis. *Cell Stem Cell* 5, 527–539. doi: 10.1016/j.stem.2009.09.014

Rodriguez-Aznar, E., Barrallo-Gimeno, A., and Nieto, M. A. (2013). Scratch2 prevents cell cycle re-entry by repressing miR-25 in postmitotic primary neurons. *J. Neurosci.* 33, 5095–5105. doi: 10.1523/JNEUROSCI.4459-12.2013

Roese-Koerner, B., Stappert, L., and Brüstle, O. (2017). Notch/Hes signaling and miR-9 engage in complex feedback interactions controlling neural progenitor cell proliferation and differentiation. *Neurogenesis* 4:e1313647. doi: 10.1080/23262133.2017.1313647

Roese-Koerner, B., Stappert, L., Koch, P., Brüstle, O., and Borghese, L. (2013). Pluripotent stem cell-derived somatic stem cells as tool to study the role of microRNAs in early human neural development. *Curr. Mol. Med.* 13, 707–722. doi: 10.2174/1566524011313050003

Roy, N. S., Wang, S., Jiang, L., Kang, J., Benraiss, A., Harrison-Restelli, C., et al. (2000). In vitro neurogenesis by progenitor cells isolated from the adult human hippocampus. *Nat. Med.* 6, 271–277. doi: 10.1038/73119

Sanai, N., Nguyen, T., Ihrie, R. A., Mirzadeh, Z., Tsai, H.-H., Wong, M., et al. (2011). Corridors of migrating neurons in the human brain and their decline during infancy. *Nature* 478, 382–386. doi: 10.1038/nature10487

Schmitz, U., Lai, X., Winter, F., Wolkenhauer, O., Vera, J., and Gupta, S. K. (2014). Cooperative gene regulation by microRNA pairs and their identification using a computational workflow. *Nucleic Acids Res.* 42, 7539–7552. doi: 10.1093/nar/gku465

Schouten, M., Fratantoni, S. A., Hubens, C. J., Piersma, S. R., Pham, T. V., Bielefeld, P., et al. (2015). MicroRNA-124 and -137 cooperativity controls caspase-3 activity through BCL2L13 in hippocampal neural stem cells. *Sci. Rep.* 5:12448. doi: 10.1038/srep12448

Schratt, G. M., Tuebing, F., Nigh, E. A., Kane, C. G., Sabatini, M. E., Kiebler, M., et al. (2006). A brain-specific microRNA regulates dendritic spine development. *Nature* 439, 283–289. doi: 10.1038/nature04367

Selbach, M., Schwanhäusser, B., Thierfelder, N., Fang, Z., Khanin, R., and Rajewsky, N. (2008). Widespread changes in protein synthesis induced by microRNAs. *Nature* 455, 58–63. doi: 10.1038/nature07228

Semerci, F., Choi, W. T., Bajic, A., Thakkar, A., Encinas, J. M., Depreux, F., et al. (2017). Lunatic fringe-mediated Notch signaling regulates adult hippocampal neural stem cell maintenance. *eLife* 6:e1002466. doi: 10.7554/eLife.24660

Seri, B., Garcia-Verdugo, J. M., Collado-Morente, L., McEwen, B. S., and Alvarez-Buylla, A. (2004). Cell types, lineage, and architecture of the germinal zone in the adult dentate gyrus. *J. Comp. Neurol.* 478, 359–378. doi: 10.1002/cne.20288

Shi, Y., Chichung Lie, D., Taupin, P., Nakashima, K., Ray, J., Yu, R. T., et al. (2004). Expression and function of orphan nuclear receptor TLX in adult neural stem cells. *Nature* 427, 78–83. doi: 10.1038/nature02211

Shimazaki, T., and Okano, H. (2018). Heterochronic microRNAs in temporal specification of neural stem cells: application toward rejuvenation. *NPJ Aging Mech Dis.* 2:15014. doi: 10.1038/npjamd.2015.14

Shin, J., Berg, D. A., Zhu, Y., Shin, J. Y., Song, J., Bonaguidi, M. A., et al. (2015). Single-cell RNA-seq with waterfall reveals molecular cascades underlying adult neurogenesis. *Stem Cell* 17, 360–372. doi: 10.1016/j.stem.2015.07.013

Siegel, G., Obernosterer, G., Fiore, R., Oehmen, M., Bicker, S., Christensen, M., et al. (2009). A functional screen implicates microRNA-138-dependent regulation of the depalmitoylation enzyme APT1 in dendritic spine morphogenesis. *Nat. Cell Biol.* 11, 705–716. doi: 10.1038/ncb1876

Sierra, A., Encinas, J. M., Deudero, J. J. P., Chancey, J. H., Enikolopov, G., Overstreet-Wadiche, L. S., et al. (2010). Microglia shape adult hippocampal neurogenesis through apoptosis-coupled phagocytosis. *Cell Stem Cell* 7, 483–495. doi: 10.1016/j.stem.2010.08.014

Smrt, R. D., Szulwach, K. E., Pfeiffer, R. L., Li, X., Guo, W., Pathania, M., et al. (2010). MicroRNA miR-137 regulates neuronal maturation by targeting ubiquitin ligase mind bomb-1. *Stem Cells* 28, 1060–1070. doi: 10.1002/stem.431

Sorrells, S. F., Paredes, M. F., Cebrian-Silla, A., Sandoval, K., Qi, D., Kelley, K. W., et al. (2018). Human hippocampal neurogenesis drops sharply in children to undetectable levels in adults. *Nature* 555, 377–381. doi: 10.1038/nature25975

Spalding, K. L., Bergmann, O., Alkass, K., Bernard, S., Salehpour, M., Huttner, H. B., et al. (2013). Dynamics of hippocampal neurogenesis in adult humans. *Cell* 153, 1219–1227. doi: 10.1016/j.cell.2013.05.002

Stankiewicz, T. R., and Linseman, D. A. (2014). Rho family GTPases: key players in neuronal development, neuronal survival, and neurodegeneration. *Front. Cell Neurosci.* 8:314. doi: 10.3389/fncel.2014.00314

Stappert, L., Roese-Koerner, B., and Brüstle, O. (2014). The role of microRNAs in human neural stem cells, neuronal differentiation and subtype specification. *Cell Tissue Res.* 359, 47–64. doi: 10.1007/s00441-014-1981-y

Sun, G., Alzayady, K., Stewart, R., Ye, P., Yang, S., Li, W., et al. (2010). Histone demethylase LSD1 regulates neural stem cell proliferation. *Mol. Cell. Biol.* 30, 1997–2005. doi: 10.1128/MCB.01116-09

Sun, G., Ye, P., Murai, K., Lang, M.-F., Li, S., Zhang, H., et al. (2011). miR-137 forms a regulatory loop with nuclear receptor TLX and LSD1 in neural stem cells. *Nat. Commun.* 2:529. doi: 10.1038/ncomms1532

Sun, G. J., Zhou, Y., Stadel, R. P., Moss, J., Yong, J. H. A., Ito, S., et al. (2015). Tangential migration of neuronal precursors of glutamatergic neurons in the adult mammalian brain. *Proc. Natl. Acad. Sci. U.S.A.* 112, 9484–9489. doi: 10.1073/pnas.1508545112

Sun, L., Zhao, M., Wang, Y., Liu, A., Lv, M., Li, Y., et al. (2017). Neuroprotective effects of miR-27a against traumatic brain injury via suppressing FoxO3a-mediated neuronal autophagy. *Biochem. Biophys. Res. Commun.* 482, 1141–1147. doi: 10.1016/j.bbrc.2016.12.001

Szulwach, K. E., Li, X., Smrt, R. D., Li, Y., Luo, Y., Lin, L., et al. (2010). Cross talk between microRNA and epigenetic regulation in adult neurogenesis. *J. Cell Biol.* 189, 127–141. doi: 10.1083/jcb.200908151

Tashiro, A., Sandler, V. M., Toni, N., Zhao, C., and Gage, F. H. (2006). NMDA-receptor-mediated, cell-specific integration of new neurons in adult dentate gyrus. *Nature* 442, 929–933. doi: 10.1038/nature05028

Terzibasi Tozzini, E., Savino, A., Ripa, R., Battistoni, G., Baumgart, M., and Cellerino, A. (2014). Regulation of microRNA expression in the neuronal stem

cell niches during aging of the short-lived annual fish *Nothobranchius furzeri*. *Front. Cell Neurosci.* 8:51. doi: 10.3389/fncel.2014.00051

Toda, T., and Gage, F. H. (2018). Review: adult neurogenesis contributes to hippocampal plasticity. *Cell Tissue Res.* 373, 693–709. doi: 10.1007/s00441-017-2735-4

Vadodaria, K. C., Brakebusch, C., Suter, U., and Jessberger, S. (2013). Stage-specific functions of the small Rho GTPases Cdc42 and Rac1 for adult hippocampal neurogenesis. *J. Neurosci.* 33, 1179–1189. doi: 10.1523/JNEUROSCI.2103-12.2013

van Praag, H., Kempermann, G., and Gage, F. H. (1999). Running increases cell proliferation and neurogenesis in the adult mouse dentate gyrus. *Nat. Neurosci.* 2, 266–270. doi: 10.1038/6368

Visvanathan, J., Lee, S., Lee, B., Lee, J. W., and Lee, S. K. (2007). The microRNA miR-124 antagonizes the anti-neural REST/SCP1 pathway during embryonic CNS development. *Genes Dev.* 21, 744–749. doi: 10.1101/gad.1519107

Vo, N., Klein, M. E., Varlamova, O., Keller, D. M., Yamamoto, T., Goodman, R. H., et al. (2005). A cAMP-response element binding protein-induced microRNA regulates neuronal morphogenesis. *Proc. Natl. Acad. Sci. U.S.A.* 102, 16426–16431. doi: 10.1073/pnas.0508448102

Wayman, G. A., Davare, M., Ando, H., Fortin, D., Varlamova, O., Cheng, H. Y., et al. (2008). An activity-regulated microRNA controls dendritic plasticity by down-regulating p250GAP. *Proc. Natl. Acad. Sci. U.S.A.* 105, 9093–9098. doi: 10.1073/pnas.0803072105

Xu, B., Woodroffe, A., Rodriguez-Murillo, L., Roos, J. L., van Rensburg, E. J., Abecasis, G. R., et al. (2009). Elucidating the genetic architecture of familial schizophrenia using rare copy number variant and linkage scans. *Proc. Natl. Acad. Sci. U.S.A.* 106, 16746–16751. doi: 10.1073/pnas.0908584106

Yoo, A. S., Sun, A. X., Li, L., Shcheglovitov, A., Portmann, T., Li, Y., et al. (2011). MicroRNA-mediated conversion of human fibroblasts to neurons. *Nature* 476, 228–231. doi: 10.1038/nature10323

Yuan, J., Huang, H., Zhou, X., Liu, X., Ou, S., Xu, T., et al. (2016). MicroRNA-132 interact with p250GAP/Cdc42 Pathway in the hippocampal neuronal culture model of acquired epilepsy and associated with epileptogenesis process. *Neural Plast.* 2016:5108489. doi: 10.1155/2016/5108489

Zhang, C.-L., Zou, Y., He, W., Gage, F. H., and Evans, R. M. (2008). A role for adult TLX-positive neural stem cells in learning and behaviour. *Nature* 451, 1004–1007. doi: 10.1038/nature06562

Zhang, Y., Liu, C., Wang, J., Li, Q., Ping, H., Gao, S., et al. (2018). MiR-299-5p regulates apoptosis through autophagy in neurons and ameliorates cognitive capacity in APPswe/PS1dE9 mice. *Sci. Rep.* 6:24566. doi: 10.1038/srep24566

Zhao, C., Sun, G., Li, S., Lang, M.-F., Yang, S., Li, W., et al. (2010). MicroRNA let-7b regulates neural stem cell proliferation and differentiation by targeting nuclear receptor TLX signaling. *Proc. Natl. Acad. Sci. U.S.A.* 107, 1876–1881. doi: 10.1073/pnas.0908750107

Zhao, C., Sun, G., Li, S., and Shi, Y. (2009). A feedback regulatory loop involving microRNA-9 and nuclear receptor TLX in neural stem cell fate determination. *Nat. Struct. Mol. Biol.* 16, 365–371. doi: 10.1038/nsmb.1576

Zhao, C., Sun, G., Ye, P., Li, S., and Shi, Y. (2013). MicroRNA let-7d regulates the TLX/microRNA-9 cascade to control neural cell fate and neurogenesis. *Sci. Rep.* 3:1329. doi: 10.1038/srep01329

Zhao, C., Teng, E. M., Summers, R. G., Ming, G.-L., and Gage, F. H. (2006). Distinct morphological stages of dentate granule neuron maturation in the adult mouse hippocampus. *J. Neurosci.* 26, 3–11. doi: 10.1523/JNEUROSCI.3648-05.2006

Zhao, X., Ueba, T., Christie, B. R., Barkho, B., McConnell, M. J., Nakashima, K., et al. (2003). Mice lacking methyl-CpG binding protein 1 have deficits in adult neurogenesis and hippocampal function. *Proc. Natl. Acad. Sci. U.S.A.* 100, 6777–6782. doi: 10.1073/pnas.1131928100

Ziebell, F., Dehler, S., Martin-Villalba, A., and Marciniak-Czochra, A. (2018). Revealing age-related changes of adult hippocampal neurogenesis using mathematical models. *Development* 145:dev153544. doi: 10.1242/dev.153544

Conflict of Interest Statement: OB is a co-founder of and has stock in Life & Brain GmbH.

The remaining authors declare that the research was conducted in the absence of any commercial or financial relationships that could be construed as a potential conflict of interest.

frontiers in Molecular Neuroscience

ORIGINAL RESEARCH
published: 15 November 2018
doi: 10.3389/fnmol.2018.00415

Long-Term Labeling of Hippocampal Neural Stem Cells by a Lentiviral Vector

Hoonkyo Suh[1], Qi-Gang Zhou[1†], Irene Fernandez-Carasa[2,3], Gregory Dane Clemenson Jr.[4], Meritxell Pons-Espinal[2,3], Eun Jeoung Ro[1], Mercè Marti[5,6], Angel Raya[5,6,7], Fred H. Gage[4] and Antonella Consiglio[2,3,8]**

[1] Department of Neurosciences, Cleveland Clinic, Lerner Research Institute, Cleveland, OH, United States, [2] Department of Pathology and Experimental Therapeutics, Institut d'Investigació Biomédica de Bellvitge, Bellvitge University Hospital, Barcelona, Spain, [3] Institute of Biomedicine of the University of Barcelona, Barcelona, Spain, [4] Gene Expression Laboratory, The Salk Institute for Biological Studies, La Jolla, CA, United States, [5] Center of Regenerative Medicine in Barcelona, Hospital Duran i Reynals, Barcelona, Spain, [6] Biomedical Research Networking Center in Bioengineering, Biomaterials and Nanomedicine, Madrid, Spain, [7] Institució Catalana de Recerca i Estudis Avançats (ICREA), Barcelona, Spain, [8] Department of Molecular and Translational Medicine, University of Brescia, Brescia, Italy

OPEN ACCESS

Edited by:
Annalisa Buffo, Università degli Studi di Torino, Italy

Reviewed by:
Mariagrazia Grilli, Università degli Studi del Piemonte Orientale "Amedeo Avogadro", Italy
Chiara Rolando, Universität Basel, Switzerland

***Correspondence:**
Hoonkyo Suh
suhh2@ccf.org
Antonella Consiglio
consiglio@ub.edu;
aconsiglio@ibub.pcb.ub.es

†Present address:
Qi-Gang Zhou, Department of Clinical Pharmacology, School of Pharmacy, Nanjing Medical University, Nanjing, China

Received: *01 June 2018*
Accepted: *25 October 2018*
Published: *15 November 2018*

Citation:
Suh H, Zhou Q-G, Fernandez-Carasa I, Clemenson GD Jr, Pons-Espinal M, Ro EJ, Marti M, Raya A, Gage FH and Consiglio A (2018) Long-Term Labeling of Hippocampal Neural Stem Cells by a Lentiviral Vector. Front. Mol. Neurosci. 11:415. doi: 10.3389/fnmol.2018.00415

Using a lentivirus-mediated labeling method, we investigated whether the adult hippocampus retains long-lasting, self-renewing neural stem cells (NSCs). We first showed that a single injection of a lentiviral vector expressing a green fluorescent protein (LV PGK-GFP) into the subgranular zone (SGZ) of the adult hippocampus enabled an efficient, robust, and long-term marking of self-renewing NSCs and their progeny. Interestingly, a subset of labeled cells showed the ability to proliferate multiple times and give rise to $Sox2^+$ cells, clearly suggesting the ability of NSCs to self-renew for an extensive period of time (up to 6 months). In addition, using GFP^+ cells isolated from the SGZ of mice that received a LV PGK-GFP injection 3 months earlier, we demonstrated that some GFP^+ cells displayed the essential properties of NSCs, such as self-renewal and multipotency. Furthermore, we investigated the plasticity of NSCs in a perforant path transection, which has been shown to induce astrocyte formation in the molecular layer of the hippocampus. Our lentivirus (LV)-mediated labeling study revealed that hippocampal NSCs are not responsible for the burst of astrocyte formation, suggesting that signals released from the injured perforant path did not influence NSC fate determination. Therefore, our studies showed that a gene delivery system using LVs is a unique method to be used for understanding the complex nature of NSCs and may have translational impact in gene therapy by efficiently targeting NSCs.

Keywords: lentiviral vectors, hippocampal neurogenesis, targeting, neural stem cells, lesion

INTRODUCTION

Evidence from several studies has shown that self-renewing and multipotent neural stem cells (NSCs) are responsible for hippocampal neurogenesis, a process that maintains a NSC pool and generates newborn neurons (Gage, 2000; Suh et al., 2007; Eisch et al., 2008; Bonaguidi et al., 2011). This life-long production and integration of newborn neurons into the hippocampal neural

circuits plays a crucial role in learning and memory as well as emotional and stress response (Deng et al., 2010). The regenerative capacity of NSCs has raised hopes that NSCs could be used to replace degenerating cells as a part of therapy for various neurodegenerative and neuropsychiatric disorders. This therapeutic potential of NSCs underscores the importance of understanding the properties of hippocampal NSCs.

The idea that hippocampal NSCs are multipotent and have a self-renewal capacity has been widely accepted. However, the details of these critical features of NSCs are still unclear. For example, although hippocampal NSCs can differentiate into both neurons and astrocytes, a series of fate-mapping studies and lineage analyses revealed that hippocampal NSCs produce predominantly neurons, whereas the generation of astrocytes and oligodendrocytes is minimal to non-existent (Seri et al., 2001; Kronenberg et al., 2003; Suh et al., 2007; Lugert et al., 2010; Bonaguidi et al., 2011; Encinas et al., 2011; Beckervordersandforth et al., 2014; Rolando et al., 2016; Pons-Espinal et al., 2017). However, it remains to be determined whether NSCs are continuously self-renewing over the long term or whether they are short-lived cells (Bonaguidi et al., 2011; Encinas et al., 2011; Beckervordersandforth et al., 2014). Both models can explain the presence of self-renewing NSCs, but they do not indicate whether NSCs are continuously self-renewing or live only for a short time. These inconclusive observations regarding key features of NSCs are partially due to the technical challenges involved in labeling and tracing complex NSC populations over time.

To address this issue directly, we used a lentivirus (LV)-mediated gene delivery system that has shown to transduce both dividing and non-dividing cells, including NSCs as well as their progeny over a long-term marking period (Consiglio et al., 2004; Suh et al., 2007). By taking advantage of LV's ability to efficiently transduce a GFP reporter gene in adult NSCs *in vivo*, we clearly demonstrated the presence of long-lasting NSCs that can proliferate multiple times when spaced by month intervals and produce cells expressing a NSC marker, Sox2. Importantly, when we isolated, cultured, and examined the properties of GFP-labeled cells 3 months after we injected LV PGK-GFP into the dentate gyrus (DG), we observed that the same population labeled by LV PGK-GFP *in vivo* could expand and produce neurons as well as astrocytes *in vitro*. Using a LV PGK-GFP, we subsequently tested whether hippocampal NSCs underlies the burst of astrocyte formation that occurs during performant path (PP) injury. In the PP injury model that induces astrocyte production in the hippocampus (Gage et al., 1988; Fagan and Gage, 1994), we found that NSCs did not contribute to the burst of astrocytes. Our studies demonstrate that a LV is a robust and efficient gene delivery system that allows us to dissect the detailed characteristics of hippocampal NSCs.

MATERIALS AND METHODS

LV Production and Stereotactic Surgery

The production and determination of LV PGK-GFP expression were previously described in detail (Consiglio et al., 2004). We used LV PGK-GFP that has 5×10^9 to 1×10^{10} transducing units per ml with an HIV-1 p24 concentration of 100 μg/ml. All procedures using animals were done in accordance with protocols approved by the Animal Care and Use Committee of the Salk Institute for Biological Studies and the Parc Cientific of Barcelona. Six- to eight-week old female C57BL/6 (Harlan) mice were used for all experiments. Mice were anesthetized with a mixture of ketamine (100 mg/kg) and xylazine (10 mg/kg), and 1 μl of vector was injected into the right hippocampal dentate gyrus at a rate of 0.2 μl/min using a Hamilton (Reno, NV, United States) syringe. Stereotactic coordinates were as follows: AP = −2, ML = +1.5, DV = −2 in mm from bregma. Mice were analyzed 15 days and 3 and 6 months after injection.

BrdU Administration

To understand the long-term proliferation of GFP-transduced cells in the adult hippocampus, 100 mg/kg of Bromodeoxyuridine (BrdU) was administrated daily by intraperitoneal (IP) injection for 7 days [83 and 173 days post injection (dpi)]. Animals were sacrificed 24 h after the last BrdU injection (90 and 180 dpi). To examine the differentiation potential of GFP-labeled cells, a group of mice received the same amount of BrdU at 30 dpi for 7 days and were analyzed 4 weeks later.

Tissue Processing and Immunohistochemistry

Detailed procedures regarding tissue processing and antibody staining, including BrdU detection, were previously described (Suh et al., 2007). Primary antibodies used were mouse anti-Neuronal Nuclei (NeuN 1:10; kindly provided by Dr. R. Mullen, University of Utah); mouse anti-Nestin (1:500; Pharmingen); goat anti-Doublecortin (DCX 1:200; Santa Cruz Biotechnologies); rabbit anti-Glial Fibrillary Acidic Protein (GFAP 1:1000; Dako); rabbit anti-S-100β (1:5000; Swant); rat anti-BrdU (1:200; Accurate Chemicals); rabbit anti-Ki67 (1:200; Novocastra); rabbit anti-Sox2 (1:200, Chemicon); rabbit anti-brain lipid binding protein (BLBP 1:1000; kindly provided by N. Heintz, Rockefeller); rat anti-MUSASHI-1 (1:1000; a kind gift from O. Hideyuki, Keiyo University, Japan); rabbit anti-GFP (1:100, Molecular Probes); and guinea pig anti-GFAP (1:1,000). Fluorescence immunohistochemistry (IHC) was performed using corresponding FITC, Cy3, or Cy5 secondary antibodies (1:200, all raised in donkey, Jackson ImmunoResearch, West Grove, PA, United States). DAPI (10 mg/ml, Sigma) was used as a fluorescent counterstain.

Confocal stack images of brain slices (40 μm) were obtained with the Confocal A1 Nikon Inverted SFC with 40× objective and the Zeiss Spinning Disk with a 20× objective. Cell quantification and analysis was performed using NIS-Elements software (Nikon) and Zen Blue (Zeiss).

Cell Counting

To quantify the percentage of labeled cells in coronal sections stained for GFP and BrdU, the number of BrdU-positive nuclei was identified in a selected optical field and counted. The fraction

of labeled nuclei showing GFP-positive cytoplasm in the same field was then assessed. The analysis was performed on three randomly chosen fields taken from two or three independent non-sequential sections from three mice per experimental group.

Perforant Path (PP) Lesion

Lentiviral vector expressing a green fluorescent protein was injected into the right side of the dentate gyrus of six- to eight-week old C57BL6 female mice (n = 5). One month later, these mice received ipsilateral aspirative lesions that resulted in the ablation of the PP as previously described (Fagan and Gage, 1994). Brains were harvested and analyzed 7 days post-surgery.

Preparation of Hippocampal Progenitors

Six- to eight-week old C57BL/6 female mice were injected with LV PGK-GFP in the DG. Three months later, hippocampi were isolated from these mice and used to prepare hippocampal progenitor cells as previously described (Ray and Gage, 2006; Suh et al., 2007). Briefly, 3–5 LV PGK-GFP injected hippocampi were isolated from these mice and digested in PPD solution [papain (2.5 U/ml, Worthington), pronage (1 U/ml, Roche), and DNase (250 U/ml, Worthington)] and sucrose gradient was applied to remove cell debris and myelin. Then cells were plated in the presence of FGF2 (Fibroblast Growth Factor, 20 ng/ml; PeproTech), EGF (Epidermal Growth Factor, 20 ng/ml; PeproTech), and heparin (5 μg/ml; Sigma) in DMEM/F12 (Life Technology) basal media supplemented with N2 (Life Technology). Once NSCs were established and expanded in the presence of FGF2 and EGF, we sorted out GFP-expressing cells via FACS and established three clonally expanded NSCs lines. The number of total GFP-expressing cells isolated by FACS was around 2 × 10^4 cells per preparation. To differentiate GFP-expressing NSCs, 10^5 cells/cm^2 were plated on the laminin-coated glass chamber slides (Nalge Nunc International) and cultured in differentiation medium consisting of DMEM/F12, N2 supplement, and 5 μM forskolin (Sigma), for 7 more days.

Immunofluorescence

The immunofluorescence staining on cell cultures was performed after fixing NSCs for 30 min with 4% paraformaldehyde (PFA) followed by extensive washings with PBS for 30 min. Cells were washed three times with PBS 0,1% Triton X-100 (PBS-T) and blocked for 2 h with PBS-T containing 5% normal goat serum (Vector laboratories), followed by overnight incubation with primary antibodies: rabbit anti- GFAP (1:1000; Dako); mouse anti-Nestin (1:500; Pharmingen); rabbit anti-Sox2 (1:200; Chemicon); anti-TUJ-1 (1:1,000; Chemicon). The next day, after washing extensively with PBS-T, cells were incubated with secondary antibodies. Cells were mounted in mounting medium and counterstained with fluorescent nuclear dye DAPI (Invitrogen). Images were obtained using the microscope Nikon Eclipse at 20 or 40× magnification and quantification was performed using a Cell-counter plugin in FIJI (Fiji is Just ImageJ).

RESULTS

LV-Mediated Long-Term Labeling of NSCs in the Hippocampus

To test the ability of LV to transduce hippocampal NSCs *in vivo*, we injected a vesicular stomatitis virus-pseudotyped, late-generation LV expressing the GFP into the right DG of the mouse hippocampus (Consiglio et al., 2004). GFP expression in the LVs was driven by the ubiquitously expressed phosphoglycerate kinase promoter and by the posttranscriptional regulatory element of the woodchuck hepadnavirus. Mice were sacrificed after 2 weeks to assess cell phenotype shortly after transduction or after 3 and 6 months as the longest time point. Robust GFP-expressing cells were identified in both DG and the hilus after 2 weeks of injection and during a six-month period (**Figures 1A,B**). Because neither the VSV-G envelope nor the PGK promoter provided neural precursor cell (NPCs) specificity, the majority of GFP-labeled cells expressed post-mitotic immature and mature neuronal markers (data not shown).

Next, we tested whether the LV successfully labeled hippocampal NSCs. Interestingly, IHC with NSCs markers showed that a population of GFP^+ cells located along the subgranular zone (SGZ) co-localized with BLBP, NESTIN, SOX2, GFAP, and MUSASH-1 2 weeks and 6 months after LV PGK-GFP injection (Suh et al., 2007; **Figures 1C–J**).

Three-dimensional confocal images revealed that 38 ± 5.3% (n = 3) of the GFP-positive cells in the SGZ expressed BLBP marker, known to label a subset of neurogenic radial glia (Filippov et al., 2003; Fukuda et al., 2003; Mignone et al., 2004; Gebara et al., 2016), and 7 ± 2.2% (n = 3) was expressed in non-radial cells ($SOX2^+$ cells), suggesting the ability of LV PGK-GFP to target NSCs that have the potential to self-renew and differentiate into neurons in the adult hippocampus (Suh et al., 2007; Bonaguidi et al., 2011; Gebara et al., 2016).

LV Marks a Cell Population That Retains Multiple Proliferation Capacity

To test whether LV PGK-GFP is successfully transduced in NSCs that have proliferation capacity over a long period of time, we introduced BrdU 6 months post LV PGK-GFP injection. The hippocampus was then examined to identify proliferating cells 24 h after the final BrdU injection. We found that 6.25 ± 1.8% of GFP^+ cells were positive for BrdU in the SGZ of the DG. This observation indicates that initially targeted cells or their progeny retain proliferation capacity over 6 months (**Figure 2A**). We identified that 10 ± 1.4% of these GFP/BrdU double-labeled cells expressed SOX2 marker (n = 3; **Figure 2B**), known to represent the self-renewing and multipotent NSCs (Suh et al., 2007). Doublecortin (DCX), a transient marker that labels both neuroblasts and immature neurons, was used to measure a continuous neurogenesis from GFP^+ cells (Steiner et al., 2006). Indeed, we observed both GFP/DCX double-labeled cells (26.8 ± 2% of GFP^+ cells; n = 3 **Figure 2C**) and GFP/BrdU/DCX cells triple-labeled cells (60 ± 2.3% n = 3; **Figure 2D**). Interestingly, these results collectively suggest that

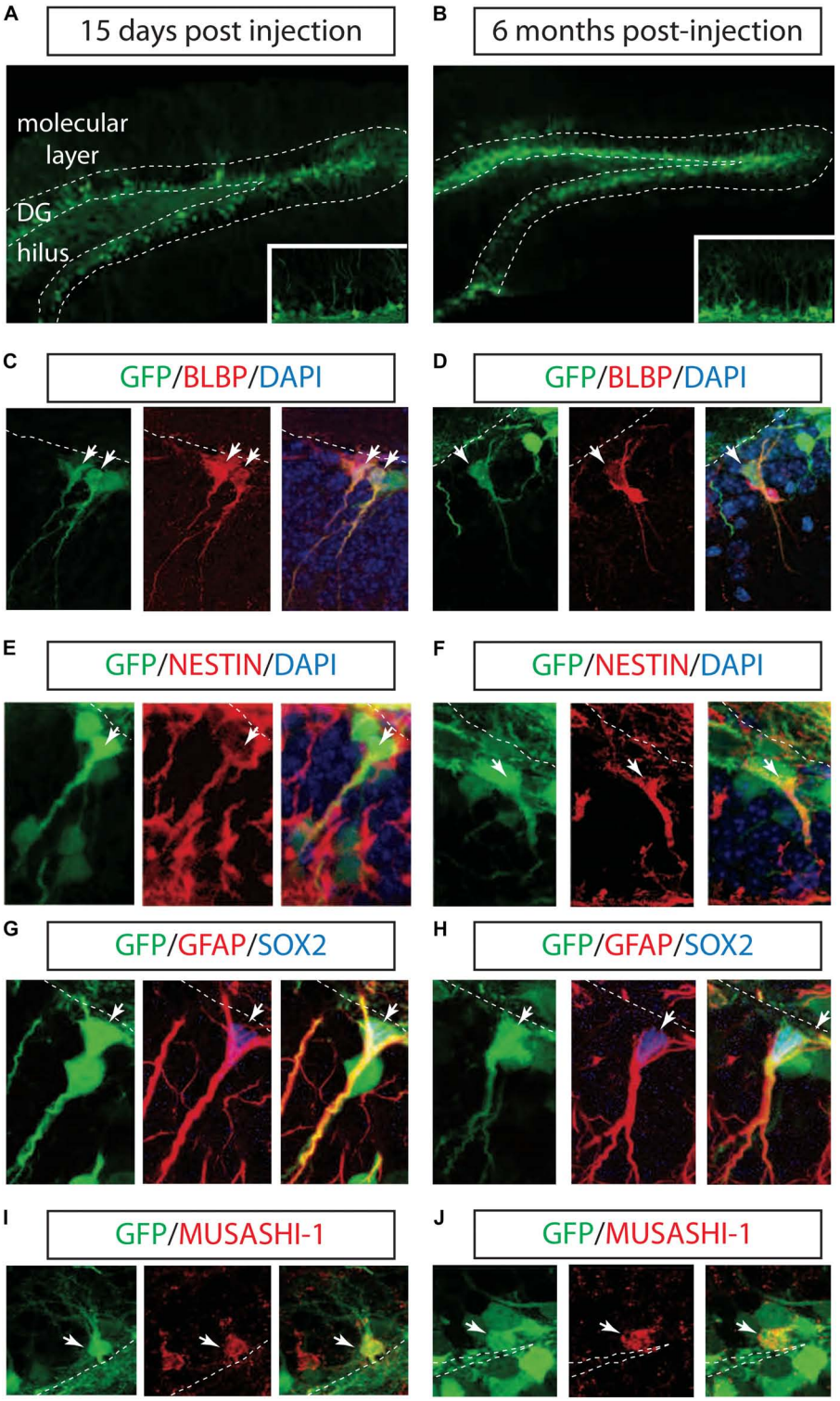

FIGURE 1 | Long-term marking of hippocampal NSCs by LV PGK-GFP. LV PGK-GFP was unilaterally injected into the hippocampal DG; brain sections were analyzed 15 days **(A)** and 6 months **(B)** later. GFP expression was evident in the DG at both time points. A higher magnification view is displayed in insets **(A,B)**. GFP-expressing cells co-labeled with NSCs markers such as BLBP **(C,D)**, NESTIN **(E,F)**, SOX2, GFAP **(G,H)**, and MUSASHI-1 **(I,J)** (arrows). Note that some GFP-positive cells stained for SOX2 showed co-localization with radial glial cell markers such as GFAP in their processes **(G,H)**. DG, dentate gyrus; SGZ is marked with dotted lines.

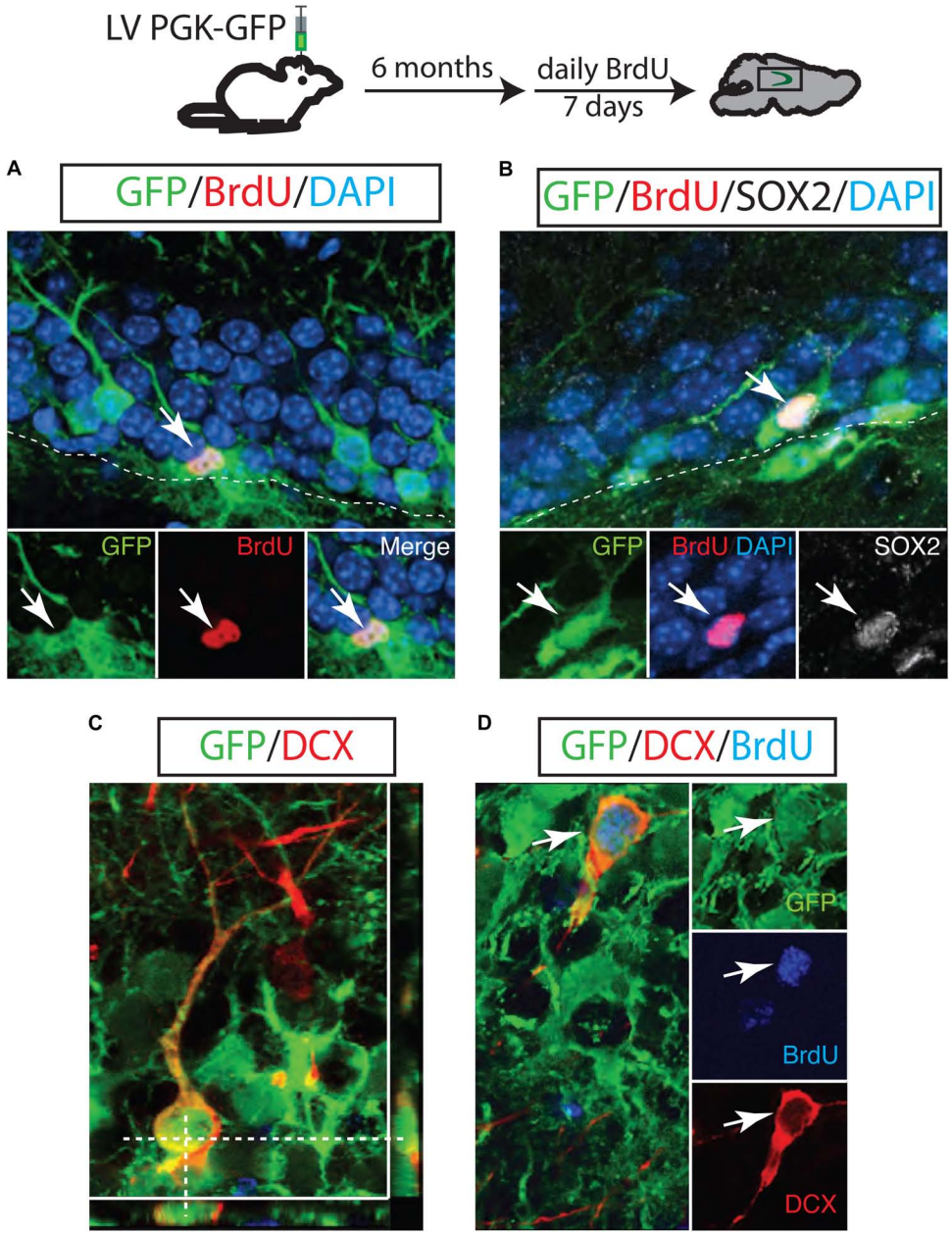

FIGURE 2 | A long-lasting NSC population in the adult hippocampus. GFP-positive neuroblasts were observed in the SGZ 6 months after LV PGK-GFP injection. Some GFP$^+$ cells incorporated BrdU **(A)** and maintained the expression of SOX2 **(B)**, indicating that LV PGK-GFP-labeled NSC populations retained the proliferation capacity over a six-month tracing period. Many of the GFP-labeled cells expressed the early neuronal marker doublecortin (DCX; **C**). Higher magnification picture of the triple-labeled cells GFP/DCX/BrdU **(D)**.

NSCs are continuously generated from targeted GFP$^+$ cells and actively produce neuroblasts even 6 months after LV injection.

Long-Term Maintenance of NSCs in the Hippocampus

Next, we investigated the cell fate of the proliferating GFP$^+$ cells and their extensive proliferation ability. One month after the LV PGK-GFP injection, mice were injected with BrdU daily for 7 days and sacrificed 4 weeks after the last BrdU injection. The majority of progeny of proliferating GFP$^+$ cells (GFP/BrdU double-labeled cells) gave rise to 87.5 ± 2.5% neurons which account for 40% DCX$^+$ and 60% NeuN$^+$ (**Figure 3A**). Specifically, neurons positive for NeuN expressed a granular neuron-specific marker, Prox1 (data not shown) and displayed distinctive morphological features of mature granular neurons in the DG. In contrast to a dominant neuronal differentiation of GFP-labeled cells, proliferating GFP$^+$ (GFP/BrdU$^+$) cells

produced a significantly lower number of mature astrocytes that co-labeled with S-100β (3.9 ± 0.49% GFP/BrdU/S-100 β+ cells) (**Figure 3B**); the generation of new oligodendrocytes was not detected in our experimental paradigm. These results are in line with those obtained by using other labeling methods (Song et al., 2002; Maslov et al., 2004; Steiner et al., 2004; Suh et al., 2007, 2009; Zhao et al., 2008; Venere et al., 2012). We also performed IHC with BrdU and MCM2 to test the proliferation capacity of GFP^+ cells (Maslov et al., 2004). A triple staining revealed a subset of GFP/BrdU double positive cells expressing MCM2 (2.3 ± 1.2%), indicating that GFP^+ cells had proliferated 1 month after LV injection and were in continuous cell cycle for an additional month (**Figure 3C**).

Our assessment of the differentiation capacity of GFP^+ cells *in vivo* was in sharp contrast to the multipotency capacity of the hippocampal NSCs *in vitro* that has been reported in many studies: while GFP^+ cells *in vivo* differentiated predominantly to neurons, cultured NSCs produced more astrocytes than neurons. This finding raised the possibility that neurogenic cells labeled by LV PGK-GFP might differ from the cell population that gives rise to hippocampal NSCs *in vitro*. To test this hypothesis, we isolated the hippocampal NSCs 3 months after we injected LV PGK-GFP into the DG and established NSCs with clonally derived GFP^+ cells. Clonally expanded GFP^+ NSCs showed their ability to propagate at least 20 times, maintaining the expression of NSC markers of NESTIN and SOX2 (**Figure 3D**). When the NSCs were induced to differentiate in the presence of forskolin, the majority of GFP^+ NSCs differentiated into astrocytes positive for GFAP, although a moderate amount of GFP+ NSCs gave rise to neurons positive for Tuj1 (**Figures 3E,F**). These results showed that LV PGK-GFP clearly targeted the same cell populations that serve as a source of both *in vitro* and *in vivo* NSCs, though the *in vitro* conditions favored astroglial differentiation.

Differentiation Potential of NSCs in the Perforant Path Injury

It has been shown that unilateral injury of the perforant path (PP) induces degeneration of axon terminals of the entorhinal neurons and a burst of astrocyte formation in the molecular layer of the ipsilateral hippocampus (Gage et al., 1988; Fagan and Gage, 1994). It has been a long lasting question whether NSCs in the dentate gyrus could contribute to the PP injury-induced astrocytes. To directly answer to this question, 1 month after LV PGK-GFP was injected to label NSCs in the DG, a unilateral transection of the PP was performed. BrdU was injected for 3 days and the brain was analyzed 4 days later.

Consistent with previous reports, the generation of astrocytes expressing GFAP increased on the ipsilateral side of the molecular layer (**Figure 4A**). Thus, by immunofluorescence analyses, we confirmed that the ablation of inputs from entorhinal cortex to the granular neurons causes degeneration of axons and results in increased astrocyte proliferation (GFAP/BrdU double positive cells), specifically in the DG-molecular layer of the lesioned side (**Figure 4A**). However, the contribution of GFP^+ cells to newly generated astrocytes was not detected, suggesting that GFP^+ NSCs were not responsible for the burst of astrocytes (**Figure 4B**).

DISCUSSION

Self-renewing and multipotent NSCs are responsible for continuous neurogenesis in the adult hippocampus. These two properties of NSCs are critical for the production of newborn neurons and maintenance of a stem cell pool throughout life. As neurogenesis occurs, adult NSCs undergo changes in their intrinsic properties such as morphology, gene expression, proliferation kinetics, and self-renewal capacity and ultimately produce differentiated neural cells (Zhao et al., 2008; Suh et al., 2009). In the normal brain, the production, and integration of newborn neurons into the preexisting neural circuits play a key role in hippocampus-dependent learning and memory (Aimone et al., 2011). In pathological conditions, however, injury-associated signals appear to affect many aspects of neurogenesis, leading to changes in the proliferation of NSCs, survival and fate determination of newborn cells (Lindvall and Kokaia, 2006; Llorens-Bobadilla et al., 2015). Dysregulated neurogenesis has been implicated in functional deficits. In this report, we investigated the precise characteristics of LV-targeted NSCs to understand how NSCs contribute to neurogenesis in normal and injured brains.

Two different models have been proposed to address the nature of the longevity of NSCs in the adult hippocampus: long-lasting and continuously self-renewing NSCs vs. one-time activated and short-living NSCs. In the former model, NSCs continuously proliferate to maintain a NSC pool and produce newborn neurons and astrocytes (Suh et al., 2007; Bonaguidi et al., 2011). In the latter model, however, NSCs are proposed to be activated only once throughout life, to proliferate a limited number of times and sequentially generate neurons and astrocytes within a period of a month (Encinas et al., 2011). This latter model of short-lived NSCs is in line with previous *in vitro* studies, suggesting that the adult hippocampus does not contain NSCs but only lineage-committed and transiently proliferating cells (Seaberg and van der Kooy, 2002; Bull and Bartlett, 2005). The key difference between these models is whether NSCs have a long-term or short-term self-renewal ability. Here, using an advanced-generation LV (Consiglio et al., 2004), we showed that a subpopulation of GFP^+ cells (indicating lentivirus-mediated labeling), retained the proliferative capacity over a six-month labeling period analyzed. Moreover, some GFP^+ cells divided multiple times (GFP/BrdU/MCM2) within a one-month interval, producing progeny expressing a NSC marker (GFP/BrdU/SOX2) over the two-month period analyzed. That NSCs were targeted *in vivo* by LVs was further validated by culturing experiments demonstrating that some of the transduced SGZ cells behaved as long-term self-renewing progenitors *in vitro* and they could propagate for up to 5 months (the latest time tested). Interestingly, when we analyzed the differentiation ability of the labeled cells *in vitro*, our results showed that while GFP^+ cells *in vivo* differentiated predominantly to neurons, cultured NSCs produced more astrocytes than neurons, indicating that *in vitro*

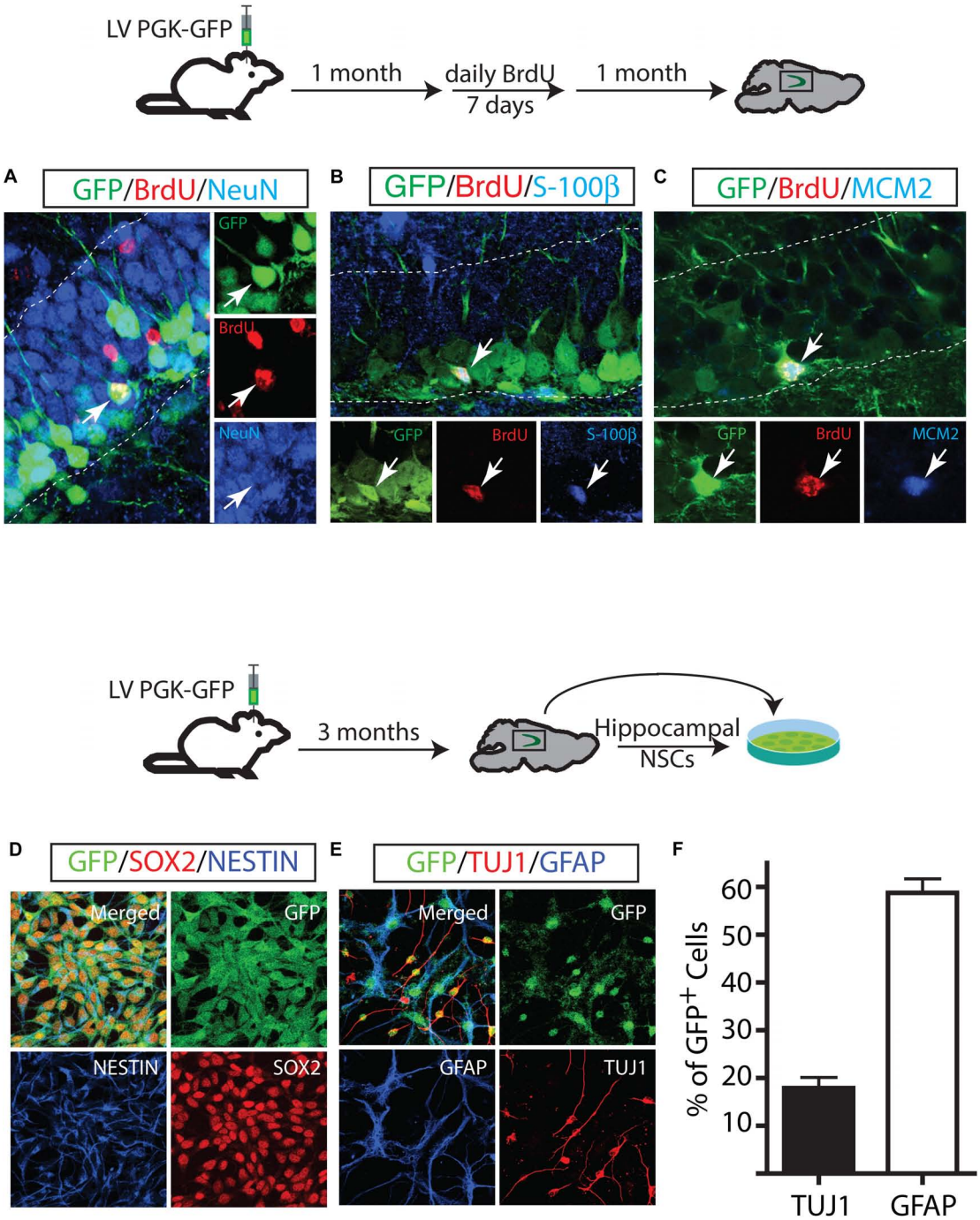

FIGURE 3 | Long-term maintenance of NSCs in the adult hippocampus. Fate mapping of GFP$^+$ identified NSCs that proliferate and produce neurons **(A)** and astrocytes **(B)**. Some NSCs underwent cell proliferation proliferated twice in a one-month interval **(C)**. GFP-labeled cells *in vivo* gave rise to *in vitro* NSCs. *In vitro*, GFP$^+$ NSCs expressed NSC markers such as NESTIN and Sox2 **(D)** and differentiated into neurons (TUJ1) and astrocytes (GFAP) **(E)**. GFP$^+$ derived-neurons and astrocytes at day 7 of differentiation **(F)**.

conditions favored astroglial differentiation. When we clonally expanded GFP+ NSCs that had already been established *in vitro*, they all showed the similar differentiation ratio of neuron and astrocytes, suggesting this preferred astrocyte differentiation is likely to reflect the general NSC properties *in vitro*.

Using our LV system, we directly asked whether NSCs in the DG directly contributed to astrocytes formation by performing a unilateral transection of the PP, which induces astrocyte production specifically in the molecular layer of the ipsilateral DG (Gage et al., 1988; Fagan and Gage, 1994). Since the site of

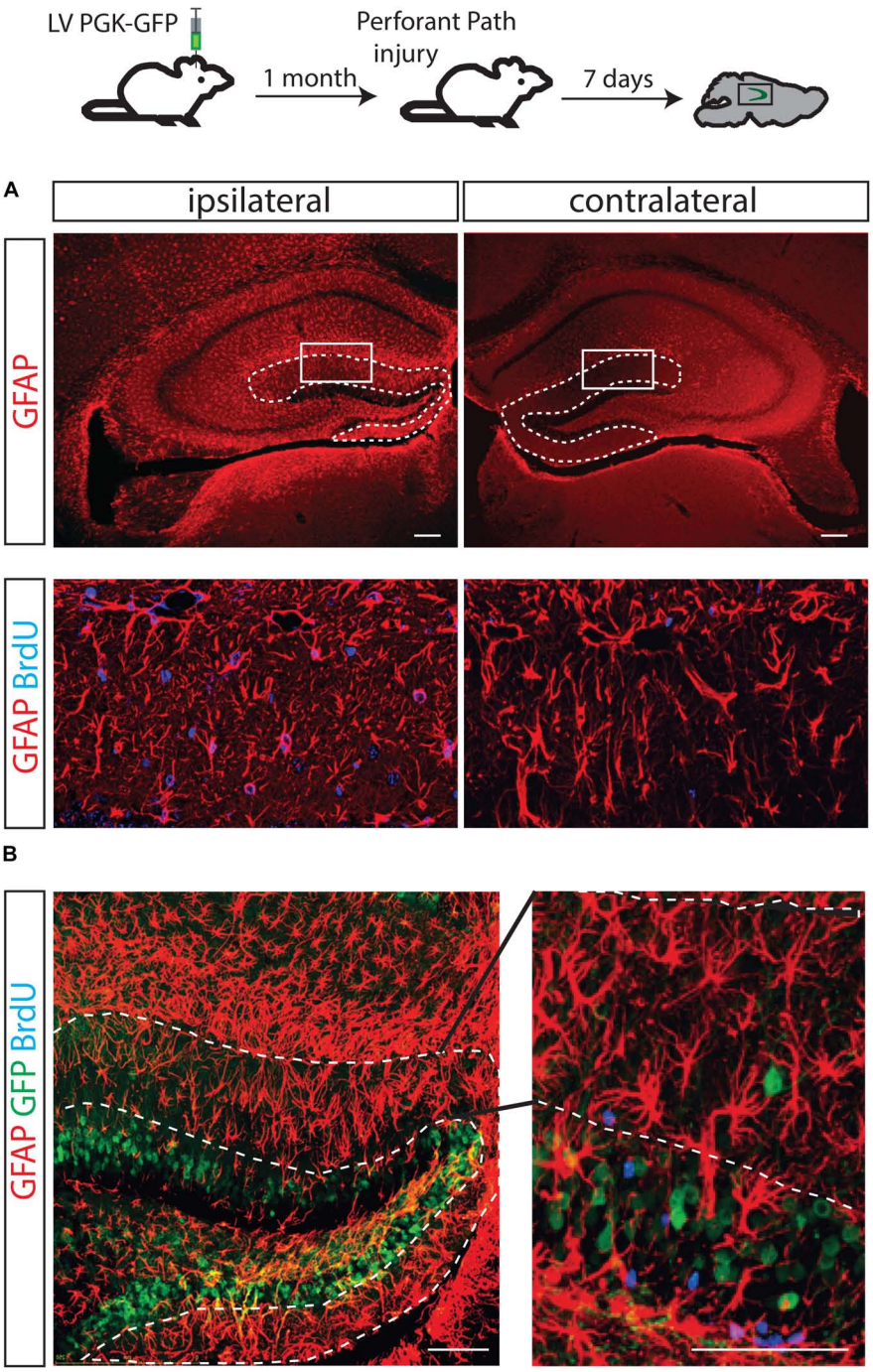

FIGURE 4 | The fate of hippocampal NSCs did not change following PP injury. A brain lesion in the perforant path resulted in over-expression of GFAP-positive cells in the molecular layer of the injury side but not the contralateral side (**A**, dotted line). As expected, an increased number of astrocytes (positively stained with BrdU) was found in the molecular layer of the ipsilateral side (**B**, left) but not in the contralateral side of these animals (**B**, right); however, GFP-labeled progenitors did not contribute to the increased astrocyte numbers.

astrocyte induction is geographically separated from the injury site, our experimental paradigm has the advantage of ruling out the possibility that the cellular phenotypes we observed were caused by the direct physical damage to the brain. In such an experimental condition that facilitates astrocyte induction, we predicted we would observe increased astrocyte formation derived from NSCs labeled by a lentiviral vector. Contrary to what was expected, our fate mapping showed that NSCs did not contribute to the formation of astrocytes. LV-mediated fate mapping revealed that the fate determination of NSCs might be

less influenced by environmental cues in the injured brains, and astrocyte progenitors located in the molecular layer might be responsible for astrocyte induction in the case of the PP injury model (Buffo et al., 2008; Zhang and Barres, 2010).

Although these findings support the conclusion that our lentiviral system is able to induce transgene expression in a long-lasting, self-renewing NSCs within the hippocampus of the adult mouse brain that continually give rise to proliferating neuronal progenitors that contribute to maintain neurogenesis in the hippocampus, the fraction of NSC that were actually transduced *in vivo* remains to be determined. An unequivocal characterization of the cell type originally transduced by the LV may require the use of cell type specific promoters restricted to NPCs. However, in spite of its uncertain identity, our findings indicate that LV, in combination with BrdU-labeling and morphological analysis, allows long-term studies of adult NSCs properties *in vivo*. In future experiments, we will test whether the combination of the usage of cell type specific promoters and different glycoprotein will improve targeting specificity, which is a critical factor also for successful gene therapy.

AUTHOR CONTRIBUTIONS

HS, FG, and AC conceived the study. HS, Q-GZ, GC, IF-C, and MP-E contributed to methodology. HS and AC performed the formal analysis. HS, Q-GZ, GC, IF-C, MP-E, ER, AR, MM, and AC investigated the analysis. HS, FG, and AC validated the results. HS, FG, and AC wrote, reviewed, and edited the manuscript. HS, FG, and AC acquired funding. HS, FG, and AC supervised the study. All authors edited and approved the final manuscript.

FUNDING

This work was supported by grants from the European Research Council-ERC (2012-StG-311736-PD-HUMMODEL) and the Spanish Ministry of Economy and Competitiveness-MINECO (BFU2013-49157-P and BFU2016-80870-P) to AC and by the Whitehall Foundation Research Grant and NIH grant (R01AA022377) to HS. Additional funding came from MINECO (SAF2015-69706-R), Instituto de Salud Carlos III-ISCIII/FEDER (Red de Terapia Celular – TerCel RD16/0011/0024 and PIE14/00061), ACCIÓ/FEDER (AdvanceCat), Generalitat de Catalunya-AGAUR (2017-SGR-899), and CERCA Programme/ Generalitat de Catalunya.

ACKNOWLEDGMENTS

We thank Lola Mulero Pérez and Haleigh Golub for bioimaging and technical assistance, and Carles Terol for help with experiments. We also thank Carles Calatayud for helpful discussion and Mary Lynn Gage for editorial comments.

REFERENCES

Aimone, J. B., Deng, W., and Gage, F. H. (2011). Resolving new memories: a critical look at the dentate gyrus, adult neurogenesis, and pattern separation. *Neuron* 70, 589–596. doi: 10.1016/j.neuron.2011.05.010

Beckervordersandforth, R., Deshpande, A., Schaffner, I., Huttner, H. B., Lepier, A., Lie, D. C., et al. (2014). In vivo targeting of adult neural stem cells in the dentate gyrus by a split-cre approach. *Stem Cell Rep.* 2, 153–162. doi: 10.1016/j.stemcr.2014.01.004

Bonaguidi, M. A., Wheeler, M. A., Shapiro, J. S., Stadel, R. P., Sun, G. J., Ming, G. L., et al. (2011). In vivo clonal analysis reveals self-renewing and multipotent adult neural stem cell characteristics. *Cell* 145, 1142–1155. doi: 10.1016/j.cell.2011.05.024

Buffo, A., Rite, I., Tripathi, P., Lepier, A., Colak, D., Horn, A. P., et al. (2008). Origin and progeny of reactive gliosis: a source of multipotent cells in the injured brain. *Proc. Natl. Acad. Sci. U.S.A.* 105, 3581–3586. doi: 10.1073/pnas.0709002105

Bull, N. D., and Bartlett, P. F. (2005). The adult mouse hippocampal progenitor is neurogenic but not a stem cell. *J. Neurosci.* 25, 10815–10821. doi: 10.1523/JNEUROSCI.3249-05.2005

Consiglio, A., Gritti, A., Dolcetta, D., Follenzi, A., Bordignon, C., Gage, F. H., et al. (2004). Robust in vivo gene transfer into adult mammalian neural stem cells by lentiviral vectors. *Proc. Natl. Acad. Sci. U.S.A.* 101, 14835–14840. doi: 10.1073/pnas.0404180101

Deng, W., Aimone, J. B., and Gage, F. H. (2010). New neurons and new memories: how does adult hippocampal neurogenesis affect learning and memory? *Nat. Rev. Neurosci.* 11, 339–350. doi: 10.1038/nrn2822

Eisch, A. J., Cameron, H. A., Encinas, J. M., Meltzer, L. A., Ming, G. L., and Overstreet-Wadiche, L. S. (2008). Adult neurogenesis, mental health, and mental illness: hope or hype? *J. Neurosci.* 28, 11785–11791. doi: 10.1523/JNEUROSCI.3798-08.2008

Encinas, J. M., Michurina, T. V., Peunova, N., Park, J. H., Tordo, J., Peterson, D. A., et al. (2011). Division-coupled astrocytic differentiation and age-related depletion of neural stem cells in the adult hippocampus. *Cell Stem Cell* 8, 566–579. doi: 10.1016/j.stem.2011.03.010

Fagan, A. M., and Gage, F. H. (1994). Mechanisms of sprouting in the adult central nervous system: cellular responses in areas of terminal degeneration and reinnervation in the rat hippocampus. *Neuroscience* 58, 705–725. doi: 10.1016/0306-4522(94)90449-9

Filippov, V., Kronenberg, G., Pivneva, T., Reuter, K., Steiner, B., Wang, L. P., et al. (2003). Subpopulation of nestin-expressing progenitor cells in the adult murine hippocampus shows electrophysiological and morphological characteristics of astrocytes. *Mol. Cell. Neurosci.* 23, 373–382. doi: 10.1016/S1044-7431(03)00060-5

Fukuda, S., Kato, F., Tozuka, Y., Yamaguchi, M., Miyamoto, Y., and Hisatsune, T. (2003). Two distinct subpopulations of nestin-positive cells in adult mouse dentate gyrus. *J. Neurosci.* 23, 9357–9366. doi: 10.1523/JNEUROSCI.23-28-09357.2003

Gage, F. H. (2000). Mammalian neural stem cells. *Science* 287, 1433–1438. doi: 10.1126/science.287.5457.1433

Gage, F. H., Olejniczak, P., and Armstrong, D. M. (1988). Astrocytes are important for sprouting in the septohippocampal circuit. *Exp. Neurol.* 102, 2–13. doi: 10.1016/0014-4886(88)90073-8

Gebara, E., Bonaguidi, M. A., Beckervordersandforth, R., Sultan, S., Udry, F., Gijs, P. J., et al. (2016). Heterogeneity of radial glia-like cells in the adult hippocampus. *Stem Cells* 34, 997–1010. doi: 10.1002/stem.2266

Kronenberg, G., Reuter, K., Steiner, B., Brandt, M. D., Jessberger, S., Yamaguchi, M., et al. (2003). Subpopulations of proliferating cells of the adult hippocampus respond differently to physiologic neurogenic stimuli. *J. Comp. Neurol.* 467, 455–463. doi: 10.1002/cne.10945

Lindvall, O., and Kokaia, Z. (2006). Stem cells for the treatment of neurological disorders. *Nature* 441, 1094–1096. doi: 10.1038/nature04960

Llorens-Bobadilla, E., Zhao, S., Baser, A., Saiz-Castro, G., Zwadlo, K., and Martin-Villalba, A. (2015). Single-cell transcriptomics reveals a population of dormant neural stem cells that become activated upon brain injury. *Cell Stem Cell* 3, 329–340. doi: 10.1016/j.stem.2015.07.002

Lugert, S., Basak, O., Knuckles, P., Haussler, U., Fabel, K., Gotz, M., et al. (2010). Quiescent and active hippocampal neural stem cells with distinct morphologies respond selectively to physiological and pathological stimuli and aging. *Cell Stem Cell* 6, 445–456. doi: 10.1016/j.stem.2010.03.017

Maslov, A. Y., Barone, T. A., Plunkett, R. J., and Pruitt, S. C. (2004). Neural stem cell detection, characterization, and age-related changes in the subventricular zone of mice. *J. Neurosci.* 24, 1726–1733. doi: 10.1523/JNEUROSCI.4608-03.2004

Mignone, J. L., Kukekov, V., Chiang, A. S., Steindler, D., and Enikolopov, G. (2004). Neural stem and progenitor cells in nestin-GFP transgenic mice. *J. Comp. Neurol.* 469, 311–324. doi: 10.1002/cne.10964

Pons-Espinal, M., de Luca, E., Marzi, M. J., Beckervordersandforth, R., Armirotti, A., Nicassio, F., et al. (2017). Synergic functions of miRNAs determine neuronal fate of adult neural stem cells. *Stem Cell Rep.* 11, 1046–1061. doi: 10.1016/j.stemcr.2017.02.012

Ray, J., and Gage, F. H. (2006). Differential properties of adult rat and mouse brain-derived neural stem/progenitor cells. *Mol. Cell. Neurosci.* 31, 560–573. doi: 10.1016/j.mcn.2005.11.010

Rolando, C., Erni, A., Grison, A., Beattie, R., Engler, A., Gokhale, P. J., et al. (2016). Multipotency of adult hippocampal NSCs in vivo is restricted by Drosha/NFIB. *Cell Stem Cell* 19, 653–662. doi: 10.1016/j.stem.2016.07.003

Seaberg, R. M., and van der Kooy, D. (2002). Adult rodent neurogenic regions: the ventricular subependyma contains neural stem cells, but the dentate gyrus contains restricted progenitors. *J. Neurosci.* 22, 1784–1793. doi: 10.1523/JNEUROSCI.22-05-01784.2002

Seri, B., Garcia-Verdugo, J. M., McEwen, B. S., and Alvarez-Buylla, A. (2001). Astrocytes give rise to new neurons in the adult mammalian hippocampus. *J. Neurosci.* 21, 7153–7160. doi: 10.1523/JNEUROSCI.21-18-07153.2001

Song, H. J., Stevens, C. F., and Gage, F. H. (2002). Neural stem cells from adult hippocampus develop essential properties of functional CNS neurons. *Nat. Neurosci.* 5, 438–445. doi: 10.1038/nn844

Steiner, B., Klempin, F., Wang, L., Kott, M., Kettenmann, H., and Kempermann, G. (2006). Type-2 cells as link between glial and neuronal lineage in adult hippocampal neurogenesis. *Glia* 54, 805–814. doi: 10.1002/glia.20407

Steiner, B., Kronenberg, G., Jessberger, S., Brandt, M. D., Reuter, K., and Kempermann, G. (2004). Differential regulation of gliogenesis in the context of adult hippocampal neurogenesis in mice. *Glia* 46, 41–52. doi: 10.1002/glia.10337

Suh, H., Consiglio, A., Ray, J., Sawai, T., D'Amour, K. A., and Gage, F. H. (2007). In vivo fate analysis reveals the multipotent and self-renewal capacities of Sox2(+) neural stem cells in the adult hippocampus. *Cell Stem Cell* 1, 515–528. doi: 10.1016/j.stem.2007.09.002

Suh, H., Deng, W., and Gage, F. H. (2009). Signaling in adult neurogenesis. *Annu. Rev. Cell Dev. Biol.* 25, 253–275. doi: 10.1146/annurev.cellbio.042308.113256

Venere, M., Han, Y. G., Bell, R., Song, J. S., Alvarez-Buylla, A., and Blelloch, R. (2012). Sox1 marks an activated neural stem/progenitor cell in the hippocampus. *Development* 139, 3938–3949. doi: 10.1242/dev.081133

Zhang, Y., and Barres, B. A. (2010). Astrocyte heterogeneity: an underappreciated topic in neurobiology. *Curr. Opin. Neurobiol.* 20, 588–594. doi: 10.1016/j.conb.2010.06.005

Zhao, C., Deng, W., and Gage, F. H. (2008). Mechanisms and functional implications of adult neurogenesis. *Cell* 132, 645–660. doi: 10.1016/j.cell.2008.01.033

Conflict of Interest Statement: The authors declare that the research was conducted in the absence of any commercial or financial relationships that could be construed as a potential conflict of interest.

frontiers in Molecular Neuroscience

ORIGINAL RESEARCH
published: 11 December 2018
doi: 10.3389/fnmol.2018.00443

An Immune-CNS Axis Activates Remote Hippocampal Stem Cells Following Spinal Transection Injury

*Sascha Dehler[1], Wilson Pak-Kin Lou[1], Liang Gao[2], Maxim Skabkin[1], Sabrina Dällenbach[1], Andreas Neumann[1] and Ana Martin-Villalba[1]**

[1]*Molecular Neurobiology, German Cancer Research Center (DKFZ), Heidelberg, Germany,* [2]*The Brain Cognition and Brain Disease Institute, ShenZhen Institutes of Advanced Technology, Chinese Academy of Sciences, Shenzhen, China*

External stimuli such as injury, learning, or stress influence the production of neurons by neural stem cells (NSCs) in the adult mammalian brain. These external stimuli directly impact stem cell activity by influencing areas directly connected or in close proximity to the neurogenic niches of the adult brain. However, very little is known on how distant injuries affect NSC activation state. In this study, we demonstrate that a thoracic spinal transection injury activates the distally located hippocampal-NSCs. This activation leads to a transient increase production of neurons that functionally integrate to improve animal's performance in hippocampal-related memory tasks. We further show that interferon-CD95 signaling is required to promote injury-mediated activation of remote NSCs. Thus, we identify an immune-CNS axis responsible for injury-mediated activation of remotely located NSCs.

Keywords: neurogenesis, neural stem cells, hippocampus, spinal cord injuries, CD95/FAS

OPEN ACCESS

Edited by:
Annalisa Buffo,
Università degli Studi di Torino, Italy

Reviewed by:
Ruth Marie Beckervordersandforth,
Institute for Biochemistry,
Faculty of Medicine,
Friedrich-Alexander-University
Erlangen-Nürnberg, Germany
Silvia De Marchis,
Università degli Studi di Torino, Italy

****Correspondence:***
Ana Martin-Villalba
a.martin-villalba@dkfz.de

Received: *03 July 2018*
Accepted: *16 November 2018*
Published: *11 December 2018*

Citation:
Dehler S, Lou WP-K, Gao L, Skabkin M, Dällenbach S, Neumann A and Martin-Villalba A (2018) An Immune-CNS Axis Activates Remote Hippocampal Stem Cells Following Spinal Transection Injury. Front. Mol. Neurosci. 11:443. doi: 10.3389/fnmol.2018.00443

INTRODUCTION

The process of generating new neurons in the adult mouse brain is best characterized in the ventricular-subventricular zone (V-SVZ) and the subgranular zone (SGZ) of the dentate gyrus (DG). Neural stem cells (NSCs) within the V-SVZ generate neuronal precursors that migrate along the rostral migratory stream into the olfactory bulbs (OBs) where they disperse radially and generate functional interneurons that fine-tune odor discrimination. NSCs within the SGZ generate neuronal precursors that migrate short distance into the inner granule cell layer of the DG where they become functionally integrated into the existing network (Gage, 2000; Taupin and Gage, 2002; Zhao et al., 2008; Ming and Song, 2011; Aimone et al., 2014; Lim and Alvarez-Buylla, 2016). Hippocampal newborn neurons contribute to the formation of certain types of memories such as episodic and spatial memory (Kropff et al., 2015), as well as regulation of mood (Sahay and Hen, 2007) or stress (Snyder et al., 2011; Anacker et al., 2018). Adult neurogenesis is increased by various stimuli like an enriched environment, running and learning via neurotransmitters, hormones or growth factors (Kempermann et al., 1997, 2002; Nilsson et al., 1999; van Praag et al., 1999a,b; Shors et al., 2001; van Praag et al., 2005; Leuner et al., 2006; Lledo et al., 2006; Kobilo et al., 2011; Mustroph et al., 2012; Alvarez et al., 2016). In addition, endogenous NSCs can be activated by traumatic brain injury (Arvidsson et al., 2002; Parent et al., 2002; Thored et al., 2006; Hou et al., 2008; Liu et al., 2009).

In this study, we show that injury of the spinal cord transiently activates distantly located hippocampal stem cells. Some activated stem cells generate neurons in the hippocampal DG that transiently improve performance of injured mice in spatial memory and stress related tasks as compared to uninjured controls. Notably, we identify the interferon-gamma/CD95

signaling as necessary for activation of NSCs by a remote injury. In summary, our study unveils an immune-CNS interaction leading to injury-mediated activation of hippocampal neurogenesis.

MATERIALS AND METHODS

Animals

For the experiments we used the following mouse lines: C57BL/6N, NesCreER^{T2}CD95flox [B6.Cg-Tg(Nestin-Cre/Ers1)#GSc Fastm1Cgn] and IFNα-/IFNγ-R-KO [B6.Cg.Ifnar1tm1Agt Ifngr1tm1Agt/Agt]. Six weeks old NesCreER^{T2}CD95flox (Cre^{+}) and respective controls (Cre^{-}) were intraperitoneally (i.p.) injected with 1 mg Tamoxifen (Sigma) twice a day for five consecutive days before operating. At the age of 12 weeks the respective group of mice received a sham or spinal transection injury as previously described (Letellier et al., 2010). For short term labeling of NSCs, mice received i.p. 5-bromo-2-deoxyuridine (BrdU; Sigma; 300 mg/kg bw) injections at 1 h, 24 h and 48 h post injury or a single shot injection 89 days post injury (**Figures 1A**, **4A,E**), followed by a chase time of 1 day, 2 weeks or 4 weeks, respectively. For the long term label retaining experiment (**Supplementary Figure S1A**), 8-week-old mice received a daily single shot injection of BrdU (50 mg/kg bw) for a total duration of 3 weeks followed by a chase time of 17 weeks after the last BrdU injection. By giving a single shot of BrdU we were able to label a precise number of proliferating cells at a very specific time point. Multiple shots of BrdU were used to label enough amount of cells at the beginning, which would then allow having enough cells at the longer time points, and thus statistical power. The same BrdU-labeling protocol was used in (Seib et al., 2013), in which caspase-3 staining excluded any increase in apoptosis. For the isolation of primary NSCs, 8 weeks old C57BL/6N mice were used. All animals were housed in the animal facilities of the German Cancer Research Center (DKFZ) at a 12 h dark/light cycle with free access to food and water. For the injury and behavioral experiments, exclusively age-matched female mice were used. All animal experiments were performed in accordance with the institutional guidelines of the DKFZ and were approved by the "Regierungspräsidium Karlsruhe," Germany.

Spinal Cord Injury

Female, age-matched animals were subjected to laminectomy at spine T7-T8 followed by a 80% transaction of the spinal cord injury by cutting the spinal cord with iridectomy scissors, as described in (Demjen et al., 2004; Stieltjes et al., 2006; Letellier et al., 2010). Sham mice were subjected only to laminectomy. Naïve mice did not face any surgical procedure.

Handling of the Animals

Mice were habituated to the handling experimenter before starting with behavioral experiments. To this end, mice were handled for 5–10 min twice a day. Handling was performed for at least 5 days until the animals showed no anxiety-related behavior when meeting the experimenter.

Spontaneous Alternation in the T-Maze

Spatial working memory performance was assessed on an elevated wooden T-Maze as described in (Corsini et al., 2009). Each animal had 4 sessions on the T-Maze (1 session/day; 4 trials/session). One trial consisted of a choice and a sample run. During the choice run one of the two target arms was blocked by a barrier according to a pseudorandom sequence, with equal numbers of left and right turns per session and with no more than two consecutive turns in the same direction. The mice were allowed to explore the accessible arm. Before the sample run (intertrial interval of ∼10 s), the barrier was removed enabling accessibility to both arms. On the sample run the mouse was replaced back into the start arm facing the experimenter. The mouse was allowed to choose one of the two target arms. The trial was classified as success if the animal chose the previously blocked arm. For analysis all trials were combined and the success rate (%) was quantified [(# successful trials/# trials)*100].

Restraint Stress Test

The mice were placed in a 50 ml canonical tube, equipped with a sufficient amount of breathing holes, for a duration of 30 min. Afterwards the mice were placed back into their housing cages for 30 min. Subsequently, blood samples of each mouse were isolated and the corticosterone (CORT) concentration was measured by using a CORT ELISA (IBL).

Immunohistochemistry

Animals were sacrificed by using an overdose of Ketamin (120 mg/kg)/Xylazine (20 mg/kg) and were subsequently transcardially perfused with 20 ml 1× HBSS (Gibco) and 10 ml of 4% paraformaldehyde (Carl Roth). The brains were dissected and postfixed in 4% paraformaldehyde overnight at 4°C. A Leica VT1200 Vibratome was used to cut the tissue in 50 μm thick coronal sections. From each mouse six identical brain sections for DG and SVZ every 100 μm along the coronal axis were used for quantification. First, the brain sections were washed 3× 15 min at room temperature in TBS, followed by a 1 h blocking step in TBS^{++} (TBS with 0.3% horse serum (Millipore) and 0.25% Triton-X100 (Sigma)) at room temperature. Tissue was transferred to 0.5 ml Safe Lock Reaction-Tubes containing 200 μl TBS^{++} including primary antibodies. Samples were incubated for 24–48 h at 4°C. After incubating with primary antibody, tissue samples were washed 3× 15 min in TBS at room temperature, followed by a 30 min blocking step in TBS^{++} at room temperature. Brain sections were transferred to 0.5 ml Safe Lock Reaction-Tubes containing 200 μl TBS^{++} including secondary antibodies. Samples were incubated in the dark, for 2 h at room temperature. Finally the brain slices were washed 4× 10 min in TBS at room temperature, before they were further floated in 0.1M PB-Buffer and mounted on glass slides with Fluoromount G (eBioscience). The following antibodies were used: rat anti-BrdU (Abcam, 1/150), goat anti-DCX (Santa Cruz, 1/200), guinea pig anti-DCX (Merck, 1/400), rabbit anti-S100b (Abcam, 1/100), mouse anti-GFAP (Merck Millipore, 1/300), goat anti-Sox2 (Abcam, 1/200) and mouse anti-NeuN (Merck Millipore, 1/800). Nuclei were counterstained with Hoechst 33342 (Biotrend, 1/4,000).

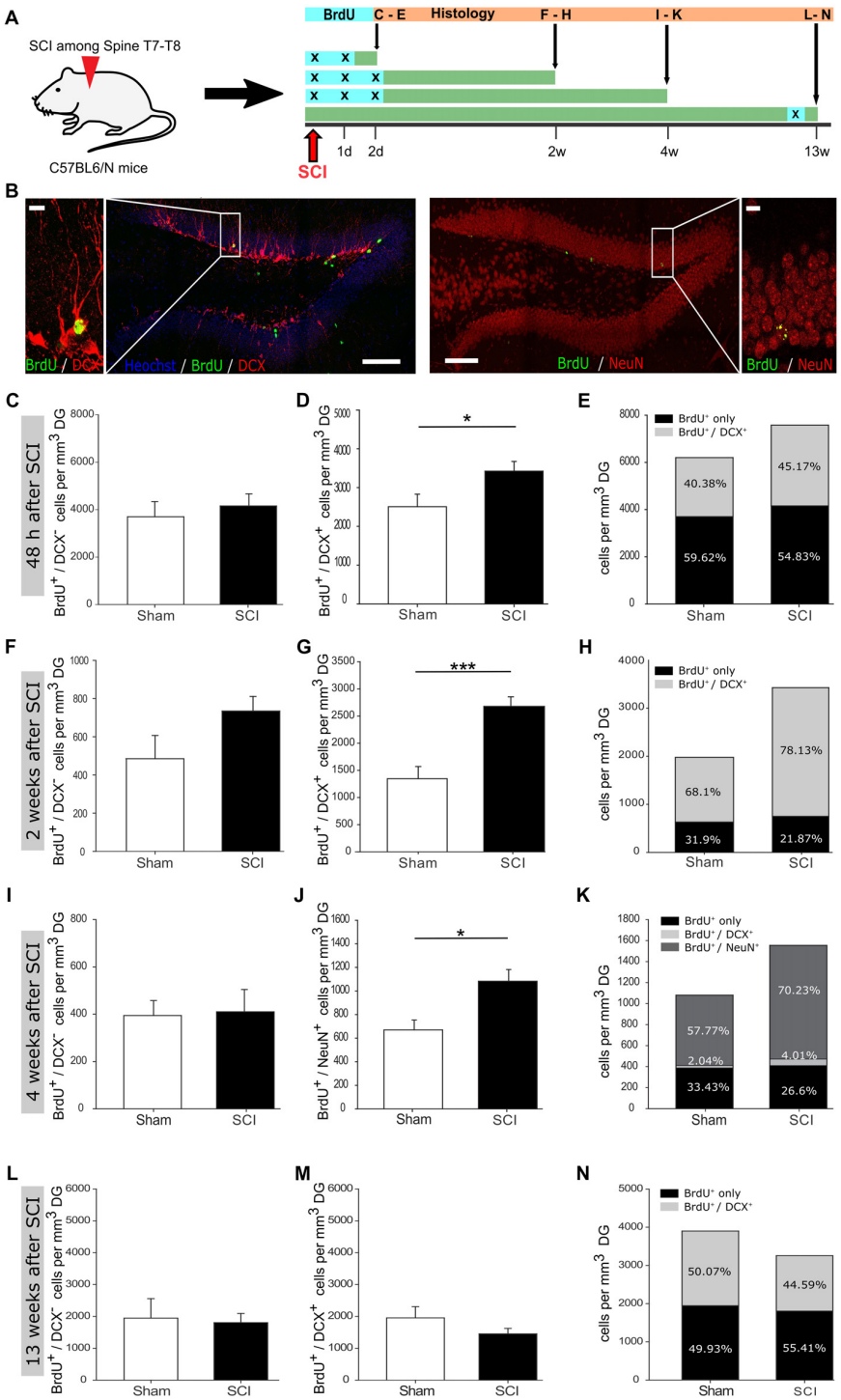

FIGURE 1 | Increased hippocampal neurogenesis upon distant spinal cord injury. **(A)** Schematic illustration of the experimental timeline performed with C57BL/6N mice. **(B)** 5-Bromo-2-deoxyuridine (BrdU) incorporation within the dentate gyrus (DG) of adult mice; scale bar is 100 μm or 10 μm, respectively. **(C)** Quantification of $BrdU^+/DCX^-$ cells 48 h post injury in sham vs. SCI mice (3,698 ± 561 vs. 4,156 ± 434 cells/mm^3 DG); $n_{sham} = 6$ vs. $n_{SCI} = 6$. **(D)** Quantification of $BrdU^+/DCX^+$ cells 48 h post injury, in sham vs. SCI mice (2,505 ± 323 vs. 3,422 ± 249 cells/mm^3 DG); $n_{sham} = 6$ vs. $n_{SCI} = 6$. **(E)** Percentage distribution of $BrdU^+/DCX^+$ cells 48 h post injury in sham vs. SCI mice (40.38% vs. 45.17%). **(F)** Quantification of $BrdU^+/DCX^-$ cells 2 weeks post injury in sham vs. SCI mice (485 ± 109 vs. 734 ± 70 cells/mm^3 DG); $n_{sham} = 5$ vs. $n_{SCI} = 6$. **(G)** Quantification of $BrdU^+/DCX^+$ cells 2 weeks post injury in sham vs. SCI mice (1,345 ± 224 vs. 2,677 ± 175 cells/mm^3 DG); $n_{sham} = 6$ vs. $n_{SCI} = 6$. **(H)** Percentage distribution of $BrdU^+/DCX^+$ cells 2 weeks post injury in sham vs. SCI mice (68.1% vs. 78.13%). **(I)** Quantification of $BrdU^+/DCX^-$ cells 4 weeks post injury in sham vs. SCI mice (394 ± 57 vs. 410 ± 86 cells/mm^3 DG); $n_{sham} = 5$ vs. $n_{SCI} = 6$. **(J)** Quantification

(*Continued*)

FIGURE 1 | Continued
of $BrdU^+/NeuN^+$ cells 4 weeks post injury in sham vs. SCI mice (669 ± 83 vs. 1,082 ± 99 cells/mm^3 DG); $n_{sham} = 6$ vs. $n_{SCI} = 6$. **(K)** Percentage distribution 4 weeks post injury of $BrdU^+/NeuN^+$ cells in sham vs. SCI mice (57.77% vs. 70.23%) and $BrdU^+/DCX^+$ cells in sham vs. SCI (2.04% vs. 4.01%). **(L)** Quantification of $BrdU^+/DCX^-$ cells 13 weeks post injury in sham vs. SCI mice (1,947 ± 558 vs. 1,805 ± 270 cells/mm^3 DG); $n_{sham} = 6$ vs. $n_{SCI} = 8$. **(M)** Quantification of $BrdU^+/DCX^+$ cells 13 weeks post injury in sham vs. SCI mice (2,005 ± 382 vs. 1,452 ± 159 cells/mm^3 DG); $n_{sham} = 5$ vs. $n_{SCI} = 8$. **(N)** Percentage distribution of $BrdU^+/DCX^+$ cells 13 weeks post injury in sham vs. SCI mice (50.07% vs. 44.59%). All mice were 12 weeks old at the time of injury/sham-injury. Cell numbers are given as mean values (±SEM); $^*p < 0.05$, $^{***}p < 0.001$; Student's *t*-test.

Microscopy and Cell Quantification

All images were acquired with a Leica TCS SP5 AOBS confocal microscope (Leica) equipped with a UV diode 405 nm laser, an argon multiline (458–514 nm) laser, a helium-neon 561 nm laser and a helium-neon 633 nm laser. Images were acquired as multichannel confocal stacks (Z-plane distance 2 μm) in 8-bit format by using a 20× (HCX PL FLUOTAR L NA0.40) oil immersion objective. Images were processed and analyzed in ImageJ (NIH). For representative images, the maximum intensity of a variable number of Z-planes was stacked, to generate the final Z-projections. Representative images were adjusted for brightness and contrast, applied to the entire image, cropped, transformed to RGB color format and assembled into figures with Inkscape. For cell quantification the entire volume of the DG was calculated by multiplying the entire area of the DG (middle plane of the total Z-stack) with the entire Z-stack size. The different cell populations were identified and counted (LOCI and Cell-Counter pug-in for ImageJ) based on their antibody labeling profile. Cell counts were either represented as cells/mm^3 DG or as cells/DG.

In vitro Culturing and Treatment of NSCs with INFγ

The lateral SVZ was microdissected as a whole mount as previously described (Mirzadeh et al., 2010). Tissue of one mouse was digested with trypsin and DNase according to the Neural Tissue Dissociation Kit (Miltenyi Biotec) in a Gentle MACS Dissociator (Miltenyi Biotec). Cells were cultured and expanded for 8–12 days in Neurobasal medium (Gibco) supplemented with B27 (Gibco), Heparine (Sigma), Glutamine (Gibco), Pen/Strep (Gibco), EGF (PromoKine) and FGF (PeloBiotech) as used in (Walker and Kempermann, 2014). For stimulation with INFγ (Millipore), 4×10^5 cells were seeded. The next day, cells were treated with 50 ng INFγ/ml media for duration of 14 h.

Flow Cytometric Analysis

The cells were harvested and were treated with Accutase (Sigma) for 5 min at 37°C, followed by filtering the cells with a 40 μm cell strainer to get a single cell suspension. Afterwards the cells were washed twice with FACS media (PBS/10%FCS) and were re-suspend in 200 μl FACS media. Cells were stained for 30 min at room temperature by using the Jo2 CD95::PECy7 antibody (BD Pharming/ 1/100). Afterwards the cells were washed three times with FACS media and were finally re-suspend in 200 μl FACS media.

Statistics

Statistical analysis was performed with SigmaPlot Student's *T*-Test, Mann-Whitney Rank Sum Test and one sided ANOVA. The respective statistical analysis as well as *p*-values is indicated in figure legends.

RESULTS

Distinct Activation of Hippocampal Neurogenesis Following Spinal Cord Injury

To assess whether a remote CNS injury would activate NSCs in the SGZ, we injured the spinal cord at thoracic level T7-T8. In order to detect the reaction of SGZ-NSCs and their neurogenic progeny, we labeled these cells with BrdU (once daily) at the time of injury and in the following 24 h, 48 h or after 89 days and examined them at 2 days, 2 weeks, 4 weeks and 13 weeks following injury (**Figure 1A**). Brains were stained for BrdU, to follow actively dividing NSCs and transient amplifying progenitors (TAPs) cells on their transition to $BrdU^+/DCX^+$ neuroblasts and $BrdU^+/NeuN^+$ newborn neurons (**Figure 1B**). Already 48 h after injury, we observed a significant increase in new-born neuroblasts (**Figures 1C–E**). Two weeks following injury, the number of neuroblasts remained significantly higher when compared to sham-injured controls (**Figure 1G**). The population of $BrdU^+/DCX^-$ that encompass NSCs and TAPs showed a clear trend towards higher numbers in injured compared to sham-operated mice (**Figures 1F,H**). We therefore, proceed to specifically addressed NSCs in the DG 2 weeks after injury by staining for BrdU and the NSC specific markers Sox2 and GFAP as well as the astrocyte marker S100b and neuroblast marker DCX (**Figures 2A,B**). The number of $BrdU^+/Sox2^+/GFAP^+$ NSCs was significantly increased in spinal cord injured mice as compared to sham controls (**Figure 2C**). We further assessed the maturation of BrdU-labeled cells to neurons ($BrdU^+/NeuN^+$) at 4 weeks after the injury. Significantly more newborn neurons were identified in the DG of the injured mice, whereas the number of $BrdU^+/DCX^-$ cells was comparable in injured and sham controls (**Figures 1I–K**). This 61.7% increase in newborn neurons is surprisingly high, since already an increase of 13% of newborn DG-neurons in the aging hippocampus through increased Wnt activity dramatically improved the performance of the animals in hippocampal-dependent memory tasks (Seib et al., 2013). Notably, at 13 weeks following injury, the number of cycling $BrdU^+/DCX^-$ cells and newborn neuroblasts was set back to basal levels, exhibiting similar numbers to that of its sham operated counterparts (**Figures 1L–N**).

Injury has been shown to activate a pool of highly dormant cells in the hematopoietic system (Wilson et al., 2008; Essers et al., 2009; Essers and Trumpp, 2010). To test if this is also the case for SGZ-NSCs, we used a 3 weeks BrdU-labeling protocol starting at the age of 8 weeks and allowed a chase time of

16 weeks after the last BrdU injection. Mice were subjected to spinal cord injury at 14 weeks chase time or left uninjured and sacrificed 2 weeks later to follow the reaction to injury of the highly dormant NSCs (**Supplementary Figure S1A**). Notably, the number of BrdU$^+$ cells in the DG was significantly reduced in injured mice as compared to sham controls (**Supplementary Figures S1B,C**). Since, it is known that a local injury to the brain activates the migration of NSCs in close vicinity out of the neurogenic niche (Nakatomi et al., 2002; Grande et al., 2013), we assessed a potential migration of BrdU-labeled cells to the neighboring regions of the fimbria-fornix (FF) and corpus callosum (CC; **Supplementary Figure S1B**). The number of BrdU-labeled cells in FF and CC regions was higher in injured than naïve counterparts (**Supplementary Figures S1D,E**). In summary our data suggest that spinal cord injury activates local neurogenesis within the SGZ of the DG, and reduces the fraction of a dormant label-retaining cells within the SGZ. Further studies shall further address the nature of these label retaining cells and whether they migrate out to nearby regions.

We next assess whether spinal cord injury would also activate neuronal production in NSCs within the other V-SVZ neurogenic niche (**Figures 2D–H**). Notably, the total numbers of BrdU-labeled cells, BrdU-NSCs or neuroblasts were comparable in sham and SCI animals (**Figures 2F–H**). Together, our data shows that distant spinal cord injury stimulates a fast but transient activation of NSCs residing in the remote SGZ of

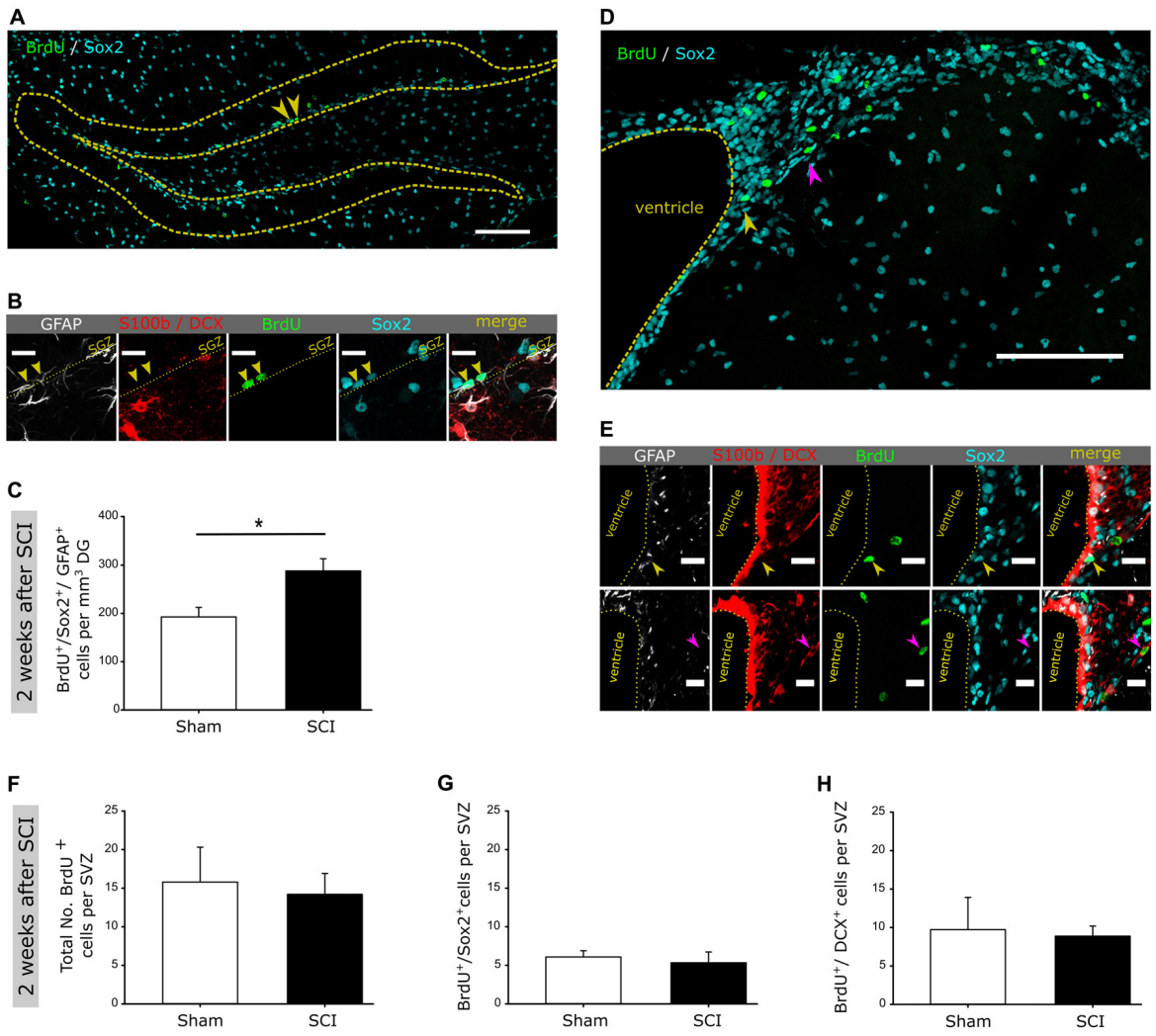

FIGURE 2 | SCI does not affect neurogenesis within the ventricular-subventricular zone (V-SVZ). **(A)** Representative image of BrdU incorporation into Sox2 positive cells within the DG; scale bar is 100 μm. **(B)** Detailed image of a BrdU$^+$/Sox2$^+$/GFAP$^+$ positive cell within the DG; scale bar is 15 μm. **(C)** Quantification of BrdU$^+$/Sox2$^+$/GFAP$^+$ cells in the DG 2 weeks post injury in sham vs. SCI mice (192 ± 39 vs. 288 ± 50 cells/mm^3 DG). **(D)** Representative image of BrdU incorporation into Sox2 positive cells within the V-SVZ; scale bar is 100 μm. **(E)** Detailed image of a BrdU$^+$/Sox2$^+$ and BrdU$^+$/DCX$^+$ cell within the V-SVZ; scale bar is 15 μm. **(F)** Quantification of the total number of BrdU$^+$ cells in the V-SVZ 2 weeks post injury in sham vs. SCI mice (16 ± 5 vs. 14 ± 3 cells per SVZ). **(G)** Quantification of the total number of BrdU$^+$/Sox2$^+$ cells in the V-SVZ 2 weeks post injury in sham vs. SCI mice (6 ± 1 vs. 5 ± 2 cells per SVZ). **(H)** Quantification of the total number of BrdU$^+$/DCX$^+$ cells in the V-SVZ 2 weeks post injury in sham vs. SCI mice (10 ± 4 vs. 8 ± 1 cells per SVZ). All mice were 12 weeks old at the time of injury/sham-injury; group size n_{naive} = 4 vs. n_{SCI} = 4. Cell numbers are given as mean values (± SEM); *$p < 0.05$; Mann-Whitney Rank Sum Test.

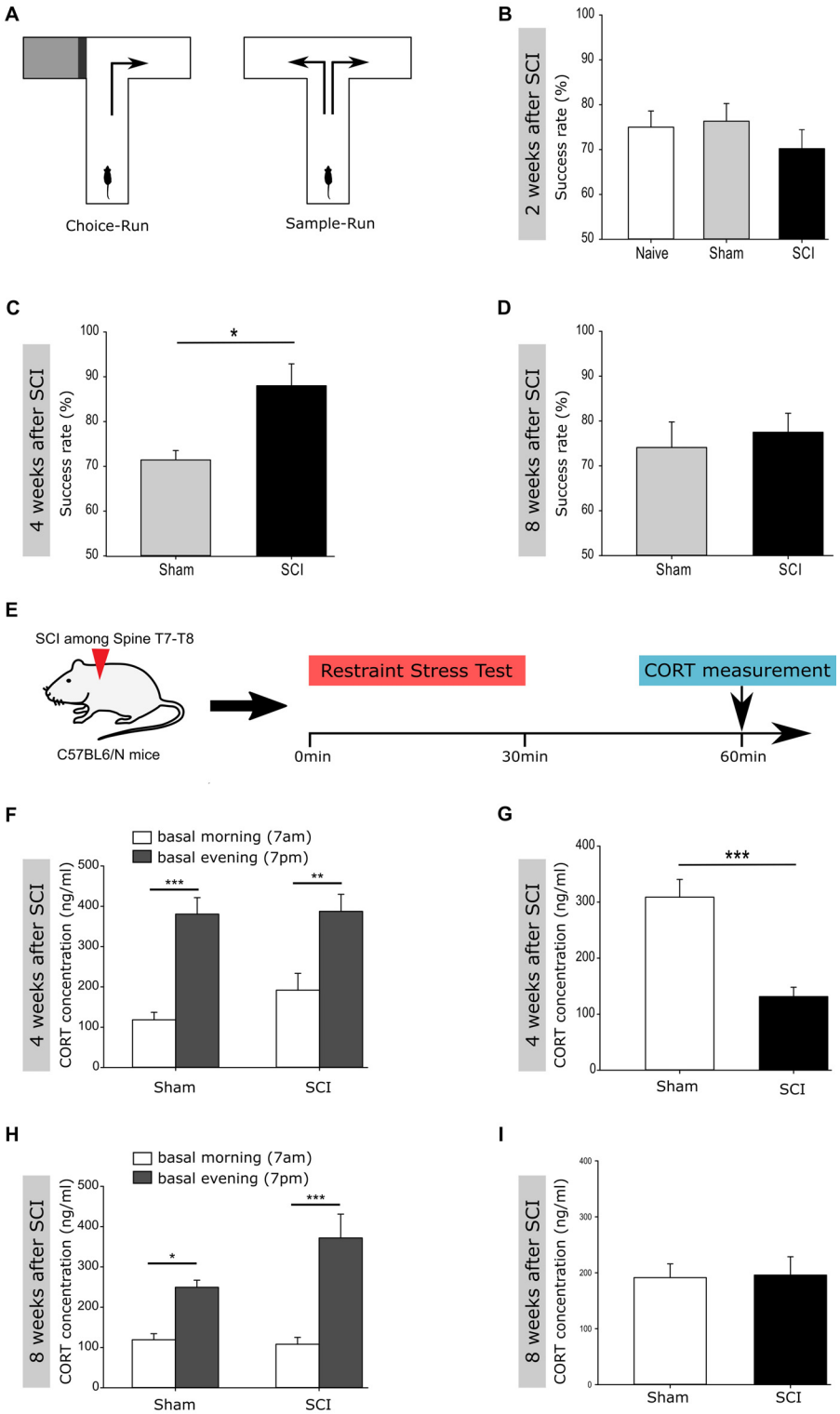

FIGURE 3 | Improved performance in a Working Memory task and in buffering acute stress following spinal cord injury. **(A)** Experimental setup for the spontaneous alternation in the T-Maze test. **(B)** Success rate 2 weeks post injury of naïve vs. sham vs. SCI mice (75% ± 3.29 vs. 76.34% ± 3.80 vs. 70.19% ± 4.09); n_{naive} = 6 vs. n_{sham} = 14 vs. n_{SCI} = 13. **(C)** Success rate 4 weeks post injury of sham vs. SCI mice (71.43% ± 5.15 vs. 88% ± 4.38); group size, n_{sham} = 7 vs. n_{SCI} = 5; Mann-Whitney Rank Sum Test. **(D)** Success rate 8 weeks post injury of sham vs. SCI mice (74.11% ± 5.27 vs. 77.5% ± 3.79); group size, n_{sham} = 7 vs. n_{SCI} = 5. **(E)** Experimental setup to perform the restraint stress test. **(F)** Basal corticosterone (CORT) concentration 4 weeks post injury in $sham_{morning}$ vs. $sham_{evening}$ (118.2 ± *(Continued)*

FIGURE 3 | Continued
18.7 vs. 380.6 ± 40.9 ng/ml) and $SCI_{morning}$ vs. $SCI_{evening}$ (191.7 ± 42 vs. 387.5 ± 42.3 ng/ml); n_{sham} = 14 vs. n_{SCI} = 14; one way ANOVA. **(G)** CORT concentration 4 weeks post injury after the restraint stress test in sham vs. SCI mice (309 ± 31.6 vs. 131.3 ± 16.8 ng/ml); n_{sham} = 14 vs. n_{SCI} = 14; Mann-Whitney Rank Sum Test. **(H)** Basal CORT concentration 8 weeks post SCI in $sham_{morning}$ vs. $sham_{evening}$ (119 ± 15.2 vs. 249.5 ± 17.6 ng/ml) and $SCI_{morning}$ vs. $SCI_{evening}$ (108 ± 17 vs. 371.9 ± 59.1 ng/ml); n_{sham} = 13 vs. n_{SCI} = 13; one way ANOVA. **(I)** CORT concentration 8 weeks post SCI after the restraint stress test in sham vs. SCI mice (191.4 ± 24.6 vs. 196 ± 32.8 ng/ml); n_{sham} = 13 vs. n_{SCI} = 13. All mice were 12 weeks old at the time of injury/sham-injury. Succes rate and CORT concentration are given as mean values (±SEM); $^{*}p < 0.05$, $^{**}p < 0.01$, $^{***}p < 0.001$.

the DG to generate neurons, but not in the V-SVZ of the lateral ventricles. How a distant injury specifically affects local hippocampal NSCs through interferons will be subject of future studies.

Spinal Cord Injury Leads to Better Working Memory and an Improved Buffering of Acute Stress

Together, we see that the injury activates both, normal homeostatic neurogenesis and decreases the pool of highly dormant stem cells potentially by activating their migration out of the DG. Therefore, we next tested the function of the injury-induced surplus of newborn neurons within the hippocampus of injured mice, homeostatic neurogenesis. Adult hippocampal neurogenesis has been shown to positively impact short- and long-term spatial working memory, navigation learning, pattern discrimination as well as trace and contextual fear conditioning (Corsini et al., 2009; Deng et al., 2010; Aimone et al., 2011), but also to counteract depression- and stress-induced behavioral responses (Sahay and Hen, 2007; Snyder et al., 2011). To test the function of injury-induced newborn neurons in the DG, we tested the performance of injured and naïve mice in a hippocampal-dependent task, the spontaneous alternation on an elevated T-Maze, used as readout of short term spatial working memory (**Figure 3A**). Even if spinal cord injured mice definitely experience motor dysfunctions, no differences between the injured and sham-injured group were detected in terms of reaction time/decision time while performing the elevated T-Maze test. Mice were tested at 2, 4 and 8 weeks following spinal cord injury. At 2 weeks post-injury naïve, sham and spinal cord injured mice showed a similar success rate of the spontaneous alternation (**Figure 3B**). Importantly, at 4 weeks following injury, the success rate of injured mice was significantly higher than the rate of Sham controls (**Figure 3C**). Notably, the improved performance of injured mice on the T-Maze disappeared at 8 weeks post-injury (**Figure 3D**).

Another reported function of newborn DG-neurons is buffering of acute stress, which would be very beneficial following injury (Snyder et al., 2011). To test the behavioral response to an acute stress situation, we performed a restraint stress test (**Figure 3E**) at 4 and 8 weeks following spinal cord or sham-injury. CORT, a corticosteroid that is produced in the cortex of the adrenal glands and released into the blood stream, is classically used as readout for various stress situations in rodents (Gong et al., 2015). The basal CORT concentration within the bloodstream of rodents is increased during daytime under homeostatic conditions, as shown in the tested groups before the stress test (**Figures 3F,H**). At 4 weeks post-injury the injured mice showed significantly lower levels of CORT in the bloodstream as compared to the sham-injured mice (**Figure 3G**). Notably, at 8 weeks following injury the CORT levels exhibit similar blood concentrations following restraint stress in both experimental groups (**Figure 3I**).

Taken together, our data demonstrated that newly generated neurons integrate into the existing hippocampal network and positively influence the performance of injured mice in a hippocampal-dependent spatial memory task and in buffering acute stress situations. However, as the observed activation of neurogenesis, the functional improvement is also transient. Interestingly, we previously observed a transient increase in neurogenesis following exercise that improved performance on the T-Maze in an equally transient mode (Corsini et al., 2009). Thus, our data suggest that newborn functionally immature neurons impact short term memory and the buffering of acute stress as long as they are young and plastic. However, this effect disappears as they become similar to their older counterparts (Kropff et al., 2015).

Loss of IFNα-/IFNγ-R and CD95 Inhibits Neural Stem Cell Activation Upon Spinal Transection Injury

Acute tissue injury activates an immediate inflammatory response that is able to rapidly affect distant locations. Notably, we previously identified interferons as an activator of NSCs in the V-SVZ following a global ischemic insult that induces damage in the nearby located striatum (Llorens-Bobadilla et al., 2015). The requirement of IFNγ signaling for SCI-mediated activation of SGZ-NSCs was further tested using mice deficient in IFNα-/IFNγ-receptor (**Figure 4A**) as compared to wt counterparts (**Figures 1F–H**). Excitingly, 2 weeks following injury, IFNα-/IFNγ-receptor deficient mice did neither show a significant increase in the population of neuroblasts ($BrdU^{+}/DCX^{+}$), nor in the population of $BrdU^{+}/DCX^{-}$ cells (**Figures 4B–D**). These observations indicated that spinal transection injury does not activate SGZ-NSCs lacking a functional IFNα/IFNγ-signaling-pathway. We next investigated the putative signaling pathways involved in local SCI-mediated activation of SGZ-NSCs. Interferons have been reported to increase the expression of CD95-ligand and CD95 (Chow et al., 2000; Kirchhoff et al., 2002; Boselli et al., 2007). In a previous study we demonstrated that the TNF-R family member, CD95, is required for the activation of SGZ-NSCs following global ischemia (Corsini et al., 2009). To test the regulation of CD95 upon IFNγ treatment in NSCs, we isolated NSCs from the V-SVZ of 8 weeks old C57BL/6N mice, cultured them *in vitro* for short time and exposed them for 14 h to IFNγ. Thereafter expression of CD95 was analyzed by Flow Cytometry. IFNγ significantly increased the expression of CD95 in NSCs as

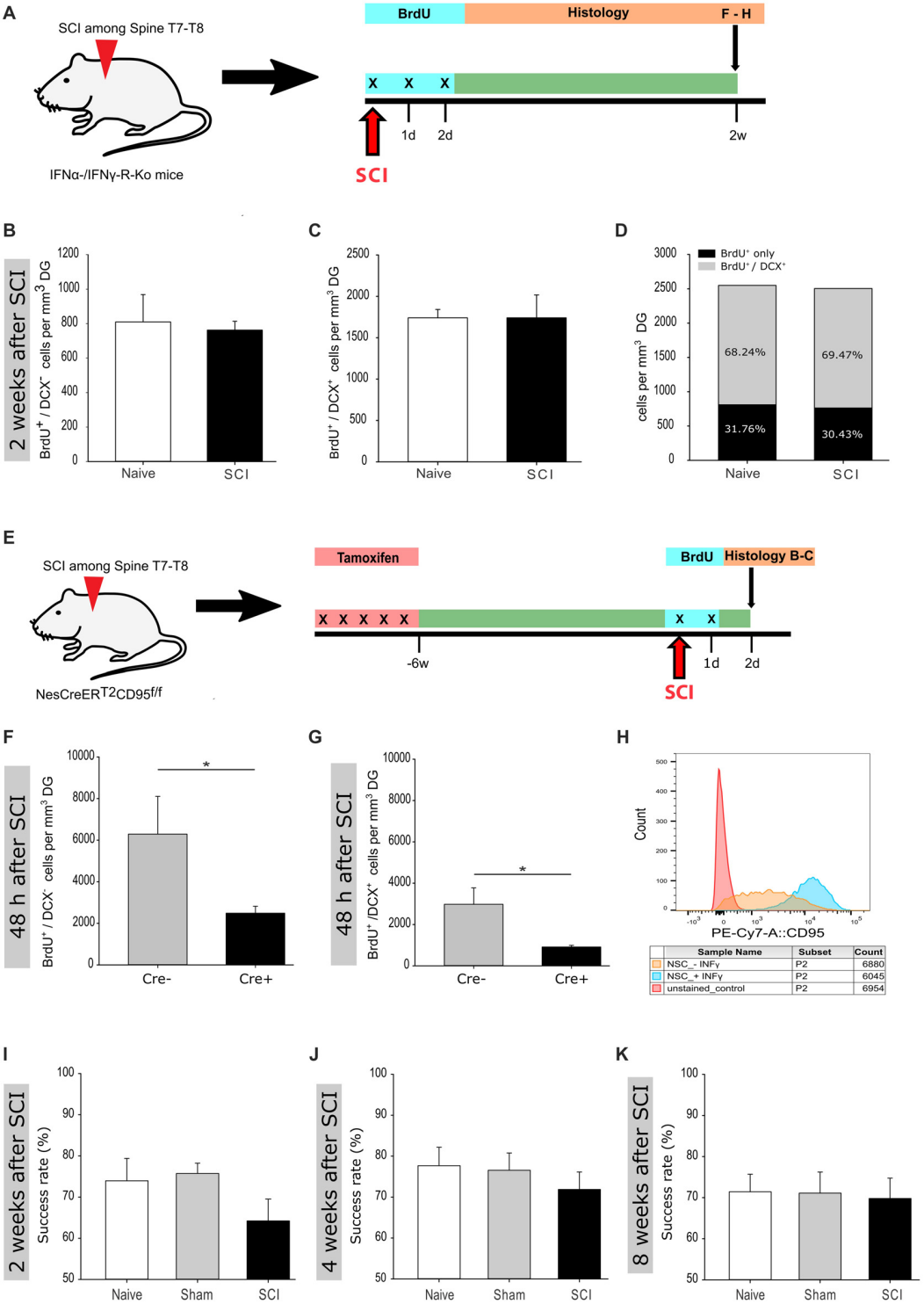

FIGURE 4 | Reduced activation of adult hippocampal neurogenesis in IFNα-/IFNγ-R and CD95-Ko upon spinal cord injury. **(A)** Illustration of the experimental timeline performed with IFNα-/IFNγ-R-Ko mice. **(B)** Quantification of $BrdU^+/DCX^-$ cells 2 weeks post injury in naïve vs. SCI mice (809 ± 158 vs. 762 ± 51 cells/mm^3 DG); $n_{naive} = 4$ vs. $n_{SCI} = 5$. **(C)** Quantification of $BrdU^+/DCX^+$ cells 2 weeks post injury in naïve vs. SCI mice (1,740 ± 101 vs. 1,741 ± 276 cells/mm^3 DG); $n_{naive} = 4$ vs. $n_{SCI} = 5$. **(D)** Percentage distribution of $BrdU^+/DCX^+$ cells 2 weeks post injury in naïve vs. SCI mice (68.24 vs. 69.47%). **(E)** Illustration of the experimental timeline performed with NesCreER^{T2}CD95$^{f/f}$ mice. **(F)** Quantification of $BrdU^+/DCX^-$ cells 48 h post injury in injured Cre^- vs. injured Cre^+ mice (6,292 ± 2,899 vs. 2,486 ± 662 cells/mm^3 DG); $n_{Cre-} = 6$ vs. $n_{Cre+} = 6$; Student's *t*-test. **(G)** Quantification of $BrdU^+/DCX^+$ cells 48 h post injury in injured Cre^- vs. injured Cre^+ mice

(*Continued*)

FIGURE 4 | Continued
(2,976 ± 1,591 vs. 910 ± 157 cells/mm^3 DG); n_{Cre-} = 6 vs. n_{Cre+} = 6; Student's *t*-test. **(H)** Relative CD95 expression in unstained control, INFγ-untreated and -treated cells are illustrated in a single parameter histogram. **(I)** Success rate 2 weeks post injury of naïve vs. sham vs. SCI mice (73.96% ± 4.98 vs. 75.75% ± 2.33 vs. 64.22% ±4.62); n_{naive} = 6 vs. n_{sham} = 8 vs. n_{SCI} = 8. **(J)** Success rate 4 weeks post injury of naïve vs. sham vs. SCI mice (77.68% ± 4.49 vs. 76.56% ± 3.95 vs. 71.88 ± 3.98); n_{naive} = 7 vs. n_{sham} = 8 vs. n_{SCI} = 8. **(K)** Success rate 8 weeks post injury of naïve vs. sham vs. SCI mice (71.43% ± 4.28 vs. 71.09% ± 4.81 vs. 69.79 ± 3.91); n_{naive} = 7 vs. n_{sham} = 8 vs. n_{SCI} = 6. All mice were 12 weeks old at the time of injury/sham-injury. Cell numbers and success rate are given as mean (±SEM); $^*p < 0.05$.

compared to untreated NSCs (**Figure 4H** and **Supplementary Figure S2**). To assess CD95's involvement in SCI-induced neurogenesis we used the NesCreER^{T2}CD95$^{f/f}$ mouse line. This mouse line enables an acute deletion of CD95 in the adult NSC compartment (Corsini et al., 2009). CD95NesCreER^{T2+} (Cre$^+$) and CD95NesCreER^{T2-} (Cre$^-$) mice received tamoxifen injections at 6 weeks of age. Their spinal cord was injured at the age of 12 weeks. Dividing cells were labeled by BrdU at the time of injury and 24 h post injury. The SGZ was further processed for staining of BrdU and DCX 48 h after the surgery (**Figure 4E**). CD95-deficient NSCs exhibit an impaired injury-induced activation, as significantly fewer BrdU$^+$/DCX$^-$cells and newborn neuroblasts (BrdU$^+$/DCX$^+$) could be detected in the SGZ of Cre$^+$ mice as compared to their injured Cre$^-$ counterparts (**Figures 4F,G**). Thus, CD95 is locally involved in activation of SGZ-NSCs by a remote injury. Next, we set out to test if the injury-induced improvement of the spatial working-memory is due to the increased activation of NSCs. Indeed, injured and sham operated IFNα-/IFNγ-receptor deficient mice showed a similar success rate in the spontaneous alternation in the elevated T-Maze (**Figures 4I–K**). Thus, interferon-related increase of homeostatic neurogenesis mediates the functional improvement in short-term working memory exhibited by spinal injured animals. Altogether, our results indicate that injury-induced IFN signaling triggers CD95 activation of SGZ-NSCs, thereby leading to a transient expansion of the pool of newborn neurons resulting in an improved working memory.

DISCUSSION

Here, we examine how a remote injury to the CNS influences distally located SGZ-NSCs, short and long term post-injury. Our data clearly show an acute and transiently increased activation of adult SGZ-NSCs to produce neurons following a remote injury and suggest that a fraction of highly dormant stem cells are activated to migrate out of the neurogenic niche. Notably, we show that the newly generated neurons functionally integrate into the existing network, as demonstrated in an elevated spatial navigation performance, spontaneous alternations on a T-Maze test, which provides a very sensitive test to detect dysfunction of the hippocampus in rodents (Deacon and Rawlins, 2006; Zhang et al., 2004). In addition, SCI mice exhibited a higher ability to buffer acute restraint stress than control counterparts, consistent with the previously reported role of hippocampal neurogenesis in regulating the hypothalamic-pituitary-adrenal axis (Snyder et al., 2011).

However, this activation of neurogenesis fades away with time. Accordingly, two studies investigated the effects of spinal cord injury to the neurogenic niches in adult *Sprague-Dawley* rats and detected a decreased level of adult V-SVZ and SGZ neurogenesis 60 days post spinal cord injury (Felix et al., 2012; Jure et al., 2017). Besides, studies of hematopoietic stem cell (HSC) activation by inflammatory signals, show that an acute exposure activates the quiescent population of HSCs, whereas chronic exposure negatively impact HSC activation (Essers et al., 2009).

As already hypothesized by Felix et al. (2012) and in line with Essers et al. (2009), we show that inflammatory signatures, released in an acute phase post spinal cord injury, play a major role in transmitting the injury signal towards the hippocampus to activate adult neurogenesis. It is known that an injury to the spinal cord would activate a multiphase immune response including macrophage/microglia activation within the spinal cord (Letellier et al., 2010; Abdanipour et al., 2013). Using single cell transcriptomics we identified activation of an interferon-gamma-response in NSCs as necessary for injury-induced activation of V-SVZ NSCs in a model of global ischemia (Llorens-Bobadilla et al., 2015). However, also in this setting we could not detect expression of the interferon transcripts in stem cells or niche cells, other than microglia. Interferon mRNAs are very low abundant and thus hardly to detect in most non-immune cells. In the aging brain interferon mRNA was detected in the plexus choroideus in rodents and humans (Baruch et al., 2014). We can only speculate that in the case of stroke and of a distant spinal injury local microglia, plexus choroideus or systemic signals provide the upstream regulator of the interferon-response in NSCs.

In the current study, we identify interferons as the main factor that transmits the injury signal from the spinal cord towards the hippocampus, where through activation of CD95 stem cells exit the quiescent state to differentiate into neurons. This results are consistent with the previously reported role of CD95 in activation of hippocampal NSCs following a global ischemic injury (Corsini et al., 2009). In NSCs CD95 does not induce apoptosis, but on the contrary, increases their survival and differentiation. Notably, transplantation of CD95-activated NSCs, but not of control non treated counterparts, rescued the hippocampal-related memory deficits following global ischemia (Corsini et al., 2009). This study also showed that CD95-deficient mice show a reduced basal level of neurogenesis within the DG. However, running activity was able to activate CD95-deficient NSCs within the DG, which makes it even more remarkable, that SCI fails to do so (Corsini et al., 2009). Expression of CD95-ligand increased following ischemic injury to the brain in humans and rodents. In a follow up study, characterizing the single cell transcriptomes of NSCs in the ischemic SVZ, we detected an injury-induced increase of cells expressing CD95 transcripts, that was lower in interferon-receptor deficient mice (Llorens-Bobadilla et al., 2015).

The observed transition from a quiescent to an active state, triggered by a distant injury site, in effects seems to be similar to the transition from G_0 to an elevated G_{alert} state in muscle

satellite cells (Rodgers et al., 2014). Interestingly, this alert state is triggered in distant stem cells in contralateral muscles, and is also observed in other tissue stem cells such as HSCs (Rodgers et al., 2014). Stem cells in an alert state are primed for cell cycle entry to react in a much faster and efficient way to incoming injuries of different nature. Here, we show that a remote CNS injury triggers different responses in actively dividing and dormant NSCs. While actively dividing NSCs are engaged in homeostasis, the fraction of dormant cells decreases, presumably to take potential alternative migratory pathways to injury-associated areas. Of course, local activation and proliferation of glia cells might play a role and should not be underestimated, but these astrocytes would have been proliferating at the time of labeling and only become reactivated by local brain injury, which is a less probable behavior. However, future studies are needed to follow up the fate of these highly dormant stem cells.

What could be the role of an increased production of granule cell neurons in the hippocampus? Certainly, spinal cord injury represents a very stressful state for the whole organism. It has been shown that adult hippocampal neurogenesis is on the one hand strongly influenced by chronic and acute stress (Conrad et al., 1999; Kirby et al., 2013; LaDage, 2015), on the other hand increased neurogenesis ameliorates stress (Snyder et al., 2011; Anacker et al., 2018). We show that spinal cord injury buffers acute restraint stress, and this buffering disappears when active neurogenesis does. Thus, we hypothesized that injury-induced neurogenesis buffers stress and thereby improves behavioral adaptation to the post-traumatic situation.

In summary, our data show that an acute injury to the spinal cord activates hippocampal neurogenesis, resulting in a transiently increased production of newborn neurons that are functional, as shown by the improved performance in spatial memory tasks of injured mice. Furthermore, we identified interferons as a major factor involved in activation via CD95 of distant stem cells.

AUTHOR CONTRIBUTIONS

SDe performed experiments involving cell counts, interferon, stress, behavioral read out following spinal injury, analyzed and interpreted data, and wrote the manuscript. WP-KL and LG performed spinal injuries. MS: experiments related to interferon in stem cell cultures. SDä and AN: cell counts following spinal injuries in wt and CD95ko mice, analyzed and interpreted related data. AM-V: project design and oversight, data interpretation, and wrote the manuscript.

FUNDING

This work was supported by the German Cancer Research Center (DKFZ), the German Science Foundation (SFB 873) and the German Federal Ministry of Education and Research (BMBF).

ACKNOWLEDGMENTS

We thank C. Pitzer and the members of the Interdisciplinary Neurobehavioral Core (INBC); M. Essers for Ifngr1$^{-/-}$ and Ifnar$^{-/-}$ mice; S. Limpert, K. Volk and M. Richter for technical assistance; the Light Microscopy Core Facility; the DKFZ Flow Cytometry Core Facility; and the members of the Martin-Villalba laboratory for critically reading the manuscript.

SUPPLEMENTARY MATERIAL

The Supplementary Material for this article can be found online at: https://www.frontiersin.org/articles/10.3389/fnmol.2018.00443/full#supplementary-material

FIGURE S1 | Dormant NSCs are activated following spinal transection injury. **(A)** Schematic illustration of the experimental timeline for labeling dormant NSCs in the DG of adult C57BL/6N mice. **(B)** Representative coronal section of the adult mouse brain with designated regions for the quantification of BrdU$^+$ labeled cells. **(C)** Quantification of BrdU$^+$ labeled cells in the DG in sham vs. SCI mice (11,437 ± 1,255 vs. 7,532 ± 1,017 cells/mm^3 DG); n_{sham} = 5 vs. n_{SCI} = 11. **(D)** Quantification of BrdU$^+$ labeled cells in the FF in naïve vs. SCI mice (4,010 ± 913 vs. 6,326 ± 906 cells/mm^3 FF); n_{naive} = 4 vs. n_{SCI} = 6. **(E)** Quantification of BrdU$^+$ labeled cells in the CC in naïve vs. SCI mice (1,848 ± 665 vs. 7,210 ± 2,829 cells/mm^3 CC); n_{naive} = 4 vs. n_{SCI} = 6. All mice were 28 weeks old at the time of injury/sham-injury. Cell numbers are given as mean (±SEM); $^*p < 0.05$; Student's *t*-test.

FIGURE S2 | Related to **Figure 4**. Strategy to determine relative CD95 expression in cultured NSCs by using Flow Cytometry. First gate uses FSC/SSC gating to exclude cellular debris; second gate excludes cell aggregates and third shows relative CD95 expression in unstained control cells **(A)**, stained IFNγ-untreated cells **(B)** and stained IFNγ-treated cells **(C)**.

REFERENCES

Abdanipour, A., Tiraihi, T., Taheri, T., and Kazemi, H. (2013). Microglial activation in rat experimental spinal cord injury model. *Iran. Biomed. J.* 17, 214–220. doi: 10.6091/ibj.1213.2013

Aimone, J. B., Deng, W., and Gage, F. H. (2011). Resolving new memories: a critical look at the dentate gyrus, adult neurogenesis and pattern separation. *Neuron* 70, 589–596. doi: 10.1016/j.neuron.2011.05.010

Aimone, J. B., Li, Y., Lee, S. W., Clemenson, G. D., Deng, W., and Gage, F. H. (2014). Regulation and function of adult neurogenesis: from genes to cognition. *Physiol. Rev.* 94, 991–1026. doi: 10.1152/physrev.00004.2014

Alvarez, D. D., Giacomini, D., Yang, S. M., Trinchero, M. F., Temprana, S. G., Büttner, K. A., et al. (2016). A disynaptic feedback network activated by experience promotes the integration of new granule cells. *Science* 354, 459–465. doi: 10.1126/science.aaf2156

Anacker, C., Luna, V. M., Stevens, G. S., Millette, A., Shores, R., Jimenez, J. C., et al. (2018). Hippocampal neurogenesis confers stress resilience by inhibiting the ventral dentate gyrus. *Nature* 559, 98–102. doi: 10.1038/s41586-018-0262-4

Arvidsson, A., Collin, T., Kirik, D., Kokaia, Z., and Lindvall, O. (2002). Neuronal replacement from endogenous precursors in the adult brain after stroke. *Nat. Med.* 8, 963–970. doi: 10.1038/nm747

Baruch, K., Deczkowska, A., David, E., Castellano, J. M., Miller, O., Kertser, A., et al. (2014). Aging. Aging-induced type I interferon response at the choroid plexus negatively affects brain function. *Science* 346, 89–93. doi: 10.1126/science.1252945

Boselli, D., Losana, G., Bernabei, P., Bosisio, D., Drysdale, P., Kiessling, R., et al. (2007). IFN-γ regulates Fas ligand expression in human CD4+ T lymphocytes and controls their anti-mycobacterial cytotoxic functions. *Eur. J. Immunol.* 37, 2196–2204. doi: 10.1002/eji.200636541

Chow, W. A., Fang, J. J., and Yee, J. K. (2000). The IFN regulatory factor family participates in regulation of Fas ligand gene expression in T cells. *J. Immunol.* 164, 3512–3518. doi: 10.4049/jimmunol.164.7.3512

Conrad, C. D., Lupien, S. J., and McEwen, B. S. (1999). Support for a bimodal role for type II adrenal steroid receptors in spatial memory. *Neurobiol. Learn. Mem.* 72, 39–46. doi: 10.1006/nlme.1998.3898

Corsini, N. S., Sancho-Martinez, I., Laudenklos, S., Glagow, D., Kumar, S., Letellier, E., et al. (2009). The death receptor CD95 activates adult neural stem cells for working memory formation and brain repair. *Cell Stem Cell* 5, 178–190. doi: 10.1016/j.stem.2009.05.004

Deacon, R. M. J., and Rawlins, J. N. P. (2006). T-maze alternation in the rodent. *Nat. Protoc.* 1, 7–12. doi: 10.1038/nprot.2006.2

Demjen, D., Klussmann, S., Kleber, S., Zuliani, C., Stieltjes, B., Metzger, C., et al. (2004). Neutralization of CD95 ligand promotes regeneration and functional recovery after spinal cord injury. *Nat. Med.* 10, 389–395. doi: 10.1038/nm1007

Deng, W., Aimone, J. B., and Gage, F. H. (2010). New neurons and new memories: how does adult hippocampal neurogenesis affect learning and memory? *Nat. Rev. Neurosci.* 11, 339–350. doi: 10.1038/nrn2822

Essers, M. A. G., Offner, S., Blanco-Bose, W. E., Waibler, Z., Kalinke, U., Duchosal, M. A., et al. (2009). IFNα activates dormant haematopoietic stem cells *in vivo*. *Nature* 458, 904–908. doi: 10.1038/nature07815

Essers, M. A. G., and Trumpp, A. (2010). Targeting leukemic stem cells by breaking their dormancy. *Mol. Oncol.* 4, 443–450. doi: 10.1016/j.molonc.2010.06.001

Felix, M.-S., Popa, N., Djelloul, M., Boucraut, J., Gauthier, P., Bauer, S., et al. (2012). Alteration of forebrain neurogenesis after cervical spinal cord injury in the adult rat. *Front. Neurosci.* 6:45. doi: 10.3389/fnins.2012.00045

Gage, F. H. (2000). Mammalian neural stem cells. *Science* 287, 1433–1438. doi: 10.1126/science.287.5457.1433

Gong, S., Miao, Y. L., Jiao, G. Z., Sun, M. J., Li, H., Lin, J., et al. (2015). Dynamics and correlation of serum cortisol and corticosterone under different physiological or stressful conditions in mice. *PLoS One* 10:e0117503. doi: 10.1371/journal.pone.0117503

Grande, A., Sumiyoshi, K., López-Juárez, A., Howard, J., Sakthivel, B., Aronow, B., et al. (2013). Environmental impact on direct neuronal reprogramming *in vivo* in the adult brain. *Nat. Commun.* 4:2373. doi: 10.1038/ncomms3373

Hou, S. W., Wang, Y. Q., Xu, M., Shen, D. H., Wang, J. J., Huang, F., et al. (2008). Functional integration of newly generated neurons into striatum after cerebral ischemia in the adult rat brain. *Stroke* 39, 2837–2844. doi: 10.1161/strokeaha.107.510982

Jure, I., Pietranera, L., De Nicola, A. F., and Labombarda, F. (2017). Spinal cord injury impairs neurogenesis and induces glial reactivity in the hippocampus. *Neurochem. Res.* 42, 2178–2190. doi: 10.1007/s11064-017-2225-9

Kempermann, G., Gast, D., and Gage, F. H. (2002). Neuroplasticity in old age: sustained fivefold induction of hippocampal neurogenesis by long-term environmental enrichment. *Ann. Neurol.* 52, 135–143. doi: 10.1002/ana.10262

Kempermann, G., Kuhn, H. G., and Gage, F. H. (1997). More hippocampal neurons in adult mice living in an enriched environment. *Nature* 386, 493–495. doi: 10.1038/386493a0

Kirby, E. D., Muroy, S. E., Sun, W. G., Covarrubias, D., Leong, M. J., Barchas, L. A., et al. (2013). Acute stress enhances adult rat hippocampal neurogenesis and activation of newborn neurons via secreted astrocytic FGF2. *Elife* 2:e00362. doi: 10.7554/eLife.00362

Kirchhoff, S., Sebens, T., Baumann, S., Krueger, A., Zawatzky, R., Li-Weber, M., et al. (2002). Viral IFN-regulatory factors inhibit activation-induced cell death via two positive regulatory IFN-regulatory factor 1-dependent domains in the CD95 ligand promoter. *J. Immunol.* 168, 1226–1234. doi: 10.4049/jimmunol.168.3.1226

Kobilo, T., Liu, Q.-R., Gandhi, K., Mughal, M., Shaham, Y., and van Praag, H. (2011). Running is the neurogenic and neurotrophic stimulus in environmental enrichment. *Learn. Mem.* 18, 605–609. doi: 10.1101/lm.2283011

Kropff, E., Yang, S. M., and Schinder, A. F. (2015). Dynamic role of adult-born dentate granule cells in memory processing. *Curr. Opin. Neurobiol.* 35, 21–26. doi: 10.1016/j.conb.2015.06.002

LaDage, L. D. (2015). Environmental change, the stress response, and neurogenesis. *Integr. Comp. Biol.* 55, 372–383. doi: 10.1093/icb/icv040

Letellier, E., Kumar, S., Sancho-Martinez, I., Krauth, S., Funke-Kaiser, A., Laudenklos, S., et al. (2010). CD95-ligand on peripheral myeloid cells activates Syk kinase to trigger their recruitment to the inflammatory site. *Immunity* 32, 240–252. doi: 10.1016/j.immuni.2010.01.011

Leuner, B., Waddell, J., Gould, E., and Shors, T. J. (2006). Temporal discontiguity is neither necessary nor sufficient for learning-induced effects on adult neurogenesis. *J. Neurosci.* 26, 13437–13442. doi: 10.1523/jneurosci.2781-06.2006

Lim, D. A., and Alvarez-Buylla, A. (2016). The adult ventricular—subventricular zone (V-SVZ) and olfactory bulb (OB) neurogenesis. *Cold Spring Harb. Perspect. Biol.* 8:a018820. doi: 10.1101/cshperspect.a018820

Liu, F., You, Y., Li, X., Ma, T., Nie, Y., Wei, B., et al. (2009). Brain injury does not alter the intrinsic differentiation potential of adult neuroblasts. *J. Neurosci.* 29, 5075–5087. doi: 10.1523/jneurosci.0201-09.2009

Lledo, P.-M., Alonso, M., and Grubb, M. S. (2006). Adult neurogenesis and functional plasticity in neuronal circuits. *Nat. Rev. Neurosci.* 7, 179–193. doi: 10.1038/nrn1867

Llorens-Bobadilla, E., Zhao, S., Baser, A., Saiz-Castro, G., Zwadlo, K., and Martin-Villalba, A. (2015). Single-cell transcriptomics reveals a population of dormant neural stem cells that become activated upon brain injury. *Cell Stem Cell* 17, 329–340. doi: 10.1016/j.stem.2015.07.002

Ming, G.-L., and Song, H. (2011). Adult neurogenesis in the mammalian brain: significant answers and significant questions. *Neuron* 70, 687–702. doi: 10.1016/j.neuron.2011.05.001

Mirzadeh, Z., Doetsch, F., Sawamoto, K., Wichterle, H., and Alvarez-Buylla, A. (2010). The subventricular zone en-face: wholemount staining and ependymal flow. *J. Vis. Exp.* 39:1938. doi: 10.3791/1938

Mustroph, M. L., Chen, S., Desai, S. C., Cay, E. B., DeYoung, E. K., and Rhodes, J. S. (2012). Aerobic exercise is the critical variable in an enriched environment that increases hippocampal neurogenesis and water maze learning in male C57BL/6J mice. *Neuroscience* 219, 62–71. doi: 10.1016/j.neuroscience.2012.06.007

Nakatomi, H., Kuriu, T., Okabe, S., Yamamoto, S., Hatano, O., Kawahara, N., et al. (2002). Regeneration of hippocampal pyramidal neurons after ischemic brain injury by recruitment of endogenous neural progenitors. *Cell* 110, 429–441. doi: 10.1016/s0092-8674(02)00862-0

Nilsson, M., Perfilieva, E., Johansson, U., Orwar, O., and Eriksson, P. S. (1999). Enriched environment increases neurogenesis in the adult rat dentate gyrus and improves spatial memory. *J. Neurobiol.* 39, 569–578. doi: 10.1002/(sici)1097-4695(19990615)39:4<569::aid-neu10>3.0.co;2-f

Parent, J. M., Vexler, Z. S., Gong, C., Derugin, N., and Ferriero, D. M. (2002). Rat forebrain neurogenesis and striatal neuron replacement after focal stroke. *Ann. Neurol.* 52, 802–813. doi: 10.1002/ana.10393

Rodgers, J. T., King, K. Y., Brett, J. O., Cromie, M. J., Charville, G. W., Maguire, K. K., et al. (2014). mTORC1 controls the adaptive transition of quiescent stem cells from G0 to G(Alert). *Nature* 510, 393–396. doi: 10.1038/nature13255

Sahay, A., and Hen, R. (2007). Adult hippocampal neurogenesis in depression. *Nat. Neurosci.* 10, 1110–1115. doi: 10.1038/nn1969

Seib, D. R. M., Corsini, N. S., Ellwanger, K., Plaas, C., Mateos, A., Pitzer, C., et al. (2013). Loss of Dickkopf-1 restores neurogenesis in old age and counteracts cognitive decline. *Cell Stem Cell* 12, 204–214. doi: 10.1016/j.stem.2012.11.010

Shors, T. J., Miesegaes, G., Beylin, A., Zhao, M., Rydel, T., and Gould, E. (2001). Neurogenesis in the adult is involved in the formation of trace memories. *Nature* 410, 372–376. doi: 10.1038/35066584

Snyder, J. S., Soumier, A., Brewer, M., Pickel, J., and Cameron, H. A. (2011). Adult hippocampal neurogenesis buffers stress responses and depressive behaviour. *Nature* 476, 458–461. doi: 10.1038/nature10287

Stieltjes, B., Klussmann, S., Bock, M., Umathum, R., Mangalathu, J., Letellier, E., et al. (2006). Manganese-enhanced magnetic resonance imaging for *in vivo* assessment of damage and functional improvement following spinal cord injury in mice. *Magn. Reson. Med.* 55, 1124–1131. doi: 10.1002/mrm.20888

Taupin, P., and Gage, F. H. (2002). Adult neurogenesis and neural stem cells of the central nervous system in mammals. *J. Neurosci. Res.* 69, 745–749. doi: 10.1002/jnr.10378

Thored, P., Arvidsson, A., Cacci, E., Ahlenius, H., Kallur, T., Darsalia, V., et al. (2006). Persistent production of neurons from adult brain stem cells during recovery after stroke. *Stem Cells* 24, 739–747. doi: 10.1634/stemcells.2005-0281

van Praag, H., Christie, B. R., Sejnowski, T. J., and Gage, F. H. (1999a). Running enhances neurogenesis, learning, and long-term potentiation in mice. *Proc. Natl. Acad. Sci. U S A* 96, 13427–13431. doi: 10.1073/pnas.96.23.13427

van Praag, H., Kempermann, G., and Gage, F. H. (1999b). Running increases cell proliferation and neurogenesis in the adult mouse dentate gyrus. *Nat. Neurosci.* 2, 266–270. doi: 10.1038/6368

van Praag, H., Shubert, T., Zhao, C., and Gage, F. H. (2005). Exercise enhances learning and hippocampal neurogenesis in aged mice. *J. Neurosci.* 25, 8680–8685. doi: 10.1523/jneurosci.1731-05.2005

Walker, T. L., and Kempermann, G. (2014). One mouse, two cultures: isolation and culture of adult neural stem cells from the two neurogenic zones of individual mice. *J. Vis. Exp.* 84:e51225. doi: 10.3791/51225

Wilson, A., Laurenti, E., Oser, G., van der Wath, R. C., Blanco-Bose, W., Jaworski, M., et al. (2008). Hematopoietic stem cells reversibly switch from dormancy to self-renewal during homeostasis and repair. *Cell* 135, 1118–1129. doi: 10.1016/j.cell.2008.10.048

Zhang, W.-N., Pothuizen, H. H. J., Feldon, J., and Rawlins, J. N. P. (2004). Dissociation of function within the hippocampus: effects of dorsal, ventral and complete excitotoxic hippocampal lesions on spatial navigation. *Neuroscience* 127, 289–300. doi: 10.1016/j.neuroscience.2004.05.007

Zhao, C., Deng, W., and Gage, F. H. (2008). Mechanisms and functional implications of adult neurogenesis. *Cell* 132, 645–660. doi: 10.1016/j.cell.2008.01.033

Conflict of Interest Statement: The authors declare that the research was conducted in the absence of any commercial or financial relationships that could be construed as a potential conflict of interest.

The reviewer SDM and handling editor declared their shared affiliation at time of review.

frontiers in Neuroscience

REVIEW
published: 26 March 2019
doi: 10.3389/fnins.2019.00283

Direct Neuronal Reprogramming Reveals Unknown Functions for Known Transcription Factors

Gaia Colasante[1†], Alicia Rubio[1,2†], Luca Massimino[1] and Vania Broccoli[1,2]*

[1] Stem Cell and Neurogenesis Unit, Division of Neuroscience, San Raffaele Scientific Institute, Milan, Italy, [2] CNR Institute of Neuroscience, Milan, Italy

In recent years, the need to derive sources of specialized cell types to be employed for cell replacement therapies and modeling studies has triggered a fast acceleration of novel cell reprogramming methods. In particular, in neuroscience, a number of protocols for the efficient differentiation of somatic or pluripotent stem cells have been established to obtain a renewable source of different neuronal cell types. Alternatively, several neuronal populations have been generated through direct reprogramming/transdifferentiation, which concerns the conversion of fully differentiated somatic cells into induced neurons. This is achieved through the forced expression of selected transcription factors (TFs) in the donor cell population. The reprogramming cocktail is chosen after an accurate screening process involving lists of TFs enriched into desired cell lineages. In some instances, this type of studies has revealed the crucial role of TFs whose function in the differentiation of a given specific cell type had been neglected or underestimated. Herein, we will speculate on how the *in vitro* studies have served to better understand physiological mechanisms of neuronal development *in vivo*.

Keywords: stem cells, cell reprogramming, neuronal differentiation, brain development, transcription factor

OPEN ACCESS

Edited by:
Annalisa Buffo,
University of Turin, Italy

Reviewed by:
Mengqing Xiang,
Sun Yat-sen University, China
Eumorphia Remboutsika,
National and Kapodistrian University of Athens Medical School, Greece

***Correspondence:**
Vania Broccoli
broccoli.vania@hsr.it

†These authors share first authorship

Specialty section:
This article was submitted to Neurogenesis, a section of the journal Frontiers in Neuroscience

Received: *12 November 2018*
Accepted: *11 March 2019*
Published: *26 March 2019*

Citation:
Colasante G, Rubio A, Massimino L and Broccoli V (2019) Direct Neuronal Reprogramming Reveals Unknown Functions for Known Transcription Factors. Front. Neurosci. 13:283. doi: 10.3389/fnins.2019.00283

INTRODUCTION

Over the years, crucial extrinsic and intrinsic mechanisms regulating the acquisition of cell fate during neural development have been elucidated. Gradients of morphogens secreted by organizer centers instruct neural progenitor cells (NPCs) to activate the expression of transcription factor (TF) cascades that guide cells through every single step of the fate acquisition process. Genetic studies *in vitro* and *in vivo*, essentially based on the gain- and loss-of-function experiments, revealed that large arrays of TF cascades are indeed responsible for the specification of different neuronal subtypes.

This mechanistic knowledge was critical for the field of cell reprogramming to emerge. Indeed, the possibility to convert a cell type into another has been strictly dependent on seminal findings accumulated over the last 30 years in neurodevelopmental biology.

Back in the 1950s, it was not yet clear whether all cells belonging to the same organism contained the same set of genes. On this line, Weismann had suggested that genes whose function was no longer required might be lost or permanently inactivated in a specific cell type, seeding the concept that cell fate acquisition is an irreversible process being associated with loss of genetic material. This concept, well represented by the famous Waddington's landscape (Waddington, 1957) was later challenged by Gurdon's work. He performed pioneer experiments of somatic nuclei transfer

in *Xenopus* oocytes during his Ph.D. studies, providing the first evidence for the preservation of genome integrity after cellular differentiation (Gurdon, 1962).

Up to date, it is consolidated the concept that epigenetic-mediated gene silencing, rather than gene loss, accompanies cell fate acquisition. This evidence opened a crack toward the plasticity of cell identity and the possibility of altering the fate of a differentiated cell.

In 1988, *MyoD* ectopic expression in mouse embryonic fibroblasts (MEFs) was revealed sufficient to convert them into muscle cells (Tapscott et al., 1988). Two decades later the breakthrough from the Yamanaka's group showed that somatic cells can be reverted to a pluripotent state forcing the expression of the four factors *Oct4, Sox2, Klf4,* and *c-Myc* (Takahashi and Yamanaka, 2006), that are mediating global chromatin remodeling allowing for the expression of the pluripotency gene machinery (Takahashi and Yamanaka, 2006; Boissart et al., 2012). First successful conversion of MEFs into functional induced neurons (iNs) was described a few years later through *Ascl1*, *Brn2,* and *Myt1l* misexpression (Vierbuchen et al., 2010). After this study, many others attempted to modify or enrich this TF combination to induce MEF differentiation toward specific neuronal subtypes localized to defined areas of the brain (reviewed in Masserdotti et al., 2016).

All these works highlighted the ability of accurately selected cocktail of TFs to alter the fate of fully differentiated cells and to obtain functional neuronal cells.

To define a cell reprogramming gene cocktail, the TFs to be tested in the screening are chosen for their capability to impose that specific neuronal fate (master regulator genes) or among genes enriched in the target cell population, but not necessarily with their functions already addressed. Very recently, unbiased screenings of TFs for neuronal conversion have been also performed with very informative results (Liu et al., 2018; Tsunemoto et al., 2018). Once the candidate TF list is selected, they are delivered in donor cells according to a "narrow down" or an "add one" strategy. Generally, TFs are delivered and expressed all simultaneously in the donor cells although they control different phases of the cell fate acquisition process. In other cases, genetic tricks (i.e., mix of constitutive promoter guided- and inducible promoter guided-TFs whose expression can be turned off at a defined time) are employed to allow sequential expression of TFs required in different phases of differentiation in a manner that tries to recapitulate the expression timing observed during *in vivo* development (Au et al., 2013; Colasante et al., 2015). Finally, in an even more sophisticated experimental setting, the endogenous loci of the desired TFs can be activated using the CRISPR/Cas9 system (Black et al., 2016; Liu et al., 2018). In all these cases, the final output of these studies can meet the initial expectations, but unpredicted results have not rarely been reported. In fact, in some instances, new features for the mechanisms of action of TFs have been emerging. In others, TFs whose role was not considered determining for a specific neuronal fate acquisition during *in vivo* development, have come out as pivotal in the neuronal specification during direct cell reprogramming. Even more surprisingly is the identification of TFs not related to neuronal development that are able to impose a neuronal identity when overexpressed in heterologous cells.

This predictive value of the direct cell reprogramming methodology can be likely explained by the fact that during this process selected TFs are forced to operate in donor cell populations that are very distant from the target neuronal cells. This is the case for the fibroblast-to-neuron conversion, as fibroblasts have a mesodermic origin in the embryo contrary to the ectoderm-derived neurons. According to this different ontogeny, fibroblasts present both divergent global gene expression profiles and chromatin states compared to neurons. In this "unfavorable environment," some neuronal TFs unexpectedly revealed to have a pioneer function being able to "open up" the chromatin and activate genes that are silenced in donor cells. Conversely, *in vivo*, their function might be facilitated by other TFs expressed earlier in the transcriptional cascades or their function might be hidden by complex gene regulation networks. With its ability to directly challenge TFs, the direct neuronal reprogramming provides a unique experimental system where to better appreciate their role in a relatively simple *in vitro* assay with a clear phenotypic analysis outcome.

NEW INSIGHTS INTO THE ROLES OF THE PRONEURAL TFs

Deepening Our Understanding of Classical Proneural TFs: *Ascl1* and *Neurog2*

Textbook developmental biology studies revealed that Achaete-scute homolog 1 (*Ascl1*) and Neurogenin2 (*Neurog2*) are the prominent pro-neural factors in charge of the neuronal identity specification in the nervous system (Horton et al., 1999; Bertrand et al., 2002; Parras et al., 2002; Mattar et al., 2004; Schuurmans et al., 2004; Britz et al., 2006; Poitras et al., 2007; Kovach et al., 2013). These two TFs are expressed in a complementary manner in the telencephalon: *Neurog*2 is expressed in dorsal progenitors and instruct them to generate glutamatergic neurons, whereas *Ascl1* is expressed in ventral progenitor cells contributing to the acquisition of GABAergic fate.

With this well-established background, it seemed pretty consistent that the forced expression of *Ascl1* was shown essential to obtain neurons from both murine and human fibroblasts (Vierbuchen et al., 2010; Caiazzo et al., 2011; Kim et al., 2011; Pfisterer et al., 2011; Torper et al., 2013; Colasante et al., 2015; **Table 1**). The relevant role of *Ascl1* has also been demonstrated in the reprogramming of other cell types that are more plastic than terminally differentiated fibroblasts or more closely related to neurons. Indeed, *Ascl1* alone can guide the conversion of murine or human embryonic stem cells (ESCs) (Chanda et al., 2014) and astrocytes (Berninger et al., 2007; Heinrich et al., 2010; Liu et al., 2015; Masserdotti et al., 2015; Chouchane et al., 2017) into neurons (**Table 1**).

Very soon in the field, an amazing difference in the ability in fibroblast-to-neuron conversion was observed between *Ascl1* and its glutamatergic *alter ego*, *Neurog2*. Indeed, several studies

indicated that the induction of *Neurog2* cannot reprogram fibroblasts efficiently while it can generate neurons when overexpressed in ESCs, induced pluripotent stem cells (iPSCs), NPCs and astrocytes (Berninger et al., 2007; Heinrich et al., 2010; Vierbuchen et al., 2010; Liu et al., 2013; Zhang et al., 2013; Busskamp et al., 2014; Chanda et al., 2014; Masserdotti et al., 2015; Ho et al., 2016; Orellana et al., 2016; Rubio et al., 2016; **Table 1**). As expected, in most of these cases the neurons acquired a glutamatergic identity. Only when it is induced in murine astrocytes of cerebellar origin, Neurog2 promotes the generation of GABAergic neurons in according to its role during embryo development where it drives the differentiation of GABAergic Purkinje cells (Florio et al., 2012; Chouchane et al., 2017).

The poor efficiency of *Neurog2* in the fibroblast-to-neuron conversion can be raised dramatically when *Neurog2* is expressed together with other transcriptional factors and/or in the presence of small molecules in the media (Son et al., 2011; Liu et al., 2012, 2013, 2015, 2016; Aravantinou-Fatorou et al., 2015; Blanchard et al., 2015).

We tried to clarify this intriguing difference between *Ascl1* and *Neurog2* in reprogramming efficiency of fibroblasts comparing side by side their direct molecular targets. To this aim, we took advantage of chromatin immunoprecipitation-sequencing (ChIP-seq) data already available in the literature. Smith et al. (2016) transduced MRC-5 human fetal fibroblasts with lentiviruses expressing either *ASCL1*, *NEUROG2,* or *NEUROG2* together with the small molecules forskolin and dorsomorphin to increase the reprogramming efficiency. Then, ChIP-seq analyses were performed at 2.5, 3, and 4 days after the infection for each condition and we cross-referenced the datasets merging all time points together (**Figure 1**). Focusing our attention on the conditions where (i) *ASCL1* or (ii) *NEUROG2* were induced, we found that *ASCL1* and *NEUROG2* share a consistent number of direct targets (1863) although maintaining many other exclusive (319+729 for ASCL1 and 811+5965 for NEUROG2) (**Figure 1A**).

Surprisingly, NEUROG2 targets are about nine times more abundant than those of ASCL1. Considering the difference in the reprogramming efficiency of these two TFs, we hypothesized that ASCL1 might be more efficient in the neuronal program activation by binding mainly neural genes among its targets. However, when we analyzed more deeply the top 30 GO (gene ontology) pathways targeted by *ASCL1,* we realized that most of them correlate with the activation of non-neural specific genes, i.e., GO related to alterations in intracellular pathways and metabolic changes (**Figure 1B**).

TABLE 1 | Summary of the TF combinations that include *Ascl1* or *Ngn2* to directly reprogram somatic or pluripotent cells into specific iN subtypes.

Factors	Source	iN main subtype	Reference
Ascl1, Brn2, Myt1l	Fibroblasts	GABA/Gluta	Vierbuchen et al., 2010; Pfisterer et al., 2011
Ascl1, Myt1l, NeuroD2, miR-9/9*, miR-124	Fibroblasts	GABA/Gluta	Yoo et al., 2011
Ascl1	Fibroblasts	GABA/Gluta	Chanda et al., 2014
Ascl1, Brn2, Myt1l	Fibroblasts	GABA/Gluta	Pereira et al., 2014
Ascl1, Brn2, Myt1l, Neurod1	Fibroblasts	Gluta	Pang et al., 2011
Ascl1, Sox2, FoxG1, Dlx5, Lhx6	Fibroblasts	GABA	Colasante et al., 2015
Ascl1, Brn2, Myt1l,Ngn2, Lhx3,Isl1, Hb9 (NeuroD1)	Fibroblasts	Motor	Son et al., 2011
Ascl1, Brn2, Myt1l, Lmx1a, Foxa2	Fibroblasts	Dopaminergic	Pfisterer et al., 2011
Ascl1, Nurr1, Lmx1a	Fibroblasts	Dopaminergic	Caiazzo et al., 2011
Ascl1, Pitx3	Fibroblasts	Dopaminergic	Kim et al., 2011
Ascl1, Brn2, Myt1l, Lmx1a, Lmx1b, FoxA2, Otx2	Fibroblasts	Dopaminergic	Torper et al., 2013
Ascl1, Dlx2	Astrocytes	GABA	Heinrich et al., 2010
Ascl1	Astrocytes	GABA	Chouchane et al., 2017
Ascl1, Nurr1, Lmx1b	Astrocytes	Dopaminergic	Addis et al., 2011
Ascl1	ESCs	GABA/Gluta	Chanda et al., 2014
Ascl1, Sox2, FoxG1, Dlx5, Lhx6	iPSCs	GABA	Colasante et al., 2015
Ascl1, Dlx2	ESCs, iPSCs	GABA	Yang et al., 2017
Ngn2, Ascl1	Fibroblasts	Gluta	Ladewig et al., 2012
Ngn2, Sox11, Isl1, Lhx3	Fibroblasts	Motor	Liu et al., 2015
Ngn2, Brn3a	Fibroblasts	Sensory	Blanchard et al., 2015
Ngn2, (Sox11)	Fibroblasts	Cholinergic	Liu et al., 2013; Smith et al., 2016
Ngn2	Astrocytes	Gluta	Heinrich et al., 2010; Chouchane et al., 2017
Ngn2, Bcl2	Astrocytes	Gluta	Gascón et al., 2016
Ngn2	Cerebellar Astrocytes	GABA	Chouchane et al., 2017
Ngn2	NPC	Gluta	Ho et al., 2016; Orellana et al., 2016
Ngn2	iPS, ESCs	Gluta	Zhang et al., 2013; Busskamp et al., 2014; Rubio et al., 2016

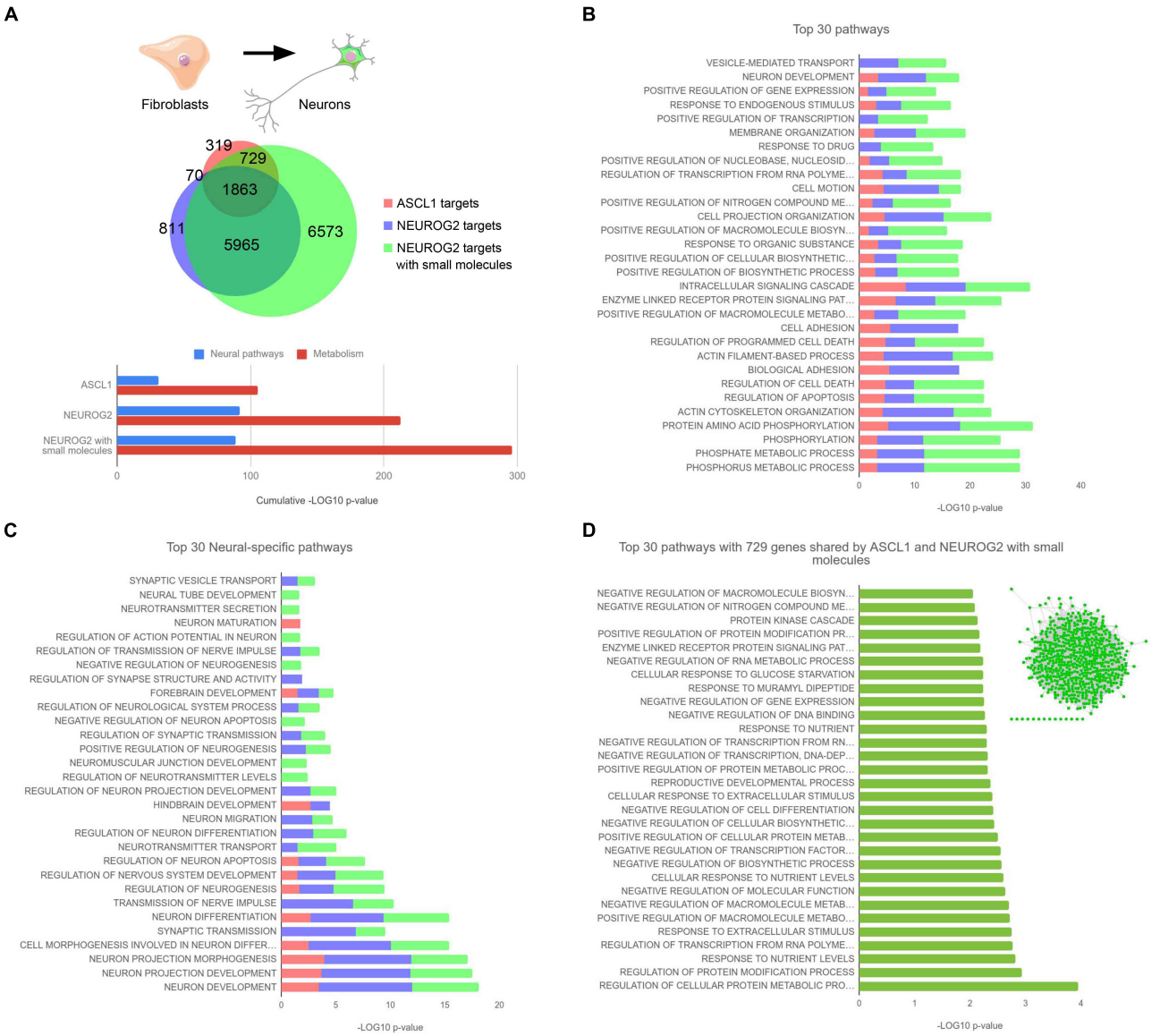

FIGURE 1 | (A) Area-proportional Venn diagram depicting the total number of ASCL1 and NEUROG2 targets. The proportion of shared targets for the 3 experimental conditions (ASCL1, NEUROG2, and NEUROG2 with small molecules) are indicated. Bottom, result summary showing the cumulative enrichment of neural or metabolic pathways in the 3 conditions. **(B)** Top 30 pathways enriched in the 3 experimental conditions. **(C)** Top 30 neural-specific pathways in the 3 experimental conditions. **(D)** Top 30 pathways of the 729 genes shared by ASCL1 and NEUROG2 with small molecules. Inset: gene network generated with the GeneMania Cytoscape plugin, built in accordance with Physical interactions, Co-expression, Co-localization, corresponding Pathway, and Genetic interactions showing one single molecular hub of 715 genes, with 636 edges and a clustering coefficient of 0.135. ChIP-seq peaks were downloaded from NCBI GEO (GSE43916, GSE63621, and GSE75912) and annotated with annotatePeaks (Heinz et al., 2010). Functional enrichment analysis was performed with DAVID (Huang da et al., 2009). Filtering, statistics, and plotting were performed within the R environment.

Very few of them were instead related to neural differentiation program, for example, neuronal development (GO 0048666) and alterations in the cytoskeleton and plasma membrane (GO 0016044, GO 0007155, GO 0030029, and GO 0030036). Interestingly, the top 30 targets of *NEUROG2* were classified in GO categories similar to the ones observed in the case of *ASCL1*. When we focused on the Top 30 neural-specific pathways, it clearly emerged that *NEUROG2* exhibited even a higher enrichment of genes promoting neuralization in comparison to *ASCL1* (**Figure 1C**), not confirming our initial hypothesis.

To add more information to this picture, we analyzed also ChIP-seq datasets of NEUROG2 in presence of small molecules: in this condition, the access of *NEUROG2* to chromatin is even more enhanced likely due to the chromatin remodeling mediated by the small molecules possibly through the activation of SOX4 (Smith et al., 2016). In particular, in the presence of forskolin and dorsomorphin, NEUROG2 is able to bind

to 729 novel genes that in the previous comparison were exclusive targets of ASCL1 (**Figure 1A**). Supposing that they contain the key genes responsible for the success of the reprogramming, we analyzed them more accurately. Again, we observed that these shared target genes do not belong mainly to neural categories (**Figure 1D**) suggesting that the activation of non-neural pathways, more than a prompt neuralization, is essential for the neuronal reprogramming in a "non-neuronal" context. Interestingly, we observe that most of these genes (715 out of 729) were either co-expressed, physically interacting, or belonging to the same molecular pathway, thus giving rise to a unique molecular network (**Figure 1D**, inset). This indicates that the activation of key regulatory genes that are connected to each other might guide the efficient conversion of fibroblasts into neurons. We also observed that 6573 targets are exclusive to the condition where the fibroblasts were treated with *NEUROG2* and the small molecules (**Figure 1A**). Since NEUROG2 in the presence of small molecules generates cholinergic neurons, differently from *ASCL1,* we believe that these genes or at least part of them might be involved in promoting the cholinergic fate. Alternatively, we cannot exclude that those targets themselves might be responsible for the acquired success of *NEUROG2* in the neuronal conversion process. In this case, the scenario would be different and would suggest that *NEUROG2* plus small molecules and *ASCL1* activate complementary gene regulatory networks that can independently reprogram fibroblasts into neurons. Further analysis is warranted to address this hypothesis.

Importantly, the prompt and massive neuralizing action of *NEUROG2* may be beneficial for the reprogramming of cells that are more closely related to neurons (such as astrocytes) or more prone to differentiate into neurons (such as ESCs, iPSCs, or NPCs). Indeed, in agreement with this speculation and assuming that the occupancy profiles would be similar using other cells, it has been reported that *NEUROG2*, when overexpressed in human ESCs, generates mature neurons faster than *ASCL1* (Chanda et al., 2014).

In synthesis, direct reprogramming enriched the classic knowledge on proneural genes highlighting different dynamics and kinetics in neural conversion mediated by *Ascl1* and *Neurog2* (summarized in **Figure 1A**, bottom). Those differences can underlie their different neuronal reprogramming efficiencies in different cellular lineages.

The Emerging Function of the Previously Overlooked Proneural TF Myt1l

In other studies, direct cell reprogramming uncovered the importance during neuronal differentiation of TFs whose roles remained overlooked or underestimated during embryonic development. This is the case of Myt1l, encoding for a member of the zinc finger superfamily of TFs. Little work was performed in the past to understand the role of Myt1l in neural development until it emerged as an important factor in direct reprogramming (Vierbuchen et al., 2010). Since Myt1l is specifically expressed in neurons (Kim et al., 1997; Matsushita et al., 2014) it was selected together with other 18 genes as candidates to achieve fibroblast-to-neuron conversion. After careful screening, the authors defined that the minimal cocktail of 3TF necessary to reprogram fibroblasts included Myt1l indicating its importance, previously neglected, in neuronal development. Since then, Myt1l has been used in numerous protocols to reprogram non-neuronal cells into neurons (Ambasudhan et al., 2011; Marro et al., 2011; Pang et al., 2011; Pfisterer et al., 2011; Son et al., 2011; Yoo et al., 2011; Torper et al., 2013; Victor et al., 2014; Wainger et al., 2015). The experimental evidence indicate that Myt1l alone is not sufficient to obtain neurons, but it improves instead the efficiency of conversion and the morphology of the neurons when used together with *Ascl1* or miRNA (for example, in MEF (Vierbuchen et al., 2010), in human ES (Pang et al., 2011), in human fibroblasts (Victor et al., 2014). The discovery of this important role for Myt1l sparked the scientific community interest to better determine its mechanism of action during reprogramming but also *in vivo* during development. Studies in the reprogramming context have demonstrated that Myt1l is not a pioneer factor since it binds mainly open and active chromatin (Wapinski et al., 2013; Mall et al., 2017). In contrast, Myt1l acts as a transcriptional repressor that downregulates different cascade of non-neuronal genes, such as Notch and Wnt pathway, to promote neurogenesis (Mall et al., 2017). Importantly, Notch repression has been also confirmed in a physiological context for both Myt1l and Myt1, a gene highly homologous to Myt1l (Vasconcelos et al., 2016; Mall et al., 2017). Other data indicate the importance of Myt1l in neuronal development: Myt1l overexpression in NSCs and *in vivo* increases neuronal differentiation (Mall et al., 2017) and mutations in Myt1l have been associated with intellectual disability, schizophrenia and autism (Li et al., 2012; De Rubeis et al., 2014; De Rocker et al., 2015).

DEFINING GENE NETWORKS RESPONSIBLE FOR NEURONAL SUBTYPE SPECIFICATION

Direct reprogramming assays have further contributed to better tracking the functional interactions among TFs during the commitment of specific neuronal subtypes.

The discovery that *Ascl1* alone or with *Brn2* and *Myt1l* is able to generate glutamatergic iN (Vierbuchen et al., 2010; Chanda et al., 2014) and that, associated with other TFs, it seems necessary to generate every type of neurons (Caiazzo et al., 2011; Kim et al., 2011; Pfisterer et al., 2011; Torper et al., 2013; Colasante et al., 2015), resulted in direct contradiction with the undebated role of *Ascl1* during development in the specification of GABAergic neurons. Indeed, *Ascl1* was clearly described as an activator of *Dlx1/2* (Casarosa et al., 1999; Yun et al., 2002) and its ectopic expression in cortical ventricular zone (VZ) is sufficient to upregulate *Dlx1/2* (Fode et al., 2000), which in turn activates GAD65/67 expression (Stuhmer et al., 2002).

Five years later the first iN derivation, Colasante et al. (2015) suggested an answer to this conundrum revealing that *Ascl1* is effective in activating the GABAergic reporter GAD67-GFP during MEF to neuron conversion only if combined with either *Sox2* or *Foxg1*. Although their role in regulating the

competence of telencephalic progenitors to adopt subpallial fates had been recently proposed (Manuel et al., 2010; Ferri et al., 2013), Colasante and colleagues, going deeper on the mechanism, showed that *Ascl1*, *Sox2*, and *Foxg1* strictly cooperate in determining the GABAergic fate. They showed that SOX2 and ASCL1- but not FOXG1-interact to bind and activate *Dlx1/2* enhancer, but the binding is allowed only when FOXG1 is also expressed. They hypothesized a chromatin pioneer role for FOXG1 that similarly to other forkhead-box TFs (Watts et al., 2011; Iwafuchi-Doi and Zaret, 2014), might open the repressed chromatin to enable SOX2 and *ASCL1* binding to the *Dlx1/2* locus.

Interestingly, cooperation between these three factors for the determination of a GABAergic fate was confirmed also *in vivo*. Cortical VZ cells express already *Sox2* and *Foxg1*, for this reason, it is sufficient to express *Ascl1* to allow a fate switch from glutamatergic to GABAergic (Fode et al., 2000). Conversely, the silencing of either *Foxg1* or *Sox2* in cortical VZ is sufficient to abolish the ability of *Ascl1* to induce a GABAergic neuronal fate when overexpressed in the same compartment. In accordance with this report, astrocytes over-expressing *Ascl1* can be converted in GABAergic neurons as they already express *Sox2* and *FoxG1* endogenously (Heinrich et al., 2010; Zhang et al., 2013; Masserdotti et al., 2015). The direct link between *FOXG1* and GABAergic fate emerged also when Mariani et al. (2015) observed that overexpression of the TF FOXG1 is responsible for the overproduction of GABAergic neurons in brain organoids modeling of autism spectrum disorders.

UNEXPECTED TFs REGULATING NEURONAL REPROGRAMMING

Some recent works in the reprogramming field have contributed to identify TFs not previously related to neurogenesis that were unexpectedly able to generate differentiated neurons. The large majority of them has emerged by carrying out unbiased screenings of TFs able to produce neurons (Liu et al., 2018; Tsunemoto et al., 2018). In both these studies, the screening is based on systematic combinatorial strategies that are not exclusively relying on testing TFs differentially expressed between starting cells and desired target cells. Tsunemoto et al. (2018) tested 598 pairs of TFs cloned in doxycycline-inducible lentiviruses. They infected MEFs and observed which TF pair generated neurons that were functional. Surprisingly some of the identified TFs that could convert MEFs into neurons have never been related to the generation of neurons before, such as: OCT4, a well-known factor for cell pluripotency; Myf5, known mostly as a regulator of myogenesis; and Pit1, an anterior pituitary-specific TF. The screening also identified Ptf1a (Pancreas TF-1a), a TF that has been recently shown to generate NSCs when overexpressed in MEFs (Xiao et al., 2018).

Liu et al. (2018) performed an activatory CRISPR screening in mouse ESCs to systematically identify regulators of neuronal-fate specification. Among the top 20 TFs or DNA binding proteins most efficient in neuronal conversion, some of them (Ezh2, Suz12, Maz, Nr3c1, and Sin3b) were not preferentially enriched in neural cells as no differential expression was observed between the obtained neurons and mESCs. Ezh2 and Suz12 are two Polycomb-group proteins that act as global epigenetic regulators (Margueron and Reinberg, 2011) and can promote neuronal differentiation. Transcriptomic analyses suggested that Ezh2, in particular, acts mainly by inhibiting alternative endodermal and mesodermal lineages. Regarding the TFs not related with the neuronal identity the specific mechanism of action is yet to be defined. One plausible possibility is that, when expressed at supra-physiological levels, they are able to activate overlapping genetic pathways by ectopic binding to the same transcriptional targets through their sequence homology with their related neurogenic factors. Alternatively, they may have a yet unknown role during only a short window of time along the whole process of neuronal differentiation. Additional work is needed to fully investigate these alternative scenarios.

CONCLUSION

Direct cell reprogramming proved to be informative in defining the dynamics and specific roles for several TFs and clarifying their molecular functions in yet unexplored gene networks. More unbiased screenings of TFs for neuronal conversion should be pursued (Liu et al., 2018; Tsunemoto et al., 2018), since they can help to better define these networks identifying remaining TFs not yet related to neuronal development but that can facilitate cell conversion. Finally, cell reprogramming studies generated a renewed interest in better deciphering TF functions during development, stimulating new studies *in vivo*. In overall, direct cell reprogramming can be considered as the first stage where newly TFs or unprecedented functions of well-known TFs can make their debut.

DATA AVAILABILITY

All datasets generated for this study are included in the manuscript and/or the supplementary files.

AUTHOR CONTRIBUTIONS

LM performed computational analysis. GC, AR, and VB wrote the manuscript.

FUNDING

This work was supported by the European Research Council (AdERC #340527).

ACKNOWLEDGMENTS

We thank Dr. Alessandro Sessa for critical reading of the manuscript.

REFERENCES

Addis, R. C., Hsu, F. C., Wright, R. L., Dichter, M. A., Coulter, D. A., and Gearhart, J. D. (2011). Efficient conversion of astrocytes to functional midbrain dopaminergic neurons using a single polycistronic vector. *PLoS One* 6:e28719. doi: 10.1371/journal.pone.0028719

Ambasudhan, R., Talantova, M., Coleman, R., Yuan, X., Zhu, S., Lipton, S. A., et al. (2011). Direct reprogramming of adult human fibroblasts to functional neurons under defined conditions. *Cell Stem Cell* 9, 113–118. doi: 10.1016/j.stem.2011.07.002

Aravantinou-Fatorou, K., Ortega, F., Chroni-Tzartou, D., Antoniou, N., Poulopoulou, C., Politis, P. K., et al. (2015). CEND1 and NEUROGENIN2 reprogram mouse astrocytes and embryonic fibroblasts to induced neural precursors and differentiated neurons. *Stem Cell Rep.* 5, 405–418. doi: 10.1016/j.stemcr.2015.07.012

Au, E., Ahmed, T., Karayannis, T., Biswas, S., Gan, L., and Fishell, G. (2013). A modular gain-of-function approach to generate cortical interneuron subtypes from ES cells. *Neuron* 80, 1145–1158. doi: 10.1016/j.neuron.2013.09.022

Berninger, B., Costa, M. R., Koch, U., Schroeder, T., Sutor, B., Grothe, B., et al. (2007). Functional properties of neurons derived from in vitro reprogrammed postnatal astroglia. *J. Neurosci.* 27, 8654–8664. doi: 10.1523/JNEUROSCI.1615-07.2007

Bertrand, N., Castro, D. S., and Guillemot, F. (2002). Proneural genes and the specification of neural cell types. *Nat. Rev. Neurosci.* 3, 517–530. doi: 10.1038/nrn874

Black, J. B., Adler, A. F., Wang, H. G., D'Ippolito, A. M., Hutchinson, H. A., Reddy, T. E., et al. (2016). Targeted epigenetic remodeling of endogenous loci by CRISPR/Cas9-based transcriptional activators directly converts fibroblasts to neuronal cells. *Cell Stem Cell.* 19, 406–414. doi: 10.1016/j.stem.2016.07.001

Blanchard, J. W., Eade, K. T., Szucs, A., Lo Sardo, V., Tsunemoto, R. K., Williams, D., et al. (2015). Selective conversion of fibroblasts into peripheral sensory neurons. *Nat. Neurosci.* 18, 25–35. doi: 10.1038/nn.3887

Boissart, C., Nissan, X., Giraud-Triboult, K., Peschanski, M., and Benchoua, A. (2012). miR-125 potentiates early neural specification of human embryonic stem cells. *Development* 139, 1247–1257. doi: 10.1242/dev.073627

Britz, O., Mattar, P., Nguyen, L., Langevin, L. M., Zimmer, C., Alam, S., et al. (2006). A role for proneural genes in the maturation of cortical progenitor cells. *Cereb. Cortex* 16(Suppl. 1), i138–i151. doi: 10.1093/cercor/bhj168

Busskamp, V., Lewis, N. E., Guye, P., Ng, A. H., Shipman, S. L., Byrne, S. M., et al. (2014). Rapid neurogenesis through transcriptional activation in human stem cells. *Mol. Syst. Biol.* 10:760. doi: 10.15252/msb.20145508

Caiazzo, M., Dell'Anno, M. T., Dvoretskova, E., Lazarevic, D., Taverna, S., Leo, D., et al. (2011). Direct generation of functional dopaminergic neurons from mouse and human fibroblasts. *Nature* 476, 224–227. doi: 10.1038/nature10284

Casarosa, S., Fode, C., and Guillemot, F. (1999). Mash1 regulates neurogenesis in the ventral telencephalon. *Development* 126, 525–534.

Chanda, S., Ang, C. E., Davila, J., Pak, C., Mall, M., Lee, Q. Y., et al. (2014). Generation of induced neuronal cells by the single reprogramming factor ASCL1. *Stem Cell Rep.* 3, 282–296. doi: 10.1016/j.stemcr.2014.05.020

Chouchane, M., Melo de Farias, A. R., Moura, D. M. S., Hilscher, M. M., Schroeder, T., Leao, R. N., et al. (2017). Lineage reprogramming of astroglial cells from different origins into distinct neuronal subtypes. *Stem Cell Rep.* 9, 162–176. doi: 10.1016/j.stemcr.2017.05.009

Colasante, G., Lignani, G., Rubio, A., Medrihan, L., Yekhlef, L., Sessa, A., et al. (2015). Rapid conversion of fibroblasts into functional forebrain gabaergic interneurons by direct genetic reprogramming. *Cell Stem Cell* 17, 719–734. doi: 10.1016/j.stem.2015.09.002

De Rocker, N., Vergult, S., Koolen, D., Jacobs, E., Hoischen, A., and Zeesman, S. (2015). Refinement of the critical 2p25.3 deletion region: the role of MYT1L in intellectual disability and obesity. *Genet. Med.* 17, 460–466. doi: 10.1038/gim.2014.124

De Rubeis, S., He, X., Goldberg, A. P., Poultney, C. S., Samocha, K., Cicek, A. E., et al. (2014). Synaptic, transcriptional and chromatin genes disrupted in autism. *Nature* 515, 209–215. doi: 10.1038/nature13772

Ferri, A., Favaro, R., Beccari, L., Bertolini, J., Mercurio, S., Nieto-Lopez, F., et al. (2013). Sox2 is required for embryonic development of the ventral telencephalon through the activation of the ventral determinants Nkx2.1 and Shh. *Development* 140, 1250–1261. doi: 10.1242/dev.073411

Florio, M., Leto, K., Muzio, L., Tinterri, A., Badaloni, A., Croci, L., et al. (2012). Neurogenin 2 regulates progenitor cell-cycle progression and Purkinje cell dendritogenesis in cerebellar development. *Development* 139, 2308–2320. doi: 10.1242/dev.075861

Fode, C., Ma, Q., Casarosa, S., Ang, S. L., Anderson, D. J., and Guillemot, F. (2000). A role for neural determination genes in specifying the dorsoventral identity of telencephalic neurons. *Genes Dev.* 14, 67–80.

Gascón, S., Murenu, E., Masserdotti, G., Ortega, F., Russo, G. L., Petrik, D., et al. (2016). Identification and successful negotiation of a metabolic checkpoint in direct neuronal reprogramming. *Cell Stem Cell* 18, 396–409. doi: 10.1016/j.stem.2015.12.003

Gurdon, J. B. (1962). Adult frogs derived from the nuclei of single somatic cells. *Dev. Biol.* 4, 256–273. doi: 10.1016/0012-1606(62)90043-X

Heinrich, C., Blum, R., Gascon, S., Masserdotti, G., Tripathi, P., Sanchez, R., et al. (2010). Directing astroglia from the cerebral cortex into subtype specific functional neurons. *PLoS Biol.* 8:e1000373. doi: 10.1371/journal.pbio.1000373

Heinz, S., Benner, C., Spann, N., Bertolino, E., Lin, Y. C., Laslo, P., et al. (2010). Simple combinations of lineage-determining transcription factors prime cis-regulatory elements required for macrophage and B cell identities. *Mol. Cell.* 38, 576–589. doi: 10.1016/j.molcel.2010.05.004

Ho, S. M., Hartley, B. J., Tcw, J., Beaumont, M., Stafford, K., Slesinger, P. A., et al. (2016). Rapid Ngn2-induction of excitatory neurons from hiPSC-derived neural progenitor cells. *Methods* 101, 113–124. doi: 10.1016/j.ymeth.2015.11.019

Horton, S., Meredith, A., Richardson, J. A., and Johnson, J. E. (1999). Correct coordination of neuronal differentiation events in ventral forebrain requires the bHLH factor MASH1. *Mol. Cell. Neurosci.* 14, 355–369. doi: 10.1006/mcne.1999.0791

Huang da, W., Sherman, B. T., and Lempicki, R. A. (2009). Systematic and integrative analysis of large gene lists using DAVID bioinformatics resources. *Nat. Protoc.* 4, 44–57. doi: 10.1038/nprot.2008.211

Iwafuchi-Doi, M., and Zaret, K. S. (2014). Pioneer transcription factors in cell reprogramming. *Genes Dev.* 28, 2679–2692. doi: 10.1101/gad.253443.114

Kim, J., Efe, J. A., Zhu, S., Talantova, M., Yuan, X., Wang, S., et al. (2011). Direct reprogramming of mouse fibroblasts to neural progenitors. *Proc. Natl. Acad. Sci. U.S.A.* 108, 7838–7843. doi: 10.1073/pnas.1103113108

Kim, J. G., Armstrong, R. C., v Agoston, D., Robinsky, A., Wiese, C., Nagle, J., et al. (1997). Myelin transcription factor 1 (Myt1) of the oligodendrocyte lineage, along with a closely related CCHC zinc finger, is expressed in developing neurons in the mammalian central nervous system. *J. Neurosci. Res.* 50, 272–290. doi: 10.1002/(SICI)1097-4547(19971015)50:2<272::AID-JNR16>3.0.CO;2-A

Kovach, C., Dixit, R., Li, S., Mattar, P., Wilkinson, G., Elsen, G. E., et al. (2013). Neurog2 simultaneously activates and represses alternative gene expression programs in the developing neocortex. *Cereb. Cortex* 23, 1884–1900. doi: 10.1093/cercor/bhs176

Ladewig, J., Mertens, J., Kesavan, J., Doerr, J., Poppe, D., Glaue, F., et al. (2012). Small molecules enable highly efficient neuronal conversion of human fibroblasts. *Nat. Methods* 9, 575–578. doi: 10.1038/nmeth.1972

Li, W., Wang, X., Zhao, J., Lin, J., Song, X. Q., Yang, Y., et al. (2012). Association study of myelin transcription factor 1-like polymorphisms with schizophrenia in Han Chinese population. *Genes Brain Behav.* 11, 87–93. doi: 10.1111/j.1601-183X.2011.00734.x

Liu, M. L., Zang, T., and Zhang, C. L. (2016). Direct lineage reprogramming reveals disease-specific phenotypes of motor neurons from human ALS patients. *Cell Rep.* 14, 115–128. doi: 10.1016/j.celrep.2015.12.018

Liu, M. L., Zang, T., Zou, Y., Chang, J. C., Gibson, J. R., Huber, K. M., et al. (2013). Small molecules enable neurogenin 2 to efficiently convert human fibroblasts into cholinergic neurons. *Nat. Commun.* 4:2183. doi: 10.1038/ncomms3183

Liu, X., Li, F., Stubblefield, E. A., Blanchard, B., Richards, T. L., Larson, G. A., et al. (2012). Direct reprogramming of human fibroblasts into dopaminergic neuron-like cells. *Cell Res.* 22, 321–332. doi: 10.1038/cr.2011.181

Liu, Y., Miao, Q., Yuan, J., Han, S., Zhang, P., Li, S., et al. (2015). Ascl1 converts dorsal midbrain astrocytes into functional neurons in vivo. *J. Neurosci.* 35, 9336–9355. doi: 10.1523/JNEUROSCI.3975-14.2015

Liu, Y., Yu, C., Daley, T. P., Wang, F., Cao, W. S., Bhate, S., et al. (2018). CRISPR activation screens systematically identify factors that drive neuronal fate and reprogramming. *Cell Stem Cell* 23, 758–771.e8. doi: 10.1016/j.stem.2018.09.003

Mall, M., Kareta, M. S., Chanda, S., Ahlenius, H., Perotti, N., Zhou, B., et al. (2017). Myt1l safeguards neuronal identity by actively repressing many non-neuronal fates. *Nature* 544, 245–249. doi: 10.1038/nature21722

Manuel, M., Martynoga, B., Yu, T., West, J. D., Mason, J. O., and Price, D. J. (2010). The transcription factor Foxg1 regulates the competence of telencephalic cells to adopt subpallial fates in mice. *Development* 137, 487–497. doi: 10.1242/dev.039800

Margueron, R., and Reinberg, D. (2011). The polycomb complex PRC2 and its mark in life. *Nature* 469, 343–349. doi: 10.1038/nature09784

Mariani, J., Coppola, G., Zhang, P., Abyzov, A., Provini, L., Tomasini, L., et al. (2015). FOXG1-dependent dysregulation of GABA/Glutamate neuron differentiation in autism spectrum disorders. *Cell* 162, 375–390. doi: 10.1016/j.cell.2015.06.034

Marro, S., Pang, Z. P., Yang, N., Tsai, M. C., Qu, K., Chang, H. Y., et al. (2011). Direct lineage conversion of terminally differentiated hepatocytes to functional neurons. *Cell Stem Cell* 9, 374–382. doi: 10.1016/j.stem.2011.09.002

Masserdotti, G., Gascon, S., and Gotz, M. (2016). Direct neuronal reprogramming: learning from and for development. *Development* 143, 2494–2510. doi: 10.1242/dev.092163

Masserdotti, G., Gillotin, S., Sutor, B., Drechsel, D., Irmler, M., Jorgensen, H. F., et al. (2015). Transcriptional mechanisms of proneural factors and REST in regulating neuronal reprogramming of astrocytes. *Cell Stem Cell* 17, 74–88. doi: 10.1016/j.stem.2015.05.014

Matsushita, F., Kameyama, T., Kadokawa, Y., and Marunouchi, T. (2014). Spatiotemporal expression pattern of Myt/NZF family zinc finger transcription factors during mouse nervous system development. *Dev. Dyn.* 243, 588–600. doi: 10.1002/dvdy.24091

Mattar, P., Britz, O., Johannes, C., Nieto, M., Ma, L., Rebeyka, A., et al. (2004). A screen for downstream effectors of Neurogenin2 in the embryonic neocortex. *Dev. Biol.* 273, 373–389. doi: 10.1016/j.ydbio.2004.06.013

Orellana, D. I., Santambrogio, P., Rubio, A., Yekhlef, L., Cancellieri, C., Dusi, S., et al. (2016). Coenzyme a corrects pathological defects in human neurons of PANK2-associated neurodegeneration. *EMBO Mol. Med.* 8, 1197–1211. doi: 10.15252/emmm.201606391

Pang, Z. P., Yang, N., Vierbuchen, T., Ostermeier, A., Fuentes, D. R., Yang, T. Q., et al. (2011). Induction of human neuronal cells by defined transcription factors. *Nature* 476, 220–223. doi: 10.1038/nature10202

Parras, C. M., Schuurmans, C., Scardigli, R., Kim, J., Anderson, D. J., and Guillemot, F. (2002). Divergent functions of the proneural genes Mash1 and Ngn2 in the specification of neuronal subtype identity. *Genes Dev.* 16, 324–338. doi: 10.1101/gad.940902

Pereira, M., Pfisterer, U., Rylander, D., Torper, O., Lau, S., Lundblad, M., et al. (2014). Highly efficient generation of induced neurons from human fibroblasts that survive transplantation into the adult rat brain. *Sci. Rep.* 4:6330. doi: 10.1038/srep06330

Pfisterer, U., Kirkeby, A., Torper, O., Wood, J., Nelander, J., Dufour, A., et al. (2011). Direct conversion of human fibroblasts to dopaminergic neurons. *Proc. Natl. Acad. Sci. U.S.A.* 108, 10343–10348. doi: 10.1073/pnas.1105135108

Poitras, L., Ghanem, N., Hatch, G., and Ekker, M. (2007). The proneural determinant MASH1 regulates forebrain Dlx1/2 expression through the I12b intergenic enhancer. *Development* 134, 1755–1765. doi: 10.1242/dev.02845

Rubio, A., Luoni, M., Giannelli, S. G., Radice, I., Iannielli, A., Cancellieri, C., et al. (2016). Rapid and efficient CRISPR/Cas9 gene inactivation in human neurons during human pluripotent stem cell differentiation and direct reprogramming. *Sci. Rep.* 6:37540. doi: 10.1038/srep37540

Schuurmans, C., Armant, O., Nieto, M., Stenman, J. M., Britz, O., Klenin, N., et al. (2004). Sequential phases of cortical specification involve Neurogenin-dependent and -independent pathways. *EMBO J.* 23, 2892–2902. doi: 10.1038/sj.emboj.7600278

Smith, D. K., Yang, J., Liu, M. L., and Zhang, C. L. (2016). Small molecules modulate chromatin accessibility to promote neurog2-mediated fibroblast-to-neuron reprogramming. *Stem Cell Rep.* 7, 955–969. doi: 10.1016/j.stemcr.2016.09.013

Son, E. Y., Ichida, J. K., Wainger, B. J., Toma, J. S., Rafuse, V. F., Woolf, C. J., et al. (2011). Conversion of mouse and human fibroblasts into functional spinal motor neurons. *Cell Stem Cell* 9, 205–218. doi: 10.1016/j.stem.2011.07.014

Stuhmer, T., Puelles, L., Ekker, M., and Rubenstein, J. L. (2002). Expression from a Dlx gene enhancer marks adult mouse cortical GABAergic neurons. *Cereb. Cortex* 12, 75–85. doi: 10.1093/cercor/12.1.75

Takahashi, K., and Yamanaka, S. (2006). Induction of pluripotent stem cells from mouse embryonic and adult fibroblast cultures by defined factors. *Cell* 126, 663–676. doi: 10.1016/j.cell.2006.07.024

Tapscott, S. J., Davis, R. L., Thayer, M. J., Cheng, P. F., Weintraub, H., and Lassar, A. B. (1988). MyoD1: a nuclear phosphoprotein requiring a Myc homology region to convert fibroblasts to myoblasts. *Science* 242, 405–411. doi: 10.1126/science.3175662

Torper, O., Pfisterer, U., Wolf, D. A., Pereira, M., Lau, S., Jakobsson, J., et al. (2013). Generation of induced neurons via direct conversion in vivo. *Proc. Natl. Acad. Sci. U.S.A.* 110, 7038–7043. doi: 10.1073/pnas.1303829110

Tsunemoto, R., Lee, S., Szucs, A., Chubukov, P., Sokolova, I., Blanchard, J. W., et al. (2018). Diverse reprogramming codes for neuronal identity. *Nature* 557, 375–380. doi: 10.1038/s41586-018-0103-5

Vasconcelos, F. F., Sessa, A., Laranjeira, C., Raposo, A., Teixeira, V., Hagey, D. W., et al. (2016). MyT1 counteracts the neural progenitor program to promote vertebrate neurogenesis. *Cell Rep.* 17, 469–483. doi: 10.1016/j.celrep.2016.09.024

Victor, M. B., Richner, M., Hermanstyne, T. O., Ransdell, J. L., Sobieski, C., Deng, P. Y., et al. (2014). Generation of human striatal neurons by microRNA-dependent direct conversion of fibroblasts. *Neuron* 84, 311–323. doi: 10.1016/j.neuron.2014.10.016

Vierbuchen, T., Ostermeier, A., Pang, Z. P., Kokubu, Y., Sudhof, T. C., and Wernig, M. (2010). Direct conversion of fibroblasts to functional neurons by defined factors. *Nature* 463, 1035–1041. doi: 10.1038/nature08797

Waddington, C. H. (1957). *The Strategy of the Genes; A Discussion of Some Aspects of Theoretical Biology*. London: Allen & Unwin.

Wainger, B. J., Buttermore, E. D., Oliveira, J. T., Mellin, C., Lee, S., Saber, W. A., et al. (2015). Modeling pain in vitro using nociceptor neurons reprogrammed from fibroblasts. *Nat. Neurosci.* 18, 17–24. doi: 10.1038/nn.3886

Wapinski, O. L., Vierbuchen, T., Qu, K., Lee, Q. Y., Chanda, S., Fuentes, D. R., et al. (2013). Hierarchical mechanisms for direct reprogramming of fibroblasts to neurons. *Cell* 155, 621–635. doi: 10.1016/j.cell.2013.09.028

Watts, J. A., Zhang, C., Klein-Szanto, A. J., Kormish, J. D., Fu, J., Zhang, M. Q., et al. (2011). Study of FoxA pioneer factor at silent genes reveals Rfx-repressed enhancer at Cdx2 and a potential indicator of esophageal adenocarcinoma development. *PLoS Genet.* 7:e1002277. doi: 10.1371/journal.pgen.1002277

Xiao, D., Liu, X., Zhang, M., Zou, M., Deng, Q., Sun, D., et al. (2018). Direct reprogramming of fibroblasts into neural stem cells by single non-neural progenitor transcription factor Ptf1a. *Nat. Commun.* 9:2865. doi: 10.1038/s41467-018-05209-1

Yang, N., Chanda, S., Marro, S., Ng, Y. H., Janas, J. A., Haag, D., et al. (2017). Generation of pure GABAergic neurons by transcription factor programming. *Nat. Methods* 14, 621–628. doi: 10.1038/nmeth.4291

Yoo, A. S., Sun, A. X., Li, L., Shcheglovitov, A., Portmann, T., Li, Y., et al. (2011). MicroRNA-mediated conversion of human fibroblasts to neurons. *Nature* 476, 228–231. doi: 10.1038/nature10323

Yun, K., Fischman, S., Johnson, J., Hrabe de Angelis, M., Weinmaster, G., and Rubenstein, J. L. (2002). Modulation of the notch signaling by Mash1 and Dlx1/2 regulates sequential specification and differentiation of progenitor cell types in the subcortical telencephalon. *Development* 129, 5029–5040.

Zhang, Y., Pak, C., Han, Y., Ahlenius, H., Zhang, Z., Chanda, S., et al. (2013). Rapid single-step induction of functional neurons from human pluripotent stem cells. *Neuron* 78, 785–798. doi: 10.1016/j.neuron.2013.05.029

Conflict of Interest Statement: The authors declare that the research was conducted in the absence of any commercial or financial relationships that could be construed as a potential conflict of interest.

frontiers in Neuroscience

ORIGINAL RESEARCH
published: 08 August 2019
doi: 10.3389/fnins.2019.00829

The Chromatin Environment Around Interneuron Genes in Oligodendrocyte Precursor Cells and Their Potential for Interneuron Reprograming

*Linda L. Boshans[1,2], Daniel C. Factor[3], Vijender Singh[4], Jia Liu[5], Chuntao Zhao[6], Ion Mandoiu[7], Q. Richard Lu[6], Patrizia Casaccia[5], Paul J. Tesar[3] and Akiko Nishiyama[1,2,8]**

[1] Department of Physiology and Neurobiology, University of Connecticut, Storrs, CT, United States, [2] Connecticut Institute for Brain and Cognitive Sciences, University of Connecticut, Storrs, CT, United States, [3] Department of Genetics and Genome Sciences, School of Medicine, Case Western Reserve University, Cleveland, OH, United States, [4] Computational Biology Core, University of Connecticut, Storrs, CT, United States, [5] Advanced Science Research Center at the Graduate Center, Neuroscience Initiative, The City University of New York, New York, NY, United States, [6] Department of Pediatrics, University of Cincinnati, Cincinnati, OH, United States, [7] Department of Computer Science and Engineering, University of Connecticut, Storrs, CT, United States, [8] Institute for Systems Genomics, University of Connecticut, Storrs, CT, United States

OPEN ACCESS

Edited by:
Annalisa Buffo, University of Turin, Italy

Reviewed by:
Fernando de Castro, Cajal Institute (CSIC), Spain
Ken Arai, Massachusetts General Hospital and Harvard Medical School, United States
Kaylene M. Young, University of Tasmania, Australia

***Correspondence:**
Akiko Nishiyama
akiko.nishiyama@uconn.edu

Specialty section:
This article was submitted to Neurogenesis, a section of the journal Frontiers in Neuroscience

Received: *27 December 2018*
Accepted: *25 July 2019*
Published: *08 August 2019*

Citation:
Boshans LL, Factor DC, Singh V, Liu J, Zhao C, Mandoiu I, Lu QR, Casaccia P, Tesar PJ and Nishiyama A (2019) The Chromatin Environment Around Interneuron Genes in Oligodendrocyte Precursor Cells and Their Potential for Interneuron Reprograming. Front. Neurosci. 13:829. doi: 10.3389/fnins.2019.00829

Oligodendrocyte precursor cells (OPCs), also known as NG2 glia, arise from neural progenitor cells in the embryonic ganglionic eminences that also generate inhibitory neurons. They are ubiquitously distributed in the central nervous system, remain proliferative through life, and generate oligodendrocytes in both gray and white matter. OPCs exhibit some lineage plasticity, and attempts have been made to reprogram them into neurons, with varying degrees of success. However, little is known about how epigenetic mechanisms affect the ability of OPCs to undergo fate switch and whether OPCs have a unique chromatin environment around neuronal genes that might contribute to their lineage plasticity. Our bioinformatic analysis of histone posttranslational modifications at interneuron genes in OPCs revealed that OPCs had significantly fewer bivalent and repressive histone marks at interneuron genes compared to astrocytes or fibroblasts. Conversely, OPCs had a greater degree of deposition of active histone modifications at bivalently marked interneuron genes than other cell types, and this was correlated with higher expression levels of these genes in OPCs. Furthermore, a significantly higher proportion of interneuron genes in OPCs than in other cell types lacked the histone posttranslational modifications examined. These genes had a moderately high level of expression, suggesting that the "no mark" interneuron genes could be in a transcriptionally "poised" or "transitional" state. Thus, our findings suggest that OPCs have a unique histone code at their interneuron genes that may obviate the need for erasure of repressive marks during their fate switch to inhibitory neurons.

Keywords: NG2, oligodendrocyte, inhibitory neuron, reprograming, chromatin, histone post-translational modification

INTRODUCTION

Oligodendrocyte precursor cells (OPCs), also known as NG2 glia, NG2 cells, or polydendrocytes, are ubiquitously present throughout the central nervous system and comprise 2-9% of total cells (Dawson et al., 2003). They represent a fourth major population of glial cells endowed with proliferative and self-renewing ability throughout life. Their most well known function is to generate oligodendrocytes in the developing and mature central nervous system, but they also exhibit some degree of lineage plasticity, as briefly reviewed below. The term NG2 glia has been used in the context where the properties of these cells other than their role as oligodendrocyte-producing cells is discussed. However, there has been no evidence that a subpopulation of OPCs generates oligodendrocytes, while other distinct subpopulations receive inputs from neurons (Bergles et al., 2000) or generate astrocytes (Zhu et al., 2008, 2011). On the contrary, accumulating evidence supports the notion that neuronal inputs onto OPCs affect the dynamics of oligodendrocyte lineage cells (Gibson et al., 2014; Hill et al., 2014). Thus, the consensus in the field is that NG2 glia are equated with OPCs and represent cells that have the potential to generate oligodendrocytes but have other functions as well (Nishiyama et al., 2016). OPCs are identified by the expression of NG2 and platelet-derived growth factor receptor alpha (PDGFRα) (Nishiyama et al., 1996, 2016). Neither protein is exclusively present in OPCs. NG2 is also expressed by vascular pericytes and a subpopulation of macrophages that enter the CNS (Stallcup et al., 2016) though not on resting ramified microglia (Nishiyama et al., 1997). *Pdgfra* transcript is also present at a low level in neurons and other unidentified cell types, though it is >60-fold more abundant in OPCs (Vignais et al., 1995; Zhang et al., 2014). Thus, it has become the convention to identify OPCs by the combinatorial expression of the oligodendrocyte transcription factor Olig2 (see below) and one of the two cell surface antigens, NG2 or PDGFRα.

Development of OPCs and Their Close Relation to Interneurons

During mid-embryonic development, OPCs arise in discrete domains in the ventral germinal zones, and this process is dependent on the basic helix-loop-helix (bHLH) transcription factor Olig2 (Lu et al., 2002; Takebayashi et al., 2002; Zhou and Anderson, 2002). Olig2 induces Sox10, a member of the SoxE family of high mobility group (HMG) box-containing transcription factors. The onset of Sox10 expression marks the commitment to the oligodendrocyte lineage (Kuhlbrodt et al., 1998; Kuspert et al., 2011). This is shortly followed by their emigration from the germinal zone and onset of expression of NG2 and PDGFRα (Nishiyama et al., 2016; Weider and Wegner, 2017). In the forebrain, a subset of OPCs is generated from ventral neural progenitor cells (NPCs) in the ganglionic eminences, which also give rise to interneurons (Spassky et al., 1998; Nery et al., 2001; Kessaris et al., 2006; Miyoshi et al., 2007). Ventral NPCs express the pro-interneuron homeodomain transcription factors Dlx1 and 2, and when Dlx1/2 expression is sustained, these cells become GABAergic interneurons. A subpopulation of these NPCs down-regulate Dlx1/2 and up-regulate Olig1/2. Cross-repression of Dlx1/2 and Olig1/2 plays an important role in the determination of interneuron and oligodendrocyte cell fates (Petryniak et al., 2007; Silbereis et al., 2014). Once specified, OPCs do not revert to a neuronal fate under physiological conditions, and they either self-renew or differentiate into oligodendrocytes (see below for more discussion on neuronal fate of OPCs) (Nishiyama et al., 2009, 2016).

Additional OPCs that arise from the dorsal germinal zones of the spinal cord expand and migrate ventrally to become intermingled with the first cohorts of OPCs that arise ventrally (Cai et al., 2005; Fogarty et al., 2005; Vallstedt et al., 2005). In the forebrain, the dorsal progenitors arise in the ventricular zone of the dorsal pallium characterized by the expression of the homeodomain transcription factor Emx1 (Kessaris et al., 2006; Winkler et al., 2018). Both populations appear to be PDGF and PDGFRα-dependent (Calver et al., 1998; Fruttiger et al., 1999). In addition, there is a small subpopulation of OPCs that appears to arise perinatally around the lateral ventricles as well as in the hindbrain in the absence of PDGF signaling (Timsit et al., 1995; Spassky et al., 1998; Zheng et al., 2018), and in the forebrain this population rapidly generates oligodendrocytes (Zheng et al., 2018). However, the exact origin of this subpopulation, its relationship to other oligodendrocytes, and the target axons they myelinate remain unclear.

OPC-Astrocyte Fate Plasticity

Oligodendrocyte precursor cells exhibit some degree of lineage plasticity under developmental and pathological conditions. For example, some OPCs in the prenatal ventral gray matter downregulate oligodendrocyte lineage genes and become protoplasmic astrocytes, contributing to as many as one-third of the local astrocyte population, while at the same time generating oligodendrocyte lineage cells in the same region (Zhu et al., 2008, 2011; Huang et al., 2014). The ability of OPCs to become astrocytes is restricted to the ventral gray matter and is never seen in white matter tracts throughout the neuraxis. OPCs also switch their fate from oligodendrocytes to protoplasmic astrocytes upon deletion of Olig2 (Zhu et al., 2012; Zuo et al., 2018). The fate switch mediated by loss of Olig2 occurs only in OPCs in the dorsal forebrain but not in the ventral gray matter and becomes less efficient with age. Deletion of histone deacetylase 3 (HDAC3) in OPCs causes downregulation of Olig2 and phenocopies Olig2 deletion (Zhang et al., 2016). Curiously, the distribution of OPCs in the postnatal brain that are converted into functional protoplasmic astrocytes by Olig2 deletion coincides with the distribution of OPCs that arise in the dorsal germinal zone defined by the expression the homeodomain transcription factor, Emx1 (Kessaris et al., 2006; Zhu et al., 2012; Winkler et al., 2018). The differences in the astrocyte fate and fate potential of OPCs in ventral and dorsal forebrain could arise from differences in the chromatin environment of OPCs from the two different sources.

The Neuronal Fate of OPCs

The neuronal fate of OPCs has been highly debated. Earlier studies showed that exposure of OPCs from postnatal rat optic

nerves to bone morphogenetic protein 2 (BMP2) caused them to revert to a neural stem cell-like state, upregulate Sox2, and subsequently differentiate into neuron-like cells in culture (Kondo and Raff, 2000, 2004). Sox2 belongs to the SoxB1 family of HMG box-containing transcription factors and is necessary for neural stem cell maintenance (Graham et al., 2003; Thiel, 2013). It is also used as one of the four transcription factors to induce pluripotency in somatic cells (Takahashi and Yamanaka, 2006). In OPCs in the postnatal rat optic nerve, Sox2 expression is repressed by methylation at lysine residue 9 of histone H3 (H3K9), and derepression of Sox2 is critical for their fate change to neuronal cells (Lyssiotis et al., 2007).

More recent genetic fate mapping studies suggest that it is unlikely that neurons comprise a significant physiological progeny of OPCs (Dimou et al., 2008; Rivers et al., 2008; Zhu et al., 2008, 2011; Kang et al., 2010). A few studies have detected a small number of neuronal cells in different CNS regions (Rivers et al., 2008; Guo et al., 2010; Robins et al., 2013), but the findings have not yet revealed a consistent rule regarding the location or the functional subtype of neurons that are generated from OPCs, and one cannot rule out the possibility that neurons are detected in the genetic fate mapping studies due to ectopic expression of the cre recombinase in common progenitor cells or mature neurons (Nishiyama et al., 2014; Tognatta et al., 2017). Since OPCs are unique from other CNS cell types in that they remain proliferative through adulthood, one can combine genetic fate mapping with continuous labeling with 5-ethynyl-2′-deoxyuridine (EdU), which results in EdU incorporation into >98% of OPCs in young adult mice. Under these conditions, although >96% of oligodendrocytes were also EdU+, none of the neurons previously interpreted to have originated from OPCs (Rivers et al., 2008) had incorporated EdU (Clarke et al., 2012). This further suggests that proliferating OPCs do not generate neurons under normal physiological conditions.

Direct Neuronal Reprograming From Oligodendrocyte Lineage Cells

Since the demonstration that four transcription factors could revert differentiated somatic cells to a pluripotent state (Takahashi and Yamanaka, 2006), efforts have shifted toward achieving direct reprograming from one differentiated cell into another differentiated cell type. Direct neuronal reprograming has been achieved by transfecting fibroblasts with three transcription factors *Ascl1*, *Brn2*, and *Myt1l* (Vierbuchen et al., 2010). Attempts have been made to directly reprogram neurons from OPCs. Glutamatergic and GABAergic neurons were reported to have been generated from reactive glial cells in the injured neocortex following retroviral transduction with the proneural bHLH transcription factor *Neurod1* (Bertrand et al., 2002; Guo et al., 2014). However, the identity of the cells that were initially transduced by *Neurod1* remains uncertain. Genetic fate mapping was used to show that Sox10-expressing OPCs in the injured but not intact neocortex could be converted into neurons by retroviral delivery of Sox2 and Ascl1, another member of the bHLH family (Heinrich et al., 2014), although most of the transduced cells were functionally immature, compared to neurons reprogramed from astrocytes (Heinrich et al., 2010). While these two studies only succeeded in reprograming from OPCs in the injured cortex, another study (Torper et al., 2015) showed that neurons could be generated from OPCs in the normal adult striatum by adeno-associated viral (AAV) delivery of a combination of three transcription factors *Ascl1*, *Lmx1a*, and *Nurr1*, known to promote reprograming of fibroblasts into dopaminergic neurons (Caiazzo et al., 2011). The converted neurons were stably integrated into the circuit, and many exhibited electrical properties of mature GABAergic neurons (Pereira et al., 2017). When oligodendrocytes in adult rats were transduced with an oligodendrocyte-tropic AAV harboring microRNA against polypyrimidine tract-binding protein, some of the transduced cells differentiated into neurons (Weinberg et al., 2017). However, the mechanisms by which direct neuronal conversion from glial cells occurs have remained unclear. Elucidation of basic mechanistic principles that promote or hinder direct neuronal reprograming would facilitate the application of reprograming strategies to rectify pathological conditions in which the balance of excitation and inhibition in the neural circuit is shifted toward too much excitation, such as epilepsy.

Transcription Factors and Chromatin Regulators in Cellular Reprograming

Somatic cell reprograming using transduction of four factors *Oct3/4*, *Sox2*, *c-Myc*, and *Klf4* resets the epigenetic state of a differentiated cell into an induced pluripotent state, with changes in DNA and histone methylation at the key transcription factors (Wernig et al., 2007). The efficiency of reprograming into a pluripotent state drastically increases when the physical barrier created by nucleosomes around the pluripotency factors is removed to create an open chromatin state that is accessible for transcription factor binding (Ehrensberger and Svejstrup, 2012). ATP-dependent chromatin remodeling enzymes and/or posttranslational modification of histones play an important role in altering the chromatin state during somatic cell reprograming to induced pluripotent state. Overexpression of the BAF complex (Brg/Brahma-associated factors), one of the four ATP-dependent chromatin remodeling complexes (Hota and Bruneau, 2016), accelerates and increases the efficiency of the generation of induced pluripotent stem cells from fibroblasts by opening the chromatin, thereby obviating the need for c-Myc in the reprograming process (Singhal et al., 2010). Moreover, histone posttranslational modifications such as methylation and acetylation serve as a "code" that is read by "histone readers" that recruit molecular complexes, leading to nucleosome reorganization and restructuring of the chromatin landscape. Inhibition of enzymes that promote chromatin condensation, such as DNA methyltransferases and histone deacetylases, can increase the efficiency of generating induced pluripotent cells (Shi and Jin, 2010). Thus, it is likely that the chromatin landscape of a differentiated cell affects the ability of the cell to undergo reprograming. However, little is known about the chromatin landscape around neuronal

genes in committed glial cells that might affect their neuronal reprograming efficiency.

Chromatin Regulators in the Oligodendrocyte Lineage

Epigenetic factors play critical roles in the oligodendrocyte lineage and have been studied primarily in the context of the regulatory mechanisms that affect terminal oligodendrocyte differentiation and myelination. Inhibiting histone deacetylases and their targets in OPCs not only compromises oligodendrocyte differentiation (Shen et al., 2005; He et al., 2007; Ye et al., 2009) but also upregulates astrocyte and neuronal genes (Liu et al., 2007). While histone methylation does not appear to have a major role in oligodendrocyte differentiation, H3K9 methylation but not H3K27 methylation increases in oligodendrocytes with age (Liu et al., 2015). In OPCs, H3K9me3 occupancy is prominent on genes involved in GABA signaling, and in mature oligodendrocytes, H3K9me3 is associated with genes involved in neuronal differentiation. H3K27me3 is also associated with genes involved in neuronal differentiation in both OPCs and oligodendrocytes.

In addition to histone posttranslational modification (histone PTM), ATP-dependent chromatin remodeling has also been implicated in the oligodendrocyte lineage. A member of the SWI/SNF complex Brg1 (Brahma-related gene 1) is associated with the regulatory region of myelin genes and forms a complex with Olig2 (Yu et al., 2013; Bischof et al., 2015; Matsumoto et al., 2016). The chromodomain-binding proteins comprise another family of ATP-dependent chromatin remodeling complex. Of these, Chd7 and Chd8 cooperatively bind to key oligodendrocyte lineage transcription factors including Olig2 and Sox10 and affect proliferation, survival, and oligodendrocyte maturation (Marie et al., 2018). Furthermore, Chd8 functions upstream of Brg1 and initiates a cascade of nucleosome remodeling events mediated by Brg1 and Chd7 (Zhao et al., 2018).

While the mechanisms that regulate chromatin landscape in OPCs are beginning to be unraveled, these studies have been conducted in the context of regulation of cellular dynamics within the oligodendrocyte lineage and have focused primarily on their function at oligodendrocyte and myelin genes. There is currently little information on how these mechanisms affect the ability of OPCs to undergo reprograming into other cell types. Chromatin immunoprecipitation sequencing (ChIP-seq) for *Ezh2*, which is the catalytic component the Polycomb Repressor Complex 2 and catalyzes histone methylation to generate H3K27me3, has revealed that *Ezh2* is enriched at many of the genes that promote neuronal fate or neuronal differentiation (Sher et al., 2012). Based on these observations and the close relationship between interneuron and oligodendrocyte development, we hypothesized that interneuron genes in OPCs are modified by histone PTMs that facilitate their reprograming into interneurons. To test this, we have systematically analyzed active, latent, bivalent, and repressive histone marks at the promoter and distal regions of interneuron genes in OPCs and compared them with those in astrocytes and fibroblasts.

MATERIALS AND METHODS

Interneuron Gene Expression in OPCs and Other Cell Types

To compile a list of interneuron genes, we curated genes that are important for interneuron development, function, and identity from four datasets (Batista-Brito et al., 2008; Zhang et al., 2014; Zeisel et al., 2015, and the Gene Expression Nervous System Atlas (GENSAT) database) (**Figure 1** and **Supplementary Table S1**). The FPKM (fragments per kilobase per million mapped reads) values corresponding to transcript levels in OPCs and astrocytes from postnatal day 7 (P7) mouse cortex were obtained from the RNA-seq database generated by Barres and colleagues (Zhang et al., 2014)[1], from which we extracted FPKM values for the curated interneuron genes (**Supplementary Table S2**). Genes with FPKM <1 were considered "not expressed". Gene Ontology analysis was performed with the web toolset g:Profiler (version r1750_e91_eg38) to identify enrichment of biological processes (Reimand et al., 2007, 2016) using the g:GOSt gene group functional profiling function. GO terms with p-value < 0.05 were considered significantly enriched.

RNA-seq data for interneuron genes expressed in normal adult skin tissue (dermal fibroblasts) were downloaded from accession GSE98157 as an FPKM transcript table (Zhao et al., 2019). Microarray expression data for interneuron genes expressed in mouse fibroblasts isolated from E13.5 embryos were downloaded from accession GSE8024 as processed data (Mikkelsen et al., 2007). RNA-seq data for mouse medial ganglionic eminence (MGE) isolated from E12.5 embryos were downloaded from accession GSE99049 as processed FPKMs (Liu et al., 2018).

Chromatin-Immunoprecipitation Sequencing (ChIP-seq) Analysis

We obtained ChIP-seq data for genomic regions that were occupied by histone 3 lysine 27 acetylation (H3K27ac) and histone 3 lysine 4 tri-methylation (H3K4me3) in P2 rat cortical OPCs (Yu et al., 2013); histone 3 lysine 27 tri-methylation (H3K27me3) and H3K9me3 in P1 rat cortical OPCs, and histone 3 lysine 4 mono-methylation (H3K4me1) in mouse epiblast stem cell-derived OPCs (Najm et al., 2011). All animal experiments were approved by the Institutional Animal Use and Care Committees. The ChIP-seq data for H3K27ac and H3K4me3 were aligned to the rat rn5 genome build using Bowtie with the following options: -p 8 –best –chunkmbs 200[2]. Peak calling was performed using Model-based Analysis[3] of ChIP-seq (MACS) with a p value cutoff of $1 \times e^{-9}$. The ChIP-seq data of histone 3 lysine 27 tri-methylation (H3K27me3) and histone 3 lysine 9 tri-methylation (H3K9me3) were obtained from OPCs isolated from P1 rat cortices of either sex (Liu et al., 2015), and MACS was used for peak calling.

For analysis of histone marks in adult human astrocytes and adult dermal fibroblasts, H3K27ac, H3K4me3, H3K4me1,

[1]https://web.stanford.edu/group/barres_lab/brain_rnaseq.html

[2]http://bowtie-bio.sourceforge.net

[3]http://liulab.dfci.harvard.edu/MACS

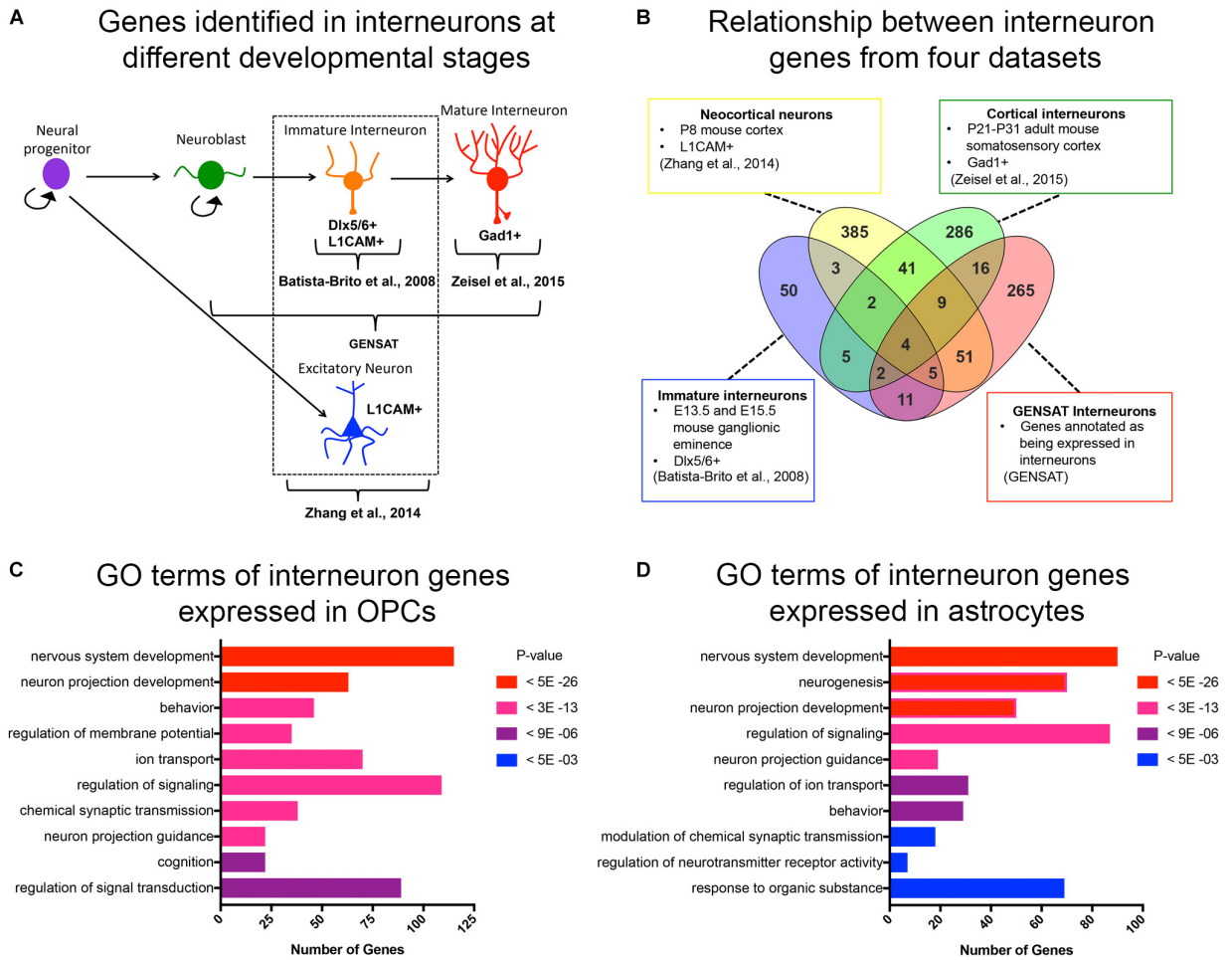

FIGURE 1 | Curated list of interneuron genes. **(A)** Diagram illustrating the stages of interneuron development and the sets of interneuron genes used. Markers used to identify interneuron populations are shown. **(B)** Venn diagram displaying the number of genes obtained from each source and the degree of overlap. A total of 500 genes from P8 neocortical neurons, 82 genes from immature neurons from embryos, 365 genes from cortical interneurons from juvenile mice, and 372 genes from GENSAT annotated interneurons. **(C,D)** Bar graphs of the top 10 significant gene ontology (GO) terms (*y*-axis) of interneuron genes expressed in OPCs **(C)** and astrocytes **(D)**. The number of genes in each GO category is shown on the *x*-axis. GO categories are ordered by *p*-values. Red represents the most significant GO terms while blue represents the least significant.

H3K27me3, and H3K9me3 ChIP-seq datasets were generated by the ENCODE Project Consortium (Consortium, 2012) and downloaded as narrowPeak files from the roadmap epigenomics project web portal[4] and converted to BED files. ChIP-seq data for mouse astrocytes were obtained from embryonic stem (ES) cell-derived NPCs that were differentiated into mature astrocytes (Tiwari et al., 2018). EncodePeak files for H3K27ac and H3K4me1 ChIP-seq datasets were downloaded from the GEO database, accession GSM2535250, and converted to BED files. H3K27me3 ChIP-seq data for cortical astrocytes that were isolated at P5, expanded for 10 days and infected with EGFR-expressing viral supernatant were downloaded from the GEO database, accession GSE76289, as BED files (Signaroldi et al., 2016). For analysis of mouse adult dermal fibroblasts, H3K4me3 and H3K27me3 ChIP-seq datasets were downloaded from the GEO database, accession GSE58965, as BedGraph files and converted to BED files (Park et al., 2017). For analysis of histone marks in E13.5 mouse embryonic fibroblasts (MEFs), H3K27ac, H3K4me1, and H3K4me3, ChIP-seq datasets, broadPeak files were downloaded from the GEO database, accession GSE31039 generated by the mouse ENCODE project, and H3K27me3 and H3K9me3 wig files were downloaded from accession GSE26657 and converted to BED files. For analysis of histone marks of the MGE region of E12.5 telencephalon, H3K27ac, H3K4me1, H3K4me3, and H3K27me3 ChIP-seq datasets were downloaded from accession GSE85704 as MACS peak output files and converted to BED files (Sandberg et al., 2016).

All ChIP-seq BED files were used to call for closest genes using the closest feature utility in bedtools. ChIP peaks were parsed based on location, with ±2 kb from the gene transcription start site (TSS) defined as promoter, 2 kb downstream from

[4]https://egg2.wustl.edu/roadmap/web_portal/

gene TSS to 2kb downstream from the end of the last exon defined as gene body, and any peaks outside those regions defined as intergenic enhancer. Significant peaks were filtered with a false discovery rate ≤5% and *p*-value $1.00e^{-05}$. To compare RNA-seq expression and peak intensity of histone PTMs across different datasets, signal intensity values within each dataset in a given cell type were converted to percentiles, ranging from 100 for the gene with the highest mRNA expression or histone modification peak signal intensity to 0 for the gene with the lowest mRNA expression or peak signal intensity or no signal (**Supplementary Table S3**).

Assay for Transposase Accessible Chromatin-Sequencing (ATAC-seq) Analysis

To assess chromatin accessibility, ATAC-seq data for open chromatin regions from P7 mouse cortical OPCs was downloaded from accession GSE116598 (Marie et al., 2018), and bigWig files were converted to BED files and BedGraph files. ATAC-seq data from adult mouse astrocytes infected with Xbp1-shRNA in an EAE model was downloaded from accession GSE121923 as BedGraph files and converted to BED files (Wheeler et al., 2019). Closest genes to ATAC-seq peaks were called as described above. For visualization of genome tracks, BedGraph files were uploaded to the Integrative Genomics Viewer (Thorvaldsdottir et al., 2013).

RESULTS

Compiling Interneuron Genes

Since OPCs share an early developmental origin with cortical interneurons, we sought to determine whether OPCs had specific histone post-translational modifications (histone PTMs) at interneuron genes, which might facilitate their conversion into interneurons. We first curated a list of genes that are expressed specifically in interneurons at different stages of their development or known to be important for differentiation and maturation of interneurons from the following four sources (**Figures 1A,B** and **Supplementary Table S1**): (1) The top 500 genes that were enriched in acutely dissociated neurons from P8 cortex compared to genes expressed by OPCs, and this list included both excitatory and inhibitory neurons (Zhang et al., 2014); (2) 82 genes expressed in immature postmitotic interneuron precursors from E13.5 and E15.5 mouse neocortex (Batista-Brito et al., 2008); (3) 365 genes expressed in mature interneurons in young adult (P21-P31) somatosensory cortex and hippocampal CA1 region identified by single cell RNA-seq (Zeisel et al., 2015); and (4) 372 genes listed as interneuron-associated genes in the GENSAT database generated using text annotation search for "interneuron." This resulted in a combined list of 890 non-duplicate genes (**Figure 1B**). We chose these four sources since they provided a diverse list of interneuron genes expressed at different developmental stages. This included genes that are important for the differentiation, function and subtype specification of interneurons (Batista-Brito et al., 2008; Rudy et al., 2011; Pla et al., 2018).

Expression of Interneuron Genes in OPCs and Astrocytes

We previously noted from published transcriptomic analyses that OPCs express low levels of transcripts encoding some neuronal genes (Nishiyama et al., 2016). To systematically determine the levels of interneuron gene expression in OPCs, we generated a list of interneuron genes that had an FPKM >1 in the RNA-seq database generated from purified P7 mouse neocortical OPCs (Zhang et al., 2014). Of the 890 curated interneuron genes described above, 46% (405 genes) were expressed (FPKM > 1) in OPCs, with an average FPKM of 15.8 and median FPKM of 6.8 (**Supplementary Table S2**). Gene ontology analysis of interneuron genes expressed in OPCs revealed an enrichment of genes involved in nervous system development, neuronal projection development, and regulating membrane potential, ion transport and signal transduction (**Figure 1C**). Some of these enriched "interneuron" genes may play a role in OPC function such as process extension and regulation of membrane potential, supporting a shared function in OPCs and interneurons. We also examined interneuron gene expression in cortical astrocytes from P7 mice (Zhang et al., 2014) and found that compared to OPCs, fewer interneuron genes were expressed in astrocytes (330 genes, 37% of the 890 interneuron genes), with an average FPKM value of 13.2 and median FPKM of 5.4 (**Supplementary Table S2**). Gene ontology analysis of the interneuron genes expressed in astrocytes revealed that 6 of the 10 top GO terms were shared with those represented in OPCs. Unique functions for interneuron genes expressed in astrocytes included neurogenesis and regulation of synaptic transmission and neurotransmitter receptor activity, consistent with the known role of astrocytes at synapses (**Figure 1D**).

Histone Post-translational Modifications (Histone PTMs) at Interneuron Genes in OPCs

We examined whether there were histone PTMs at a subset of interneuron genes in OPCs that could facilitate their reprograming into inhibitory neurons. Specifically, we were interested in determining whether interneuron genes in OPCs had an enrichment of bivalent histone PTMs. Bivalent genes are defined as genes that are occupied by both active and repressive histone PTMs. Many of the bivalently modified genes are developmentally important genes that regulate cell fate, and the bivalent marks are often resolved into either active or repressive marks as the cell differentiates into a more mature cell type, leading to transcriptional activation or silencing of the genes, respectively (Bernstein et al., 2006; Zhou et al., 2011). Thus, genes that are bivalently marked are considered to be repressed but "poised" for activation.

To determine the key categories of histone PTMs associated with interneuron genes in OPCs, we analyzed ChIP-seq datasets from postnatal rodent OPCs for H3K4me1, H3K4me3, H3K27ac, and H3K27me3 (Yu et al., 2013; Liu et al., 2015; Factor and

Tesar, unpublished) at the promoter and distal regions of the 890 interneuron genes in OPCs (**Figure 2A**). The promoter was defined as ±2kb from TSS (Roh et al., 2006), and distal region included gene body and intergenic regions. We used the following criteria to classify histone PTMs at interneuron genes. Promoter regions were classified into, (1) active histone PTM defined by H3K27ac occupancy with or without H3K4me3 (Barski et al., 2007; Creyghton et al., 2010; Sandberg et al., 2016); (2) bivalent histone PTM defined by the dual occupancy of the active mark H3K4me3 and the repressive mark H3K27me3 (Barski et al., 2007; Creyghton et al., 2010; Rada-Iglesias et al., 2011; Young et al., 2011; Zentner et al., 2011; Matsumura et al., 2015); and (3) repressive histone PTM defined by H3K27me3 occupancy without any of the above active marks (Bannister et al., 2001; Boyer et al., 2006; Barski et al., 2007; Zhu et al., 2013). Distal regions were classified into (1) active histone PTM defined by H3K27ac occupancy with or without H3K4me1 (Barski et al., 2007; Creyghton et al., 2010); (2) latent histone PTM defined by H3K4me1 occupancy alone (Barski et al., 2007; Guenther et al., 2007; Bogdanovic et al., 2012; Rada-Iglesias et al., 2012); (3) bivalent histone PTM defined by occupancy of H3K27ac alone or in combination with H3K4me1 and/or H3K27me3 (Zentner et al., 2011; King et al., 2016); and (4) repressive histone PTM defined by H3K27me3 occupancy alone or in combination with H3K4me1 (Attanasio et al., 2014). Genes marked with latent histone PTMs are considered to be 'primed' for activation, and this modification typically precedes H3K27ac deposition. Interneuron genes that lacked any of the above histone PTMs were grouped as "no marks," and interneuron genes that were not found in the ChIP-seq data were classified as "not found."

When we examined the histone PTMs at the 890 curated interneuron genes in postnatal mouse or rat OPCs, surprisingly none of the interneuron genes were bivalently marked at the promoter, and only 6.3% were bivalently marked at distal regions (**Figure 2B**). None of these were transcription factors known to be important for interneuron differentiation (**Table 1**). Among the interneuron genes, 17.5 and 21.5% had active histone modifications at promoter and distal regions, respectively (**Figure 2B**). While genes with H3K27ac had the highest transcript levels, those with H3K27ac positioned at both the promoter and gene body had higher transcript levels (average FPKM 32.87) than those with H3K27ac positioned at the promoter (average FPKM 24.42) or gene body (average FPKM 19.74) alone. Of the key interneuron transcription factor genes, Dlx2, Lhx6, and Sp9 were in this distal active category (**Table 1**).

Only 0.5% of the interneuron gene promoters and 5.7% of distal regions were repressively marked in OPCs. The majority of interneuron genes (55.4%) lacked any of the analyzed histone PTMs at the promoter, and 21% of the genes also lacked the analyzed PTMs at distal regions. This group of interneuron genes in OPCs with "no marks" at the promoter included all but one of the ten key interneuron transcription factor genes (Dlx1, Dlx2, Dlx5, Lhx6, Lhx8, Lhx9, Sp8, and Sp9). Dlx1, Dlx5, and Dlx6 also lacked the analyzed histone PTMs at distal sites (**Table 1**). One-fifth of interneuron genes were latently marked at distal regions, including transcription factors Lhx5, Lhx8, Lhx9 and Sp8, suggesting these genes were in a chromatin state "primed for activation."

Histone PTMs at Interneuron Genes in Astrocytes

We next examined whether the number and extent of histone PTMs at interneuron genes differed between OPCs and astrocytes, which represent another non-neuronal neuroectodermally derived cell type. We first compared human adult astrocytes with OPCs because ChIP-seq data for all four histone PTMs at the promoter were not available for mouse astrocytes. The most striking difference between mouse OPCs and human astrocytes was the abundance of bivalent histone PTMs at the 890 interneuron genes in astrocytes both at promoter and distal regions, which represented one-third of the interneuron genes (**Figure 2C**), compared to that in OPCs. A significantly larger proportion of the interneuron genes had repressive marks in astrocytes than in OPCs at the promoter or distal sites. All the key interneuron transcription factor genes had either bivalent or repressive marks in astrocytes (**Table 1**). Two other major differences between OPCs and human astrocytes were the larger proportion of interneuron genes in OPCs with no marks at the promoter or distal sites and those with distal latent marks compared with astrocytes. More interneuron genes in astrocytes had active marks at the promoter than those in OPCs, while at distal regions, the proportion of actively marked interneuron genes was slightly lower in astrocytes than in OPCs.

To determine whether the observed differences in histone PTMs at interneuron genes between murine OPCs and human astrocytes were due to species differences or a reflection of the differences between the cell types, we performed a similar analysis on mouse cells. Since a comparable ENCODE ChIP-seq datasets from acutely isolated mouse astrocytes was not available, we used H3K27ac and H3K4me1 ChIP-seq datasets from ES cell-derived NPCs that had been further differentiated into astrocytes (Tiwari et al., 2018) and H3K27me3 ChIP-seq dataset from astrocytes isolated from P5 mouse cortex and expanded for 10 days in culture (Signaroldi et al., 2016). These astrocytes exhibited some phenotype of mature astrocytes, such as the expression of Aquaporin-4 and genes involved in signaling and cytokine response (Tiwari et al., 2018). Since H3K4me3 ChIP-seq data was unavailable for mouse astrocytes, we analyzed distal regions only. The abundance of bivalently and repressively marked genes was similar in human and mouse astrocytes and much greater than that in OPCs (**Figures 2B–D**). A notable difference between mouse and human astrocytes was the higher proportion of interneuron genes that were latently marked (**Figure 2D**), which was comparable to that in OPCs and could reflect the degree of cell maturity rather than species difference. The proportions of actively marked interneuron genes in mouse astrocytes was slightly higher compared to human astrocytes and comparable to that in OPCs. The key interneuron transcription factor gene Dlx2 had a distal active mark in both OPCs and mouse astrocytes, while the other two transcription factor genes Lhx6 and Sp9 that had active distal PTMs in OPCs had distal bivalent marks in mouse astrocytes, and those with latent marks

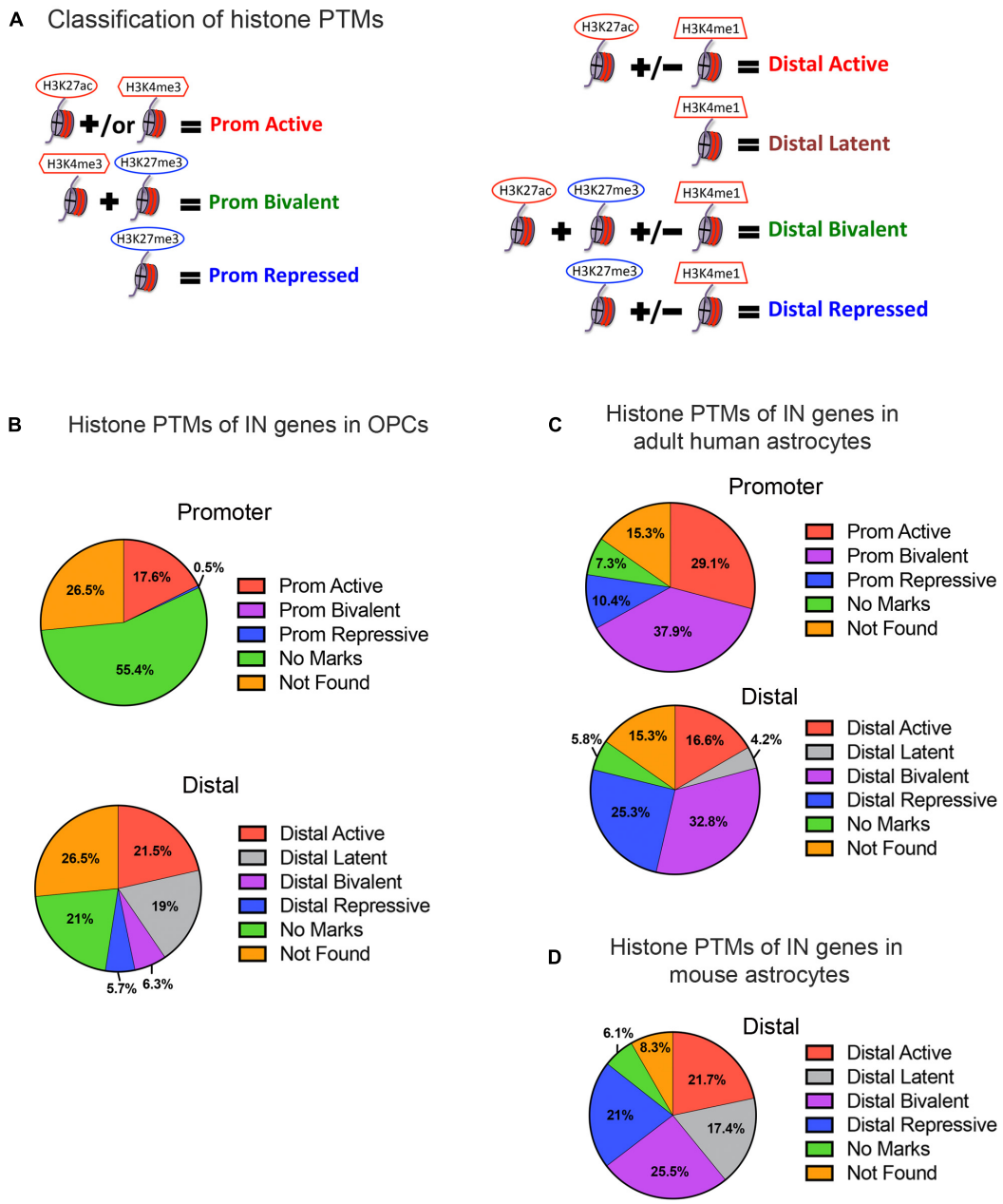

FIGURE 2 | Histone post-translational modifications (PTMs) at interneuron genes in OPCs and astrocytes. **(A)** Diagram illustrating the operational classification of histone PTMs at the promoter and distal regions of interneuron genes used in this study. Red marks indicate active histone PTMs and blue marks indicate repressive histone PTMs. **(B)** The proportion of the 890 curated interneuron genes with each category of histone PTMs at promoter and distal regions in postnatal OPCs. **(C,D)** The proportion of interneuron genes with each category of histone PTMs at promoter and distal regions in adult human astrocytes **(C)**, and at the distal regions in mouse astrocytes derived from neural stem cells and matured in culture **(D)**.

in OPCs (Lhx5, 8, 9, and Sp8) had distal repressive marks in mouse astrocytes. The proportion of interneuron genes with no marks was similar between human and mouse astrocytes and represented a significantly lower fraction than those with no marks in OPCs. Overall, the distribution of histone PTMs at interneuron genes was highly conserved between the mouse and human, and the most significant differences in histone PTMs at interneuron genes between OPCs and astrocytes were the higher occupancy of bivalent and repressive marks in astrocytes and the paucity of genes with no marks.

Histone PTMs at Interneuron Genes in Fibroblasts

We next compared histone PTMs at interneuron genes between OPCs and fibroblasts. Fibroblasts are mesodermally derived

TABLE 1 | Histone post-translational modifications at key interneuron transcription factor genes in different cell types.

	OPC		Mouse astrocyte		Mouse adult fibroblast	
Gene	**Promoter**	**Distal**	**Gene**	**Distal**	**Gene**	**Promoter**
Dlx1	No Marks	No Marks	Dlx1	No Marks	Dlx1	Bivalent
Dlx2	No Marks	Active	Dlx2	Active	Dlx2	Active
Dlx5	No Marks	No Marks	Dlx5	Repressive	Dlx5	Repressive
Dlx6	Not Found	No Marks	Dlx6	Repressive	Dlx6	Repressive
Lhx5	No Marks	Latent	Lhx5	Repressive	Lhx5	Repressive
Lhx6	No Marks	Active	Lhx6	Bivalent	Lhx6	Active
Lhx8	No Marks	Latent	Lhx8	Repressive	Lhx8	Repressive
Lhx9	No Marks	Latent	Lhx9	Repressive	Lhx9	Bivalent
sp8	No Marks	Latent	Sp8	Repressive	Sp8	Bivalent
sp9	No Marks	Active	Sp9	Bivalent	Sp9	Repressive

	MEF		MGE		
Gene	**Promoter**	**Distal**	**Gene**	**Promoter**	**Distal**
Dlx1	Active	Latent	Dlx1	Bivalent	Bivalent
Dlx2	Active	Bivalent	Dlx2	Bivalent	Bivalent
Dlx5	Bivalent	Repressive	Dlx5	Bivalent	Bivalent
Dlx6	Bivalent	Repressive	Dlx6	Bivalent	Bivalent
Lhx5	Active	Repressive	Lhx5	Bivalent	Bivalent
Lhx6	Active	Active	Lhx6	Bivalent	Bivalent
Lhx8	Active	Active	Lhx8	Bivalent	Bivalent
Lhx9	Active	Bivalent	Lhx9	Bivalent	Bivalent
Sp8	Active	Latent	Sp8	Bivalent	Bivalent
Sp9	Active	Repressive	Sp9	Bivalent	Bivalent

	Human Astrocyte		Human Adult Fibroblast		
Gene	**Promoter**	**Distal**	**Gene**	**Promoter**	**Distal**
Dlx1	Bivalent	Repressive	Dlx1	Bivalent	Repressive
Dlx2	Bivalent	Bivalent	Dlx2	Active	Active
Dlx5	Bivalent	Repressive	Dlx5	Bivalent	Repressive
Dlx6	Bivalent	Repressive	Dlx6	Bivalent	Repressive
Lhx5	Repressive	Repressive	Lhx5	Repressive	Repressive
Lhx6	Repressive	Bivalent	Lhx6	Repressive	Repressive
Lhx8	Repressive	Repressive	Lhx8	Bivalent	Repressive
Lhx9	Repressive	Bivalent	Lhx9	Bivalent	Repressive
Sp8	Bivalent	Repressive	Sp8	Bivalent	Repressive
Sp9	Bivalent	Repressive	Sp9	Active	Active

Red, active marks; orange, latent mark; green, bivalent marks; blue, repressive marks; gray, no marks; purple, gene not found in the ChIP-seq dataset.

and are often targeted for direct reprograming. We reasoned that the mesodermal origin of fibroblasts would result in a more closed chromatin environment around interneuron genes, with greater repressive and lower bivalent or active marks. We first examined adult human dermal fibroblasts, for which ChIP-seq data for all the histone PTMs were available. The proportion of repressive and bivalent marks at interneuron genes was significantly higher both at the promoter and distal regions in adult human fibroblasts compared to murine OPCs (**Figure 3A**). The proportion of these marks was highly conserved in adult (8-week-old) mouse dermal fibroblasts (**Figures 3A,B**). Surprisingly, about one-third of the interneuron genes in mouse and human fibroblasts had active marks at the promoter, similar to astrocytes and higher than that in OPCs. Fibroblasts had a similar proportion of latently marked genes to astrocytes, which was lower than that in OPCs. The interneuron transcription factor Dlx2 had active promoter marks in both mouse and human dermal fibroblasts, while the other interneuron transcription factor genes had either repressive or bivalent marks in fibroblasts, with the exception of active promoter marks on Lhx6 in mouse fibroblasts and active promoter marks on Sp9 in human fibroblasts (**Table 1**).

In addition to adult fibroblasts, we examined histone PTMs at interneuron genes in fibroblasts isolated from E13.5 mouse embryos to explore age-dependent differences (**Figure 3C**). Mouse embryonic fibroblasts (MEFs) are a population of immature fibroblasts that have been widely used as a starting population for reprograming. The most notable characteristic of histone PTMs in MEFs was that two-thirds of interneuron genes had active modifications at the promoter, which was significantly higher than that in any other cell types examined, including OPCs. This was accompanied by a lower proportion of bivalent and repressive marks at the promoter compared to adult fibroblasts, though they were higher than in OPCs. The distal histone PTMs in MEFs were similar to those in adult fibroblasts except for the larger proportion of latently marked genes in MEFs, which was comparable to that in OPCs. In MEFs, the key interneuron transcription factor genes Dlx1, Dlx2, Lhx5, Lhx6, Lhx8, Lhx9, Sp8 and Sp9 had active modifications at the promoter, while Dlx5 and Dlx6 were bivalently modified at the promoter (**Table 1**). These findings suggest that cells from developmentally immature animals tended to have more active promoter and latent distal histone PTMs and fewer genes with repressive marks than those from more mature animals.

Histone PTMs in Cells From Mouse Medial Ganglionic Eminence (MGE)

We examined histone PTMs at interneuron genes in cells from E12.5 MGE as an example of progenitors that were fated to become inhibitory neurons. The MGE at this developmental age consists of neural progenitors, neuroblasts, post-mitotic differentiating inhibitory neurons and a small population of progenitor cells that are becoming committed to the oligodendrocyte lineage. The most striking feature of the histone PTMs in MGE cells was the abundance of interneuron genes with bivalent marks, particularly at the promoter, which comprised almost half of the interneuron genes (**Figure 3D**) and was higher than in any other cell types, consistent with the presence of multipotent progenitors in this region. Notably, all the key interneuron transcription factor genes had bivalent marks at the promoter and distal sites (**Table 1**). MGE cells also had a higher proportion of interneuron genes with active marks at the promoter and distal regions compared with OPCs, though this was lower than that in MEFs. The proportion of repressive modification at the promoter region of interneuron genes was similar to that in MEFs and OPCs and slightly higher than in

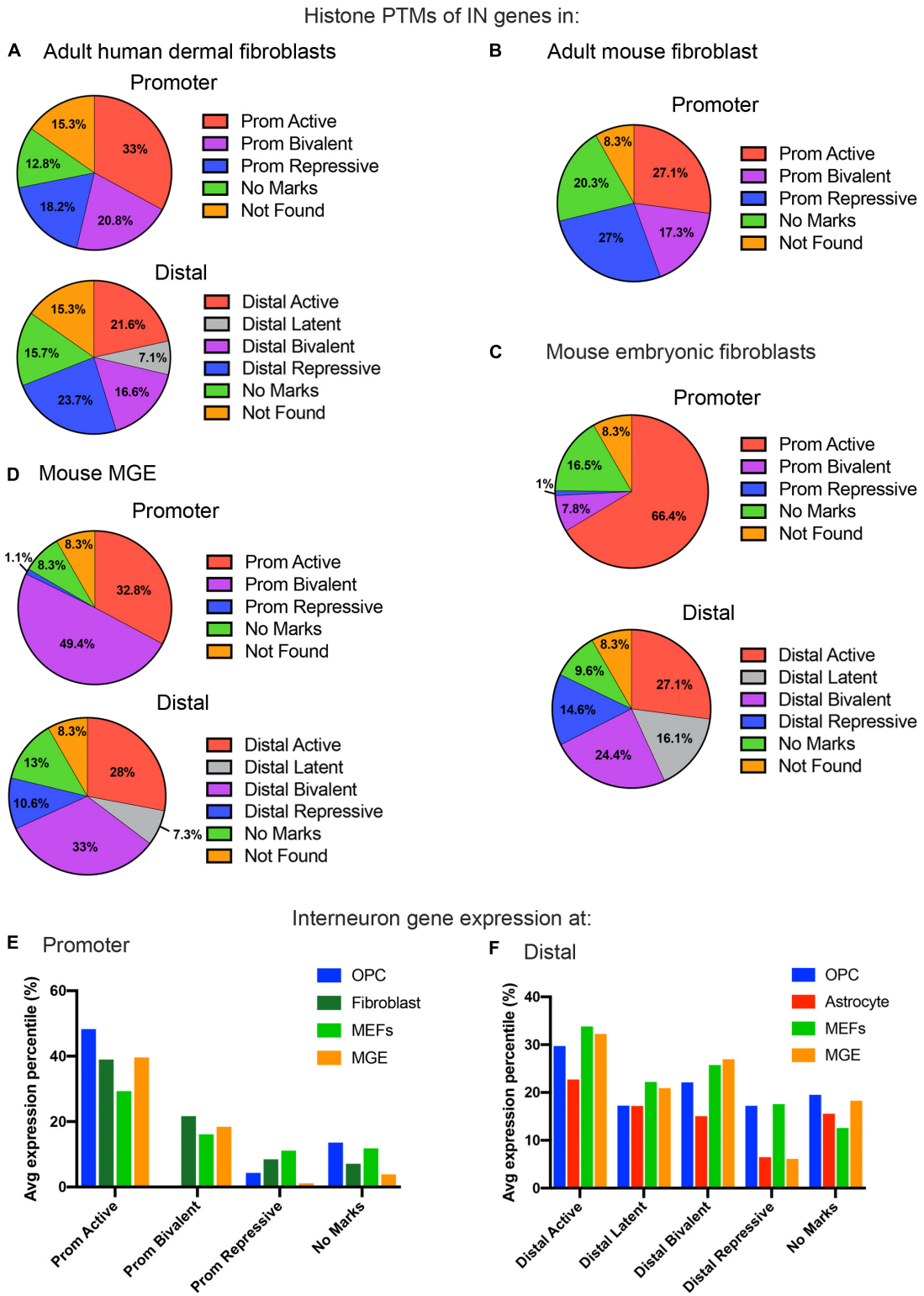

FIGURE 3 | Histone PTMs at interneuron genes in embryonic and adult fibroblasts and MGE cells. Distribution of histone PTMs at promoter and distal regions of all 890 curated interneuron genes in adult human fibroblasts **(A)**, mouse fibroblasts **(B)**, mouse embryonic fibroblasts **(C)**, and mouse MGE **(D)**. Bar graph of average expression percentiles (*y*-axis) of interneuron genes expressed in OPCs (blue), astrocytes (red), adult fibroblasts (dark green), and embryonic fibroblasts (light green) for each histone PTM category (*x*-axis) at the promoter **(E)** and distal regions **(F)** of interneuron genes.

OPCs at distal regions. These findings suggest that interneuron genes were more highly decorated with bivalent histone PTMs in MGE cells than in other cell types, consistent with previous reports on bivalent marks in uncommitted progenitor cells (Bernstein et al., 2006; Boyer et al., 2006; Mikkelsen et al., 2007).

Expression of Interneuron Genes in Mouse OPCs, Astrocytes, Fibroblasts, and MGE Cells

To determine if the histone PTM occupancy at interneuron genes were correlated with transcription, we compared interneuron genes in each histone PTM category to the RNA-seq data of different cell types. The FPKM values of interneuron genes in P7 cortical OPCs and astrocytes (Zhang et al., 2014) and the histone PTM patterns for OPCs are shown in **Supplementary Table S2**. We extended the analysis of interneuron gene expression levels with histone PTM occupancy across the different mouse cell types. Since the different methods of transcriptome analyses of the various mouse cell types precluded a direct comparison of FPKM values, we normalized the range of FPKM or microarray expression values within each RNA-seq or microarray dataset to obtain percentiles of transcript expression for each cell type, ranging from highest at 100th percentile to lowest at 0th percentile, and compared the percentile values for interneuron genes among OPCs, mouse astrocytes, adult mouse fibroblasts, MEFs, and MGE.

Overall, the levels of interneuron transcripts with each histone PTM category tended to be higher in OPCs than in astrocytes, with the exception of latently marked interneuron genes, which were expressed at comparable levels in OPCs and astrocytes (**Figures 3E,F**). When comparing transcript levels of interneuron genes marked by the different histone PTMs, interneuron genes with active modifications at either the promoter or distal regions had the highest average expression percentile in all cell types, as expected. In OPCs, 83% of the interneuron genes with active marks at the promoter had FPKM values above 1, and the majority of interneuron genes with FPKM values above 100 had an active modification at the promoter and/or distal region (**Supplementary Table S2**).

Generally, there was a good correlation between histone PTMs at the promoter and transcript levels (**Figure 3E**). Those with active marks had the highest level of expression, those with repressive marks had the lowest expression, and those with bivalent marks had intermediate levels of expression. Interneuron genes with no marks at the promoter had a wide range of expression, from <1 to >100 FPKM, but the average expression levels of these genes were significantly lower than those with active marks, and this was true for all cell types. The average expression level of interneuron genes with no marks at the promoter was higher than those with repressive marks. However, in OPCs, the nine key interneuron transcription factor genes described above that had no marks at the promoter all had FPKM values of <1, which is consistent with the non-neuronal phenotype of OPCs.

In OPCs, the expression levels of interneuron genes with different types of histone PTMs at distal sites did not segregate as cleanly as the promoter marks. While the genes with distal active marks had the highest levels of expression, those with latent, bivalent, repressive or no marks at distal sites were expressed at similar levels in OPCs. By contrast, in astrocytes, there was a tighter correlation between expression levels and distal histone PTMs, similar to the histone PTMs at the promoter. Thus, interneuron genes with bivalent or repressive marks were more repressed in astrocytes than in OPCs.

Quantitative Analysis of Histone PTMs at Interneuron Genes With Bivalent and Repressive Marks

We explored further into the nature of the bivalent modification that was detected at an unexpectedly large number of interneuron genes in astrocytes and fibroblasts from both human and mouse. The analysis described above did not take into account the ChIP-seq peak signal intensity of each kind of histone PTM. To more quantitatively examine the histone PTMs at interneuron genes, we normalized the range of signal intensities within a histone PTM dataset to obtain percentiles of signal intensities, ranging from highest at 100th percentile to lowest at 0th percentile, and compared the percentile values for each type of histone PTM at the interneuron genes among murine OPCs, human adult astrocytes, mouse astrocytes, and human adult dermal fibroblasts. We were unable to include the MEFs in this comparison because there was no quantitative output from the available ChIP-seq data. We limited our analysis to distal sites because there were too few interneuron genes with bivalent or repressive marks at the promoter region in OPCs for a meaningful comparison.

The most notable difference between OPCs and astrocytes or adult dermal fibroblasts was that the signal intensity of H3K27me3 at distal regions of interneuron genes with both bivalent and purely repressive histone PTMs was significantly lower in OPCs compared to human and mouse astrocytes and adult human fibroblasts (**Figures 4A,B**). When comparing the range of the occupancy of the H3K27me3 mark at distal sites in both bivalently and repressively marked interneuron genes, the majority of the genes with H3K27me3 in OPCs had signal intensity values of less than 50th percentile, whereas some of the highest degrees of enrichment for H3K27me3 at interneuron genes were found in astrocytes and fibroblasts. We included an analysis of H3K9me3 as another repressive modification and an indicator of heterochromatin. The difference between the depth of H3K9me3 enrichment at interneuron genes in OPCs and astrocytes was not as prominent as the difference in H3K27me3, while fibroblasts had a significantly greater deposition of H3K9me3 compared to OPCs. These observations indicated a tendency for many of the interneuron genes to be more heavily enriched for the repressive histone PTM H3K27me3 in astrocytes and fibroblasts than in OPCs, consistent with lower levels of interneuron transcripts in astrocytes compared with OPCs.

Chromatin Accessibility in Murine OPCs and Mouse Astrocytes

We have shown that OPCs have the highest proportion of interneuron genes that lacked the four histone modifications

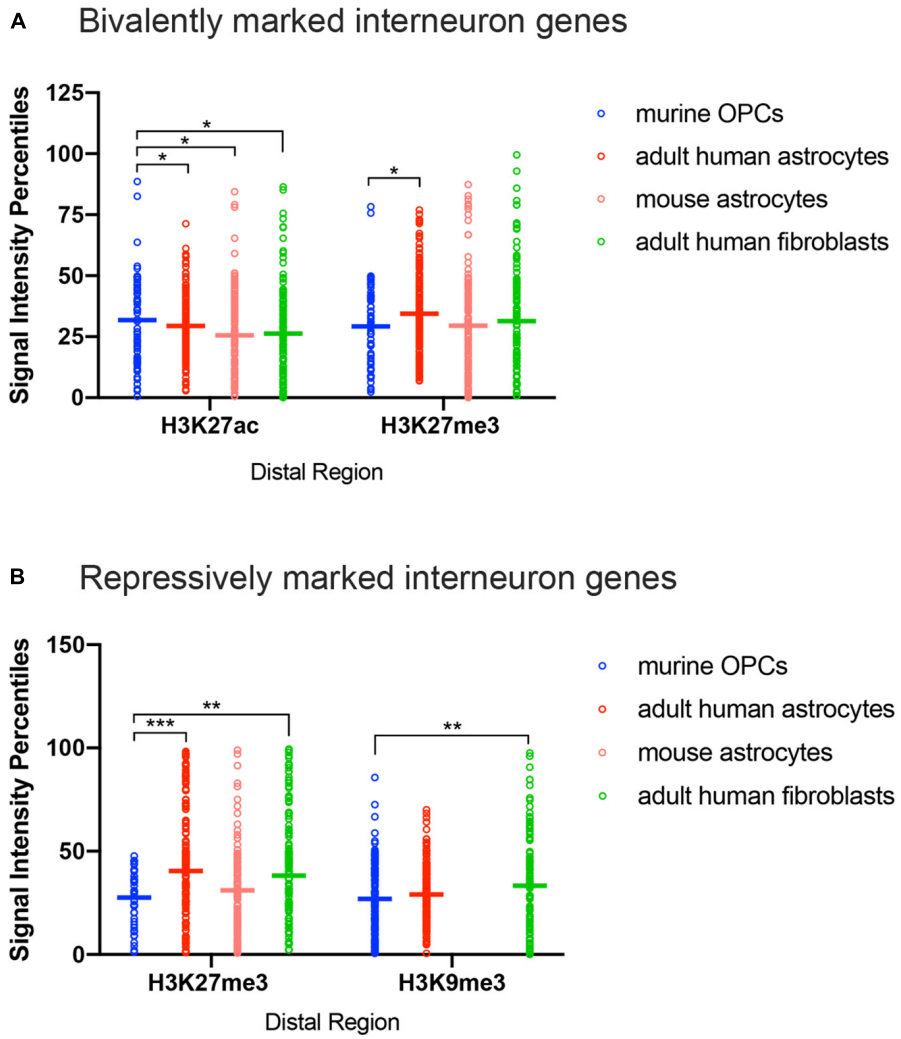

FIGURE 4 | ChIP-seq peak signal intensity at interneuron genes in OPCs and other cell types. Dot plots show signal intensity percentiles (*y*-axis) for histone PTMs (*x*-axis) at interneuron genes in OPCs (blue), human astrocytes (red), mouse astrocytes (pink), and adult human fibroblasts (light green) among the bivalently marked **(A)** and repressively marked **(B)** interneuron genes. Each circle represents the signal intensity percentile data after binning of two adjacently ranked genes. Horizontal bars represent the means of the signal intensity percentiles within each histone PTM dataset. $*p < 0.05$, $**p < 0.01$, $***p < 0.001$, two-way ANOVA, Fisher's LSD.

analyzed, particularly at key interneuron transcription factors (**Table 1**), while this group of "unmarked" genes had the highest expression of interneuron genes among all mouse cell types analyzed (**Figures 3E,F**). In addition to histone PTMs, the chromatin structure also critically affects transcription by modulating accessibility of transcription factors (Thurman et al., 2012). ATAC-seq is a method that uses a mutant Tn5 transposase to interrogate across the genome for accessible and hence open chromatin, which can be quantified by degree of transposase-mediated insertion of sequencing adaptors, measured by the number of sequencing reads. We analyzed available ATAC-seq datasets from P7 mouse cortical OPCs (Marie et al., 2018) and adult mouse cortical astrocytes (Wheeler et al., 2019) to examine chromatin accessibility around the key interneuron transcription factors. OPCs had sizeable open chromatin peaks around the TSS and the first exons of Dlx1, Dlx2 and Dlx6 genes that were largely absent or very sporadic in astrocytes (**Figure 5**). This is consistent with the previous report that genes that are transcribed typically have a large chromatin peak at the TSS as well as the transcription termination site (Teif et al., 2012), and suggests a more transcription-conducive environment at these genes in OPCs. Other key interneuron transcription factor genes that were unmarked in OPCs, including Dlx5, Lhx5, Lhx6, and Sp8 also had significant ATAC-seq reads in OPCs but the peaks appeared similar between OPCs and astrocytes and seemed more randomly distributed throughout the genes. Both OPCs and astrocytes had a chromatin peak around the first exon of the Sp9 gene, but the intensity was much greater in OPCs. This supports the notion that interneuron genes lacking the four histone modifications have a permissive environment and thus may be "poised" for transcription.

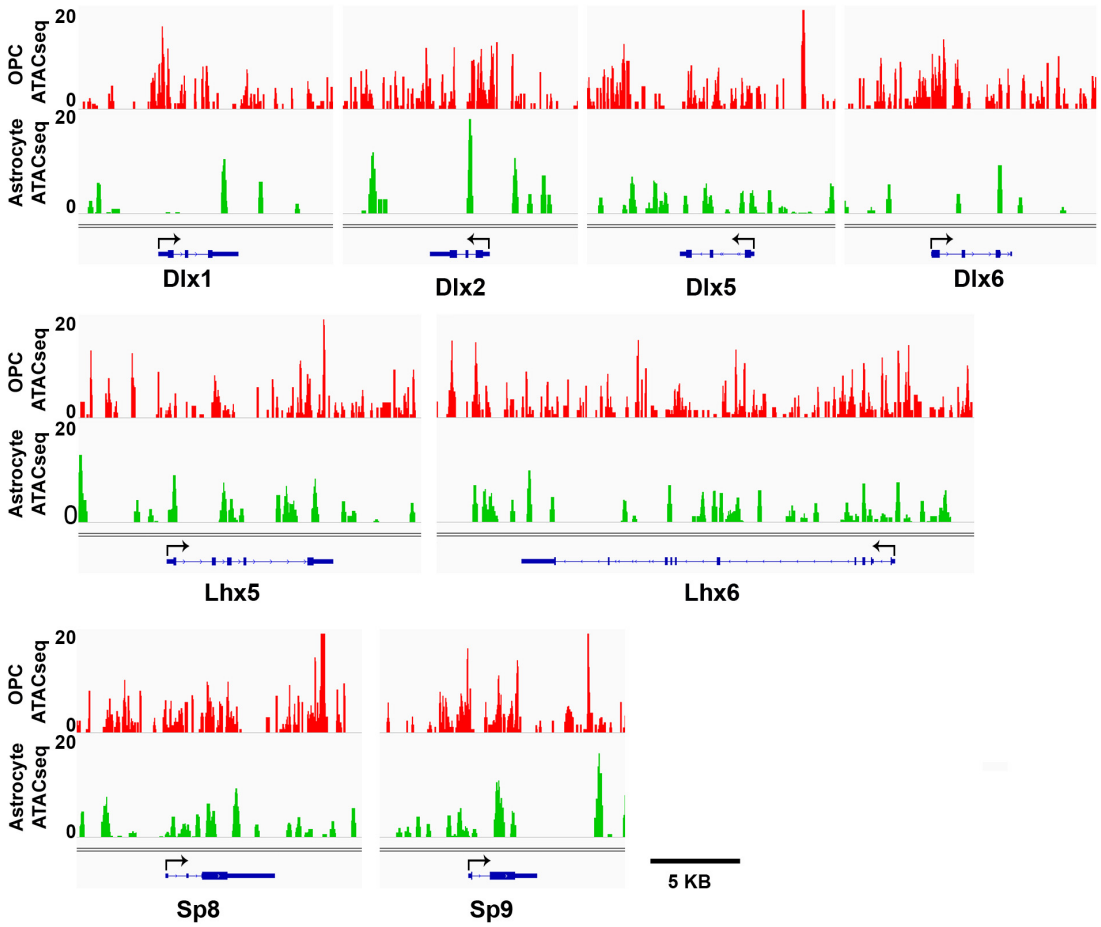

FIGURE 5 | ATAC-seq genome tracks showing open or closed chromatin regions at key interneuron transcription factor genes. Tracks show peak signal intensity (*y*-axis) for open chromatin regions of interneuron genes (*x*-axis) in mouse OPCs (red, **top**) and mouse astrocytes (green, **bottom**). Individual gene maps are shown in blue. Tracks span +5 kb from first exon and –5 kb from last exon of each gene. Black arrows indicate transcription start site and direction of transcription. Scale bar = 5 kb.

DISCUSSION

Gene expression is globally regulated by transcription factor availability and the chromatin environment. Histone PTMs and ATP-dependent chromatin remodeling complexes play key roles in defining the chromatin landscape of a given cell type under different conditions. We focused this study on examining histone PTMs at interneuron genes in OPCs as a first step toward gaining a mechanistic insight into how OPCs can be reprogramed toward an interneuron fate. We were particularly interested in determining whether histone PTMs at interneuron genes in OPCs were distributed in a way that marked them in a "poised state". Bivalent histone modifications are characterized by the presence of both active and repressive histone PTMs. During development, the bivalent marks are often resolved into either active or repressive marks as the cell differentiates from a progenitor state into a mature cell type, resulting in transcriptional activation or silencing of the genes, respectively (Bernstein et al., 2006; Zhou et al., 2011). Since OPCs that arise from ventral sources, which comprise about half of those in the neocortex and are lineally closely related to interneurons, our initial hypothesis was that OPCs have an enrichment of bivalent histone PTMs at interneuron genes, making them "poised for activation," compared to other cell types such as astrocytes and fibroblasts, which are developmentally more distant from interneurons. However, contrary to our expectations, we found that bivalent modifications were the least abundant in OPCs at interneuron genes, and a large majority of interneuron genes either had active or no histone PTMs at their promoter, while bivalent marks were a prominent feature of the promoter of interneuron genes in the MGE.

Active and Latent Histone PTMs at Interneuron Genes

Using the available transcriptomic data, we found that interneuron genes were expressed at a higher level in OPCs than in astrocytes. This led us to closely examine active histone PTMs in these cells. H3K27ac is a well-characterized active

histone mark correlated with enhancer activity (Barski et al., 2007), and H3K4me3 has traditionally been associated with active promoters, although it is also deposited at 59% of silent promoters (Barski et al., 2007; Guenther et al., 2007). H3K4me1 is associated with active enhancers but also functions as a 'priming' mark, identifying genes that will become active (Creyghton et al., 2010; Rada-Iglesias et al., 2011). For this reason, we classified promoters with H3K4me3 and/or H3K27ac and distal regions of genes with H3K27ac with or without H3K4me1 as active. Distal regions associated with H3K4me1 without the other active PTMs were classified as latent. The presence of H3K27ac at both the promoter and gene body showed the greatest correlation with higher transcript levels, as was the presence of active promoter PTMs, consistent with previous reports. The proportion of interneuron genes with active histone PTMs was unexpectedly high in fibroblasts, as we had predicted that interneuron genes would be more permanently repressed in mesodermally derived cells. It is possible that histone marks do not affect chromatin structure by themselves but influence the binding or activity of other chromatin regulators, such as ATP-dependent chromatin remodeling enzymes (Zentner and Henikoff, 2013). The abundance of genes with active promoter marks in fibroblasts was even greater in MEFs, which could reflect the generally high degree of open chromatin and active transcriptional state in embryos.

In OPCs, there were more interneuron genes with latent marks than in other cell types, particularly those from adults, suggesting that this could be a PTM that has a more significant function in cells during development. Consistent with the "priming" function known for the H3K4me1 mark, the transcript levels of these genes were comparable to those of distal bivalently marked genes and lower than those of actively marked genes.

Bivalent and Repressive Histone PTMs at Interneuron Genes

Contrary to our prediction that many of the interneuron genes have bivalent marks in OPCs, none of the interneuron genes had bivalent marks at the promoter in OPCs, and bivalent marks were more frequently detected in all the other cell types. Moreover, the relative abundance of bivalent marks was highly conserved in human and mouse astrocytes. When we examined quantitatively the degree of enrichment of each of the specific histone PTMs classified as bivalent marks, the repressive H3K27me3 mark was significantly more enriched at interneuron genes in adult human astrocytes than in OPCs. This was not the case with mouse astrocytes, which had been cultured from NPCs and matured *in vitro* for 5 days. Thus, the higher H3K27me3 deposition at bivalently marked genes in astrocytes could reflect age-dependent differences, rather than a species difference, and it is possible that OPCs from the adult brain have a greater enrichment of H3K27me3 at interneuron genes. While H3K27me3 or Ezh2, the Polycomb group methyltransferase that catalyzes the deposition of this PTM, has been detected at some interneuron genes (Sher et al., 2012; Liu et al., 2015), our analyses revealed a greater occupancy of the active H3K27ac mark at distal bivalently modified interneuron genes in OPCs compared to other cell types. Collectively, these observations indicate that the interneuron genes were less repressed in OPCs, consistent with the higher average FPKM of bivalently marked interneuron genes in OPCs than in astrocytes. Similarly, among the repressively marked genes, there was a greater enrichment of H3K27me3 in adult astrocytes and fibroblasts than in OPCs. In contrast to H3K27me3, H3K9me3 occupancy at interneuron genes in OPCs was similar to that in astrocytes but lower than that in fibroblasts. It is possible that this modification plays a more important role in permanently repressing interneuron genes in non-neurectodermally derived cells. Compared to OPCs, H3K9me3 has been shown to be more abundant in mature oligodendrocytes, and many of the genes occupied by H3K9me3 in oligodendrocytes are genes related to GABAergic transmission and neuronal differentiation (Liu et al., 2015). Thus, it appears that in the terminally differentiated oligodendrocytes, H3K9me3-mediated repression of interneuron genes occurs more prominently than in astrocytes and that the interneuron fate is more tightly sealed. This is consistent with the observation that astrocytes can be reprogramed into interneurons under certain conditions (Heinrich et al., 2010; Niu et al., 2013).

No Histone PTMs at Many Interneuron Genes in OPCs, Particularly the Key Transcription Factor Genes

A major unexpected observation was the large number of interneuron genes in OPCs that had none of the four histone marks at either their promoter or distal regions. It was intriguing that all but one of the ten key interneuron transcription factors in OPCs had no marks at their promoter (**Table 1**). Several observations make it highly unlikely that this group arose from technical reasons such as inadequate peak detection of the ChIP-seq data. First, other modifications, such as active marks were detected at the promoters in OPCs. Second, 7 out of 10 of these transcription factor genes had latent or distal active marks that were distinct from those in other cell types. Third, ATAC-seq data revealed greater chromatin accessibility around the transcription initiation sites of these genes in OPCs compared to that in astrocytes in which these genes were more prominently marked by bivalent and repressive marks. Collectively, these observations indicate that interneuron genes with no promoter marks represent a specific functional state that can be considered as a 'poised' state, somewhat similar to bivalently or latently marked genes. It is possible that they represent a transition from an active to a more repressed state or the converse as the cells develop further along the oligodendrocyte lineage, analogous to the bivalent marks in multipotent stem cells. Notably, all ten key interneuron transcription factor genes were bivalently marked in E12.5 MGE cells, which is consistent with the original description of bivalent histone PTMs prior to lineage restriction from multipotent stem cells, which are resolved to either active or repressive marks upon lineage commitment (Bernstein et al., 2006; Boyer et al., 2006). It would be interesting to examine the evolution of the PTMs at these genes throughout different stages of oligodendrocyte development.

The OPCs that were used for ChIP-seq analyses in this study were mostly derived from neocortical OPCs from perinatal rodents, which represent a mixture of OPCs derived from ventral germinal zones and those from the dorsal Emx1 domain (Kessaris et al., 2006; Winkler et al., 2018). The paucity of repressive histone PTMs at interneuron genes in OPCs could reflect a unique property of ventrally derived OPCs that share their origin with interneurons, and that this signal is diluted by dorsally derived OPCs with a different histone PTM signature. Conversely, interneuron genes in OPCs from the ventral sources might require tighter repression when their fate diverges from a common precursor to firmly establish their oligodendrocyte lineage identity, and that the paucity of repressive marks in cortical OPCs reflects the property of dorsally derived OPCs diluted by ventrally derived OPCs with a different PTM signature. It is also possible that the histone modifications do not reflect the origin of OPCs but rather the function of OPCs and the necessity to transcribe some genes expressed in interneurons to maintain OPC functions. Comparison of ChIP-seq data of OPCs from ventral and dorsal germinal zones should provide a clearer answer as to whether the developmental origin and relation to interneurons plays a significant role in their chromatin landscape. Regardless of the possible heterogeneity among OPCs in their histone modifications, the lack of repressive histone PTMs and the open chromatin state at these key interneuron transcription factor genes found in the neocortical OPCs could give OPCs a significant advantage over other cell types for reprograming into interneurons.

Species-Dependent Differences in Histone PTMs

We initially compared histone modifications of murine OPCs and human astrocytes and fibroblasts, which was supplemented with data from mouse astrocytes and fibroblasts where available. Although a comprehensive analysis of all four histone modifications of the different cell types done within the same species would have been ideal to fully validate the findings of this study, such a study was not feasible with the currently available datasets, and our findings suggested a high degree of species conservation of histone PTMs at interneuron genes. For example, the proportional distribution of the histone modifications was similar between mouse and human astrocytes, with the exception of more distal latent modified genes in mouse astrocytes. Furthermore, there was a higher proportion of genes that were bivalently and repressively marked in both mouse and human astrocytes compared to OPCs, also suggesting species conservation. A similar conservation was observed for fibroblasts, which showed similar extent of active marks at the promoter in mouse and human. Regardless of the species, more interneuron genes were repressively marked and bivalently marked in fibroblasts than in OPCs. Consistent with our findings, a study on the direct comparison of histone PTMs between mouse and human brain tissue showed 90% conservation at promoter regions, 84% at enhancers, and 33% of heterochromatin regions (Gjoneska et al., 2015). A separate group performed a similar study and found a strong association between stability and conservation of histone modifications in mouse and human species (Woo and Li, 2012). Thus, the observed differences seen among histone PTMs at interneuron genes between mouse and human cells are more likely due to cell type-dependent and age-dependent differences than inherent interspecies differences.

In summary, we have identified a characteristic histone PTM signature at interneuron genes in OPCs, which consisted of an enrichment of active histone PTMs and a paucity of bivalent and repressive modifications, particularly H3K27me3, compared with adult astrocytes and fibroblasts. In both OPCs and astrocytes, the histone PTM signature was highly correlated with transcript levels. MEFs, on the other hand, had a greater enrichment of active histone PTMs at their interneuron genes, suggesting that age significantly influences the chromatin landscape. Most somatic cell reprograming strategies require the bHLH transcription factor Ascl1 (Wapinski et al., 2013), which is considered a pioneer transcription factor capable of opening nucleosome-bound chromatin (Zaret and Carroll, 2011; Wapinski et al., 2017). Our findings that OPCs had a more accessible chromatin environment around their key interneuron transcription factor genes and lacked repressive marks could be partially explained by the expression of Ascl1 in OPCs (Nakatani et al., 2013; Zhang et al., 2014), suggesting that OPCs could more readily switch their fate into interneurons than adult fibroblasts or astrocytes, given the correct signals. The observation that OPCs in the ventral telencephalon (striatum) were readily reprogramed into interneurons (Torper et al., 2015; Pereira et al., 2017), while similar attempts in the neocortex, were only successful in the injured environment (Guo et al., 2014; Heinrich et al., 2014), could be related to differences in their epigenetic landscape around interneuron genes that could reflect their developmental origin. Further explorations on age-, cell type-, and cell origin-dependent differences in the chromatin landscape could lead to rational approaches for manipulating the fate of OPCs and exploiting the lineage plasticity of this ubiquitous and abundant self-renewing cell population.

STATEMENT OF DATA SHARING

We have provided the key datasets as **Supplementary Tables**. Additional datasets that we have generated will be shared upon request.

ETHICS STATEMENT

The study was approved by the Institutional Animal Care and Usage Committee.

AUTHOR CONTRIBUTIONS

LB and AN conceived the study and wrote the manuscript. DF, JL, CZ, QL, PC, and PT provided the ChIP-seq data.

VS extracted the ChIP-seq data. LB analyzed the data with the help of VS and IM.

FUNDING

This work was supported by funds from the NIH (R01 NS074870 and R01 NS073425 to AN, R01 NS072427 and R01 NS075243 to QL, and R35 NS111604 and R01 NS52738 to PC), the National Multiple Sclerosis Society (RG1612-26501 to AN), an Innovator Grant #414253 from the CURE Foundation (Citizens United for Research on Epilepsy) to AN, and a fellowship from the University of Connecticut Institute of Brain and Cognitive Science to LB.

ACKNOWLEDGMENTS

We thank the ENCODE project consortium for the astrocyte and dermal fibroblast ChIP-seq datasets. We thank Dr. Yin Shen and Dr. Richard Young for the MEF ChIP-seq datasets. We also thank Dr. William Wood (Department of Physiology and Neurobiology, University of Connecticut) for many helpful discussions and his critical comments on the manuscript.

SUPPLEMENTARY MATERIAL

The Supplementary Material for this article can be found online at: https://www.frontiersin.org/articles/10.3389/fnins.2019.00829/full#supplementary-material

TABLE S1 | List of interneuron genes obtained from the four sources.

TABLE S2 | Expression levels of the interneuron genes expressed in OPCs and astrocytes and histone PTMs in OPCs. Histone PTM categories are color coded as follows: red, active marks; orange, latent mark: blue, repressive marks; green, bivalent marks; gray, no marks detected; and purple, genes not found in the ChIP-seq datasets. Specific histone PTMs are indicated in red font for active modifications and blue font for repressive modifications.

TABLE S3 | Signal intensities of the ChIP-seq peaks for each of the histone modifications at the 890 curated interneuron genes in different cell types. Signal intensity values within a histone PTM dataset were obtained by converting the ChIP peaks to percentiles, ranging from 100 (highest signal intensity) to 0 (no signal). The datasets for OPCs, astrocytes and fibroblasts are in separate worksheets.

REFERENCES

Attanasio, C., Nord, A. S., Zhu, Y., Blow, M. J., Biddie, S. C., Mendenhall, E. M., et al. (2014). Tissue-specific Smarca4 binding at active and repressed regulatory elements during embryogenesis. *Genome Res.* 24, 920–929. doi: 10.1101/gr.168930.113

Bannister, A. J., Zegerman, P., Partridge, J. F., Miska, E. A., Thomas, J. O., Allshire, R. C., et al. (2001). Selective recognition of methylated lysine 9 on histone H3 by the HP1 chromo domain. *Nature* 410, 120–124. doi: 10.1038/35065138

Barski, A., Cuddapah, S., Cui, K., Roh, T. Y., Schones, D. E., Wang, Z., et al. (2007). High-resolution profiling of histone methylations in the human genome. *Cell* 129, 823–837. doi: 10.1016/j.cell.2007.05.009

Batista-Brito, R., Machold, R., Klein, C., and Fishell, G. (2008). Gene expression in cortical interneuron precursors is prescient of their mature function. *Cereb. Cortex* 18, 2306–2317. doi: 10.1093/cercor/bhm258

Bergles, D. E., Roberts, J. D., Somogyi, P., and Jahr, C. E. (2000). Glutamatergic synapses on oligodendrocyte precursor cells in the hippocampus. *Nature* 405, 187–191. doi: 10.1038/35012083

Bernstein, B. E., Mikkelsen, T. S., Xie, X., Kamal, M., Huebert, D. J., Cuff, J., et al. (2006). A bivalent chromatin structure marks key developmental genes in embryonic stem cells. *Cell* 125, 315–326. doi: 10.1016/j.cell.2006.02.041

Bertrand, N., Castro, D. S., and Guillemot, F. (2002). Proneural genes and the specification of neural cell types. *Nat. Rev. Neurosci.* 3, 517–530. doi: 10.1038/nrn874

Bischof, M., Weider, M., Kuspert, M., Nave, K. A., and Wegner, M. (2015). Brg1-dependent chromatin remodelling is not essentially required during oligodendroglial differentiation. *J. Neurosci.* 35, 21–35. doi: 10.1523/jneurosci.1468-14.2015

Bogdanovic, O., Fernandez-Minan, A., Tena, J. J., de la Calle-Mustienes, E., Hidalgo, C., van Kruysbergen, I., et al. (2012). Dynamics of enhancer chromatin signatures mark the transition from pluripotency to cell specification during embryogenesis. *Genome Res.* 22, 2043–2053. doi: 10.1101/gr.134833.111

Boyer, L. A., Plath, K., Zeitlinger, J., Brambrink, T., Medeiros, L. A., Lee, T. I., et al. (2006). Polycomb complexes repress developmental regulators in murine embryonic stem cells. *Nature* 441, 349–353. doi: 10.1038/nature04733

Cai, J., Qi, Y., Hu, X., Tan, M., Liu, Z., Zhang, J., et al. (2005). Generation of oligodendrocyte precursor cells from mouse dorsal spinal cord independent of nkx6 regulation and Shh signaling. *Neuron* 45, 41–53. doi: 10.1016/j.neuron.2004.12.028

Caiazzo, M., Dell'Anno, M. T., Dvoretskova, E., Lazarevic, D., Taverna, S., Leo, D., et al. (2011). Direct generation of functional dopaminergic neurons from mouse and human fibroblasts. *Nature* 476, 224–227. doi: 10.1038/nature10284

Calver, A. R., Hall, A. C., Yu, W.-P., Walsh, F. S., Heath, J. K., Betsholtz, C., et al. (1998). Oligodendrocyte population dynamics and the role of PDGF in vivo. *Neuron* 20, 869–882. doi: 10.1016/s0896-6273(00)80469-9

Clarke, L. E., Young, K. M., Hamilton, N. B., Li, H., Richardson, W. D., and Attwell, D. (2012). Properties, and fate of oligodendrocyte progenitor cells in the corpus callosum, motor cortex, and piriform cortex of the mouse. *J. Neurosci.* 32, 8173–8185. doi: 10.1523/JNEUROSCI.0928-12.2012

Consortium, E. P. (2012). An integrated encyclopedia of DNA elements in the human genome. *Nature* 489, 57–74. doi: 10.1038/nature11247

Creyghton, M. P., Cheng, A. W., Welstead, G. G., Kooistra, T., Carey, B. W., Steine, E. J., et al. (2010). Histone H3K27ac separates active from poised enhancers and predicts developmental state. *Proc. Natl. Acad. Sci. U.S.A.* 107, 21931–21936. doi: 10.1073/pnas.1016071107

Dawson, M. R., Polito, A., Levine, J. M., and Reynolds, R. (2003). NG2-expressing glial progenitor cells: an abundant and widespread population of cycling cells in the adult rat cns. *Mol. Cell. Neurosci.* 24, 476–488. doi: 10.1016/s1044-7431(03)00210-0

Dimou, L., Simon, C., Kirchhoff, F., Takebayashi, H., and Gotz, M. (2008). Progeny of Olig2-expressing progenitors in the gray and white matter of the adult mouse cerebral cortex. *J. Neurosci.* 28, 10434–10442. doi: 10.1523/JNEUROSCI.2831-08.2008

Ehrensberger, A. H., and Svejstrup, J. Q. (2012). Reprogramming chromatin. *Crit. Rev. Biochem. Mol. Biol.* 47, 464–482. doi: 10.3109/10409238.2012.697125

Fogarty, M., Richardson, W. D., and Kessaris, N. (2005). A subset of oligodendrocytes generated from radial glia in the dorsal spinal cord. *Development* 132, 1951–1959. doi: 10.1242/dev.01777

Fruttiger, M., Karlsson, L., Hall, A. C., Abramsson, A., Calver, A. R., Bostrom, H., et al. (1999). Defective oligodendrocyte development and severe hypomyelination in PDGF-A knockout mice. *Development* 126, 457–467.

Gibson, E. M., Purger, D., Mount, C. W., Goldstein, A. K., Lin, G. L., Wood, L. S., et al. (2014). Neuronal activity promotes oligodendrogenesis and adaptive myelination in the mammalian brain. *Science* 344:1252304. doi: 10.1126/science.1252304

Gjoneska, E., Pfenning, A. R., Mathys, H., Quon, G., Kundaje, A., Tsai, L. H., et al. (2015). Conserved epigenomic signals in mice and humans reveal immune basis of Alzheimer's disease. *Nature* 518, 365–369. doi: 10.1038/nature14252

Graham, V., Khudyakov, J., Ellis, P., and Pevny, L. (2003). Sox2 functions to maintain neural progenitor identity. *Neuron* 39, 749–765. doi: 10.1016/s0896-6273(03)00497-5

Guenther, M. G., Levine, S. S., Boyer, L. A., Jaenisch, R., and Young, R. A. (2007). A chromatin landmark and transcription initiation at most promoters in human cells. *Cell* 130, 77–88. doi: 10.1016/j.cell.2007.05.042

Guo, F., Maeda, Y., Ma, J., Xu, J., Horiuchi, M., Miers, L., et al. (2010). Pyramidal neurons are generated from oligodendroglial progenitor cells in adult piriform cortex. *J. Neurosci.* 30, 12036–12049. doi: 10.1523/JNEUROSCI.1360-10.2010

Guo, Z., Zhang, L., Wu, Z., Chen, Y., Wang, F., and Chen, G. (2014). In vivo direct reprogramming of reactive glial cells into functional neurons after brain injury and in an alzheimer's disease model. *Cell Stem Cell* 14, 188–202. doi: 10.1016/j.stem.2013.12.001

He, Y., Sandoval, J., and Casaccia-Bonnefil, P. (2007). Events at the transition between cell cycle exit and oligodendrocyte progenitor differentiation: the role of HDAC and YY1. *Neuron Glia Biol.* 3, 221–231. doi: 10.1017/S1740925X08000057

Heinrich, C., Bergami, M., Gascon, S., Lepier, A., Vigano, F., Dimou, L., et al. (2014). Sox2-mediated conversion of NG2 glia into induced neurons in the injured adult cerebral cortex. *Stem Cell Rep.* 3, 1000–1014. doi: 10.1016/j.stemcr.2014.10.007

Heinrich, C., Blum, R., Gascon, S., Masserdotti, G., Tripathi, P., Sanchez, R., et al. (2010). Directing astroglia from the cerebral cortex into subtype specific functional neurons. *PLoS Biol.* 8:e1000373. doi: 10.1371/journal.pbio.1000373

Hill, R. A., Patel, K., Goncalves, C. M., Grutzendler, J., and Nishiyama, A. (2014). Modulation of oligodendrocyte generation during a critical temporal window after NG2 cell division. *Nat. Neurosci.* 17, 1518–1527. doi: 10.1038/nn.3815

Hota, S. K., and Bruneau, B. G. (2016). Atp-dependent chromatin remodeling during mammalian development. *Development* 143, 2882–2897. doi: 10.1242/dev.128892

Huang, W., Zhao, N., Bai, X., Karram, K., Trotter, J., Goebbels, S., et al. (2014). Novel NG2-CreERT2 knock-in mice demonstrate heterogeneous differentiation potential of NG2 glia during development. *Glia* 62, 896–913. doi: 10.1002/glia.22648

Kang, S. H., Fukaya, M., Yang, J. K., Rothstein, J. D., and Bergles, D. E. (2010). NG2+ CNS glial progenitors remain committed to the oligodendrocyte lineage in postnatal life and following neurodegeneration. *Neuron* 68, 668–681. doi: 10.1016/j.neuron.2010.09.009

Kessaris, N., Fogarty, M., Iannarelli, P., Grist, M., Wegner, M., and Richardson, W. D. (2006). Competing waves of oligodendrocytes in the forebrain and postnatal elimination of an embryonic lineage. *Nat. Neurosci.* 9, 173–179. doi: 10.1038/nn1620

King, A. D., Huang, K., Rubbi, L., Liu, S., Wang, C. Y., Wang, Y., et al. (2016). Reversible regulation of promoter and enhancer histone landscape by DNA methylation in mouse embryonic stem cells. *Cell Rep.* 17, 289–302. doi: 10.1016/j.celrep.2016.08.083

Kondo, T., and Raff, M. (2000). Oligodendrocyte precursor cells reprogrammed to become multipotential CNS stem cells. *Science* 289, 1754–1757. doi: 10.1126/science.289.5485.1754

Kondo, T., and Raff, M. (2004). Chromatin remodeling and histone modification in the conversion of oligodendrocyte precursors to neural stem cells. *Genes Dev.* 18, 2963–2972. doi: 10.1101/gad.309404

Kuhlbrodt, K., Herbarth, B., Sock, E., Hermans-Borgmeyer, I., and Wegner, M. (1998). Sox10, a novel transcriptional modulator in glial cells. *J. Neurosci.* 18, 237–250. doi: 10.1523/jneurosci.18-01-00237.1998

Kuspert, M., Hammer, A., Bosl, M. R., and Wegner, M. (2011). Olig2 regulates Sox10 expression in oligodendrocyte precursors through an evolutionary conserved distal enhancer. *Nucleic Acids Res.* 39, 1280–1293. doi: 10.1093/nar/gkq951

Liu, A., Han, Y. R., Li, J., Sun, D., Ouyang, M., Plummer, M. R., et al. (2007). The glial or neuronal fate choice of oligodendrocyte progenitors is modulated by their ability to acquire an epigenetic memory. *J. Neurosci.* 27, 7339–7343. doi: 10.1523/jneurosci.1226-07.2007

Liu, J., Magri, L., Zhang, F., Marsh, N. O., Albrecht, S., Huynh, J. L., et al. (2015). Chromatin landscape defined by repressive histone methylation during oligodendrocyte differentiation. *J. Neurosci.* 35, 352–365. doi: 10.1523/JNEUROSCI.2606-14.2015

Liu, Z., Zhang, Z., Lindtner, S., Li, Z., Xu, Z., Wei, S., et al. (2018). Sp9 regulates medial ganglionic eminence-derived cortical interneuron development. *Cereb. Cortex* 29, 2653–2667. doi: 10.1093/cercor/bhy133

Lu, Q. R., Sun, T., Zhu, Z., Ma, N., Garcia, M., Stiles, C. D., et al. (2002). Common developmental requirement for Olig function indicates a motor neuron/oligodendrocyte connection. *Cell* 109, 75–86. doi: 10.1016/s0092-8674(02)00678-5

Lyssiotis, C. A., Walker, J., Wu, C., Kondo, T., Schultz, P. G., and Wu, X. (2007). Inhibition of histone deacetylase activity induces developmental plasticity in oligodendrocyte precursor cells. *Proc. Natl. Acad. Sci. U.S.A.* 104, 14982–14987. doi: 10.1073/pnas.0707044104

Marie, C., Clavairoly, A., Frah, M., Hmidan, H., Yan, J., Zhao, C., et al. (2018). Oligodendrocyte precursor survival and differentiation requires chromatin remodeling by Chd7 and Chd8. *Proc. Natl. Acad. Sci. U.S.A.* 115, E8246–E8255. doi: 10.1073/pnas.1802620115

Matsumoto, S., Banine, F., Feistel, K., Foster, S., Xing, R., Struve, J., et al. (2016). Brg1 directly regulates Olig2 transcription and is required for oligodendrocyte progenitor cell specification. *Dev. Biol.* 413, 173–187. doi: 10.1016/j.ydbio.2016.04.003

Matsumura, Y., Nakaki, R., Inagaki, T., Yoshida, A., Kano, Y., Kimura, H., et al. (2015). H3K4/H3K9me3 bivalent chromatin domains targeted by lineage-specific DNA methylation pauses adipocyte differentiation. *Mol. Cell* 60, 584–596. doi: 10.1016/j.molcel.2015.10.025

Mikkelsen, T. S., Ku, M., Jaffe, D. B., Issac, B., Lieberman, E., Giannoukos, G., et al. (2007). Genome-wide maps of chromatin state in pluripotent and lineage-committed cells. *Nature* 448, 553–560. doi: 10.1038/nature06008

Miyoshi, G., Butt, S. J., Takebayashi, H., and Fishell, G. (2007). Physiologically distinct temporal cohorts of cortical interneurons arise from telencephalic Olig2-expressing precursors. *J. Neurosci.* 27, 7786–7798. doi: 10.1523/jneurosci.1807-07.2007

Najm, F. J., Zaremba, A., Caprariello, A. V., Nayak, S., Freundt, E. C., Scacheri, P. C., et al. (2011). Rapid and robust generation of functional oligodendrocyte progenitor cells from epiblast stem cells. *Nat. Methods* 8, 957–962. doi: 10.1038/nmeth.1712

Nakatani, H., Martin, E., Hassani, H., Clavairoly, A., Maire, C. L., Viadieu, A., et al. (2013). Ascl1/mash1 promotes brain oligodendrogenesis during myelination and remyelination. *J. Neurosci.* 33, 9752–9768. doi: 10.1523/JNEUROSCI.0805-13.2013

Nery, S., Wichterle, H., and Fishell, G. (2001). Sonic hedgehog contributes to oligodendrocyte specification in the mammalian forebrain. *Development* 128, 527–540.

Nishiyama, A., Boshans, L., Goncalves, C. M., Wegrzyn, J., and Patel, K. D. (2016). Lineage, fate, and fate potential of NG2-glia. *Brain Res.* 1638, 116–128. doi: 10.1016/j.brainres.2015.08.013

Nishiyama, A., Komitova, M., Suzuki, R., and Zhu, X. (2009). Polydendrocytes (NG2 cells): multifunctional cells with lineage plasticity. *Nat. Rev. Neurosci.* 10, 9–22. doi: 10.1038/nrn2495

Nishiyama, A., Lin, X. H., Giese, N., Heldin, C. H., and Stallcup, W. B. (1996). Co-localization of NG2 proteoglycan and PDGF alpha-receptor on O2A progenitor cells in the developing rat brain. *J. Neurosci. Res.* 43, 299–314. doi: 10.1002/(sici)1097-4547(19960201)43:3<299::aid-jnr5>3.0.co;2-e

Nishiyama, A., Suzuki, R., and Zhu, X. (2014). NG2 cells (polydendrocytes) in brain physiology and repair. *Front. Neurosci.* 8:133. doi: 10.3389/fnins.2014.00133

Nishiyama, A., Yu, M., Drazba, J. A., and Tuohy, V. K. (1997). Normal and reactive NG2+ glial cells are distinct from resting and activated microglia. *J. Neurosci. Res.* 48, 299–312. doi: 10.1002/(sici)1097-4547(19970515)48:4<299::aid-jnr2>3.0.co;2-6

Niu, W., Zang, T., Zou, Y., Fang, S., Smith, D. K., Bachoo, R., et al. (2013). In vivo reprogramming of astrocytes to neuroblasts in the adult brain. *Nat. Cell Biol.* 15, 1164–1175. doi: 10.1038/ncb2843

Park, J., Kwon, Y. W., Ham, S., Hong, C. P., Seo, S., Choe, M. K., et al. (2017). Identification of the early and late responder genes during the generation of induced pluripotent stem cells from mouse fibroblasts. *PLoS One* 12:e0171300. doi: 10.1371/journal.pone.0171300

Pereira, M., Birtele, M., Shrigley, S., Benitez, J. A., Hedlund, E., Parmar, M., et al. (2017). Direct reprogramming of resident NG2 glia into neurons with

properties of fast-spiking parvalbumin-containing interneurons. *Stem Cell Rep.* 9, 742–751. doi: 10.1016/j.stemcr.2017.07.023

Petryniak, M. A., Potter, G. B., Rowitch, D. H., and Rubenstein, J. L. (2007). Dlx1 and Dlx2 control neuronal versus oligodendroglial cell fate acquisition in the developing forebrain. *Neuron* 55, 417–433. doi: 10.1016/j.neuron.2007.06.036

Pla, R., Stanco, A., Howard, M. A., Rubin, A. N., Vogt, D., Mortimer, N., et al. (2018). Dlx1 and Dlx2 promote interneuron gaba synthesis, synaptogenesis, and dendritogenesis. *Cereb. Cortex* 28, 3797–3815. doi: 10.1093/cercor/bhx241

Rada-Iglesias, A., Bajpai, R., Prescott, S., Brugmann, S. A., Swigut, T., and Wysocka, J. (2012). Epigenomic annotation of enhancers predicts transcriptional regulators of human neural crest. *Cell Stem Cell* 11, 633–648. doi: 10.1016/j.stem.2012.07.006

Rada-Iglesias, A., Bajpai, R., Swigut, T., Brugmann, S. A., Flynn, R. A., and Wysocka, J. (2011). A unique chromatin signature uncovers early developmental enhancers in humans. *Nature* 470, 279–283. doi: 10.1038/nature09692

Reimand, J., Arak, T., Adler, P., Kolberg, L., Reisberg, S., Peterson, H., et al. (2016). G:Profiler-a web server for functional interpretation of gene lists (2016 update). *Nucleic Acids Res.* 44, W83–W89. doi: 10.1093/nar/gkw199

Reimand, J., Kull, M., Peterson, H., Hansen, J., and Vilo, J. (2007). G:Profiler–a web-based toolset for functional profiling of gene lists from large-scale experiments. *Nucleic Acids Res.* 35, W193–W200.

Rivers, L. E., Young, K. M., Rizzi, M., Jamen, F., Psachoulia, K., Wade, A., et al. (2008). PDGFRA/NG2 glia generate myelinating oligodendrocytes and piriform projection neurons in adult mice. *Nat. Neurosci.* 11, 1392–1401. doi: 10.1038/nn.2220

Robins, S. C., Trudel, E., Rotondi, O., Liu, X., Djogo, T., Kryzskaya, D., et al. (2013). Evidence for NG2-glia derived, adult-born functional neurons in the hypothalamus. *PLoS One* 8:e78236. doi: 10.1371/journal.pone.0078236

Roh, T. Y., Cuddapah, S., Cui, K., and Zhao, K. (2006). The genomic landscape of histone modifications in human t cells. *Proc. Natl. Acad. Sci. U.S.A.* 103, 15782–15787. doi: 10.1073/pnas.0607617103

Rudy, B., Fishell, G., Lee, S., and Hjerling-Leffler, J. (2011). Three groups of interneurons account for nearly 100% of neocortical gabaergic neurons. *Dev. Neurobiol.* 71, 45–61. doi: 10.1002/dneu.20853

Sandberg, M., Flandin, P., Silberberg, S., Su-Feher, L., Price, J. D., Hu, J. S., et al. (2016). Transcriptional networks controlled by Nkx2-1 in the development of forebrain gabaergic neurons. *Neuron* 91, 1260–1275. doi: 10.1016/j.neuron.2016.08.020

Shen, S., Li, J., and Casaccia-Bonnefil, P. (2005). Histone modifications affect timing of oligodendrocyte progenitor differentiation in the developing rat brain. *J. Cell Biol.* 169, 577–589. doi: 10.1083/jcb.200412101

Sher, F., Boddeke, E., Olah, M., and Copray, S. (2012). Dynamic changes in Ezh2 gene occupancy underlie its involvement in neural stem cell self-renewal and differentiation towards oligodendrocytes. *PLoS One* 7:e40399. doi: 10.1371/journal.pone.0040399

Shi, G., and Jin, Y. (2010). Role of Oct4 in maintaining and regaining stem cell pluripotency. *Stem Cell Res. Ther.* 1:39. doi: 10.1186/scrt39

Signaroldi, E., Laise, P., Cristofanon, S., Brancaccio, A., Reisoli, E., Atashpaz, S., et al. (2016). Polycomb dysregulation in gliomagenesis targets a Zfp423-dependent differentiation network. *Nat. Commun.* 7:10753. doi: 10.1038/ncomms10753

Silbereis, J. C., Nobuta, H., Tsai, H. H., Heine, V. M., McKinsey, G. L., Meijer, D. H., et al. (2014). Olig1 function is required to repress Dlx1/2 and interneuron production in mammalian brain. *Neuron* 81, 574–587. doi: 10.1016/j.neuron.2013.11.024

Singhal, N., Graumann, J., Wu, G., Arauzo-Bravo, M. J., Han, D. W., Greber, B., et al. (2010). Chromatin-remodeling components of the Baf complex facilitate reprogramming. *Cell* 141, 943–955. doi: 10.1016/j.cell.2010.04.037

Spassky, N., Goujet-Zalc, C., Parmantier, E., Olivier, C., Martinez, S., Ivanova, A., et al. (1998). Multiple restricted origin of oligodendrocytes. *J. Neurosci.* 18, 8331–8343. doi: 10.1523/jneurosci.18-20-08331.1998

Stallcup, W. B., You, W. K., Kucharova, K., Cejudo-Martin, P., and Yotsumoto, F. (2016). NG2 proteoglycan-dependent contributions of pericytes and macrophages to brain tumor vascularization and progression. *Microcirculation* 23, 122–133. doi: 10.1111/micc.12251

Takahashi, K., and Yamanaka, S. (2006). Induction of pluripotent stem cells from mouse embryonic and adult fibroblast cultures by defined factors. *Cell* 126, 663–676. doi: 10.1016/j.cell.2006.07.024

Takebayashi, H., Nabeshima, Y., Yoshida, S., Chisaka, O., and Ikenaka, K. (2002). The basic helix-loop-helix factor Olig2 is essential for the development of motoneuron and oligodendrocyte lineages. *Curr. Biol.* 12, 1157–1163. doi: 10.1016/s0960-9822(02)00926-0

Teif, V. B., Vainshtein, Y., Caudron-Herger, M., Mallm, J. P., Marth, C., Hofer, T., et al. (2012). Genome-wide nucleosome positioning during embryonic stem cell development. *Nat. Struct. Mol. Biol.* 19, 1185–1192. doi: 10.1038/nsmb.2419

Thiel, G. (2013). How Sox2 maintains neural stem cell identity. *Biochem. J.* 450, e1–e2. doi: 10.1042/BJ20130176

Thorvaldsdottir, H., Robinson, J. T., and Mesirov, J. P. (2013). Integrative genomics viewer (IGV): high-performance genomics data visualization and exploration. *Brief. Bioinform.* 14, 178–192. doi: 10.1093/bib/bbs017

Thurman, R. E., Rynes, E., Humbert, R., Vierstra, J., Maurano, M. T., Haugen, E., et al. (2012). The accessible chromatin landscape of the human genome. *Nature* 489, 75–82.

Timsit, S., Martinez, S., Allinquant, B., Peyron, F., Puelles, L., and Zalc, B. (1995). Oligodendrocytes originate in a restricted zone of the embryonic ventral neural tube defined by DM-20 mRNA expression. *J. Neurosci.* 15, 1012–1024. doi: 10.1523/jneurosci.15-02-01012.1995

Tiwari, N., Pataskar, A., Peron, S., Thakurela, S., Sahu, S. K., Figueres-Onate, M., et al. (2018). Stage-specific transcription factors drive astrogliogenesis by remodeling gene regulatory landscapes. *Cell Stem Cell* 23, 557.e8–571.e8. doi: 10.1016/j.stem.2018.09.008

Tognatta, R., Sun, W., Goebbels, S., Nave, K. A., Nishiyama, A., Schoch, S., et al. (2017). Transient Cnp expression by early progenitors causes cre-lox-based reporter lines to map profoundly different fates. *Glia* 65, 342–359. doi: 10.1002/glia.23095

Torper, O., Ottosson, D. R., Pereira, M., Lau, S., Cardoso, T., Grealish, S., et al. (2015). In vivo reprogramming of striatal NG2 glia into functional neurons that integrate into local host circuitry. *Cell Rep.* 12, 474–481. doi: 10.1016/j.celrep.2015.06.040

Vallstedt, A., Klos, J. M., and Ericson, J. (2005). Multiple dorsoventral origins of oligodendrocyte generation in the spinal cord and hindbrain. *Neuron* 45, 55–67. doi: 10.1016/j.neuron.2004.12.026

Vierbuchen, T., Ostermeier, A., Pang, Z. P., Kokubu, Y., Sudhof, T. C., and Wernig, M. (2010). Direct conversion of fibroblasts to functional neurons by defined factors. *Nature* 463, 1035–1041. doi: 10.1038/nature08797

Vignais, L., Nait Oumesmar, B., and Baron-Van Evercooren, A. B. (1995). PDGF-alpha receptor is expressed by mature neurones of the central nervous system. *Neuroreport* 6, 1993–1996. doi: 10.1097/00001756-199510010-00010

Wapinski, O. L., Lee, Q. Y., Chen, A. C., Li, R., Corces, M. R., Ang, C. E., et al. (2017). Rapid chromatin switch in the direct reprogramming of fibroblasts to neurons. *Cell Rep.* 20, 3236–3247. doi: 10.1016/j.celrep.2017.09.011

Wapinski, O. L., Vierbuchen, T., Qu, K., Lee, Q. Y., Chanda, S., Fuentes, D. R., et al. (2013). Hierarchical mechanisms for direct reprogramming of fibroblasts to neurons. *Cell* 155, 621–635. doi: 10.1016/j.cell.2013.09.028

Weider, M., and Wegner, M. (2017). Soxe factors: transcriptional regulators of neural differentiation and nervous system development. *Semin. Cell Dev. Biol.* 63, 35–42. doi: 10.1016/j.semcdb.2016.08.013

Weinberg, M. S., Criswell, H. E., Powell, S. K., Bhatt, A. P., and McCown, T. J. (2017). Viral vector reprogramming of adult resident striatal oligodendrocytes into functional neurons. *Mol. Ther.* 25, 928–934. doi: 10.1016/j.ymthe.2017.01.016

Wernig, M., Meissner, A., Foreman, R., Brambrink, T., Ku, M., Hochedlinger, K., et al. (2007). In vitro reprogramming of fibroblasts into a pluripotent ES-cell-like state. *Nature* 448, 318–324. doi: 10.1038/nature05944

Wheeler, M. A., Jaronen, M., Covacu, R., Zandee, S. E. J., Scalisi, G., Rothhammer, V., et al. (2019). Environmental control of astrocyte pathogenic activities in CNS inflammation. *Cell* 176, 581.e18–596.e18. doi: 10.1016/j.cell.2018.12.012

Winkler, C. C., Yabut, O. R., Fregoso, S. P., Gomez, H. G., Dwyer, B. E., Pleasure, S. J., et al. (2018). The dorsal wave of neocortical oligodendrogenesis begins embryonically and requires multiple sources of Sonic hedgehog. *J. Neurosci.* 38, 5237–5250. doi: 10.1523/JNEUROSCI.3392-17.2018

Woo, Y. H., and Li, W. H. (2012). Evolutionary conservation of histone modifications in mammals. *Mol. Biol. Evol.* 29, 1757–1767. doi: 10.1093/molbev/mss022

Ye, F., Chen, Y., Hoang, T., Montgomery, R. L., Zhao, X. H., Bu, H., et al. (2009). HDAC1 and HDAC2 regulate oligodendrocyte differentiation by disrupting the beta-catenin-Tcf interaction. *Nat. Neurosci.* 12, 829–838. doi: 10.1038/nn.2333

Young, M. D., Willson, T. A., Wakefield, M. J., Trounson, E., Hilton, D. J., Blewitt, M. E., et al. (2011). Chip-seq analysis reveals distinct H3K27me3 profiles that correlate with transcriptional activity. *Nucleic Acids Res.* 39, 7415–7427. doi: 10.1093/nar/gkr416

Yu, Y., Chen, Y., Kim, B., Wang, H., Zhao, C., He, X., et al. (2013). Olig2 targets chromatin remodelers to enhancers to initiate oligodendrocyte differentiation. *Cell* 152, 248–261. doi: 10.1016/j.cell.2012.12.006

Zaret, K. S., and Carroll, J. S. (2011). Pioneer transcription factors: establishing competence for gene expression. *Genes Dev.* 25, 2227–2241. doi: 10.1101/gad.176826.111

Zeisel, A., Munoz-Manchado, A. B., Codeluppi, S., Lonnerberg, P., La Manno, G., Jureus, A., et al. (2015). Brain structure. Cell types in the mouse cortex and hippocampus revealed by single-cell RNA-seq. *Science* 347, 1138–1142. doi: 10.1126/science.aaa1934

Zentner, G. E., and Henikoff, S. (2013). Regulation of nucleosome dynamics by histone modifications. *Nat. Struct. Mol. Biol.* 20, 259–266. doi: 10.1038/nsmb.2470

Zentner, G. E., Tesar, P. J., and Scacheri, P. C. (2011). Epigenetic signatures distinguish multiple classes of enhancers with distinct cellular functions. *Genome Res.* 21, 1273–1283. doi: 10.1101/gr.122382.111

Zhang, L., He, X., Liu, L., Jiang, M., Zhao, C., Wang, H., et al. (2016). HDAC3 interaction with p300 histone acetyltransferase regulates the oligodendrocyte and astrocyte lineage fate switch. *Dev. Cell* 36, 316–330. doi: 10.1016/j.devcel.2016.01.002

Zhang, Y., Chen, K., Sloan, S. A., Bennett, M. L., Scholze, A. R., O'Keeffe, S., et al. (2014). An RNA-sequencing transcriptome and splicing database of glia, neurons, and vascular cells of the cerebral cortex. *J. Neurosci.* 34, 11929–11947. doi: 10.1523/JNEUROSCI.1860-14.2014

Zhao, C., Dong, C., Frah, M., Deng, Y., Marie, C., Zhang, F., et al. (2018). Dual requirement of Chd8 for chromatin landscape establishment and histone methyltransferase recruitment to promote CNS myelination and repair. *Dev. Cell* 45, 753.e8–768.e8. doi: 10.1016/j.devcel.2018.05.022

Zhao, X., Psarianos, P., Ghoraie, L. S., Yip, K., Godstein, D., Gilbet, R., et al. (2019). Metabolic regulation of dermal fibroblasts contributes to skin extracellular matrix homeostasis and fibrosis. *Nat. Metabol.* 1, 147–157. doi: 10.1038/s42255-018-0008-5

Zheng, K., Wang, C., Yang, J., Huang, H., Zhao, X., Zhang, Z., et al. (2018). Molecular and genetic evidence for the PDGFR alpha-independent population of oligodendrocyte progenitor cells in the developing mouse brain. *J. Neurosci.* 38, 9505–9513. doi: 10.1523/jneurosci.1510-18.2018

Zhou, Q., and Anderson, D. J. (2002). The bHLH transcription factors Olig2 and Olig1 couple neuronal and glial subtype specification. *Cell* 109, 61–73. doi: 10.1016/s0092-8674(02)00677-3

Zhou, V. W., Goren, A., and Bernstein, B. E. (2011). Charting histone modifications and the functional organization of mammalian genomes. *Nat. Rev. Genet.* 12, 7–18. doi: 10.1038/nrg2905

Zhu, X., Bergles, D. E., and Nishiyama, A. (2008). NG2 cells generate both oligodendrocytes and gray matter astrocytes. *Development* 135, 145–157. doi: 10.1242/dev.004895

Zhu, X., Hill, R. A., Dietrich, D., Komitova, M., Suzuki, R., and Nishiyama, A. (2011). Age-dependent fate and lineage restriction of single NG2 cells. *Development* 138, 745–753. doi: 10.1242/dev.047951

Zhu, X., Zuo, H., Maher, B. J., Serwanski, D. R., LoTurco, J. J., Lu, Q. R., et al. (2012). Olig2-dependent developmental fate switch of NG2 cells. *Development* 139, 2299–2307. doi: 10.1242/dev.078873

Zhu, Y., Sun, L., Chen, Z., Whitaker, J. W., Wang, T., and Wang, W. (2013). Predicting enhancer transcription and activity from chromatin modifications. *Nucleic Acids Res.* 41, 10032–10043. doi: 10.1093/nar/gkt826

Zuo, H., Wood, W. M., Sherafat, A., Hill, R. A., Lu, Q. R., and Nishiyama, A. (2018). Age-dependent decline in fate switch from NG2 cells to astrocytes after Olig2 deletion. *J. Neurosci.* 38, 2359–2371. doi: 10.1523/JNEUROSCI.0712-17.2018

Conflict of Interest Statement: The authors declare that the research was conducted in the absence of any commercial or financial relationships that could be construed as a potential conflict of interest.

frontiers in Neuroscience

ORIGINAL RESEARCH
published: 03 September 2019
doi: 10.3389/fnins.2019.00914

Laminin and Environmental Cues Act in the Inhibition of the Neuronal Differentiation of Enteric Glia *in vitro*

*Carla Pires Veríssimo[1,2,3], Juliana da Silva Carvalho[1], Fábio Jorge Moreira da Silva[2], Loraine Campanati[2], Vivaldo Moura-Neto[1,2] and Juliana de Mattos Coelho-Aguiar[1,2]**

[1] Instituto Estadual do Cérebro Paulo Niemeyer, Secretaria de Estado de Saúde do Rio de Janeiro, Rio de Janeiro, Brazil, [2] Instituto de Ciências Biomédicas, Universidade Federal do Rio de Janeiro, Rio de Janeiro, Brazil, [3] Pós-graduação em Anatomia Patológica, Faculdade de Medicina, Universidade Federal do Rio de Janeiro, Rio de Janeiro, Brazil

The enteric glia, a neural crest-derived cell type that composes the Enteric Nervous System, is involved in controlling gut functions, including motility, gut permeability, and neuronal communication. Moreover this glial cell could to give rise to new neurons. It is believed that enteric neurons are generated up to 21 days postnatally; however, adult gut cells with glial characteristics can give rise to new enteric neurons under certain conditions. The factors that activate this capability of enteric glia to differentiate into neurons remain unknown. Here, we followed the progress of this neuronal differentiation and investigated this ability by challenging enteric glial cells with different culture conditions. We found that, *in vitro*, enteric glial cells from the gut of adult and neonate mice have a high capability to acquire neuronal markers and undergoing morphological changes. In a co-culture system with 3T3 fibroblasts, the number of glial cells expressing βIIItubulin decreased after 7 days. The effect of 3T3-conditioned medium on adult cells was not significant, and fewer enteric glial cells from neonate mice began the neurogenic process in this medium. Laminin, an extracellular matrix protein that is highly expressed by the niche of the enteric ganglia, seemed to have a large role in inhibiting the differentiation of enteric glia, at least in cells from the adult gut. Our results suggest that, in an *in vitro* approach that provides conditions more similar to those of enteric glial cells *in vivo*, these cells could, to some extent, retain their morphology and marker expression, with their neurogenic potential inhibited. Importantly, laminin seemed to inhibit differentiation of adult enteric glial cells. It is possible that the differentiation of enteric glia into neurons is related to severe changes in the microenvironment, leading to disruption of the basement membrane. In summary, our data indicated that the interaction between the enteric glial cells and their microenvironment molecules significantly affects the control of their behavior and functions.

Keywords: enteric glia, neurogenesis, laminin, cell culture, microenvironment

OPEN ACCESS

Edited by:
Annalisa Buffo,
University of Turin, Italy

Reviewed by:
Werend Boesmans,
Hasselt University, Belgium
Eric D. Laywell,
Florida State University, United States

***Correspondence:**
Juliana de Mattos Coelho-Aguiar
jumcoelho@gmail.com

Specialty section:
This article was submitted to Neurogenesis, a section of the journal Frontiers in Neuroscience

Received: *26 March 2019*
Accepted: *16 August 2019*
Published: *03 September 2019*

Citation:
Veríssimo CP, Carvalho JS, Silva FJM, Campanati L, Moura-Neto V and Coelho-Aguiar JM (2019) Laminin and Environmental Cues Act in the Inhibition of the Neuronal Differentiation of Enteric Glia in vitro. Front. Neurosci. 13:914. doi: 10.3389/fnins.2019.00914

INTRODUCTION

The enteric nervous system (ENS) controls the motor, secretory and vascular functions of the gastrointestinal tract. The ENS is composed of neurons and enteric glial cells derived from the vagal and sacral neural crest. Enteric glial cells are involved in regulating the main functions of the gut, such as the regulation of the intestinal epithelial barrier, communication between

neurons by modulating neurotransmission, and affect inflammation and many other gut diseases and alterations (Coelho-Aguiar Jde et al., 2015). The enteric glia is a highly plastic cell type, and the phenotype of these cells is dictated by cues from their specific location, i.e., intraganglionic, interganglionic, along nerve fibers in muscle layers, or in mucosa (Boesmans et al., 2015). Glia can assume a reactive phenotype in response to a specific stimulus, and can readily proliferate, both under steady-state conditions and after injury (Joseph et al., 2011).

Neural crest-derived progenitors exist in the adult peripheral nervous system (Dupin and Coelho-Aguiar, 2013). In the adult ENS, neural progenitors can give rise to neurons *in vitro* (Kruger et al., 2002; Bondurand et al., 2003) and in grafts to murine gut explants (Lindley et al., 2008; Metzger et al., 2009; Hetz et al., 2014). In *in vivo* experiments, Laranjeira et al. (2011) chemically destroyed ganglia with benzalkonium chloride (BAC) detergent and demonstrated the neurogenic capability of enteric glial cells in this specific damage condition. Enteric glial cell neurogenesis could also be induced *in vivo* through activation of the serotonin receptor (Liu et al., 2009). Some studies have shown that colitis can lead mouse and human enteric glial cells to undergo neurogenesis (Belkind-Gerson et al., 2015, 2017). Recently, Kulkarni et al. (2017) suggested that constitutive neurogenesis exists in the gut, although this study does not agree with data obtained by other groups that have investigated the matter (Pham et al., 1991; Young et al., 2003; Sasselli et al., 2012), which support the paradigm that intestinal neurons are stable and not easily replaced under healthy conditions. Moreover, the cited study evidences a population of nestin-positive adult progenitor cells that would be the source of these newborn neurons, different from that of GFAP-positive enteric glia, in contrast to previous work that had shown nestin and GFAP co-expression by enteric glial cells (Joseph et al., 2011).

It has been proposed that in cases of ganglion rupture and disruption of contact between cells (Gershon, 2011), such as in cell culture or in the chemical ganglion destruction with BAC detergent (Laranjeira et al., 2011), enteric glial cells have their neurogenic potential activated. However, this hypothesis has never been directly confirmed, and other factors may be involved. How would environmental changes be involved in this neurogenic differentiation of enteric glia?

One possibility is that changes in the extracellular matrix (ECM) in the ganglia niche can trigger the neuronal differentiation of enteric glia. The basement membranes of the muscle cells as well as that of the mucosal layer are rich in laminin, and the glial cells are located nearby. Enteric glia do not produce ECM proteins, but are surrounded by the basement membrane proteins including type IV collagen, laminin and a heparan sulfate proteoglycan (Bannerman et al., 1986; Neunlist et al., 2007). Previous investigations of laminin suggested that laminin-1 promotes migration of sox-10-positive enteric neural crest cells in mice (Nakazawa et al., 2013). Another study cultured neural progenitor cells from the adult rabbit jejunum on substrates composed by different combinations of ECM molecules, including laminin, heparin sulfate and collagen; and found that these molecules did not seem to inhibit the neuronal or glial fate after 5 and 15 days in culture (Raghavan et al., 2013). The composition of the ECM in engineered intestinal smooth-muscle sheets modulates the subtype of neurons differentiated from progenitor neural cells isolated from adult rabbit jejunum (Raghavan and Bitar, 2014). Moreover, a laminin-511 substrate enabled self-renewal in an undifferentiated state of other progenitor cell types, as cultured human embryonic stem cells and induced pluripotent stem cells (Domogatskaya et al., 2008; Miyazaki et al., 2008; Rodin et al., 2010). The engagement of postnatal hippocampal neural progenitor cells with a laminin substrate causes changes in the expression of connexin types and is associated with decreased neurogenesis of these cells in culture (Imbeault et al., 2009).

In spite of the known neurogenic potential of enteric glia, no study has addressed the question of how enteric glia are activated to differentiate in neurons. Here, we challenged enteric glial cells from adult and neonate mice with different cell culture conditions. We described the initial steps of neuronal differentiation of enteric glia in cell culture and investigated the role of the crosstalk between enteric neural cells and mesenchymal cells, in a co-culture with embryonic fibroblasts, as well as the role of the factors secreted by this fibroblasts lineage. Subsequently, we investigated the role of the main basement membrane protein, laminin. Our observations suggested that enteric glial cells in culture without the proper substrate were stimulated to initiate neuronal differentiation. Therefore, it seems that the proper contact of adult enteric glial cells with laminin plays a crucial role in inhibiting their potential for neuronal differentiation.

MATERIALS AND METHODS

Animals

Newborn (P0 or P1) and adult (P90–P120) male Swiss mice were used. This research project was approved by the Animal Use Ethics Committee of the Centro de Ciências da Saúde-Universidade Federal do Rio de Janeiro (CCS-UFRJ) (protocol no. 129/16).

Murine Enteric Neural Cells Culture

ENS cells were obtained from the final portion of the ileum (except the cecum) and the whole colon of adult mice in a culture of adult enteric glia, or the whole intestine of neonatal animals. We collected and thoroughly washed the tissue with phosphate-buffered saline solution (PBS) containing fungizone and penicillin/streptomycin, and removed the mesentery and mucosa with the aid of a stereoscopic microscope. The tissue containing the muscle layers and myenteric and submucous plexuses was cut into smaller pieces and incubated with the enzymes collagenase II (Gibco) and DNAse I (Sigma Chemical Co., St. Louis, MO, United States) for 1 h at 37°C. The tissue pieces were then mechanically dissociated and centrifuged twice (1200 rpm for 5 min). Dissociated cells were plated onto glass coverslips previously coated with poly-L-lysin (Sigma-Aldrich, St. Louis, MO, United States) in DMEM-F12 medium (Gibco, Carlsbad, CA, United States) containing glutamine

(2 mM; Calbiochem, San Diego, CA, United States), sodium bicarbonate (3 mM; Merck, Gibbstown, NJ, United States), penicillin/streptomycin (0.5 mg/ml; Sigma-Aldrich, St. Louis, MO, United States), 10% fetal bovine serum (FBS) and 2% chicken embryo extract (CEE). Cultures were maintained at 37°C in a humidified chamber with 5% CO_2, 95% air. In order to distribute the cells homogeneously, the cells were re-plated, either on the first (neonatal cells) or third (adult cells) day of culture. Cells were trypsinized and cultures were established by plating 1.5-2.0 $\times$ 10^4 cells onto 24-well plates containing glass coverslips coated with poly-L-lysin, laminin, fibronectin or 3T3 feeder-layer substrates. The coating of glass coverslips with the different substrates and preparation of 3T3-conditioned medium (3T3-CM) are described in the following topics.

ENS Cell Co-culture on NIH/3T3 Fibroblast Feeder-Layer

The NIH/3T3 cell lineage monolayer was prepared with 8 $\times$ 10^4 cells per well of the 24-well plate. After 48 h, 1.5 $\times$ 10^4 cells from the passage of enteric glial-cell cultures (from neonatal or adult mice) were plated on a 3T3 feeder-layer. These co-cultures were maintained for 4 (cells from adult mice) or 5 days (cells from neonate mice), fixed, and analyzed by immunofluorescence.

Culture of ENS Cells With NIH/3T3 Fibroblast-Conditioned Medium

The NIH/3T3 cells (1.3 $\times$ 10^6 cells) were plated into 25 cm^2 culture flasks. After 48 h, the culture medium (as described for murine enteric neural cells culture) was conditioned for 24 h, centrifuged at 1500 rpm for 5 min to remove dead cells, and collected for culture of ENS cells.

Preparation of Laminin and Fibronectin Substrates

The poly-laminin substrate (Sigma-Aldrich, St. Louis, MO, United States) was prepared in a concentration of 50 μg/ml, in acid buffer (pH = 4) containing 20 mM sodium acetate and 1 mM calcium chloride according to Freire et al. (2012). This poly-laminin substrate was prepared and added to the plate on the previous day. After at least 12 h at 37°C, the wells with laminin were washed three times with PBS. The ENS cells were then plated and maintained at 37°C and 5% CO_2.

Fibronectin (Sigma-Aldrich, St. Louis, MO, United States) was prepared in a concentration of 50 μg/mL in DMEM-F12 culture medium, added to the plate for 1 h at 37°C and then removed from the wells, which were allowed to dry. Then, the ENS cells were plated and maintained at 37°C and 5% CO_2.

Preparation of Frozen Histological Sections

The intestine sample obtained was fixed with 4% formaldehyde for 16 h at 4°C. After washing with PBS, the sample was incubated in 30% sucrose (diluted in PBS) for at least 16 h. The sample was then transferred to an OCT (Tissue-Tek, Sakura Finetek, United States) mold, and rapidly frozen by immersion in liquid nitrogen. We set the Leica CM1860 cryostat to a temperature of −20°C and made 15-μm sections of the frozen block. The sections were transferred to histology slides previously treated with poly-L-lysine (Sigma-Aldrich, St. Louis, MO, United States).

Immunocytochemistry and Immunofluorescence in Histological Slides

For cells in culture (fixed in 4% paraformaldehyde for 5 min) or histological sections, the material was permeabilized with 0.2% Triton X-100 for 5 min at room temperature, and unspecific sites were blocked with 5% bovine serum albumin (Sigma) for 1 h before immunoreactions with the following primary antibodies: rabbit anti-GFAP (1:400; DAKO Cytomation), rabbit anti-S100β (1:100; Dako Cytomation), mouse anti-Sox10 (1:50; Santa Cruz Biotechnology), mouse anti-p75 (1:60; Millipore); mouse anti-βIIItubulin (1:500; Promega), mouse anti-HuC/D (1:50; Molecular Probes), rabbit anti-Peripherin (1:500; Millipore), mouse anti-smooth muscle actin (SMA) (1:400; Sigma), rabbit anti-Ki67 (1:200; BD pharmigen), rabbit anti-laminin (1:100; Sigma-Aldrich), rabbit anti-fibronectin (1:100; Sigma-Aldrich). After incubation with the primary antibody, the material was thoroughly washed with PBS and incubated with secondary antibodies for 1 h at room temperature. Secondary antibodies were: goat anti-mouse Alexa Fluor 546 (1:500) or goat anti-rabbit Alexa Fluor 488 (1:500) (Molecular Probes). Nuclei were counterstained with DAPI (4′,6-diamidino-2-phenyindole, dilactate; Sigma-Aldrich). The images were obtained with a Leica DMi8 inverted fluorescent microscope. Deconvolution of the images and Z projection analysis were performed. The images were obtained with the projection of 5 or more photos along the *Z* axis.

Immunofluorescence *in toto*

The longitudinal muscle layer of the colon or ileum was dissected using a stereoscope microscope, and then the tissue containing the myenteric plexus adhered to the muscle tunica was fixed in 4% formaldehyde for 16 h at 4°C. The material was then permeabilized and blocked by incubating with 0.2% triton-X100 and 5% BSA for 1 h, and after several washes with PBS, was incubated with the primary antibody for 16 h at 4°C. Specific antibodies were used for glial (GFAP and S100β), neuronal proteins (βIIItubulin, Peripherin and HuC/D), and for laminin at the same dilution as in the immunocytochemistry protocol. Then, after washes with PBS, the material was incubated with the specific secondary antibody for 2 h at room temperature. Nuclei were counterstained with DAPI and the tissues mounted as histological sections. The images were obtained with a Leica DMi8 inverted fluorescent microscope.

RT-PCR Experiments

RNA was extracted from the cultured cells using TrizolVR (Invitrogen), according to the manufacturer's instructions. Complementary DNAs (cDNAs) were synthesized using a High-Capacity cDNA Reverse Transcription kit (Applied Biosystems) according to the supplier's instructions, and were used as templates for the polymerase chain reaction (PCR). Primers

were designed and synthesized by Sigma or IDT. Reverse and forward specific oligonucleotides were: GFAP: (F) TGC AAG AGA CAG AGG AGT GG, (R) CTC CAG ATC GCA GGT CAA GG; βIIItubulin: (F) CCC AGC GGC AAC TAT GTA GGG, (R) CCA GGT TCC AAG TCC ACC AGA A; P75: (F) CCA ACC AGA CCG TGT GTG AA, (R) CAC AGG GAG CGG ACA TAC TC; Sox10: (F) GCT GGA CCG CAC ACC TTG, (R) TCC TCG TGA AGA GCC CAA CG; Synaptophysin: (F) GTG TTT GCC TTC CTC TAC TC, (R) CAC ATA GGC ATC TCC TTG ATA A; Psd95: (F) TGC CAG ATG GAC AAG GAG ACC AAA, (R) TGT TGG CCT TGA GGT GGT AGA GTT; β-actin: (F) TGG ATC GGT TCC ATC CTG G, (R) GCA GCTCAG TAA CAG TCC GCC TAG A. PCR parameters were 94°C for 30 s (first cycle 2 min) for the denaturing step, 60°C for 30 s for the annealing step, and 72°C for 60 s for the elongation step, with a total number of 35 cycles. PCR included beta-actin as a control and reaction in the absence of the cDNA prepared in the reverse transcriptase reaction step (RT−).

Statistical Analysis

GraphPad Prism version 5.0 (GraphPad Software, La Jolla, CA, United States) was used for statistical analysis of quantitative data. An Analysis of Variance (ANOVA) was followed by a Bonferroni post-test for multiple comparisons, and a *t*-test was performed for each pair of means. The results represent the mean of the quantification of three independent experiments. In each experiment, cells from 10 or more photos (using the 20x magnification objective) from different fields of the cell culture were quantified. A value of $P < 0.05$ was considered statistically significant. The data are reported as mean ± standard deviation; the error bars in the graphs represent the standard deviation.

RESULTS

Enteric Glial Cells Migrate to Each Other and Acquire Neuronal Markers When Cultured *in vitro*

Cells of the enteric nervous system were obtained from mouse colon and ileum, from dissociated tissue containing the myenteric and submucous plexus after mucosa removal. After 3 days, the cultured cells were analyzed (**Figures 1A–C**'), or they were harvested, individualized and re-plated. In these conditions, after re-plating, enteric neural cells proliferated and tended to organize themselves in groups (**Figure 1D**).

In addition to enteric neural cells, the target of this study, we found many cells that were negative for the neural markers at all times analyzed. Most of them were fibroblasts and expressed SMA protein (**Supplementary Figure S1**). After 3 days in cultures, neural cells accounted for 51.1–73.5%, and after 7 days they represented 29.4–48.9%. We represented in the graphics only the neural cells stained for the analyzed markers.

To evaluate the presence of enteric glial and neuronal cells, we analyzed the expression of the glial marker GFAP, and of βIIItubulin, a marker of early neuroblasts and mature neurons, at different culture times. In these cultures of ENS cells from adult mice, many GFAP-positive cells were detected at day 3 (**Figures 1A,B**). Cells positive for GFAP+βIIItubulin+ comprised 86.1 ± 4.3%, and only 11.6 ± 5.0% of the neural cells consisted of cells double-labeled with both the glial and neuronal markers. GFAP-βIIItubulin+ cells comprised only 2.2 ± 1.5% (**Figure 1H**). At day 7 (**Figures 1D–G**), 73.8 ± 12.9% of the neural cells co-expressed GFAP and the neuronal marker βIIItubulin (**Figures 1G,G**'), either isolated or in groups. Cells that expressed only GFAP comprised 17.6 ± 14.0%. Relatively few cells (about 8.4 ± 3.3%) expressed only the neuronal marker and correspond to neurons arising to the cell culture directly from intestinal tissue, that do not appear from the differentiation *in vitro* of enteric glial cells. Neurons obtained directly from the gut tissue were easily identified morphologically and had a clearly higher fluorescence intensity of βIIItubulin staining (arrow in **Figure 1B**, for example), compared to the GFAP and βIIItubulin double-labeled cells. They correspond to the GFAP-βIIItubulin+ cells found at days 3 and 7 of culture.

These initial results suggest that GFAP-positive enteric glial cells are in the initial steps of directly convertion into neurons *in vitro*, and co-expressed both markers. To better characterize this event, we investigated other glial markers. We found that most of the GFAP-positive cells also expressed Sox10 (**Figures 1I–J**') and nestin (data not shown), and few cells expressed only one of these markers. Even at day 7, Sox10 was expressed by most of the GFAP-positive cells, which were also labeled with anti-βIIItubulin (**Figures 1J,J**').

This acquisition of the neuronal marker by enteric glia was also observed in cells from the neonate gut. **Figure 2D** shows the quantification of enteric neural cells expressing glial and neuronal markers after 2 and 6 days in culture.

We also obtained in culture of neonate enteric neural cells many negative cells for the neural markers. After 2 days in cultures, neural cells accounted for 14.4–18.8%, and after 6 days they represented only 14.4–21.2%. We represented in the graphics only the neural cells stained for the analyzed markers.

After 2 days (**Figure 2A**), most of the neural cells were enteric glia (GFAP+βIIItubulin−) (49.0 ± 6.0%), and 38.9 ± 7.3% were double-labeled. At day 6 (**Figures 2B,C**), 89.7 ± 7.4% of the cells co-expressed both GFAP and βIIItubulin. Once again, after replating the neural cells migrated to maintain contact with each other and were mainly organized in groups (**Figure 2D**). GFAP-βIIItubulin + cells represent a small percentage after 2 and 6 days.

After 14 and 21 days of adult enteric neural cells culture, neural cells that expressed both GFAP and βIIItubulin still predominated (**Figure 3**). However, βIIItubulin expression had a generally higher fluorescence level in most of positive cells. After 21 days in culture, the cells were replated three times, and we could not identify neurons arising to the cell culture directly from intestinal tissue, that do not appear from the differentiation *in vitro* of enteric glial cells (neither by the high expression of βIIItubulin nor by morphology), probably because of the culture passage procedures. Nevertheless, at days 14 and 21, GFAP-βIIItubulin+ cells were easily found

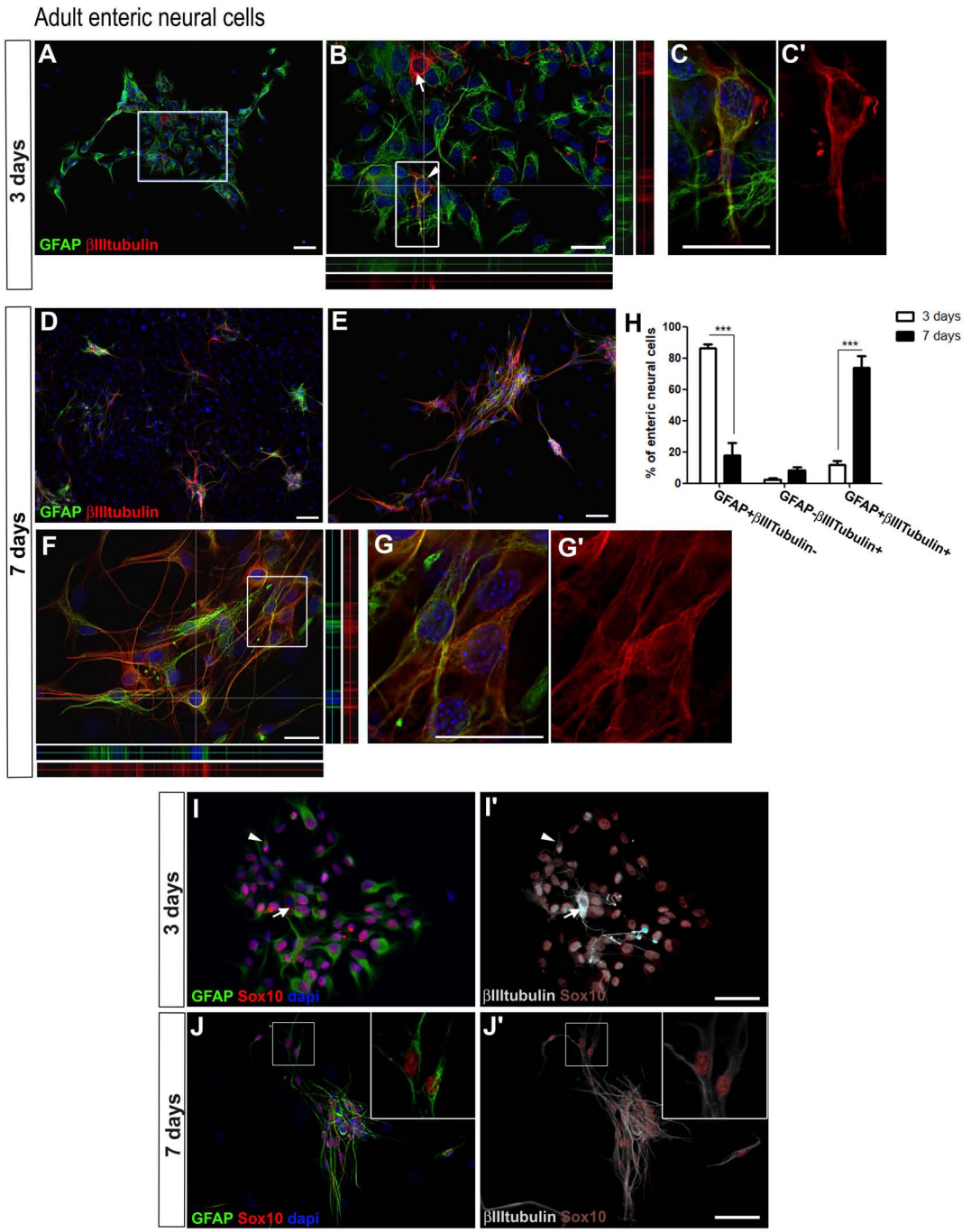

FIGURE 1 | Adult enteric glial cells acquire βIIItubulin expression *in vitro*. **(A–G')** Enteric neural cells immunostained for GFAP and βIIItubulin. **(A–C')** At day 3, most of the cells were GFAP-positive. βIIItubulin expression was observed in neurons arising to the cell culture directly from intestinal tissue (arrow in **B**) or in few cells that were also positive for GFAP (arrowhead in **B**). **(B)** Higher magnification of selected field in **(A)**. Orthogonal view confirms the expression of GFAP, βIIItubulin or both at a given point. **(C,C')** Double-labeled cell depicted in **(B)** (arrowhead) shown in higher magnification. **(D–G')** At day 7, after replating than at day 3, most of the neural cells were organized in groups **(D,E)**, and most enteric neural cells showed expression of both GFAP and βIIItubulin. **(F)** Orthogonal view confirms the expression of GFAP, βIIItubulin or both at a given point. **(G,G')** Double-labeled cells depicted in **(F)** shown in higher magnification. **(H)** Quantification of GFAP and/or βIIItubulin-expressing adult enteric neural cells at days 3 and 7 in cell culture. Cells expressing only GFAP showed a significant reduction from day 3 to day 7. Instead, the number of double-labeled cells increased markedly over the period. The results represent the mean of three independent experiments. $^{***}P < 0.001$. **(I–J')** Sox10 expression by cultured adult enteric nervous system cells at days 3 and 7. Same field is shown in **(I,I')**. Same field is shown in **(J,J')**. Most glial cells showed GFAP and Sox10 expression, but some expressed only Sox10 or GFAP. At day 3, βIIItubulin expression **(I')** was rarely observed in neurons arising to the cell culture directly from intestinal tissue (arrow) or in cells that were also positive for GFAP and Sox10 (arrowhead). At day 7, most neural cells were labeled for both the glial markers and βIIItubulin. Two GFAP+Sox10+βIIItubulin+ cells are shown in higher magnification **(J,J')**. Scale bars: 100 μm **(D,I–J')**, 50 μm **(A,E)**, and 25 μm **(B,C',F,G')**.

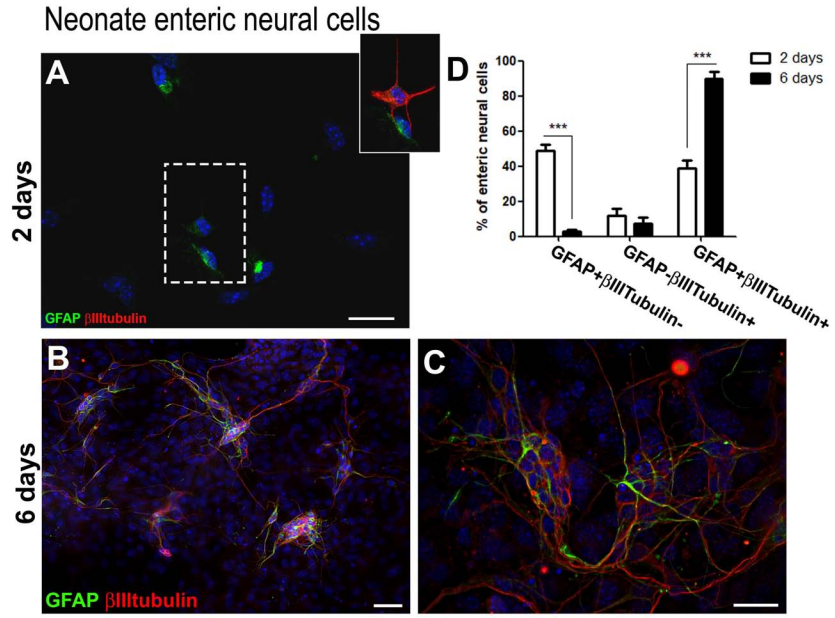

FIGURE 2 | Neonate enteric glial cells acquire βIIItubulin expression *in vitro*. **(A–C)** Enteric neural cells immunostained for GFAP and βIIItubulin. **(A)** At day 2, a great proportion of GFAP-positive cells already expressed βIIItubulin. βIIItubulin expression was also observed in some neurons arising to the cell culture directly from intestinal tissue. The selected field, in higher magnification, shows a cell expressing only GFAP and other expressing both markers. **(B,C)** At day 6, most of the neural cells were organized in groups after replating than at day 1, and most enteric neural cells expressed both GFAP and βIIItubulin. **(D)** Quantification of numbers of GFAP and/or βIIItubulin-expressing neonate enteric neural cells at days 2 and 6 in cell culture. As occurred with the adult cells, neonate cells expressing only GFAP showed a significant reduction from day 2 to day 6. Instead, the number of double-labeled cells increased markedly over the period. The results represent the mean of three independent experiments. $^{***}P < 0.001$. Scale bars: 50 μm **(B)** and 25 μm **(A,C)**.

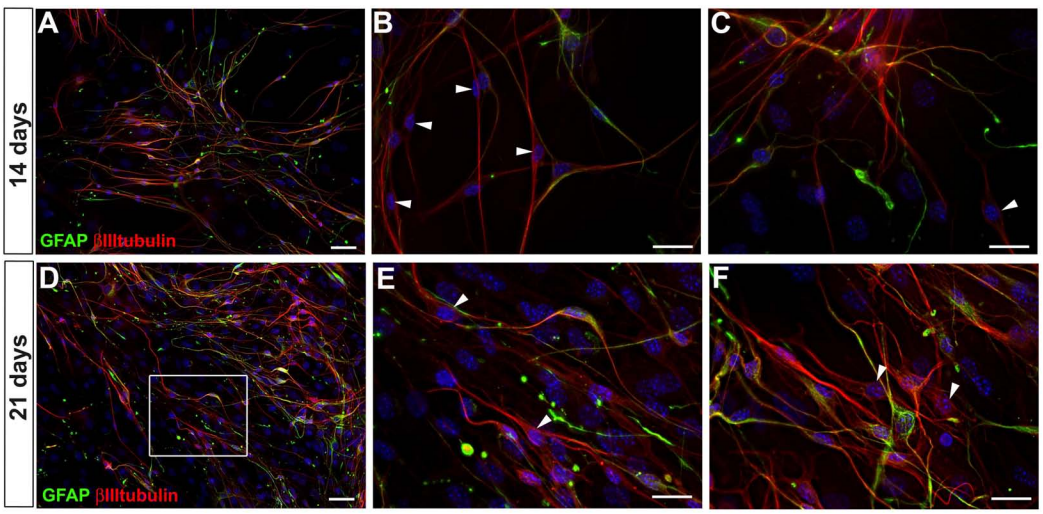

FIGURE 3 | GFAP and βIIItubulin expression by adult mouse enteric nervous system cells at days 14 and 21 in culture. **(A–C)** Culture at day 14. **(D–F)** Culture at day 21. Stronger expression of βIIItubulin per cell. Cells expressing only βIIItubulin indicated by arrowheads in **(B,C,E,F)**. Scale bars: 50 μm **(A,D)** and 25 μm **(B,C,E,F)**.

(arrowheads in **Figures 3B,C,E,F**), suggesting that they had lost the GFAP expression in the neurogenic differentiation process. In fact, it was difficult to find a cell expressing GFAP that did not also express βIIItubulin. Even those with strong GFAP expression and glia morphology had at least a basal expression of βIIItubulin.

To investigate whether enteric glial GFAP-positive cells could progress toward acquiring neuronal markers, the cultures were further investigated for the presence of other mature neuronal markers at 7, 14 (data not shown) and 21 days (**Figure 4**). HuC/D, the RNA-binding protein that is present in immature and mature neurons, and Peripherin, an intermediate filament of mature

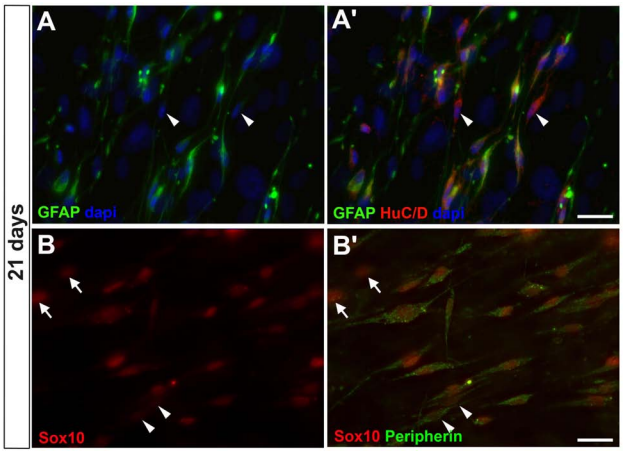

FIGURE 4 | Enteric glial cells undergoing neurogenesis *in vitro* expressed HuC/D and peripherin after 21 days. **(A,A')** Same field is shown in **(A,A')**. Image shows cells expressing GFAP and HuC/D and some expressing only HuC/D (arrowheads). **(B,B')** Same field is shown in **(B,B')**. Cells expressing Sox10 and peripherin. Some of them expressed only peripherin (arrowheads), and others did not yet express peripherin, only Sox10 (arrows). Scale bars: 25 μm.

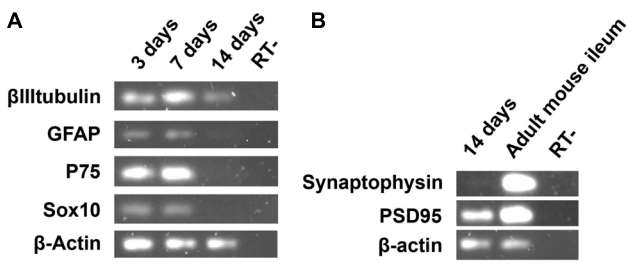

FIGURE 5 | Semi-quantitative RT-PCR analysis of adult ENS cells in culture at days 3, 7, and 14. **(A)** The expression of βIIItubulin, neuron marker gene, and glial marker genes were evaluated. **(B)** The synaptic protein Psd95 was highly expressed after 14 days of enteric glial cell culture.

neurons, could be observed at 7 days in only a few GFAP-negative cells (data not shown), corresponding to neurons arising directly from intestinal tissue. In cells cultured for 21 days, HuC/D was detected with a weak fluorescence intensity in GFAP-positive cells and some GFAP-negative cells (arrowheads in **Figures 4A,A'**). Peripherin was weakly expressed in most of Sox10-positive cells.

The *in vitro* development of enteric glia in the course of the neuronal fate was further characterized by semi-quantitative RT-PCR of cultures harvested from day 3 to day 14 (**Figure 5**). Data from the RT-PCR experiments confirmed the different levels of genes expressed by ENS cells over the course of the cell culture, as observed through immunocytochemical experiments. The level of βIIItubulin mRNA expression increased noticeably from 3 to 7 days, although the βactin level was slightly lower at 7 days, and even with the number of non-neural cells having grown considerably in this period, as mentioned before. At 14 days, βIIItubulin was notably higher than GFAP,

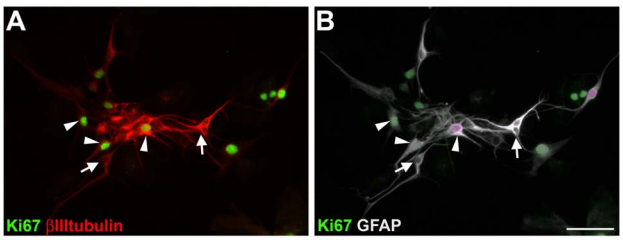

FIGURE 6 | Proliferation of cultured adult mouse enteric nervous system cells. After 7 days *in vitro*, cells were immunostained for Ki67, βIIItubulin **(A)** and GFAP **(B)**. Same field is shown in **(A,B)**. GFAP and βIIItubulin double-labeled cells with (arrowheads) or without (arrows) Ki67 staining. Scale bar: 50 μm.

which showed a basal expression (the low expression of GFAP at 14 days was probably due to a larger number of non-neural cells that proliferated from days 7 to 14). Sox10 and p75 showed similar levels of expression between days 3 and 7, and, similarly to GFAP, almost no expression after day 14, indicating the presence of βIIItubulin-positive cells that had lost their glial marker expression, as also observed by immunocytochemistry.

In addition to the glial and neuronal markers, we investigated the presence of a synaptic gene expression in our ENS cell cultures (**Figure 5B**). At day 14 we found no expression of synaptophysin, a protein that is usually present in neuronal synaptic density. Curiously, we observed expression of psd95, a protein involved in the organization of postsynaptic density, suggesting the development of neuronal activity of the glial cells that were becoming neurons.

Taken together, these data suggest that cultured enteric glia can undergo a process of neuronal differentiation.

Enteric GFAP-Positive Cells Acquire βIIItubulin Expression *in vitro* Independently of Their Proliferative State

We analyzed the proliferative state of adult enteric neural cells cultured for 7 days (**Figure 6**). In our culture conditions, we observed many neural and non-neural proliferative cells. Double-labeled cells for GFAP and βIIItubulin could be in a proliferative state (arrowheads) or not (arrows). These results are consistent with a transdifferentiation process, since we observed βIIItubulin expression in most of the cells that were positive for GFAP and Sox10 (**Figures 1I–J'**).

In vivo Enteric Glial Cells Do Not Express βIIItubulin

Histological stains were used to evaluate the expression of the glial marker GFAP and the neuronal markers βIIItubulin, HuC/D and Peripherin, directly in the tissue. We observed that glial and neuronal markers did not usually co-localize. In the longitudinal muscle with the adherent myenteric plexus (LMMP) preparations (**Figures 7A–C**), GFAP did not co-localize with βIIItubulin (**Figures 7A–A"**) or with HuC/D (**Figures 7B,C**). In transverse

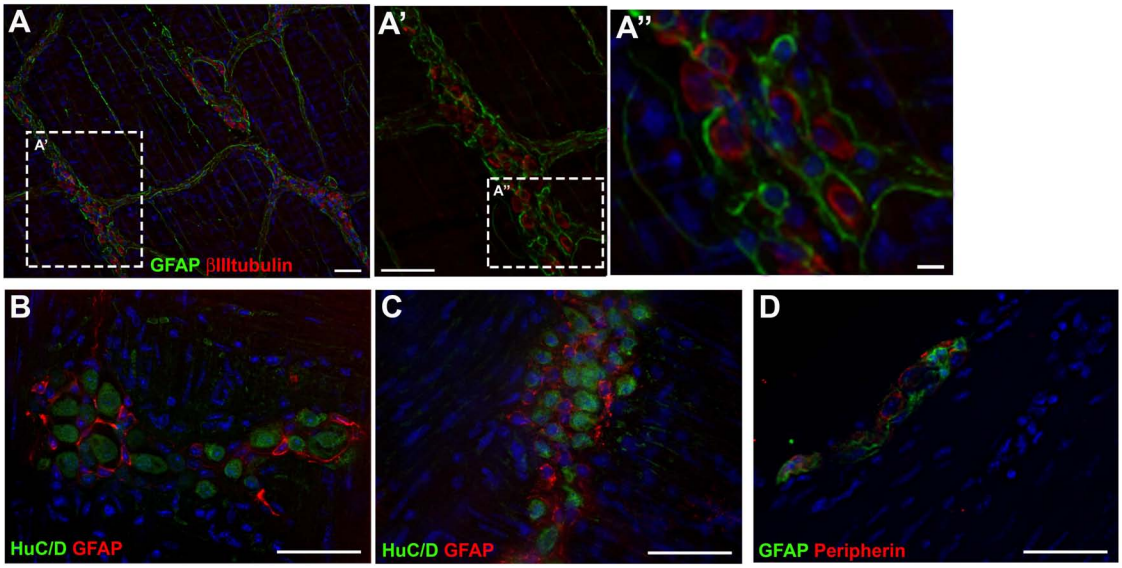

FIGURE 7 | Expression of glial and neuronal markers in mouse gut tissue. **(A,A')** Longitudinal muscle with the adherent myenteric plexus (LMMP) of adult mouse colon stained for GFAP and βIIItubulin. **(B,C)** LMMP of adult mouse ileum stained for GFAP and HuC/D. **(D)** Transverse section of mouse colon stained for GFAP and Peripherin. Scale bars: 25 μm **(A")** and 50 μm **(A,A',B–D)**.

sections of adult mouse colon, GFAP did not co-localize with peripherin (**Figure 7D**).

Co-culture With Embryonic Fibroblasts Limits the Neuronal Differentiation Process of Enteric Glia

In vivo, the enteric neural cells are influenced by different secreted molecules and in contact with specific substrates, influenced by muscle, fibroblastic, immune and other cell types. Feeder cells can be used to support the indifferentiated growth of stem cells. They provide an environment with several secreted molecules, adhesion molecules, and ECM proteins (Li et al., 2017). We cultured the ENS cells on a feeder-layer of the 3T3 lineage of mouse embryonic fibroblasts. On 3T3 feeder-layers, the glial cells did not underwent neuronal differentiation to the same extent, nor did enteric glial cells from adult or neonate mice (**Figure 8**). In this condition, fewer cells from adult mice were positive for both GFAP and βIIItubulin after 7 days in culture, comprising only 40.0 ± 9.8% (**Figures 8A,C**), whereas in the control they comprised 73.8 ± 12.9%, as we showed previously (**Figure 1H**); and the cells expressing only GFAP comprised 53.8 ± 10.8%, against 17.6 ± 14.0% in the control cultures. To determine whether soluble factors released by 3T3 could play a role in this differentiation-inhibition effect, we treated the enteric neural cells with the 3T3-conditioned medium (3T3-CM) (**Figure 8B**). No significant inhibition was observed compared to the control condition and 67.3 ± 14.2% were double-labeled cells (**Figures 8B,C**).

Neonate enteric glial cells cultured on the 3T3 feeder-layer also had their differentiation potential inhibited (**Figure 8D**). Cells double-labeled for GFAP+βIIItubulin+ comprised only 32.8 ± 9.9% after 6 days of co-culture (**Figure 8F**), while in the control they comprised 89.7 ± 7.4%, as mentioned above (**Figure 2D**). Cells expressing only GFAP comprised 53.3 ± 12.6%, and in the control comprised 2.8 ± 1.6%. With 3T3-CM the inhibition was not as marked as on the 3T3 substrate, but still this condition led to a significant reduction of cells expressing both the glial and neuronal markers (**Figure 8E**). 3T3-CM reduced the percentage of GFAP+βIIItubulin+ cells to 68.8 ± 7.2% after 6 days in culture (**Figure 8F**).

Laminin Is Expressed by Basement Membranes of the Muscular and Epithelial Cells of the Gut and Contact With It Reduces the Number of Enteric Glial Cells in Neuronal Differentiation Process *in vitro*

We observed that 3T3-CM did not significantly regulate the neurogenesis of adult enteric glial cells. Another possibility is that this effect was produced by the physical contact of enteric glial cells with 3T3 and the deposited proteins produced by this cell lineage.

One must consider the role of laminin, a protein of the ECM, that similarly to the fibroblast feeder-layers, may support the undifferentiated growth of some cell types, such as ES cells (Miyazaki et al., 2008). Accordingly, we also analyzed the expression of the ECM proteins laminin and fibronectin by the 3T3 fibroblasts. Our results showed that 3T3 cells expressed laminin and fibronectin (**Supplementary Figure S2**). We observed some neuronal and glial projections that followed the same pathway designated by laminin deposition (data not shown).

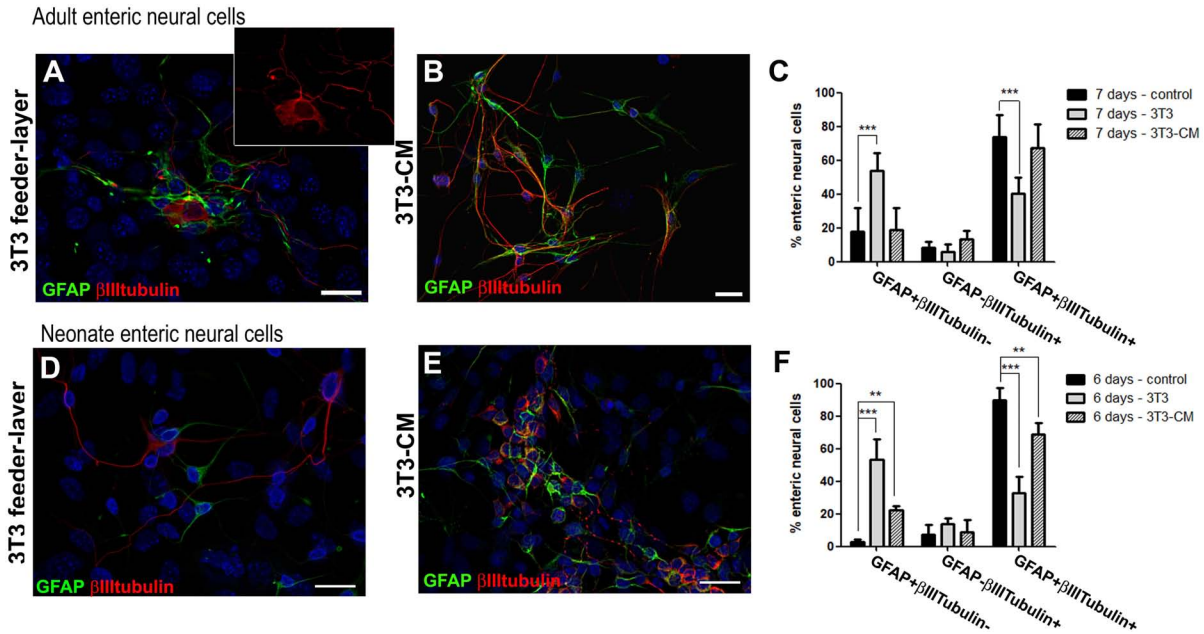

FIGURE 8 | Culture of enteric glial cells on 3T3 fibroblast feeder-layer inhibits neurogenesis. Analysis by immunostaining for GFAP and βIIItubulin. **(A–C)** After cell passage on day 3, the adult enteric neural cells were maintained for more 4 days on 3T3 feeder-layer **(A)** or with 3T3-CM **(B)**. Quantification **(C)** of GFAP and/or βIIItubulin expressing adult enteric neural cells in control, on 3T3-feeder-layer, or with 3T3-CM treatment. Significantly fewer cells expressed both GFAP and βIIItubulin when cultured on 3T3 feeder-layer. The results represent the mean of 3 independent experiments. ***$P < 0.001$. **(D–F)** After cell passage on day 1, neonate enteric neural cells were maintained for 5 more days on 3T3 feeder-layer **(D)** or with 3T3-CM **(E)**. Quantification **(F)** of GFAP and/or βIIItubulin expressing neonate enteric neural cells in control, on 3T3 feeder-layer, or with 3T3-CM treatment. Cells expressing only GFAP significantly increased in the 2 new conditions. The number of double-labeled cells showed a significant reduction with 3T3-CM and even more on the 3T3 feeder-layer. The results represent the mean of 3 independent experiments. **$P < 0.01$, ***$P < 0.001$. Scale bars: 25 μm.

The expression of laminin and fibronectin by 3T3 suggests that contact with these ECM could be involved in the maintenance of enteric glia that do not undergo neuronal differentiation. The next step was to investigate how the basement membrane produced by the gut cells is related to the enteric neural cells. We performed immunofluorescence analyses of adult and neonate gut tissue. We observed that laminin composes the basement membranes of epithelial and muscular layers of mucosa and also of muscle cells of the circular and longitudinal layers (**Figures 9A,B**). Longitudinal and circular muscle layers of the adult gut express large amounts of laminin (**Figure 9A**), while the laminin network of muscle layers of the neonate mouse gut is still sparse, suggesting that the ganglion cells may not necessarily be in contact with laminin at that time (**Figure 9B**). ENS ganglionic cells seem to not express laminin (arrow at **Figure 9A**), but in the adult mouse they are in close contact with it, especially the cells composing the myenteric ganglia, located between the laminin layers.

Therefore, in order to understand the real function of the contact of enteric glia with laminin in the differentiation process, we prepared a poly-laminin substrate (Freire et al., 2012) to culture the enteric neural cells of adult (**Figures 9C,D**) and neonate (**Figures 9H,I**) mice. The fibronectin substrate was also used in the ENS cell culture (**Figures 9F,G**). The number of enteric glial cells from adult mice who acquired the expression of βIIItubulin decreased markedly during the 7 days of culture. GFAP+βIIItubulin+ cells comprised 31.8 ± 6.1%, while in the absence of the substrate they comprised 73.8 ± 12.9% (**Figure 9E**). Cells expressing only GFAP comprised 17.6 ± 14.0% in the control and 63.3 ± 7.2% on laminin. When cultured on the fibronectin substrate, the neural cells showed a quite different morphology, with longer neural projections (**Figures 9F,G**), and the cell culture contained a markedly larger number of cells, suggesting a role in proliferation. However, the fibronectin substrate showed no observable function in the neuronal differentiation process, and the cells acquired βIIItubulin expression, as occurred in the control conditions. These observations reinforce the specific role of laminin in this function of inhibiting enteric glia differentiation.

For enteric glial cells of neonate mice, on the other hand, neurogenesis was not significantly inhibited by contact with the laminin substrate (**Figures 9H,I**). Although the GFAP+βIIItubulin+ double-labeled cells showed a lower fluorescence intensity than the control cells, they were still very numerous, comprising 79.6 ± 4.0% of the neural cells found in cultures at 6 days. Cells expressing only GFAP comprised only 5.8 ± 4.5% in this condition (**Figure 9J**).

Our *in vitro* results strongly suggest that the cell microenvironment acts to maintain the differentiation potential of enteric glia, and that the laminin deposits located around the

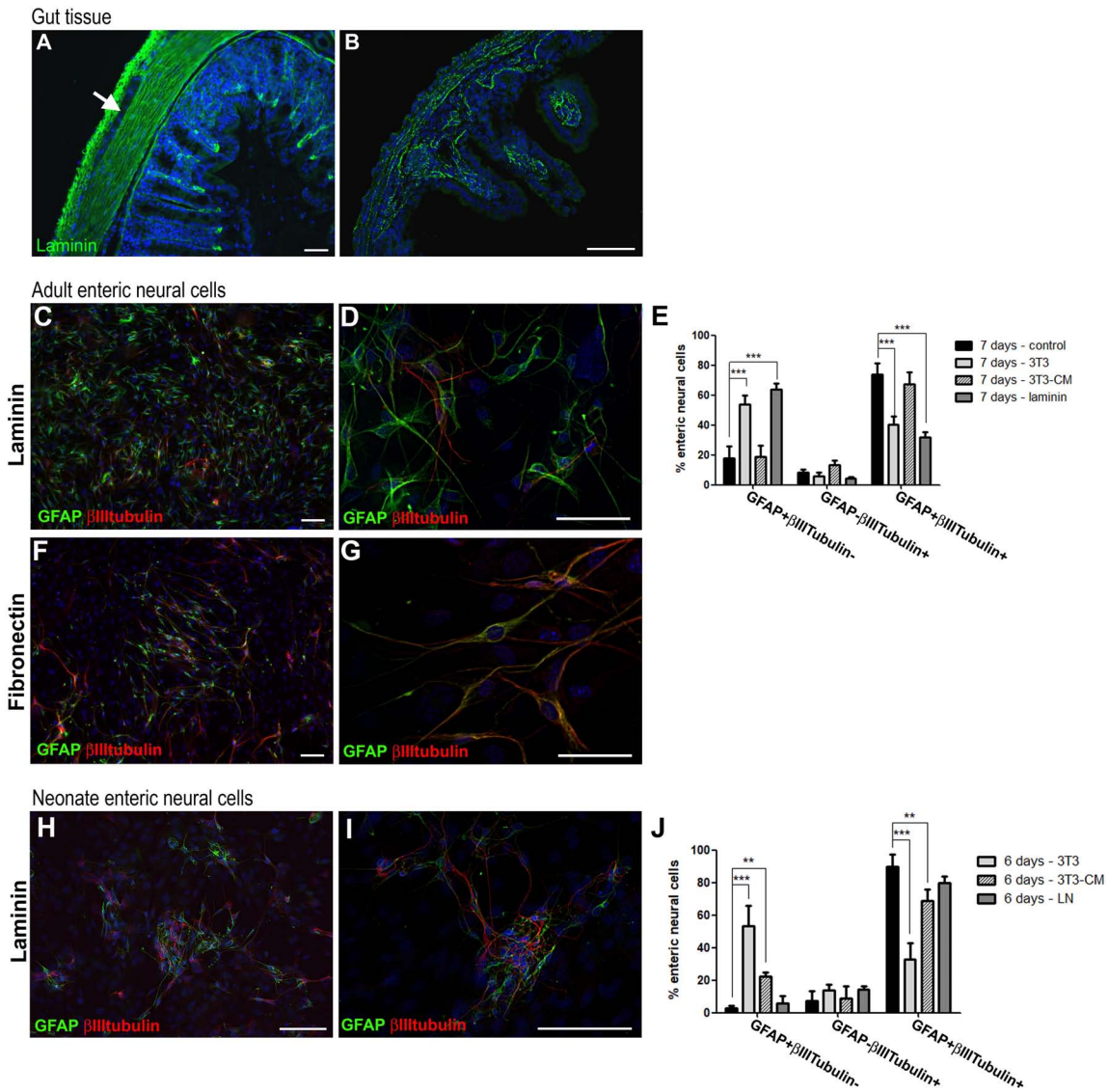

FIGURE 9 | Culture of adult mouse enteric glial cells on laminin substrate inhibits neurogenesis. Analysis by immunostaining for GFAP and βIII-tubulin. **(A,B)** Muscle layers of adult mouse colon expressed high amounts of laminin **(A)**, and muscle layers from neonate mice showed sparse deposition of laminin **(B)**. Laminin expression can also be observed on basement membranes of adult and neonate mucosal layers. **(C,D)** Adult mouse enteric glial cells cultured on laminin substrate. **(E)** Graph shows the data of **Figure 8C**, plus the culture condition on laminin. On laminin, fewer cells expressed both GFAP and βIIItubulin, at a similar rate found in the co-culture with 3T3 fibroblasts. At the same time, a much larger number of cells expressed only GFAP. The results represent the mean of 3 independent experiments. $^{***}P < 0.001$. **(F,G)** Adult enteric glial cells cultured on fibronectin substrate. As in the control condition, most of the cells expressed both GFAP and βIIItubulin after 7 days in culture. **(H,I)** Neonate enteric glial cells cultured on laminin substrate. **(J)** Graph shows the data of **Figure 8F**, plus the culture condition on laminin. The number of cells expressing only GFAP or both GFAP and βIIItubulin did not change significantly on laminin. The results represent the mean of 3 independent experiments. $^{**}P < 0.01$, $^{***}P < 0.001$. Scale bars: 50 μm **(A,B,D,G)** and 100 μm **(C,F,H,I)**.

ganglia are a newly recognized factor in controlling the process of differentiation of adult enteric glia into neurons.

DISCUSSION

By culturing enteric glial cells *in vitro*, we observed that after a few days most of the enteric neural cells naturally showed both the glial marker GFAP and the neuronal marker βIIItubulin. The proportion of these double-labeled cells increased gradually in the first days of culture, reaching 73.8 ± 12.9% of the neural cells in the 7-day adult cell cultures and 89.7 ± 7.4% in the 6-day neonatal cell cultures (**Figures 1H**, **2D**).

Some cells double-labeled for GFAP and βIIItubulin were in a proliferative state, and others were not. These observations together with the fact that the cells express the glial and neuronal markers in the same exact moment, indicate that the glial cells were in the process of transdifferentiating into neurons,

which is in agreement with a previous study that observed transdifferentiation of enteric glial cells *in vivo* in cases of colitis (Belkind-Gerson et al., 2017). In that study, with *in vivo* experiments, the Sox2-positive enteric glial cells also showed double labeling with the HuC/D neuronal marker during the differentiation process, and were negative for RET, which is typically present in neurons and progenitor cells. Laranjeira et al. (2011) demonstrated that the glial marker GFAP was lost before the acquisition of the βIIItubulin marker. While in our experiments a transdifferentiation process seemed to occur without the need for proliferation, that study indicated dedifferentiation followed by differentiation initiated by Mash1, at least in part of the neurons.

The ability of glial cells to become neurons has also been observed in the central nervous system by some studies. It has already been shown that astrocytes of the subventricular zone of the adult mice brain give rise to neurons of the olfactory bulb. They are also able to generate immature progenitors and neuroblasts in the region, after elimination of neurons and progenitors with antimitotic treatment, and form multipotent neurospheres *in vitro* (Doetsch et al., 1999). Astrocytes of the cerebral cortex, spinal cord, cerebellum and subependymal zone of neonatal mice of up to 2 weeks form neurospheres that give rise to both neurons and glia. In adult mice this capacity was observed only in the astrocytes of the subependymal zone (Laywell et al., 2000). Cells differentiated from neurospheres generated from cells of the subependymal zone or cerebellar cortex of postnatal mice also present from 3 days in culture the expression of both GFAP and βIIItubulin markers (Laywell et al., 2005).

We also analyzed the presence of Sox10 in those glial cells that initiated neuronal differentiation with βIIItubulin expression. During development, neuronal differentiation of the enteric neural crest involves the inhibition of Sox10, which continues to be expressed only in glial cells. Interestingly, a distinct majority of GFAP+βIIItubulin+ cells continued to express Sox10. The GFAP+βIIItubulin+Sox10- or GFAP-βIIItubulin+Sox10+ cells were rare.

Our RT-PCR experiments reinforce this sequential program of differentiation. Interestingly, at 3 days, when βIIItubulin-positive cells correspond to only 13.8% of the neural cells (and 8.8% of total cell number, including non-neural cells), before overt morphological differentiation, we found a high RNA expression of βIIItubulin when compared with GFAP expression (97.7% of the neural cells and 62.7% of total cell number), which suggest that neurogenesis starts *in vitro* before the production of βIIItubulin protein by the glial cells.

Recently, Kulkarni et al. (2017) suggested that neural progenitors exist in the gut of healthy adult mice, and replace most of the enteric neurons lost by apoptosis every 2 weeks. According to the authors, these progenitor cells express nestin, but not Sox10, thus composing a nestin+Sox10- cell population different from the sox10-positive enteric glial cells. In contrast, Joseph et al. (2011), characterizing the enteric glial cells isolated from the myenteric plexus of the mouse colon by CD49b expression, showed that 98% of them expressed Sox10 and 93% expressed nestin, making it clear that most glial cells show both markers, contrary to the findings of Kulkarni et al. (2017). Our results showed that nestin was expressed *in vitro* by most enteric glial cells (**Supplementary Figure S3**), which also expressed GFAP and Sox10 (**Figures 1I–J'**). In addition, a study in mice, that received pulses of thymidine analogs at regular intervals, showed that enteric neurons arise from E8 until the first 3 weeks of life only (Pham et al., 1991).

In long-term cultures of 14 and 21 days it was possible to detect the presence of HuC/D and peripherin (**Figure 4**), neuronal markers that arise later than βIIItubulin. This was not observed in the 7-day cultures, where only neurons from the primary culture were positive for these markers (data not shown). In later cultures, we readily observed the presence of cells expressing only the βIIItubulin marker, indicating that by continuing the neurogenesis process, the original glial cells lose the GFAP expression (neurons arising to the cell culture directly from intestinal tissue, that do not appear from the *in vitro* differentiation of enteric glial cells, are mostly lost in the 7-day passage).

The markers analyzed *in vitro* were also evaluated directly in the intestinal tissue, in the colon and/or ileum of adult mice. We did not find co-localization of the glial and neuronal markers when we analyzed the myenteric plexus ganglia adhered to the longitudinal muscular layer (LMMP), confirming that *in vivo* these markers are not commonly co-expressed.

It is known that stem cells cultured on fibroblasts monolayers can maintain their undifferentiated growth (Domogatskaya et al., 2008; Rodin et al., 2010). Our results showed that a co-culture system with 3T3 fibroblasts also restricted the differentiation of enteric glial cells from neonatal mice, where only 32.8 ± 9.9% expressed GFAP and βIIItubulin; and from adults, where only 40.0 ± 9.8% were double-labeled. In this way this culture condition does seem to more closely resemble the condition of enteric glial cells *in vivo*.

According to Gershon (2011), the disruption of contact between cells may initiate neurogenesis from precursors that express enteric glial markers. However, our data showed that even after the dissociation of the neural cells performed in the culture protocol, enteria glial cells showed a significantly lower rate of differentiation when they were dispersed on the 3T3 monolayer. What property of 3T3 fibroblasts might be responsible for causing the smallest number of cells in neurogenesis? One might consider the possibility of an effect of secreted soluble growth factors. However, we did not observe a significant change in the differentiation rate when we cultured the adult ENS cells in the presence of conditioned medium from 3T3 fibroblasts. Only co-cultured enteric glia from newborn mice showed a significant reduction in the number of cells expressing both GFAP and βIIItubulin, although smaller than the inhibition promoted by the substrate of 3T3 fibroblasts.

Connective tissue cells typically secrete large amounts of ECM proteins. Another reason why 3T3 reduced the differentiation in relation to the control, might be through the action of secreted proteins that compose the ECM. In fact, the fibroblast lineage used secretes the ECM protein laminin, as well as fibronectin (**Supplementary Figure S2**). When we analyzed cells grown on the laminin substrate, we found that this condition caused greater

inhibition of the neuronal differentiation of enteric glia from adult mice, reducing the number of GFAP+βIIItubulin+ cells by more than 50% after 7 days (from 73.8 to 31.8%). In addition, we did not observe inhibition of neuronal differentiation when the enteric glial cells of adult individuals were cultured on the fibronectin substrate, which serves as a control for the specific role of laminin. Interestingly, the inhibition of the neurogenesis of enteric glia from neonate mice on laminin substrate was not significant, decreasing only about11.2% the percentage of GFAP + βIIItubulin + cells (from 89.7 to 79.6%). Our findings differ from those previously found, where neither laminin nor other ECM molecules investigated were able to inhibit the neuronal fate of neural progenitor cells from the adult rabbit gut (Raghavan et al., 2013). These results allow us to hypothesize that 3T3 promotes inhibition of neuronal differentiation of enteric glia by different mechanisms in cells from adult or neonate mice.

This study suggests that the rupture of contact between the adult enteric glial cells and laminin composing the ECM produced by the cells located around them is able to trigger neurogenesis. Given this first step, it is important that further studies look at the intracellular molecular processes that follow. Results obtained with *ex vivo* culture of longitudinal muscle and myenteric plexus tissue suggest that ENS neurogenesis can occur in a PTEN-dependent manner (Becker et al., 2013). Liu et al. (2009) demonstrated that it is possible to induce neurogenesis in myenteric plexus ganglia through activation of the serotonin receptor with the 5-hydroxytryptamine agonist 4 (5-HT 4). It is possible that these mechanisms are involved in the neurogenesis of enteric glial cells when they lose their contact with laminin. Understanding how the neurogenic potential of enteric glia is activated is the first step in thinking about inducing the generation of new neurons in damaged areas, which could possibly lead to ENS regeneration.

Taking the above into consideration, our results reinforce the importance of the microenvironment molecules in inhibiting the neuronal differentiation of enteric glia. Culturing these cells in a more similar condition to the *in vivo* environment appears to hold the glial phenotype and to keep inhibited the neurogenic potential of the enteric glial cells, suggesting that, in normal conditions and with appropriate interactions with the microenvironment molecules, enteric glia can act in its glial functions without undergoing neuronal differentiation, and only severe disruption can alter significantly the balance of soluble and ECM molecules and trigger this phenomenon.

DATA AVAILABILITY

All datasets generated for this study are included in the manuscript and/or the **Supplementary Files**.

ETHICS STATEMENT

Newborn (P0 or P1) and adult (P90–P120) male Swiss mice were used. This research project was approved by the Animal Use Ethics Committee of the Centro de Ciências da Saúde-Universidade Federal do Rio de Janeiro (CCS-UFRJ) (protocol no. 129/16).

AUTHOR CONTRIBUTIONS

JC-A was responsible for the overall project conception and design. JC-A, LC, and VM-N supervised the project. CV, JC, FS, and JC-A performed the experiments. CV and JC-A wrote the manuscript.

FUNDING

This study was supported by the National Institute for Translational Neuroscience (INNT) of the Ministry of Science and Technology, Brazilian Federal Agency for the Support and Evaluation of Graduate Education (CAPES) of the Ministry of Education, National Council for Technological and Scientific Development (CNPq), Rio de Janeiro State Research Foundation (FAPERJ), and Ary Frauzino Foundation for Cancer Research.

SUPPLEMENTARY MATERIAL

The Supplementary Material for this article can be found online at: https://www.frontiersin.org/articles/10.3389/fnins.2019.00914/full#supplementary-material

FIGURE S1 | Culture of adult mouse ENS cells show the presence of myofibroblats. Cells at day 7 in cell culture on laminin substrate. Scale bar: 25 μm.

FIGURE S2 | Cells from the 3T3 fibroblast lineage express laminin **(A)** and fibronectin **(B)**. Scale bar: 50 μm.

FIGURE S3 | Enteric glial cells from adult mice express Nestin *in vitro*. **(A)** At day 3, Nestin expression was observed in most cells. **(B)** Cells at day 7 in cell culture on laminin substrate. Scale bar: 50 μm.

REFERENCES

Bannerman, P. G., Mirsky, R., Jessen, K. R., Timpl, R., and Duance, V. C. (1986). Light microscopic immunolocalization of laminin, type IV collagen, nidogen, heparan sulphate proteoglycan and fibronectin in the enteric nervous system of rat and guinea pig. *J. Neurocytol.* 15, 733–743. doi: 10.1007/bf01625191

Becker, L., Peterson, J., Kulkarni, S., and Pasricha, P. J. (2013). Ex vivo neurogenesis within enteric ganglia occurs in a PTEN dependent manner. *PLoS One* 8:e59452. doi: 10.1371/journal.pone.0059452

Belkind-Gerson, J., Graham, H. K., Reynolds, J., Hotta, R., Nagy, N., Cheng, L., et al. (2017). Colitis promotes neuronal differentiation of Sox2+ and PLP1+ enteric cells. *Sci. Rep.* 7:2525. doi: 10.1038/s41598-017-02890-y

Belkind-Gerson, J., Hotta, R., Nagy, N., Thomas, A. R., Graham, H., Cheng, L., et al. (2015). Colitis induces enteric neurogenesis through a 5-HT4-dependent mechanism. *Inflamm. Bowel Dis.* 21, 870–878. doi: 10.1097/MIB.0000000000000326

Boesmans, W., Lasrado, R., Vanden Berghe, P., and Pachnis, V. (2015). Heterogeneity and phenotypic plasticity of glial cells in the mammalian enteric nervous system. *Glia* 63, 229–241. doi: 10.1002/glia.22746

Bondurand, N., Natarajan, D., Thapar, N., Atkins, C., and Pachnis, V. (2003). Neuron and glia generating progenitors of the mammalian enteric nervous system isolated from foetal and postnatal gut cultures. *Development* 130, 6387–6400. doi: 10.1242/dev.00857

Coelho-Aguiar Jde, M., Bon-Frauches, A. C., Gomes, A. L. T., Verissimo, C. P., Aguiar, D. P., Matias, D., et al. (2015). The enteric glia: identity and functions. *Glia* 63, 921–935. doi: 10.1002/glia.22795

Doetsch, F., Caille, I., Lim, D. A., Garcia-Verdugo, J. M., and Alvarez-Buylla, A. (1999). Subventricular zone astrocytes are neural stem cells in the adult mammalian brain. *Cell* 97, 703–716. doi: 10.1016/s0092-8674(00)80783-7

Domogatskaya, A., Rodin, S., Boutaud, A., and Tryggvason, K. (2008). Laminin-511 but Not -332, -111, or -411 enables mouse embryonic stem cell self-renewal In Vitro. *Stem Cells* 26, 2800–2809. doi: 10.1634/stemcells.2007-0389

Dupin, E., and Coelho-Aguiar, J. M. (2013). Isolation and differentiation properties of neural crest stem cells. *Cytometry A* 83, 38–47. doi: 10.1002/cyto.a.22098

Freire, E., Barroso, M. M. S., Klier, R. N., and Coelho-Sampaio, T. (2012). Biocompatibility and structural stability of a laminin biopolymer. *Macromol. Biosci.* 12, 67–74. doi: 10.1002/mabi.201100125

Gershon, M. D. (2011). Behind an enteric neuron there may lie a glial cell. *J. Clin. Investig.* 121, 3386–3389. doi: 10.1172/JCI59573

Hetz, S., Acikgoez, A., Voss, U., Nieber, K., Holland, H., Hegewald, C., et al. (2014). In vivo transplantation of neurosphere-like bodies derived from the human postnatal and adult enteric nervous system: a pilot study. *PLoS One* 9:e93605. doi: 10.1371/journal.pone.0093605

Imbeault, S., Gauvin, L. G., Toeg, H. D., Pettit, A., Sorbara, C. D., Migahed, L., et al. (2009). The extracellular matrix controls gap junction protein expression and function in postnatal hippocampal neural progenitor cells. *BMC Neurosci.* 10:13. doi: 10.1186/1471-2202-10-13

Joseph, N. M., He, S., Quintana, E., Kim, Y.-G., Nunez, G., and Morrison, S. J. (2011). Enteric glia are multipotent in culture but primarily form glia in the adult rodent gut. *J. Clin. Investig.* 121, 3398–3411. doi: 10.1172/JCI58186

Kruger, G. M., Mosher, J. T., Bixby, S., Joseph, N., Iwashita, T., Morrison, S. J., et al. (2002). Neural crest stem cells persist in the adult gut but undergo changes in self-renewal, neuronal subtype potential, and factor responsiveness. *Neuron* 35, 657–669. doi: 10.1016/s0896-6273(02)00827-9

Kulkarni, S., Micci, M.-A., Leser, J., Shin, C., Tang, S.-C., Fu, Y.-Y., et al. (2017). Adult enteric nervous system in health is maintained by a dynamic balance between neuronal apoptosis and neurogenesis. *Proc. Natl. Acad. Sci. U.S.A.* 114, E3709–E3718. doi: 10.1073/pnas.1619406114

Laranjeira, C., Sandgren, K., Kessaris, N., Richardson, W., Potocnik, A., Vanden Berghe, P., et al. (2011). Glial cells in the mouse enteric nervous system can undergo neurogenesis in response to injury. *J. Clin. Investig.* 121, 3412–3424. doi: 10.1172/JCI58200

Laywell, E. D., Kearns, S. M., Zheng, T., Chen, K. A., Deng, J., Chen, H.-X., et al. (2005). Neuron-to-astrocyte transition: phenotypic fluidity and the formation of hybrid asterons in differentiating neurospheres. *J. Comp. Neurol.* 493, 321–333. doi: 10.1002/cne.20722

Laywell, E. D., Rakic, P., Kukekov, V. G., Holland, E. C., and Steindler, D. A. (2000). Identification of a multipotent astrocytic stem cell in the immature and adult mouse brain. *Proc. Natl. Acad. Sci. U.S.A.*97, 13883–13888. doi: 10.1073/pnas.250471697

Li, P., Wang, S., Zhan, L., He, X., Chi, G., Lv, S., et al. (2017). Efficient feeder cells preparation system for large-scale preparation and application of induced pluripotent stem cells. *Sci. Rep.* 7:12266. doi: 10.1038/s41598-017-10428-5

Lindley, R. M., Hawcutt, D. B., Connell, M. G., Almond, S. L., Vannucchi, M.-G., Faussone-Pellegrini, M. S., et al. (2008). Human and mouse enteric nervous system neurosphere transplants regulate the function of aganglionic embryonic distal colon. *Gastroenterology* 135, 205–216.e6. doi: 10.1053/j.gastro.2008.03.035

Liu, M.-T., Kuan, Y.-H., Wang, J., Hen, R., and Gershon, M. D. (2009). 5-HT4 receptor-mediated neuroprotection and neurogenesis in the enteric nervous system of adult mice. *J. Neurosci.?* 29, 9683–9699. doi: 10.1523/JNEUROSCI.1145-09.2009

Metzger, M., Caldwell, C., Barlow, A. J., Burns, A. J., and Thapar, N. (2009). Enteric nervous system stem cells derived from human gut mucosa for the treatment of aganglionic gut disorders. *Gastroenterology* 136, 2213–2214. doi: 10.1053/j.gastro.2009.02.048

Miyazaki, T., Futaki, S., Hasegawa, K., Kawasaki, M., Sanzen, N., Hayashi, M., et al. (2008). Recombinant human laminin isoforms can support the undifferentiated growth of human embryonic stem cells. *Biochem. Biophys. Res. Commun.* 375, 27–32. doi: 10.1016/j.bbrc.2008.07.111

Nakazawa, N., Miyahara, K., Okawada, M., Yamataka, A., Suzuki, R., Akazawa, C., et al. (2013). Laminin-1 promotes enteric nervous system development in mouse embryo. *Pediatr. Surg. Int.* 29, 1205–1208. doi: 10.1007/s00383-013-3388-3

Neunlist, M., Aubert, P., Bonnaud, S., Van Landeghem, L., Coron, E., Wedel, T., et al. (2007). Enteric glia inhibit intestinal epithelial cell proliferation partly through a TGF-beta1-dependent pathway. *Am. J. Physiol. Gastrointest. Liver Physiol.* 292, G231–G241. doi: 10.1152/ajpgi.00276.2005

Pham, T. D., Gershon, M. D., and Rothman, T. P. (1991). Time of origin of neurons in the murine enteric nervous system: sequence in relation to phenotype. *J. Comp. Neurol.* 314, 789–798. doi: 10.1002/cne.903140411

Raghavan, S., and Bitar, K. N. (2014). The influence of extracellular matrix composition on the differentiation of neuronal subtypes in tissue engineered innervated intestinal smooth muscle sheets. *Biomaterials* 35, 7429–7440. doi: 10.1016/j.biomaterials.2014.05.037

Raghavan, S., Gilmont, R. R., and Bitar, K. N. (2013). Neuroglial differentiation of adult enteric neuronal progenitor cells as a function of extracellular matrix composition. *Biomaterials* 34, 6649–6658. doi: 10.1016/j.biomaterials.2013.05.023

Rodin, S., Domogatskaya, A., Ström, S., Hansson, E. M., Chien, K. R., Inzunza, J., et al. (2010). Long-term self-renewal of human pluripotent stem cells on human recombinant laminin-511. *Nat. Biotechnol.* 28, 611–615. doi: 10.1038/nbt.1620

Sasselli, V., Pachnis, V., and Burns, A. J. (2012). The enteric nervous system. *Dev. Biol.* 366, 64–73. doi: 10.1016/j.ydbio.2012.01.012

Young, H. M., Bergner, A. J., and Muller, T. (2003). Acquisition of neuronal and glial markers by neural crest-derived cells in the mouse intestine. *J. Comp. Neurol.* 456, 1–11. doi: 10.1002/cne.10448

Conflict of Interest Statement: The authors declare that the research was conducted in the absence of any commercial or financial relationships that could be construed as a potential conflict of interest.

frontiers in Neuroscience

BRIEF RESEARCH REPORT
published: 26 November 2019
doi: 10.3389/fnins.2019.01242

Dimethylsulfoxide Inhibits Oligodendrocyte Fate Choice of Adult Neural Stem and Progenitor Cells

*Anna O'Sullivan[1,2,3], Simona Lange[2,4], Peter Rotheneichner[1,2], Lara Bieler[1,2], Ludwig Aigner[2,4,5], Francisco J. Rivera[2,4,6,7] and Sebastien Couillard-Despres[1,2,5]**

[1] Institute of Experimental Neuroregeneration, Paracelsus Medical University, Salzburg, Austria, [2] Spinal Cord Injury and Tissue Regeneration Center Salzburg (SCI-TReCS), Salzburg, Austria, [3] Department of Otorhinolaryngology, Paracelsus Medical University, Salzburg, Austria, [4] Institute of Molecular Regenerative Medicine, Paracelsus Medical University, Salzburg, Austria, [5] Austrian Cluster for Tissue Regeneration, Vienna, Austria, [6] Laboratory of Stem Cells and Neuroregeneration, Institute of Anatomy, Histology and Pathology, Faculty of Medicine, Universidad Austral de Chile, Valdivia, Chile, [7] Center for Interdisciplinary Studies on the Nervous System (CISNe), Universidad Austral de Chile, Valdivia, Chile

OPEN ACCESS

Edited by:
Fraser James Sim,
University at Buffalo, United States

Reviewed by:
Carlos Vicario-Abejón,
Spanish National Research Council (CSIC), Spain
Myriam Cayre,
UMR 7288 Institut de Biologie du Développement de Marseille (IBDM), France

***Correspondence:**
Sebastien Couillard-Despres
s.couillard-despres@pmu.ac.at

Specialty section:
This article was submitted to Neurogenesis, a section of the journal Frontiers in Neuroscience

Received: 15 June 2019
Accepted: 04 November 2019
Published: 26 November 2019

Citation:
O'Sullivan A, Lange S, Rotheneichner P, Bieler L, Aigner L, Rivera FJ and Couillard-Despres S (2019) Dimethylsulfoxide Inhibits Oligodendrocyte Fate Choice of Adult Neural Stem and Progenitor Cells. Front. Neurosci. 13:1242. doi: 10.3389/fnins.2019.01242

Several clinical trials address demyelinating diseases via transplantation of mesenchymal stromal cells (MSCs). Published reports detail that administration of MSCs in patients may provide a beneficial immunomodulation, and that factors secreted by MSCs are potent inducers of oligodendrogenesis. Dimethylsulfoxide (DMSO) is widely used in life science and medicine as solvent, vehicle or cryoprotectant for cells used in transplantation. Importantly, most transplantation protocols do not include the removal of DMSO before injecting the cell suspension into patients. This indifferent application of DMSO is coming under increasing scrutiny following reports investigating its potential toxic side-effects. While the impact of DMSO on the central nervous system (CNS) has been partially studied, its effect on oligodendrocytes and oligodendrogenesis has not been addressed yet. Consequently, we evaluated the influence of DMSO on oligodendrogenesis, and on the pro-oligodendrogenic effect of MSCs' secreted factors, using adult rat neural stem and progenitor cells (NSPCs). Here, we demonstrate that a concentration of 1% DMSO robustly suppressed oligodendrogenesis and drove the fate of differentiating NSPCs toward astrogenesis. Furthermore, the pro-oligodendrogenic effect of MSC-conditioned medium (MSCCM) was also nearly completely abolished by the presence of 1% DMSO. In this condition, inhibition of the Erk1/2 signal transduction pathway and high levels of Id2 expression, a specific inhibitor of oligodendrogenic differentiation, were detected. Furthermore, inflammatory demyelinating diseases may even potentiate the impact of DMSO on oligodendrogenesis. Our results demonstrate the imperative of considering the strong anti-oligodendrogenic activity of DMSO when designing future clinical trial protocols.

Keywords: oligodendrogenesis, neural stem cells, myelination, DMSO, Id2, Olig2, astrocyte, oligodendrocytes

INTRODUCTION

In young adults, the most common neurological disease leading to permanent disability is multiple sclerosis (MS). The latter is a neuroinflammatory disorder of the central nervous system (CNS) characterized by the progressive destruction of myelin sheaths. Although MS patients can recover from their first demyelinating episodes through a process known as remyelination, the regenerative capacity of the CNS declines through the course of the disease. This leads to physical and cognitive deficits over time due to insufficient axon insulation and neuronal loss. Despite new drug developments, the repair of CNS damage still constitutes a challenging problem (Wingerchuk and Carter, 2014). As our understanding of the mechanisms underlying the process of remyelination grows, there is increasing interest in cell-based therapies to address the issue.

We previously reported that factors secreted by mesenchymal stromal cells (MSCs) induce oligodendrogenic fate decision in neural stem and progenitor cells (NSPCs) and oligodendrocyte precursor cells (OPCs) (Rivera et al., 2006, 2008, 2019; Jadasz et al., 2013), both of which represent natural sources for new oligodendrocytes in the CNS (Menn et al., 2006; Franklin and Ffrench-Constant, 2008; Etxeberria et al., 2010; Jablonska et al., 2010; Kazanis et al., 2017). Furthermore, MSCs are potent immunomodulators (Uccelli and Mancardi, 2010), are easily accessible from the bone marrow, and their administration has been proven safe (Dahbour et al., 2017).

These properties encouraged the development of multiple clinical trials involving the application of MSCs to patients suffering from a demyelinating disease (summary of published studies of MSC transplantation in MS in Scolding et al., 2017). However, diverging results between studies raise questions about the efficacy of this MSC-based strategy and warrant standardized protocols, which should include the origin of cell product, the route of delivery, the dose, and the trial design (Scolding et al., 2017). Consideration should also be given to the presence or removal of the cryoprotectant dimethylsulfoxide (DMSO) from the cell preparation administered. While it has been demonstrated that a standard dose of 10% DMSO in the cell suspension administered is generally well tolerated, adverse reactions to cell applications could significantly be reduced when DMSO was removed or its concentration reduced prior to injection (Windrum et al., 2005). Moreover, case reports describing neurological adverse events like epileptic seizures, stroke, encephalopathy or leukoencephalopathy, following administration of DMSO suggest that it might be harmful for the CNS (Dhodapkar et al., 1994; Higman et al., 2000; Hoyt et al., 2000; Bauwens et al., 2005). Previous studies explored the influence of DMSO on neurons and astrocytes and reported concerning results about cell toxicity even at low DMSO concentrations (Hanslick et al., 2009; Tamagnini et al., 2014; Yuan et al., 2014; Zhang et al., 2017). However, DMSO's effect on other CNS resident precursor cells has not been addressed yet.

Our study demonstrates that a concentration of 1% DMSO almost completely obliterates the generation of oligodendrocytes from adult rat NSPCs in favor of astrocytic differentiation. These results substantiate the assumption that DMSO could have a negative impact on oligodendrogenesis, and we therefore call for further investigation of its potential hazard when applied in the context of demyelinating disorders.

MATERIALS AND METHODS

Animal Works

Experiments were performed in accordance to the guidelines of the "Directive 2010/63/EU of the European Parliament and of the Council of 22 September 2010 on the protection of animals used for scientific purposes." According to the European Directive 2010/63/EU Article 3 and the Austrian legislation for experiments on living animals Tierversuchsgesetz 2012 §2c, no additional approval was required for the killing of animals with the aim of collecting tissues.

MSC Cultures and MSCCM

Mesenchymal stromal cell cultures and MSC-conditioned medium (MSCCM) were generated as described by Rivera et al. (2006). In brief, bone marrow plugs from tibias and femurs of 6–8 weeks old female Fischer-344 rats were harvested and mechanically dissociated in α-MEM. After centrifugation and resuspension, dissociated bone marrow cells were seeded at 1×10^6 cells/cm^2 in α-MEM containing 10% FBS, 100 U/mL penicillin and 100 μg/mL streptomycin (thereafter aMEM) and grown in a humidified incubator at 37°C with 5% CO_2. Medium was changed every third day until a confluent cell layer was reached. For MSCCM production, MSCs were seeded at a density of 12,000 cells/cm^2 in aMEM. After 3 days of incubation, the supernatant (conditioned medium) was collected and filtered using a 0.22 μm pore filter (Rivera et al., 2006).

NSPC Cultures

Neural stem and progenitor cells cultures from the adult hippocampus (HC) and subventricular zone (SVZ) were established as described by Wachs et al. (2003). Briefly, 6–8 weeks old female Fischer-344 rats were decapitated and their HC and SVZ dissected. The tissue was transferred to 4°C cold PBS containing 4.5 mg/L D-glucose, then mechanically minced and enzymatically digested. Dissociated cells were collected and resuspended in Neurobasal A medium (NBA, Gibco) supplemented with B27 (Gibco), 2 mM L-glutamine, 100 U/mL penicillin, 100 μg/mL streptomycin, as well as 2 μg/mL heparin, 20 ng/mL human recombinant EGF and 20 ng/mL human recombinant FGF (thereafter referred to as NBA+all). Neurosphere cultures were kept in a humidified incubator with 5% CO_2 at 37°C and half of the medium was changed every third day.

For passaging, the medium containing floating neurospheres was centrifuged at 120 × *g* for 5 min. The supernatant was discarded and the pellet dissociated with Accutase (PAN Biotech). The single cells were then reseeded into NBA+all at a density of 1×10^5 cells/mL. Passaging took place every 7–9 days.

For freezing, the cell suspension was centrifuged 3 days after passaging and the supernatant was discarded. The cells were then

transferred into cryomedium (10% DMSO, 20% FBS, 70% NBA supplemented with B27, 2 mM L-glutamine, 100 U/mL penicillin, 100 μg/mL streptomycin) and frozen at −150°C until further use. After thawing, cells were immediately washed with NBA+all to remove remnants of the cryomedium, and cultured in NBA+all.

All NSPCs used in the experiments were frozen at passage 1 or 2, and employed for the various experiments in passage number 2–6. No difference in fate choice was observed during differentiation between fresh cells, and cultures derived from frozen stocks (data not shown). Data provided in the main figures were generated with hippocampal NSCs. Differentiation of NSCs obtained from the SVZ was not significantly different (**Supplementary Figure S1**).

Treatment of NSPCs

Neurospheres were dissociated using Accutase (PAN Biotech) and seeded onto 100 μg/mL poly-L-ornithine and 5 μg/mL laminin coated coverslips at a density of 8000–10,000 cells/cm^2 in aMEM. After 16 h, medium was replaced with aMEM or MSCCM containing the final concentration of DMSO. After 3 or 6 days of differentiation, the NSPCs were fixed with 4% paraformaldehyde and processed for immunofluorescence stainings.

For RNA-isolation, NSPCs were grown as mentioned above on poly-L-ornithine and laminin coated petri dishes in aMEM and MSCCM containing either 0 or 1% of DMSO. After 3 days of differentiation, NSPCs were lysed with Tri Reagent (Sigma-Aldrich) and total RNA was isolated using the RNeasy plus mini RNA isolation kit (Qiagen) (see below).

For protein isolation, NSPCs were seeded onto poly-L-ornithine and laminin coated petri dishes for 16 h. After that, the NSPCs were stimulated with aMEM or MSCCM with 0 or 1% DMSO. After 10 min of treatment, protein isolation was performed using a RIPA-buffer.

Immunofluorescence Analysis and Quantification

Immunofluorescence analysis and quantification were performed as described by Oberbauer et al. (2013). Following primary antibodies and concentrations were used: guinea pig anti-Glial Acidic Fibrillary Protein (GFAP) 1:500 (Progen); mouse anti-2′,3′-cyclic-nucleotide-3′-phosphodieesterase (CNP) 1:200 (Millipore); rabbit anti-Caspase3 (Casp3) 1:200 (Abcam); goat anti-oligodendrocyte transcription factor 2 (Olig2) 1:20 (R&D Systems); mouse anti-neural/glial antigen 2 (NG2) 1:500 (Sigma-Aldrich). Secondary antibodies: donkey anti-guinea pig Alexa Fluor 647 1:500 (Dianova); donkey anti-rabbit Alexa Fluor 488 1:1000 (Thermo Fisher Scientific); donkey anti-mouse Alexa Fluor 568 1:1000 (Thermo Fisher Scientific). Nuclear counterstaining was performed with 0.25 μg/mL 4′,6′-diamidino-2-phenylindole dihydrochloride hydrate (DAPI; Sigma). Epifluorescence was observed using an Olympus IX81 (Olympus) equipped with a Hamamatsu digital camera (Hamamatsu Photonics) and CellSense Software (Olympus) for documentation. Ten observation fields were chosen randomly, containing between 300 and 1300 cells, and photographed for analysis of cell fate decision.

Protein Extraction and Western Blots

Neural stem and progenitor cells were treated as mentioned above and after washing with PBS, cells were lysed with RIPA buffer supplemented with protease inhibitors (cOmplete, Roche) and phosphatase inhibitors (PhosSTOP, Roche). The suspensions were homogenized through a 27-gauge needle and samples placed on ice for 30 min. Protein concentrations of lysates were determined with a Pierce BCA Protein Assay Kit (Thermo Fisher Scientific). Equal amounts (10 μg) of protein samples were loaded on Mini-PROTEAN TGX Stain-free precast gel (Bio-Rad) and run with 120 V. Precision Plus Protein Dual Color Standard (Bio-Rad) as well as SeeBlue Plus2 Pre-stained Protein Standard (Thermo Fisher Scientific) were used as protein standard markers. Blotting was performed using a Trans-Blot Turbo Transfer System (Bio-Rad) with Trans-Blot Turbo Mini Transfer Packs (Bio-Rad).

Membranes were blocked using 5% BSA in Tris–buffered saline with 0.1% Triton X-100 (TBST) for 1 h at room temperature prior to incubation with the primary antibodies diluted in the same buffer overnight at 4°C. Following primary antibodies were used: rabbit anti-Erk1/2 1:1000 (p44/42 MAPK (Erk1/2) mAb #4695, Cell Signaling Technologies); rabbit anti-pErk1/2 1:1000 (Phospho-p44/42 MAPK (Erk1/2) (Thr202/Tyr204), mAb #4370, Cell Signaling Technologies); mouse anti-beta actin 1:2000 (Sigma). The membranes were then washed with TBST and incubated with secondary antibodies diluted in blocking solution for 2 h at room temperature: donkey anti-rabbit Alexa Fluor 568 1:1000 (Thermo Fisher Scientific); donkey anti-mouse Alexa Fluor 488 1:1000 (Thermo Fisher Scientific). Immunocomplexes were visualized using a Chemidoc (Bio-Rad) and the Bio-Rad ImageLab software was used for analysis and quantification.

Quantitative Gene Expression Analyses

Neural stem and progenitor cells were differentiated for 3 days as mentioned above. RNA-extractions were performed using TRI Reagent (Sigma) followed by the use of an RNeasy plus mini RNA isolation kit (Qiagen). The cDNA synthesis was performed with iScript Reverse Transcription Supermix for RT-qPCR (Bio-Rad). Quantitative gene expression analyses were performed using TaqMan RT-PCR technology. Technical duplicates containing 10 ng of cDNA were amplified with the GoTAQ Probe qPCR Master Mix (Promega) using a two-step cycling protocol (95°C for 15 s, 60°C for 60 s; 40 cycles, Bio-Rad CFX 96 Cycler).

The following gene expression assays were employed: Id2 (Rn01495280_m1, Applied Biosystems), Olig2 (Rn0056603_m1, Applied Biosystems), DCX (Rn00584505_m1, Applied Biosystems) as well as the following housekeepers: Hprt1 (Rn01527840_m1, Applied Biosystems), Sdha (Rn00590475_m1, Applied Biosystems), Heatr3 (Rn.PT.56a.5120057, Integrated DNA Technologies, United States); TBP (Rn.PT.39a.22214837, Integrated DNA Technologies, United States) Ywhaz (Rn.PT.56a.8368619, Integrated DNA Technologies,

United States). Only validated housekeepers were included in the analysis.

Quantification analyses were performed with qBase Plus (Biogazelle, Belgium) using geNorm algorithms for multi-reference gene normalization followed by normalization to average.

Statistical Analysis

Data are presented as means ± SD. Statistical analysis was performed using RStudio (RStudio Inc., Boston, MA, United States). Data sets were analyzed according to the general factorial design included in the GFD-package in R (Friedrich et al., 2017) using the ANOVA-type approximation for the calculation of p-values. P-values of <0.05 were considered significant. Significance: ns, $p \geq 0.05$; $^{*}p < 0.05$; $^{**}p < 0.01$; $^{***}p < 0.001$.

RESULTS

DMSO Inhibits Oligodendrogenic Fate Decision of NSPCs

Novel strategies for remyelination strive to take advantage of the pro-oligodendrogenic effect of MSCs, while the mechanisms behind this activity are still being resolved. As DMSO is frequently used as a vehicle, solvent or cryoprotectant for cells, we analyzed its influence on the pro-oligodendrogenic properties of MSCs. NSPCs were incubated during differentiation in aMEM, MSCCM or MSCCM containing 1% of DMSO. After 3 days in these differentiation conditions, the expression of GFAP (astrocytes), CNP (oligodendrocytes) and Olig2 (entire oligodendroglial lineage) were examined by immunohistology (**Figure 1**). While the expression of GFAP was not different in aMEM and MSCCM (aMEM: 14.0 ± 10.0% and MSCCM: 28.4 ± 13.5%, $p = 0.216$, $n = 3$), differences in CNP expression were already evident after 3 days of differentiation (aMEM: 11.2 ± 3.1% and MSCCM: 34.9 ± 4.2%, $p = 0.002$, $n = 3$). Addition of 1% DMSO to MSCCM did not show significant changes in the number of GFAP-expressing cells (MSCCM + 1% DMSO: 42.0 ± 18.1%, compared to MSCCM: $p = 0.361$ or aMEM $p = 0.097$, $n = 3$). In contrast, following application of 1% DMSO, the percentage of CNP-expressing oligodendrocytes was substantially reduced compared to MSCCM (MSCCM + 1% DMSO: 13.2 ± 3.1%, $p = 0.003$, $n = 3$). Expression of Olig2, a lineage marker for oligodendrocytes, robustly increased in the presence of MSCCM (MSCCM: 54.1 ± 8.6% compared aMEM: 11.7 ± 2.5%, $p = 0.009$, $n = 3$). The addition of 1% DMSO to MSCCM significantly reduced the percentage of cells expressing Olig2, however, their abundance was still significantly higher than in aMEM (MSCCM + 1% DMSO: 34.5 ± 4.0%, compared to MSCCM: $p = 0.041$ compared aMEM: $p = 0.002$, $n = 3$).

We evaluated the expression of the neurogenic marker DCX after 3 days of differentiation in aMEM and MSCCM, with or without 1% DMSO. As previously described, neuronal differentiation of adult rat NSPCs in aMEM and MSCCM takes place at very low levels (Rivera et al., 2006; Couillard-Despres et al., 2008; Ladewig et al., 2008; Steffenhagen et al., 2012) and expression of the neuronal markers Map2ab or DCX remain in the low single-digit percentages. We therefore addressed the impact of DMSO on neuronal differentiation based on the expression of DCX mRNA levels. Addition of 1% DMSO to aMEM significantly decreased the relative expression of DCX mRNA (aMEM: 2.92 ± 0.82 to aMEM + 1% DMSO 1.30 ± 0.44, $p = 0.037$, $n = 3$). Furthermore, also MSCCM had a detrimental effect on DCX expression compared to aMEM (MSCCM: 0.48 ± 0.10, $p = 0.034$, $n = 3$). The addition of DMSO to MSCCM did not further decrease DCX mRNA relative expression (MSCCM + 1% DMSO: 0.59 ± 0.11, $p = 0.285$, $n = 3$) (see **Supplementary Figure S2**). Hence, in the absence of a neuronal induction stimuli, the influence of DMSO on neuronal differentiation remained marginal.

To further evaluate the glial differentiation in these conditions, the expression of the astrocyte marker GFAP and the oligodendrocyte marker CNP were examined after 6 days of differentiation. In aMEM ($n = 9$), the majority of NSPCs differentiated into GFAP-expressing astrocytes, while the abundance of CNP^{+} oligodendrocytes remained similar to the level observed after 3 day of differentiation (CNP^{+} cells: 11.6 ± 5.0% and $GFAP^{+}$ cells: 63.2 ± 9.0%) (**Figures 2A,B**). On the contrary, differentiation for 6 days in MSCCM ($n = 9$) significantly enhanced oligodendrogenesis, whereas astrogenesis was comparable to the level observed after 3 days (CNP^{+} cells: 62.1 ± 8.9% and $GFAP^{+}$ cells: 22.9 ± 9.0%). The addition of 1% DMSO ($n = 6$) to differentiating cells nearly completely inhibited the MSCCM-induced oligodendrogenesis after 6 days (CNP^{+} cells: 24.4 ± 17.4%, $p = 0.002$; $GFAP^{+}$ cells: 57.3 ± 20.8%, $p = 0.008$ as compared to MSCCM) (**Figures 2A,B**). We examined whether lower concentrations of DMSO also have an impact on the MSCCM pro-oligodendrogenic effect using DMSO concentrations of 0.05, 0.1, 0.2, 0.4, or 1% ($n = 3$; 3; 3; 3; 6, respectively). We observed that increasing concentrations of DMSO progressively inhibited the MSCCM-derived pro-oligodendrogenic activity, however, only a concentration of 1% DMSO significantly inhibited the oligodendroglial cell fate of differentiating NSPCs, in favor of astrocytes (**Figure 2C**).

Next, we extended our analyses to the spontaneous oligodendrocytic differentiation potential of NSPCs in aMEM to determine whether DMSO only neutralizes the activity of MSCCM or restricts the intrinsic capacity of NSPCs to undergo oligodendroglial differentiation. Following differentiation in aMEM with 1% DMSO ($n = 3$), the percentage of CNP-expressing NPSCs was significantly reduced as compared to cultures maintained in aMEM only ($n = 9$) (aMEM: 11.6 ± 5.0% compared to aMEM + 1% DMSO: 3.4 ± 2.8%; $p = 0.011$), whereas GFAP levels remained stable (aMEM: 69.4 ± 9.8% compared to aMEM + 1% DMSO: 58.1 ± 5.1%; $p = 0.264$) (**Figures 2A,D**). Furthermore, DMSO's inhibitory effect on oligodendrogenesis was not limited to NSPCs from the hippocampal neurogenic niche, since NSPCs from the SVZ were affected in the same manner following addition of 1% DMSO during their differentiation (see **Supplementary Figures S1A,B**).

To exclude the possibility that the loss of oligodendrocytes results from an early selection through lineage-specific apoptosis, we quantified the frequency of active Caspase 3 in NG2+, Olig2+

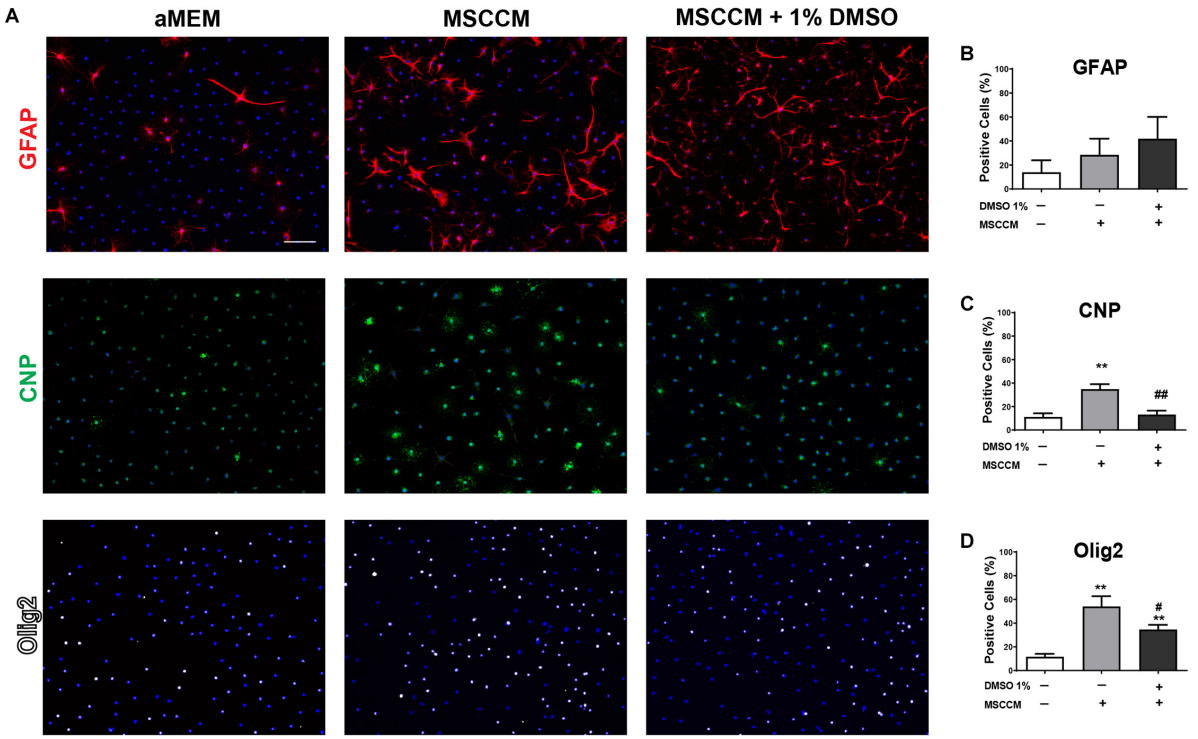

FIGURE 1 | Impact of MSCCM and DMSO on early differentiation of NSPCs (3 days). **(A)** Representative immunodetection of markers for astrocytes (GFAP, red), oligodendrocytes (CNP, green) and cells of the oligodendrocytic lineage (Olig2, white) in NSPCs under the various differentiation conditions for 3 days. Nuclei were counterstained with DAPI (blue). Scale bar = 100 μm. Quantification of the number of cells expressing **(B)** GFAP, **(C)** CNP, and **(D)** Olig2 after 3 days of differentiation. Data represented as mean ± SD. Asterisks mark significant differences in relation to aMEM, pound signs mark significant differences in relation to MSCCM, $^{**}p < 0.01$, $\#p < 0.05$, $\#\#p < 0.01$.

or NG2/Olig2+ progenitor cells after 3 days of differentiation. Neither in aMEM, nor in MSCCM, the addition of 1% DMSO was leading to an increase in apoptosis in the subpopulations of oligodendrocyte progenitor cells (**Supplementary Figure S3** and **Supplementary Table S1**). These results suggest that DMSO blocked the oligodendrogenic activity of MSCCM by suppressing the intrinsic capacity of NSPCs to undergo oligodendroglial differentiation in favor of an astrocytic fate.

DMSO Alters the Balance of the Transcription Factors Olig2 and Id2

The transcription factors Olig2 (oligodendroglial lineage) and Id2 (astroglial lineage) are key determinants of NSPC's glial lineage commitment (Samanta and Kessler, 2004; Steffenhagen et al., 2012). Overexpression of Id2 can thereby lead to the inhibition of oligodendrogenesis and sequestration of Olig2 (Wang et al., 2001; Samanta and Kessler, 2004). To evaluate the gene expression of these glial fate determinants, we quantified the relative expression levels of Olig2 and Id2 in NSPCs after 3 days of differentiation in aMEM or MSSCM, with or without 1% DMSO (**Figure 3A**). In NSPCs exposed to MSCCM, Id2 expression levels were significantly reduced compared to aMEM (MSCCM: 0.3 ± 0.1, aMEM: 1.5 ± 0.3, $p = 0.013$, $n = 3$). Addition of 1% DMSO in MSCCM prevented this decrease (MSCCM + 1% DMSO: 1.0 ± 0.4; $p = 0.117$ compared to aMEM, $n = 3$). In aMEM on the other hand, DMSO induced an upregulation of Id2 mRNA (aMEM + 1% DMSO: 3.1 ± 0.5; $p = 0.018$ compared to aMEM, $n = 3$). The expression levels of Olig2 did not differ significantly throughout the conditions. Hence, these results suggest that DMSO mainly impacted differentiation through an increase of the expression of the astroglial fate determinant Id2, thereby inhibiting oligodendroglial fate decision in NSPCs.

In addition to their absolute levels of expression, the ratio between Olig2 and Id2 in the NSPCs is also crucial for fate decision. We have previously reported that pretreatment with MSCCM during proliferation enhanced the Olig2/Id2 ratio in NSPCs and this high ratio promotes an oligodendrocytic fate (Steffenhagen et al., 2012). Comparing the ratio calculated for various conditions used to differentiate the NSPCs, it is conspicuous that the addition of 1% DMSO, either in aMEM or in MSCCM, robustly decreased the Olig2/Id2 ratio, in correlation with the inhibition of the oligodendrogenic activity (**Figure 3B**).

DMSO Reduces Phosphorylation of Erk1/2 in NSPCs During Differentiation

Erk1/2 is activated by phosphorylation during oligodendrocyte differentiation (Fyffe-Maricich et al., 2011; Guardiola-Diaz et al., 2012). To evaluate whether the presence of DMSO modulates this crucial signaling pathway, we analyzed the level of Erk1/2 phosphorylation compared to total Erk1/2 (tErk1/2)

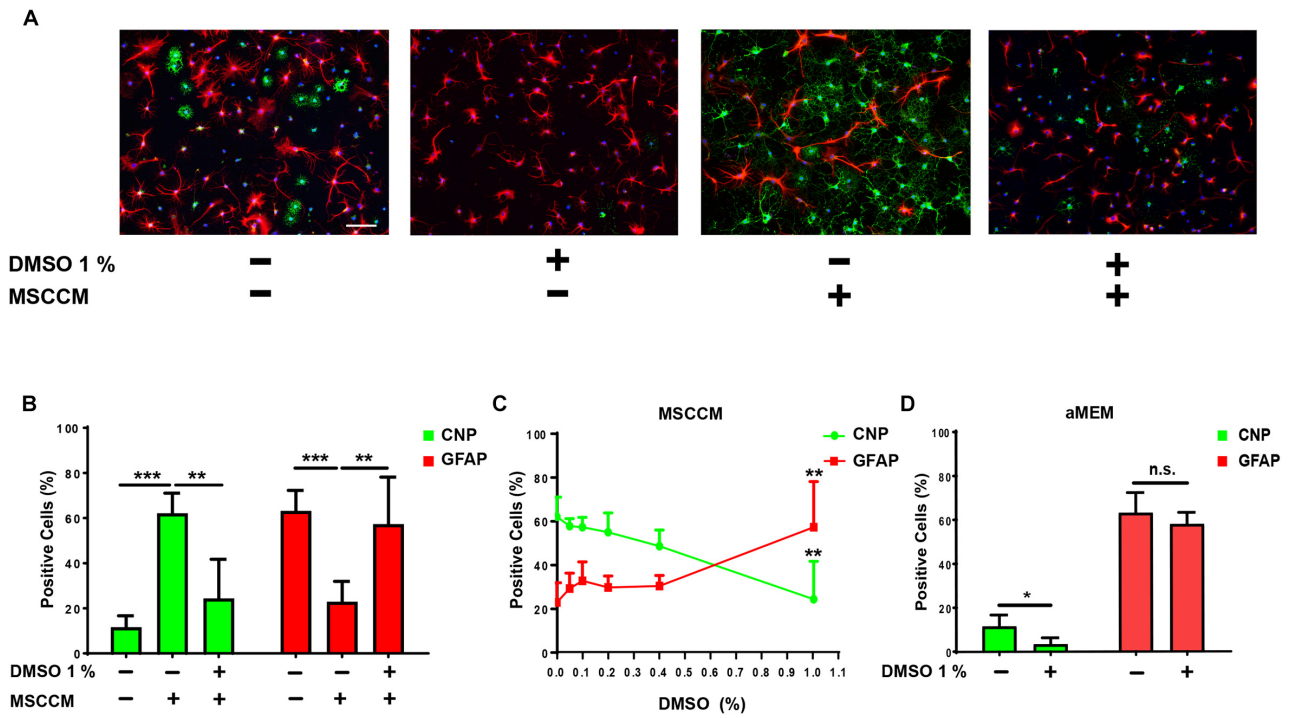

FIGURE 2 | DMSO blocks the pro-oligodendrogenic effect of MSCCM and inhibits oligodendrocytic fate in NSPCs. **(A)** Representative immunodetection of CNP (green) and GFAP (red) expression in NSPCs differentiated for 6 days in aMEM and MSCCM, ±1% DMSO. Nuclei were counterstained with DAPI (blue). Note the decline of CNP^+ cells in the presence of DMSO. Scale bar 100 μm. **(B)** Quantification of glial marker expression in NSPCs differentiated for 6 days in aMEM, MSCCM and MSCCM + 1% DMSO. **(C)** Analysis of glial marker expression in MSSCM with increasing concentrations of DMSO. **(D)** Quantification of glial marker expression in NSPCs differentiated for 6 days in aMEM and aMEM + 1% DMSO. Data represented as mean ± SD, $*p < 0.05$, $**p < 0.01$, $***p < 0.001$, n.s.: not significant.

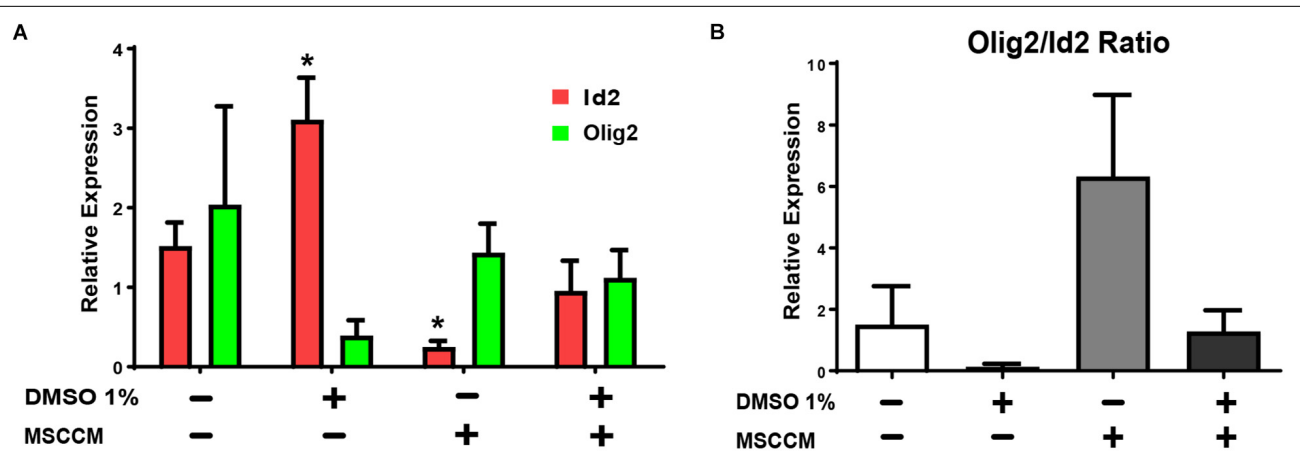

FIGURE 3 | Expression of glial fate determinants after treatment with 1% DMSO. RT-PCRs of pro-oligodendrogenic Olig2 and pro-astrocytic Id2 gene expression were performed on NSPCs differentiating for 3 days. **(A)** Relative levels of mRNA expression for Id2 (red) and Olig2 (green) detected in NSPCs cultivated in aMEM or MSCCM, with or without 1% DMSO. **(B)** Ratio of Olig2/Id2. Data are shown as mean ± SD. Asterisks mark significant difference compared to aMEM, $*p < 0.05$.

in the various culture conditions. Erk1/2 phosphorylation, which is a strong oligodendrocytic fate inducer (Hu et al., 2004; Shi et al., 2014), was significantly elevated in NSPCs exposed to MSCCM (2.3 ± 0.8 fold change compared to aMEM, $p = 0.026$, $n = 5$) (**Figure 4**). In contrast, adding 1% DMSO to MSCCM reduced the levels of phosphorylated Erk1/2 (pErk1/2) back to the levels detected in NSPCs maintained in aMEM (MSCCM + 1% DMSO: 0.8 ± 0.3 fold change, $p = 0.014$ compared to MSCCM, $n = 5$). The lowest pErk1/2 levels were detected in aMEM with 1% DMSO (aMEM + 1% DMSO: 0.6 ± 0.3 fold change compared to aMEM, $p = 0.044$, $n = 5$). These results demonstrate the inhibition

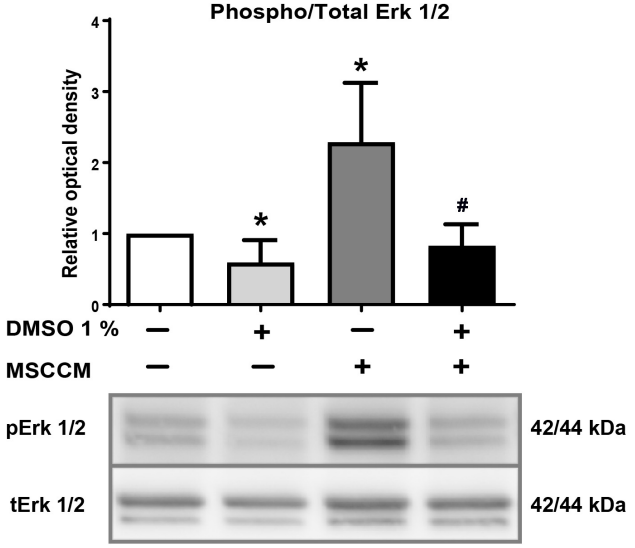

FIGURE 4 | DMSO blocks phosphorylation of Erk1/2. Detection of phospho- and total Erk1/2 after exposure of NSPCs to DMSO. **(Upper panel)** The ratio of relative levels of pErk1/2 in relation to tErk1/2 quantified on western blots is shown for the various conditions. Addition of 1% DMSO significantly decreased phosphorylation of Erk1/2 in aMEM and MSCCM. Data represented as mean ± SD. Asterisks mark significant differences in relation to aMEM, pound sign marks significant differences in relation to MSCCM, $^{*}p < 0.05$, $\#p < 0.05$. **(Lower panel)** Representative western blots for tErk1/2 and pErk1/2 are shown.

of a well-known oligodendrogenic pathway by the addition of DMSO (**Figure 4**).

DISCUSSION

For decades, DMSO has probably been the most utilized solvent for lipophilic agents in *in vitro* and *in vivo* studies. Due to its unique chemical properties, DMSO enables miscibility of hydrophobic substances and serves as a drug carrier enabling penetration into mammalian tissues. In addition, DMSO is widely used as cryoprotectant, e.g., for storage of stem cells. Unlike previous assumptions describing DMSO as inert in low concentrations, recent reports suggested an impact on the cell cycle, differentiation patterns, cell survival and epigenetic changes, even for concentration of DMSO below 1% (Santos et al., 2003; Iwatani et al., 2006). In the past years, additional studies have demonstrated that DMSO induces neurotoxic effects (Hanslick et al., 2009; Yuan et al., 2014), neurophysiological alterations in pyramidal neurons (Tamagnini et al., 2014) and activation of astrocytes (Zhang et al., 2017). Even though concerns over potential risks of using DMSO are growing, its impact on NSPCs residing in the CNS has not been carefully addressed yet.

In the present study, we investigated the impact of DMSO on the differentiation and glial fate decision of NSPCs. As previously reported (Rivera et al., 2006), under standard culture conditions (aMEM), the vast majority of NSPCs spontaneously differentiated into the astrocytic lineage, whereas addition of MSCCM strongly directed the fate choice toward oligodendrocytes. We could demonstrate that this pro-oligodendrogenic effect was inhibited to a large extent by the presence of DMSO during differentiation. This inhibitory activity of DMSO was not limited to NSPCs from the hippocampus, but also applied to NSPCs from the other adult neurogenic niche, i.e., the SVZ. We further observed a progressive inhibition of oligodendrogenesis with increasing concentrations of DMSO, however, significant inhibition in our *in vitro* conditions was observed at a concentration of 1% DMSO. As the detailed mode of action of DMSO on cell fate remains elusive, a significant inhibition of oligodendrogenesis at lower concentrations cannot be ruled out in the presence of additional factors or under pathological conditions.

We further investigated key determinants of oligodendrogenesis and found that the application of DMSO elevated the expression of Id2 in differentiating NSPCs cultivated either in aMEM, or in MSCCM. An overall decrease in the Olig2/Id2 ratio resulted in a shift of NSPCs fate decision away from oligodendrocytes and toward astrocytes. We also investigated the extracellular signal regulated kinases 1/2 (Erk1/2) pathway, which has been shown to regulate oligodendrogenic differentiation in NSPCs (Hu et al., 2004; Shi et al., 2014). We examined the phosphorylation status of Erk1/2 and detected a strong upregulation of the phosphorylated isoform following application of MSCCM. In contrast, the addition of DMSO in MSCCM blocked the phosphorylation of Erk1/2. Whether Erk1/2 dephosphorylation directly modulates Id2 expression under the influence of DMSO still needs to be evaluated.

Although remyelination is mainly achieved by OPC differentiation (Franklin and Goldman, 2015), NSPCs in the adult neurogenic niches have been shown to proliferate and migrate toward lesion sites and locally differentiate into oligodendrocytes as well (Menn et al., 2006; Etxeberria et al., 2010; Jablonska et al., 2010; Kazanis et al., 2017) As our results demonstrate strong anti-oligodendrogenic properties mediated by DMSO for cells of different neurogenic niches, even in the presence of MSCCM, the simultaneous application of MSCs and DMSO in transplantations might inhibit the MSC-mediated pro-oligodendrogenic activity. Furthermore, it would be of interest to evaluate, if OPC differentiation is similarly affected by DMSO, as documented in NSPCs, since upregulation of Id2 and dephosphorylation of Erk1/2 have been shown to block differentiation of OPCs as well (Wang et al., 2001; Fyffe-Maricich et al., 2011; Guardiola-Diaz et al., 2012).

In summary, our study demonstrates a robust anti-oligodendrogenic effect of DMSO on fate decision when present during NSPCs' differentiation *in vitro*. Due to its broad use in cell culture, *in vivo* experiments and clinical trials, future studies evaluating the differentiation of NSPCs, oligodendrogenesis or remyelination should consider the impact of DMSO carefully and, whenever its removal is not possible, emphasize the use of appropriate controls.

DATA AVAILABILITY STATEMENT

All datasets generated for this study are included in the article/**Supplementary Material**.

ETHICS STATEMENT

Ethical review and approval was not required for the animal study because the legislation does not require ethics approval for the killing of animals with the aim of collecting tissues.

AUTHOR CONTRIBUTIONS

AO'S, SL, PR, and LB conducted and analyzed the experiments. AO'S, PR, and LB performed the statistical analysis. AO'S, FR, and SC-D wrote the manuscript. All authors contributed to the conception, design, and finalizing of the study, and approved the submitted version.

FUNDING

This work was supported by the Chilean Comisión Nacional de Investigación Científica y Tecnológica (CONICYT) FONDECYT Program Regular Grant N° 1161787 (FR), Chilean CONICYT PCI Program Grant N° REDES170233 (FR) and REDES180139, and Chilean CONICYT FONDEF-IDeA Program Grant N° ID17AM0043 (FR).

ACKNOWLEDGMENTS

The authors are grateful for the support of Georg Zimmermann (Department of Neurology, Spinal Cord Injury and Tissue Regeneration Center Salzburg, Paracelsus Medical University, Salzburg, Austria) for his support to the statistical analysis.

SUPPLEMENTARY MATERIAL

The Supplementary Material for this article can be found online at: https://www.frontiersin.org/articles/10.3389/fnins.2019.01242/full#supplementary-material

FIGURE S1 | SVZ and HC NSPCs react equally to DMSO exposure. Quantification of glial marker expression in NSPCs differentiated for 6 days in aMEM (HC $n = 9$, SVZ $n = 3$), aMEM + 1% DMSO (HC $n = 3$; SVZ $n = 3$), MSCCM (HC $n = 9$; SVZ $n = 3$) and MSCCM + 1% DMSO (HC $n = 6$; SVZ $n = 3$). Comparison of HC and SVZ NSPCs marker expression: **(A)** CNP and **(B)** GFAP. No statistical difference was detected between the two groups. Data represented as mean ± SD, n.s.: not significant.

FIGURE S2 | DMSO and MSCCM decrease DCX expression. RT-PCRs of DCX gene expression were performed on NSPCs differentiating for 3 days. Relative mRNA expression level of DCX detected in NSPCs cultivated in aMEM or MSCCM, with or without 1% DMSO respectively. Data are shown as mean ± SD. Asterisks mark significant difference compared to aMEM, $^*p < 0.05$, n.s.: not significant.

FIGURE S3 | Detection of Caspase 3 after 3 days of differentiation. Representative immunodetection of NG2 (green), Olig2 (white) and Caspase3 (red) in NSCs after 3 days of differentiation in **(A)** aMEM, **(B)** aMEM + 1% DMSO, **(C)** MSCCM, and **(D)** MSCCM + 1% DMSO. Nuclear counterstained with DAPI (blue). Scale bar in **D**: 100 μm. Example of cells positive for Caspase3 are identified with arrows.

TABLE S1 | DMSO does not induce specific cell death in cells of oligodendrocyte lineage. Percentages of NG2/Casp3$^+$, Olig2/Casp3$^+$ and NG2/Olig2/Casp3$^+$ cells in relation to their respective population (NG2$^+$, Olig2$^+$, NG2/Olig2$^+$) after 3 days of differentiation. Percentages of CNP/Casp3+ and GFAP/Casp3+ cells in relation to their respective population (CNP+ and GFAP+). *P*-values comparing fractions of Casp3$^+$ cells of specific NG2$^+$, Olig2$^+$ and NG2/Olig2$^+$ cell populations in aMEM or MSCCM with and without 1% DMSO. Data represented as mean ± SD. $n = 3$. ND: not determined. DMSO did not significantly affected Casp3 frequency in the subpopulations.

REFERENCES

Bauwens, D., Hantson, P., Laterre, P. F., Michaux, L., Latinne, D., De Tourtchaninoff, M., et al. (2005). Recurrent seizure and sustained encephalopathy associated with dimethylsulfoxide-preserved stem cell infusion. *Leuk Lymphoma* 46, 1671–1674. doi: 10.1080/10428190500235611

Couillard-Despres, S., Quehl, E., Altendorfer, K., Karl, C., Ploetz, S., Bogdahn, U., et al. (2008). Human *in vitro* reporter model of neuronal development and early differentiation processes. *BMC Neurosci.* 9:31. doi: 10.1186/1471-2202-9-31

Dahbour, S., Jamali, F., Alhattab, D., Al-Radaideh, A., Ababneh, O., Al-Ryalat, N., et al. (2017). Mesenchymal stem cells and conditioned media in the treatment of multiple sclerosis patients: clinical, ophthalmological and radiological assessments of safety and efficacy. *CNS Neurosci. Ther.* 23, 866–874. doi: 10.1111/cns.12759

Dhodapkar, M., Goldberg, S. L., Tefferi, A., and Gertz, M. A. (1994). Reversible encephalopathy after cryopreserved peripheral blood stem cell infusion. *Am. J. Hematol.* 45, 187–188. doi: 10.1002/ajh.2830450218

Etxeberria, A., Mangin, J. M., Aguirre, A., and Gallo, V. (2010). Adult-born SVZ progenitors receive transient synapses during remyelination in corpus callosum. *Nat. Neurosci.* 13, 287–289. doi: 10.1038/nn.2500

Franklin, R. J., and Ffrench-Constant, C. (2008). Remyelination in the CNS: from biology to therapy. *Nat. Rev. Neurosci.* 9, 839–855. doi: 10.1038/nrn2480

Franklin, R. J., and Goldman, S. A. (2015). Glia disease and repair-remyelination. *Cold Spring Harb Perspect Biol.* 7, a020594. doi: 10.1101/cshperspect.a020594

Friedrich, S., Konietschke, F., and Pauly, M. (2017). GFD: an r package for the analysis of general factorial designs. *J. Stat. Softw.* 79, 1–18. doi: 10.18637/jss.v079.c01

Fyffe-Maricich, S. L., Karlo, J. C., Landreth, G. E., and Miller, R. H. (2011). The ERK2 mitogen-activated protein kinase regulates the timing of oligodendrocyte differentiation. *J. Neurosci.* 31, 843–850. doi: 10.1523/JNEUROSCI.3239-10.2011

Guardiola-Diaz, H. M., Ishii, A., and Bansal, R. (2012). Erk1/2 MAPK and mTOR signaling sequentially regulates progression through distinct stages of oligodendrocyte differentiation. *Glia* 60, 476–486. doi: 10.1002/glia.22281

Hanslick, J. L., Lau, K., Noguchi, K. K., Olney, J. W., Zorumski, C. F., Mennerick, S., et al. (2009). Dimethyl sulfoxide (DMSO) produces widespread apoptosis in the developing central nervous system. *Neurobiol. Dis.* 34, 1–10. doi: 10.1016/j.nbd.2008.11.006

Higman, M. A., Port, J. D., Beauchamp, N. J. Jr., and Chen, A. R. (2000). Reversible leukoencephalopathy associated with re-infusion of DMSO preserved stem cells. *Bone Marrow Transpl.* 26, 797–800. doi: 10.1038/sj.bmt.1702589

Hoyt, R., Szer, J., and Grigg, A. (2000). Neurological events associated with the infusion of cryopreserved bone marrow and/or peripheral blood progenitor cells. *Bone Marrow Transpl.* 25, 1285–1287. doi: 10.1038/sj.bmt.1702443

Hu, X., Jin, L., and Feng, L. (2004). Erk1/2 but not PI3K pathway is required for neurotrophin 3-induced oligodendrocyte differentiation of post-natal neural stem cells. *J. Neurochem.* 90, 1339–1347. doi: 10.1111/j.1471-4159.2004.02594.x

Iwatani, M., Ikegami, K., Kremenska, Y., Hattori, N., Tanaka, S., Yagi, S., et al. (2006). Dimethyl sulfoxide has an impact on epigenetic profile in mouse embryoid body. *Stem Cells* 24, 2549–2556. doi: 10.1634/stemcells.2005-2427

Jablonska, B., Aguirre, A., Raymond, M., Szabo, G., Kitabatake, Y., Sailor, K. A., et al. (2010). Chordin-induced lineage plasticity of adult SVZ neuroblasts after demyelination. *Nat. Neurosci.* 13, 541–550. doi: 10.1038/nn.2536

Jadasz, J. J., Kremer, D., Gottle, P., Tzekova, N., Domke, J., Rivera, F. J., et al. (2013). Mesenchymal stem cell conditioning promotes rat oligodendroglial cell maturation. *PLoS One* 8:e71814. doi: 10.1371/journal.pone.0071814

Kazanis, I., Evans, K. A., Andreopoulou, E., Dimitriou, C., Koutsakis, C., Karadottir, R. T., et al. (2017). Subependymal zone-derived oligodendroblasts respond to focal demyelination but fail to generate myelin in young and aged mice. *Stem Cell Rep.* 8, 685–700. doi: 10.1016/j.stemcr.2017.01.007

Ladewig, J., Koch, P., Endl, E., Meiners, B., Opitz, T., Couillard-Despres, S., et al. (2008). Lineage selection of functional and cryopreservable human embryonic stem cell-derived neurons. *Stem Cells* 26, 1705–1712. doi: 10.1634/stemcells.2008-2007

Menn, B., Garcia-Verdugo, J. M., Yaschine, C., Gonzalez-Perez, O., Rowitch, D., and Alvarez-Buylla, A. (2006). Origin of oligodendrocytes in the subventricular zone of the adult brain. *J. Neurosci.* 26, 7907–7918. doi: 10.1523/JNEUROSCI.1299-06.2006

Oberbauer, E., Urmann, C., Steffenhagen, C., Bieler, L., Brunner, D., Furtner, T., et al. (2013). Chroman-like cyclic prenylflavonoids promote neuronal differentiation and neurite outgrowth and are neuroprotective. *J. Nutr. Biochem.* 24, 1953–1962. doi: 10.1016/j.jnutbio.2013.06.005

Rivera, F. J., Couillard-Despres, S., Pedre, X., Ploetz, S., Caioni, M., Lois, C., et al. (2006). Mesenchymal stem cells instruct oligodendrogenic fate decision on adult neural stem cells. *Stem Cells* 24, 2209–2219. doi: 10.1634/stemcells.2005-2614

Rivera, F. J., de la Fuente, A. G., Zhao, C., Silva, M. E., Gonzalez, G. A., Wodnar, R., et al. (2019). Aging restricts the ability of mesenchymal stem cells to promote the generation of oligodendrocytes during remyelination. *Glia* 67, 1510–1525. doi: 10.1002/glia.23624

Rivera, F. J., Kandasamy, M., Couillard-Despres, S., Caioni, M., Sanchez, R., Huber, C., et al. (2008). Oligodendrogenesis of adult neural progenitors: differential effects of ciliary neurotrophic factor and mesenchymal stem cell derived factors. *J. Neurochem.* 107, 832–843. doi: 10.1111/j.1471-4159.2008.05674.x

Samanta, J., and Kessler, J. A. (2004). Interactions between ID and OLIG proteins mediate the inhibitory effects of BMP4 on oligodendroglial differentiation. *Development* 131, 4131–4142. doi: 10.1242/dev.01273

Santos, N. C., Figueira-Coelho, J., Martins-Silva, J., and Saldanha, C. (2003). Multidisciplinary utilization of dimethyl sulfoxide: pharmacological, cellular, and molecular aspects. *Biochem. Pharmacol.* 65, 1035–1041. doi: 10.1016/s0006-2952(03)00002-9

Scolding, N. J., Pasquini, M., Reingold, S. C., Cohen, J. A., and International Conference on Cell-Based Therapies for Multiple for Multiple Sclerosis, (2017). Cell-based therapeutic strategies for multiple sclerosis. *Brain* 140, 2776–2796. doi: 10.1093/brain/awx154

Shi, B., Ding, J., Liu, Y., Zhuang, X., Zhuang, X., Chen, X., et al. (2014). ERK1/2 pathway-mediated differentiation of IGF-1-transfected spinal cord-derived neural stem cells into oligodendrocytes. *PLoS One* 9:e106038. doi: 10.1371/journal.pone.0106038

Steffenhagen, C., Dechant, F. X., Oberbauer, E., Furtner, T., Weidner, N., Kury, P., et al. (2012). Mesenchymal stem cells prime proliferating adult neural progenitors toward an oligodendrocyte fate. *Stem Cells Dev.* 21, 1838–1851. doi: 10.1089/scd.2011.0137

Tamagnini, F., Scullion, S., Brown, J. T., and Randall, A. D. (2014). Low concentrations of the solvent dimethyl sulphoxide alter intrinsic excitability properties of cortical and hippocampal pyramidal cells. *PLoS One* 9:e92557. doi: 10.1371/journal.pone.0092557

Uccelli, A., and Mancardi, G. (2010). Stem cell transplantation in multiple sclerosis. *Curr. Opin. Neurol.* 23, 218–225. doi: 10.1097/WCO.0b013e328338b7ed

Wachs, F. P., Couillard-Despres, S., Engelhardt, M., Wilhelm, D., Ploetz, S., Vroemen, M., et al. (2003). High efficacy of clonal growth and expansion of adult neural stem cells. *Lab Invest* 83, 949–962. doi: 10.1097/01.lab.0000075556.74231.a5

Wang, S., Sdrulla, A., Johnson, J. E., Yokota, Y., and Barres, B. A. (2001). A role for the helix-loop-helix protein Id2 in the control of oligodendrocyte development. *Neuron* 29, 603–614. doi: 10.1016/s0896-6273(01)00237-9

Windrum, P., Morris, T. C., Drake, M. B., Niederwieser, D., Ruutu, T., and Subcommittee, E. C. L. W. P. C. (2005). Variation in dimethyl sulfoxide use in stem cell transplantation: a survey of EBMT centres. *Bone Marrow Transpl.* 36, 601–603. doi: 10.1038/sj.bmt.1705100

Wingerchuk, D. M., and Carter, J. L. (2014). Multiple sclerosis: current and emerging disease-modifying therapies and treatment strategies. *Mayo Clin. Proc.* 89, 225–240. doi: 10.1016/j.mayocp.2013.11.002

Yuan, C., Gao, J., Guo, J., Bai, L., Marshall, C., Cai, Z., et al. (2014). Dimethyl sulfoxide damages mitochondrial integrity and membrane potential in cultured astrocytes. *PLoS One* 9:e107447. doi: 10.1371/journal.pone.0107447

Zhang, C., Deng, Y., Dai, H., Zhou, W., Tian, J., Bing, G., et al. (2017). Effects of dimethyl sulfoxide on the morphology and viability of primary cultured neurons and astrocytes. *Brain Res. Bull.* 128, 34–39. doi: 10.1016/j.brainresbull.2016.11.004

Conflict of Interest: The authors declare that the research was conducted in the absence of any commercial or financial relationships that could be construed as a potential conflict of interest.

frontiers in Neuroscience

METHODS
published: 18 June 2020
doi: 10.3389/fnins.2020.00607

A Guide to Extract Spinal Cord for Translational Stem Cell Biology Research: Comparative Analysis of Adult Human, Porcine, and Rodent Spinal Cord Stem Cells

Ahmad Galuta[1,2], Ryan Sandarage[1,3], Diana Ghinda[2,4], Angela M. Auriat[2], Suzan Chen[2], Jason C. S. Kwan[1,5] and Eve C. Tsai[1,2,4]**

[1] Department of Neurosciences, Faculty of Medicine, University of Ottawa, Ottawa, ON, Canada, [2] Neuroscience Program, Ottawa Hospital Research Institute, The Ottawa Hospital, Ottawa, ON, Canada, [3] Faculty of Medicine, The University of British Columbia, Vancouver, BC, Canada, [4] Division of Neurosurgery, Department of Surgery, The Ottawa Hospital, Ottawa, ON, Canada, [5] Faculty of Medicine, University of Toronto, Toronto, ON, Canada

OPEN ACCESS

Edited by:
Fraser James Sim, University at Buffalo, United States

Reviewed by:
Eric D. Laywell, Florida State University, United States
Tal Burstyn-Cohen, The Hebrew University of Jerusalem, Israel

***Correspondence:**
Ahmad Galuta
agalu083@uottawa.ca
Eve C. Tsai
etsai@toh.ca

Specialty section:
This article was submitted to Neurogenesis, a section of the journal Frontiers in Neuroscience

Received: *14 June 2019*
Accepted: *18 May 2020*
Published: *18 June 2020*

Citation:
Galuta A, Sandarage R, Ghinda D, Auriat AM, Chen S, Kwan JCS and Tsai EC (2020) A Guide to Extract Spinal Cord for Translational Stem Cell Biology Research: Comparative Analysis of Adult Human, Porcine, and Rodent Spinal Cord Stem Cells. Front. Neurosci. 14:607. doi: 10.3389/fnins.2020.00607

Improving the clinical translation of animal-based neural stem/progenitor cell (NSPC) therapies to humans requires an understanding of intrinsic human and animal cell characteristics. We report a novel *in vitro* method to assess spinal cord NSPCs from a small (rodent) and large (porcine) animal model in comparison to human NSPCs. To extract live adult human, porcine, and rodent spinal cord tissue, we illustrate a strategy using an anterior or posterior approach that was simulated in a porcine model. The initial expansion of primary NSPCs is carried out using the neurosphere assay followed by a pharmacological treatment phase during which NSPCs derived from humans, porcines, and rodents are assessed in parallel using the same defined parameters. Using this model, NSPCs from all species demonstrated multi-lineage differentiation and self-renewal. Importantly, these methods provide conditions to enable the direct comparison of species-dependent cell behavior in response to specific exogenous signals.

Keywords: human, spinal cord, translation, neural stem/progenitor cells, proliferation, differentiation

INTRODUCTION

Spinal cord injury research has relied largely on animal models to understand the mechanisms of disease and develop pre-clinical models of treatment (Cheriyan et al., 2014). Currently, there are no effective treatments for spinal cord injury which promote regeneration and restore function in humans despite numerous attempts which include physical rehabilitation, anti-inflammatory, and anti-apoptotic drugs, stem cell transplants and the use of bio-scaffolds (Varma et al., 2013; Silva et al., 2014; Badhiwala et al., 2018). The lack of successful translation from pre-clinical to patient interventions can be widely attributed to the limited understanding of biological differences between human and animal model systems, which is due to the scarcity of studies conducted with human tissue (Varma et al., 2013; Ramer et al., 2014; Silva et al., 2014; Chhabra and Sarda, 2017). Understandably, acquiring human spinal cord tissue for study is difficult for ethical and technical reasons. We report a technique of obtaining viable spinal cord tissue from neurologically deceased

organ donors to enable the study of live human tissue and cell physiology. Importantly, this will also allow the direct comparison with the small and large animal models that have been advocated for translation of animal therapies to humans (Kwon et al., 2011).

One promising strategy to repair the spinal cord that has proven useful in animal studies involves the utilization of spinal cord neural stem and progenitor cells (NSPCs) (Ohori et al., 2006; Moreno-Manzano et al., 2009; Panayiotou and Malas, 2013; Kadoya et al., 2016; Yousefifard et al., 2016; Kumamaru et al., 2018). Spinal cord NSPCs are predominately located surrounding the central canal in the ependymal layer and possess the inherent ability to self-renew and differentiate into the different cell types of the central nervous system (Weiss et al., 1996; Sabelström et al., 2014). Therefore, given the correct conditions, NSPCs may be capable of regenerating the neurons, oligodendrocytes, and astrocytes that have undergone cellular death following neural insult. NSPCs may also beneficially modulate their surroundings by secreting trophic factors and providing anatomical support for cellular regeneration (Goldshmit et al., 2012; Hawryluk et al., 2012; Sabelström et al., 2013). As such, understanding the factors controlling NSPC proliferation and their differentiation is pivotal for their application in regenerative strategies. However, the majority of research into NSPC behavior has been conducted in rodent cells with limited comparison to primary human NSPCs (Dromard et al., 2008; Varghese et al., 2009; Mothe et al., 2011), thereby limiting clinical translatability. Consequently, a method to allow direct comparisons between human and animal NSPC differentiation and proliferation would enhance the clinical translation of regenerative interventions.

Rodent NSPCs have been well characterized for their differentiation and proliferation profiles using neurosphere assays, which involve the selective culture and study of NSPCs in controlled environments (Meletis et al., 2008; Hamilton et al., 2009; Kulbatski and Tator, 2009; Grégoire et al., 2015). Self-renewing NSPCs give rise to neurospheres which can be treated under defined conditions to assess the influence of exogenous signaling. NSPCs from adult human organ donors with a neurological determination of death (NDD) can be cultured in a similar manner for characterizing differentiation and self-renewal properties (Dromard et al., 2008; Varghese et al., 2009; Mothe et al., 2011). However, primary human NSPCs require an adherent basement membrane matrix such as Matrigel to expand (Mothe et al., 2011) while primary rodent NSPCs have historically been cultured as neurospheres in suspension (Weiss et al., 1996). The use of different *in vitro* models (adherent vs. suspension) impacts NSPC phenotype (Walker and Kempermann, 2014), thus a direct comparison between human and rodent NSPC studies cannot be made. Therefore, it is not clear if human and animal NSPCs differ in their differentiation and proliferation profiles.

Within this methods manuscript, we demonstrate an *in vitro* protocol to assess the intrinsic and extrinsic directed differentiation and proliferation of adult human, porcine, and rodent spinal cord NSPCs. This direct comparison of human and animal stem cell behavior is necessary to further our understanding of human NSPC regeneration potential and expands our understanding of how basic therapeutic advancements translate to clinical interventions. Human spinal cords were obtained from NDD organ donors and were processed immediately for cell culture using the neurosphere assay. NDD organ donors were identified as detailed in the Trillium Gift of Life Donor Resource Manual (Trillium Gift of Life Network, 2015). We selected porcine and rodent as our comparative species due to their predominance in previous preclinical and basic science research animal models (Cheriyan et al., 2014; Kim et al., 2018). Here, we processed primary NSPCs from humans, porcines, and rodents identically as an adherent layer to eliminate potential confounding cell culture differences and allow a direct comparison. Our culture protocol involves an expansion of primary NSPCs and allows an assessment of the proliferation and differentiation responses of human, porcine, and rodent NSPCs to extrinsic factors in parallel.

MATERIALS AND EQUIPMENT

All procedures and experiments are performed using a sterile technique. Quantities mentioned represent the minimum requirements for the extraction and culture of one human, porcine, or rodent spinal cord.

Spinal Cord Extraction

(1) 100 mL dissection buffer: Hank's balanced salt solution (HBSS, Ca^{2+} and Mg^{2+} free) + 2% Penicillin-Streptomycin (PS) + 0.6% D-glucose.
(2) Tiletamine/zolazepam (Telazol®).
(3) Sodium pentobarbital (Fatal-Plus®).
(4) 50 mL falcon tube (x1; Falcon™).
(5) Surgical tools for humans: Sternal saw (System 7 Sternum Saw – Stryker™ 7207-000-000), bone osteotome, 32 mm, 9 ½″ (Blacksmith Surgical, BS-13-34329), mallet (Blacksmith Surgical, BS-13-34011), Deaver Retractor #3 (Sklar Surgical Instruments, 60-3212), Debakey tissue forceps (Sklar Surgical Instruments, 52-5307), Mayo scissors, straight (Sklar Surgical Instruments, 15-1555), Metzenbaum scissors (Sklar Surgical Instruments, 22-1057), Harrington-Mixter clamp (Sklar Surgical Instruments, 55-3012), scalpel handle #3 (BS-01-10001), surgical Scalpel Blade No. 10 (Bard-Parker® Cat. No. 37110).
(6) Surgical tools for porcines: Autopsy saw (Stryker™ Model #810 – Mopec, BD001), spinal column blade (Mopec, BD112), large section blade (Mopec, BD101), bone osteotome, 15 mm, 8″(Blacksmith Surgical, BS-13-34270), mallet (Blacksmith Surgical, BS-13-34011), scalpel handle #4 (BS-01-10003), surgical Scalpel Blade No. 23 (Swann-Morton® No. 0310), scalpel handle #3 (BS-01-10001), surgical Scalpel Blade No. 10(Bard-Parker® Cat. No. 37110), Adson needle holder (Blacksmith Surgical, BS-09-26025), Adson tissue forceps (Blacksmith Surgical, BS-9024), microscissors (McPherson-Vannas Micro Scissors, straight, 8 cm long, 0.1 mm tips, 5 mm blades; Kent Scientific Corporation, INS600124), paddle retractors (Kelly Retractors 64 × 76 mm, 10.5″; Medline Industries,

Inc., MDS1815630), finger retractors (Finger Volkmann Retractors 6 prong, 4 1/2″; Medline Industries, Inc., MDS1838106).
(7) Surgical tools for rodents: Curved standard operating scissors (Medline Industries, Inc., MDS0812115), tissue forceps with teeth (Medline Industries, Inc., TRI66190H), fine operating with scissors straight blades (Medline Industries, Inc., MDS0800411), hemostat forceps (Medline Industries, Inc., MDS1222310), fine forceps (Medline Industries, Inc., DYND04046H), micro-dissection scissors (Medline Industries, Inc., MDG3860761).

Central Canal Dissection

(1) 100 mm Petri dishes (x3) with 15 mL HBSS in each.
(2) 1.5 mL microcentrifuge tube (x1).
(3) Dissection microscope.
(4) Tray with ice.
(5) Surgical tools for human and porcine: fine forceps (x3) (Medline Industries, Inc., DYND04046H), scalpel handle (Medline Industries, Inc., MDS10801), scalpel blade No. 13 (Swann-Morton® No. 0239), Iris scissors with straight edges (Medline Industries, Inc., MDS0859411), Wescott micro-scissors with curved blades (Medline Industries, Inc., MDS0910311).
(6) Surgical tools for rodent: fine forceps (x3) (Medline Industries, Inc., DYND04046H), scalpel handle (Medline Industries, Inc., MDS10801), scalpel blade No. 13 (Swann-Morton® No. 0239), micro Iris scissors with straight edges (Medline Industries, Inc., MDS0729836), McPherson-Vannas micro Iris scissors with curved blades (Medline Industries, Inc., MDS0707764).

Tissue Dissociation, Purification and Primary Cell Seeding

(1) Papain Dissociation kit (Worthington biochemical Inc., LK003150).
(2) Rotary Shaker.
(3) Centrifuge.
(4) 15 and 50 mL canonical tubes (Falcon™).
(5) Serological pipettes (5, 10, and 25 mL, Corning™).
(6) 40 μm nylon cell strainer (VWR, 10054-462).
(7) Hemocytometer.
(8) Matrigel (Growth factor reduced; Corning™, 354230) coated six-well plates (see note 1).
(9) Neurobasal-A medium (Thermo Fisher Scientific, 10888022).
(10) L-glutamine, 200 mM (Gibco, A2916801).
(11) Penicillin-Streptomycin (PS), 10,000 U/mL (Gibco, 15140122).
(12) B27™ minus vitamin A (B27), 50X (Gibco, 12587010).
(13) Human recombinant epidermal growth factor (EGF, Sigma, E9644).
(14) Human recombinant basic fibroblast growth factor (bFGF2, Sigma, F3685).
(15) Heparin (Sigma, H3149).
(16) 1:1DMEM/F12 (Sigma, D8900).
(17) Hormone mix: 1:1 DMEM/F12, 0.6% glucose, 3 mM $NaHCO_3$, 5 mM HEPES, 25 μg/mL insulin, 100 μg/mL apo-transferrin, 10 μM putrescine, 30 nM selenium, and 20 nM progesterone in distilled water.
(18) Serum-free media (SFM): Neurobasal-A medium, 2 mM L-glutamine, 100 U/mL PS, 1% B27, and 10% hormone mix.
(19) Proliferation media (EFH): SFM + 20 ng/mL EGF + 20 ng/mL bFGF2 + 2 μg/mL heparin.

NSPC Culture and Passaging

(1) Proliferation media (EFH).
(2) Ultra-low attachment six-well plates (Corning™, C3516).
(3) StemProAccutase (Gibco, A1110501).
(4) Hemocytometer.
(5) 15 mL canonical tubes.

NSPC Treatment Assay

(1) Proliferation media (EFH).
(2) Fetal bovine serum (FBS) (Corning™, 35015CV).
(3) 96 well plate with black wells (Thermo Fisher Scientific, 137101) coated with Matrigel-growth factor reduced.
(4) 1X Phosphate buffer saline (PBS): [NaCl] = 137 mM, [KCl] = 2.7 mM, $[Na_2HPO_4]$ = 10 mM, $[KH_2PO_4]$ = 1.8 mM, pH 7.4.
(5) Bromodeoxyuridine (BrdU, Sigma, B5002).
(6) StemProAccutase.
(7) Hemocytometer.
(8) 15 mL canonical tubes.

NSPC Characterization

(1) 4% paraformaldehyde (Sigma, P6148) in 1X PBS, pH 7.4.
(2) 1X PBS.
(3) Normal goat serum (NGS, Thermo Fisher Scientific, P131873).
(4) 0.3% Triton-X (Sigma, X100) in1X PBS.
(5) 2 M hydrochloric acid.
(6) Borax buffer, pH 9.2.
(7) Hoechst 33342, trihydrochloride, trihydrate – 10 mg/mL (Invitrogen, H3570).
(8) Primary antibodies: β-III tubulin (STEMCELL Technologies, 01409), GFAP (EMD Millipore, Ab5804), O4 (R&D Systems, MAB1326), Sox2 (Abcam, Ab97959), BrdU (EMD Millipore, MAB4072) (see note 2).
(9) Secondary antibodies: Goat anti-mouse IgG AlexaFlour®488 and 594 (Abcam, ab150113 and ab150116), Goat anti-Rabbit IgG AlexaFlour488 and 594 (Abcam, ab150077 and ab150080) (see note 2).

METHODOLOGY

This protocol, summarized in **Figure 1**, describes the extraction of human, porcine, and rodent spinal cord tissue using an anterior approach for humans and a posterior approach for porcines and rodents. It also describes how to culture NSPCs

FIGURE 1 | Experimental work-flow depicting spinal cord extraction (20–40 min), central canal dissection (20–40 min), tissue dissociation and purification (2–3 h), NSPC culture (up to 10 weeks), treatment (up to 3 weeks), and characterization (2 days).

from all species using identical methods to allow the direct comparison of cellular behavior.

All animals were treated in strict compliance with the Canadian Council on Animal Cares guidelines for the Care and Use of Experimental Animals, all protocols were approved by the Animal Care Committee of the Ottawa Hospital Research Institute. For the extraction of human spinal cord tissue, ethics approval was obtained from the Ottawa Health Science Network Research Ethics Board. The consent form and process complied with the template provided by the University of Ottawa[1] and followed the Tri-Council Policy Statement Guidelines (Canadian Institutes of Health Research, 2018). Informed written consent was obtained from the next of kin of the deceased organ donor.

Spinal Cord Extraction for Humans (20–40 min), Porcines (30–40 min), and Rodents (10–20 min)

Human spinal cord is extracted from adult (≥18 years old) NDD following aortic cross-clamping and removal of other transplant organs, approximately 2 h after cessation of circulation. If the heart and lungs are retrieved for transplant, then the rostral thoracic spinal cord is more easily attained. The spinal cord tissue is extracted using the same anterior exposure that was used for transplant organ removal (simulated in porcine, **Figures 2A–C**).

(1) Contain the remaining tissues and organs with a green towel and use a Deaver retractor to retract and expose the spinal column.
(2) Identify the sacral promontory and count the lumbar vertebrae to determine the L2 level.
(3) Using an osteotome and the mallet, perform a transverse wedged-shaped osteotomy through the L2 vertebral body to expose the spinal canal and allow the footplate of the sternal saw to be placed under the posterior aspect of the vertebral body.
(4) Using the sternal saw angled 45° medially (**Figure 2A**), cut through the vertebral bodies in a caudal to rostral direction holding the footplate of the sternal saw up against the posterior aspect of the vertebral body to ensure the cord and thecal sac are not damaged. Take care not to change the angle of the sternal saw as this could result in difficulty retrieving the sternal saw. Then, mobilize the tissues and organs to the contralateral side and perform the same maneuvers on the contralateral side.
(5) After performing the transverse cuts bilaterally with the sternal saw, remove the vertebral bodies using an osteotome to detach the rostral attachment (**Figure 2C**).
(6) Starting at the second lumbar vertebral level, use a closed Harrington-Mixter clamp to dissect the thecal sac circumferentially. Using the Harrington-Mixter clamp, gently retract the thecal sac ventrally. Use the Mayo or Metzenbaum scissors to transect the thecal sac at the L2 level. Then, retract the dura ventrally with forceps and use the Metzenbaum or Mayo scissors to cut the nerve roots bilaterally in a caudal to cranial direction. This allows the thecal sac containing the spinal cord to be mobilized and minimizes trauma to the spinal cord tissue itself. Once the thecal sac has been dissected to the rostral end of the vertebral exposure, transect the rostral end of the thecal sac with the spinal cord using Metzenbaum or Mayo scissors or a number 10 blade.
(7) Incise the dura with Metzenbaum scissors and place the extracted spinal cord tissue in the sterile cold (4°C) dissection media in a 50 mL conical tube on ice for transport to the tissue culture room. Typically, the spinal cord is sectioned in 20–25 cm long sections. If the thoracic organs were removed, the spinal cord can be more easily extracted to the higher thoracic levels.

While an anterior approach was used in humans because of the organ donation positioning and exposure, the extraction of porcine spinal cord described here utilizes a posterior approach given the ease of this approach and that the porcines did not undergo organ tissue retrieval and exposure.

(1) First, sedate porcines with 4 mg/kg of intramuscular tiletamine/zolazepam (Telazol®) and anesthetize with 2% isoflurane in 100% oxygen. Then, euthanize porcines by administrating sodium pentobarbital (Fatal-Plus®) intravenously at ≥100 mg/kg according to institution approved animal protocol.
(2) Orient porcine in the prone position. Using a No. 4 scalpel handle with No. 23 blade, make a longitudinal incision over the spinous processes starting from the T1 thoracic vertebrae and ending at the L2 lumbar vertebrae (see note 3). Make two transverse incisions perpendicular to the longitudinal incisions at the first thoracic vertebrae and last lumbar vertebrae (**Figure 2D**).
(3) Make deep incisions running adjacent to the spinous processes, lamina, and transverse processes to expose the spinous processes of the vertebrae (**Figure 2E**). For this cut, ensure that the incisions are deep to expose the ribs

[1]"Consent Process and Templates," University of Ottawa, accessed November 13, 2019, https://research.uottawa.ca/ethics/guidelines/consent-process

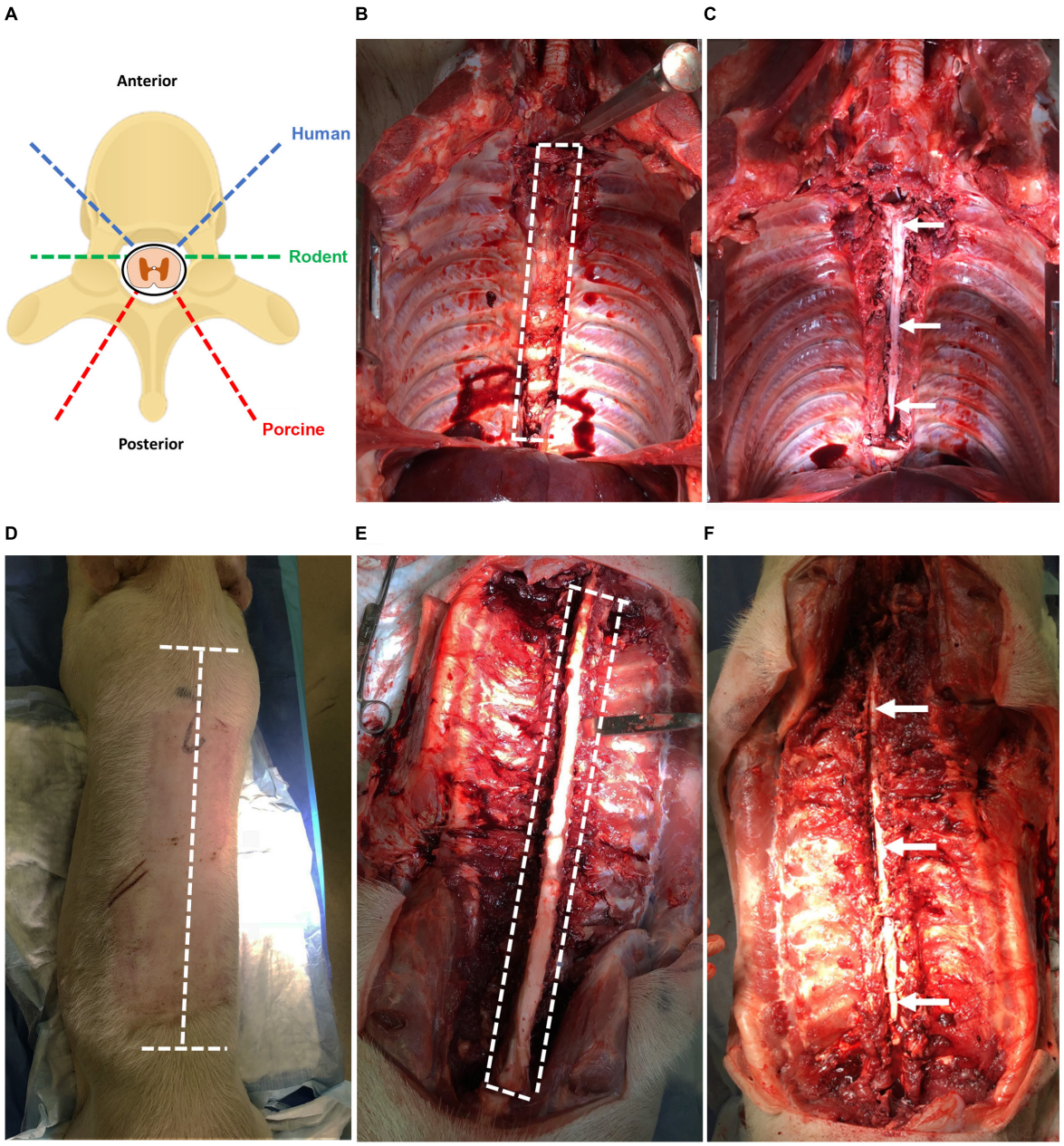

FIGURE 2 | (A) Angles of approach for laminectomy in human, rodent, and porcine to extract the spinal cord. The dashed blue line indicates humans; green indicates rodents; red indicates porcines. **(B)** Laminectomy of the human spinal cord using anterior approach simulated in a porcine (T2–T12). Heart, lungs, esophagus, and major vessels have been removed for improved visibility. The dashed white line indicates the region of the spinal cord to be cut. **(C)** Exposed spinal cord post-laminectomy using the anterior approach from T2–T12. The thecal sac containing the spinal cord tissue is indicated by the arrow. **(D)** Laminectomy of the porcine spinal cord using a posterior approach with incisions lines marked. The dashed white line indicates incisions required to expose the vertebral column. **(E)** Laminectomy of the porcine spinal cord using the posterior approach with vertebral column exposed and paraspinal muscles removed for clarity. The dashed white line indicates cuts required to expose the spinal cord. **(F)** Exposed spinal cord post-laminectomy using the posterior approach from T1 to L2. The thecal sac containing the spinal cord tissue is indicated by the arrows.

and such that all the paraspinal muscles are severed from their insertions.

(4) Expose the posterior spinal column through retraction of the paraspinal muscles with paddle or sharp prong finger retractors. If retraction is not possible, excise the para-spinal muscles and overlying skin by dissecting the fascia of the muscles using a scalpel with No. 23 blade. After the para-spinal muscles have been separated from underlying

fascia, make a longitudinal incision lateral to the muscle such that the muscle can be removed.

(5) Cut through the lamina using an autopsy saw mounted with a large section or spinal column blade. Cut a through the lamina by angling the saw orthogonal to the lamina and stopping before the spinal canal (**Figure 2A**). Cut the vertebral column with the desired spinal cord length to be extracted.

(6) Sever the rostral and caudal ends of the spinous processes using an osteotome and mallet being cautious as to not sever the spinal cord. Remove the spinous processes and lamina using an osteotome and mallet taking care to avoid damaging the cord (**Figure 2F**). Then, lift the dura covered spinal cord using tooth forceps and carefully dissect rostrally. Sharply cut the spinal cord at the exposed rostral end with a No. 3 scalpel handle with No. 10 blade. Use Metzenbaum or Mayo scissors and forceps to cut the nerve roots bilaterally in a caudal to cranial direction.

(7) Place the extracted spinal cord tissue in the sterile cold (4°C) dissection media in a 50 mL conical tube on ice for transport to the tissue culture room. A 25–30 cm spinal cord section from the upper thoracic to lower lumbar region can be obtained under usual conditions. The time elapsed between euthanasia and extraction of the spinal cord is 30–40 min.

The extraction of rodent spinal cord tissue also uses a posterior approach.

(1) Anesthetize rodents with 4% isoflurane in 100% oxygen and euthanize by decapitation according to institution approved animal protocol.

(2) Place rodents on their ventral surface and sterilize skin on the dorsal surface with 70% ethanol.

(3) Excise the skin on the dorsal surface around and along the vertebral column using operating scissors.

(4) Make a bilateral incision around the vertebral column at the caudal end of the lumbar spinal cord using operating scissors and then cut the vertebral column transversely.

(5) Perform a bilateral laminectomy from the point of transection toward the rostral direction. Use dissection scissors to cleave the lamina and retract the dorsal vertebral column throughout the process until the entire spinal cord length is exposed.

(6) Gently lift the spinal cord from the caudal end using fine forceps and cleave the spinal nerves in the rostral direction. Place the extracted spinal cord tissue in the sterile cold (4°C) dissection media in a petri dish on ice.

Dissection of the Human, Porcine, and Rodent Spinal Cord (20–40 min)

The procedure outlined here describes the excision of the ependymal cell containing region of the central canal of the spinal cord. This technique is novel compared to previous methods (Dromard et al., 2008; Mothe and Tator, 2015) and may be advantageous given the considerable reduction of contaminating white and gray matter. Briefly, the spinal cord is cleansed of its meninges, sectioned into thin slices (∼1–2 mm) using a scalpel blade then micro-dissected to excise a cuboidal tissue sample containing the central canal (**Figure 3**). Consistency in the dissection technique is necessary to obtain a similar primary cell population between biological replicates and to minimize contamination from progenitor cells in the surrounding gray and white matter tissue.

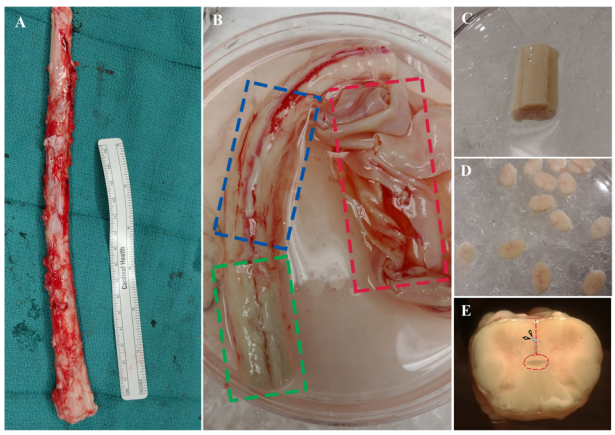

FIGURE 3 | (A) Spinal cord is extracted from NDD adult human organ donors. **(B)** The three layers of meninges are indicated by dashed boxes; dura in red, arachnoid in blue, and pia in green. **(C)** Spinal cord segment after removal of meninges and ready for sectioning. **(D)** ∼1–2 mm thick sections to be dissected. **(E)** A cross-sectional view of the spinal cord; dashed line in red indicating direction of central canal dissection.

(1) Transfer the spinal cord segment using tissue forceps into the first sterile petri dish containing cold dissection buffer.

(2) Clean the spinal cord of the dura using straight-edge dissection scissors. Proceed to remove the underlying arachnoid under a dissection microscope by holding the tissue in place with fine forceps and cutting away the meninges using curved edge microscissors. Start from either end of the whole spinal cord tissue, pull away the meninges with forceps, then place one edge of microscissors between the meninges and the underlying tissue and cut all the way down to the opposite end (**Figure 3B**, see note 4).

(3) Once cleaning is complete (**Figure 3C**), wash the spinal cord in cold dissection buffer and place it in a new petri dish with cold dissection buffer for sectioning.

(4) Proceed to section the tissue into thin ∼1–2 mm sections using a scalpel blade and forceps. Start at either end of the tissue and orient the forceps downwards to hold the tissue on its lateral ends. Using the perpendicular edge of the forceps as a guide for the blade, proceed to section the tissue transversely. Sectioning is facilitated by the removal of meninges in the previous steps.

(5) Transfer the thin sections to a new petri dish with cold dissection for central canal dissection (**Figure 3D**). Initiate dissection from the ventral sulcus and cut toward the central canal using curved edge microscissors; use

forceps to hold tissue sections in place during dissection. Stop cutting just before reaching the central canal and start cutting toward either lateral direction. Complete the dissection by cutting around the central canal region to excise a cuboidal piece (**Figure 3E**). It is important to use curved edge micro-scissors in this step to avoid excision of the central canal region from the underside of the section.

(6) Ensure enough spinal cord is sectioned to yield enough primary cells for culture. Typically, 5–7 sections yield 1–5 $\times$ 10^6 cells. Alternatively, one gram of dissected central canal tissue yields 5 $\times$ 10^7 cells.

(7) Transfer the dissected central canal tissue into sterile 1.5 mL microcentrifuge tubes and mechanically dissociate the tissue using scissors until completely minced. Keep the microcentrifuge tubes on ice while preparing the tissue dissociation kit.

Tissue Dissociation, Purification and NSPC Seeding (2–3 h)

(1) The minced central canal tissue is dissociated into single cells using a papain / DNase treatment from Worthington Biochemicals, according to the manufacturer's instructions. Transfer the minced tissue into a 15 mL conical tube containing the papain solution and place it on a rocker platform at 37 degrees. Use 0.2–0.4 g of tissue per vial provided in the kit and incubate for 1–2 h. This should yield 1–2 $\times$ 10^7 cells per vial.

(2) Following digestion, triturate using a 10 mL pipette until the tissue fragments are disintegrated to form a cloudy solution.

(3) Centrifuge at 500 $\times$ *g* for 5 min, discard the supernatant, and resuspend the cells in an ovomucoid/albumin solution from the dissociation kit to inhibit papain activity.

(4) Set up a discontinuous gradient centrifugation to purify NSPCs of contaminant (post-mitotic and glial) cells and debris. Using a 10 mL pipette, gently layer the resuspended cells in step 3 onto 5 mL of albumin-ovomucoid solution from the dissociation kit.

(5) Centrifuge at 70 $\times$ *g* for 6 min, discard the supernatant, and resuspend the cells in 10 mL of warm EFH.

(6) Filter the cells through a 40 μm sterile filter using 100–1000 μL tips, add 30 mL of warm EFH, and then centrifuge at 300 $\times$ *g* for 5 min.

(7) Resuspend the cells in 1 mL of warm EFH and count the cell density using a hemocytometer.

(8) Seed the primary cells in 6-well plates pre-coated with Matrigel at a density of 20 cells/μL in a total of 4 mL EFH then incubate at 37°C, 5% CO_2, 20% O_2 for 1 week undisturbed.

Feeding (15–30 min) and Passaging (30–45 min) Primary NSPC Cultures

The protocol described in this section is based on Mothe and Tator (2015), who have optimized *in vitro* culture conditions and techniques to successfully propagate adult human spinal cord NSPCs through multiple passages. They also demonstrated that human primary NSPCs require an adherent substrate to be successfully passaged, which can then be assessed as neurospheres. Rodent NSPCs do not require an adherent substrate for expansion of primary cells; but since the type of culture (adherent vs. suspension) is known to influence population phenotype, they are cultured similarly as human NSPCs.

(1) After 1 week, replace 50% of the medium with warm EFH containing double the concentration of mitogens (40 ng/mL EGF and FGF2). NSPCs are fed this way every 2 or 3 days for the next 1–3 weeks until adherent cultures are visibly expanding (see note 5).

(2) Once proliferating NSPCs are visible (**Figure 4**), remove 100% of the media, wash with warm PBS, and replace media with 2 mL of fresh warm EFH. Cultures are fed by replacing 100% of the media every 2–3 days while monitoring their growth (see note 6).

(3) Passage the cells before they reach confluence using Accutase (see note 7). Add enough Accutase to cover the surface (1 mL per well of a 6-well plate). Incubate at room temperature for 5–10 min while regularly observing to see if cells have lifted. Knock the plate on the side to detach cells.

(4) Transfer the lifted cells into a sterile conical tube, wash each well with warm PBS and transfer washes into the tube.

(5) Centrifuge at 300 $\times$ *g* for 5 min, discard the supernatant and resuspend in 1 mL of warm EFH.

(6) Count the cell density to seed NSPCs for secondary expansion or conditioned treatment.

Generating Neurospheres (30–45 min)

To further select for self-renewing NSPCs and eradicate progenitors, cultures must be passaged and seeded in suspension. Under these conditions, self-renewing stem cells will form neurospheres that can be separated from non-stem cells by mass centrifugation. However, it is important to note that NSPC behavior changes with increased time spent in culture and away from their physiological niche. The steps below can be used to culture secondary (and beyond) neurospheres of human, porcine, and rodent NSPCs (**Figure 4**).

(1) Seed secondary NSPCs in 6 well plates at a density of 10 cells/μL in a total of 2 mL EFH then incubate at 37°C, 5% CO_2, 20% O_2.

(2) Allow NSPCs to grow for 1 week unperturbed to prevent neurosphere aggregation (see note 8).

(3) After 1 week, transfer the media containing neurospheres into a 15 mL conical flask. Wash the wells with warm PBS and transfer washes into the 15 mL conical flask.

(4) Centrifuge at 300 rpm for 5 min, discard the supernatant containing dead/single cells and resuspend in 1–2 mL Accutase. Triturate using a 1000 μL pipette tip and incubate for 5–10 min at room temperature.

(5) Centrifuge the cell suspension at 1500 rpm for 5 min, discard the supernatant, and resuspend in 1 mL warm EFH.

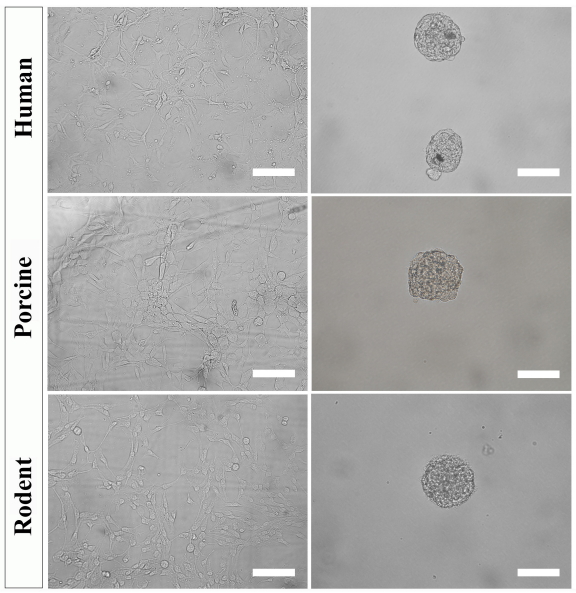

FIGURE 4 | Primary NSPC cultures from adult human, porcine, and rodent spinal cord are cultured under identical conditions as an adherent layer (column 1). NSPCs can be passaged and cultured in suspension at low cell density to form neurospheres (column 2). Images were taken at 20x magnification. Scale bar = 100 μm.

(6) Count the cell density and seed NSPCs for tertiary expansion (10 cells/μL) or conditioned treatment.

Treatment and Direct Comparison of Species NSPC (Up to 3 Weeks)

Here, we propose a flexible high throughput assay to treat human, porcine, and rodent NSPCs identically and to characterize NSPC proliferation and differentiation. The parameters of this assay (cell density, culture conditions, and time spent in culture) were all optimized for the treatment of NSPCs for up to 2 weeks without becoming over confluent. Importantly, this assay is versatile to allow the assessment of various exogenous factors.

(1) Seed primary derived NSPCs onto Matrigel-coated 96-well plates in a total of 150 μL EFH. The cell density used (1–5 cells/μL) will depend on the treatment (see note 9). Leave cultures incubated at 37°C, 5% CO_2, 20% O_2 for 3 days undisturbed. This step is to further select for NSPCs and allow enough time for NSPCs to adhere to the basement surface.
(2) Aspirate the media and wash with warm PBS (50 μL). Ensure that conditioned media/treatments are prepared and warmed at 37°C.
(3) To induce differentiation, replace the PBS wash with 1% FBS in 150 μL SFM. To induce proliferation, replace the PBS wash with 150 μL EFH. Incubate at 37°C, 5% CO_2, 20% O_2 and replace media with corresponding fresh media every 2–3 days. NSPCs can be treated up to 2 weeks in 1% FBS or EFH without reaching confluency.
(4) To assess proliferation, a DNA analog (e.g., BrdU, EdU) can be used as a marker for the S-phase of the cell cycle. In our experiments, BrdU (10 μM) is added 24 h before fixing.
(5) Fix NSPC cultures at desired time points (up to 2 weeks) using 4% PFA. Incubate cultures with PFA for 20 min at room temperature, followed by three PBS (50 μL) washes. Cultures need not be characterized immediately; add a total of 100 μL PBS into each well and store the plate at 4 degrees.

Characterization of NSPC Proliferation and Differentiation (2 Days)

A method of NSPC characterization by immunocytochemistry is proposed here. This involves the fluorescent labeling of specific cell phenotypes according to their molecular signatures (see **Table 1**). A working volume of 50 μL/well is used for a 96 well plate.

(1) Remove PBS from each well to be stained and add 50 μL of PBS for 10 min at room temperature to equilibrate.
(2) Pre-treat with 10% NGS to prevent non-specific antibody binding and with 0.3% Triton-X to permeabilize cells for 30 min at room temperature. If staining for membrane receptors, such as O4, skip the permeabilization step. Wash each well three times with PBS for 5 min at room temperature.
(3) For BrdU staining only, DNA denaturation is required by incubating cultures with 2 M HCl at 37 degrees for 30 min. Wash twice with borax for 5 min each followed by three washes with PBS for 5 min each.
(4) Dilute the primary antibody in 10% NGS in PBS according to the optimized dilution (see **Table 1**) and incubate at 4 degrees overnight.
(5) The next day, wash each well three times with PBS for 5 min at room temperature.
(6) Dilute the secondary antibody (1:500) in PBS and incubate for 2 h at room temperature (see note 10). Wash three times with PBS.
(7) Counterstain nuclei with Hoechst (1:2000 dilution in PBS) for 5 min at room temperature. Wash twice with PBS, add 100 μL PBS into each well for storage. NSPCs are now ready to be visualized by immunofluorescence.

DISCUSSION

We have successfully cultured primary spinal cord NSPCs from three species using comparable dissection techniques and identical culture conditions. Here, we describe a model to treat NSPCs with exogenous factors using the same defined parameters for all species, allowing for a direct comparison of species NSPC proliferation and differentiation. We also describe a means to characterize NSPC proliferation and differentiation using immunocytochemistry (**Table 1**) which permits the visualization and quantification of cellular phenotypes. We confirmed that human, porcine, and rodent NSPCs are self-renewing (**Figure 4**) and maintain high expression of neural stem cell marker

TABLE 1 | Descriptions of the antibodies used for NSPC characterization including antibody specificity, dilution used, and source.

Marker	Specificity	Dilution	Antibody manufacturer
β-iii tubulin	Cytoskeletal protein abundant in neural precursors	1:500	STEMCELL Technologies
GFAP	Intermediate filament cytoskeletal protein expressed in astrocytes and brain stem cells	1:1000	EMD Millipore
O4	Membrane receptor in mature oligodendrocytes	1:500	R&D Systems
BrdU	Cell cycle (S-phase) checkpoint used as a proliferation marker	1:2000	EMD Millipore
Sox2	Transcription factor necessary for the self-renewal of neural stem cells	1:1000	Abcam

GFAP, glial fibrillary acidic protein; BrdU, bromodeoxyuridine; Sox2, SRY-related HMG box.

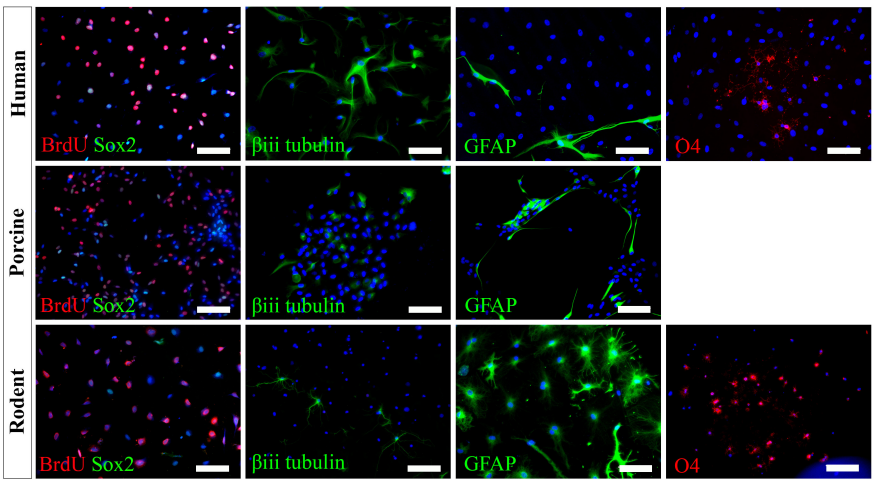

FIGURE 5 | Human, porcine, and rodent primary NSPCs grew in EFH proliferate ($BrdU^+$) and express neural stem cell marker Sox2. Upon differentiation, NSPCs are multipotent and generate β-iii $tubulin^+$ neural precursors, $GFAP^+$ astrocytes, and $O4^+$ oligodendrocytes. No $O4^+$ staining was observed from porcine NSPCs. Scale bar = 100 μm.

TABLE 2 | Expected differentiation profile of primary-derived spinal cord NSPCs that have been treated with 1% FBS for 7 days for humans, porcines, and rodents.

	Human	Porcine	Rodent
Neurons	≈45%	≈20%	≈10%
Astrocytes	≈5%	≈35%	≈40%
Oligodendrocytes	<1%	*	≈5%

* *Oligodendrocytes were not detected with the O4 antibody and under the conditions tested.*

Sox2 when stimulated to proliferate with mitogen treatment (**Figure 5**). Unlike NSPCs in the brain that co-express Sox2 and GFAP, NSPCs in the mammalian spinal cord express Sox2 but not GFAP, allowing for the characterization of spinal cord NSPCs using Sox2 alone (Meletis et al., 2008; Becker et al., 2018). We've shown that human and rodent NSPCs are multipotent and differentiate into β-iii $tubulin^+$ neurons, $GFAP^+$ astrocytes, and $O4^+$ oligodendrocytes (**Figure 5** and **Table 2**). We also found that porcine NSPCs differed in that they did not form identifiable $O4^+$ oligodendrocytes under the conditions tested. Therefore, our model, for the first time, can allow direct comparisons of human and animal NSPC proliferation and differentiation utilizing identical culture conditions so that intrinsic differences between the human and animal cells can be identified.

Initially, primary NSPCs from all species were stimulated to proliferate with mitogen treatment (EGF, FGF2) and grown on Matrigel, a necessity for human (Mothe et al., 2011) and porcine but not rodent NSPCs. We have cultured NSPCs from all species on Matrigel as an adherent mono-layer since the culture system (adherent vs. suspension) may affect the proportion of stem, progenitor, and mature cells in the final population (Walker and Kempermann, 2014). Also, the adherent layout results in a uniform distribution of primary derived NSPCs with minimal cell-to-cell contact allowing the direct assessment of exogenous factors. The advantage of this setting is that the causal mechanisms can be easily examined by modifying the chemical composition of the media. This model, however, presents an important limitation in the interpretation of data and inference to *in vivo* behavior where cell-to-cell contact is present.

To further select for self-renewing NSPCs, primary NSPCs can be passaged and seeded at low cell density (≤10 cells/μL) to form clonal neurospheres. These neurospheres arise from the proliferation of a single stem cell and thus may better portray the NSPC lineage profile (Narayanan et al., 2016). Secondary (and beyond) neurospheres can be dissociated into single cells and assessed similarly as primary derived NSPCs using our model. It is important to note, however, that NSPC behavior is expected to change with increased time in culture and with an increased passage. Therefore, assessment of primary NSPCs portrays *in vivo*

behavior best since they spend minimal time outside their natural niche (Gil-Perotín et al., 2013).

The proposed model can serve to evaluate and compare human, porcine, and rodent NSPC responses concerning many physiological and disease processes. For example, response to physiologically and clinically relevant exogenous factors can be assessed; we can treat human and rodent NSPCs with factors that are upregulated in spinal cord injury and drive known cellular responses in rodent NSPCs (Okada et al., 2004; Kang and Kang, 2008; Moreno-Manzano et al., 2009; Lacroix et al., 2014) to determine if a similar response occurs in human NSPCs. A functional assay as such could depict causal mechanisms that would be impossible to obtain otherwise from living patients or post-mortem samples. This model can also be used to optimize a combination of growth factors to promote human NSPC survival and differentiation following transplant. Growth factors are commonly used with rodent and human NSPC transplants (Karimi-Abdolrezaee et al., 2010; Lu et al., 2012; Kadoya et al., 2016; Kumamaru et al., 2018), but potential differences in signaling mechanisms between species (Mothe et al., 2011) may hinder the translation of such treatments. As such, it is important to consider how human NSPCs would respond to exogenous factor treatments, which can be assessed *in vitro* using our proposed model and with the consideration that the factors utilized in this protocol to obtain NSPCs may also have an effect due to differences in signaling mechanisms between species. Ultimately, the evaluation of human NSPCs and comparison with animal NSPCs can clarify human NSPC response to spinal cord injury and advance the translation of regenerative strategies.

According to our knowledge, adult porcine spinal cord NSPCs have not been previously characterized for oligodendrocyte differentiation. In this study, we did not observe any oligodendrocyte differentiation from our porcine cultures using the O4 antibody and under the conditions tested. While O4 has been reported to label oligodendrocytes obtained from the brains of adult porcines (Liard et al., 2009), their protocol differed in that they obtained NSPCs from the brain rather than the spinal cord, cultured their NSPCs as neurospheres rather than in a monolayer, and utilized a different O4 antibody. It is also possible that the O4 antibody used in this study does not recognize the porcine epitope and further characterization using alternative antibodies may be beneficial. This finding highlights a challenge for conducting cross-species comparisons in which reagents that cross-react with all species being tested are needed to further understand the translational assessment of animal studies to humans. Besides, we have used NG2 and Olig2 for rodent cell labeling. However, because they are markers for early oligodendrocyte progenitors and do not exclusively label the oligodendrocyte lineage, we did not pursue further assessment in humans and porcines. We also tried CNPase and PDGFR, however, while we were able to get labeling in rodents, we were unable to get labeling in humans. Thus, in the end, since we wanted to identify terminally differentiated oligodendrocytes, and because more preclinical studies are done with rodents rather than porcines, we used O4 for labeling of oligodendrocytes.

In conclusion, the model described here is the first which allows a direct comparison of the differentiation and proliferation characteristics of primary adult human and animal spinal cord NSPCs. This assay uses the same parameters for all species, is reproducible, and allows for high-throughput testing. This model can help with the identification of species-dependent cell-intrinsic mechanisms which would be important for the translation of regenerative strategies targeting human spinal cord NSPCs.

NOTES

(1) Matrigel plates should be prepared in advance and kept at 4°C until ∼1 h before use. Use a dilution of 1:25 in SFM to coat a thin Matrigel basement layer. We recommend warming the Matrigel plates at room temperature immediately after papain digestion is initiated. Matrigel polymerizes slowly at room temperature to form a basement membrane and is required for the expansion of primary human primary NSPCs. Matrigel can be replaced by other surface coatings such as laminin, poly-D-lysine, and collagen (Mothe et al., 2011).

(2) Optimization of antibody dilutions (primary and secondary) is necessary before immunostaining, especially if antibodies are purchased from a different manufacturer or lot number.

(3) Generally, the first thoracic vertebrae are the first palpable spinous process at the rostral end and the last lumbar vertebrae are the last palpable spinous process at the caudal end. There are 14 thoracic and 6 lumbar vertebrae in porcines.

(4) The spinal cord must be removed of its meninges (dura and arachnoid) to facilitate sectioning of the spinal cord into thin segments. The dura is relatively easy to remove and does not require a dissection microscope while removal of the arachnoid requires closer attention and should be performed under a dissection microscope. The spinal cord with the dura and arachnoid removed will also minimize endothelial contamination.

(5) It is important to observe cultures regularly and track any areas with cell growth. Human NSPCs start to proliferate in small patches and grow radially outward. However, cell growth is not uniformly distributed throughout the wells and is not consistent between human cultures. Therefore, each primary human culture must be frequently observed and treated uniquely.

(6) Do not allow cells to reach confluence (over-crowding) as it becomes difficult to lift NSPCs during the passage. At this stage (near confluence), we recommend having your NSPC treatment protocol and reagents ready.

(7) Accutase is a milder dissociation enzyme than trypsin and is preferred for the delicate treatment of NSPCs.

(8) It is recommended to seed NSPCs at a low cell density and expand for 1 week to minimize sphere aggregation. This would render results more variable and reduce cell viability.

(9) The cell density used depends on the conditions. For example, EFH will stimulate NSPC self-renewal while FBS will induce differentiation. The latter process involves

rapid division of progenitor cells and thus NSPCs will attain confluence quicker in FBS than NSPCs stimulated to self-renewal. For this reason, it is recommended to seed NSPCs at a lower cell density (1 cell/μL) when stimulating differentiation compared to when stimulating self-renewal (5 cells/μL).

(10) Co-staining using several antibodies is possible, if all primary antibodies are generated in different animals and all secondary antibodies bear different fluorophores.

DATA AVAILABILITY STATEMENT

The datasets generated for this study are available on request to the corresponding author.

ETHICS STATEMENT

The animal study was reviewed and approved by the Animal Care Committee of the Ottawa Hospital Research Institute. Written informed consent was obtained from the owners for the participation of their animals in this study. The studies involving human participants were reviewed and approved by Ottawa Health Science Network Research Ethics Board. Written informed consent to participate in this study was provided by the participants' legal guardian/next of kin.

AUTHOR CONTRIBUTIONS

AG, ET, DG, RS, JK, and SC contributed to the design and conception. AG, RS, and JK contributed to the acquisition of data. AG implemented the study. All authors contributed to the drafting of the manuscript.

FUNDING

This study was funded by the Ottawa Hospital Department of Surgery Research Program Award and the Ontario Graduate Scholarship.

ACKNOWLEDGMENTS

We would like to acknowledge the Ottawa Hospital Department of Neurosurgery and TGLM for permitting spinal cord extractions from organ donors and the University of Ottawa Heart Institute Animal Care and Veterinary Service for providing porcines. We would also like to thank Isaac Kim, Ellen Doney, Hesham Ismail, Annemarie Dedek, and Tongda Li for assisting during the porcine spinal cord harvests.

REFERENCES

Badhiwala, J. H., Wilson, J. R., Kwon, B. K., Casha, S., and Fehlings, M. G. (2018). A review of clinical trials in spinal cord injury including biomarkers. *J. Neurotraum.* 35, 1906–1917. doi: 10.1089/neu.2018.5935

Becker, C. G., Becker, T., and Hugnot, J. P. (2018). The spinal ependymal zone as a source of endogenous repair cells across vertebrates. *Prog. Neurobiol.* 170, 67–80. doi: 10.1016/j.pneurobio.2018.04.002

Canadian Institutes of Health Research (2018). *Natural Sciences and Research Council of Canada and Social Sciences and Humanities Research Council. Tri-Council Policy Statement: Ethical Conduct for Research Involving Humans.* Ottawa: Canadian Institutes of Health Research.

Cheriyan, T., Ryan, D. J., Weinreb, J. H., Cheriyan, J., Paul, J. C., Lafage, V., et al. (2014). Spinal cord injury models: a review. *Spinal Cord* 52, 588–595. doi: 10.1038/sc.2014.91

Chhabra, H. S., and Sarda, K. (2017). Clinical translation of stem cell based interventions for spinal cord injury — are we there yet ? *Adv. Drug Deliv. Rev.* 120, 41–49. doi: 10.1016/j.addr.2017.09.021

Dromard, C., Guillon, H., Rigau, V., Ripoll, C., Sabourin, J. C., Perrin, F. E., et al. (2008). Adult human spinal cord harbors neural precursor cells that generate neurons and glial cells in vitro. *J. Neurosci. Res.* 86, 1916–1926. doi: 10.1002/jnr.21646

Gil-Perotín, S., Duran-Moreno, M., Cebrián-Silla, A., Ramírez, M., García-Belda, P., and García-Verdugo, J. M. (2013). Adult neural stem cells from the subventricular zone: a review of the neurosphere assay. *Anatom. Record* 296, 1435–1452. doi: 10.1002/ar.22746

Goldshmit, Y., Sztal, T. E., Jusuf, P. R., Hall, T. E., Nguyen-Chi, M., and Currie, P. D. (2012). Fgf-dependent glial cell bridges facilitate spinal cord regeneration in zebrafish. *J. Neurosci.* 32, 7477–7492. doi: 10.1523/JNEUROSCI.0758-12.2012

Grégoire, C.-A., Goldenstein, B. L., Floriddia, E. M., Barnabé-Heider, F., and Fernandes, K. J. L. (2015). Endogenous neural stem cell responses to stroke and spinal cord injury. *Glia* 63, 1469–1482. doi: 10.1002/glia.22851

Hamilton, L. K., Truong, M. K. V., Bednarczyk, M. R., Aumont, A., and Fernandes, K. J. L. (2009). Cellular organization of the central canal ependymal zone, a niche of latent neural stem cells in the adult mammalian spinal cord. *Neuroscience* 164, 1044–1056. doi: 10.1016/j.neuroscience.2009.09.006

Hawryluk, G. W. J., Mothe, A. J., Chamankhah, M., Wang, J., Tator, C., and Fehlings, M. G. (2012). In vitro characterization of trophic factor expression in neural precursor cells. *Stem Cells Dev.* 21, 432–447. doi: 10.1089/scd.2011.0242

Kadoya, K., Lu, P., Nguyen, K., Lee-Kubli, C., Kumamaru, H., Yao, L., et al. (2016). Spinal cord reconstitution with homologous neural grafts enables robust corticospinal regeneration. *Nat. Med.* 22, 479–487. doi: 10.1038/nm.4066

Kang, M. K., and Kang, S. K. (2008). Interleukin-6 induces proliferation in adult spinal cord-derived neural progenitors via the JAK2/STAT3 pathway with EGF-induced MAPK phosphorylation. *Cell Prolif.* 41, 377–392. doi: 10.1111/j.1365-2184.2008.00537.x

Karimi-Abdolrezaee, S., Eftekharpour, E., Wang, J., Schut, D., and Fehlings, M. G. (2010). Synergistic effects of transplanted adult neural stem/progenitor cells, chondroitinase, and growth factors promote functional repair and plasticity of the chronically injured spinal cord. *J. Neurosci.* 30, 1657–1676. doi: 10.1523/JNEUROSCI.3111-09.2010

Kim, K. T., Streijger, F., Manouchehri, N., So, K., Shortt, K., Okon, E. B., et al. (2018). Review of the UBC porcine model of traumatic spinal cord injury. *J. Korea. Neurosurg. Soc.* 61, 539–547. doi: 10.3340/jkns.2017.0276

Kulbatski, I., and Tator, C. H. (2009). Region-specific differentiation potential of adult rat spinal cord neural stem/precursors and their plasticity in response to in vitro manipulation. *J. Histochem. Cytochem.* 57, 405–423. doi: 10.1369/jhc.2008.951814

Kumamaru, H., Kadoya, K., Adler, A. F., Takashima, Y., Graham, L., Coppola, G., et al. (2018). Generation and post-injury integration of human spinal cord neural stem cells. *Nat. Methods* 15, 723–731. doi: 10.1038/s41592-018-0074-73

Kwon, B. K., Okon, E. B., Tsai, E., Beattie, M. S., Bresnahan, J. C., Magnuson, D. K., et al. (2011). A grading system to evaluate objectively the strength of pre-clinical data of acute neuroprotective therapies for clinical translation in spinal cord injury. *J. Neurotrau.* 28, 1525–1543. doi: 10.1089/neu.2010.1296

Lacroix, S., Hamilton, L. K., Vaugeois, A., Beaudoin, S., Breault-Dugas, C., Pineau, I., et al. (2014). Central canal ependymal cells proliferate extensively in response to traumatic spinal cord injury but not demyelinating lesions. *PLoS One* 9:e085916. doi: 10.1371/journal.pone.0085916

Liard, O., Segura, S., Pascual, A., Gaudreau, P., Fusai, T., and Moyse, E. (2009). In vitro isolation of neural precursor cells from the adult pig subventricular zone. *J. Neurosci. Methods* 182, 172–179. doi: 10.1016/j.jneumeth.2009.06.008

Lu, P., Wang, Y., Graham, L., McHale, K., Gao, M., Wu, D., et al. (2012). Long-distance growth and connectivity of neural stem cells after severe spinal cord injury. *Cell* 150, 1264–1273. doi: 10.1016/j.cell.2012.08.020

Meletis, K., Barnabé-Heider, F., Carlén, M., Evergren, E., Tomilin, N., Shupliakov, O., et al. (2008). Spinal cord injury reveals multilineage differentiation of ependymal cells. *PLoS Biol.* 6:e060182. doi: 10.1371/journal.pbio.0060182

Moreno-Manzano, V., Rodriguez-Jimenez, F. J., Garcia-Rosello, M., Lainez, S., Erceg, S., Calvo, M. T., et al. (2009). Activated spinal cord ependymal stem cells rescue neurological function. *Stem Cells* 27, 733–743. doi: 10.1002/stem.24

Mothe, A., and Tator, C. H. (2015). Isolation of neural stem/progenitor cells from the periventricular region of the adult rat and human spinal cord. *J. Vis. Exper.* 99, 1–8. doi: 10.3791/52732

Mothe, A. J., Zahir, T., Santaguida, C., Cook, D., and Tator, C. H. (2011). Neural stem/progenitor cells from the adult human spinal cord are multipotent and self-renewing and differentiate after transplantation. *PLoS One* 6:27079. doi: 10.1371/journal.pone.0027079

Narayanan, G., Yu, Y. H., Tham, M., Gan, H. T., Ramasamy, S., Sankaran, S., et al. (2016). Enumeration of neural stem cells using clonal assays. *J. Vis. Exper.* 116, 1–8. doi: 10.3791/54456

Ohori, Y., Yamamoto, S.-I., Nagao, M., Sugimori, M., Yamamoto, N., Nakamura, K., et al. (2006). Growth factor treatment and genetic manipulation stimulate neurogenesis and oligodendrogenesis by endogenous neural progenitors in the injured adult spinal cord. *J. Neurosci.* 26, 11948–11960. doi: 10.1523/JNEUROSCI.3127-06.2006

Okada, S., Nakamura, M., Mikami, Y., Shimazaki, T., Mihara, M., Ohsugi, Y., et al. (2004). Blockade of interleukin-6 receptor suppresses reactive astrogliosis and ameliorates functional recovery in experimental spinal cord injury. *J. Neurosci. Res.* 76, 265–276. doi: 10.1002/jnr.20044

Panayiotou, E., and Malas, S. (2013). Adult spinal cord ependymal layer: a promising pool of quiescent stem cells to treat spinal cord injury. *Front. Physiol.* 4:340. doi: 10.3389/fphys.2013.00340

Ramer, L. M., Ramer, M. S., and Bradbury, E. J. (2014). Restoring function after spinal cord injury: towards clinical translation of experimental strategies. *Lancet Neurol.* 13, 1241–1256. doi: 10.1016/S1474-4422(14)70144-70149

Sabelström, H., Stenudd, M., and Frisén, J. (2014). Neural stem cells in the adult spinal cord. *Exp. Neurol.* 260, 44–49. doi: 10.1016/j.expneurol.2013.01.026

Sabelström, H., Stenudd, M., Réu, P., Dias, D. O., Elfineh, M., Zdunek, S., et al. (2013). Resident neural stem cells restrict tissue damage and neuronal loss after spinal cord injury in mice. *Science* 342, 637–640. doi: 10.1126/science.1242576

Silva, N. A., Sousa, N., Reis, R. L., and Salgado, A. J. (2014). From basics to clinical: a comprehensive review on spinal cord injury. *Prog. Neurobiol.* 114, 25–57. doi: 10.1016/j.pneurobio.2013.11.002

Trillium Gift of Life Network (2015). Trillium Gift of Life Network - Ontario's Organ and Tissue Donation Agency : Public Reporting. Ontario. 2015. Available online at: https://www.giftoflife.on.ca/en/professionals.htm (accessed November 29, 2019).

Varghese, M., Olstorn, H., Berg-Johnsen, J., Moe, M. C., Murrell, W., and Langmoen, I. A. (2009). Isolation of human multipotent neural progenitors from adult filum terminale. *Stem Cells Dev.* 18, 603–613. doi: 10.1089/scd.2008.0144

Varma, A. K., Das, A., Wallace, I. V. G., Barry, J., Vertegel, A. A., Ray, S. K., et al. (2013). Spinal cord injury: a review of current therapy, future treatments, and basic science frontiers. *Neurochem. Res.* 38, 895–905. doi: 10.1007/s11064-013-0991-996

Walker, T. L., and Kempermann, G. (2014). One mouse, two cultures: isolation and culture of adult neural stem cells from the two neurogenic zones of individual mice. *J. Vis. Exp.* 84, 1–9. doi: 10.3791/51225

Weiss, S., Dunne, C., Hewson, J., Wohl, C., Wheatley, M., Peterson, A. C., et al. (1996). Multipotent cns stem cells are present in the adult mammalian spinal cord and ventricular neuroaxis. *J. Neurosci.* 16, 7599–7609. doi: 10.1002/CNE.902890106

Yousefifard, M., Rahimi-Movaghar, V., Nasirinezhad, F., Baikpour, M., Safari, S., Saadat, S., et al. (2016). Neural stem/progenitor cells transplantation for spinal cord injury treatment; a systematic review and meta-analysis. *Neuroscience* 322, 377–397. doi: 10.1016/j.neuroscience.2016.02.034

Conflict of Interest: The authors declare that the research was conducted in the absence of any commercial or financial relationships that could be construed as a potential conflict of interest.

Advantages of publishing in Frontiers

OPEN ACCESS
Articles are free to read for greatest visibility and readership

FAST PUBLICATION
Around 90 days from submission to decision

HIGH QUALITY PEER-REVIEW
Rigorous, collaborative, and constructive peer-review

TRANSPARENT PEER-REVIEW
Editors and reviewers acknowledged by name on published articles

Frontiers
Avenue du Tribunal-Fédéral 34
1005 Lausanne | Switzerland

Visit us: www.frontiersin.org
Contact us: frontiersin.org/about/contact

REPRODUCIBILITY OF RESEARCH
Support open data and methods to enhance research reproducibility

DIGITAL PUBLISHING
Articles designed for optimal readership across devices

FOLLOW US
@frontiersin

IMPACT METRICS
Advanced article metrics track visibility across digital media

EXTENSIVE PROMOTION
Marketing and promotion of impactful research

LOOP RESEARCH NETWORK
Our network increases your article's readership